TECHNISCHE UNIVERSITÄT MÜNCHEN

Fakultät für Chemie
Lehrstuhl für Physikalische Chemie

Photochemical and Photocatalytic Reaction Pathways of Alcohols on Bare and Metal-Loaded TiO_2(110)

Carla Courtois

Vollständiger Abdruck der von der Fakultät für Chemie der Technischen Universität München zur Erlangung des akademischen Grades eines

Doktors der Naturwissenschaften (Dr. rer. nat.)

genehmigten Dissertation.

Vorsitzende	Prof. Dr. Barbara Lechner
Prüfer der Dissertation	1. Prof. Dr. Ulrich K. Heiz
	2. Prof. Dr. Ian Sharp
	3. Prof. Dr. Jennifer Strunk

Die Dissertation wurde am 19.05.2021 bei der Technischen Universität München eingereicht und durch die Fakultät für Chemie am 06.07.2021 angenommen.

Abstract

Photocatalytic alcohol reforming is prospective for providing 'green' hydrogen and value-added oxygenates. However, heterogeneous photocatalysis is currently neither efficient nor selective enough to be applied on industrial scale. The aim of this thesis is to elucidate individual reaction steps in the photocatalytic conversion of alcohols on an atomically defined model system: size-selected Pt or Ni clusters on TiO_2(110). Surface science methods in combination with catalytic concepts enable for the disentanglement of reaction pathways and the establishment of a complete catalytic cycle for alcohol photoreforming.

The photo-conversion of large alcohols on bare titania is investigated and the fundamental process leading to a limited conversion is elucidated. It is found that the temperature is a key factor to determine selectivity. A new mechanism for alcohol photoreforming on metal-loaded TiO_2(110) is established: the hole-mediated oxidation proceeds on the semiconductor surface, whereas the metal clusters act as thermal recombination centers. The mechanism is validated for various alcohols and a detailed analysis of the surface species provides further evidence for the mechanism. The photocatalytic conversion of tertiary alcohols involves a selective C-C bond cleavage by abstracting a radical. Whereas the methyl radical is directly ejected into the gas-phase, ethyl- or propyl-radicals recombine with a hydrogen atom to an alkane.

While Pt clusters exhibit a long-term stability and a specific size effect in the photocatalytic hydrogen evolution, Ni clusters are less efficient and deactivate over reaction time. However, bigger Ni clusters are more resistant against photo-corrosion than smaller ones. Finally, a perspective on protecting Pt clusters by exploiting the strong metal-support interaction is presented.

Zusammenfassung

Photokatalytische Alkoholreformierung ist eine äußerst vielversprechende Herstellungsmethode von "grünem" Wasserstoff und wertvollen sauerstoffhaltigen Chemikalien. Die heterogene Photokatalyse ist derzeit jedoch weder effizient noch selektiv genug, um im industriellen Maßstab angewendet zu werden. Ziel dieser Arbeit ist es, einzelne Reaktionsschritte in der photokatalytischen Umsetzung von Alkoholen auf einem atomar definierten Modellsystem bestehend aus größenselektierten Pt- oder Ni-Clustern auf TiO_2(110) aufzuklären. Methoden der Oberflächenwissenschaften in Kombination mit Konzepten der Katalyse ermöglichen es, Reaktionsschritte zu identifizieren und einen vollständigen Katalysezyklus für die Photoreformierung von Alkoholen zu entwickeln.

Es werden Photoreaktionen größerer Alkohole auf Titandioxid untersucht und der grundlegende Prozess, der zu einer limitierten Umsetzung dieser führt, aufgeklärt. Es zeigt sich, dass Veränderungen der Temperatur einen maßgeblichen Einfluss auf die Selektivität haben. Außerdem wird ein neuer Mechanismus für die photokatalytische Umsetzung von Alkoholen auf metallbeladenem TiO_2(110) postuliert: Die lochgetriebene Oxidation verläuft auf der Halbleiteroberfläche, während Metallcluster die thermische Rekombination von H_2 ermöglichen. Der Mechanismus wird für verschiedene Alkohole bestätigt, und eine detaillierte Analyse der auftretenden Oberflächenspezies liefert weitere Belege für das Vorherrschen dieses. Die photokatalytische Umsetzung von tertiären Alkoholen beinhaltet eine selektive Spaltung einer C-C-Bindung durch Abstraktion eines Radikals. Ethyl- oder Propylradikale rekombinieren mit einem Wasserstoffatom zu einem Alkan, während Methylradikale direkt in die Gasphase übergehen.

Pt-Cluster weisen eine Langzeitstabilität und einen spezifischen Größeneffekt bei der photokatalytischen Wasserstoffentwicklung auf, wohin gegen Ni-Cluster weniger effizient sind und ihre Aktivität sich über die Reaktionszeit verringert. Hinzu kommt, dass größere Ni-Cluster aktiver und widerstandsfähiger gegen Photokorrosion sind als kleinere. Abschließend wird noch eine Möglichkeit zum Schutz der Pt-Cluster unter Ausnutzung der starken Wechselwirkung zwischen Metall und Träger präsentiert.

Contents

Acknowledgements

Als Erstes möchte ich Prof. Ueli Heiz dafür danken, dass er mir die Möglichkeit gab an diesem spannenden Thema und in dieser besonderen Gruppe zu arbeiten. Er bringt es fertig eine außergewöhnlich gute Atmosphäre am Lehrstuhl zu schaffen, in der ich mich bei der Arbeit sehr wohl fühlte und mir die Freiheit und auch den Mut gab mich immer weiterzuentwickeln.

Ein besonderer Dank gilt Dr. Martin Tschurl für seine herausragende Betreuung und unermüdliche Unterstützung. Danke Martin, dass du der beste Mentor, Lehrer und Chef warst, den ich mir hätte vorstellen können und ebenfalls ein herzliches Dankeschön für die etlichen Dolchstöße beim Kicker!

Ein spezieller Dank geht an Dr. Constantin Walenta und Dr. Sebastian Kollmannsberger, die mir vom ersten Tag an die Welt der Photokatalyse beigebracht haben – und vielleicht auch ein bisschen Kicker spielen. Ihr habt mich bei euch in der Photokat aufgenommen und mir immer das Gefühl gegeben Teil der Gruppe zu sein. Die morgendlichen Kaffeerunden waren mir eine Ehre! Cons, vielen Dank für die andauernde Unterstützung während meiner gesamten Doktorarbeit.

Außerdem bedanke ich mich herzlichst bei meinem Laborkollegen Moritz Eder, mit dem jede Messung doppelt so viel Spaß gemacht hat und der jedes Problem, sei es an der Anlage, in der Diskussion der Daten oder bei der kritischen Frage wer für Kaffee machen zuständig ist lösbar gemacht hat. Dreckseder, es war mir eine Ehre mit dir zusammenzuarbeiten, vielen Dank für die täglichen Lachanfälle und vielen Dank für die Freundschaft.

Kevin Bertrang und Tobias Hinke, meine liebsten und geschätzten Kollegen aus der Nanokat, vielen Dank für das dauernde fertigmachen beim Kicker, die gute und humorvolle Atmosphäre und die Feierabendbiere. Ohne euch wäre es nur halb so lustig gewesen.

Nico Bock, vielen Dank für die guten Gespräche bei dem ein oder anderen Kaffee. Du hattest immer ein offenes Ohr für mich.

Des weiteren, möchte ich mich noch gerne bei all den Studenten für die Hilfe und Unterstützung im Labor bedanken, insbesondere bei Philipp Petzoldt, Sonia Mackewicz und Natalie Rosen. Petzi, Zukunft der Photokat, ich wünsche dir viel Erfolg und viel Spaß. Rosi, es hat mich gefreut mit dir zusammen arbeiten zu dürfen. Sonia, vielen Dank für schweißtreibenden Sportstunden nach der Arbeit.

Ich möchte mich herzlichst bei der gesamten Heizgruppe für die gute Atmosphäre und die stets vorhandene Hilfsbereitschaft bedanken.

Ein großer Dank gilt den Feinmechanik- und Elektronikwerkstätten, die mir bei jedem Problem und auch beim Aufbau neuer Projekte stets eine große Hilfe waren, ohne euch wäre es nicht möglich die Forschung auf diesem Niveau zu betreiben.

I want to thank Prof. Cynthia Friend for providing me with the opportunity of a research internship in her lab. Thanks to her entire group for the warm welcome and the friendly atmosphere. Thanks again Cons; you made this stay possible and unforgettable.

Zu guter Letzt möchte ich mich besonders bei meiner Familie und meinen Freunden für die große Unterstützung bedanken. Ohne euch wäre all dies nie möglich gewesen.

Eidesstattliche Erklärung

Ich erkläre an Eides statt, dass ich bei der promotionsführenden Einrichtung Fakultät für Chemie der TUM zur Promotionsprüfung vorgelegte Arbeit mit dem Titel *Photochemical and Photocatalytic Reaction Pathways of Alcohols on Bare and Metal-Loaded TiO_2(110)* in der Fakultät für Chemie am Lehrstuhl für Physikalische Chemie unter der Anleitung und Betreuung durch Prof. Dr. Ueli Heiz ohne sonstige Hilfe erstellt und bei der Abfassung nur die gemäß § 6 Ab. 6 und 7 Satz 2 angebotenen Hilfsmittel benutzt habe.

Ort, Datum, Unterschrift

List of Figures

List of Tables

List of Abbreviations

2PPE . . . . . two-photon photoemission spectroscopy

(a) . . . . . adsorbed

(g) . . . . . gaseous

O_{ad} . . . . . oxygen adatom

AFM . . . . . atomic force microscopy

BBO-H . . . . . bridge-bonded oxygen hydroxyl

BBO . . . . . bridge-bonded oxygen

DFT . . . . . density functional theory

FP . . . . . fragmentation pattern

ICS . . . . . electron-impact ionisation cross section

IRRAS . . . . . infrared reflexion absorption spectroscopy

lab-air . . . . . laboratory air

LEIS . . . . . low-energy ion scattering

MBD . . . . . molecular beam doser

ML . . . . . monolayer

OPO . . . . . optical parametric oscillator

PSD . . . . . photon-stimulated desorption

PSR . . . . . photon-stimulated reaction

QMF . . . . . quadrupole mass filter

QMS . . . . . quadrupole mass spectrometer

RF . . . . . radio frequency

RFA . . . . . retarding-field-analysis

SEM . . . . . secondary electron multiplier

SFG . . . . . sum frequency generation

SHG . . . . . second harmonic generator

SMSI . . . . . strong metal-support interaction

SPV . . . . . surface potential voltage

STM . . . . . scanning tunneling microscopy

syn-air . . . . . synthetic air

TD-2PPE . . . time-dependent two-photon photoemission

TOF . . . . . turn-over-frequency

TPD . . . . . thermal-programmed desorption

TPR . . . . . thermal-programmed reaction

UHV . . . . . ultra-high vacuum

UPS . . . . . ultraviolet photoelectron spectroscopy

1 Introduction

Photocatalysis facilitates an exceptional way for chemical transformations. It exploits the energy supplied by light to drive reactions that would only be possible in the dark under harsh conditions or sometimes even impossible. Applications range from the renewable energy sector, over waste-water treatment and self-cleaning devices, to a selective synthesis of fine chemicals.

The German Federal Government introduced the National Hydrogen Strategy in 2020 to initiate the energy transition towards a 'clean, secure and affordable energy supply'.[1] Hydrogen can be used as a renewable energy source, e.g. in fuel cells, or as an energy storage medium to ensure a flexible and transportable energy supply. Furthermore, many industrial processes require hydrogen as base substance, as e.g. the ammonia production. However, up to now most of the hydrogen is produced in carbon-emitting processes like steam reforming of natural gas.[2] Therefore, alternative ways must be found to generate 'green' hydrogen. The National Hydrogen Strategy envisage to produce this 'green' hydrogen through electrolysis from renewable electricity. This means that electricity produced with e.g. a wind turbine or photovoltaics drives the electrolyser that splits water into hydrogen and oxygen. Photocatalysis would skip the detour of electricity production and directly convert photonic energy into hydrogen with solar light.[3–5]

Unfortunately, the concept of photocatalytic hydrogen production has not been integrated into the National Hydrogen Strategy due to low solar-to-hydrogen conversion efficiency and the high costs, which currently hamper it from being applicable on a large-scale in the near future.[6–8] Yet, photocatalysis has already demonstrated that it can be utilised in common applications: nanoparticle photocatalysts are often used in products like self-cleaning

glasses with a hydrophilic coating based on titania that degrades dirt, or in self-sterilising photocatalytic or anti-fouling coatings.[9–11] Moreover, organic contaminations in waste-water are decomposed with photoactive catalysts.[12] The coatings and the waste-water treatment processes are based on the photocatalytic transformation of organic compounds.

The 'Holy Grail' in photocatalysis is the overall water splitting, but the potential for a selective synthesis of organic compounds should not be underestimated. For instance, photocatalysis allows for a selective oxidation of biomass-derived substances into value-added chemicals.[13, 14] A selective synthesis increases the yield and prevents expensive and complex purification processes. In addition, a controlled oxidation avoids a partial over-oxdiation and thus the formation of toxic CO and climate-damaging CO_2. Moreover, photocatalysis may facilitate the production of food additives, pharmaceuticals and fine chemicals under mild and energy-saving conditions in contrast to thermal catalysis with its harsh conditions. For example, the selective oxidation of glucose over a titanium photocatalyst supplies valuable glucaric acid, gluonic acid and arabitol at 30° C and atmospheric pressure.[15] Though, underlying reaction pathways must be understand for a precise and controlled selective up-conversion of biomass-derived chemicals, such as alcohols.

Unfortunately, the research over the past 30 years was not able to achieve a successful and commercially competitive application in the photocatalytic hydrogen production and the selective synthesis of chemicals. One reason might be that the research mainly focused on material screening, so that the photocatalysts become more and more complex.[3, 8, 16, 17] Simultaneously, the underlying mechanisms were usually neglected. Only in recent times, the concept of 'photocatalysis by design' has emerged.[18] Even though almost the entire periodic table has been applied in the design for photocatalysts, only one picture is considered to explain the photocatalytic reactivity: a mechanism derived from electrochemistry based on two electrochemical half-cells for which only the energetics of the materials are considered.[19] Although some publications include a chemical point of view, they mainly focus on the analysis of the observed intermediates and products based in this 'electrochemical' picture.[20–22] Instead, the surface chemistry of the applied photocatalyst should also be taken into account in order to increase the efficiency and especially the selectivity of photo-reactions. The identification and comprehension of individual reaction pathways may enable to 'design' a synthesis. For example, the temperature controls the residence time of a substance on the surface and its variation may change dramatically the selectivity.

Therefore, the goal of this thesis is to understand the photochemical and photocatalytic conversion of various alcohols on bare and metal-loaded TiO_2(110). Surface science

methods are utilised on the one hand to illustrate reaction pathways of different alcohols on bare titania, and on the other hand to elucidate a completely new mechanism that fully explains the photocatalytic conversion of alcohols and hydrogen evolution on metal-loaded TiO_2(110). The influence of different parameters, such as temperature, pressure and light intensity, on the reactivity of alcohols is also investigated. For this purpose, a model system that consists of size-selected metal clusters deposited on an atomically controlled surface is applied to gain insights on a fundamental level. The choice of the semiconductor is a single-crystal of TiO_2(110) because titania is one of the most applied and at the same time, the most studied metal oxide.[23, 24]

The present work reveals, that the oxidation of tertiary alcohols is facilitated on the semiconductor surface upon illumination. For different tertiary alcohols, either the temperature or the addition of a Pt co-catalysts influences the overall selectivity, which demonstrates the complexity of alleged 'simple' systems. The photo-conversion of primary and secondary alcohols is limited without a metal co-catalyst because titania is not able to evolve H_2 and thus the thermal back-reaction towards the reactant is eventually favoured at prolonged illumination. Therefore, size-controlled Pt clusters are deposited on TiO_2(110) as Pt is commonly used as 'benchmark' co-catalyst in the photocatalytic hydrogen evolution. This helps to initially understand the system and establish a mechanism that completely explains the catalytic cycle by accounting for all related fields as e.g. surface chemistry and semiconductor physics. This understanding sets the stage for an investigation of the use of more abundant materials, as Ni clusters, which are studied in a second part before specific cluster size-effects of Pt and Ni clusters are investigated.

2 Literature Review

This chapter gives an overview of the known literature. In a first section, the physical and surface properties of rutile titania is discussed, especially with a focus on the relevant properties in heterogeneous photocatalysis. Then, the morphology and reactivity of size-selected Pt and Ni clusters on TiO_2(110) is elucidated before a general overview of the photochemical reaction pathways of alcohols, aldehydes and ketones on TiO_2(110) is presented.

2.1 Properties of Titania

Titania is one of the most studied semiconductors in the form of nanoparticles and crystals in heterogeneous photocatalysis.[23, 24] Especially, the rutile (110) surface, which is the most stable facet, is thoroughly investigated for its surface structure and properties, and its thermal and photochemical reactivity. Therefore, it is a good model system to elucidate fundamental photoreaction pathways. The surface structure and properties are described in detail in the review by Diebold[23], while a review about the photocatalysis of TiO_2 for example is given in [24].

2.1.1 Surface and Defects

As written above, TiO_2(110)-(1x1) is the most stable crystal facet.[23] Two different kinds of Ti atoms form alternating rows, one of them are 5-fold coordinated Ti^{3+} atoms (also referred as Ti_{5c}) with a dangling bond perpendicular to the surface. The other ones are 6-fold coordinated Ti atoms underneath the BBO row, as they are found in the bulk

structure. The BBO rows consist of out-of-plane oxygen atoms located on top of the 6-fold coordinated Ti atoms. A surface model is shown in figure 2.1.

A perfect stoichiometric surface is never obtained; different kinds of defects are always present, such as bridge-bonded oxygen vacancies, oxygen adatoms, hydroxyls or Ti-interstitials.[23] The preparation method determines the majority defect, but it never produces only one kind of defect. BBO vacancies are created through annealing the crystal in vacuum, but Ti^{3+} interstitials also diffuse from the bulk to the sub-surface or surface above 400 K.[25–27] Thus the creation of BBO vacancies is always accompanied by the emergence of Ti^{3+} interstitials. Consequently, the interstitials are present to a certain degree on all $TiO_2(110)$ surfaces since every preparation method involves an annealing step.[28] Furthermore, interstitials and BBO vacancies may influence themselves; for example the group of Lyubinetsky showed that BBO vacancies are virtually absent near a subsurface point defect as Ti-interstitial.[29] In addition, Ti-interstitials can have an effect on bonding geometries or the formation of intermediates.[30] For example, they are relevant in reductive coupling reactions or in the high temperature reactivity of alcohols.[31–34] Furthermore, the O_2 adsorption and dissociation is driven by Ti-interstitials from the near-surface region, as they may provide the necessary charge for the O_2 adsorption and dissociation.[35] That is why during annealing in O_2 atmosphere, Ti-interstitials from the bulk react with oxygen to grow new islands and strands that finally lead to a complete (1x1) surface.[25, 27, 36–38]

Oxygen adatoms are created by adsorbing O_2 in BBO vacancies at room temperature, which fill the vacancies and leave one oxygen atom on top of a Ti_{5c}.[25, 39] Though, O_2 does not fill every vacancy at room temperature.[35, 40] The same phenomenon is observed for the formation of hydroxyls. Water is adsorbed in BBO vacancies creating two distinct hydroxyls, but water does not fill every vacancy.[39, 41] Different preparation methods vary the relative amount of different defects, so that the active site for a reaction may be identified, but it is not possible to create solely one defect species.

2.1.2 Band Bending in Photocatalysis

In the Dark

Titania is a semiconductor with a band gap of $3.0 - 3.2\,\text{eV}$ which corresponds to a wavelength of $387 - 413\,\text{nm}$.[42] In this work, the semiconductor is a bulk material with an extended surface, that is why a band bending model from semiconductor physics is considered. Band bending towards the surface may be induced by adsorbates, metal contacts, field effects or surface states.[43] The latter stem from dangling bonds of

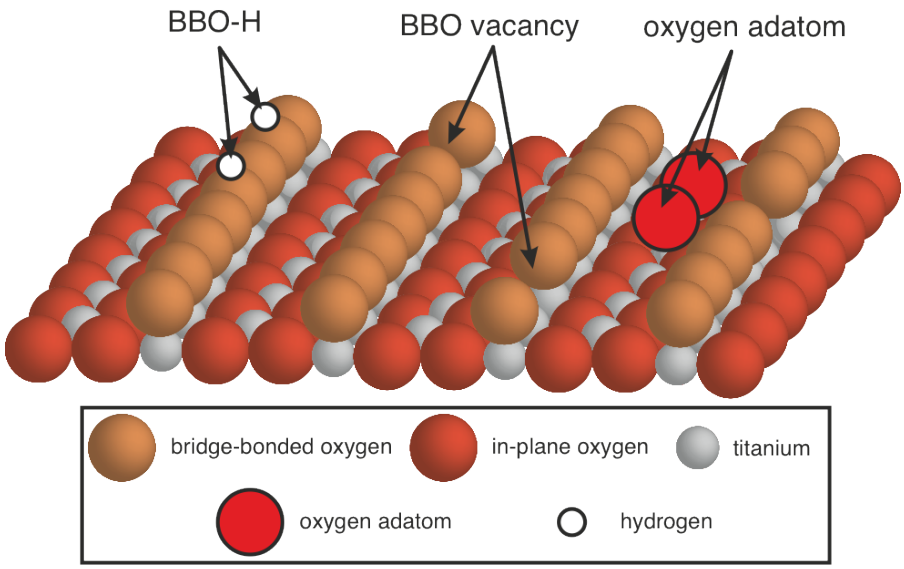

Figure 2.1. Ball model of the rutile TiO_2(110)-(1x1) with different surface defects. BBO vacancies are missing one BBO oxygen atom. Oxygen adatoms are located on top of 5-fold coordinated Ti atoms. Hydroxyls are formed with BBO atoms.

the 5-fold coordinated Ti^{3+} surface atoms and surface defects. The under-coordinated Ti_{5c} atoms are formally negatively charged, which makes TiO_2(110) an intrinsic n-type semiconductor. In fact all different types of defects presented above have in common that they are negatively charged. BBO vacancies are assumed to be double-negatively charged and may add to the surface band-gap states.[44–46] Ti^{3+} interstitials are under-coordinated and may, thus be single-negatively charged and contribute to the Ti3d defect state in the band gap.[26, 35] Different studies debate, whether the Ti-interstitials or the BBO vacancies are the dominant origin for the surface band-gap state.[35, 46] Hydroxyls are formed through adsorption in a BBO vacancy which is believed to not affect the charge of the vacancy, so that it correlates them to a negative charge.[35, 46]

In any case, all these negatively charged defects contribute to the upward band-bending in the semiconductor towards the surface.[42] The dangling bonds of the 5-fold coordinated Ti^{3+} surface atoms and surface defects introduce states in the band gap of titania. Both contribute to an accumulation of electrons in the surface region what causes a local imbalance in charge neutrality compared to the bulk. An electric field is established in the space charge region and causes the electrostatic potential to go up towards the surface; this is called band bending.

Under Illumination

Upon illumination with a photon energy above the band gap of titania, an electron is excited from the valence band into the conduction band creating a photo-hole in the

valence band. Photo-electrons preferentially flow to the bulk, because they are repelled by the negative surface states. Whereas, the upward band-bending favours the hole migration to the surface, because the negative surface charges, e.g. BBO vacancies or Ti-interstitials, attract the positively charged holes. The holes may recombine with these surface charges and neutralises them. This charge recombination in the surface region causes that bands are flattened, so that the photo-holes and photo-electrons are experiencing a reduced driving force.

Alternatively, the photo-holes migrating to the surface may interact with an adsorbate to drive a photo-reaction or photo-desorption. It is generally accepted that the photo-hole initiates the photo-oxidation of organics, or neutralises a negative surface charge, which e.g. leads to the desorption of specific O_2^- species.[30, 47–52] However, the electrons may also play a role in the O_2 photochemistry; e.g. the dissociation of molecular oxygen is attributed to be caused by electrons.[53–55]

Band bending, band flattening and surface states can be measured with surface photovoltage measurements.[43, 56] The photo-electron and photo-hole move in opposite directions under illumination due to electric field in the space charge region and the photo-holes neutralise negative charges on the surface. This causes a band flattening and a change of the surface potential. This surface potential is measured before and during illumination and determines the change in SPV. Ideally, the bands may be completely flattened for a high enough photon flux and the resulting SPV may indicate the initial band bending. Typical band bending values for titania are in the range of several hundred meV and strongly depend on adsorbates and the surface preparation.[43, 57]

2.2 Size-selected Pt and Ni Clusters on TiO_2(110)

Studies of size-selected Pt or Ni clusters on titania single crystals so far, mainly address the morphology and stability of the clusters. Reaction studies are limited to CO oxidation reactions. This section outlines the main results from those studies.

The group of Watanabe studied the morphology and CO oxidation of size-selected Pt clusters ($Pt_{4,7\text{-}10,15}$) on r-TiO_2(110) using STM and XPS.[58–60] Pt clusters were synthesised with a DC-magnetron sputter source and were randomly deposited on r-TiO_2(110). Atomic-resolution STM shows that the clusters do not diffuse at 300 K and do not occupy a specific site.[61, 62] Small clusters as Pt_4 and Pt_7 have a planar structure and lie flat on the surface. A DFT study by Jiang *et al.* confirms a preferential flat structure of Pt_4 but claims that larger clusters $Pt_{5\text{-}8}$ prefer a two-layered structure.[63] STM studies by Watanabe reveal a geometric transition from planar-to-3D transition

that occurs between Pt_8 and Pt_9. Both cluster sizes have isomers and are present as both, flat and two-layered clusters. Larger clusters as Pt_{10} and Pt_{15} are only found as 3D structures with two atomic layers. XPS studies confirm the planar-to-3D transition; an inflection point of the Pt core-level is observed at Pt_8.[59] The geometric transition is also reflected in the CO oxidation activity in a high-pressure reaction cell.[60] The activity[1] increases up to Pt_8 and has its maximum at Pt_7, which are all planar clusters. Watanabe and co-workers attribute this behaviour to the presence of a second layer of Pt atoms. They speculate that the second layer, consisting of low coordinated Pt atoms, decrease the activation energy for the CO oxidation but, simultaneously, block the reaction sites of the first layer. The reaction rate decreases as soon as a second layer occurs, so that they assume that the site blocking effect dominates.

Bonanni *et al.* deposited Pt_3, Pt_5, and Pt_{10} on r-TiO_2(110) and found an opposite trend: the catalytic CO oxidation activity[2] decreases with increasing cluster size.[62] This differences may have other origins than a specific size effect. The significant pressure difference of 10^{-7} mbar[62], compared to tens of mbars[59] may change the reactivity and is a good example for the need to close the pressure gap. Another source might be the difference in cluster coverage, Bonanni *et al.* deposited 2.5% ML[3] whereas the group of Watanabe loaded titania with $5 - 10\%$ ML[3] of clusters.

Thirdly, the reduction degree of titania may play a critical role as the group of Harbich has demonstrated. The CO oxidation rate with Pt_7 is strongly enhanced on a slightly reduced crystal in comparison to highly reduced TiO_2(110).[64] Ti^{3+} interstitials, mobile at the reaction temperature, consume the spilled-over oxygen atoms and form TiO_x structures. Consequently, less reactant O_2 is available and the reaction rate decreases. As the bulk reduction degree increases the amount of Ti^{3+} interstitials, the effect is more pronounced on highly reduced supports.[65]

Another discrepancy concerns the stability of Pt_{10} clusters. Watanabe *et al.* reports no shift in the Pt 4f XPS spectra before and after CO oxidation, which indicates no cluster ripening.[60] In contrast, Bonanni *et al.* demonstrate with STM that a morphology change upon annealing in CO and O_2 atmosphere results.[62] Monodisperse Pt clusters sinter to larger clusters during the oxidation of CO. CO and O_2 induce the ripening process because the Pt clusters are otherwise stable upon annealing to 600 K in UHV. A theoretical study by the group of Alexandrova supports the Ostwald ripening of monodisperse Pt clusters on TiO_2(110).[66] Size-selection is thought to suppress the

[1] The production rate of CO_2 is related to the total number of Pt atoms.
[2] The activity is related to the total number Pt atoms.
[3] With respect to a closed-packed monolayer.

Ostwald ripening, but small clusters $Pt_{1\text{-}8}$ may populate many low-energy metastable isomers at 700 K which favours the sintering process.[66]

However, those groups completely neglected the potential encapsulation of Pt clusters by a thin TiO_x layer.[67] The strong metal-support interaction, where platinum group metals supported on reducible oxides are overgrown by a thin reduced support-oxide layer, is commonly known since its oberservation by Tauster *et al.* in 1978.[67] Many studies focused on the high-temperature behaviour of Pt/TiO_2 systems and all observed the encapsulation of Pt particles.[68–72]

Yet a few years earlier, the same group of Harbich studied the strong-metal support interaction on the $Pt_1/TiO_2(110)$ system.[73] Deposited Pt atoms on a strongly reduced rutile (110) are annealed to 1100 K and form two-layered clusters that are encapsulated by a reduced titania layer. The thin titania layer suppresses the CO oxidation activity completely. A sputter-anneal procedure removes the titania overlayer and re-establishes the oxidation reactivity.

Only one group has investigated hitherto the behaviour of size-selected nickel clusters on titania.[74] $Ni_{1,2,5,10,15}$ are synthesised with a laser vaporisation cluster source and landed with different impact energies (soft-landing or hard-landing conditions) on $TiO_2(110)$. XPS shows that soft-landed Ni clusters are stable on the reduced $TiO_2(110)$, but increasing impact energies oxidise the Ni clusters upon deposition. Further, Aizawa *et al.* suggest that the clusters do not fragment or agglomerate upon deposition at room temperature. Low energy ion scattering spectroscopy shows a preferential adsorption of small clusters on oxygen sites and a 3D structure for larger ones. No significant CO desorption features from Ni clusters are observed in a TPD. The authors attribute this to a strong Ni-TiO_2 binding. XPS data before and after TPD indicate that a little fraction of Ni is oxidised to +3, but $> 90\%$ remains in its metallic state. Comparable to the strong metal-support interaction fo Pt, Ni might undergo encapsulation with a thin titania layer. Low energy ion scattering spectroscopy before and after TPD suggests that Ni clusters are partially encapsulated and are significantly sintering. The authors speculate that the sintering is more pronounced than the encapsulation and is the dominant effect leading to the data.

In summary, even though size-selected clusters on single crystalline surface in UHV conditions is one of the best achievable model systems, it is very difficult to compare qualitatively, and even harder quantitatively, different data. The data is very sensitive to preparation methods and reaction conditions. It is established that Pt clusters do not occupy a specific site and that small clusters prefer a flat structure while larger ones exhibit a two-layered structure. This structural behaviour is comparable for Ni clusters. A size effect in the CO oxidation on Pt clusters is not evident and Ni ones do not even bind CO significantly. Sintering and the encapsulation of Pt or Ni clusters are playing a role at higher temperature but the exact mechanism remains elusive.

2.3 Photochemistry on TiO_2(110)

This section discusses the photo-active site on rutile (110), as well as the photo-active species in alcohol photochemistry. A short overview of the photochemical conversion of alcohols, aldehydes and ketones on TiO_2(110) is presented in the second part.

2.3.1 Alcohols

Active Species and Active Site

An ongoing discussion addresses the photo-active species and photo-active site on titania.[75] The debate mostly involves the simplest alcohol, namely methanol. Methanol adsorbs molecularly and dissociatively on TiO_2(110).[41, 76] There is consensus that methanol thermally dissociates in BBO vacancies to methoxy and BBO-H.[76–80] Yet, the dissociation degree of methanol on regular Ti_{5c} is unclear. Coverage-dependent TPD series show a peak shift characteristic for second-order kinetics that is possibly caused by the co-existence of molecular and dissociated methanol.[76, 81] Certainly, the dissociation equilibrium between methoxy and methanol depends on the coverage as SFG vibrational spectroscopy studies suggests.[82, 83] The temperature also has a strong effect on the methoxy formation, as e.g. methanol diffuses above 200 K on the TiO_2(110) surface and is able to 'find' a site for its thermal dissociation to form methoxy.[84] In addition, co-adsorbed O_2 promotes methoxy formation on regular Ti_{5c} sites as an oxygen adatom may catch a hydrogen atom and break the O–H bond.[48, 76]

The groups of Yang and Huang claim that the O–H bond dissociation in methanol and ethanol is a photon-driven process.[79, 85–87] These groups have conducted several studies supposedly demonstrating the photon-induced O–H bond cleavage using amongst others PI-TPD, XPS, STM, SFG vibrational spectroscopy, TD-2PPE, and isotopic labeling methods.[79, 85–91] They assume a two-photon process in the reaction from methanol to formaldehyde: a first photon cleaves the O–H bond and a second photon oxidises the methoxy to formaldehyde by breaking the C–H bond.

Though in recent publications, Yang and co-workers refrain from this interpretation and follow the interpretation that methanol is thermally dissociated into methoxy and that a photo-hole oxidises this methoxy.[92] They claim that the methoxy species formed in BBO vacancies are not photo-active, whereas methoxys formed on Ti_{5c} are photo-active.[92] The group by Yang demonstrated with UPS that the thermally formed methoxy species are favoured over methanol to trap holes by increasing the band bending on the TiO_2 surface.[93] In the photoconversion of methanol on Pt- or Au-loaded TiO_2(110),

the authors suggest that the metal-TiO_2 interface promotes the thermal formation of the photo-active methoxy species.[94, 95] These recent publications do not mention a photon-induced O–H bond cleavage anymore.

This interpretation goes more in line with Henderson, Friend and other groups.[48, 80, 84, 96–100] Henderson and co-workers convincingly identified thermally methoxy as the photo-active species, that undergo a hole-mediated oxidation.[48] The purely methoxy-covered surface is prepared by co-dosing O_2, which promote the O–H bond cleavage, and annealing the surface to 350 K so that undissociated methanol desorbs.[48, 76, 101] Further, Henderson points out that molecular methanol is not photo-active.[96] The group around Idriss also speculates that thermally formed ethoxies are the photo-active species in the photo-oxidation of ethanol on TiO_2(110).[99, 100]

Summing up, these different groups generally agree that methoxy (or alkoxide) is the hole-scavenging intermediate to yield formaldehyde (or aldehyde), though they do not completely agree if the O–H bond cleavage is a purely thermal or photon-induced process. The photo-active site at which the methoxy is adsorbed is also still controversial.

Several studies show that methanol adsorbs dissociatively in BBO vacancies yielding methoxy and a BBO-H, as already mentioned above.[41, 102, 103] The group by Henderson follows the interpretation that those methoxy species in BBO vacancies are photo-active. In contrast, Ren and co-workers claim in a study using SFG that exactly those methoxys are not photo-active.[92] According to them, only methoxy formed on regular Ti_{5c} sites are photo-active.[92] Oxygen adatoms promote the methoxy formation on regular Ti_{5c} sites. The group of Ren state that these are more prone to get photo-oxidised than 'normal' methoxy species.[104] This argumentation line is not conclusive as it is not clear how to distinguish between these two methoxy species. However, it is undisputed that an oxidative surface preparation leading to adsorbed oxygen, i.e. oxygen adatoms on Ti_{5c}, enhances the amount of methoxy species. That is why oxidised TiO_2(110) surfaces exhibit a higher photochemical activity in alcohol conversion.[48, 80, 96, 105] Hansen *et al.* reveal in an STM study that ethoxy species on Ti_{5c} have a higher probability to get photo-oxidised than ethoxies adsorbed in BBO vacancies.[105]

To conclude, there is still a controversial discussion about the exact photo-active site, but the literature agrees that methoxies are the photo-active species to yield formaldehyde. However, it remains to be seen, how methoxies have been formed. These insights may be adapted to other alcohols as already studies show a comparable adsorption behaviour of all relatively simple alcohols.[106–109] Therefore, this thesis follows the interpretation of Henderson and Friend, that alkoxides are formed thermally and that they are the photo-active species. These interpretations are adapted for metal-loaded TiO_2(110) as

well, since results indicate that the photo-oxidation itself takes place on the titania surface and is not influenced by metal clusters.

A profound discussion about the photo-active species and site is found in the review by Walenta *et al.*.[75]

Reactivity

Primary and secondary alcohols adsorb on $TiO_2(110)$ and thermally dissociate to a certain degree to form alkoxides and BBO-Hs (see *Active Species and Active Site* for details).[41] The alkoxide formation takes place either on regular Ti_{5c} sites or in BBO vacancies where in each case an adjacent BBO atom captures the hydrogen atom to form a hydroxyl. Or, the alkoxide formation is assisted by O_{ad} atoms where O_{ad} forms a hydroxyl with the abstracted hydrogen.[41, 76] In the following reaction equations, $O_{(ad)}$ stands for a surface oxygen atom that includes a BBO or oxygen adatom.

$$R_2HCOH_{(ad)} + O_{(ad)} \xrightarrow{\Delta T} R_2HCO_{(ad)} + OH_{(ad)} \tag{2.1}$$

Upon UV illumination, an electron-hole pair is created and the hole migrates to the surface (see subsection 2.1.2). The alkoxide is oxidised *via* a direct hole transfer that leads to an α-H abstraction and the formation of an aldehyde or ketone.[48] The abstracted hydrogen again forms a surface hydroxyl with a BBO. Both hydroxyls desorb from the surface as H_2O by leaving a BBO vacancy behind in the case of a reduced surface and an oxygen adatom on a Ti_{5c} site in the case of an oxidised surface.[85, 110–112]

$$R_2HCO_{(ad)} + O_{(ad)} \xrightarrow{h\nu} R_2CO_{(ad)\,or\,(g)} + OH_{(ad)} \tag{2.2}$$

$$2OH_{(ad)} \xrightarrow{\Delta T} H_2O_{(g)} + O_{(ad)} \tag{2.3}$$

For the photochemical conversion of methanol, the primary photo-product, formaldehyde, either remains intact or partially undergoes a consecutive photo-reaction.[50, 80, 111, 113] Guo *et al.* irradiated the methanol-covered reduced-$TiO_2(110)$ surface at cryogenic temperatures with UV light.[50] As a result, formaldehyde is thermally trapped on the surface and partially further reacts in a second photo-oxidation.[50] The second photo-reaction is a hole-driven coupling between formaldehyde and residual methoxy to produce methyl formate.[50] Both photo-products only desorb upon heating in a subsequent PI-TPD.[50] The yield of methyl formate increases and the yield of formaldehyde decreases with UV-illumination time.[50] Friend and co-workers observe the same cross-coupling that

yields methyl formate on oxidised-TiO_2(110) during illumination at cryogenic temperatures (PI-TPD) and at room temperature (PSR).[80] For the latter one, formaldehyde and methyl formate desorb immediately upon illumination whereas the irradiation at cryogenic temperatures again traps both photo-products on the surface.[80] Formaldehyde is identified as an intermediate in the photo-coupling reaction and both groups agree that it forms a photo-activated $H_2CO{-}O$ complex, either with a BBO or an O_{ad}.[50, 80]

$$H_3CO_{(ad)} + H_2CO_{(ad)} \xrightarrow{h\nu} HCOOCH_{3\,(ad)\text{ or }(g)} \tag{2.4}$$

Ethanol reacts in the first photo-oxidation analogously to methanol. Ethoxy is photo-oxidised *via* an α-H abstraction to acetaldehyde.[110, 114] In contrast to methanol, acetaldehyde does not undergo a consecutive photo-reaction in an anaerobic environment.[85, 105, 110] Walenta *et al.* and Hansen *et al.* do not observe any side-products expect of the concomitant hydroxyls and the resulting water formation on reduced- and oxidised surfaces.[105, 110]. Both groups agree that the thermally formed ethoxy is the photo-active species and that the overall reaction from ethanol to acetaldehyde is a 1-photon process.

In contrast, Yang and co-workers argue with 2PPE experiments and DFT calculations in addition to PI-TPDs that the reaction from ethanol to acetaldehyde is a 2-photon process where the O–H and α-C–H bond cleavages are photo-induced.[85] Furthermore, they observe an increased yield of the typical thermal deoxygenation product ethylene, at around 600 K in the PI-TPD.[85] The abstracted hydrogen atoms from the photo-oxidation recombine to water and create a BBO vacancy by desorbing at 450 K. Unreacted ethoxy residing on BBO rows may diffuse to those BBO vacancies and desorb at around 600 K as ethylene what may increase the yield. In TPDs, ethoxy typically recombine with a hydroxyl leaving the surface as ethanol. According to the authors, the increased yield of ethylene is also due to insufficient hydroxyls available for the ethanol recombination. However, the photo-reaction from ethanol to acetaldehyde and water is stoichiometric and should not deplete hydroxyls.

The group of Idriss follows the 2-photon process interpretation in studying the photo-reactivity of ethanol on TiO_2(110) in an O_2 atmosphere.[99, 100, 112] Contradicting Yang and co-workers, Idriss and co-workers are congruent with the other works mentioned in this section that the dissociative adsorption , i.e. O–H bond cleavage, is a thermal process. Though, they state that a first hole is needed to form an ethoxy radical and a second hole is required for the α-H abstraction to yield acetaldehyde.[99] The presence of O_2 under illumination enables a consecutive reaction under the consumption of one hole. In contrast to methanol photochemistry, acetaldehyde does not couple with an ethoxy but a fraction of the molecules follows the acetaldehyde photochemistry. Acetaldehyde forms

a photo-active carboxylate on the surface involving oxygen species, wherefore the yield increases with O_2 partial pressure. The carboxylate traps a hole and ejects a methyl radical into the gas-phase leaving behind a formate species.[112] An increased partial pressure of O_2 shifts the selectivity of the gas-phase products towards methyl radicals.[112]

Engel and Brinkley investigated the photochemical conversion of *iso*-propanol on $TiO_2(110)$ in an O_2 atmosphere, which yields acetone and water.[115, 116] The photochemical dehydrogenation may involve an electron trapping of molecular oxygen. However, the presented mechanism stems from early stages and is nowadays not convincing anymore.

The ethylene glycol photochemistry on reduced-$TiO_2(110)$ exhibits a coverage-dependent reaction behaviour.[117] Ethylene glycol possesses two alcohol groups which dissociatively adsorb by cleaving two O–H bonds. At high coverages ($> 0.6\,\mathrm{ML}$), ethylene glycol dominantly reacts to acetaldehyde and water under UV illumination at cryogenic temperatures. Acetaldehyde formation involves a $-CH_2-CH_2-O-$ intermediate that is yielded through a C–H and C–O bond scission in the deprotonated ethylene glycol.

$$OH-CH_2-CH_2-OH \xrightarrow{h\nu} CH_3CHO + H_2O \quad \text{at high coverages} \tag{2.5}$$

A second reaction channel opens up at low coverages ($< 0.2\,\mathrm{ML}$): the two alcohol groups of the dissociatively adsorbed ethylene glycol are oxidised leading to a C–C bond cleavage and the formation of two formaldehydes. At low coverages, the selectivity of the first to second reaction pathway is 1:1. At high coverages, the production of acetaldehyde and water significantly prevails the formation of formaldehyde. The dominance of the first reaction pathway yielding acetaldehyde at high coverages is attributed by the authors to an increased coverage of hydroxyls and the steric hindrance of ethylene glycol.

$$OH-CH_2-CH_2-OH + O \xrightarrow{h\nu} 2CH_2O + 2OH \quad \text{at low coverages} \tag{2.6}$$

The photochemistry of the presented alcohols have in common that its first photo-reaction involves an alkoxide that is oxidised *via* a C–H or C–C bond scission. A possible consecutive reaction strongly differs for the alcohols and no conclusive trend is observed. This extract from the alcohol photochemistry on titania demonstrates the complexity of reaction pathways under highly-defined conditions of even presumed simple alcohols.

2.3.2 Aldehydes and Ketones

Aldehydes and ketones adsorb *via* the oxygen atom from the carbonyl group to the Ti_{5c} sites in an η^1-configuration.[118–120] On the oxidised surface containing O_{ad} atoms the η^1-configuration may thermally react with an O_{ad} to form a bridging diolate species, in an η^2-configuration.[113, 119] In the absence of O_{ad} atoms on a reduced titania surface, the bidentate species is formed with BBO atoms.[120] According to Henderson, the η^1-configuration is photo-inactive whereas the diolate species may undergo a hole-mediated reaction.[113, 119]

$$\begin{gathered}\eta^1\text{–}R_1R_2O + O \xrightarrow{\Delta T} \eta^2\text{–}R_1R_2O\text{–}O \\ \text{with } R_1 = \text{ alkyl chain and } R_2 = \text{ alkyl chain or H}\end{gathered} \tag{2.7}$$

Upon UV illumination, the diolate is decomposed with a hole *via* the ejection of an alkyl radical into the gas-phase. The remaining species forms a carboxylate on the surface. This η^2-configuration and radical ejection has been described for acetaldehyde[119, 120] and various ketones[113, 119], e.g. acetone[121–123], butanone [124], or butyrophenone[125]. The radical abstraction may be highly selective, as e.g. the butyrophenone-O bidentate selectively abstracts the propyl radical upon UV illumination and leaves behind a benzoate species.[80]

$$\begin{gathered}\eta^2\text{–}R_1R_2O\text{–}O \xrightarrow{h\nu} \eta^2\text{–}R_2O\text{–}O + R_1^{\cdot} \\ \text{with } R_1 = \text{ alkyl chain and } R_2 = \text{ alkyl chain or H}\end{gathered} \tag{2.8}$$

Petrik *et al.* identified a second photo-active species next to the η^2-diolate that abstracts a radical in the photochemistry of acetone using angle-resolved PSR and IRRAS. The η^1-acetone that thermally forms a η^2-diolate with an O_{ad} atom ejects the methyl radical off-normal at $\sim \pm 66°$ to the surface normal upon UV illumination. The second species in contrast ejects the methyl radical normal to the surface into the gas-phase. The authors assign this species to a photo-produced η^2-enolate that stems from the reaction of η^1-acetone and an O_{ad} atom. In the η^2-enolate, the oxygen atom from the carbonyl group and a β-C bind to a Ti_{5c} site respectively. The η^2-diolate dominates at low acetone coverages (< 0.2 ML) and remains constant with higher coverages whereas the η^2-enolate becomes important with higher coverages up to 0.6 ML.

The photo-oxidation of formaldehyde on $TiO_2(110)$ does not lead to a desorption of any photo-products due to the lack of an alkyl chain.[30, 126, 127] Instead, the main reaction channel is the photo-decomposition of formaldehyde to formate by abstracting a hydrogen atom that forms a hydroxyl with a BBO.[126] Both products, the formate

and the hydroxyl, remain on the surface.[30] In a subsequent TPD, formate decomposes thermally, analogously to the thermal formic acid chemistry.[30, 127, 128] Similar to higher aldehydes, formaldehyde forms a photo-active η^2-diolate species ($H_2CO{-}O$) either with an O_{ad} on the oxidised surface or with a BBO on the reduced surface.[30, 126] The oxidised surface is significantly more efficient than the reduced one.[30] Xu *et al.* observes a second and minor photo-reaction pathway: the methylene group from the η^2-diolate is transferred to a BBO atom whereas the oxygen atom from the carbonyl group remains on the Ti_{5c} site.[126] In a subsequent TPD, the second BBO-methylene species couples to form ethylene or decompose by leaving the surface as methyl radical.[126]

In general, the photochemistry of aldehydes and ketones follows a trend. The main photo-reaction channel involves a thermal activation leading to a η^2-diolate. Upon UV illumination, the α-C–C bond is cleaved leaving a formate species behind and ejecting an alkyl radical into the gas-phase. In the absence of an alkyl chain, which is the case for formaldehyde, the α-H is abstracted. It forms a hydroxyl and the remnants stay on the surface as formates.

3 Experimental

The chapter describes the experimental setup and the utilised techniques and procedures. An overview of the UHV setup is given in figure 3.1. The setup consists of a high-frequency laser evaporation cluster source for the synthesis of atomically precise nanoparticles and an analysis chamber for the characterisation of the catalyst and the reactivity measurements. The synthesised clusters are deposited on a single crystal in the analysis chamber. Both chambers are separated by a vacuum gate except for the time of deposition to ensure UHV conditions in the analysis chamber. The whole setup is differentially pumped, ranging from a pressure of 10^{-1} mbar at the skimmer to 10^{-7} mbar in the analysis chamber during cluster deposition. The UHV analysis chamber with a base pressure of $< 8.0 \cdot 10^{-11}$ mbar is equipped with a liquid-N_2 cooled (x, y, z, ϕ)-manipulator (VAB Vakuum) with three substrate holders, an Ar^+-sputter gun (IQE 11/35, SPECS) for crystal cleaning, an Auger Electron Spectrometer (CMA 100, Omicron Nanotechnology), a quadrupole mass spectrometer (QMA 430, Pfeiffer Vacuum) for thermal and photon-stimulated desorption and reaction studies, leak valves (Pfeiffer Vacuum), a molecular beam doser and a home-built gasline. A Nd:YAG (Innolas, Spitlight 1200, 20 Hz) pumped optical parametric oscillator (GWU, premiScan ULD/400) laser system can be used as light source for photo-experiments. More details are given in the following.

3.1 Cluster Source

The metal co-catalysts are synthesised with a laser vaporisation cluster source. The setup allows for a formation of atomically-precise clusters in the range of 1 to ~ 100 atoms, depending on the atomic mass ($1 - 16000$ amu). The clusters are deposited on a single crystal

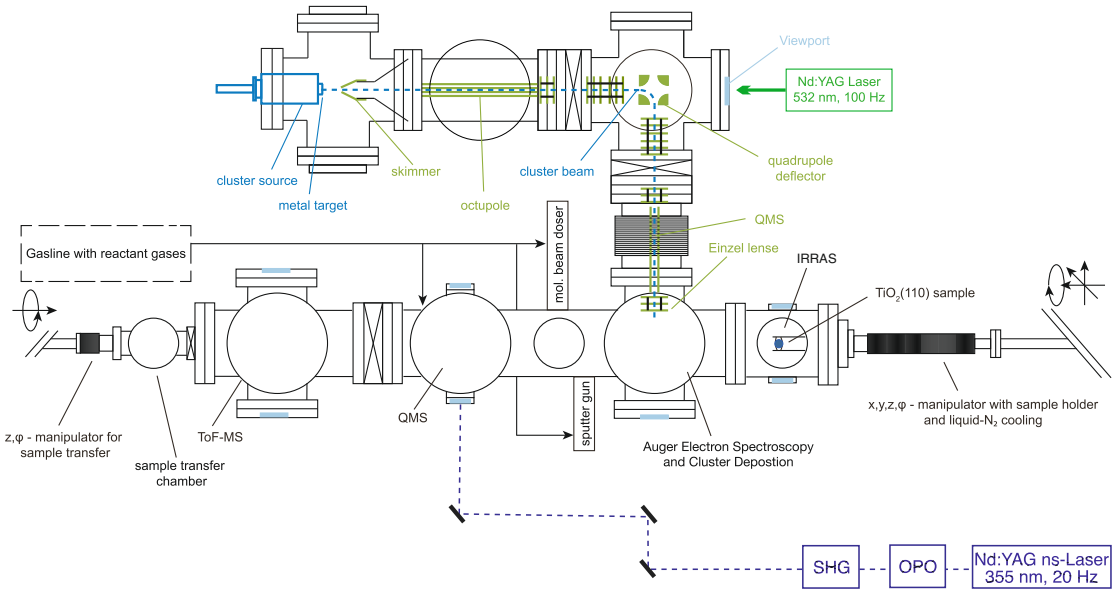

Figure 3.1. Schematic overview of the experimental setup from a top-view. The setup is divided into two parts: the laser vaporisation cluster source for the synthesis of the metal co-catalysts (top) and the analysis chamber for the surface preparation and characterisation and the reactivity measurements (bottom). Adapted with permission from [129]. Copyright 2018 American Chemical Society.

under soft-landing conditions (1 eV/atom).[130] The deposition time governs the cluster coverage so that cluster size and coverage can be chosen independently from each other.

The high-frequency laser evaporation cluster source is based on the design by Heiz *et al.* which has been adapted from a cluster source developed by Smalley.[131, 132] The 2^{nd} harmonic (532 nm) of a diode-pumped solid state Nd:YAG laser (DPPS Spitlight, InnoLas, 100 Hz, 6 W, 9 ns pulse width) enters the chamber counter-propagating to the cluster beam through a viewport and is focused onto a metal target (Pt > 99.95% purity, ESG Edelmetalle; Ni with a high purity[1]). The metal target is rotated in a hypocycloidal way and the speed is altered during one rotation to ensure a uniform ablation.[133] The produced metal plasma is cooled by two processes: through collisions with He atoms and by adiabatic expansion leading to a supersonic jet.[134, 135] The helium (He 4.7 or 6.0 Westfalen Gas[2]) gas pulse (40 μs), generated with a piezo-valve[3], is introduced in the thermalisation chamber directed to the target with a delay to the laser pulse (8.828 ms with respect to the previous laser pulse[4]). The helium gas enables the cluster formation.

[1] The mass scan shows no impurities apart from nickel oxides (see figure 3.2).
[2] The 6.0 gas purity is used for Ni clusters because they might be more prone to contaminations. 4.7 gas purity is used for Pt clusters.
[3] The back-pressure of the piezo valve varies from $3 - 5$ bar and is one parameter to regulate the cluster size distribution during their formation.
[4] Such settings are required because the laser trigger is used as pulse generator and the piezo valve features rather long times.

A possible mechanism is that He atoms catch the released binding energy during cluster formation and prevent fragmentation. The He-metal plasma adiabatically expands through a nozzle (3 mm) into the vacuum typically leading to clusters below room temperature.[136]

The cluster beam is comprising positively and negatively charged, and uncharged clusters and passes through a skimmer. Further, the cations are guided through a differentially pumped vacuum system to reduce the pressure from $1.18 \cdot 10^{-1}$ mbar at the skimmer to 10^{-7} mbar in the analysis chamber during cluster deposition. The ion beam is guided through a radio-frequency driven linear octupole (Kenwood HT Transceiver, TS-5700) in the first pumping stage before it reaches the bender passing three stacks of ion optics, each containing $3-4$ electrostatic lenses. The bender is a 90° quadrupole deflector and is operated to separate positively charged clusters from neutral ones. Subsequently several stacks of electrostatic lenses direct the positively charged ion beam into a QMF (Extrel, 150 QC). The QMF allows for the selection of one single cluster size in the mass range from $1-16000\,m/z$. It can also be operated as high-pass mass filter in the RF-only mode. Thereby, masses with more than $\frac{7}{9}$ of the preset m/z-ratio are able to pass the QMF.[137] This RF-only mode is used for the deposition of a distribution of clusters sizes rather than one single size, and is denominated as 'unselected clusters' in the following. Additional stacks of electrostatic lenses guide the mass-selected cluster beam through a pin hole (6 mm) after which the clusters are soft-landed on the single crystal in the analysis chamber. The soft-landing condition (1 eV/atom) ensures an intact cluster deposition and prevent the clusters and the substrate from fragmentation upon impact.[130] The kinetic energy distribution is determined by a retarding-field analysis, where the cluster current is measured as a function of the applied voltage on the sample holder[5]. The positively charged clusters are neutralised with an electron from the TiO_2 support. This neutralisation current is measured with a picoammeter (6487 Picoammeter/Voltage, Keithley GmbH), monitored and evaluated with a home-written LabView program in order to determine the amount of deposited clusters. The cluster coverage is given in %-ML with respect to the total number of surface atoms. The accessible surface area for the clusters is estimated to be about the size of the pin hole (6 mm) and thus does not change for different samples. The total number of surface atoms for TiO_2(110)-(1x1) is $1.56 \cdot 10^{15}$ surface atoms per cm^2, thus $4.42 \cdot 10^{14}$ surface atoms in total. Typical currents during the deposition are in the range of $100-300$ pA for size-selected and $1-2$ nA for unselected clusters. The optimisation of the cluster current is a multi-parameter problem with i.a. the voltages of the lenses, bender, skimmer, octupole or the He back pressure, the delay and pulse width of the laser and He. During the optimisation process,

[5]The retarding-field analysis is performed on the molybdenum sample holder without a titania crystal in order not to contaminate the sample.

the cluster current is measured on an electrostatic lens with an applied negative voltage ($-200\,\mathrm{V}$) and a positive voltage ($+500\,\mathrm{V}$) on the subjacent lens to attract on respectively repel the cationic clusters. More details about the experimental setup can be found in [135, 137] and in [138, 139] for this specific cluster source.

3.1.1 Ni and Pt Cluster Size Distribution

Size-selected and various size distributions of Pt and Ni clusters are used in the experiments. The size distribution is determined by the nucleation conditions, in particular the He buffer gas, laser power and He-laser pulse delay. The cluster size distribution is manipulated through an interplay with the He back-pressure and the opening of the piezo valve[6] so that the pressure of $1.1 - 1.3 \cdot 10^{-1}\,\mathrm{mbar}$ is kept at the skimmer to ensure a high cluster current. Mass scans are recorded by measuring the current on an electrostatic lens as function of size. The QMF is operated to scan over a size distribution during such measurements.

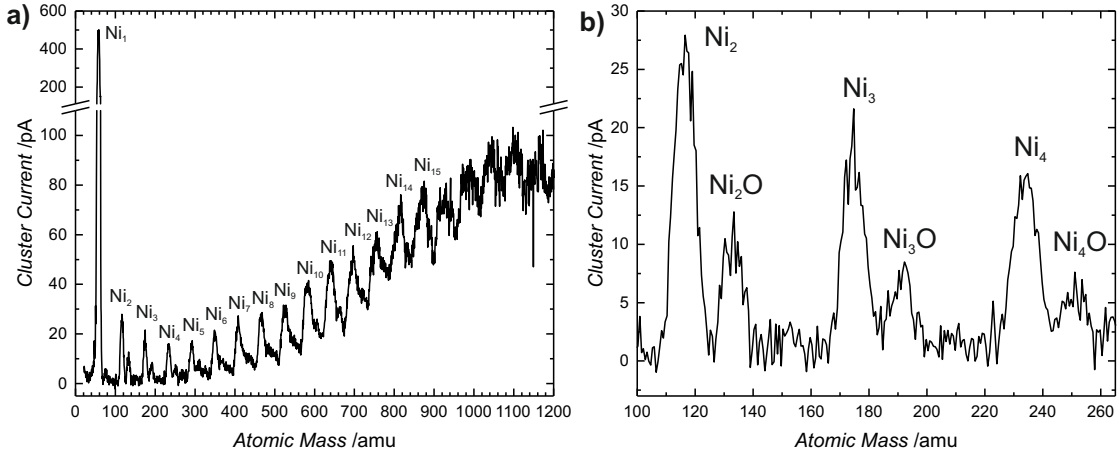

Figure 3.2. $Ni_{1\text{-}15}$ mass scan with settings for small Ni clusters shortly after having switched on the cluster source. **a)** gives an overview of the mass scan ranging from Ni_1 to Ni_{15} after which the peaks are not resolved sufficiently. Ni_xO_x peaks are next to the sharp metallic Ni peaks. **b)** is a zoom showing Ni_2, Ni_3, Ni_4 and their oxides. The Ni_xO are separated by 16 amu from their metallic cluster confirming the assumption of monoxide formation.

Even when the metal targets are stored in high-vacuum ($\sim 10^{-8}\,\mathrm{mbar}$), a native oxide layer is formed on the surface. Figure 3.2 shows a mass scan of $Ni_{1\text{-}15}$ clusters and their oxides immediately after turning on the cluster source. The small clusters $Ni_{2\text{-}4}$ form an oxide containing one single oxygen atom. This is demonstrated in figure 3.2**b)**, where the oxide peaks are next to the sharp metallic Ni peaks and are separated by a multiple of 16 amu. The oxide peaks vanish after running the cluster source for $\sim 30\,\mathrm{min}$. The

[6] The opening of the piezo valve is controlled by the applied voltage.

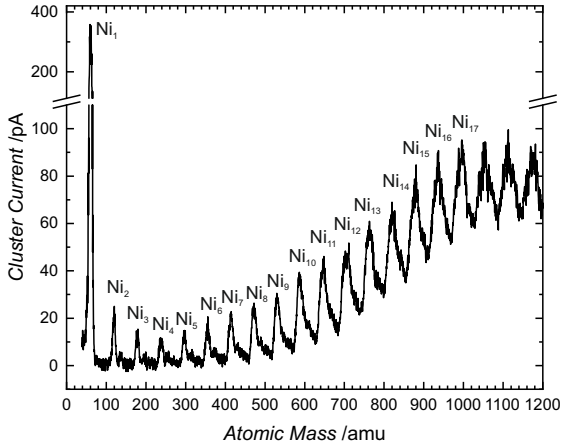

Figure 3.3. $Ni_{1\text{-}17}$ mass scan with settings for small Ni clusters after operating the cluster source for > 30 min. The scan gives an overview ranging from Ni_1 to Ni_{17} after which the peaks are not resolved sufficiently. No significant Ni_xO peaks are observed.

laser may ablate the native oxide layer resulting in a pure metallic $Ni_{1\text{-}15}$ mass scan, shown in figure 3.3. Therefore, the cluster source is operated for > 30 min prior to cluster deposition. The resolution[7] of the QMF is adjusted so that the desired single size cluster peak is completely resolved, which means that the baseline reaches 0 pA between two peaks. The peak width originates from slightly different trajectories, but is mostly caused by the isotopic distribution of nickel (^{58}Ni, ^{60}Ni, ^{61}Ni, ^{62}Ni, ^{64}Ni).

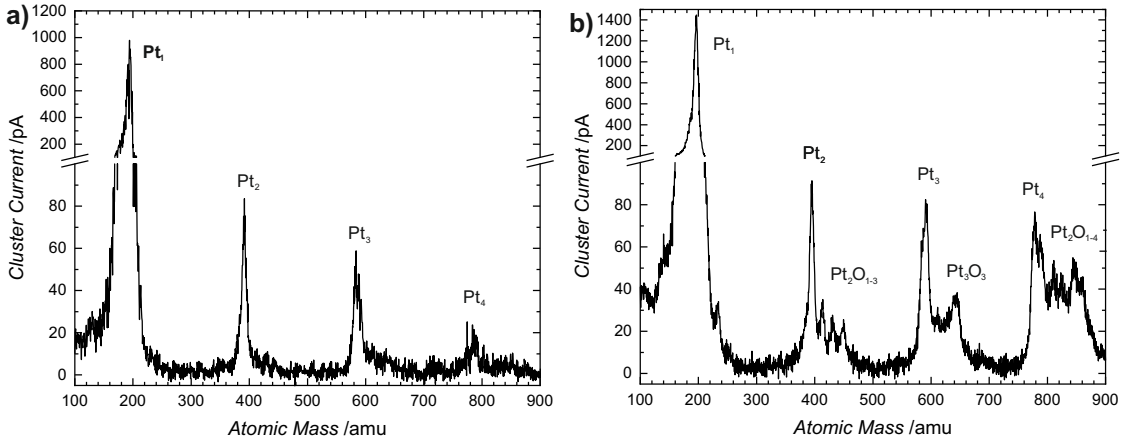

Figure 3.4. $Pt_{1\text{-}4}$ mass scans with settings for small Pt clusters. **a)** shows a mass scan after operating the cluster source for > 30 min. Only peaks assigned to pure Pt clusters are observed. **b)** shows a mass scan briefly after having turned on the cluster source. Different $Pt_xO_{1\text{-}4}$ peaks appear at higher masses next to their respective metallic peak, identified by their separation by multiples of 16 amu from their metallic cluster.

A similar behaviour is observed for Pt clusters, the mass scan shows platinum oxides shortly after having turned on the cluster source. An exemplary mass scan for small

[7]The set value given on the instrument for the resolution is typically varied from $5.0 - 6.0$.

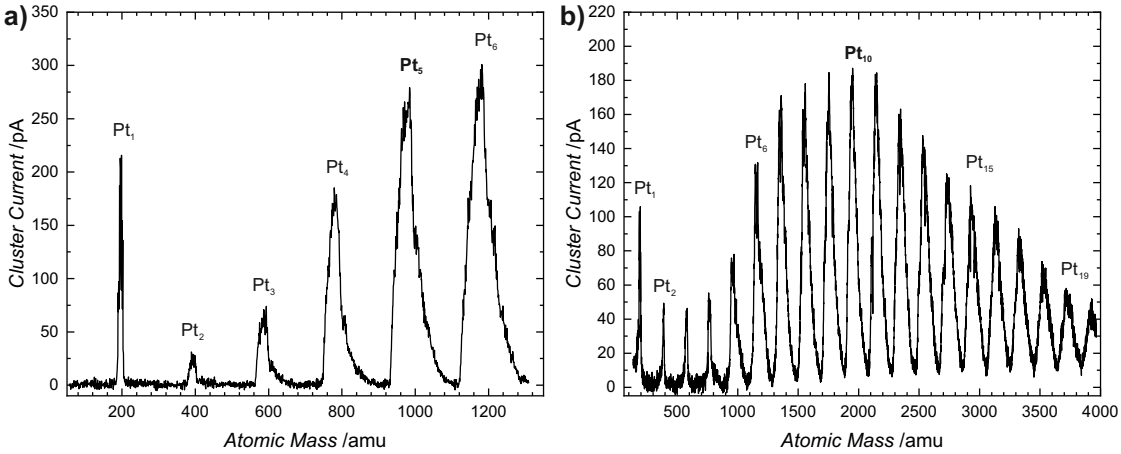

Figure 3.5. $Pt_{1\text{-}6}$ mass scans with settings for small Pt clusters. **a)** $Pt_{1\text{-}6}$ mass scan operating the cluster source optimised for the deposition of Pt_5. **b)** $Pt_{1\text{-}19}$ mass scan operating the cluster source optimised for the deposition of Pt_{10}.

Pt clusters is given in figure 3.4, where even different oxides are resolved. Pt_2^+ clusters form different oxides containing one to three oxygen atoms whereas for Pt_3^+ only oxides with three oxygen atoms are observed. The peaks broaden towards higher masses as can be seen in figure 3.5 due to the natural isotope distribution of Pt (^{1}94Pt, ^{195}Pt, ^{196}Pt, ^{198}Pt). The mass scans in figure 3.5, only showing clean metal clusters, are recorded prior to the deposition of Pt_5 or, respectively, Pt_{10} used in the experiments. The nucleation parameters are optimised for each cluster size in order to maximise its current.

3.2 Analysis Chamber

All experiments have been performed in the home-built ultra-high vacuum chamber at a base pressure below $8.0 \cdot 10^{-11}$ mbar. Briefly summarised, the surface of the single crystal TiO_2(110) is prepared by sputter-anneal cycles and analysed with different methods, prior to any experiments to ensure comparable conditions. Most of the experiments consist of thermal- and photo-induced reactivity measurements with a quadrupole mass spectrometer as main tool of investigation. The chapter is divided into a methodological and technical part including all the details. For more information, the analysis chamber is described extensively in previous dissertations.[138–141]

3.2.1 Technical Setup

Sample Holders and Sample Transfer

A single crystal TiO_2(110)-(1x1) is mounted on molybdenum rods of a liquid-N_2 cooled (x, y, z, ϕ)-manipulator (VAB Vakuum). Two different sample holders are used in the

course of this work, one for a fast sample transfer and one for a permanently installed crystal. Both sample holders are heated up to 1000 K indirectly *via* resistive heating with tungsten-26% rhenium (W-26%Re) wires with a thickness of 0.35 mm. Besides the heating, the W-26%Re wires clamp the sample holders to the Mo rods.

A permanently installed TiO_2(110)-(1x1) (⌀10 mm×2 mm, SurfaceNet) crystal with a cylindrical shape is fixed with two Ta clamps on a Ta base plate, shown in figure 3.6**a)**. For an optimal heat transfer, a gold foil is placed between the crystal and the Ta base plate. The W-26%Re heating wires fix the Ta-crystal mounting on the Mo rods. Type-C thermocouples are twisted and inserted into a hole in the crystal. This sample mounting allows for a fast liquid-N_2 cooling down to 90 K.

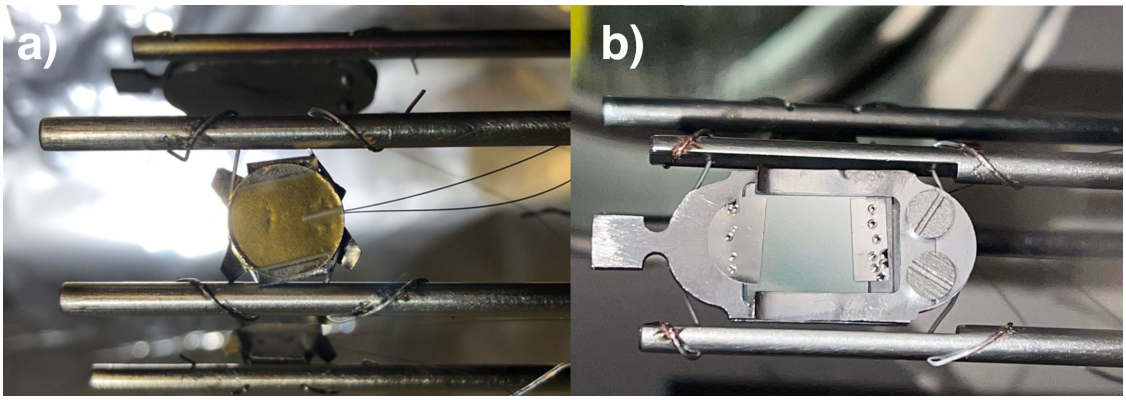

Figure 3.6. a) A fresh cylindrical TiO_2(110) crystal is permanently mounted on a Ta heating plate. The twisted thermocouples are inserted into a hole in the crystal. The crystal is completely transparent because it has not been bulk-reduced yet.[65] **b)** The transfer sample holder with a square shaped reduced TiO_2(110) platelet allows for a fast sample exchange. The thermocouples are spot-welded beneath the fixed base plate. The light blue colour of the crystal results from several sputter-anneal cycles which increases the degree of reduction.[65]

The transfer sample holder shown in figure 3.6**b)** allows for a fast exchange of samples without venting the entire chamber. The sample holder is made completely out of Ta and is composed of two parts: one part is fixed on the Mo rods (called the 'garage') *via* the heating wires and consists of a Ta base plate with type-C thermocouples spot-welded beneath and retaining springs. The second part (called 'car') contains a square-shaped TiO_2(110)-(1x1) crystal ($9.95 \times 9.95 \times 0.3\,mm^3$, SurfaceNet) and can be removed with a transfer manipulator. A thin gold foil (0.025 mm) is placed between the crystal and the car to ensure an optimal heat transfer. One drawback of this sample holder is the desorption of reactants and its outgasing during the thermal- and photo-measurements. Another one is a slower cooling process down to only 130 K.

Table 3.1. Summary and application of the rutile TiO_2(110)-(1x1) crystals employed during this thesis.

Type	Nickname	Project
cylindrical	*platinisiert*	different alcohols with unselected Pt on TiO_2
cylindrical	*virgin*	tertiary alcohols on TiO_2
platelet	*Plättchen 1*	bad heat transfer and broke eventually
platelet	*Plättchen 2*	Ni clusters on TiO_2
platelet	*Plättchen 3*	size-selected Pt_x on TiO_2

The transfer procedure starts with removing the car from the garage with a transfer manipulator (z, ϕ)-manipulator (Ferrovac MDG40). The car is picked up with a rotation-locking mechanism (SH2/12 ISR from SPECS Surface Nano Analysis) from the garage and moved to the transfer chamber. The gate between the analysis chamber and transfer chamber is closed and the transfer chamber is vented either with air from the lab or synthetic air *via* a venting valve. After the crystals have been exchanged, the transfer chamber is pumped down to $< 1.0 \cdot 10^{-8}$ mbar to not contaminate the analysis chamber. The car is then transferred back to the garage. The sample holders and transfer system have also been described in detail in previous dissertations.[138–140]

Five different rutile TiO_2(110) crystals were employed in the course of this thesis, which were all purchased from SurfaceNet. Table 3.1 gives an overview of the crystals and their applications. Cylindrical crystals are fixed permanently to the W-26%Re wires and platelet crystals are mounted on the transfer sample holder.

Reactant Dosage

The molecules required for the sample preparation or the reactivity experiments are introduced into the analysis chamber either *via* a leak valve or a molecular beam doser. The gas bottles are connected with pressure regulators to the gasline and liquids are stored in glas fingers whereby their vapour pressure is employed for the dosage. The liquids are degassed and purified by several pump-thaw-freeze cycles until no bubbles are evolving during the thawing. The gasline is able to carry five different reactants which can also be mixed in the gasline. Prior to any dosage, the gasline is flushed three times with the reactant. A base pressure of $5.0 \cdot 10^{-9}$ mbar can usually be obtained in the gasline.

For the dosage *via* the leak valve, a defined pressure ranging from $5.0 \cdot 10^{-10} - 1.0 \cdot 10^{-5}$ mbar is set whereby the entire analysis chamber is filled with the reactant. Therefore, the reactant is not only adsorbing on the crystal surface but on every component inside

the chamber in particular on the LN_2-cooled sample holder and manipulator. For the Langmuir dosage, that is the dosage *via* filling the background with a reactant, the defined pressure is hold for a certain time[8]. For the continuous catalytic experiments, the background is filled with the reactant over the whole course of the experiment.

The molecular beam doser enables for a directed dosing onto the sample surface *via* a micro capillary plate, whereby the pressure in the analysis is not significantly increased at all. This is in particular necessary for water to avoid an increasing partial pressure of water in the chamber. The MBD can be calibrated and allows for the dosage of a defined amount of molecules. Further details can be found elsewhere.[137]

In this work, all the reactants except of water are dosed *via* a leak valve.

QMS

The main tool for investigation in this thesis is a differentially pumped electron-impact quadrupole mass spectrometer (QMA 430, Pfeiffer Vacuum) monitoring the reactants and products. The sample is placed in line-of-sight to the QMS at a distance of $\sim 2 - 10\,\mathrm{mm}$ to the entrance skimmer in order to reach the highest sensitivity and to minimise signals from the background. For photochemical experiments, the distance between the sample and the skimmer is higher than for thermal experiments because the laser beam must be able to illuminate the entire crystal surface. During a day of measurements, water and hydrogen accumulate in the QMS chamber. Although the QMS is differentially pumped, the background of those mass fragments is constantly rising. Water and hydrogen are originating from the outgasing of the ionization filament and additional hydrogen stems from the reaction and alcohol fragmentation upon ionization. The QMS is equipped with a secondary electron multiplier (here a channeltron) where the very low ion currents (ionised mass fragments) are physically pre-amplified and detected, subsequently the signal is amplified electronically. In this work, the amplifier is set to either 10^{-9} for high signals or 10^{-10} for low signals. The SEM amplification is changing due to contaminations and a chemical change in the active layer. Therefore, the voltage is increased from 1800 V to 2000 V in the course of the thesis. One must thus pay attention when comparing quantitatively data from a prolonged period and frequent calibration is needed when doing so.

The QMS is operated in two different modes: mass scans and mass monitoring. In the first mode, all masses (usually $1 - 200\,\mathrm{amu}$) are recorded successively. Therefore the reaction and conditions must be very stable. The different mass scans reveal that the

[8] A pressure of $1.0 \cdot 10^{-8}\,\mathrm{mbar}$ is held for 2 min 13 s for dosing 1 L.

amplifier settings from 10^{-9} to 10^{-10} do not change the intensity of the resolved peaks. The sole difference is that mass fragments with a high intensity reach the saturation of the detector while low signals get resolved. Under stable conditions[9], one can record two comparable mass scans with amplifier settings of 10^{-9} and 10^{-10} to resolve all signals. In the second mode, preset masses are recorded as a function of time so that the QMS is only switching between those mass channels during one its measurement cycles.

Laser System

A laser system is used for a defined illumination of the crystal surface for photochemical experiments. The setup allows for a tuneable wavelength range in the UV/VIS, as well as NIR. The third harmonic of a Nd:YAG laser (355 nm, 20 Hz, 7 ns pulse width, 4 W at 355 nm, Spitlight HighPower 1200, Innolas) pumps an optical parametric oscillator (premiScan ULD/400, GWU, with modifications from Innolas) with a β-bariumborate crystal as active laser medium for wavelengths between $420 - 500$ nm. The OPO process is a second-order non-linear optical interaction in which pump photons cause the emission of two types of other photons (signal and idler) with different energies lower than that of the pump photons. Phase matching thus governs the signal and idler wavelengths and their tuning is achieved by varying the angle of incidence (by rotating the β-bariumborate crystal). Afterwards the idler beam is finally separated from the signal beam by a Pellin-Broca prism. For this work, the OPO is adjusted in order to emit a wavelength of 480 nm with an energy of 20 ± 2 mJ per pulse for the idler laser beam. The idler beam enters a second harmonic generation unit equipped with another non-linear crystal, in order to double the photon frequency and attain a UV laser beam. This means that two pump photons are converted to one photon with twice the energy. The 241 nm beam, which is separated by the same Pellin-Broca prism again from the pump wave, has a pulse energy of $500 - 1000 \pm 100\,\mu$J and can be adjusted to lower energies with grey filters. The UV beam is guided into the UHV chamber with different mirrors and a periscope (CVI Melles Griot) onto the crystal surface at an angle of 30° with respect to the surface normal. The resulting energy on the crystal surface is approximatively 1/3 of the energy measured after the laser housing output. The OPO and the SHG units are controlled by an in-house built LabView program, which controls the motor positions of the crystals and the prism in order to adjust the transmission of the wavelength of interest.

For the purpose of maintaining a constant laser power, the flash lamps of the Nd:YAG pump laser need to be changed after approx. 1 mio. shots or every second year. Therewith, the deioniser cartouche is also replaced and highly deionised water (Milli-Q water) must be filled into the cooling system to prevent a short circuit between the flash lamps.

[9] The background pressure must be highly stable as it has a tremendous effect on the signal intensity.

3.2.2 Methodological Part

This part describes the different experimental working principles and the crystal preparation. The measurement principles are either of a thermal or photochemical nature, or a combination of both, to disentangle thermal and photochemical pathways. Furthermore, photo-reactions are conducted either in a discontinuous, with a single adsorbate coverage, or continuous manner. For the latter, the reaction is conducted in a continuous alcohol background so that the reactant is constantly replenished.

Temperature-programmed desorption and reaction

Temperature-programmed desorption (TPD) and reaction experiments (TPR) are experimental techniques observing the desorbing molecules from a surface as function of temperature.[142, 143] With the TPD, the desorption temperature of an adsorbate is monitored while the TPR additionally is investigating a chemical reaction. The TPD gives access to the type of bonding of molecules to the surface, bonding strength and adsorption site. In addition, the TPR provides information about the thermal reaction pathways and products formed on the surface.

A defined amount of adsorbates for TPD/R experiments is dosed on the substrate at cryogenic temperatures *via* background dosing or in case of water with the MBD. The sample is placed underneath the skimmer of the QMS. The crystal is heated *via* resistive heating with a linear heating ramp of $1-2\,\mathrm{K/s}$ from the adsorption temperature to 800 K. The linear heating ramp is realised by a current gradient which is programmed manually due to the non-linear thermal behaviour of oxides.[139] The desorbing species enter the skimmer and are detected with the QMS. The measurement principle is shown in figure 3.7.

Photon-stimulated desorption and reaction

Photon-stimulated desorption (PSD) and reaction experiments (PSR) are investigating photo-activated processes on the surface upon illumination and in this work with a photon energy higher than the band gap of the semiconductor. Upon illumination, an electron-hole pair is excited and the minority charge carrier, in the case of titania the hole migrates to the surface where it initiates a desorption or reaction.[24, 52, 144–146] The PSD might reveal informations about the photo-activity, photo-active surface sites and surface composition. Insights about photochemical pathways and processes are additionally gained with the PSR. For the PSD, the desorption itself is photon-stimulated while for the PSR the formation of the product is photon-driven, but the desorption itself may also be thermally-driven.[52, 110, 147]

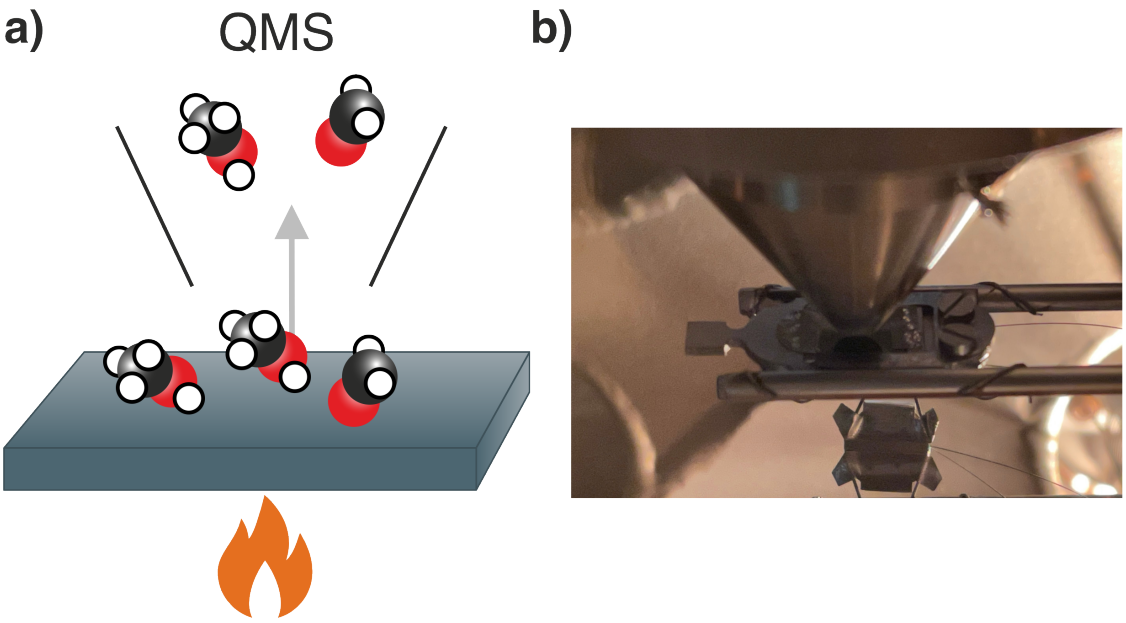

Figure 3.7. **a)** Sketch of the TPD and TPR measurement principle. Methanol is adsorbed on the single crystal. Upon heating of the crystal with a linear ramp, methanol undergoes either desorption (TPD) or reaction with subsequent desorption (TPR). The desorbing species diffuse to the skimmer and into the QMS. Note that the sketch is solely illustrative and not chemically correct. **b)** Photo of the TPD/R setup inside the UHV analysis chamber.

The experimental procedure is similar to the TPD/R ones, the surface is covered with a defined amount of adsorbates at cryogenic temperatures. The sample is placed underneath the skimmer of the QMS so that the laser beam is able to illuminate the crystal surface. For the O_2 PSD, the surface is illuminated at LN_2 temperatures for a certain amount of time. O_2 then desorbs and is recorded by the QMS.[42] In the case of PSR, two measurement procedures are distinguished. In the first case, the surface is illuminated for variable times at cryogenic temperatures that means below the desorption temperature of the products. This leads to an accumulation of the products on the surface depending on the illumination time. The photo-products are desorbing thermally or undergo a potential consecutive thermal reaction in a subsequent TPD/R. This procedure is also denominated as post-illuminated TPD/R (PI-TPD/R). In the second case, the sample is heated to a temperature above the desorption temperature of at least of the products and below the desorption temperature of the reactant. In an illumination step at isothermal conditions, the photo-products are formed and desorbing. The isothermal PSD/R at different temperatures and subsequent TPD/R elucidate photochemical reaction pathways and disentangle thermal from photochemical reaction steps. The temperature influences the adsorption coverage, possibly the site and geometry, and the diffusion of reactants.

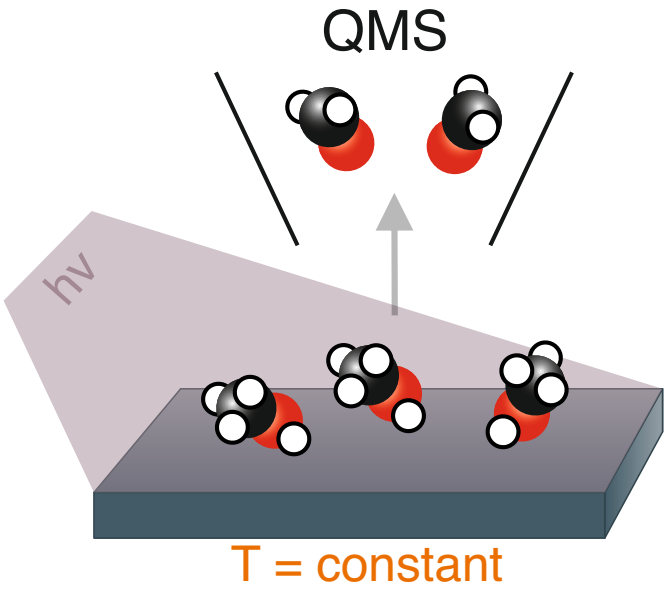

Figure 3.8. Sketch of the isothermal PSR measurement principle. Methanol is adsorbed on the surface. Upon UV illumination, methanol is photo-oxidised to formaldehyde and is thermally desorbing and diffusing to the QMS. Note that, the sketch is solely illustrative and it is not chemically correct.

Photocatalytic Measurements

The photocatalytic measurements are conducted analogously to isothermal PSR experiments. The sample is kept at a certain temperature above the desorption temperature of all the products and is illuminated for a certain amount of time. In contrast to PSR experiments, the sample is illuminated in a constant reactant background so that the surface is constantly refilled with reactants. This might mimic a flow reactor with very low reactant pressures because a re-adsorption of product is very unlikely. The background pressure is established at least 10 minutes prior to the start of the reaction in order to ensure a saturation coverage of the adsorbate. The reactant consumption and the products evolution is monitored with the QMS as a function of time. A turn-over-frequency can be calculated from the integration of the product signals. A detailed description is given in the section 3.3.

3.2.3 Crystal Preparation

In order to ensure reproducible and comparable data, the crystal surface is controlled on an atomic level and prepared constantly to the same condition. A new untreated rutile crystal has several contaminations like cerium, carbon and calcium as can be seen in the AES in figure 3.9**a)** which are removed by several sputter/anneal cycles. Figure 3.9**b)** shows a typical AES of a clean TiO_2(110) revealing only characteristic Ti and O peaks.

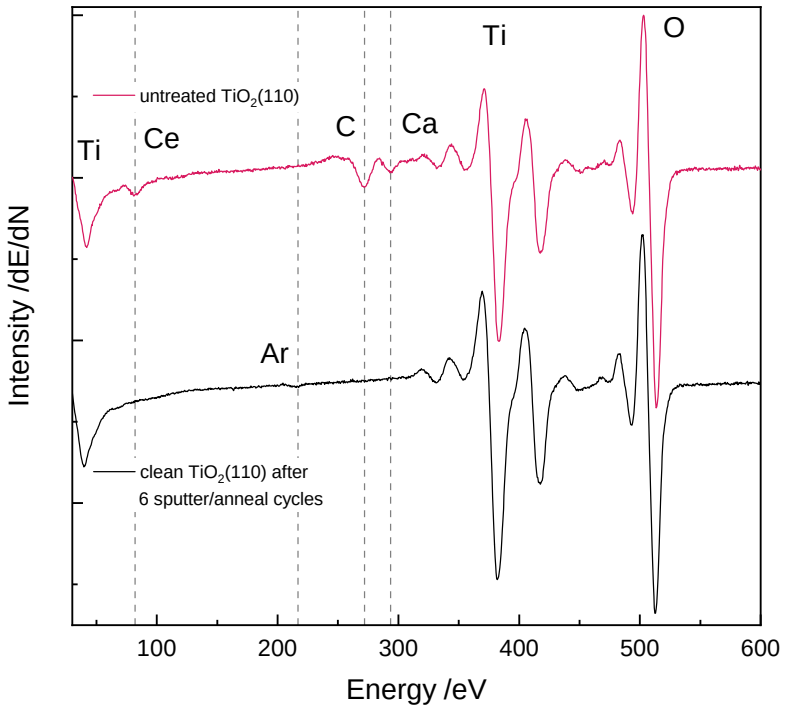

Figure 3.9. **a)** AES of a new untreated $TiO_2(110)$ with significant cerium, carbon and calcium contaminations. **b)** AES of a prepared rutile $TiO_2(110)$ after several sputter/anneal cycles shows no significant contaminations. The Ar peak stems from Ar embedded due to Ar^+-sputtering.

One sputter/anneal cycle consists of 30 min Ar^+-sputtering (1 keV, $5 \cdot 10^{-6}$ mbar Ar, $I_{sample} = 13\,\mu A$, T= $150 - 300$ K) and 20 min O_2-annealing (800 K, $1.0 \cdot 10^{-6}$ mbar O_2). The reduced surface (r-$TiO_2(110)$) is received through vacuum annealing (800 K, 10 min) after the last sputter-anneal cycle. The oxidised titania surface (o-$TiO_2(110)$) is achieved by adsorption of > 10 L O_2 at cryogenic temperatures on the r-$TiO_2(110)$ followed by an annealing step to 300 K, which leads to O_{ad} on Ti_{5c} rows and some filled bridge-bonded oxygen vacancies.[148, 149]. The hydroxylated surface (h-$TiO_2(110)$) is realised by dosing a multilayer of H_2O at cryogenic temperature on the r-$TiO_2(110)$. The sample is subsequently annealed to 300 K to desorb molecular water and leaving behind only surface hydroxyls.[150, 151]

A fresh crystal is transparent (figure 3.6**a)**) and has no significant Ti^{3+} related bulk defects.[65] The bulk reduction state, that means the bulk defect concentration, is increased through Ar^+-sputtering and annealing in vacuum ($800 - 900$ K) leading to a colour change to light blue (figure 3.6**b)**).[65] The bulk reduction correlates somehow with the concentration of surface oxygen vacancies in the bridging oxygen row, which play an import role for the reactivity and are indispensable for the photo-activity. [23, 33, 65, 75] The bridge-bonded oxygen vacancy concentration is determined and monitored constantly

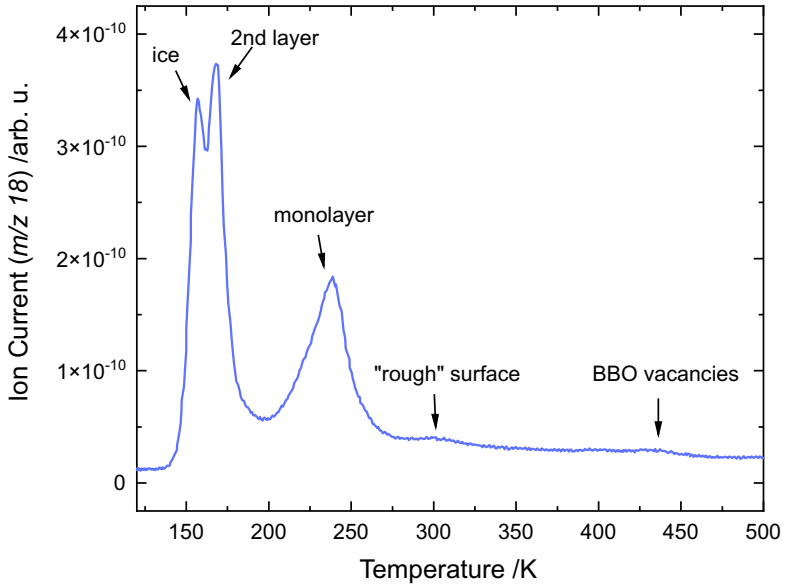

Figure 3.10. H_2O TPD from a highly reduced rough r-TiO_2(110) surface. A multilayer of water is dosed at 120 K. Water adsorbs dissociatively at BBO vacancies leading to the formation of two hydroxyls, which are desorbing at 450 K as water. Higher coordinated molecular water is desorbing at 300 K from step-edges and kinks. Molecular water bound to Ti_{5c} sites desorbs at 250 K. The second monolayer and the multilayer called 'ice' are desorbing < 200 K. The peak assignment is following that of Henderson.[152, 153]

by the evaluation of the high-temperature feature in the H_2O TPD.[138, 152, 154] Water adsorbs dissociatively in BBO vacancies forming two hydroxyls by healing the vacancy. Two hydroxyls recombine at 450 K leaving the surface as water. The relation of the area underneath the high-temperature signal with the area of molecular adsorbed water at Ti_{5c} lattice sites gives the concentration of BBO vacancies. The defect concentration in this work varies for different crystals from $1-6\pm1$%ML. The cleaning procedure leads to stable BBO vacancy concentration over a long period. A new crystal is used for each project and is employed for the entire project; a summary of the crystals is found in table 3.1.

The cleaning procedure is applied extensively to fully remove metal clusters. Especially Pt clusters are persistent towards Ar^+-sputtering. H_2O TPDs serve as detection tool for Pt residues. Even smallest amounts of Pt lead to H_2 evolution in the course of a H_2O TPD, similar as shown in figure 3.11**b)**.[155] Up to 15 sputter/anneal cycles are employed until no H_2 feature is detectable (figure 3.11**a)**). This leads to a rougher surface morphology, islands are formed and the size of terraces are reduced and thus the amount of step-edges and kinks are increased.[36, 65, 156] This 'highly' reduced rough surface shows an additional H_2O desorption feature at slightly higher temperatures than 300 K with respect to molecular water desorbing from regular Ti_{5c} sites shown in figure 3.10. Molecular water is stronger bound at kinks and step-edges due to a higher coordination.[124]

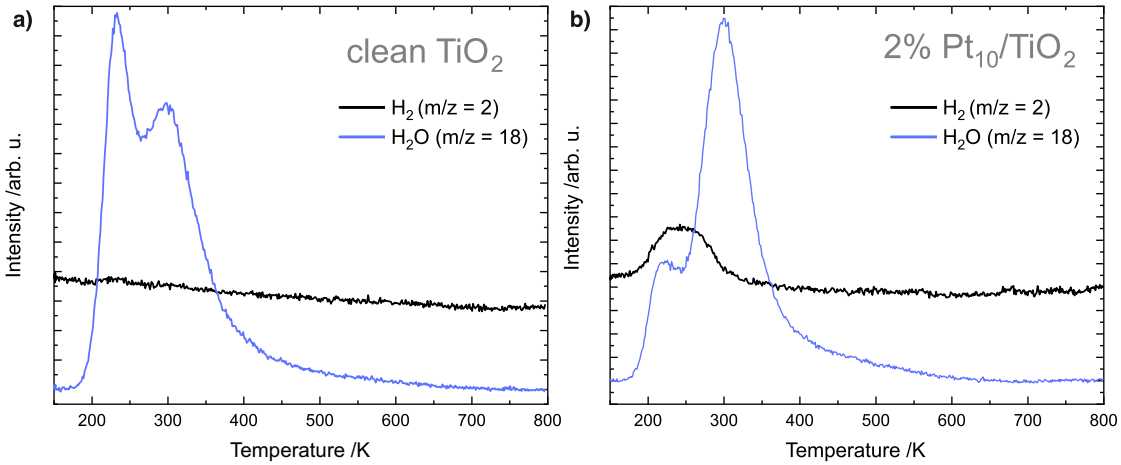

Figure 3.11. H_2O TPDs from **a)** r-TiO_2(110) and **b)** 2%ML Pt_5/r-TiO_2(110). A multilayer of water is dosed at 180 K. Water adsorbs dissociatively at BBO vacancies leading to the formation of two hydroxyls, which are able to recombine on Pt clusters to form H_2.

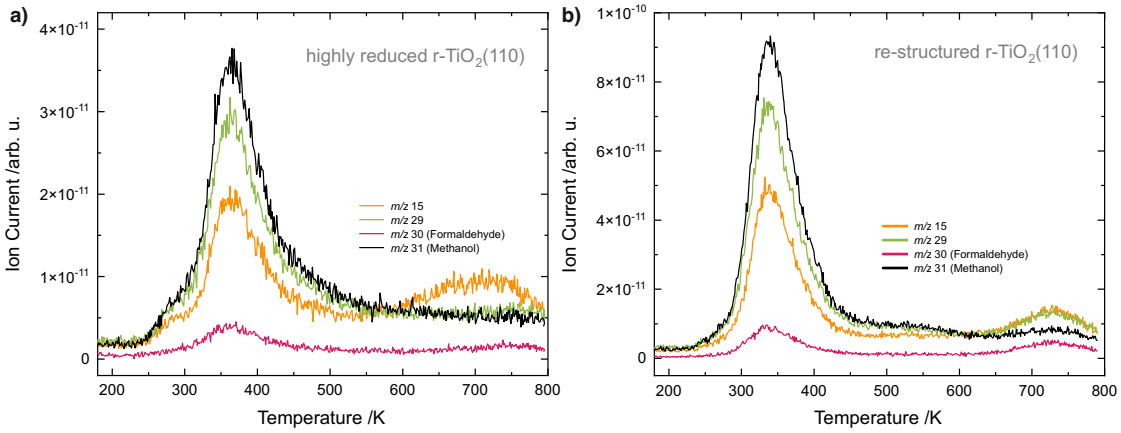

Figure 3.12. TPDs of 1.5 L methanol from **a)** a rough highly reduced TiO_2(110) and **b)** re-structured TiO_2(110) surface. On the highly reduced surface, methoxys are decomposed to CH_3 or CH_3 containing species, where as on a flat re-structured surface methoxys are disproportionated to formaldehyde (m/z 30) and methanol (m/z 31).

Furthermore, this rough surface exhibits a different high-temperature reactivity of methanol. Dissociatively adsorbed methanol, resulting in a methoxy and hydroxyl, decomposes at 700 K to a species containing a CH_3-fragment (m/z 15). On a rough surface, no features in $m/z = 16, 29, 30, 31$ are observed[10], as can be seen in figure 3.12**a)**. This indicates that methoxy is deoxygenated into a methyl radical. In contrast, methoxy is disproportionated to formaldehyde and methanol at 700 K on a flat (110)-(1x1) surface.[152] Several re-oxidation sputter/anneal cycles (1 min Ar^+-sputtering, 1 h O_2-annealing) re-establish the flat surface. Figure 3.12 shows a methanol TPD of the re-

[10] A feature in $m/z = 16, 29, 30, 31$ would be observed if methane, formaldehyde or methanol respectively would be desorbing.

structured surface and shows the typical methanol disproportionation reaction occurring at high-temperatures.

The photoconversion of 2-methyl-2-pentanol to acetone and propane (more informations are found in the results section) on a rough highly reduced TiO_2(110) and a re-structured TiO_2(110) demonstrates that the roughness does not influence the photo-activity of the sample. Figure 3.13 shows that the TOFs are unaffected by the surface condition.

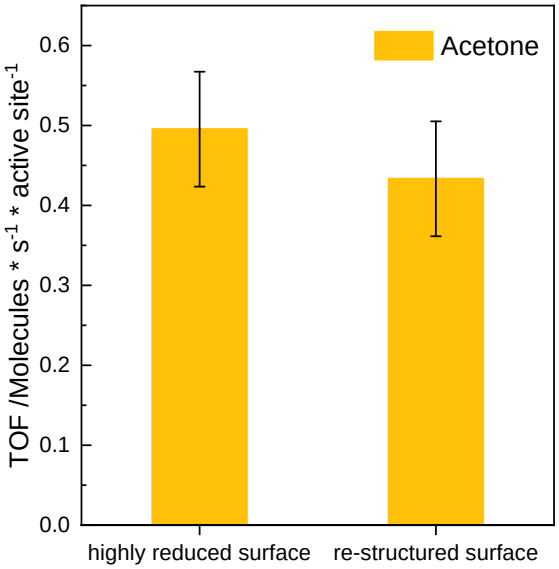

Figure 3.13. TOF of the photocatalytic conversion of 2-methyl-2-pentanol on highly reduced r-TiO_2 and re-structured r-TiO_2 through several re-oxidation sputter/anneal cycles. The photoactivity towards the oxidation of 2-methyl-2-pentanol is independent of the surface condition. 2-methyl-2-pentanol is converted to acetone and propane at 330 K with a background pressure of $5.0 \cdot 10^{-8}$ mbar, more informations are presented in the results in section 4.7.

3.3 Data Evaluation

Discontinuous Measurements

In TPD/R and PSD/R, the QMS records an ion current of specific m/z-ratios as a function of temperature or time. In order to obtain qualitative and quantitative informations from the ion current, the QMS signal is processed and calibrated. A detailed description of TPD/R data analysis is found in a previous dissertation, wherefore this section in this thesis only outlines the main points.[139]

The ion current is evaluated to take into account the fragmentation pattern FP, the electron-impact ionisation cross-section σ and the transmission coefficient T and is

Table 3.2. Transmission probability of m/z-ratios for the apparatus Hiden Analytical at Harvard University.

m/z	T
0-20	1.5
21-30	1
31-40	0.9
41-50	0.8
51-60	0.7
61-70	0.6

corrected for contributions from other molecules. The neutral molecule fragments into cationic fragments upon electron-impact ionisation. The fragmentation pattern and the ionisation probability upon electron-impact are substance-specific. The transmission through the QMS decreases exponentially for higher m/z-ratio fragments. First, the ion current ($m/z = a$) of substance A is deconvoluted from contributions from substance B, which is only possible if substance B fragments into a unique $m/z = i$ fragment. The mass scans from the NIST database or self-recorded mass scans are exploited as to determine the fragmentation pattern and the contribution to one mass signal of a specific substance. In this way, the ratio of $(m/z = a :)(m/z = i) = \frac{a}{i}$ (> 1) gives the contribution of substance B to the mass signal $m/z = a$. Thus the intensity arising from substance A to the mass signal $m/z = a$ is given by equation 3.1.

$$I(A) = I(m/z = a) - \frac{a}{i} \cdot I(m/z = i) \ \text{[A]} \tag{3.1}$$

The deconvoluted mass signal is further corrected for its fragmentation pattern, ionisation cross-section and transmission probability through the QMS. The transmission function is determined experimentally. It is given by equation 3.2 for the apparatus at the TUM and listed in table 3.2 for the apparatus at Harvard University.

$$T = 3.198 \cdot e^{-0.034 \cdot m/z} \tag{3.2}$$

In a second part, the ion current of a specific substance is referenced to a signal originating from the desorption of one monolayer. A coverage-dependent TPD serie is conducted to determine the integral of this monolayer exactly. In this work, methanol is used as reference the ion current to a monolayer. A more detailed description is found in the appendix of a previous dissertation.[138] A monolayer is defined as $5.2 \cdot 10^{14}$ molecules/cm^{-2} for the

TiO_2(110)-(1x1) surface; this assumes one adsorbed molecule per surface unit cell.[81] This is a reasonable assumption since methanol is adsorbing molecularly on Ti_{5c} sites and one unit cell contains one Ti_{5c} surface atom. The mass signal $m/z = 31$, which is a unique mass signal in a methanol TPD, is corrected for its fragmentation pattern, ionisation cross-section and transmission. The mass signals are plotted versus time, not temperature, because the ion current is time-dependent and a plot versus temperature would only be valid with a heating ramp of 1 K/s. The integration of the area $Area_{ML}$ of the feature stemming from molecular methanol desorption at ~ 300 K gives the amount of electric charges in [C] corresponding to one monolayer.

The unique mass signals or the deconvoluted mass signals are converted into a rate with the unit [ML/s] by equation 3.3. The ionisation-cross sections, fragmentation pattern factors and employed unique mass signals for the substances used in this work are found in the different publications or Supporting Informations related to the publications.

$$rate = \frac{I(A) \cdot FP}{T \cdot \sigma \cdot Area_{ML}} \text{ [ML/s]} \tag{3.3}$$

Photocatalytic Measurements

The QMS monitors preset m/z-ratios as a function of time in photocatalytic measurements. The baselines of the mass signals is determined by the background pressure, this is the signal in the 'dark'. UV illumination initialise the photo-reaction. The mass signals reflecting the photo-products increase abruptly. This is the 'illuminated' signal. The mass signals are calibrated and corrected with equation 3.3 in order to obtain the rate. The turn-over-frequency, that means the number of converted molecules per time and per active site is calculated by the mathematical integration of the illuminated signal, named 'integral', divided by the time difference Δt and the percentage of active sites per monolayer with equation 3.4. In this work, the active site is assumed to be the BBO vacancies, which are titrated with a H_2O TPD (see subsection 3.2.3).[48, 75]

$$TOF = \frac{integral}{\Delta t \cdot \%BBO_{vac} \cdot 100} \left[\frac{\text{molecules}}{\text{s}^{-1} \cdot \text{active sites}^{-1}}\right] \tag{3.4}$$

Product Analysis - Mass Scans

In the best case, products are identified unambiguously by the evaluation of mass scans in a steady-state photocatalytic measurement. To achieve this, the reaction must be driven in a steady-state and the catalysts must not be deactivating. Further, the reactant

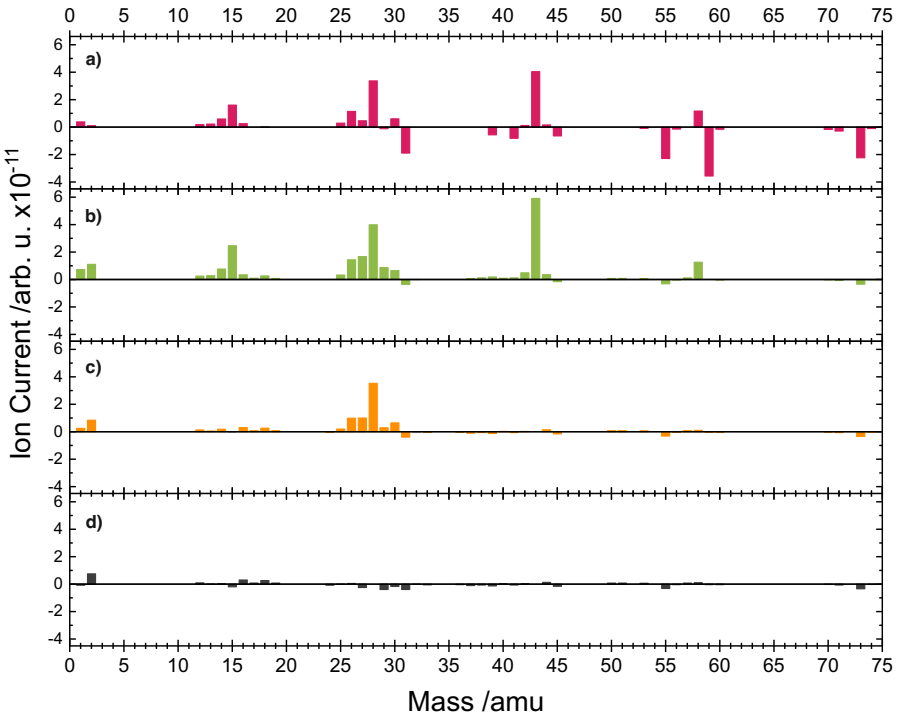

Figure 3.14. Exemplary mass spectra for demonstrating the product analysis of the photocatalytic reforming of the alcohol 2-methyl- 2-butanol (0.1%ML Pt_x/TiO_2, 263 K, alcohol background pressure $2.0 \cdot 10^{-7}$ mbar). **a)** shows the difference spectrum, where positive peaks originate from the products (here acetone and ethane), and the negative peaks stem from the consumption of the alcohol (here 2-methyl-2-butanol). The mass spectra of the alcohol is added to the difference spectrum shown in **b)**, both spectra have been normalised to $m/z = 59$ prior to the addition. Spectrum **c)** shows the subtraction of the product (here acetone), here the spectra have been normalised to $m/z = 43$. **d)** shows the subtraction of ethane (normalised to $m/z = 29$) leading to the baseline.

background pressure must be highly stable. If those requirements are fulfilled, even complex reaction products and pathways are elucidated.

At a determined alcohol background pressure a mass scan **D** (for 'dark') over a complete mass range (i.e. $1 - 200$ amu), where potential products masses occur, is performed. This mass scan **D** includes all the m/z-fragments stemming from the ionisation of the alcohol as well as all possible contaminations from the residual gas in the UHV chamber (H_2, CO, CO_2 and H_2O). Subsequently, the sample is illuminated and the photo-reaction is initialised. A steady-state of the reaction is reached latest after several minutes. Then, a second mass scan **I** (for 'illuminated') is recorded and it includes the fragmentation pattern of the alcohol and its photo products. A pure mass scan of the photocatalytic reaction is received through the subtraction of **D** from mass scan **I**. In this difference mass spectrum in figure 3.14 **a)**, positive values indicate the mass peaks arising from photo-products and the negative values originate from the consumption of the alcohol.

In order to identify explicitly all the photo-products and to not overlook a product, self-recorded mass spectra of the reactant and products are subtracted or added from the difference spectrum **a)**. Prior to every addition or subtraction, the two spectra are normalised to a unique mass of the product in order to account for the abundance of the species. In figure 3.14, the mass scan of the alcohol is added to the difference spectrum from **a)** to **b)**. The resulting spectrum **b)** solely includes reaction products. Further, the mass scan of one product after the other is subtracted from **b)** until only the baseline is reached.

4 Results and Discussion

This chapter comprises published and unpublished research about alcohol photo-conversion on bare and metal-loaded titania. The combination of surface science and heterogeneous catalysis concepts provides fundamental mechanistic insights into photocatalytic processes. The first part focuses on the individual reaction pathways of alcohols on bare titania and elucidates fundamental processes. In the second part, the role of size-selected platinum and nickel co-catalysts is clarified and a catalytic cycle is established, which is validated for several alcohols. A detailed analysis of the surface species further elucidates the mechanism. The pressure and temperature influence is investigated and their impact on the selectivity in the photocatalytic conversion of both small and larger alcohols is elaborated. A brief outlook is given about the SMSI effect on the photocatalytic activity and the cluster's stability.

The sections 4.1-4.8 represent respectively summaries of published articles in peer-reviewed journals. The sections only give an overview of the data and their interpretation; the data itself is given in the respective publication and Supporting Information. Section 4.9 discusses recent and unpublished data, and section 4.10 presents preliminary studies and gives an outlook for the future. Every section comprises cross-references, but they can also be read independently from other sections.

The results from section 4.4, 4.5, and 4.6 are to some extent based on data from my preceding Master thesis.[157] However, the thorough interpretation of these results, together with additional experiments during the course of this work, led to new fundamental insights and the publication of three articles. The results from the remaining chapters were conducted and elaborated during my PhD project. The experiments from

section 4.2 were conducted at Harvard University in the lab of Prof. Cynthia Friend in a three-month research exchange.

4.1 Photocatalytic Selectivity Switch to C-C Scission: α-Methyl Ejection of *tert*-Butanol on TiO_2(110)

Title	Photocatalytic Selectivity Switch to C-C scission: α-Methyl Ejection of *tert*-Butanol on TiO_2(110)
Authors	Constantin A. Walenta, Sebastian L. Kollmannsberger, Carla Courtois, Martin Tschurl and Ueli Heiz
Journal	*Phys. Chem. Chem. Phys.* **2018**, *20*, 7105 - 7111.
DOI	`https://doi.org/10.1039/C8CP00223A`
Status	published online February 6, 2018

The photocatalytic degradation of organic pollutants over titania has been given considerable attention in the past three decades.[12] Titania exhibits a rich oxidation chemistry but the decomposition of complex organics is still lacking the desired selectivity because elementary chemical processes are largely unknown.[24] In this regard, the thermal and photochemical reaction pathways of *tert*-butanol on rutile TiO_2(110) is investigated as model system. Dohnalek et al. already showed that the main thermal reaction pathway is the dehydration of *tert*-butanol to isobutene *via* a concerted E2-elimination of water.[102] In this work, it is demonstrated how the product distribution of the reaction of *tert*-butanol on rutile titania is governed by the contribution of thermal and photochemical reaction steps.

A portion of *tert*-butanol adsorbs dissociatively, predominantly in BBO-vacancies forming a *tert*-butoxy and a hydroxyl with a BBO (BBO-H).[96, 159] Several studies report that alkoxies are the photo-active species for the hole-driven oxidation, as already described in section subsection 2.3.1. This interpretation is adopted for *tert*-butanol and all other alcohols occurring in this thesis, as alcohols show comparable adsorption and reactivity.[48, 80, 81, 97, 98, 103]

The UV illumination of the reactant-covered surface at 100 K leads to the oxidation of *tert*-butoxy to acetone by a photo-hole and the ejection of a methyl radical into the gas-phase. The tertiary alcohol is missing the α-H that is typically cleaved upon oxidation of primary and secondary alcohols; instead the C-C bond is cleaved. Acetone and *tert*-butanol remain on the surface at this cryogenic temperatures. In a consecutive PI-TPD, the photo-product acetone is desorbing. To some extent, unreacted *tert*-butanol replenishes the BBO-vacancies during annealing forming *tert*-butoxy, which thermally

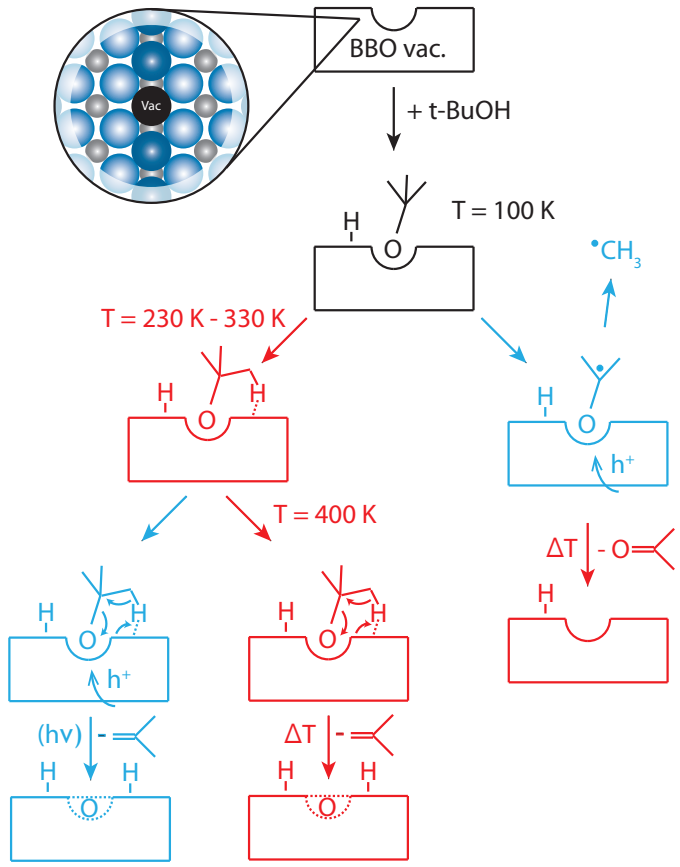

Figure 4.1. Scheme of the thermal (red) and photochemical (blue) reaction steps of *tert*-butanol on r-TiO_2(110). A fraction of *tert*-butanol adsorbs at 100 K in BBO-vacancies as *tert*-butoxy. The BBO-vacancy (black) is illustrated in-plane. The Ti atoms are represented in grey and the oxygen atoms in blue. One reaction pathway involves the thermal activation of a cyclic transition state of the alkoxy between $230 - 330$ K. Then, the photo-reaction leads to the dehydration of the activated alkoxy to isobutene and its photodesorption. Isobutene is also formed thermally from the transition state but only above 400 K. The photo-reaction pathway at cryogenic temperatures is initiated by the photo-oxidation of *tert*-butoxy with a hole leading to a C-C bond scission, the ejection of a methyl radical into the gas-phase, and the formation of acetone. Subsequently, acetone is desorbing at higher temperatures. Reproduced from Ref. [158] with permission from the PCCP Owner Societies.

reacts to isobutene, while most of *tert*-butanol is desorbing intactly. Longer illumination times increase acetone production and decrease the amount of unreacted *tert*-butanol and isobutene until 30 min UV illumination, above which saturation is observed.

The change of the reaction temperature to 293 K, which is above the desorption temperature of acetone, changes the reaction behaviour. As expected, acetone and methyl radicals are instantly formed and desorbed upon UV illumination. Unexpectedly, isobutene desorption is additionally observed immediately after the photo-reaction is initiated, although the thermal formation of isobutene is only enabled at higher temperatures above

400 K. This, together with the absence of isobutene formation during the photo-reaction at 100 K, indicates that only a thermally activated adsorption state is active for the photo-induced reaction to isobutene and/or photo-assisted desorption. Varying the photo-reaction temperature between 239 − 330 K reveals that the acetone yield is increasing and the isobutene yield remains relatively constant with higher temperature. The higher reaction temperature favours the thermal desorption of acetone, which is the rate-limiting step, and thus increases the yield. In contrast, the desorption of isobutene is not thermally hindered as isobutene already desorbs below 250 K.[160] Instead, a minimum temperature is required to form a cyclic transition state of *tert*-butanol, which is accessible for the UV-induced dehydration to isobutene. The UV irradiation may cause a redistribution of charges, which may enable the dehydration reaction and desorption.

The analysis of individual decay curves at 293 K confirms the assumption that different mechanisms are responsible for the formation of isobutene, acetone and methyl radicals. The methyl radical ejection occurs in every isothermal photo-reaction experiment (100 − 330 K) and is evidently a photo-reaction. While the concomitant photo-product acetone is formed at every temperature, too, its desorption is hindered thermally, which is why its yield during illumination increases with higher reaction temperature. Acetone shows the slowest exponential decay closely followed by the methyl radical. Isobutene exhibits a much faster decay, which indicates that the UV illumination facilitates the formation of isobutene from the thermally activated alcohol, whereas the desorption is either UV-induced or at least not thermally hindered.

In conclusion, the hole-driven photoconversion of *tert*-butanol shows a new mechanistic pathway involving the scission of a C-C bond or a dehydration reaction, both of which are photo-induced. While at cryogenic temperatures, UV illumination only leads to the formation of acetone and methyl radicals, a second reaction pathway opens up for the photo-reaction above 230 K. A thermally activated cyclic structure of *tert*-butanol involving the BBO-vacancy facilitates the UV-induced dehydration pathway and desorption. It is demonstrated, that the temperature plays a crucial role in photocatalysis and may govern strongly the product selectivity.

4.2 Regulating Photochemical Selectivity with Temperature: Isobutanol on TiO_2(110)

Title	Regulating Photochemical Selectivity with Temperature: Isobutanol on TiO_2(110)
Authors	Carla Courtois*, Constantin A. Walenta*, Martin Tschurl, Ueli Heiz, and Cynthia M. Friend
Journal	*J. Am. Chem. Soc.* **2020**, *142*, 13072 - 13080.
DOI	`https://dx.doi.org/10.1021/jacs.0c04411`
Status	published online June 26, 2020

*These authors contributed equally to this work.

The photocatalytic conversion of alcohols to hydrogen and valuable oxidation products is an attractive approach for a sustainable energy supply because alcohols are potential fuels made from biomass.[20, 162] Especially, isobutanol has arousen interest because of the recent developments in biologically assisted fermentation of cellulose to produce energetically dense alcohols.[163, 164] However, the reaction pathways of longer-chain alcohols are not well understood and the influence of temperature is often neglected.[165, 166] This work demonstrates the temperature-dependent selectivity for the photochemical decomposition of isobutanol. A second, consecutive photo-oxidation step competes with the thermal desorption of the initial photoproduct.

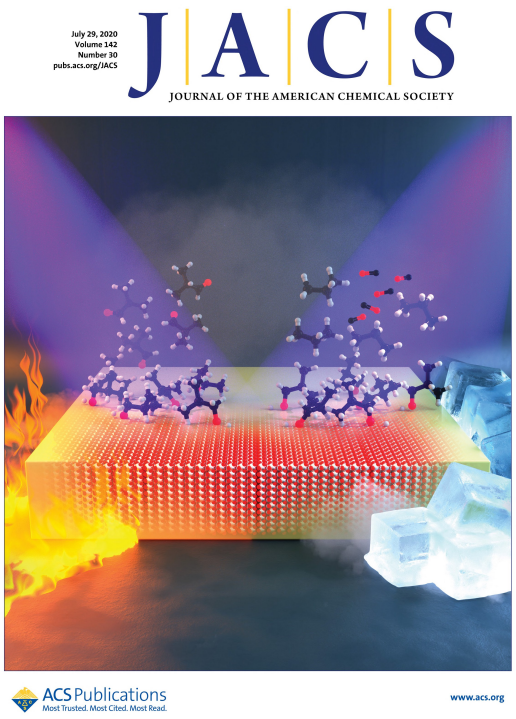

Figure 4.2. Front cover art from this publication. The photochemical conversion of isobutanol over titania shows a temperature-dependent selectivity. Reprinted with permission from [161]. Copyright 2020 American Chemical Society.

The thermal chemistry of isobutanol on oxidised, reduced, and hydroxylated TiO_2(110) is comparable to other small alcohols.[76, 102, 103] A small portion of isobutanol adsorbs dissociatively forming isobutoxy and BBO-H. The isobutoxy formation

is related to defects such as BBO vacancies or oxygen adatoms (O_{ad}), as described in more detail in subsection 2.3.1. The isobutoxy species may undergo two thermal reaction pathways, namely a dehydration or a disproportionation reaction. Most of isobutanol desorbs moleculary from Ti_{5c} sites. In a TPR experiment, isobutoxy reacts around 600 K in two parallel reaction pathways to yield either isobutanal and isobutanol, or isobutene and water. Both reaction pathways, the disproportionation and dehydration one, occur independently of the surface preparation. The dehydration reaction is attributed to occur at BBO vacancies.[103]

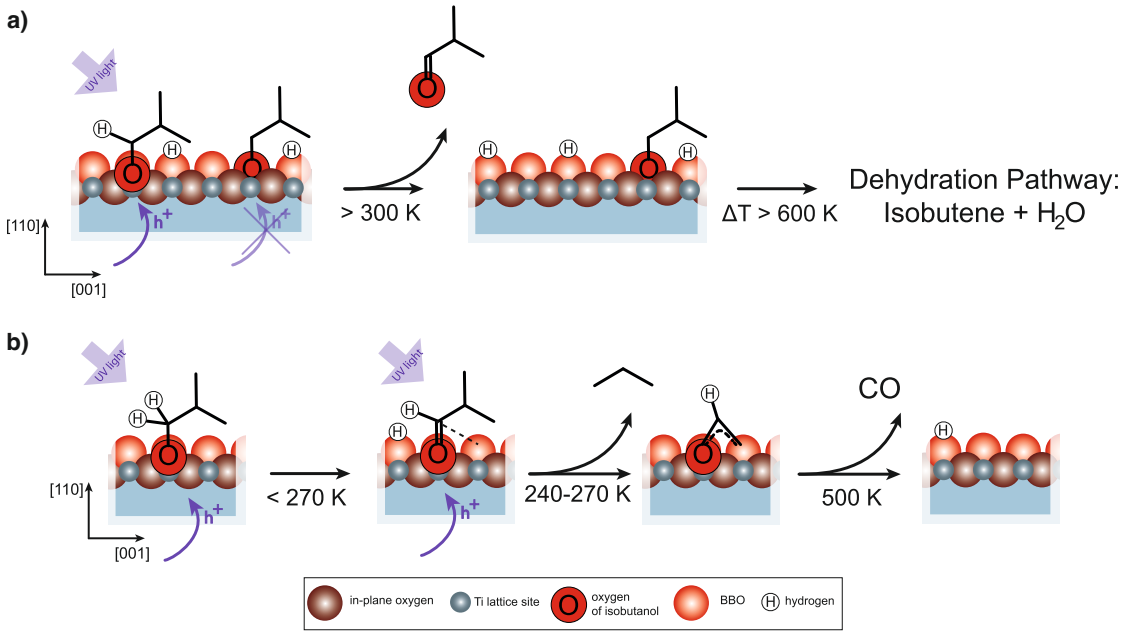

Figure 4.3. Schemes of temperature-dependent photochemical reaction steps of isobutanol on r-TiO_2(110). **a)** shows the thermal- and photochemical reaction pathways of two different isobutoxy species adsorbed on TiO_2(110) (side-view) above 300 K. The photo-active isobutoxy reacts with a photo-hole and is oxidised to isobutanal. Isobutanal immediately desorbs thermally. The remaining isobutoxy undergoes a dehydration reaction above 600 K. The formed isobutene and water desorb thermally above room temperature. **b)** shows the photo-reaction pathway of isobutoxy adsorbed on TiO_2(110) (side-view) at 240 K. Isobutoxy is photo-oxidised to isobutanal, which is thermally trapped on the surface. Isobutanal undergoes a second photo-oxidation yielding propane and formyl species. Propane is leaving the surface at this temperature. The formyl species decomposes and is mainly leaving the surface as CO at 500 K. Adapted with permission from [161]. Copyright 2020 American Chemical Society.

A photo-hole oxidises the isobutoxy to isobutanal *via* an α-H abstraction upon UV illumination. The photo-oxidation proceeds in the same way as for other alcohols described in this thesis, e.g. methanol, ethanol, benzyl alcohol, where the primary photo-products are the aldehyde and BBO-H.[48, 80, 105] Isobutanal immediately desorbs from the surface upon illumination above 300 K. The BBO-Hs originating from

dissociative adsorption and photo-oxidation recombine to water and desorb at 450 K leaving a BBO vacancy behind.[110]

The illumination at cryogenic temperatures changes substantially the product distribution. The low temperature traps the primary photo-product on the surface and enables a secondary photo-reaction. Isobutanal is further oxidised *via* a C-C scission to a propyl radical and a formyl species. The abstracted propyl radical recombines with a hydrogen atom from the surface leaving the surface as alkane at 240 K. The radical-hydrogen recombination on bare titania is also observed in the photoconversion of longer-chain tertiary alcohols and is discussed in more detail in section 4.7. The formyl species may form a formate with a lattice oxygen analogously to formaldehyde and acetaldehyde.[30, 145] In a subsequent TPR, formate decomposes to mainly CO, that desorbs at 550 K. Some additional minor signals may be assigned to CO_2 and formaldehyde at 550 K in accordance with the formate decomposition observed by Henderson *et al.*.[128] Propane is directly desorbing into the gas-phase upon illumination at 240 K whereas isobutanol, isobutanal and the formyl specie are trapped on the surface. Note that the single crystal is barely reduced and has < 1 %ML BBO vacancies. Therefore isobutanol-covered samples are heated to 300 K prior to any photo-experiment below 300 K to promote the thermal isobutoxy formation.

The PI-TPDs reveal that the high-temperature disproportionation reaction is suppressed in all the photo-experiments indicating that the same isobutoxy species are involved. The dehydration pathway to form isobutene and BBO-H persists to some extent after UV illumination indicating that some isobutoxy species are not photo-active.

The temperature governs the overall selectivity of the photochemical conversion of isobutanol. The temperature determines the surface residence time of the primary photo-product isobutanal and only a minimum surface residence time enables the photo-oxidation of the aldehyde to form propane and a formyl species. This requirement is not matched at room temperature in contrast to 240 K.

The various surface preparations mimicking realistic conditions, i.e. the presence of oxygen or water, do not have a qualitative effect on the thermal and photochemical reactions. They do not influence the selectivity, but they have an effect on the overall product yield. The highest yield is achieved on o-TiO_2(110) for both, thermal and photochemical conversions. Oxygen adatoms are known to promote the alkoxy formation, which are the reactive species.[48] Consequently, a larger amount of reactive species leads to a higher yield.

The results demonstrate that the surface temperature determines the overall selectivity and plays an important role in photochemistry. The thermal desorption directly competes with a secondary photo-reaction. The alkane does not result from a reduction with

photoelectrons, as often assumed in photochemistry, but stems from a radical-hydrogen recombination. Those insights highlight the relevance of understanding individual reaction steps in photochemistry and photocatalysis to control the selective transformations of alcohols.

4.3 Origin of Poisoning in Methanol Photoreforming on TiO_2(110): The Importance of Thermal Back-Reaction Steps in Photocatalysis

Title	Origin of Poisoning in Methanol Photoreforming on TiO_2(110): The Importance of Thermal Back-Reaction Steps in Photocatalysis
Authors	Carla Courtois*, Moritz Eder*, Sebastian L. Kollmannsberger, Martin Tschurl, Constantin A. Walenta, and Ueli Heiz
Journal	*ACS Catal.* **2020**, *10*, 7747 - 7752.
DOI	`https://dx.doi.org/10.1021/acscatal.0c01615`
Status	published online June 25, 2020

*These authors contributed equally to this work.

The primary photo-oxidation of different alcohols on rutile TiO_2(110) is now quite well understood, e.g. for methanol, ethanol, isobutanol (see section 4.2) or even *tert*-butanol (see section 4.1).[48, 104, 108, 110] The photo-reaction pathway seems generally valid for α-H containing alcohols. The alcohol adsorbs dissociatively forming a photo-active alkoxy and a BBO-H. The alkoxy is oxidised through a direct photo-hole transfer leading to a C-H bond cleavage. The primary photo-products are the aldehyde and a hydroxyl BBO-H. However, their conversions range from $5-20\%$ of a monolayer-covered sample and the origin of this upper limit in the conversion on the bare titania still remains elusive.[48, 50, 91, 110, 138]

The accompanying hydroxylation of this reaction is thought to be responsible for the restricted conversion as titania is not able to desorb surface hydroxyls (neither as H_2O nor as H_2) at room temperature. It was believed that the hydroxyls either act as electron traps and thereby facilitate the charge recombination or are blocking the active sites (or both).[104, 167] However, this work demonstrates that these assumptions can be excluded by comparing the photocatalytic reforming of 2-methyl-2-pentanol and methanol. This way, the origin of poisoning is attributed to the thermal back-reactions of alkoxies and surface hydroxyls (BBO-H).

The photochemical conversion of methanol deactivates under illumination in a steady alcohol background at room temperature. Formaldehyde desorbs upon illumination but the conversion is steadily decreasing over time. The second photo-product hydroxyl is not able to desorb leading to its accumulation on the surface. This deactivated surface is named 'poisoned'. Quite the contrary is the case for the catalytic photoreforming of

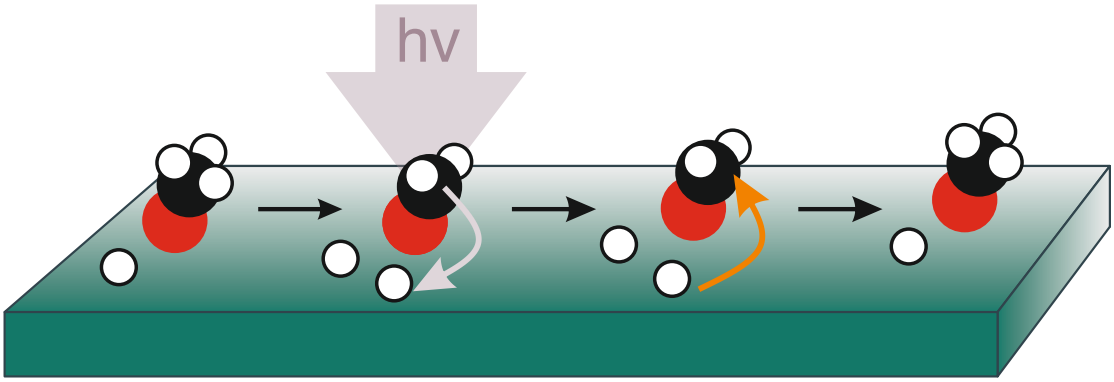

Figure 4.4. Scheme demonstrating the thermal back-reaction in the photochemical conversion of methanol. Methanol adsorbs dissociatively on the bare semiconductor surface leading to a methoxy and hydroxyl. UV illumination induces the α-H abstraction by a direct hole transfer to yield formaldehyde and another hydroxyl. A surface hydroxyl may then thermally react with a formaldehyde to yield the initial reactant methoxy.

the tertiary alcohol 2-methyl-2-pentanol[1], that disproportionates to propane and acetone which fully desorb upon illumination at room temperature. The photo-reaction occurs *via* a C-C bond cleavage abstracting a propyl radical. This propyl recombines on the surface with the hydrogen atom of BBO-Hs originating from the dissociative adsorption. The reaction proceeds stoichiometrically and does not accumulate hydroxyls on the surface so that the reaction is catalytic on the bare titania.

Surprisingly, the disproportionation reaction even occurs catalytically on the poisoned surface with the same photo-activity[2] compared to a fresh one. In addition, the disproportionation of 2-methyl-2-pentanol does not even change in the poisoned state, while the photo-reaction remains deactivated for a succeeding methanol photo-conversion. The fact that 2-methyl-2-pentanol is totally independent of surface hydroxylation by methanol conversion proves that BBO-Hs do not have a strong enough effect on the electronic processes, namely their role as electron traps or recombination centres, to affect the photo-activity significantly. It equally shows that BBO-Hs do not block photo-active sites as 2-methyl-2-pentanol is still photo-active on the poisoned surface. It is also unlikely that the mutual repulsion of BBO-H are responsible for the decline in methanol conversion because that would also hamper the dissociative adsorption of 2-methyl-2-pentanol.[104] Instead, the continuous accumulation of surface hydroxyl may favour the two thermal back-reactions involving hydroxyls: the dissociative adsorption yielding methanol as well as the reaction of formaldehyde with a hydroxyl yielding the reactant methoxy.

[1] Details on the reaction pathways are found in section 4.7.
[2] The photo-activity is expressed by the TOF, more details are found in section 3.3.

The potential thermal back-reaction of hydroxyl with methoxy to form the photo-inactive methanol is not likely the main reason for the deactivation since the dissociative adsorption step precedes in the photo-conversion of methanol and 2-methyl-2-pentanol. The unaltered photo-activity of 2-methyl-2-pentanol on the poisoned, i.e. hydroxylated, surface, demonstrates that the concentration of photo-active alkoxy species is not significantly affected by the hydroxylation.

These findings strongly point out that the thermal back-reaction of formaldehyde and BBO-H is the origin of poisoning in primary alcohol photoreforming. Indeed, Mao et al. observed this reaction of formaldehyde with hydrogen back-reaction with STM.[168] Moreover, this reaction is exothermic in contrast to the forward hole-driven oxidation reaction.

In conclusion, the differences and similarities of the reaction pathways of methanol and 2-methyl-2-pentanol strongly suggest that the back-reaction from formaldehyde to methoxy is the main origin for the vanishing photo-activity of alcohols on titania. These findings points out that individual back-reaction steps must be considered for a comprehensive understanding of photocatalytic systems.

In addition to the findings presented in the article, the photochemical conversion of *tert*-butanol presented in section 4.1 supports the arguments since the conversion is limited to 36 % of a monolayer. *tert*-Butanol is a tertiary alcohol but in contrast to 2-methyl-2-pentanol, the abstracted radical, in this case methyl, is directly ejected into the gas-phase and does not recombine with a surface hydrogen atom. This leads to an accumulation of surface hydroxyls that deactivates the photocatalyst.

4.4 Why Co-Catalyst-Loaded Rutile Facilitates Photocatalytic Hydrogen Evolution

Title	Why Co-Catalyst-Loaded Rutile Facilitates Photocatalytic Hydrogen Evolution
Authors	Constantin A. Walenta, Sebastian L. Kollmannsberger, Carla Courtois, Rui N. Pereira, Martin Stutzmann, Martin Tschurl and Ueli Heiz
Journal	*Phys. Chem. Chem. Phys.* **2019**, *21*, 1491-1496.
DOI	`https://doi.org/10.1039/C8CP05513K`
Status	published online December 17, 2018

The rutile (110) surface alone is not able to evolve molecular hydrogen. The photochemical conversion of primary and secondary alcohols leads to a hydroxylation of the surface that drastically limits alcohol conversion (see previous section 4.3). So far all previous sections of this thesis describe the photo-oxidation of alcohols on bare TiO_2(110). However, a co-catalyst is indispensable to run the reaction catalytically at room temperature. The laser vaporisation cluster source available at the apparatus (see section 3.1) allows for variable loadings of the semiconductor with size-controlled Pt co-catalysts.

The common mechanistic picture of alcohol photoreforming and full water-splitting is based on redox-couple reactions. Alcohol (or water) is oxidised by photo-holes and the hydrogen evolution is driven by the photo-electrons. The separation in two half-cell reactions implies that the oxidation potential of the alcohol (or water) is below the valence band edge and the reduction potential of hydrogen is above the band edge of rutile. However, it is still a long-lasting discussion if the latter one is true for rutile titania. For example, negative surface states in the band gap, that may be involved in the reaction, are energetically evenly located below the conduction band edge and, thus below the reduction potential of hydrogen.[169, 170] This photoelectrochemical mechanistic picture often motivates a research for efficient semiconductors that is mainly based on the energetics of the materials and widely ignores the surface chemistry. This work presents a different reaction mechanism of methanol photoreforming on Pt-loaded TiO_2(110) in the UHV, which considers the surface chemistry and semiconductor physics.

Similar to other alcohols presented previously, the photochemical conversion of methanol on TiO_2(110) yields formaldehyde and BBO-H. At 260 K, formaldehyde desorbs and hydroxyls remain on the surface. The deposition of Pt clusters (size distribution Pt_7-Pt_{32}) enables the hydrogen evolution upon illumination. Methanol is converted stoichiometrically

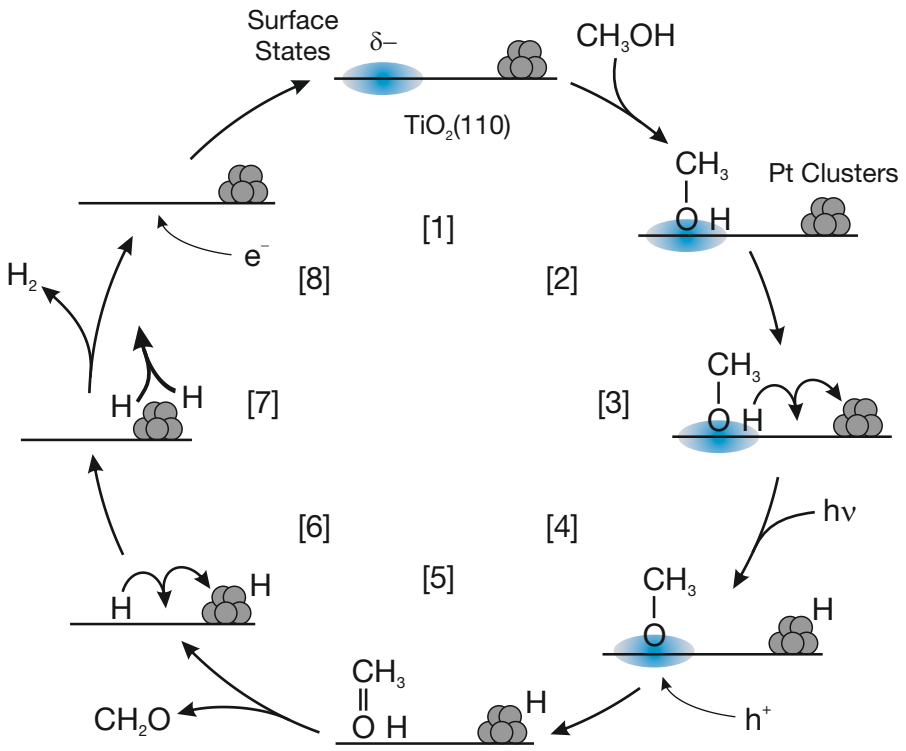

Figure 4.5. Photocatalytic reaction cycle for methanol photoreforming on Pt_x cluster loaded TiO_2(110). Methanol adsorbs dissociatively at negative surface states as methoxy and hydroxyl, which is a thermal process. The hydroxyl diffuses on the surface. Upon UV illumination, a photo-hole oxidises the methoxy yielding formaldehyde and another hydroxyl. Formaldehyde desorbs thermally. The hydroxyl diffuses on the surface until it reaches a Pt cluster where it thermally recombines with another hydrogen atom. The photo-electron refills the negative surface state so that the overall reaction is charge-neutral and the catalysts remains unchanged after one cycle. Reproduced from Ref. [171] with permission from the PCCP Owner Societies.

to CH_2O and H_2 under illumination in a constant methanol background. The conversion of methanol does not decline and is strongly enhanced compared to bare titania. The thermal-back reaction of methoxy and hydroxyls is suppressed since hydroxyls are removed from the surface and the chemical equilibrium is pushed towards the product side (see section 4.3).

The Pt_x neither seem to block active sites, nor influence the charge carrier dynamics, as the O_2 PSD is unchanged compared to a bare TiO_2 surface. The laser power dependent TOF indicates a one-photon process of the reaction of methanol. The TOF increases with higher methanol background pressure, which means that the reaction is adsorption-limited at 260 K. The TOF slightly increases with higher Pt_x loadings, but not linearly. These behaviours indicate that the photo-oxidation of methoxy to formaldehyde, which takes place on the rutile surface, is the rate-limiting step. The hydrogen diffusion towards and its recombination on the clusters are consecutive processes as the hydrogen trace is tailing while the formaldehyde production abruptly stops with the end of illumination.

Pt-decorated rutile evolves molecular hydrogen in a methanol TPD in contrast to bare titania. This together with the tailing of the hydrogen trace indicate that the H_2 recombination is a thermal process.

The comparison of the reaction behaviour of bare titania and $Pt_x/TiO_2(110)$, the indication of a one-photon process and the reaction conditions in UHV lead to the catalytic cycle in figure 4.5. In a first step, methanol adsorbs dissociatively on the negatively charged surface state forming the photo-active methoxy species and a BBO-H. Secondly, the photo-hole oxidises the methoxy to formaldehyde *via* an α-H cleavage, which forms again a BBO-H. The formaldehyde thermally desorbs. Both surface hydroxyls are undistinguishable and diffuse on the surface until they reach a Pt cluster. Thirdly, hydrogen that migrated to the Pt cluster thermally recombine as H_2. The surface hydrogen species are considered rather as radical species than H^+. The charge balance is closed by the photo-electron that fills the surface state in order to restore the initial conditions.

The photocatalytic reforming of other alcohols, e.g. ethanol, cyclohexanol, benzyl alcohol or *tert*-butanol, generalises this mechanism, and is presented in section 4.6. It takes into account the complete reaction behaviour by considering the surface chemistry and individual reaction pathways, is in agreement with semiconductor physics, and closes the catalytic cycle. This reaction mechanism outlines that photoelectrocatalytic mechanisms are not the only ones in heterogeneous photocatalysis.

4.5 Surface Species in Photocatalytic Methanol Reforming on $Pt/TiO_2(110)$: Learning from Surface Science Experiments for Catalytically Relevant Conditions

Title	Surface Species in Photocatalytic Methanol Reforming on $Pt/TiO_2(110)$: Learning from Surface Science Experiments for Catalytically Relevant Conditions
Authors	Constantin A. Walenta, Carla Courtois, Sebastian L. Kollmannsberger, Moritz Eder, Martin Tschurl, and Ueli Heiz
Journal	*ACS Catal.* **2020**, *10*, 4080 - 4091.
DOI	`https://dx.doi.org/10.1021/acscatal.0c00260`
Status	published online March 4, 2020

The general mechanism of the photocatalytic conversion of methanol on Pt_x-loaded $TiO_2(110)$ is elucidated in the previous section 4.4. This study takes a closer look at the chemical processes occurring on the surface to disentangle thermal from photochemical reaction steps. In order to recall the key steps of the mechanism: methanol adsorbs dissociatively at negatively charged surface states forming methoxy and a surface hydroxyl. Methoxy is oxidised to formaldehyde on the semiconductor surface *via* a direct hole transfer. The abstracted hydrogen atoms diffuse on the surface until they reach a Pt cluster, where they thermally recombine leaving the catalyst as H_2. The photo-electron fills the empty surface state so that the catalytic cycle is closed. While the previous section focuses on the general mechanistic understanding, this work completes the mechanistic interpretation and describes the individual steps in the catalytic cycle to identify the surface species present on the catalyst. In addition to several surface science methods presented in chapter 3, isotopic labelling and a kinetic analysis is conducted to determine the surface species, their stability, and the driving force for the product selectivity under catalytic conditions.

While it is evident that the Pt co-catalysts's role is the thermal evolution of H_2, consecutive isothermal PSR of methanol strongly suggest that Pt co-catalysts undergo an initial conditioning that is attributed to the thermal dehydrogenation of methanol to CO species. The Pt clusters are most probably covered with CO under catalytic reaction conditions. Isothermal PSR experiments of methanol on conditioned and artificially CO-precovered $Pt_x/TiO_2(110)$ show similar desorption characteristics, which confirms this assumption.

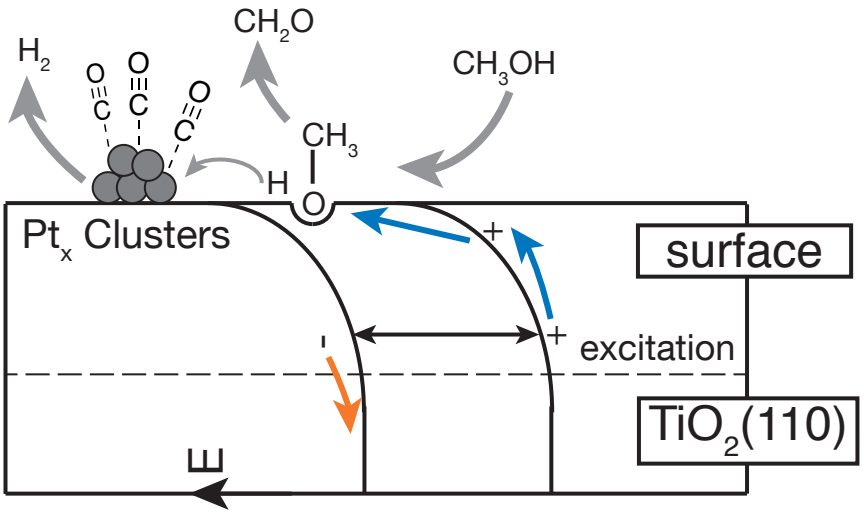

Figure 4.6. Photocatalytic mechanism of methanol conversion on a Pt_x-loaded TiO_2(110) single crystal. Upon illumination of the catalysts, a photo-hole migrates to the surface and oxidises the methoxy to formaldehyde *via* a direct hole transfer. The abstracted hydrogen atoms migrate on the surface and recombine to H_2 on the Pt cluster. The co-catalyst is covered with CO species originating from the thermal decomposition of methanol on the Pt cluster. Thermal steps are displayed with grey arrows while the charge carrier pathways are displayed with blue and orange arrows. Reprinted with permission from [172]. Copyright 2020 American Chemical Society

The catalyst reveals a long-term stability[3] under these reaction conditions. CO species are presumably spectator species and do not influence the H_2 recombination, CO might even protect the clusters which lead to its high stability.

The TPR of methanol on Pt-loaded TiO_2 suggests that the conditioning of the co-catalyst is a thermal process. Methanol shows a typical desorption chemistry compared to bare TiO_2 except that CO is desorbing at 450 K, which is characteristic for Pt(111), and molecular hydrogen is evolving at around 250 K. [76, 173] CO and H_2 stem from the dehydrogenation of methanol at the Pt clusters, which means that methanol decomposition already occurs below 250 K. These findings demonstrate that Pt co-catalysts dehydrogenate methanol and thermally recombine H_2.

Pt co-catalyst loadings in the range of 1%ML do not significantly affect the photo-oxidation properties of titania. The decay analysis of isothermal PSR experiments reveal that the photo-oxidation kinetics are not affected by the deposition of Pt clusters and suggest that the photo-oxidation is the rate-determining step.

A second photo-product, namely methyl formate, is produced if the photocatalytic conversion of methanol is conducted below 258 K. If formaldehyde resides long enough

[3] No decline in activity is observed during methanol photoreforming for 4 h in a $7 \cdot 10^{-8}$ mbar methanol atmosphere. In addition, the activity does not decline in subsequent catalytic experiments and is not altered after a storage in vacuum for 70 h.

on the surface after its formation, it will react with methanol under consumption of a photo-hole to form methyl formate.[80] The temperature, which dictates the residence time of the primary photo-product formaldehyde, governs the overall selectivity of the reaction. Kinetic insights from PI-TPD/Rs enable the calculation of the surface residence time of methanol and formaldehyde, that help to explain the observed selectivities. Furthermore, a comparison of methanol PI-TPD/R on bare and Pt-loaded TiO_2(110) reveal that Pt does not change the selectivity.

This work leads to a detailed understanding of the surface chemistry under truly catalytic conditions. The individual surface species have been identified and their influence to the overall reaction can be distinguished. This may help for future microkinetic modelling or ab initio theory investigations of co-catalyst loaded model systems. These insights gained from surface science techniques may be extended to more applied conditions and other materials.

4.6 Thermal Control of Selectivity in Photocatalytic, Water-Free Alcohol Photoreforming

Title Thermal Control of Selectivity in Photocatalytic, Water-Free Alcohol Photoreforming

Authors Sebastian L. Kollmannsberger*, Constantin A. Walenta*, Carla Courtois, Martin Tschurl, and Ueli Heiz

Journal *ACS Catal.* **2018**, *12*, 11076 - 11084.

DOI https://doi.org/10.1021/acscatal.8b03479

Status published online October 17, 2018

*These authors contributed equally to this work.

The selective oxidation of alcohols has gained great attention in the last decade.[174, 175] The previous sections 4.4 and 4.5 elucidate a detailed mechanism for methanol photoreforming on $Pt_x/TiO_2(110)$. This work validates the mechanism for different alcohols and focuses on the oxidation reaction rather than the hydrogen evolution under catalytic conditions. Water-free alcohol photoreforming around room temperature may provide value-added oxygenates with a 100% selectivity under anaerobic conditions. Light-driven reactions, which require low amounts of energy, may replace thermal inefficient processes, like the formox one. The stable photocatalytic conversion of five different alcohols, namely methanol, ethanol, cyclohexanol, benzyl alcohol and *tert*-butanol, is investigated. An overview of the reactions is found in figure 4.7.

Generally, the first reaction of these alcohols, except for *tert*-butanol, follows the mechanism presented in 4.4 and 4.5: a hole-mediated oxidation of the carbonyl species on the semiconductor surface leads to an α-H abstraction to form the respective aldehyde or ketone, and hydrogen atoms thermally recombine on the Pt clusters. While acetaldehyde and cyclohexanal are produced with a 100% selectivity[4], formaldehyde and benzaldehyde may undergo a consecutive reaction. The second photo-reaction yielding the ester, that is a coupling of the aldehyde with the alcohol under the consumption of a photo-hole, is strongly temperature-dependent. Above a certain temperature, the consecutive photo-reaction is completely suppressed because the desorption of the aldehyde is faster than the coupling reaction. This is also observed in the photochemical conversion of isobutanol on bare $TiO_2(110)$ (see section 4.2), a higher residence time increases the probability to further react.

[4]The selectivity is referenced to the oxidation products (e.g. aldehyde, ketone, ester) and does not take into account the concomitant hydrogen evolution.

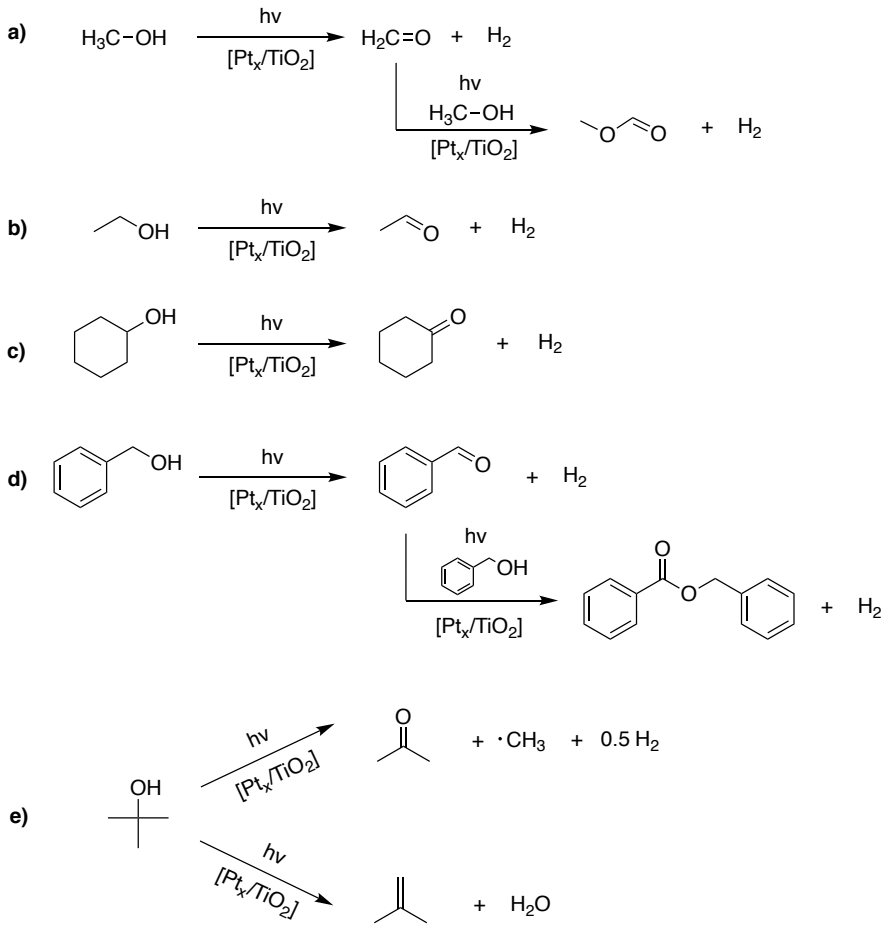

Figure 4.7. Overview of the reaction equations in the alcohol photoreforming on $Pt_x/TiO_2(110)$. The catalytic mechanism is generally valid in each case for the first reaction. All products are formed stoichiometrically. **a)** Methanol reacts to formaldehyde and hydrogen in a first reaction. The occurrence of a consecutive photo-reaction, which yields methyl formate, is temperature-dependent. **b)** Ethanol is exclusively converted to acetaldehyde and hydrogen. **c)** Cyclohexanol solely reacts to cyclohexanon and hydrogen. **d)** Benzyl alcohol reacts to benzaldehyde and hydrogen in a first photon-driven reaction. Benzaldehyde couples with benzyl alcohol to form the ester benzyl benzoate in a consecutive photo-reaction. This reaction is temperature-dependent. **e)** *tert*-Butanol reacts in two parallel reactions: the oxidative pathway leading to acetone, methyl radical and hydrogen; and the dehydration pathway leading to isobutene and water.

tert-butanol, which does not possess an α-H, undergoes two parallel reactions under catalytic conditions, in a constant alcohol background. The first pathway involves the photo-oxidation of *tert*-butoxy *via* a homolytic C-C bond scission yielding acetone and a methyl radical. Both products are also observed on the bare $TiO_2(110)$ (see section 4.1). In addition, the Pt clusters enable the thermal recombination of H-atoms stemming from the dissociative adsorption (from the O-H group). The second reaction pathway is the photon-induced dehydration forming isobutene and water stoichiometrically. Water

is desorbing under catalytic conditions in contrast to single-coverage experiments of *tert*-butanol on bare TiO_2(110), where only isobutene desorbs. The first reaction pathway exhibits a strong temperature dependence. In the investigated temperature range, the amount increases with higher temperature until approximately 300 K after which it decreases again. The conversion is alcohol adsorption-limited at high temperatures and product desorption-limited at low temperatures. On the contrary, the temperature does not influence the yield of isobutene and water significantly since only a small decrease is observed at high temperatures. The dehydration pathway may involve a specific thermally activated adsorption geometry of *tert*-butanol, a higher temperature increases the entropy and may impede the required adsorption geometry. Hence, the product ratio of the two parallel reaction pathways is controlled by the temperature.

The reactions of methanol, ethanol and *tert*-butanol imply that the oxidation pathways and selectivities are dominated by the semiconductor surface and are not influenced by the Pt cluster because the findings reflect the photochemistry on bare TiO_2(110).[110] Neither of the reaction pathways nor the respective selectivities are changed by the deposition of Pt clusters. The cluster's sole role is the thermal recombination of H_2. An exception is water desorption in the dehydration pathway of *tert*-butanol, but this may be rather caused by the catalytic conditions than the presence of Pt clusters.

In general, the selectivity is tuned by the temperature, and a suitable choice of reaction conditions allows for the photoreforming of α-H containing alcohols with a 100% selectivity towards the aldehyde, respective the ketone. The consecutive photo-reaction is suppressed by a significantly high temperature and the absence of O_2 inhibits the over-oxidation to acids, CO or CO_2. The pressure-normalised TOFs decrease with the size of the alcohol, that means that larger alcohols have lower conversion rates.

This study shows that the highly selective oxidation to water-free aldehydes and ketones is possible under mild conditions. The elucidation of the different reaction pathways offers a tool to tune and control the selectivities.

4.7 Reactions in the Photocatalytic Conversion of Tertiary Alcohols on Rutile TiO_2(110)

Title	Reactions in the Photocatalytic Conversion of Tertiary Alcohols on Rutile TiO_2(110)
Authors	Carla Courtois*, Moritz Eder*, Kordula Schnabl, Constantin A. Walenta, Martin Tschurl and Ulrich Heiz
Journal	*Angew. Chem. Int. Ed.* **2019**, *58*, 114255 - 14259.
DOI	`https://doi.org/10.1002/anie.201907917`
Status	published online August 7, 2019

*These authors contributed equally to this work.

Tertiary alcohols are chemically inert for selective oxidation reactions according to the general perception. Yet, the previous sections 4.1 and 4.6 demonstrated that the photo-oxidation of *tert*-butanol is indeed facilitated on bare and Pt-loaded TiO_2(110). *tert*-Butanol is oxidised to acetone *via* a C-C bond scission and a methyl radical is ejected into the gas-phase. Interestingly, tertiary alcohols with different chain-lengths alkyl groups reveal a different and new reaction behaviour, namely the hole-mediated disproportionation into an alkane and the respective ketone.

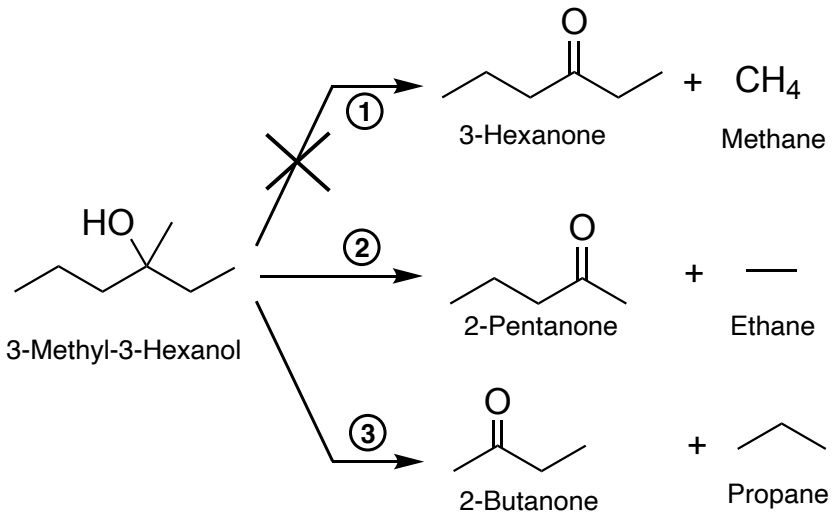

Figure 4.8. Reaction scheme for the photocatalytic conversion of 3-methyl-3-hexanol on bare and Pt-loaded TiO_2(110). The hole-mediated reaction is a disproportionation of 3-methyl-3-hexanol into an alkane and the respective ketone. However, the C-C bond to the methyl group is not cleaved, so that methane and 3-hexanone are not formed. Reprinted with permission from [176].

Similarly to primary and secondary alcohols, tertiary alcohols adsorb dissociatively to some extent on the bare titania surface yielding the photo-active alkoxies and a BBOHs, as described in subsection 2.3.1. Under UV illumination, the alkoxy reacts to the respective ketone *via* a homolytic C-C bond cleavage. 3-Methyl-3-hexanol possesses three different alkyl chains, a methyl, an ethyl, and a propyl group. Astonishingly, the bond to the methyl group is not cleaved at all[5] upon UV illumination. The photo-reforming of 2-methyl-2-butanol and 2-methyl-2-pentanol, which both possesses two methyl groups and either an ethyl or a propyl group, confirm this reaction behaviour. The abstraction of methyl groups does not take place and only the bond to a longer alkyl chain is selectively split. Consequently, the products in the disproportionation of 3-methyl-3-hexanol are 2-pentanone and ethane, and 2-butanone and propane. An overview of the reaction scheme for 3-methyl-3-hexanol is provided in figure 4.9. A dehydration pathway is not observed for those three alcohols other than in the photoconversion of *tert*-butanol.

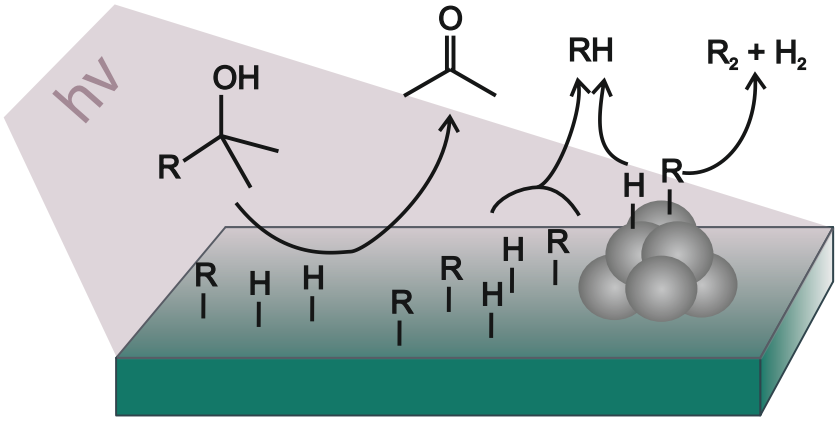

Figure 4.9. Scheme of the photocatalytic reforming of 2-methyl-2-propanol and 2-methyl-2-butanol on $Pt_x/TiO_2(110)$ at increasing alcohol pressures. The main reaction pathway is the selective disproportionation into an alkane and the respective ketone. The alcohol is oxidised *via* a C-C bond cleavage. The abstracted radical remains on the surface and recombines with a hydrogen atom. Pt clusters enable an additional reaction channel, namely the hydrogen recombination and the recombination of two alkyl radicals to form a long-chain alkane.

Thermochemistry may serve to explain the observed selectivity of 2:1 for pentanone to butanone, respectively the preferred cleavage of ethyl to propyl groups and the absence of the methyl group bond scission. All three reactions shown in figure 4.9 are endothermic, but model reactions predict that the formation of methyl radicals requires substantially more energy than the formation of ethyl and propyl radicals. In addition, the abstracted radical, ethyl or propyl, resides on the surface until it recombines thermally on bare

[5]Methane and 3-hexanone are not observed with the QMS within its detection limit.

titania with the BBO-H, that stems from the dissociative adsorption, to an alkane. Subsequently, the alkane desorbs from the surface. Ethyl and propyl radicals may exhibit stronger interactions with the titania surface than methyl radicals, which is why the methyl radical is directly ejected into the gas-phase in the photo-oxidation of *tert*-butanol. Thermochemically seen, a stronger interaction with the surface may stabilises the ethyl and propyl radicals and may add to their preferred cleavage.

As the reaction is fully stoichiometric, surface hydroxyls do not poison the surface. Consequently, the reaction can be conducted fully catalytically on the bare $TiO_2(110)$ conversely to the photoreforming of *tert*-butanol, or primary and secondary alcohols. Thereby a Pt cluster is indispensable to remove the surface hydroxyls by evolving H_2.

The deposition of small amounts of unselected Pt_x clusters increases the overall reaction rate. However, neither the TOF of the ketones, nor the selectivity for pentanone to butanone is affected when the amount of Pt clusters is increased from 0.02%ML to 1%ML. This means that Pt clusters increase the overall reaction rate but they do not influence the oxidation itself. Apart from that, the Pt clusters open up another reaction channel above a certain alcohol pressure, namely the thermal recombination of hydrogen and the recombination of two alkyl radicals yielding long-chain alkanes. For example, the photo-reforming of 2-methyl-2-pentanol unambiguously demonstrates the formation of hexane at increasing pressures.

In summary, the photocatalytic conversion of tertiary alcohols on bare and Pt-loaded $TiO_2(110)$ reveals a new reaction pathway: the hole-mediated disproportionation yielding an alkane and the respective ketone. The reaction is fully catalytic even on bare titania without co-catalyst as it does not involve the recombination of two hydrogen atoms. The C-C bond cleavage is selective in a way that only longer alkyl chains are abstracted, whereas the C-C bond to a methyl group is not cleaved. The observed selectivity is explained with the thermochemistry of radical formation. Pt clusters increase the overall reaction rate and enable another reaction pathway: the hydrogen recombination and the recombination of two alkyl radicals. This work shows that heterogeneous photocatalysis may introduce new synthetic routes under mild conditions and demonstrates the important role of co-catalysts for the product distribution.

4.8 Nickel Clusters on TiO_2(110): Thermal Chemistry and Photocatalytic Hydrogen Evolution of Methanol

Title	Nickel Clusters on TiO_2(110): Thermal Chemistry and Photocatalytic Hydrogen Evolution of Methanol
Authors	Moritz Eder*, Carla Courtois*, Tim Kratky, Sebastian Günther, Martin Tschurl and Ueli Heiz
Journal	*Catal. Sci. Technol.* **2020**, *10*, 7630 - 7639.
DOI	https://doi.org/10.1039/D0CY01465Fs
Status	published online September 9, 2020

*These authors contributed equally to this work.

The role and influence of the Pt co-catalyst in the photocatalytic conversion of alcohols is thoroughly elucidated in the previous chapters. Platinum is a rare metal and its high cost and low abundance impede the application on larger scales. Therefore, the research is intensified towards the use of more abundant and cheaper metals. The co-catalysts sole role in the catalytic cycle is the thermal recombination of two hydrogen atoms to H_2, so that nickel might also be a suitable candidate because early surface science studies show that it is indeed able to thermally desorb hydrogen.[177, 178] Moreover, Ni has already been applied as hydrogen evolution co-catalyst in several photocatalytic studies on TiO_2 powder mixtures. However, there is no consensus about its activity and its active phase (metallic nickel, nickel oxide or nickel hydroxide).[179–185] This work investigates the thermal chemistry and photocatalytic hydrogen evolution capability of Ni co-catalysts on a model system with size-controlled Ni-clusters deposited on TiO_2(110).

Methanol decomposes thermally on the Ni clusters to, amongst others, CO and H_2, whereas the two molecules are able to desorb. This is shown in consecutive methanol TPDs on Ni_x/TiO_2. Desorbing CO and H_2 stem from the partial dehydrogenation of methanol adsorbed on Ni clusters. This demonstrates that Ni clusters are indeed able to evolve molecular hydrogen. However, the intensity of CO and H_2 declines with every TPD run, which indicates a substantial change of the Ni clusters. The Ni clusters may agglomerate on the surface to a stable size upon annealing that leads to a lower number of sites for the methanol dehydrogenation.[74, 187] Alternatively, Ni clusters may get encapsulated with a thin TiO_x layer due to the strong-metal support interaction.[67]

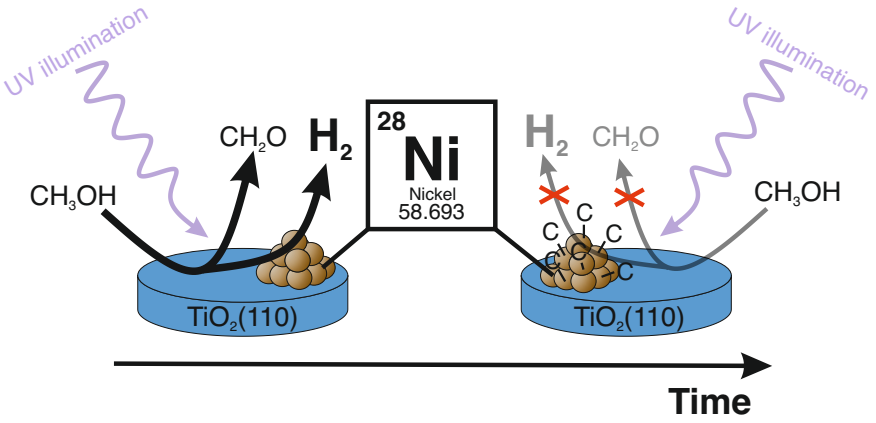

Figure 4.10. Graphical table of content from the publication. Ni clusters enable the H_2 evolution in the photoreforming of methanol on Ni_x/TiO_2. Methanol is converted to formaldehyde and H_2 under UV illumination. The photo-activity decreases for prolonged illumination times. The nickel clusters undergo a photon-driven deactivation process that involves the formation of carbon deposits. Reprinted with permission from [186].

Photocatalytic methanol reforming on Ni_x-loaded TiO_2 produces hydrogen and formaldehyde at room temperature. In other words, the same products are formed over on Ni_x/TiO_2 upon UV illumination as for Pt-loaded $TiO_2(110)$, so that the mechanism found for Pt co-catalysts is most likely also valid for Ni_x/TiO_2. However, conversely to Pt-loaded titania, the traces of formaldehyde and hydrogen decrease over time for prolonged illumination times. The product yield declines until the system resembles the activity of bare $TiO_2(110)$, i.e. no hydrogen evolution and a limited formation of formaldehyde. The amount of hydrogen desorbing steadily decreases over time. This leads to an accumulation of hydrogen atoms on the surface, which causes a limited formaldehyde desorption because the surface hydrogen atoms favour the thermal back-reaction of formaldehyde to methoxy (section 4.3). Ni clusters do not influence the photo-active sites on the titania surface, as evidenced by O_2-PSD. Thus, the deactivation most probably originates from a decreased hydrogen recombination activity of Ni clusters.

AES of the Ni-loaded titania evidence that Ni clusters are dominantly present in its metallic state Ni^0 before and after catalysis. Neither the deposition on the metal oxide nor the reaction conditions lead to a significant oxidation of the metallic clusters. The thermodynamic consideration supports these insights as the Ni oxidation through the reduction of TiO_2 is thermodynamically not favourable[6].[188] Metallic Ni clusters are the active species for the H_2 evolution and are not oxidised under catalytic conditions. Hence a change in the oxidation state of Ni clusters is ruled out as the origin for the deactivation.

[6]The standard enthalpy of formation for NiO is higher in energy than the change in standard free energy for $Ti^{3+} + 1e^- \longrightarrow Ti^{2+}$.

The catalytic activity can be recuperated to a certain extent by annealing the sample after catalysis to 800 K. A clear carbon signal remains in the AES after the heat treatment that indicates a strongly bound carbon species. In contrast, methanol only decomposes to CO and H_2 on the Pt clusters, and all the decomposition products desorb upon annealing. The heat treatment only removes C-species from the Ni clusters to a certain extent and those remaining are most likely the reason for the decreased H_2 evolution activity. The carbon residues may block the recombination sites for the H_2 formation.

The carbon deposit is a photon-driven dynamic process since the exposure of the freshly deposited Ni_x on $TiO_2(110)$ to a methanol background at room temperature does not lead to the deactivation of the Ni clusters. The thermal decomposition of methanol on Ni clusters is thus not responsible for the decreased H_2 evolution activity. The deactivation process only occurs under illumination in the methanol background and it may involve intermediate species and products. Such photo-driven deactivation processes are known as photo-corrosion.

In summary, Ni clusters are indeed able to evolve H_2 in the photoreforming of methanol. However, the activity decreases for prolonged illumination times, that is different for Pt, for which no decomposition has been observed after several hours. AES and reactivity studies in UHV identify carbon deposits as the reason for the decrease in activity. The deactivation pathway is a photo-driven process as it does not occur in the absence of light. Annealing leads to a partial desorption of carbonaceous deposits such as CO and a partial restoration of the H_2 evolution activity.

4.9 Size and Coverage Effects of Ni and Pt Co-Catalysts in the Photocatalytic Hydrogen Evolution from Methanol on TiO_2(110)

Co-authors: Moritz Eder, Philipp Petzoldt, Sonia Mackewicz, Martin Tschurl, Ueli Heiz

The previous sections qualitatively describe the role and behaviour of Pt and Ni co-catalysts in the methanol photoreforming on TiO_2(110). A wide distribution of clusters sizes as $Pt_{7\text{-}32}$ and $Ni_{10\text{-}30}$ are employed at different loadings in those studies. This section focuses on size-selected Pt and Ni clusters at different loadings.

Most common deposition methods based on wet chemistry inhibit the disentanglement of cluster size and coverage. This is most probably the main reason why literature results often do not agree on the quality of different co-catalyst materials (e.g. Pt, Au, or Ni) and their optimum particle size and coverage.[189, 190] This study investigates the photocatalytic activity of size-selected Ni and Pt clusters deposited TiO_2(110) and elucidates the effects of cluster sizes and coverages. The laser vaporisation cluster source allows for the deposition of clusters with different sizes and at different coverages independently (see section 3.1) so that such studies can be performed.

In order to quantitatively identify cluster size and coverage effects and enable a direct comparison of the performance as co-catalyst for both metals, the product formation rate on cluster-loaded TiO_2(110) is determined by quantifying the TOFs of formaldehyde and H_2 during photocatalytic methanol oxidation (see section 3.3). For Ni, single atoms and clusters with sizes of 10 and >47 atoms were deposited with different coverages. For the atom, coverages of 1%, and 3% of a ML were chosen. The better performance of clusters in comparison to the atoms in the photocatalytic reaction enabled the study with a significantly lower coverage of 0.3%ML. The product formation rates of the respective photocatalytic experiments are shown in figure 4.11.

Independent of cluster size and coverage, the behaviour of all mass traces in the photo-experiments is qualitatively the same. Upon illumination, the formaldehyde trace shows a prompt increase of high intensity but it subsequently tapers off to much lower values. This behaviour stems from an accumulation of reactant in the dark, leading to a higher surface reactant concentration for the photo-reaction. This phenomenon similarly occurs in this reaction with platinum-loaded TiO_2 as can be found in the publications presented in the previous sections 1.4-1.8. By blocking the light flux, the traces drop back to the baseline level in the dark. Desorption of H_2 is known to inhibit the thermal back-reaction

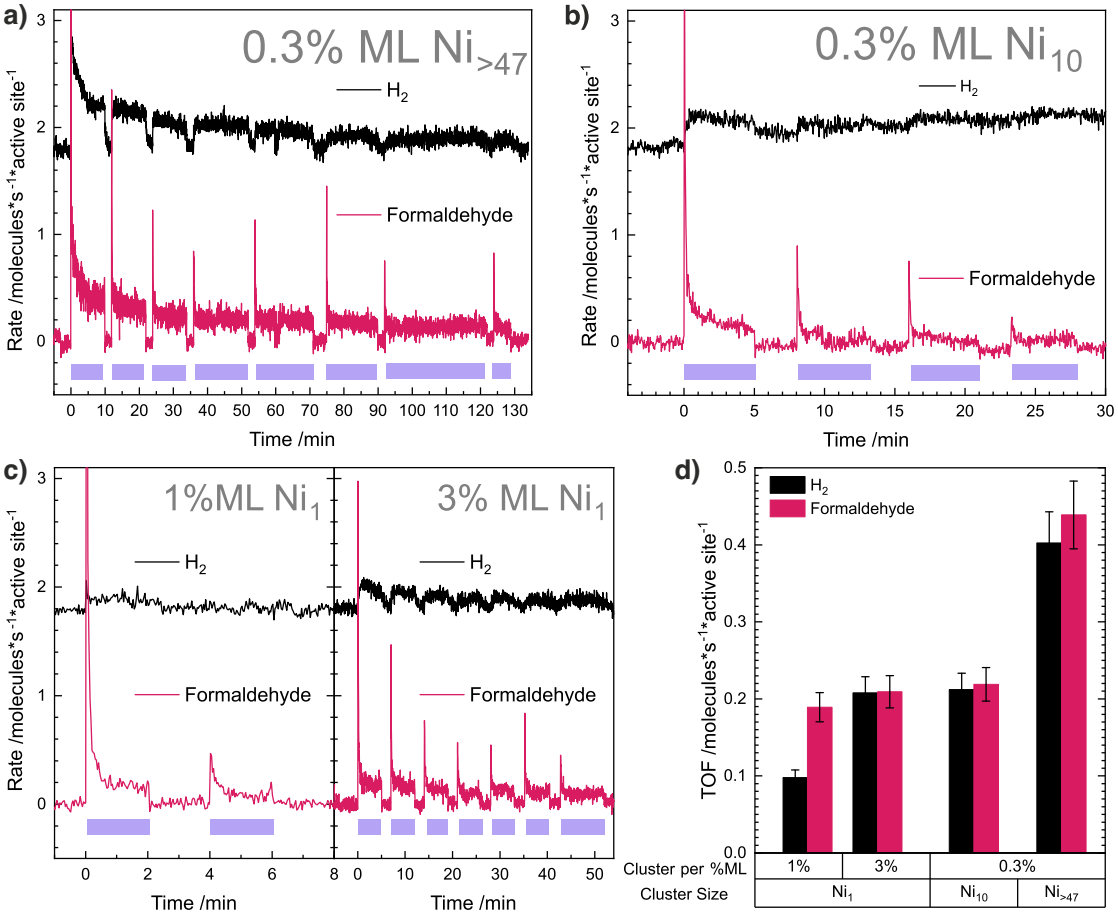

Figure 4.11. Product formation rates of hydrogen (m/z 2, black) and formaldehyde (m/z 30, red) from photocatalytic methanol oxidation on $Ni_x/TiO_2(110)$ with x= 1, 10,>47 at 300 K in a methanol background pressure of $5.0 \cdot 10^{-7}$ mbar. Violet bars indicate periods of light exposure. The experiment was conducted for **a)** 0.3%ML $Ni_{>47}$, **b)** 0.3%ML Ni_{10}, and **c)** 1% as well as 3%ML atomic nickel. The TOFs of the first illumination period for hydrogen and formaldehyde are shown in **d)**. The traces are offset for clarity. Larger clusters and higher coverages lead to enhanced TOFs and longer overall lifetimes of the photocatalyst.

of formaldehyde and hydroxyls, which is why the reaction only occurs catalytically when hydrogen can leave the titania surface as described in section 4.3.

Over the whole time range of the Ni experiments, the steady-state signal of products decreases slightly, but constantly, during illumination. While for example the formaldehyde trace on $Ni_{>47}/TiO_2(110)$ (figure 4.11**a)**) exhibits an average steady-state at roughly 0.2 molecules/(active site · s) during the first illumination period, the rate amounts to only 0.1 molecules/(active site · s) on average during the last. This photocorrosion phenomenon on $Ni_x/TiO_2(110)$ is described in section 4.8 and attributed to catalyst deactivation by carbonaceous deposits. These block the Ni clusters, so that H_2 recombination and desorption sites become inaccessible for hydrogen.

In all cases and even for nickel atoms, hydrogen evolution is facilitated, but it occurs with significantly different rates in the different systems. The H_2 and formaldehyde TOFs (figure 4.11**d)**) in general benefit from larger Ni clusters and higher coverages. $Ni_{>47}$ clusters lead to the highest, almost stoichiometric formation rate of photo-products. 0.3%ML Ni_{10} shows the same TOFs as 3%ML atomic Ni. Thus, the same amount of the co-catalyst metal leads to the same product formation rate. The formation rate of H_2 seems to be directly correlated to the total amount and size (i.e., total area) of the metal. Larger areas of H_2 recombination sites allow for higher amounts being formed over a longer time span and the total amount of Ni atoms on the surface seem to correlate directly with the product formation rate. Since the role of the co-catalyst is only thermal H_2 evolution, the availability of more hydrogen recombination sites apparently favours an increase of the overall reaction rate. Furthermore, the longer catalyst lifetimes for higher amounts of Ni is explained by the increase in time, which is required for the blocking of a bigger area with carbon. Independent of cluster size and coverage, eventual deactivation seems to be inevitable. For all studied clusters, a size which does not feature this unwanted property is not identified. Each TOF for $Ni_x/TiO_2(110)$ (figure 4.11**d)**) was thus determined in the steady-state of the first illumination period.

For Ni atoms (figure 4.11**c)**), only traces of H_2 are detected for a 1%ML coverage. After two minutes of illumination, no H_2 formation is observed anymore. Apart from that, the formation of photo-products does not even seem to be stoichiometric (figure 4.11**d)**). Thus, no significant photocatalytic behaviour of low amounts of atomic Ni is found, and the use of Ni atoms as co-catalyst in alcohol photoreforming is questionable. The reaction behaviour is almost very similar to the bare $TiO_2(110)$ surface in alcohol photoreforming, where H_2 desorption is not possible at all.

These results on $Ni_x/TiO_2(110)$ lead to the conclusion that a higher total amount of Ni on the surface (i.e. larger clusters and higher coverages) directly enhances the product formation rate in photocatalytic alcohol conversion. This again implies the absence of detectable cluster size-dependent effects for $Ni_x/TiO_2(110)$, which also concerns the catalyst deactivation, but different to what is typically observed on similar systems in thermal catalysis.[191]

Since Pt and Ni play the same mechanistic role in alcohol photooxidation on $TiO_2(110)$, their performances can be directly compared quantitatively with each other. Figure 4.12 shows the product formation rates obtained from methanol photoreforming using Pt_{10} and Ni_{10} as co-catalyst, respectively, with a coverage of 0.3%ML.

It is found that the activity of platinum clusters exceeds that of nickel clusters by more than an order of magnitude. This is in good agreement with observations made in

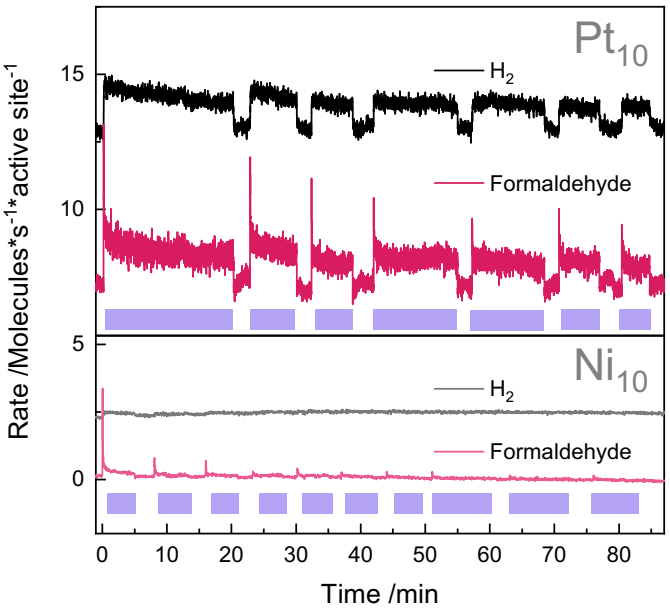

Figure 4.12. Product formation rates for hydrogen (m/z 2, black) and formaldehyde (m/z 30, red) from photocatalytic methanol reforming on 0.3%ML $Pt_{10}/TiO_2(110)$ and 0.3%ML $Ni_{10}/TiO_2(110)$ at 300 K in a methanol background pressure of $5.0 \cdot 10^{-7}$ mbar. Violet bars indicate light exposure. The traces are offset for clarity. The activity of platinum clusters is more than an order of magnitude higher than that of nickel clusters.

alcohol photoconversion experiments under ambient conditions using Ni and Pt as co-catalysts on TiO_2.[185] The higher product formation rate of platinum can be explained with its much higher hydrogen evolution capability. This probably originates from differences in the metal-hydrogen bond strength, as volcano plots from electrochemical studies suggest, although they have to be interpreted with caution.[192–194] Unlike Ni-decorated titania, $Pt_x/TiO_2(110)$ does not deactivate by photocorrosion and shows stable catalytic activity over hours (see section 4.5). While the Auger spectra of $Ni_x/TiO_2(110)$ revealed persistent carbon deposits on the surface after catalysis and even after heating to 800 K, no carbon is observed in comparable Auger spectra of $Pt_{>47}/TiO_2(110)$ after catalysis (see figure 4.13). Overall, the high activity and stability of the Pt-loaded titania makes Pt a more attractive co-catalyst material than Ni for the photocatalytic hydrogen evolution from alcohols on $TiO_2(110)$.

This observation corroborates the methanol photoreforming using 1%ML Pt atoms as co-catalyst (see figure 4.14). While 1%ML Ni_1 shows negligible amounts of hydrogen evolution during illumination (figure 4.11**c**)), the same amount of platinum atoms on $TiO_2(110)$ gives a considerable, steady H_2 formation activity. However, 0.3%ML atomic Pt does also not exhibit detectable H_2 evolution activity during methanol photooxidation. This observation demonstrates that the amount of metal co-catalyst apparently needs to be above a critical threshold concentration for significant H_2 evolution. The same

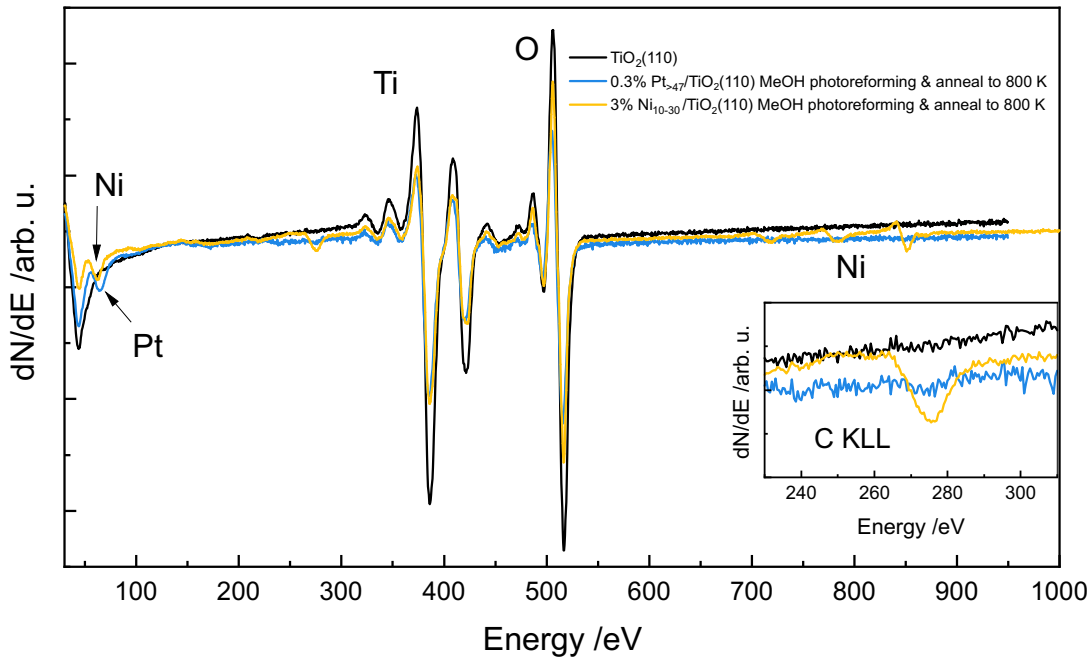

Figure 4.13. Auger spectra of bare $TiO_2(110)$ (black), 0.3%ML $Pt_{>47}/TiO_2(110)$ (blue) and 3%ML $Ni_x/TiO_2(110)$ (yellow) after methanol photoreforming experiments at 300 K and subsequent annealing to 800 K in order to desorb any surface species. The latter one was measured above 380 K to show the persistence of the carbon KLL peak at 272 eV (inset on the bottom right). The peaks are assigned using [195].

phenomenon is observed for 1%ML atomic Ni (figure 4.11**c**)), although the amount of metal is three times higher than for 0.3%ML Pt atoms, corroborating an intrinsically higher activity of Pt as co-catalyst material when compared to Ni.

To further determine the impact of Pt cluster size and loading on its activity in methanol photoreforming, Pt atoms and clusters of 5, 10, and >47 atoms were deposited between 0.1% and 2%ML on $TiO_2(110)$. The corresponding H_2 and formaldehyde TOFs are shown in figure 4.14. A green, yellow and brown background colour denotes equal amounts of Pt atoms on the surface among different size-coverage combinations.

As a general trend, it can be stated that a higher coverage leads to a higher TOF within a given cluster size, in agreement with a study by Hao *et al.*.[95] This is conceivable since the clusters act merely as H_2 recombination centers irrespective of their size; a higher cluster coverage therefore enhances the product formation rate. Coverages of 0.3%ML and below show rather small TOFs. Hence, at low coverages, the catalytic activity is dominated by the amount of clusters rather than their size. This holds also true for 0.3%ML $Pt_{>47}$, which shows relatively low TOFs albeit the total amount of Pt is the highest of all examples shown. Furthermore, different coverages with equal amounts of Pt atoms (coloured bars) often give similarly high TOFs. This suggests that the amount

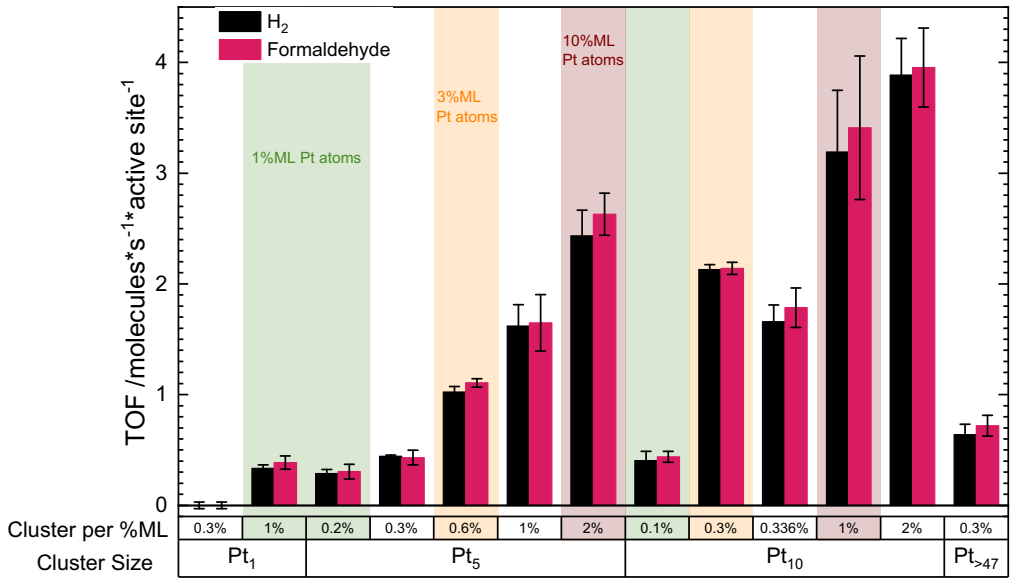

Figure 4.14. TOFs for hydrogen (black bars) and formaldehyde (red bars) from photocatalytic methanol reforming on $Pt_x/TiO_2(110)$ with x= 1, 5, 10,>47 at 300 K and different loadings in a methanol background pressure of $5.0 \cdot 10^{-7}$ mbar after one hour. A background coloured in green, yellow and brown indicates the same total amount of Pt atoms among different coverage-size combinations.

of Pt clusters (i.e. the cluster concentration) on the surface is an important parameter for H_2 evolution, but not the total amount of Pt atoms. This is completely different for Ni, where 0.3%ML $Ni_{>47}$ showed the highest TOF.

An exception in these general trends is Pt_{10}, which facilitates significant product evolution already at a low coverage of 0.3%ML. Nevertheless, the activity of $Pt_{10}/TiO_2(110)$ cannot be arbitrarily enhanced by higher loadings. From 0.3%ML, the three-fold amount (1%ML Pt_{10}) and the almost seven-fold amount (2%ML Pt_{10}) both lead to a roughly doubled product formation rate. The similarly high TOFs of the latter two cases suggest that above 0.3%ML Pt_{10}, the amount of co-catalyst is no longer limiting the kinetics. At a loading of 1% and higher, the reactant supply most probably has a much stronger impact on the reaction rate than the removal of surface hydrogen atoms. In that case, higher TOFs will rather be reached at higher methanol background pressures than at higher cluster coverages. Apart from that, the TOF of 0.3%ML Pt_{10} exceeds the one of 0.6%ML Pt_5 (which contains the same total amount of Pt atoms) two-fold.

These findings can be rationalised by an impact of size-effects on the hydrogen recombination activity. In this regard, the TOF results are generally in very good agreement with the recent literature. A first principles study by Wei and Liu predicted that Pt clusters without core atoms should show the highest H_2 formation activity.[196] Small particles with a high concentration of five or six coordinated apex sites per surface

area (i.e. sizes below 20 atoms) are ascribed a dramatically higher activity than bigger clusters. Wang *et al.* calculated electronic properties of Pt clusters on anatase and conclude that two Pt layer structures of $0.7 - 1.5\,\mathrm{nm}$ in size are the ideal shape for photocatalytic hydrogen evolution.[190] These results corroborate a recent experimental study by Dessal *et al.* under ambient conditions.[197] In a theoretical study by Jiang *et al.*, $Pt_{5\text{-}10}$ clusters on $TiO_2(110)$ are indeed found to have two-layer structures.[63] Experimentally, two-layer structures for $Pt_{>7}$ on $TiO_2(110)$ are observed by Watanabe *et al.* with STM, although not for Pt_5.[60] Thus, two-layer structures can be expected for Pt_{10} and possibly Pt_5 in this study, whose comparably high activity agrees well with the theoretical predictions. Neuberger *et al.* investigated different sizes of Pt co-catalysts for the electrocatalytic hydrogen evolution on titania.[198] They found that bulk Pt, Pt nanoparticles, Pt_{13}, Pt_{10}, and atomic Pt are all capable of H_2 production, whereas Pt_{10} and Pt_{13} outperform the others. Pt atoms shows the lowest activities. The results are explained with the overall amount of accessible Pt, whereas no clear trend in the electronic structure emerges with respect to the Pt $4f_{7/2}$ core levels.

These theoretical and experimental results explain the behaviour depicted in figure 4.14 thoroughly. The low or almost absent activity of Pt atoms is rationalised as follows: first, there is a low number of Pt sites when compared to a cluster at equal coverage. Second, a two-layer structure is absent, which is apparently favourable for H_2 evolution.[190] Third, the interaction of single Pt atoms with adsorbates and support is most likely unfavourable for efficient H_2 evolution, because the $Pt_1{-}TiO_2$ interaction is stronger than for bigger particles.[63] The H_2 formation activity for Pt_5 is higher, due to a larger total number of available Pt sites and probably one second-layer Pt atom as calculated by Jiang *et al.*.[63] Pt_{10} shows a two-layer structure and the parameters governing the activity are combined optimally among the cluster sizes investigated herein (similar as in the work by Neuberger *et al.*).[60, 190, 196, 198] $Pt_{>47}$ instead shows a high number of available Pt sites, but the particle size leads to a distinct metallic character of the majority of Pt atoms, which seems less favourable for H_2 evolution than it is the case for small particles.[190, 198]

In addition to the studies cited above, size effects are in general not uncommon for reactions involving hydrogen on metal cluster-loaded surfaces.[199, 200] Since H_2 formation on $Pt_x/TiO_2(110)$ expectedly proceeds via a reverse spillover mechanism from the support to the cluster, the system shows distinct similarities to thermal size-sensitive clusters.[201] For example, some studies suggest an enhanced catalytic activity on the cluster perimeter.[199, 202] The differences in activity would then not only rely on the electronic structure and accessibility of certain cluster sites, but also on the width of the capture zone (that is, the area around the clusters where hydrogen can efficiently be scavenged). Clearly,

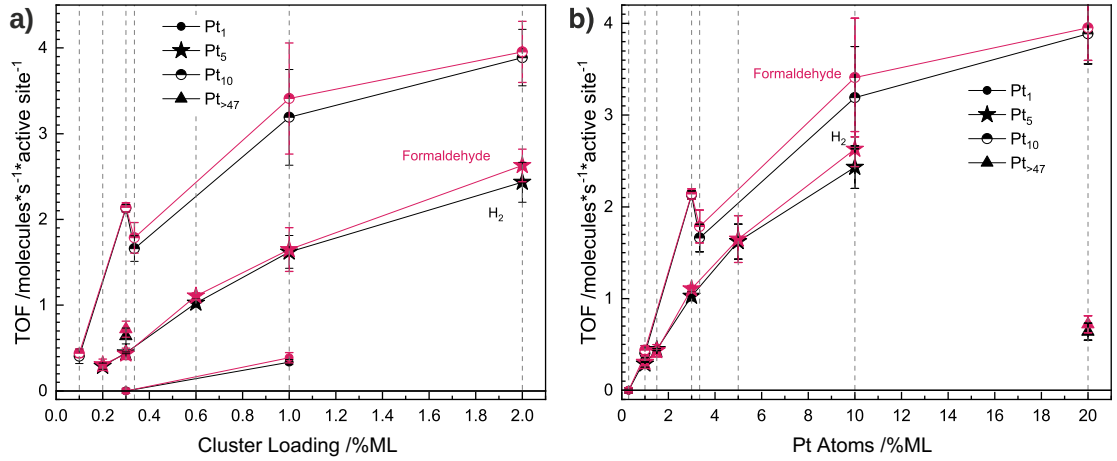

Figure 4.15. TOFs for hydrogen (black) and formaldehyde (red) from photocatalytic methanol reforming on $Pt_x/TiO_2(110)$ with x= $1, 5, 10, >47$ at 300 K in a methanol background pressure of $5.0 \cdot 10^{-7}$ mbar after one hour. **a)** TOFs for different Pt cluster sizes as a function of cluster loading. **b)** TOFs for different Pt cluster sizes as a function of total amount of Pt atoms.

this capture zone would be larger for Pt_{10} than for Pt_5 particles, affecting the H_2 evolution capability more beneficially.

When plotting the TOF versus cluster loading (figure 4.15**a)**) or over the total amount of Pt atoms (figure 4.15**b)**), the curve's progression follows a logarithmic behaviour for each cluster size. As a result, the product formation rate increases initially fast, then abates and asymptotically approaches an upper value. For example, in the case of Pt_{10}, the H_2 and formaldehyde TOFs seem to approach a value of 4 molecules/(active site·s). Notably, the curve progressions of Pt_5 and Pt_{10} (which contain the most data points) of **a)** and **b)** of figure 4.15 are equal but differ in the overall slope and height. For an equal amount of Pt surface atoms (figure 4.15**b)**), the curve of Pt_5 runs slightly but constantly below the curve of Pt_{10}. Thus, Pt_{10} TOFs are even higher if the total amount of Pt is the same as for Pt_5. Furthermore, although $Pt_{>47}$ has a similarly high amount of Pt atoms as 2%ML Pt_{10}, its TOF is only one fourth of the latter. This further indicates an intrinsically high activity of Pt_{10}, which is most likely associated to the electronic structure and beyond a simple model considering the number of surface atoms only. The general trends between cluster size and activity agree with the size dependencies found in the literature, as discussed above.[190, 196, 198]

The asymptotic behaviour of the Pt_{10} curve in figure 4.15 indicates that an upper TOF value of roughly four molecules per second and active site can be achieved, putting the benefits of higher cluster coverages into perspective. In fact, it has already been observed that high metal loadings are detrimental for the photocatalytic activity and for titania

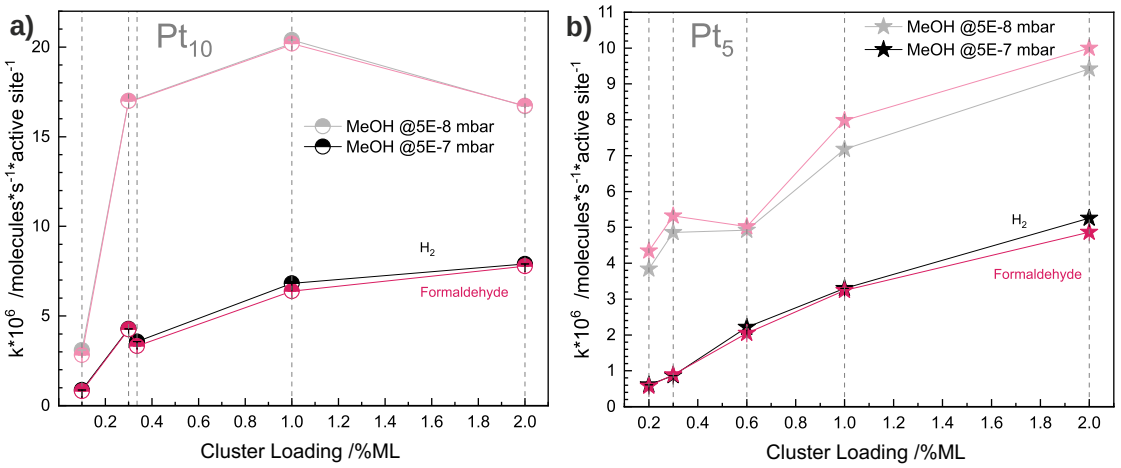

Figure 4.16. Pressure-normalised TOFs for hydrogen (black) and formaldehyde (red) from photocatalytic methanol reforming on **a)** $Pt_{10}/TiO_2(110)$ and **b)** $Pt_5/TiO_2(110)$ for different cluster loadings ($0.1 - 2.0$%ML) at 300 K in a methanol background pressure of $5.0 \cdot 10^{-8}$ mbar (light colour) and $5.0 \cdot 10^{-7}$ mbar (dark colour) after one hour.

nanoparticles, optimal values usually do not exceed more than only a few weight percents of platinum.[203, 204] An increase of reactant supply, as already speculated above, will be more beneficial for higher reaction rates than an increase of the surface coverage of co-catalyst. Indeed, this is clearly visualised when the TOF is normalised by (and therefore independent of) the pressure, as exemplified for Pt_{10} and Pt_5 in figure 4.16). The kinetic limitation by reactant adsorption also leads to a saturation of the TOF at much lower cluster coverages for a lower pressure of methanol and only much lower maximal values are achieved as can be seen in figure 4.17. These impacts of cluster loading and reactant supply on the maximum TOF corroborate the mechanistic picture of thermal H_2 formation by surface hydroxyl recombination. This reaction step occurs solely at the metal clusters and is a consecutive reaction step succeeding the photon-driven α-H cleavage of the alcohol, which takes place on the semiconductor. Consequently, if the concentration of surface hydrogen is too low due to insufficient supply of reactant, increasing the number of hydrogen recombination sites by a higher cluster density does not lead to notable changes in the overall reaction rate.

Throughout the experiments, the formaldehyde trace constantly shows an intensive burst when illumination begins, irrespective of the overall catalyst activity. Similarly, the trace drops immediately back to the baseline level in the dark when stopping the illumination. This is not the case for the hydrogen trace, indicating different desorption kinetics of these two photo-products. As the formation of H_2 is achieved by a consecutive reaction step on the metal clusters, it exhibits a different behaviour than the preceding photo-reaction yielding formaldehyde and can be regarded as an isolated reaction step. Consequently,

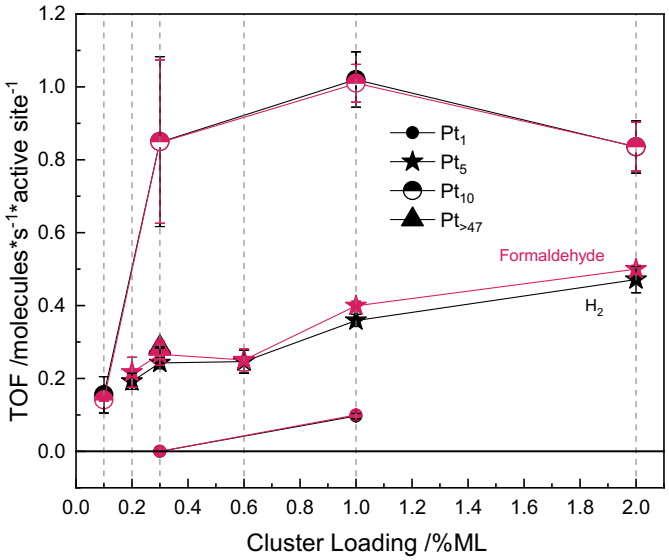

Figure 4.17. TOFs for hydrogen (black) and formaldehyde (red) from photocatalytic methanol reforming on $Pt_x/TiO_2(110)$ with x= $1, 5, 10, >47$ at 300 K in a methanol background pressure of $5.0 \cdot 10^{-8}$ mbar after one hour as a function of cluster loading.

a more detailed evaluation of the H_2 trace may provide further information about the formation kinetics of this molecule. Figure 4.18 shows excerpts from photocatalytic experiments after illumination on 1%ML Pt_{10} (**a)**) and 0.3%ML $Ni_{>47}$ (**b)**) on $TiO_2(110)$ at 300 K to illustrate the resulting effect.

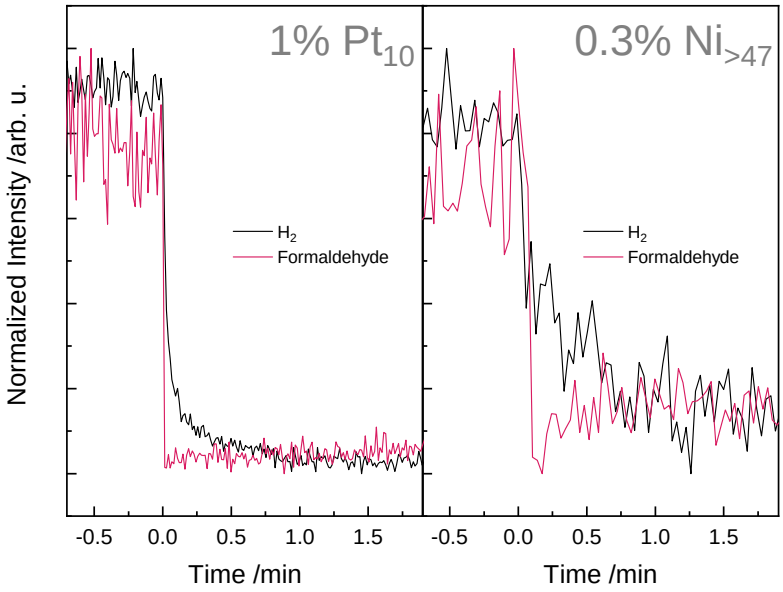

Figure 4.18. Excerpts of traces for hydrogen (black) and formaldehyde (red) after illumination in photocatalytic methanol reforming experiments on **a)** 1%ML $Pt_{10}/TiO_2(110)$ and **b)** 0.3%ML $Ni_{>47}/TiO_2(110)$ at 300 K in a methanol background pressure of $5.0 \cdot 10^{-7}$ mbar. 0 min is defined as the moment when the light flux was blocked.

For both co-catalysts, the formaldehyde trace shows a sharp drop when the illumination is stopped (set to 0 min), while the hydrogen trace tails off to the baseline in the dark. Although more clearly visible for the platinum-loaded sample due to the much better signal-to-noise ratio, the phenomenon is clearly evident on $Ni_{>47}/TiO_2(110)$, too. This further evidences that the desorption mechanisms are presumably identical for both co-catalysts and the H_2 evolution reaction represents a consecutive reaction step to the photo-reaction, which is formally independent of methanol photo-oxidation. As a consequence, the rate of this partial reaction depends on the clusters surface concentration and their capability for hydrogen recombination and desorption, which may be expressed as a rate constant. Figure 4.19 shows baseline-corrected data extracted from different experiments with different amounts of co-catalyst loadings. The curves were fitted with an exponential decay function $r(t) = R_0 \cdot e^{-kt}$, where $r(t)$ is the rate at a certain time t during the decay, k is the rate constant and R_0 is the pre-exponential factor and fixed to the last recorded molecular ion current value before stopping the illumination.

Figure 4.19 shows the decaying of the hydrogen trace after stopping the light flux for different coverages of Pt_5 and Pt_{10} on titania. Clearly, a higher co-catalyst loading involves a higher rate constant, which gives a faster decay. For Pt_5, a two-fold loading leads to a doubling of the rate constant. Obviously, a higher loading has a stronger beneficial effect on H_2 recombination for the smaller clusters. This agrees well with the results from figure 4.15 discussed above. For Pt_5, the regime of co-catalyst saturation is not reached at a 2%ML coverage, in contrast to Pt_{10}. Increasing the Pt_5 loading leads to a more pronounced change of the decay of the H_2 trace and thus of k. These results confirm the significance of sufficiently fast H_2 formation from surface hydrogen species to prevent the thermal back-reaction with formaldehyde to methoxy, which hampers the overall product formation rate. In comparison, Pt_{10} shows faster decays than Pt_5 at equal coverages, agreeing with the higher TOFs of Pt_{10} compared to Pt_5 at equal loadings and reflecting the different capabilities of removing hydrogen from the titania surface. In other words, the surface chemistry displayed in the TOFs are also observed in the H_2 formation kinetics. A kinetically fast removal of hydrogen as H_2 is expressed in high k values and a concomitant high TOF of product formation (figure 4.14).

In summary, a different impact of size-selected Ni and Pt co-catalysts on photocatalytic methanol oxidation on $TiO_2(110)$ is revealed. For Ni, catalyst deactivation occurs for all cluster sizes and coverages studied, which is not observed for Pt clusters. Moreover, Pt as co-catalyst on $TiO_2(110)$ generally leads to a higher product formation rate than Ni. Regarding the cluster size and coverage effects, an increase of the total amount of Ni on the surface, i.e. larger clusters or higher coverages, results in a TOF enhancement

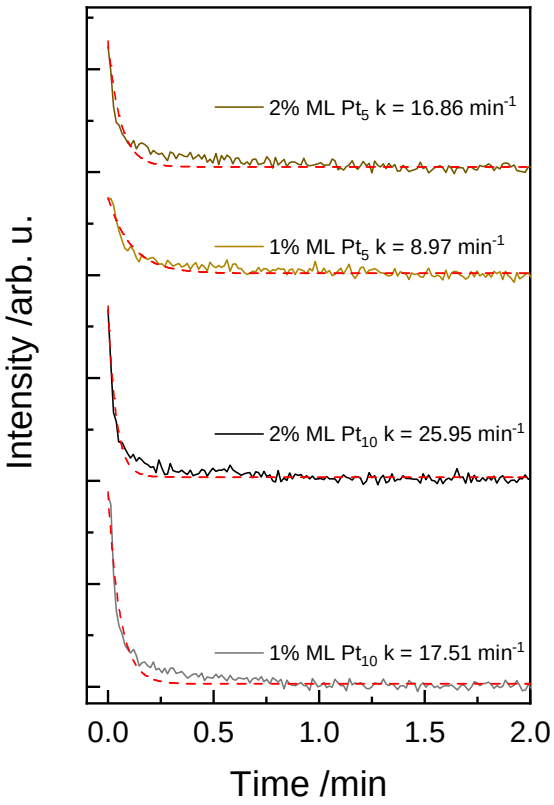

Figure 4.19. Excerpts of traces for hydrogen after illumination in photocatalytic methanol reforming experiments for 1%ML and 2%ML of Pt_5 (yellow) and Pt_{10} (grey) at 300 K in a methanol background pressure of $5.0 \cdot 10^{-7}$ mbar. The dashed red lines fit the exponentially decaying traces according to $r(t) = R_0 \cdot e^{-kt}$, where $r(t)$ is the rate at a certain time t during the decay. The resulting k values resemble the respective rate constants. The pre-exponential factor R_0 is fixed to the last recorded molecular ion current value before stopping the illumination.

without size-specific effects. In contrast, such effects must be taken into account for Pt, where the choice of a particular size is important to improve the H_2 formation, in addition to the total amount of metal on the semiconductor. In general, the findings suggest that a two-layered geometry of small Pt clusters may to be highly beneficial for H_2 evolution. These results are confirmed by an analysis of the decay of the hydrogen QMS trace occuring when the illumination is stopped. An exponential fit enables the quantification of rate constants for the hydrogen evolution reaction and their behaviour agrees well with the TOFs determined in the photocatalytic experiments. Furthermore, the decay of the signal again demonstrates that the H_2 evolution is indeed a consecutive thermal reaction to the photo-reaction.

4.10 Outlook: Effect of Strong Metal-Support Interaction on the Photocatalytic Activity of Size-Selected Pt Clusters on TiO_2(110)

In 1978, Tauster *et al.* were the first to observe a significant decrease in H_2 and CO chemisorption after reducing the catalysts, consisting of group VIII metal nanoparticles supported on TiO_2 powder, at 800 K in an H_2 atmosphere.[67] The authors attributed this phenomena to a strong metal-support interaction that may change the morphology and electronic structure of the catalyst. In the next years, it became evident that the suppression of H_2 and CO uptake results from the growth of a thin TiO_x layer over group VIII metal nanoparticles.[205] Nowadays, the strong metal-support interaction of Pt-decorated titania catalysts, as well as other group VIII metals supported on reducible oxides, is relatively good understood.[206, 207] The encapsulation effect is actually commonly exploited in heterogeneous catalysis and electrocatalysis to improve the catalytic performance and enhance the stability.[207–211]

Pesty *et al.* reported that grown Pt islands are encapsulated by a thin TiO_x suboxide layer above 450 K in UHV on TiO_2(110).[212] Whereas the group of Diebold observe that Pt nanoparticles get encapsulated after annealing to 775 K.[71]

The results of a preliminary study presented here want to exploit the SMSI to protect presumed highly reactive Pt clusters by encapsulating them with a thin titania layer. The thin titania oxide layer might protect the Pt clusters from any contaminations, while this film may still be permeable for hydrogen atoms so that the photocatalyst remains active for the hydrogen evolution. This assumption is supported by electrochemical studies, where encapsulated Pt nanoparticles suppress the oxygen evolution reaction and the CO oxidation, but still exhibit a high hydrogen oxidation activity.[210, 211]

This work compares the photocatalytic activity in methanol reforming of as-deposited and encapsulated Pt_5 and Pt_{10} supported on TiO_2(110) and probes the photocatalyst's stability in air. For this purpose, two different samples, 2%ML Pt_5 and 1%ML Pt_{10}, are investigated. In a first part, the photoactivity of the 'fresh' catalyst is determined in a methanol photoreforming experiment, analogously to experiments presented in section 4.9. Subsequently, the sample is heated for 5 min at 800 K to build a thin TiO_x overlayer; afterwards the photoactivity is measured again. In a second part, the annealed photocatalysts are exposed to either laboratory or synthetic air. Subsequently, the catalytic activity in the methanol photoreforming is probed again and compared to each other.

The mechanism of methanol photoreforming on a freshly prepared photocatalyst is extensively described in section 4.4. Briefly, upon UV illumination, the photo-active

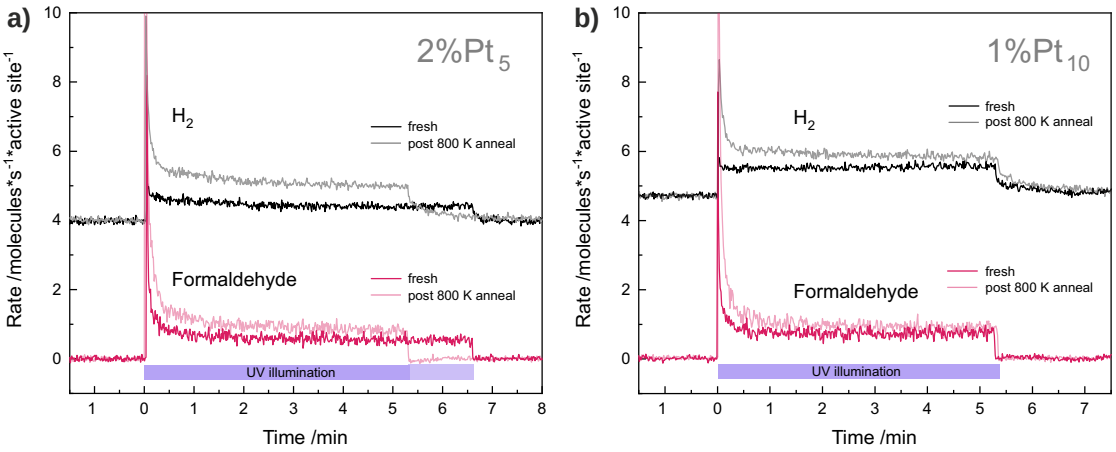

Figure 4.20. Photocatalytic methanol reforming on 'fresh', i.e. as-deposited, and annealed to 800 K **a)** 2%ML Pt_5- and **b)** 1%ML Pt_{10}-loaded TiO_2(110). The methanol is converted to H_2 (m/z 2) and formaldehyde (m/z 30) at 300 K in a $5 \cdot 10^{-8}$ mbar reactant background. The dark traces represent the formation of H_2 and formaldehyde with the fresh catalyst and the bright traces represent those with the post-annealed to 800 K catalyst. The annealed sample is still able to form H_2 and formaldehyde. The purple bars represent the period of UV illumination. Note that the traces are offset for clarity.

methoxy adsorbed on the semiconductor surface is oxidised to formaldehyde. The abstracted hydrogen atom diffuses on the surface to a Pt cluster, where it thermally recombines with another hydrogen to leave the co-catalyst as H_2.

Figure 4.20 demonstrates that the formation of formaldehyde and H_2 is not reduced by annealing the 2%ML Pt_5 or 1%ML Pt_{10}-loaded TiO_2(110) sample to 800 K. At 800 K, a thin TiO_x suboxide should be formed.[71, 212] Apparently, this overlayer does not affect the photocatalytic activity and is permeable for hydrogen atoms. Actually, the photocatalytic activity even seems to be slightly increased by the annealing step.[7] As the oxidation reaction occurs on the bare titania surface, it is not remarkable that the hole-driven reaction is not altered by the annealing step. However, a suppressed hydrogen evolution activity would increase the back-reaction of formaldehyde to methoxy and thus decrease the desorbing amount of formaldehyde. As this is not the case and H_2 is desorbing upon illumination, encapsulated Pt clusters are indeed able to evolve H_2 comparable to as-deposited clusters. This is in accordance with results from the group of Navio and Urbano. They report that the photocatalytic oxidation activity of *iso*-propanol to acetone and H_2 in the gas-phase on Pt/TiO_2 powder is increased for the annealed sample.[213] Furthermore, they observe an increased photocatalytic hydrogen evolution from a glucose/water solution of the annealed Pt/TiO_2 sample.[214]

[7] One must be very careful in a quantitative analysis because a slightly different crystal position might already change the amount of species entering the skimmer of the QMS. Therefore, it will be refrained from a more quantitative interpretation because this would require significantly more data for better statistics.

The encapsulated samples are by following recipes from literature.[71, 212] However, all the SMSI studies so far in the literature are based on evaporated Pt atoms that are grown to nanoparticles or islands upon annealing to high temperatures. Size-selected cluster might behave differently. In addition, the titania surface and the Pt clusters are covered with reactants, intermediates, and decomposition products, this may change the behaviour of the clusters upon annealing. For example, Bonanni *et al.* observed a significant ripening of Pt_7 clusters in an CO and O_2 atmosphere.[62] Therefore cluster ripening, migration and/or coalescence needs to be considered. The clusters might undergo Smoluchowski ripening and dimers, trimers might be formed upon annealing. An STM and/or AFM study might reveal the stability of reactant-covered size-selected clusters upon annealing.

Moreover, it is still under debate, whether small nanoparticles of only a few atoms are also completely encapsulated by a TiO_x layer.[68, 69, 215] The group of Weixin grow Pt particles of different sizes *via* evaporation and annealing on TiO_2(110) and they claim that small Pt clusters of about 1.4 nm do not exhibit barely any SMSI, whereas bigger particles of 20 nm do. Conversely, Han *et al.* report even a SMSI state upon annealing to 900 K of single Pt atoms on TiO_2 powder.

With the given apparatus, CO TPDs of the annealed sample would clarify if sites on Pt clusters are accessible for CO adsorption and whether the clusters are fully or partially encapsulated. A feature at around 500 K stemming from 'bare' Pt clusters will be apparent in the CO TPD if the clusters are not fully encapsulated.[62, 67, 68, 212, 216] A subsequent H_2O TPD will demonstrate that Pt clusters are still present on the surface if a H_2 feature arises (see figure 3.11).[68] In cooperation with another group, LEIS measurements would further provide evidence, whether the Pt clusters are also physically encapsulated by a thin titania layer or if they are only coordinated by TiO_x so that they are not accessible anymore for CO adsorption.

The encapsulated 2%ML Pt_5 and 1%ML Pt_{10}-loaded TiO_2(110) photocatalyts are exposed for several hours to respectively synthetic or laboratory air at ambient pressures. Afterwards, the samples are introduced in the UHV chamber again followed by an annealing step to 800 K in order to desorb all possible adsorbates. The syn-air exposured catalyst displays identical photocatalytic activity as can be seen in figure 4.21**a)**; formaldehyde and H_2 are produced in the same amounts as before this exposure. Consequently, the encapsulated Pt-TiO_2 sample is stable in an atmosphere of O_2, N_2 and traces of water (5 vol-ppm). The protected Pt clusters are thus resistant towards oxidation by O_2, or at least it does not affect the hydrogen evolution activity.

This is different for an exposure to laboratory air at atmospheric pressure. The lab-air exposed photocatalyst exhibits a strongly reduced photo-activity compared to the annealed

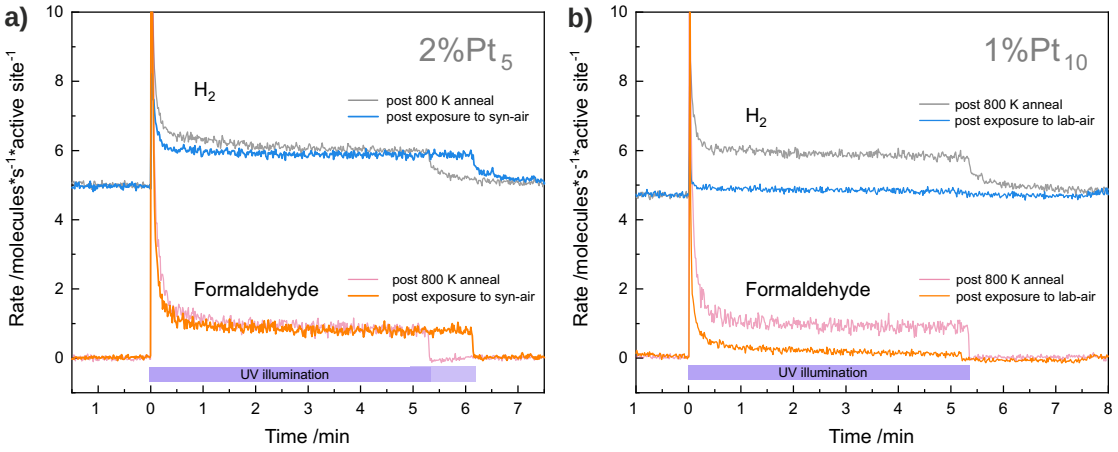

Figure 4.21. Photocatalytic methanol reforming on annealed to 800 K and exposed to **a)** laboratory air 2%ML Pt_5- and **b)** syn-air 1%ML Pt_{10}-loaded TiO_2(110). The methanol is converted to H_2 (m/z 2) and formaldehyde (m/z 30) at 300 K in a $5 \cdot 10^{-8}$ mbar reactant background. The grey and magenta traces represent the formation of H_2 and formaldehyde with the annealed catalyst and the blue and orange traces represent those with the air-exposed catalyst. The sample exposed to syn-air is still able to form H_2 and formaldehyde whereas the catalyst exposed to laboratory air reduces significantly the H_2 and formaldehyde production. The purple bars represent the period of UV illumination. Note that the traces are offset for clarity.

one, displayed in figure 4.21**b)**. H_2 is barely evolving from the lab-air sample suggesting that the Pt clusters, i.e. the H_2 evolution sites, are poisoned different to a poisoning of the photo-oxidation sites on the titania surface. This matches that the formaldehyde production is comparable to bare TiO_2(110) (see section 4.3 for more details).

Assuming comparable sensitivity towards contaminations of both 2%ML Pt_5 and 1%ML Pt_{10}-loaded TiO_2(110) samples, it is unlikely that O_2, N_2 or traces of water (5 vol-ppm) cause the deactivation of the lab-air exposed catalyst. Other components, which are found in the lab-air must be responsible for the Pt cluster poisoning.

AES spectra of both samples recorded after exposure to syn-air and lab-air reveal that a distinct sulphur peak (152 eV) appears in the spectrum of the poisoned sample (lab-air), shown in figure 4.22**b)**. For the rest, both spectra show the expected Pt, Ti, O and C signals. Sulphur species might adsorb on the titania-covered Pt clusters considering the strong affinity of sulphur to Pt and inhibit the H_2 evolution.[217–219] Sulphur is a typical poisoning agent, especially known in the automobile exhaust catalysts.[217, 220] The laboratory air might contain small amounts of sulphur compounds, as sulphur oxides, sulphuric acids, or thiols. In addition, hydrosulphide compounds might evaporate from rotary vane pumps in the laboratory, that are driven with mineral oil.

More experiments must be performed to confirm the first assumption that sulphur species inhibit the H_2 evolution on the Pt clusters. Gaseous sulphur compounds, like SO_2 or

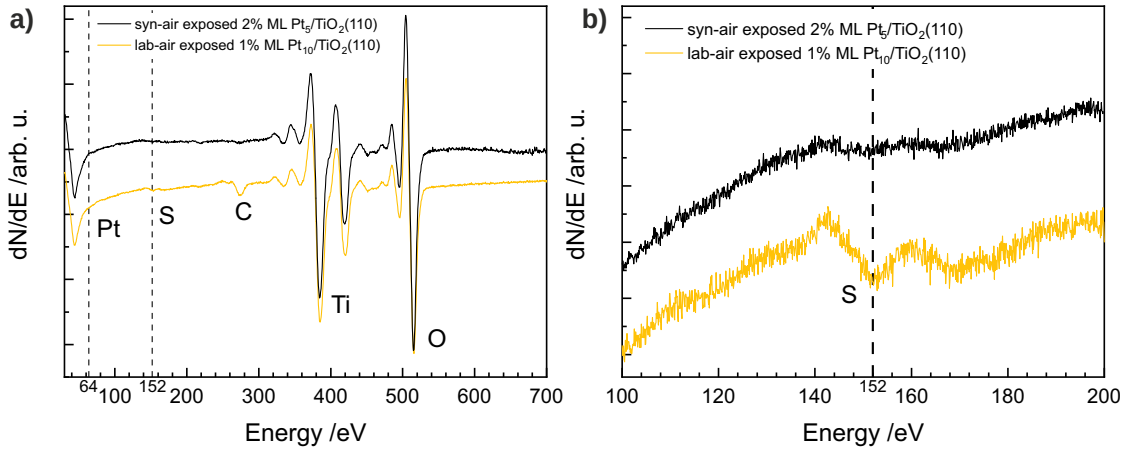

Figure 4.22. AES spectra of syn-air exposed 2%ML $Pt_5/TiO_2(110)$ and lab-air exposed 1%ML $Pt_{10}/TiO_2(110)$ recorded **a)** from $30-700\,eV$ and **b)** from $100-200\,eV$ with a higher sensitivity. **a)** and **b)** are recorded one after the other respectively. **a)** shows the the excepted Pt, Ti, O, and C peaks for the lab-air and syn-air exposed samples. **b)** highlights that the lab-air exposed sample features a sulphur peak at 152 eV which is not present in the syn-air exposed spectrum. The spectra are recorded after the photoreforming of methanol from $30-700\,eV$ at about $200-300\,K$. The carbon peak is attributed to residual carbon species from the photocatalytic reforming of methanol.

H_2O, could be dosed in very low amounts onto the annealed catalyst in order to verify a possible poisoning by sulphur compounds. A clear relation between sulphur adsorption at Pt clusters and a deactivation in photocatalytic activity may be established in this way.

To summarise, photocatalytic methanol reforming is enabled on the annealed 2%ML Pt_5 and 1%ML Pt_{10}-loaded $TiO_2(110)$ photocatalysts in the same amount. Annealing to 800 K is intended to encapsulate and thus protect the Pt clusters with a thin titania layer. Syn-air exposed samples do not show any deactivation, whereas lab-air drastically deteriorates the photocatalytic activity. AES spectra suggest that sulphur is poisoning the H_2 evolution co-catalyst. Encapsulated Pt clusters may indeed be applied in photocatalysis, but its stability should be investigated in more detail.

5 Conclusion and Outlook

This thesis provides mechanistic insights into the photochemical and photocatalytic alcohol conversion on bare and metal-loaded TiO_2(110). The model system consisting of size-selected metal clusters deposited on a single-crystal facilitated the study of surface processes on a molecular scale. Moreover, studies under UHV conditions combined with the synthesis of metal clusters with the laser vaporisation cluster source ensured an atomically-precise manipulation of the surface, and the size and loading of the co-catalysts. This allows to study the influence of the size and the loading of the co-catalyst individually. The independent variation of different parameters, such as temperature, pressure, or light intensity allowed for a deconstruction of reaction pathways and catalytic cycles into 'snapshots' to gain a profound understanding on a molecular level. In this way, it became possible to elucidate photochemical reaction pathways of various alcohols on bare titania and to establish a catalytic cycle for the photocatalytic conversion of alcohols on Pt- and Ni-loaded titania.

The product distribution for the photochemical conversion of isobutanol on bare TiO_2(110) strongly depends on the temperature. The temperature determines whether a consecutive photo-oxidation reaction of the primary product, the aldehyde, is enabled or the thermal desorption of the primary photo-product results. Below room temperature, the aldehyde is trapped on the surface and gets further oxidised to propane and CO. This second photo-reaction involves a C-C bond scission that leads to the abstraction of a propyl radical. The propyl radical resides on the surface until it recombines with a hydrogen atom to form propane. Above room temperature, the desorption of isobutanal is faster than the sequential photo-reaction.

The overall selectivity for the hole-driven oxidation of *tert*-butanol on bare titania is also temperature-dependent, but in contrast to isobutanol two individual reaction pathways proceed in parallel. The photo-oxidation pathway leads to the formation of acetone and the ejection of a methyl radical into the gas-phase, unlike to propyl radicals that reside on the surface. The photo-oxidation reaction occurs at every investigated temperature though the yield increases with temperature as the product desorption is favoured. In contrast, the dehydration pathway requires a certain temperature to activate a proposed cyclic transition state. The photochemical conversions of both, isobutanol and *tert*-butanol, exhibit a significant temperature-dependence; however, the underlying mechanisms are completely different. These examples showcase the richness in photochemical processes and demonstrate the importance of a mechanistic understanding of individual thermal- and photochemical reaction steps.

Tertiary alcohols that possess at least one alkyl chain longer than methyl do selectively abstract the longer alkyl chains and not the methyl group in the photo-oxidation reaction on TiO_2(110). This is in contrast to the photo-oxidation of *tert*-butanol, where a cleavage of bonds to methyl groups are enabled. The abstracted radical, ethyl or propyl, resides on the surface and recombines with a hydrogen atom to leave the surface as the respective alkane, comparable to the propyl radical in the sequential photo-reaction of isobutanol. The reaction that can be described as disproportionation reaction to ketones and alkanes, is fully stoichiometric and since all the products are desorbing at the reaction temperature, the conversion can be performed catalytically on bare titania. Further, the photoreforming of 3-methyl-3-hexanol reveals that ethane and pentanone is preferably formed over propane and butanone, which can be explained with the thermochemistry of radical formation.

The photoreforming of primary and secondary alcohols on bare TiO_2(110) is accompanied by a hydroxylation of the surface resulting from the dissociative adsorption and the α-H abstraction. The hydrogen atoms accumulate on the surface because titania is not able to facilitate the recombination of two hydrogen atoms at room temperature. A comparison of the different reaction steps of methanol and 2-methyl-2-pentanol indicates that the origin of poisoning in methanol photoreforming results from the back-reaction of formaldehyde with surface hydroxyls and is not caused by changes in the charge carrier dynamics. This demonstrates that every single reaction- and back-reaction step must be considered for a thorough modelling of photocatalytic systems.

The photo-conversion of various primary and secondary alcohols and *tert*-butanol can be driven catalytically in a constant alcohol background by the addition of Pt co-catalysts. Pt clusters deposited on titania enable the recombination and desorption of hydrogen atoms in contrast to bare titania and, thereby, facilitate a stoichiometric reaction. A

thorough interpretation of the results gained from catalytic measurements and a detailed analysis of surface species lead to a reaction mechanism that explains the observed one-photon dependence and considers the surface chemistry and semiconductor physics. The commonly mechanistic picture derived from photoelectrochemistry implies that the hydrogen evolution reaction on Pt is driven by photo-electrons, whereas the results in this thesis indicate that the hydrogen recombination on Pt is a thermal process. This mechanism may even be valid for other reducible oxide semiconductors and showcases that photocatalytic concepts may be different to those derived from (photo)electrochemistry.

Generally, the photo-oxidation of different alcohols to aldehydes or ketones occurs on the titania surface, whose chemistry also determines, together with the temperature, the product distribution. The deposition of Pt clusters under anaerob conditions does not qualitatively alter the photo-oxidation reaction. Certainly, since the Pt clusters prevent a surface hydroxylation and thus an increase in the rate of thermal back-reaction, the alcohol conversion is drastically enhanced. Besides this, water-free alcohol photoreforming at room temperatures allows for a highly selective generation of aldehydes and ketones when suitable conditions were chosen carefully, as e.g. the absence of O_2 and the temperature. While Pt clusters do not change the photoreaction itself, they can induce additional reaction channels as observed in the photoreforming of tertiary alcohols with longer alkyl chains. Pt clusters enable hydrogen evolution, which leads to a decrease of the concentration of surface hydrogen. The low hydrogen concentration leads to increasing alkyl species on the surface, which makes the alkyl radical dimerisation more probable to form a longer alkane so that the overall reaction remains stoichiometric. These findings demonstrate the complexity of presumed simples systems and may to some extent explain the variety of products in liquid and ambient pressure photocatalytic studies.

The $Pt_x/TiO_2(110)$ exhibits a high stability in the alcohol photoreforming, but Pt is rare and expensive. Here, it is demonstrated that also cheap and abundant nickel co-catalysts facilitate the photocatalytic hydrogen evolution from methanol. Moreover, the behaviour suggests that the mechanism proposed for $Pt_x/TiO_2(110)$ is also valid for Ni co-catalysts on $TiO_2(110)$. However, conversely to Pt-loaded titania, the photo-activity of $Ni_x/TiO_2(110)$ is declining at longer illumination times under reaction conditions. Non-desorbing carbonaceous deposits on Ni clusters are hold responsible for the reduced hydrogen evolution capability. The carbon deposition only occurs under illumination and the decrease in photo-activity represents a photocorrosion process. This deactivation process is observed for all investigated cluster sizes, though larger clusters and higher coverages exhibit a slower deactivation process in addition to a higher product formation rate. However, the activity of Ni-loaded titania with the same size and loading significantly

underperforms that of Pt by more than an order of magnitude. Unlike Ni clusters, whose activity increases with the absolute amount of Ni, size-selected Pt clusters show a size-specific effect. The H_2 evolution rate exhibits a maximum for Pt_{10} within the investigated sizes. This is attributed to a 3D-layer geometry of the cluster. However, larger cluster sizes do not simply increase the H_2 evolution rate, whereas a higher loading increases the H_2 evolution rate for the same size. These findings clarify that one material cannot be readily exchanged by another material although the role in the catalytic cycle is the same. This especially concerns specific size effects, which are supposed to be highly material specific. Theoretical calculations may serve on the one hand to explain the observed size-effect and on the other hand help to find the optimum co-catalyst size for a particular material.

The titania surface itself is relatively inert towards any contaminations, but clusters comprising only a few atoms may presumably be not.[23] Hitherto, all photocatalytic experiments have been performed in an ultra-high vacuum chamber under ideal conditions and in the absence of any unwanted substances, as e.g. H_2O, O_2 or CO_2, which are usually present under more applied conditions. Therefore, preliminary studies have been performed pertaining to the protection of Pt, and possibly even Ni clusters, by exploiting the strong metal-support interaction. The clusters may get encapsulated by annealing the sample above a certain temperature.[206, 207] The encapsulation may even prevent Ni clusters from carbon deposits during the photo-reaction as the thin TiO_x layer is permeable for hydrogen atoms, but not for carbonaceous molecules, such as methanol, formaldehyde, CO or other intermediates.[210, 211] Hence, encapsulated Ni, as highly abundant and cheap material, could be used as stable co-catalyst in the photocatalytic alcohol reforming. Though, the cluster's stability and the degree of encapsulation upon annealing must be investigated in more detail.

For future experiments, infrared reflection absorption spectroscopy, that is currently being implemented into the setup, could be a helpful analytic tool to investigate the surface species in photo-reactions in more detail, as it allows the identification of adsorbates and the elucidation of their binding behaviour. Furthermore, adsorbed CO can be used as probe molecule to investigate the degree of encapsulation.[221, 222] Besides, carbon deposits can be analysed by the evaluation of the CO stretch position as they are supposed to cause a redshift in the CO stretch frequency due to electron donation to the metal.[199, 223–225] Further, the CO frequency may provide insights into the oxidation state of the clusters as the latter one changes the bonding strength of CO, which in turn is reflected in the CO stretch frequency.[226] Presumably, the doping of the semiconductor may also induce a shift in the CO stretch frequency as the bonding of CO to the cluster may be affected. For example, e.g. Crampton *et al.* showed that a change of the support acidity

causes a change in the CO bonding strength and consequently a shift in the CO stretch frequency.[223] Similarly, Rötzer *et al.* revealed that the electronic modification of a thin SiO_2 support influences its charge transfer to cluster and thus induces a shift in the CO absorption.[227] Therefore, a different doping of the semiconductor support may give rise to a different charging of the metal cluster that is reflected in the CO bonding.[228]

Beyond the study of the clusters, IRRAS also enables to identify adsorbed intermediates during a reaction to get even more profound insights into the reaction mechanism.[32] In addition, adsorption geometries may be identified so that e.g. the cyclic transition state in *tert*-butanol photo-reaction to isobutene may be confirmed. The group of Al-Shamery showed that this is indeed possible with IRRAS for the photo-conversion of 2-propanol.[229] The implementation of the IRRAS setup will thus provide a complete new tool for *in situ* investigations of the co-catalysts and surface species. This could be especially helpful for the study of semiconductors other than titania, whose surface chemistry is much less investigated and must be understood before mechanistic photocatalytic studies can be fully interpreted.

A promising candidate for such a semiconductor is $SrTiO_3$ as $SrTiO_3$-based photocatalysts promote photocatalytic full water splitting into H_2 and O_2.[4, 230–232] For example, the group of Takanabe demonstrated that Pt-decorated $SrTiO_3$ evolves H_2 and O_2 under UV illumination from pure water; presumably, Pt acts as H_2 evolution catalysts and $SrTiO_3$ enables the O_2 evolution.[231] All those studies were performed on powder photocatalysts in aqueous solutions or pure water, but to the best of my knowledge no photochemical studies have been done on $SrTiO_3$ single crystals up to now. Though several thermal surface science studies have been performed on the (100) facet which indicate that the stoichiometric TiO_2-termination might behave similarly to TiO_2(110) with the difference that $SrTiO_3$ might evolve O_2.[233–235] Photocatalytic mechanistic studies on $SrTiO_3$(100) will be challenging, but possibly reveal the intermediates involved in the O_2 evolution and the mechanism behind full water splitting on this material.

Bibliography

[1] German Federal Ministry for Economic Affairs and Energy, "The national hydrogen strategy", *www.bmwi.de/Redaktion/EN/Publikationen/Energie/the-national-hydrogen-strategy.html, (accessed on 12.04.2021).*

[2] I. E. A., "Technology roadmap hydrogen and fuel cells", *www.iea.org, accessed on 26.03.2020).*

[3] Z. Wang, C. Li, K. Domen, "Recent developments in heterogeneous photocatalysts for solar-driven overall water splitting", *Chem. Soc. Rev.* **2019**, *48*, 2109–2125.

[4] T. Takata, J. Jiang, Y. Sakata, M. Nakabayashi, N. Shibata, V. Nandal, K. Seki, T. Hisatomi, K. Domen, "Photocatalytic water splitting with a quantum efficiency of almost unity", *Nature* **2020**, *581*, 411–414.

[5] K. Takanabe, "Photocatalytic water splitting: quantitative approaches toward photocatalyst by design", *ACS Catal.* **2017**, *11*, 8006–8022.

[6] T. Hisatomi, K. Domen, "Reaction systems for solar hydrogen production via water splitting with particulate semiconductor photocatalysts", *Nat. Catal.* **2019**, *2*, 387–399.

[7] C. Acar, I. Dincer, "Impact assessment and efficiency evaluation of hydrogen production methods", *Int. J. Energy Res.* **2015**, *39*, 1757–1768.

[8] Q. Wang, K. Domen, "Particulate photocatalysts for light-driven water splitting: mechanisms, challenges, and design strategies", *Chem. Rev.* **2020**, *120*, 919–985.

[9] N. T. Padmanabhan, H. John, "Titanium dioxide based self-cleaning smart surfaces: a short review", *J. Environ. Chem. Eng.* **2020**, *8*, 104211.

[10] S. Noimark, C. W. Dunnill, I. P. Parkin, "Shining light on materials - A self-sterilising revolution", *Adv. Drug Deliv. Rev.* **2013**, *65*, 570–580.

[11] A. J. Haider, Z. N. Jameel, I. H. M. Al-Hussaini, "Review on: titanium dioxide applications", *Energy Procedia* **2019**, *157*, 17–29.

[12] U. I. Gaya, A. H. Abdullah, "Heterogeneous photocatalytic degradation of organic contaminants over titanium dioxide: a review of fundamentals, progress and problems", *J. Photochem. Photobiol., C* **2008**, *9*, 1–12.

[13] B. Zhou, J. Song, Z. Zhang, Z. Jiang, P. Zhang, B. Han, "Highly selective photocatalytic oxidation of biomass-derived chemicals to carboxyl compounds over Au/TiO_2", *Green Chem.* **2017**, *19*, 1075–1081.

[14] F. Parrino, M. Bellardita, E. I. García-López, G. Marcì, V. Loddo, L. Palmisano, "Heterogeneous photocatalysis for selective formation of high-value-added molecules: some chemical and engineering aspects", *ACS Catal.* **2018**, *8*, 11191–11225.

[15] J. C. Colmenares, A. Magdziarz, A. Bielejewska, "High-value chemicals obtained from selective photo-oxidation of glucose in the presence of nanostructured titanium photocatalysts", *Bioresour. Technol.* **2011**, *102*, 11254–11257.

[16] S. Chen, T. Takata, K. Domen, "Particulate photocatalysts for overall water splitting", *Nat. Rev. Mater.* **2017**, *2*, 17050.

[17] A. A. Ismail, D. W. Bahnemann, "Photochemical splitting of water for hydrogen production by photocatalysis: a review", *Sol. Energy Mater. Sol. Cells* **2014**, *128*, 85–101.

[18] A. T. Garcia-Esparza, T. Shinagawa, S. Ould-Chikh, M. Qureshi, X. Peng, N. Wei, D. H. Anjum, A. Clo, T.-C. Weng, D. Nordlund, D. Sokaras, J. Kubota, K. Domen, K. Takanabe, "An oxygen-insensitive hydrogen evolution catalyst coated by a molybdenum-based layer for overall water splitting", *Angew. Chem. Int. Ed.* **2017**, *56*, 5780–5784.

[19] D. M. Fabian, S. Hu, N. Singh, F. A. Houle, T. Hisatomi, K. Domen, F. E. Osterloh, S. Ardo, "Particle suspension reactors and materials for solar-driven water splitting", *Energy Environ. Sci.* **2015**, *8*, 2825–2850.

[20] K. C. Christoforidis, P. Fornasiero, "Photocatalytic hydrogen production: a rift into the future energy supply", *ChemCatChem* **2017**, *9*, 1523–1544.

[21] M. Murdoch, G. I. N. Waterhouse, M. Nadeem, J. B. Metson, M. A. Keane, R. F. Howe, J. Llorca, H. Idriss, "The effect of gold loading and particle size on photocatalytic hydrogen production from ethanol over Au/TiO_2 nanoparticles", *Nat. Chem.* **2011**, *3*, 489 –492.

[22] A. Luken, M. Muhler, J. Strunk, "On the role of gold nanoparticles in the selective photooxidation of 2-propanol over Au/TiO_2", *Phys. Chem. Chem. Phys.* **2015**, *17*, 10931–10397.

[23] U. Diebold, "The surface science of titanium dioxide", *Surf. Sci. Rep.* **2003**, *48*, 53 –229.

[24] M. A. Henderson, "A surface science perspective on TiO_2 photocatalysis", *Surf. Sci. Rep.* **2011**, *66*, 185 –297.

[25] U. Diebold, J. Lehman, T. Mahmoud, M. Kuhn, G. Leonardelli, W. Hebenstreit, M. Schmid, P. Varga, "Intrinsic defects on a $TiO_2(110)(1\times1)$ surface and their reaction with oxygen: a scanning tunneling microscopy study", *Surf. Sci.* **1998**, *411*, 137–153.

[26] Z. Zhang, J. Lee, J. T. Yates, R. Bechstein, E. Lira, J. Ø. Hansen, S. Wendt, F. Besenbacher, "Unraveling the diffusion of bulk Ti interstitials in rutile $TiO_2(110)$ by monitoring their reaction with O adatoms", *J. Phys. Chem. C* **2010**, *114*, 3059–3062.

[27] M. Bowker, R. A. Bennett, "The role of Ti^{3+} interstitials in $TiO_2(110)$ reduction and oxidation", *J. Phys.: Condens. Matter* **2009**, *21*, 474224.

[28] L. E. Walle, A. Borg, P. Uvdal, A. Sandell, "Probing the influence from residual Ti interstitials on water adsorption on $TiO_2(110)$", *Phys. Rev. B* **2012**, *86*, 205415.

[29] Y. Yoon, Y. Du, J. C. Garcia, Z. Zhu, Z.-T. Wang, N. G. Petrik, G. A. Kimmel, Z. Dohnalek, M. A. Henderson, R. Rousseau, N. A. Deskins, I. Lyubinetsky, "Anticorrelation between surface and subsurface point defects and the impact on the redox chemistry of $TiO_2(110)$", *ChemPhysChem* **2015**, *16*, 313–321.

[30] T. Cremer, S. C. Jensen, C. M. Friend, "Enhanced photo-oxidation of formaldehyde on highly reduced o-TiO_2(110)", *J. Phys. Chem. C* **2014**, *118*, 29242–29251.

[31] L. Benz, J. Haubrich, R. G. Quiller, S. C. Jensen, C. M. Friend, "McMurry chemistry on TiO_2(110): reductive C-C coupling of benzaldehyde driven by titanium interstitials", *J. Am. Chem. Soc.* **2009**, *131*, 15026–15031.

[32] P. M. Clawin, C. M. Friend, K. Al-Shamery, "Defects in surface chemistry - Reductive coupling of benzaldehyde on rutile TiO_2(110)", *Chem. - Eur. J.* **2014**, *20*, 7665–7669.

[33] M. Osmic, L. Mohrhusen, K. Al-Shamery, "Bulk defect dependence of low-temperature partial oxidation of methanol and high-temperature hydrocarbon formation on rutile TiO_2(110)", *J. Phys. Chem. C* **2019**, *123*, 7615–7626.

[34] L. Benz, J. Haubrich, R. G. Quiller, C. M. Friend, "Acrolein coupling on reduced TiO_2(110): the effect of surface oxidation and the role of subsurface defects", *Surf. Sci.* **2009**, *603*, 1010–1017.

[35] S. Wendt, P. T. Sprunger, E. Lira, G. K. H. Madsen, Z. Li, J. Ø. Hansen, J. Matthiesen, A. Blekinge-Rasmussen, E. Lægsgaard, B. Hammer, F. Besenbacher, "The role of interstitial dites in the Ti3d defect state in the band gap of titania", *Science* **2008**, *320*, 1755–1759.

[36] M. Li, W. Hebenstreit, U. Diebold, M. A. Henderson, D. R. Jennison, "Oxygen-induced restructuring of rutile TiO_2(110): formation mechanism, atomic models, and influence on surface chemistry", *Faraday Discuss.* **1999**, *114*, 245–258.

[37] H. Onishi, Y. Iwasawa, "Reconstruction of TiO_2(110) surface: STM study with atomic-scale resolution", *Surf. Sci.* **1994**, *313*, 783–789.

[38] J. Gaberle, A. Shluger, "The role of surface reduction in the formation of Ti interstitials", *RSC Adv.* **2019**, *9*, 12182–12188.

[39] J.-M. Pan, B. L. Maschhoff, U. Diebold, T. E. Madey, "Interaction of water, oxygen, and hydrogen with TiO_2(110) surfaces having different defect densities", *J. Vac. Sci. Technol., A* **1992**, *10*, 2470 –2476.

[40] Y. Du, N. A. Deskins, Z. Zhang, Z. Dohnalek, M. Dupuis, I. Lyubinetsky, "Formation of O adatom pairs and charge transfer upon O_2 dissociation on reduced TiO_2(110)", *Phys. Chem. Chem. Phys.* **2010**, *12*, 6337–6344.

[41] Z. Zhang, O. Bondarchuk, J. M. White, B. D. Kay, Z. Dohnalek, "Imaging adsorbate O-H bond cleavage: methanol on TiO_2(110)", *J. Am. Chem. Soc.* **2006**, *128*, 4198–4199.

[42] A. L. Linsebigler, G. Lu, J. T. Yates, "Photocatalysis on TiO_2 surfaces: principles, mechanisms, and selected results", *Chem. Rev.* **1995**, *95*, 735 –758.

[43] Z. Zhang, J. T. Yates, "Band bending in semiconductors: chemical and physical consequences at surfaces and interfaces", *Chem. Rev.* **2012**, *112*, 5520–5551.

[44] M. A. Henderson, W. S. Epling, C. H. F. Peden, C. L. Perkins, "Insights into photoexcited electron scavenging processes on TiO_2 obtained from studies of the reaction of O_2 with OH groups adsorbed at electronic defects on TiO_2(110)", *J. Phys. Chem. B* **2003**, *107*, 534–545.

[45] A. C. Papageorgiou, N. S. Beglitis, C. L. Pang, G. Teobaldi, G. Cabailh, Q. Chen, A. J. Fisher, W. A. Hofer, G. Thornton, "Electron traps and their effect on the surface chemistry of TiO_2(110)", *Proc. Natl. Acad. Sci. U.S.A.* **2010**, *107*, 2391–2396.

[46] C. M. Yim, C. L. Pang, G. Thornton, "Oxygen vacancy origin of the surface band-gap state of TiO_2(110)", *Phys. Rev. Lett.* **2010**, *104*, 036806.

[47] M. Setvin, X. Shi, J. Hulva, T. Simschitz, G. S. Parkinson, M. Schmid, C. Di Valentin, A. Selloni, U. Diebold, "Methanol on anatase TiO_2 (101): mechanistic insights into photocatalysis", *ACS Catal.* **2017**, 7081–7091.

[48] M. Shen, M. A. Henderson, "Identification of the active species in photochemical hole scavenging reactions of methanol on TiO_2", *J. Phys. Chem. Lett.* **2011**, *2*, 2707–2710.

[49] G. A. Tritsaris, D. Vinichenko, G. Kolesov, C. M. Friend, E. Kaxiras, "Dynamics of the photogenerated hole at the rutile TiO_2(110)/water interface: a nonadiabatic simulation study", *J. Phys. Chem. C* **2014**, *118*, 27393–27401.

[50] Q. Guo, C. Xu, W. Yang, Z. Ren, Z. Ma, D. Dai, T. K. Minton, X. Yang, "Methyl formate production on TiO_2(110), initiated by methanol photocatalysis at 400 nm", *J. Phys. Chem. C* **2013**, *117*, 5293–5300.

[51] T. L. Thompson, J. T. Yates, "Monitoring hole trapping in photoexcited TiO_2(110) using a surface photoreaction", *J. Phys. Chem. B* **2005**, *109*, 18230–18236.

[52] M. A. Henderson, M. Shen, Z.-T. Wang, I. Lyubinetsky, "Characterization of the active surface species responsible for UV-induced desorption of O_2 from the rutile TiO_2(110) surface", *J. Phys. Chem. C* **2013**, *117*, 5774–5784.

[53] N. G. Petrik, G. A. Kimmel, "Photoinduced dissociation of O_2 on rutile TiO_2(110)", *J. Phys. Chem. Lett.* **2010**, *1*, 1758–1762.

[54] N. G. Petrik, G. A. Kimmel, "Electron- and hole-mediated reactions in UV-irradiated O_2 adsorbed on reduced rutile TiO_2(110)", *J. Phys. Chem. C* **2011**, *115*, 152–164.

[55] Z.-T. Wang, N. A. Deskins, I. Lyubinetsky, "Direct imaging of site-specific photocatalytical reactions of O_2 on TiO_2(110)", *J. Phys. Chem. Lett.* **2012**, *3*, 102–106.

[56] K. Ozawa, S. Yamamoto, R. Yukawa, R. Liu, M. Emori, K. Inoue, T. Higuchi, H. Sakama, K. Mase, I. Matsuda, "What determines the lifetime of photoexcited carriers on TiO_2 surfaces?", *J. Phys. Chem. C* **2016**, *120*, 29283–29289.

[57] A. Rothschild, A. Levakov, Y. Shapira, N. Ashkenasy, Y. Komem, "Surface photovoltage spectroscopy study of reduced and oxidized nanocrystalline TiO_2 films", *Surf. Sci.* **2003**, *532-535*, 456–460.

[58] N. Isomura, X. Wu, Y. Watanabe, "Atomic-resolution imaging of size-selected platinum clusters on TiO_2(110) surfaces", *J. Chem. Phys.* **2009**, *131*.

[59] N. Isomura, X. Wu, H. Hirata, Y. Watanabe, "Cluster size dependence of Pt core-level shifts for mass-selected Pt clusters on TiO_2(110) surfaces", *J. Vac. Sci. Technol., A* **2010**, *28*, 1141–1144.

[60] Y. Watanabe, X. Wu, H. Hirata, N. Isomura, "Size-dependent catalytic activity and geometries of size-selected Pt clusters on TiO_2(110) surfaces", *Catal. Sci. Technol.* **2011**, *1*, 1490–1495.

[61] Y. Watanabe, N. Isomura, "A new experimental setup for high-pressure catalytic activity measurements on surface deposited mass-selected Pt clusters", *J. Vac. Sci. Technol., A* **2009**, *27*, 1153–1158.

[62] S. Bonanni, K. Aït-Mansour, W. Harbich, H. Brune, "Reaction-induced cluster ripening and initial size-dependent reaction rates for CO oxidation on $Pt_n/TiO_2(110)$-(1×1)", *J. Am. Chem. Soc.* **2014**, *136*, 8702–8707.

[63] D.-e. Jiang, S. H. Overbury, S. Dai, "Structures and energetics of Pt clusters on TiO_2: interplay between metal-metal bonds and metal-oxygen bonds", *J. Phys. Chem. C* **2012**, *116*, 21880–21885.

[64] S. Bonanni, K. Aït-Mansour, W. Harbich, H. Brune, "Effect of the TiO_2 reduction state on the catalytic CO oxidation on deposited size-selected Pt clusters", *J. Am. Chem. Soc.* **2012**, *134*, 3445–3450.

[65] M. Li, W. Hebenstreit, U. Diebold, A. M. Tyryshkin, M. K. Bowman, G. G. Dunham, M. A. Henderson, "The influence of the bulk reduction state on the surface structure and morphology of rutile $TiO_2(110)$ single crystals", *J. Phys. Chem. B* **2000**, *104*, 4944–4950.

[66] B. Zandkarimi, P. Poths, A. N. Alexandrova, "When fluxionality beats size selection: acceleration of ostwald ripening of sub-nano clusters", *Angew. Chem. Int. Ed.*, *Accepted Author Manuscript.*

[67] S. Tauster, S. Fung, "Strong metal-support interactions: occurrence among the binary oxides of groups IIA-VB", *J. Catal.* **1978**, *55*, 29–35.

[68] Z. Wu, Y. Li, W. Huang, "Size-dependent Pt-TiO_2 strong metal–support interaction", *J. Phys. Chem. Lett.* **2020**, *11*, 4603–4607.

[69] B. Han, Y. Guo, Y. Huang, W. Xi, J. Xu, J. Luo, H. Qi, Y. Ren, X. Liu, B. Qiao, T. Zhang, "Strong metal-support interactions between Pt single atoms and TiO_2", *Angew. Chem. Int. Ed.* **2020**, *59*, 11824–11829.

[70] M. Spencer, "Models of strong metal-support interaction (SMSI) in Pt on TiO_2 catalysts", *J. Catal.* **1985**, *93*, 216–223.

[71] D. Jennison, O Dulub, W Hebenstreit, U Diebold, "Structure of an ultrathin TiO_x film, formed by the strong metal support interaction (SMSI), on Pt nanocrystals on $TiO_2(110)$", *Surf. Sci.* **2001**, *492*, L677–L687.

[72] O. Dulub, W. Hebenstreit, U. Diebold, "Imaging cluster surfaces with atomic resolution: the strong metal-support interaction state of Pt supported on $TiO_2(110)$", *Phys. Rev. Lett.* **2000**, *84*, 3646–3649.

[73] Simon Bonanni and Kamel Ait-Mansour and Harald Brune and Wolfgang Harbich, "Overcoming the strong metal - support interaction state: CO oxidation on $TiO_2(110)$-supported Pt nanoclusters", *ACS Catal.* **2011**, *1*, 385–389.

[74] M. Aizawa, S. Lee, S. L. Anderson, "Sintering, oxidation, and chemical properties of size-selected nickel clusters on $TiO_2(110)$", *J. Chem. Phys.* **2002**, *117*, 5001–5011.

[75] C. A. Walenta, M. Tschurl, U. Heiz, "Introducing catalysis in photocatalysis: what can be understood from surface science studies of alcohol photoreforming on TiO_2", *J. Phys.: Condens. Matter* **2019**, *31*, 473002.

[76] M. A. Henderson, S. Otero-Tapia, M. E. Castro, "The chemistry of methanol on the $TiO_2(110)$ surface: the influence of vacancies and coadsorbed species", *Faraday Discuss.* **1999**, *114*, 313 –329.

[77] Z. Zhang, R. Rousseau, J. Gong, S.-C. Li, B. D. Kay, Q. Ge, Z. Dohnálek, "Vacancy-assisted diffusion of alkoxy species on rutile TiO_2(110)", *Phys. Rev. Lett.* **2008**, *101*, 156103.

[78] C. Xu, W. Yang, Z. Ren, D. Dai, Q. Guo, T. K. Minton, X. Yang, "Strong photon energy dependence of the photocatalytic dissociation rate of methanol on TiO_2(110)", *J. Am. Chem. Soc.* **2013**, *135*, 19039–19045.

[79] C. Xu, W. Yang, Q. Guo, D. Dai, M. Chen, X. Yang, "Molecular hydrogen formation from photocatalysis of methanol on TiO_2(110)", *J. Am. Chem. Soc.* **2013**, *135*, 10206–10209.

[80] K. R. Phillips, S. C. Jensen, M. Baron, S.-C. Li, C. M. Friend, "Sequential photo-oxidation of methanol to methyl formate on TiO_2(110)", *J. Am. Chem. Soc.* **2013**, *135*, 574–577.

[81] Z. Li, R. S. Smith, B. D. Kay, Z. Dohnálek, "Determination of absolute coverages for small aliphatic alcohols on TiO_2(110)", *J. Phys. Chem. C* **2011**, *115*, 22534–22539.

[82] S. Liu, A. an Liu, B. Wen, R. Zhang, C. Zhou, L.-M. Liu, Z. Ren, "Coverage dependence of methanol dissociation on TiO_2(110)", *J. Phys. Chem. Lett.* **2015**, *6*, 3327–3334.

[83] A.-a. Liu, S. Liu, R. Zhang, Z. Ren, "Spectral identification of methanol on TiO_2(110) surfaces with sum frequency generation in the C–H stretching region", *J. Phys. Chem. C* **2015**, *119*, 23486–23494.

[84] M. Shen, D. P. Acharya, Z. Dohnálek, M. A. Henderson, "Importance of diffusion in methanol photochemistry on TiO_2(110)", *J. Phys. Chem. C* **2012**, *116*, 25465–25469.

[85] Z. Ma, Q. Guo, X. Mao, Z. Ren, X. Wang, C. Xu, W. Yang, D. Dai, C. Zhou, H. Fan, X. Yang, "Photocatalytic dissociation of ethanol on TiO_2(110) by near-band-gap excitation", *J. Phys. Chem. C* **2013**, *117*, 10336–10344.

[86] Q. Yuan, Z. Wu, Y. Jin, L. Xu, F. Xiong, Y. Ma, W. Huang, "Photocatalytic cross-coupling of methanol and formaldehyde on a rutile TiO_2(110) Surface", *J. Am. Chem. Soc.* **2013**, *135*, 5212–5219.

[87] C. Zhou, Z. Ma, Z. Ren, X. Mao, D. Dai, X. Yang, "Effect of defects on photocatalytic dissociation of methanol on TiO_2(110)", *Chem. Sci.* **2011**, *2*, 1980–1983.

[88] C. Zhou, Z. Ren, S. Tan, Z. Ma, X. Mao, D. Dai, H. Fan, X. Yang, J. LaRue, R. Cooper, A. M. Wodtke, Z. Wang, Z. Li, B. Wang, J. Yang, J. Hou, "Site-specific photocatalytic splitting of methanol on TiO_2(110)", *Chem. Sci.* **2010**, *1*, 575–580.

[89] D. Wei, X. Jin, C. Huang, D. Dai, Z. Ma, W.-X. Li, X. Yang, "Direct imaging single methanol molecule photocatalysis on titania", *J. Phys. Chem. C* **2015**, *119*, 17748–17754.

[90] T. Wang, Q. Hao, Z. Wang, X. Mao, Z. Ma, Z. Ren, D. Dai, C. Zhou, X. Yang, "Deuterium kinetic isotope effect in the photocatalyzed dissociation of methanol on TiO_2(110)", *J. Phys. Chem. C* **2018**, *122*, 26512–26518.

[91] Q. Guo, C. Xu, Z. Ren, W. Yang, Z. Ma, D. Dai, H. Fan, T. K. Minton, X. Yang, "Stepwise photocatalytic dissociation of methanol and water on TiO_2(110)", *J. Am. Chem. Soc.* **2012**, *134*, 13366–13373.

[92] X. Peng, R. Zhang, R.-r. Feng, A.-a. Liu, C. Zhou, Q. Guo, X. Yang, Y. Jiang, Z. Ren, "Active species in photocatalytic reactions of methanol on TiO_2(110) identified by surface sum frequency generation vibrational spectroscopy", *J. Phys. Chem. C* **2019**, *123*, 13789–13794.

[93] S. Dong, J. Hu, S. Xia, B. Wang, Z. Wang, T. Wang, W. Chen, Z. Ren, H. Fan, D. Dai, J. Cheng, X. Yang, C. Zhou, "Origin of the adsorption-state-dependent photoactivity of methanol on TiO_2(110)", *ACS Catal.* **2021**, *11*, 2620–2630.

[94] F. Li, X. Chen, Q. Guo, X. Yang, "Hydrogen production via methanol photocatalysis on Au/rutile-TiO_2(110)", *J. Phys. Chem. C* **2020**, *124*, 26965–26972.

[95] Q. Hao, ZhiqiangWang, T. Wang, Z. Ren, C. Zhou, X. Yang, "Role of Pt loading in the photocatalytic chemistry of methanol on rutile TiO_2(110)", *ACS Catal.* **2019**, *9*, 286–294.

[96] M. Shen, M. A. Henderson, "Role of water in methanol photochemistry on rutile TiO_2(110)", *J. Phys. Chem. C* **2012**, *116*, 18788–18795.

[97] G. Kolesov, D. Vinichenko, G. A. Tritsaris, C. M. Friend, E. Kaxiras, "Anatomy of the photochemical reaction: excited-state dynamics reveals the C–H acidity mechanism of methoxy photo-oxidation on titania", *J. Phys. Chem. Lett.* **2015**, *6*, 1624–1627.

[98] W. Chu, W. A. Saidi, Q. Zheng, Y. Xie, Z. Lan, O. V. Prezhdo, H. Petek, J. Zhao, "Ultrafast dynamics of photongenerated holes at a CH_3OH/TiO_2 rutile interface", *J. Am. Chem. Soc.* **2016**, *138*, 13740–13749.

[99] A. M. Nadeem, J. M. R. Muir, K. A. Connelly, B. T. Adamson, B. J. Metson, H. Idriss, "Ethanol photo-oxidation on a rutile TiO_2(110) single crystal surface", *Phys. Chem. Chem. Phys.* **2011**, *13*, 7637 –7643.

[100] P. M. Jayaweera, E. L. Quah, H. Idriss, "Photoreaction of ethanol on TiO_2(110) single-crystal surface", *J. Phys. Chem. C* **2007**, *111*, 1764 –1769.

[101] S. A. Tenney, B. A. Cagg, M. S. Levine, W. He, K. Manandhar, D. A. Chen, "Enhanced activity for supported Au clusters: methanol oxidation on Au/TiO_2(110)", *Surf. Sci.* **2012**, *606*, 1233–1243.

[102] Y. Kim, B. D. Kay, J. White, Z. Dohnálek, "Inductive effect of alkyl chains on alcohol dehydration at bridge-bonded oxygen vacancies of TiO_2(110)", *Catal. Lett.* **2007**, *119*, 1–4.

[103] Y. K. Kim, B. D. Kay, J. M. White, Z. Dohnalek, "Alcohol chemistry on rutile TiO_2(110): the influence of alkyl substituents on reactivity and selectivity", *J. Phys. Chem. C* **2007**, *111*, 18236–18242.

[104] R. Zhang, H. Wang, X. Peng, R.-r. Feng, A.-a. Liu, Q. Guo, C. Zhou, Z. Ma, X. Yang, Y. Jiang, Z. Ren, "In situ studies on temperature-dependent photocatalytic reactions of methanol on TiO_2(110)", *J. Phys. Chem. C* **2019**, *123*, 9993–9999.

[105] J. Ø. Hansen, R. Bebensee, U. Martinez, S. Porsgaard, E. Lira, Y. Wei, L. Lammich, Z. Li, H. Idriss, F. Besenbacher, B. Hammer, S. Wendt, "Unravelling site-specific photo-reactions of ethanol on rutile TiO_2(110)", *Sci. Rep.* **2016**, *6*, 21990.

[106] Z. Zhang, O. Bondarchuk, B. D. Kay, J. M. White, Z. Dohnálek, "Direct visualization of 2-butanol adsorption and dissociation on TiO_2(110)", *J. Phys. Chem. C* **2007**, *111*, 3021–3027.

[107] Z. Zhang, R. Rousseau, J. Gong, B. D. Kay, Z. Dohnálek, "Imaging hindered rotations of alkoxy species on TiO_2(110)", *J. Am. Chem. Soc.* **2009**, *131*, 17926–17932.

[108] J. Ø. Hansen, P. Huo, U. Martinez, E. Lira, Y. Y. Wei, R. Streber, E. Lægsgaard, B. Hammer, S. Wendt, F. Besenbacher, "Direct evidence for ethanol dissociation on rutile TiO_2(110)", *Phys. Rev. Lett.* **2011**, *107*, 136102–136106.

[109] L. Gamble, L. S. Jung, C. T. Campbell, "Decomposition and protonation of surface ethoxys on TiO_2(110)", *Surf. Sci.* **1996**, *348*, 1–16.

[110] C. A. Walenta, S. L. Kollmannsberger, J. Kiermaier, A. Winbauer, M. Tschurl, U. Heiz, "Ethanol photocatalysis on rutile TiO_2(110): the role of defects and water", *Phys. Chem. Chem. Phys.* **2015**, *17*, 22809–22814.

[111] Q. Guo, C. Zhou, Z. Ma, Z. Ren, H. Fan, X. Yang, "Elementary photocatalytic chemistry on TiO_2 surfaces", *Chem. Soc. Rev.* **2016**, *45*, 3701–3730.

[112] G. Harrison, K. Katsiev, Y. Alsalik, G. Thornton, H. Idriss, "Switch in photocatalytic reaction selectivity: the effect of oxygen partial pressure on carbon-carbon bond dissociation over hydroxylated TiO_2(110) surfaces", *J. Catal.* **2018**, *363*, 117–127.

[113] M. A. Henderson, I. Lyubinetsky, "Molecular-level insights into photocatalysis from scanning probe microscopy studies on TiO_2(110)", *Chem. Rev.* **2013**, *113*, 4428 –4455.

[114] R. Su, N. Dimitratos, J. Liu, E. Carter, S. Althahban, X. Wang, Y. Shen, S. Wendt, X. Wen, J. W. H. Niemantsverdriet, B. B. Iversen, C. J. Kiely, G. J. Hutchings, F. Besenbacher, "Mechanistic insight into the interaction between a titanium dioxide photocatalyst and Pd cocatalyst for improved photocatalytic performance", *ACS Catal.* **2016**, *6*, 4239–4247.

[115] D. Brinkley, T. Engel, "Photocatalytic dehydrogenation of 2-propanol on TiO_2(110)", *J. Phys. Chem. B* **1998**, *102*, 7596 –7605.

[116] D. Brinkley, T. Engel, "Evidence for structure sensitivity in the thermally activated and photocatalytic dehydrogenation of 2-propanol on TiO_2", *J. Phys. Chem. B* **2000**, *104*, 9836 –9841.

[117] F. Xu, X. Chen, W. Yang, X. Wang, X. Yang, Q. Guo, "Coverage-dependent ethylene glycol photochemistry on rutile-TiO_2(110)", *J. Phys. Chem. C* **2020**, *124*, 14632–14639.

[118] J. Plata, V. Collico, A. M. Márquez, J. F. Sanz, "Understanding acetaldehyde thermal chemistry on the TiO_2 (110) rutile surface: from adsorption to reactivity", *J. Phys. Chem. C* **2011**, *115*, 2819–2825.

[119] M. Henderson, N. Deskins, R. Zehr, M. Dupuis, "Generation of organic radicals during photocatalytic reactions on TiO2", *J. Catal.* **2011**, *279*, 205–212.

[120] C. Xu, W. Yang, Q. Guo, D. Dai, X. Yang, "Photoinduced decomposition of acetaldehyde on a reduced TiO_2(110) surface: involvement of lattice oxygen", *Phys. Chem. Chem. Phys.* **2016**, *18*, 30982–30989.

[121] N. G. Petrik, M. A. Henderson, G. A. Kimmel, "Insights into acetone photochemistry on rutile TiO_2(110). 2. New photodesorption channel with CH_3 ejection along the surface normal", *J. Phys. Chem. C* **2015**, *119*, 12273–12282.

[122] N. G. Petrik, M. A. Henderson, G. A. Kimmel, "Insights into acetone photochemistry on rutile TiO_2(110). 1. Off-normal CH_3 ejection from acetone diolate", *J. Phys. Chem. C* **2015**, *119*, 12262–12272.

[123] M. A. Henderson, "Photooxidation of acetone on TiO_2(110): conversion to acetate via methyl radical ejection", *J. Phys. Chem. B* **2005**, *109*, 12062 –12070.

[124] M. A. Henderson, "Relationship of O_2 photodesorption in photooxidation of acetone on TiO_2", *J. Phys. Chem. C* **2008**, *112*, 11433 –11440.

[125] S. C. Jensen, K. R. Phillips, M. Baron, E. C. Landis, C. M. Friend, "Norrish Type I surface photochemistry for butyrophenone on TiO_2(110)", *Phys. Chem. Chem. Phys.* **2013**, *15*, 5193–5201.

[126] C. Xu, W. Yang, Q. Guo, D. Dai, T. K. Minton, X. Yang, "Photoinduced decomposition of formaldehyde on a TiO_2(110) surface, assisted by bridge-bonded oxygen atoms", *J. Phys. Chem. Lett.* **2013**, *4*, 2668–2673.

[127] Q. Yuan, Z. Wu, Y. Jin, F. Xiong, W. Huang, "Surface chemistry of formaldehyde on rutile TiO_2(110) surface: photocatalysis vs thermal-Catalysis", *J. Phys. Chem. C* **2014**, *118*, 20420–20428.

[128] M. A. Henderson, "Complexity in the decomposition of formic acid on the TiO_2(110) surface", *J. Phys. Chem. B* **1997**, *101*, 221–229.

[129] S. L. Kollmannsberger, C. A. Walenta, C. Courtois, M. Tschurl, U. Heiz, "Thermal control of selectivity in photocatalytic, water-free alcohol photoreforming", *ACS Catal.* **2018**, *8*, 11076–11084.

[130] V. N. Popok, I. Barke, E. E. Campbell, K.-H. Meiwes-Broer, "Cluster-surface interaction: from soft landing to implantation", *Surf. Sci. Rep.* **2011**, *66*, 347 –377.

[131] U. Heiz, F. Vanolli, L. Trento, W.-D. Schneider, "Chemical reactivity of size-selected supported clusters: an experimental setup", *Rev. Sci. Instrum.* **1997**, *68*, 1986–1994.

[132] J. B. Hopkins, P. R. R. Langridge-Smith, M. D. Morse, R. E. Smalley, "Supersonic metal cluster beams of refractory metals: spectral investigations of ultracold Mo_2", *J. Chem. Phys.* **1983**, *78*, 1627–1637.

[133] M. König, PhD thesis, Technische Universität München, **2015**.

[134] W. A. de Heer, "The physics of simple metal clusters: experimental aspects and simple models", *Rev. Mod. Phys.* **1993**, *65*, 611–676.

[135] U. Heiz, U. Landman, *Nanocatalysis (Nanoscience and Technology)*, 1., Springer Berlin / Heidelberg, **2007**.

[136] T. Masubuchi, J. F. Eckhard, K. Lange, B. Visser, M. Tschurl, U. Heiz, "An efficient laser vaporization source for chemically modified metal clusters characterized by thermodynamics and kinetics", *Rev. Sci. Instrum.* **2018**, *89*, 023104.

[137] F. F. Schweinberger, PhD thesis, Technische Universität München, **2013**.

[138] C. A. Walenta, PhD thesis, Technische Universität München, **2018**.

[139] S. L. Kollmannsberger, PhD thesis, Technische Universität München, **2015**.

[140] J. Kiermaier, PhD thesis, Technische Universität München, **2013**.

[141] A. Winbauer, PhD thesis, Technische Universität München, **2014**.

[142] J. W. Niemantsverdriet, I. Chorkendorff, *Concepts of Modern Catalysis and Kinetics*, 2., Wiley-VCH, **2007**.

[143] J. John T. Yates, *Experimental Innovations in Surface Science*, 2nd Edition, Springer International Publishing, **2015**.

[144] N. G. Petrik, G. A. Kimmel, "Off-normal CO_2 desorption from the photooxidation of CO on reduced TiO_2(110)", *J. Phys. Chem. Lett.* **2010**, *1*, 2508–2513.

[145] R. Zehr, M. Henderson, "Acetaldehyde photochemistry on TiO_2(110)", *Surf. Sci.* **2008**, *602*, 2238–2249.

[146] N. G. Petrik, R. Mu, A. Dahal, Z. Wang, I. Lyubinetsky, G. A. Kimmel, "Diffusion and photon stimulated desorption of CO on TiO_2(110)", *J. Phys. Chem. C* **2018**.

[147] D. P. Wilson, D. Sporleder, M. G. White, "Final state distributions of methyl photoproducts from the photooxidation of acetone on TiO_2(110)", *J. Phys. Chem. C* **2012**, *116*, 16541–16552.

[148] Dohnalek, Z. and Lyubinetsky, I. and Rousseau, R., "Thermally-driven processes on rutile TiO_2(110)-(1×1): a direct view at the atomic scale", *Prog. Surf. Sci.* **2010**, *85*, 161–205.

[149] W. S. Epling, C. H. Peden, M. A. Henderson, U. Diebold, "Evidence for oxygen adatoms on TiO_2(110) resulting from O_2 dissociation at vacancy sites", *Surf. Sci.* **1998**, *412-413*, 333–343.

[150] M. A. Henderson, "An HREELS and TPD study of water on TiO_2(110): the extent of molecular versus dissociative adsorption", *Surf. Sci.* **1996**, *355*, 151–166.

[151] I. M. Brookes, C. A. Muryn, G. Thornton, "Imaging water dissociation on TiO_2(110)", *Phys. Rev. Lett.* **2001**, *87*, 266103.

[152] M. A. Henderson, "Structural sensitivity in the dissociation of water on TiO_2 single-crystal surfaces", *Langmuir* **1996**, *12*, 5093–5098.

[153] R. T. Zehr, M. A. Henderson, "Influence of O_2-induced surface roughening on the chemistry of water on TiO_2(110)", *Surf. Sci.* **2008**, *602*, 1507–1516.

[154] R. Schaub, P. Thostrup, N. Lopez, E. Lægsgaard, I. Stensgaard, J. K. Nørskov, F. Besenbacher, "Oxygen vacancies as active sites for water dissociation on rutile TiO_2(110)", *Phys. Rev. Lett.* **2001**, *87*, 266104.

[155] Z. Geng, X. Jin, R. Wang, X. Chen, Q. Guo, Z. Ma, D. Dai, H. Fan, X. Yang, "Low-temperature hydrogen production via water conversion on Pt/TiO_2", *J. Phys. Chem. C* **2018**, *122*, 10956–10962.

[156] M. Li, W. Hebenstreit, L. Gross, U. Diebold, M. Henderson, D. Jennison, P. Schultz, M. Sears, "Oxygen-induced restructuring of the TiO_2(110) surface: a comprehensive study", *Surf. Sci.* **1999**, *437*, 173–190.

[157] C. Courtois, Master's thesis, Technische Universität München, **2017**.

[158] C. A. Walenta, S. L. Kollmannsberger, C. Courtois, M. Tschurl, U. Heiz, "Photocatalytic selectivity switch to C-C scission: α-methyl ejection of tert-butanol on TiO_2(110)", *Phys. Chem. Chem. Phys.* **2018**, *20*, 7105–7111.

[159] E. Farfan-Arribas, R. J. Madix, "Role of defects in the adsorption of aliphatic alcohols on the TiO_2(110) surface", *J. Phys. Chem. B* **2002**, *106*, 10680–10692.

[160] M. A. Henderson, "Photooxidation and photodesorption in the photochemistry of isobutene on TiO_2(110)", *J. Phys. Chem. C* **2013**, *117*, 14113 –14124.

[161] C. Courtois, C. A. Walenta, M. Tschurl, U. Heiz, C. M. Friend, "Regulating photochemical selectivity with temperature: Isobutanol on TiO_2(110)", *J. Am. Chem. Soc.* **2020**, *142*, 13072–13080.

[162] L. I. Granone, F. Sieland, N. Zheng, R. Dillert, D. W. Bahnemann, "Photocatalytic conversion of biomass into valuable products: a meaningful approach?", *Green Chem.* **2018**, *20*, 1169–1192.

[163] S. Y. Lee, H. U. Kim, T. U. Chae, J. S. Cho, J. W. Kim, J. H. Shin, D. I. Kim, Y.-S. Ko, W. D. Jang, Y.-S. Jang, "A comprehensive metabolic map for production of bio-based chemicals", *Nat. Catal.* **2019**, *2*, 18–33.

[164] P. P. Peralta-Yahya, F. Zhang, S. B. del Cardayre, J. D. Keasling, "Microbial engineering for the production of advanced biofuels", *Nature* **2012**, *488*, 320–328.

[165] M. Cargnello, A. Gasparotto, V. Gombac, T. Montini, D. Barreca, P. Fornasiero, "Photocatalytic H_2 and added-value by-products – The role of metal oxide systems in their synthesis from oxygenates", *Eur. J. Inorg. Chem.* **2011**, *28*, 4309–4323.

[166] R. Rinaldi, F. Schüth, "Design of solid catalysts for the conversion of biomass", *Energy Environ. Sci.* **2009**, *2*, 610–626.

[167] Z.-T. Wang, M. A. Henderson, I. Lyubinetsky, "Origin of coverage dependence in photoreactivity of carboxylate on TiO_2(110): hindering by charged coadsorbed hydroxyls", *ACS Catal.* **2015**, *11*, 6463–6467.

[168] X. Mao, D. Wei, Z. Wang, X. Jin, Q. Hao, Z. Ren, D. Dai, Z. Ma, C. Zhou, X. Yang, "Recombination of formaldehyde and hydrogen atoms on TiO_2(110)", *J. Phys. Chem. C* **2015**, *119*, 1170–1174.

[169] S. Chen, L.-W. Wang, "Thermodynamic oxidation and reduction potentials of photocatalytic semiconductors in aqueous solution", *Chem. Mat.* **2012**, *24*, 3659–3666.

[170] T. R. Esch, T. Bredow, "Band positions of rutile surfaces and the possibility of water splitting", *Surf. Sci.* **2017**, *664*, 20–27.

[171] C. A. Walenta, S. L. Kollmannsberger, C. Courtois, R. N. Pereira, M. Stutzmann, M. Tschurl, U. Heiz, "Why co-catalyst-loaded rutile facilitates photocatalytic hydrogen evolution", *Phys. Chem. Chem. Phys.* **2019**, *21*, 1491–1496.

[172] C. A. Walenta, C. Courtois, S. L. Kollmannsberger, M. Eder, M. Tschurl, U. Heiz, "Surface species in photocatalytic methanol reforming on Pt/TiO_2(110): learning from surface science experiments for catalytically relevant conditions", *ACS Catal.* **2020**, *10*, 4080–4091.

[173] B. A. Sexton, "Methanol decomposition on platinum (111)", *Surf. Sci.* **1981**, *102*, 271–281.

[174] S. E. Davis, M. S. Ide, R. J. Davis, "Selective oxidation of alcohols and aldehydes over supported metal nanoparticles", *Green Chem.* **2013**, *15*, 17–45.

[175] C. P. Vinod, K. Wilson, A. F. Lee, "Recent advances in the heterogeneously catalysed aerobic selective oxidation of alcohols", *J. Chem. Technol. Biotechnol.* **2011**, *86*, 161–171.

[176] C. Courtois, M. Eder, K. Schnabl, C. A. Walenta, M. Tschurl, U. Heiz, "Reactions in the photocatalytic conversion of tertiary alcohols on rutile TiO_2(110)", *Angew. Chem. Int. Ed.* **2019**, *58*, 14255–14259.

[177] I. Chorkendorff, J. N. Russell, J. T. Yates, "Hydrogen implantation in Ni(111) - a study of H_2 desorption dynamics from the bulk", *Surf. Sci.* **1987**, *182*, 375–389.

[178] B. E. Koel, D. E. Peebles, J. M. White, "Low temperature coadsorption of hydrogen and carbon monoxide on Ni(100): I. TPD, Δ, and UPS studies", *Surf. Sci.* **1983**, *125*, 709–738.

[179] W.-T. Chen, A. Chan, D. Sun-Waterhouse, T. Moriga, H. Idriss, G. I. Waterhouse, "Ni/TiO_2: a promising low-cost photocatalytic system for solar H_2 production from ethanol-water mixtures", *J. Catal.* **2015**, *326*, 43–53.

[180] H. Bahruji, M. Bowker, P. R. Davies, J. Kennedy, D. J. Morgan, "The importance of metal reducibility for the photo-reforming of methanol on transition metal-TiO_2 photocatalysts and the use of non-precious metals", *Int. J. Hydrogen Energy* **2015**, *40*, 1465–1471.

[181] E. P. Melián, M. N. Suárez, T. Jardiel, J. M. D. Rodríguez, A. C. Caballero, J. Araña, D. G. Calatayud, O. G. Díaz, "Influence of nickel in the hydrogen production activity of TiO_2", *Appl. Catal., B: Environ.* **2014**, *152-153*, 192–201.

[182] J. B. Joo, R. Dillon, I. Lee, Y. Yin, C. J. Bardeen, F. Zaera, "Promotion of atomic hydrogen recombination as an alternative to electron trapping for the role of metals in the photocatalytic production of H2", *Proc. Natl. Acad. Sci. U.S.A.* **2014**, *111*, 7942–7947.

[183] P. D. Tran, L. Xi, S. K. Batabyal, L. H. Wong, J. Barber, J. S. Chye Loo, "Enhancing the photocatalytic efficiency of TiO_2 nanopowders for H_2 production by using non-noble transition metal co-catalysts", *Phys. Chem. Chem. Phys.* **2012**, *14*, 11596–11599.

[184] J. Yu, Y. Hai, B. Cheng, "Enhanced photocatalytic H_2-production activity of TiO_2 by $Ni(OH)_2$ cluster modification", *J. Phys. Chem. C* **2011**, *115*, 4953–4958.

[185] L. T. Prahov, J. Disdier, J. M. Herrmann, P. Pichat, "Room temperature hydrogen production from aliphatic alcohols over UV-illuminated powder Ni/TiO_2 catalysts", *Int. J. Hydrogen Energy* **1984**, *9*, 397–403.

[186] M. Eder, C. Courtois, T. Kratky, S. Günther, M. Tschurl, U. Heiz, "Nickel clusters on TiO_2(110): thermal chemistry and photocatalytic hydrogen evolution of methanol", *Catal. Sci. Technol.* **2020**, *10*, 7630–7639.

[187] R. E. Tanner, I. Goldfarb, M. R. Castell, G. A. D. Briggs, "The evolution of Ni nanoislands on the rutile TiO_2(110) surface with coverage, heating and oxygen treatment", *Surf. Sci.* **2001**, *486*, 167–184.

[188] C. T. Campbell, "Ultrathin metal films and particles on oxide surfaces: structural, electronic and chemisorptive properties", *Surf. Sci. Rep.* **1997**, *27*, 1–111.

[189] Z. H. N. Al-Azri, M. AlOufi, A. Chan, G. I. N. Waterhouse, H. Idriss, "Metal particle size effects on the photocatalytic hydrogen ion reduction", *ACS Catal.* **2019**, *9*, 3946–3958.

[190] D. Wang, Z.-P. Liu, W.-M. Yang, "Revealing the size effect of platinum cocatalyst for photocatalytic hydrogen evolution on TiO_2 support: a DFT study", *ACS Catal.* **2018**, *8*, 7270–7278.

[191] U. Heiz, "Size-selected, supported clusters: the interaction of carbon monoxide with nickel clusters", *Appl. Phys. A* **1998**, *67*, 621–626.

[192] B. E. Conway, G. Jerkiewicz, "Relation of energies and coverages of underpotential and overpotential deposited H at Pt and other metals to the 'volcano curve'for cathodic H_2 evolution kinetics", *Electrochimi. Acta* **2000**, *45*, 4075–4083.

[193] J. K. Norskov, T. Bligaard, J. Rossmeisl, C. H. Christensen, "Towards the computational design of solid catalysts", *Nat. Chem.* **2009**, *1*, 37 –46.

[194] P. Quaino, F. Juarez, E. Santos, W. Schmickler, "Volcano plots in hydrogen electrocatalysis - uses and abuses", *Beilstein J. Nanotechnol.* **2014**, *5*, 846–854.

[195] K. D. Childs, B. A. Carlson, L. A. Vanier, J. F. Moulder, D. F. Paul, W. F. Stickle, D. G. Watson, *Handbook of Auger Electron Spectroscopy*, Physical Electronics Industries, **1995**.

[196] G.-F. Wei, Z.-P. Liu, "Restructuring and hydrogen evolution on Pt nanoparticle", *Chem. Sci.* **2015**, *6*, 1485–1490.

[197] C. Dessal, L. Martínez, C. Maheu, T. Len, F. Morfin, J. L. Rousset, E. Puzenat, P. Afanasiev, M. Aouine, L. Soler, J. Llorca, L. Piccolo, "Influence of Pt particle size and reaction phase on the photocatalytic performances of ultradispersed Pt/TiO_2 catalysts for hydrogen evolution", *J. Catal.* **2019**, *375*, 155–163.

[198] F. Neuberger, J. Baranyai, T. Schmidt, T. Cottre, B. Kaiser, W. Jaegermann, R. Schäfer, "From bulk to atoms: the influence of particle and cluster size on the hydrogen evolution reaction", *Z. Phys. Chem.* **2020**, *234*, 847–865.

[199] A. S. Crampton, M. D. Rötzer, C. J. Ridge, F. F. Schweinberger, U. Heiz, B. Yoon, U. Landman, "Structure sensitivity in the nonscalable regime explored via catalysed ethylene hydrogenation on supported platinum nanoclusters", *Nat. Commun.* **2016**, *7*.

[200] H. Wang, J. Lu, "A review on particle size effect in metal-catalyzed heterogeneous reactions", *Chinese J. Chem.* **2020**, *38*, 1422–1444.

[201] M. A. Röttgen, S. Abbet, K. Judai, J.-M. Antonietti, A. S. Wörz, M. Arenz, C. R. Henry, U. Heiz, "Cluster chemistry: size-dependent reactivity induced by reverse spill-over", *J. Am. Chem. Soc.* **2007**, *129*, 9635 –9639.

[202] T. Ishida, T. Murayama, A. Taketoshi, M. Haruta, "Importance of size and contact structure of gold nanoparticles for the genesis of unique catalytic processes", *Chem. Rev.* **2020**, *120*, 464–525.

[203] G. R. Bamwenda, S. Tsubota, T. Nakamura, M. Haruta, "Photoassisted hydrogen production from a water-ethanol solution: a comparison of activities of $Au\text{-}TiO_2$ and $Pt\text{-}TiO_2$", *J. Photochem. Photobiol., A* **1995**, *89*, 177 –189.

[204] A. Mills, M. Bingham, C. O'Rourke, M. Bowker, "Modelled kinetics of the rate of hydrogen evolution as a function of metal catalyst loading in the photocatalysed reforming of methanol by Pt (or Pd)/TiO_2", *J. Photochem. Photobiol., A* **2019**, *373*, 122–130.

[205] S. J. Tauster in *Strong Metal-Support Interactions*, *Vol. 298*, American Chemical Society, **1986**, pp. 1–9.

[206] X. Y. Shi, W. Zhang, C. Zhang, W. T. Zheng, H. Chen, J. G. Qi, "Real-space observation of strong metal-support interaction: state-of-the-art and what's the next", *J. Micros.* **2016**, *262*, 203–215.

[207] T. W. van Deelen, C. Hernández Mejía, K. P. de Jong, "Control of metal-support interactions in heterogeneous catalysts to enhance activity and selectivity", *Nat. Catal.* **2019**, *2*, 955–970.

[208] K. Liu, X. Zhao, G. Ren, T. Yang, Y. Ren, A. F. Lee, Y. Su, X. Pan, J. Zhang, Z. Chen, J. Yang, X. Liu, T. Zhou, W. Xi, J. Luo, C. Zeng, H. Matsumoto, W. Liu, Q. Jiang, K. Wilson, A. Wang, B. Qiao, W. Li, T. Zhang, "Strong metal-support interaction promoted scalable production of thermally stable single-atom catalysts", *Nat. Commun.* **2020**, *11*, 1263.

[209] I. Jiménez-Morales, S. Cavaliere, D. Jones, J. Rozière, "Strong metal–support interaction improves activity and stability of Pt electrocatalysts on doped metal oxides", *Phys. Chem. Chem. Phys.* **2018**, *20*, 8765–8772.

[210] B. M. Stühmeier, S. Selve, M. U. M. Patel, T. N. Geppert, H. A. Gasteiger, H. A. El-Sayed, "Highly selective Pt/TiO_x catalysts for the hydrogen oxidation reaction", *ACS Appl. Energy Mater.* **2019**, *2*, 5534–5539.

[211] T. N. Geppert, M. Bosund, M. Putkonen, B. M. Stühmeier, A. T. Pasanen, P. Heikkilä, H. A. Gasteiger, H. A. El-Sayed, "HOR activity of Pt-TiO_{2-Y} at unconventionally high potentials explained: the influence of SMSI on the electrochemical behavior of Pt", *J. Electrochem. Soc.* **2020**, *167*, 084517.

[212] F. Pesty, H.-P. Steinrück, T. E. Madey, "Thermal stability of Pt films on TiO_2(110): evidence for encapsulation", *Surf. Sci.* **1995**, *339*, 83–95.

[213] M. A. Aramendía, J. C. Colmenares, A. Marinas, J. M. Marinas, J. M. Moreno, J. A. Navío, F. J. Urbano, "Effect of the redox treatment of Pt/TiO_2 system on its photocatalytic behaviour in the gas phase selective photooxidation of propan-2-ol", *Catal. Today* **2007**, *128*, 235–244.

[214] J. C. Colmenares, A. Magdziarz, M. A. Aramendia, A. Marinas, J. Marinas, F. J. Urbano, J. Navio, "Influence of the strong metal support interaction effect (SMSI) of Pt/TiO_2 and Pd/TiO_2 systems in the photocatalytic biohydrogen production from glucose solution", *Catal. Commun.* **2011**, *16*, 1–6.

[215] F. Rieboldt, S. Helveg, R. Bechstein, L. Lammich, F. Besenbacher, J. V. Lauritsen, S. Wendt, "Formation and sintering of Pt nanoparticles on vicinal rutile TiO_2 surfaces", *Phys. Chem. Chem. Phys.* **2014**, *16*, 21289–21299.

[216] W. E. Kaden, W. A. Kunkel, F. S. Roberts, M. Kane, S. L. Anderson, "CO adsorption and desorption on size-selected Pd_n/TiO_2(110) model catalysts: size dependence of binding sites and energies, and support-mediated adsorption", *J. Chem. Phys.* **2012**, *136*, 204705.

[217] M. Moldovan, S. Rauch, G. M. Morrison, M. Gómez, M. Antonia Palacios, "Impact of ageing on the distribution of platinum group elements and catalyst poisoning elements in automobile catalysts", *Surf. Interface Anal.* **2003**, *35*, 354–359.

[218] G. Somorjai, "On the mechanism of sulfur poisoning of platinum catalysts", *J. Catal.* **1972**, *27*, 453–456.

[219] J. H. Pazmiño, C. Bai, J. T. Miller, F. H. Ribeiro, W. N. Delgass, "Effects of support on sulfur tolerance and regeneration of Pt catalysts measured by ethylene hydrogenation and EXAFS", *Catal. Lett.* **2013**, *143*, 1098–1107.

[220] H. S. Gandhi, M. Shelef, "Effects of sulphur on noble metal automotive catalysts", *Appl. Catal.* **1991**, *77*, 175–186.

[221] M. A. Vannice, C. C. Twu, S. H. Moon, "SMSI effects on CO adsorption and hydrogenation on Pt catalysts: I. Infrared spectra of adsorbed CO prior to and during reaction conditions", *J. Catal.* **1983**, *79*, 70–80.

[222] A. Maeda, F. Yamakawa, K. Kunimori, T. Uchijima, "Effect of strong metal-support interaction (SMSI) on ethylene hydroformylation over niobia-supported palladium catalysts", *Catal. Lett.* **1990**, *4*, 107–112.

[223] A. S. Crampton, M. D. Rötzer, U. Landman, U. Heiz, "Can support acidity predict sub-nanometer catalyst activity trends?", *ACS Catal.* **2017**.

[224] T. P. Beebe, J. T. Yates, "Spectroscopic detection of (111) facets on supported Pd crystallites: site blocking by ethylidyne on Pd/Al_2O_3", *Surf. Sci.* **1986**, *173*, 606–612.

[225] M. J. Lundwall, S. M. McClure, D. W. Goodman, "Probing terrace and step sites on Pt nanoparticles using CO and ethylene", *J. Phys. Chem. C* **2010**, *114*, 7904–7912.

[226] D. C. Meier, D. W. Goodman, "The influence of metal cluster size on adsorption energies: CO adsorbed on Au clusters supported on TiO_2", *J. Am. Chem. Soc.* **2004**, *126*, 1892–1899.

[227] M. D. Rötzer, M. Krause, M. Huber, F. F. Schweinberger, A. S. Crampton, U. Heiz, "Ethylene hydrogenation on supported Pd nanoparticles: influence of support on catalyst activity and deactivation", *J. Catal.* **2021**, *397*, 90–97.

[228] S. Schäfer, S. A. Wyrzgol, R. Caterino, A. Jentys, S. J. Schoell, M. Hävecker, A. Knop-Gericke, J. A. Lercher, I. D. Sharp, M. Stutzmann, "Platinum nanoparticles on gallium nitride surfaces: effect of semiconductor doping on nanoparticle reactivity", *J. Am. Chem. Soc.* **2012**, *134*, 12528–12535.

[229] J. Kräuter, L. Mohrhusen, F. Waidhas, O. Brummel, J. Libuda, K. Al-Shamery, "Photoconversion of 2-propanol on rutile titania: a combined liquid-phase and surface science study", *J. Phys. Chem. C* **2021**, *125*, 3355–3367.

[230] K. Domen, A. Kudo, T. Onishi, "Mechanism of photocatalytic decomposition of water into H_2 and O_2 over $NiO/SrTiO_3$", *J. Catal.* **1986**, *102*, 92–98.

[231] M. Qureshi, A. T. Garcia-Esparza, G. Jeantelot, S. Ould-Chikh, A. Aguilar-Tapia, J.-L. Hazemann, J.-M. Basset, D. Loffreda, T. Le Bahers, K. Takanabe, "Catalytic consequences of ultrafine Pt clusters supported on SrTiO3 for photocatalytic overall water splitting", *J. Catal.* **2019**, *376*, 180–190.

[232] K. E. Sanwald, T. F. Berto, A. Jentys, D. M. Camaioni, O. Y. Gutiérrez, J. A. Lercher, "Kinetic coupling of water splitting and photoreforming on $SrTiO_3$-based photocatalysts", *ACS Catal.* **2018**.

[233] L.-Q. Wang, K. F. Ferris, G. S. Herman, "Interactions of H_2O with $SrTiO_3(100)$ surfaces", *J. Vac. Sci. Technol., A* **2002**, *20*, 239–244.

[234] S. Azad, M. H. Engelhard, L.-Q. Wang, "Adsorption and reaction of CO and CO_2 on oxidized and reduced $SrTiO_3(100)$ surfaces", *J. Phys. Chem. B* **2005**, *109*, 10327–10331.

[235] L.-Q. Wang, K. F. Ferris, S. Azad, M. H. Engelhard, "Adsorption and reaction of methanol on stoichiometric and defective $SrTiO_3(100)$ surfaces", *J. Phys. Chem. B* **2005**, *109*, 4507–4513.

Appendices

A Publications

A.1 Photocatalytic Selectivity Switch to C-C Scission: α-Methyl Ejection of *tert*-butanol on $TiO_2(110)$

PCCP

PAPER

View Article Online
View Journal | View Issue

Cite this: *Phys. Chem. Chem. Phys.*, 2018, **20**, 7105

Photocatalytic selectivity switch to C–C scission: α-methyl ejection of *tert*-butanol on TiO_2(110)†

Constantin A. Walenta,‡[ab] Sebastian L. Kollmannsberger,‡[a] Carla Courtois,[a] Martin Tschurl[a] and Ueli Heiz*[ab]

The thermal and photochemical mechanistic pathways for tertiary alcohols on the rutile TiO_2(110)-surface are studied with the example of *tert*-butanol. While the thermal reaction is known to yield isobutene, the photochemical ejection of a methyl radical is observed at 100 K. The C–C scission, which is accompanied by the formation of acetone, is the only photochemical reaction pathway at this temperature and can be attributed to the reaction of photoholes that are created upon UV-light illumination at the surface of the n-type semiconductor. At 293 K the selectivity of the reaction changes, as isobutene is additionally formed photochemically. A comparison of the kinetics of the different reactions reveals further insights. Together with the quantitative evaluation of the reaction products at low temperatures and the comparison of the reaction pathways at different temperatures it is demonstrated how thermal effects can influence the selectivity of the reactions in photocatalysis.

Received 11th January 2018,
Accepted 6th February 2018

DOI: 10.1039/c8cp00223a

rsc.li/pccp

1 Introduction

While photocatalysis is currently increasingly studied in the context of energy production and storage, it is also an often used approach for the decomposition of organic pollutants.[1] In this regard, titania is one of the most often applied materials, as this substance offers a rich oxidation catalysis of organics. The underlying reaction pathways may also be exploited in other fields of chemistry as for example, biomass conversion to fuels or high-value chemicals. These chemical processes are still limited by a lack of selectivity and new reaction pathways are highly desired.[2] In this regard, primary, secondary and tertiary alcohols are structural motifs that are often found in the conversion of biomass. Furthermore, *tert*-butanol, which is studied in this work, is a common additive to fuels as a gasoline octane booster, although its effects on the environment are still under investigation.[3,4] While titania exists in different modifications, rutile TiO_2(110) is by far the most researched surface.[1,5] While the detailed mechanisms *via* α-H abstraction of alkoxy species are known for methanol,[6,7] ethanol[8] and iso-propanol[9] on this surface, tertiary alcohols have hitherto been neglected in photocatalytic studies on single crystal surfaces. This may be because textbooks about organic chemistry usually state that tertiary alcohols are inert towards oxidation.[10] Nevertheless, attempts have been tried to use platinum-loaded TiO_2 (P25) particles for the photochemical conversion of *tert*-butanol.[11,12] It was shown that the alcohol can indeed be converted into a variety of products. However, the exact reaction pathways remained elusive, which was also the case when this alcohol was added to steer the selectivity of the photooxidation towards aldehydes in a different study.[13]

The thermal chemistry of *tert*-butanol exhibits a dehydration pathway to isobutene *via* a concerted E2-elimination of water instead of an oxidation reaction.[14] Furthermore, Dohnalek and co-workers have only recently reported a new thermal reaction pathway of phenylmethanol to methylbenzene and benzylradicals, because the benzene ring stabilizes the radical species.[15] As in the case of *tert*-butanol an α-hydride elimination is disabled, similarly direct deoxygenation occurs in the thermal reaction.[14] In this work, we study the photochemical reaction mechanism of the rutile reduced TiO_2(110) surface [r-TiO_2(110)] for *tert*-butanol. It is shown how the thermal and photochemical reaction steps contribute to the selectivity of the overall reaction outcome.

2 Experimental

The experiments were carried out in an ultrahigh vacuum (UHV) apparatus equipped for photochemical measurements

[a] *Chair of Physical Chemistry, Department of Chemistry and Catalysis Research Center, Technische Universität München, Lichtenbergstrasse 4, 85748 Garching, Germany. E-mail: ulrich.heiz@mytum.de; Fax: +49 (0)89 289 13389; Tel: +49 (0)89 289 13391*

[b] *Nanosystems Initiative Munich (NIM), Schellingstr. 4, 80799 Munich, Germany*

† Electronic supplementary information (ESI) available: detailed description of the product analysis, coverage dependent TPD experiments of *tert*-butanol, a product analysis of a TPD experiment as well as the coverage-dependent product distribution of the *tert*-butanol thermal experiments. Furthermore, the ratio of formed methyl-radical and methane is shown and isothermal illumination experiments at different temperatures are presented. See DOI: 10.1039/c8cp00223a

‡ Contributed equally to this work.

View Article Online
Paper PCCP

as described previously.[16,17] The cylindrical TiO_2(110) single crystal (Surface-net GmbH) is mounted on a 1 mm thick tantalum plate with tantalum clamps and a very thin gold foil to ensure good thermal conductivity. Crystal cleaning was accomplished by cycles of Ar^+-sputtering (5.0×10^{-6} mbar, 20 min, 100 K, 11.8 μA), annealing in oxygen (1×10^{-6} mbar, 820 K, 20 min) and vacuum annealing (820 K, 10 min) and no impurities were detected in the Auger electron spectra. The defect concentration of the reduced, blue crystal (denoted r-TiO_2(110)) was determined by H_2O temperature programmed desorption (TPD) to be about 6% ± 1%.[18] Thermal and photo-desorption experiments were carried out in a line of sight geometry with respect to the quadrupole mass spectrometer (QMA 430, Pfeiffer Vacuum GmbH) with a distance of about 4 mm to the skimmer. UV illumination of the sample was accomplished by a frequency doubled OPO laser (GWU, premiScan ULD/400) that is pumped by the third harmonic of a Nd:YAG-laser (Innolas Spitlight HighPower 1200, 7 ns pulse width, 20 Hz repetition rate). The as-generated light pulses (700 μJ per pulse, 242 nm) illuminate the sample entirely. Laser induced thermal heating effects were not observed and *tert*-butanol did not show any absorption in the UV-vis spectra in the spectral region of the illumination. The *tert*-Butanol (2-methyl-2-propanol, Sigma-Aldrich, ≥99.5%) and *tert*-butanol-OD (2-methyl-2-propan(ol-d), Sigma Aldrich, 99 atom% D) were cleaned by pump–thaw cycles and dosed *via* background dosing. The coverages are referenced to the number of Ti^{4+}-sites, for which a monolayer is normalized to the H_2O desorption yield from all Ti-sites (1 ML ≡ 5.2×10^{14} sites per cm^{-2}). Further experimental details including product identification, cracking pattern correction and ionization sensitivities are given in the ESI.† The photon-stimulated desorption (PSD) experiments are carried out by recording mass traces of products desorbing from the semiconductor under isothermal conditions at a given temperature.

3 Results and discussion

While the photochemical reaction behavior of tertiary alcohols has so far not been investigated on single crystalline surfaces, the thermal reaction pathway of *tert*-butanol is already quite well understood. In good agreement with the literature,[14,19] it is found that *tert*-butanol reacts *via* dehydration to isobutene, which occurs at around 425 K. In experiments with the deuterated *tert*-butanol-OD, HDO is identified as a by-product at the reaction temperature of 425 K (Fig. S1 and S2, ESI†). The coverage dependent molecule yields (Fig. S3, ESI†) show that the thermal reactivity levels off after the coverage of all Ti-sites on the surface.[14] When the n-type semiconductor r-TiO_2(110)-surface, which has been previously covered with 0.18 ML of *tert*-butanol, is illuminated with UV light, photon-generated holes reach the surface and methyl-radical ejection is observed at 100 K (Fig. 1a). While a similar photochemical methyl-ejection from organic compounds has been observed previously for ketones[20–25] and acetaldehyde[26] on oxidized TiO_2(110) [o-TiO_2(110)] or in an oxygen atmosphere,[27] this pathway has so far not been identified for the reaction of alcohols. This signal is

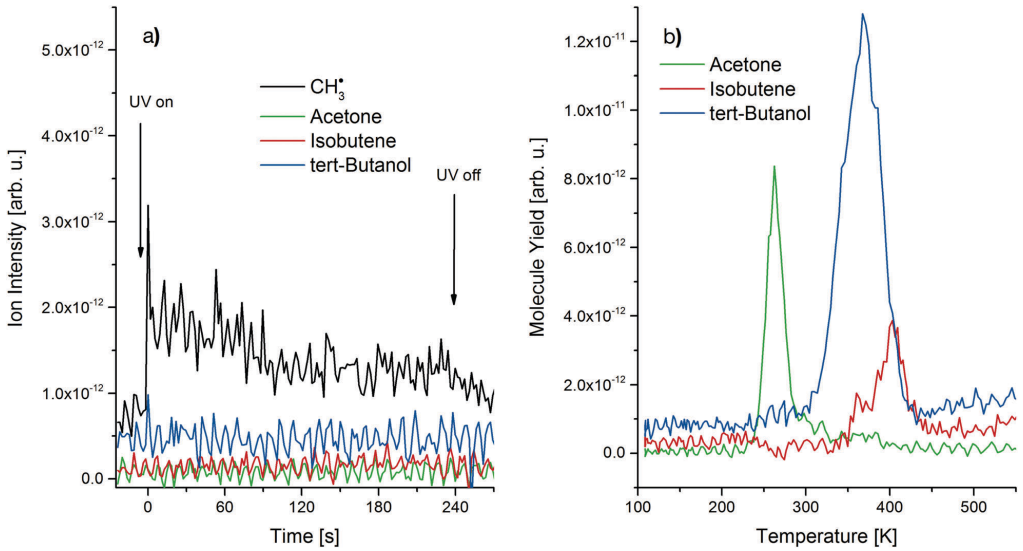

Fig. 1 (a) Isothermal photodesorption yield *vs.* time for 0.18 ML *tert*-butanol-OD at 100 K on a r-TiO_2(110) surface. When the sample is irradiated with UV light, a CH_3-radical is ejected from the *tert*-butanol, but further molecules do not desorb either due to the thermal or the photochemical reactions. In the right panel (b), a post-irradiation TPD experiment is shown after 20 min of UV illumination. The photo product acetone is observed around 270 K as well as the thermal dehydration product isobutene and unreacted *tert*-butanol.

indeed a methyl-radical as verified by a comparison of the masses 15 and 16 (Fig. S4, ESI†).

As for tertiary alcohols the usual photochemical reaction pathway[6–8,29] *via* the abstraction of an α-H is intrinsically excluded, the reaction with photoholes instead initiates the cleavage of a C–C bond. More detailed insights into the reaction pathways are obtained by subsequent post-irradiation TPD experiments (see Fig. 1b for 20 min illumination). These experiments reveal the formation of three different species: acetone is identified as the resulting product from the photocatalytic methyl radical ejection. In addition, unreacted *tert*-butanol and isobutene, which is similarly observed in the TPDs without illumination (Fig. S2, ESI†), are detected. Auger electron spectroscopy after the TPD experiments (data not shown) indicates that neither the alcohols nor the ketones result in a coking of the TiO_2(110) surface and, consequently, the carbon balance can be closed.

While other reaction products are not observed, their ratio of acetone/isobutene/*tert*-butanol significantly changes over illumination times at 100 K (Fig. 2). With an increasing illumination duration, the acetone production increases, while both the *tert*-butanol and the isobutene yields diminish. Finally, the acetone production saturates after about 30 min, yielding 36% for an initial *tert*-butanol coverage of 0.18 ML.

This amounts to a conversion of 0.065 ML of *tert*-butanol. Alcoxy species have previously been found to be the photoactive species.[6,7,30,31] While the actual active site for photooxidation still remains under discussion, we follow the interpretation of Henderson, who reports that methoxy formation occurs either on defects, co-adsorbed oxygen adatoms or terminal OH groups.[30] As on the r-TiO_2(110)-surface, only defects occur in significant amounts, and we assign the *tert*-butoxy formation to occur predominantly in bridge-bonding oxygen (BBO) defects, as attributed by the saturation value, which is in excellent agreement with the concentration of BBO-vacancies of 0.06 ± 0.01 ML on the r-TiO_2(110)-surface as determined by water-TPD.[18] Furthermore, scanning tunneling microscopy (STM) images of 2-butanol reveal the butoxy formation only occurs in the defect.[32]

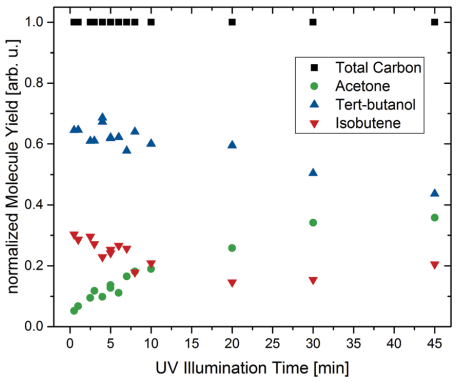

Fig. 2 Normalized integrated molecule yields *vs.* illumination time. Each of the data points represents the integrated molecule yields from a consecutive post-irradiation TPD run. Prior to this illumination, the r-TiO_2(110) surface is exposed to 0.18 ML *tert*-butanol-OD at 100 K. The carbon balance is closed, because coking is not observed in the experiments. With increasing UV illumination time, the photochemical yield of acetone increases, while both the isobutene and *t*-butanol yields are extenuated. After 30 min, the photoreaction saturates.

Interestingly, in the present work and the previously mentioned studies, some thermal dehydration-reactivity of the alcohol is still observed in the TPD after the photoproduct-accumulation experiment at cryogenic temperatures. As the thermal reaction has been attributed by Dohnalek and co-workers to also take place in the BBO-vacancies, these alkenes stem from diffusion of the alcohol into the cleared BBO-vacancies during the TPD experiments.

Therefore, the amount of acetone formed in the photoreaction sites scales with the defect concentration, but not the sum of the overall reaction products. The thermal reaction pathway is not expected to be strongly affected by the photoreaction. This is also supported by the behavior of the isobutene signal for different illumination times (Fig. 2), for which a drop from about 30% to only somewhat below 20% is observed.

In a subsequent experiment, the photoreaction was investigated at 293 K (Fig. 3a). This particular temperature was chosen, as on the one hand significant desorption of *tert*-butanol is not expected to occur. On the other hand, desorption of acetone should be enabled according to the post-irradiation TPD experiments (Fig. 1b) and the desorption behavior reported in the literature.[9,33] Similar as in case of Fig. 1, the methyl radical ejection is observed from *tert*-butanol, while the desorption of *tert*-butanol is indeed completely suppressed. In addition, some acetone desorption is observed, although with significantly lower intensity during the beginning of the illumination. Unexpectedly, desorption of isobutene is also observed under UV illumination. While it has been shown that this molecule can even be photodesorbed below 100 K on the r-TiO_2(110) surface,[28] it is detected at least 50 K below its first desorption feature in the *tert*-butanol TPD experiment (Fig. S2, ESI†). When the resulting decay curves are normalized to their maximum value (Fig. 3b), the kinetics of the different processes can readily be compared with each other. All desorption traces show multi-exponential decay kinetics, which is generally found for photochemical processes on TiO_2 indicating complex reaction pathways.[34,35]

However, the individual decay curves are significantly different from each other, which depends on the respective desorbing species: while isobutene clearly exhibits the fastest reaction kinetics, the ejection of methyl is somewhat faster than the acetone formation and desorption. This behavior indicates that different mechanisms play a role, which is a combination of the thermal and photochemical processes. The photochemistry at 100 K and 293 K as well as the thermal reactivity enable detailed insights into the different reaction mechanisms: the methyl radical ejection observed in all isothermal UV-illumination experiments is clearly a photon-induced reaction. However, this reaction is less efficient at 100 K than at 293 K, which

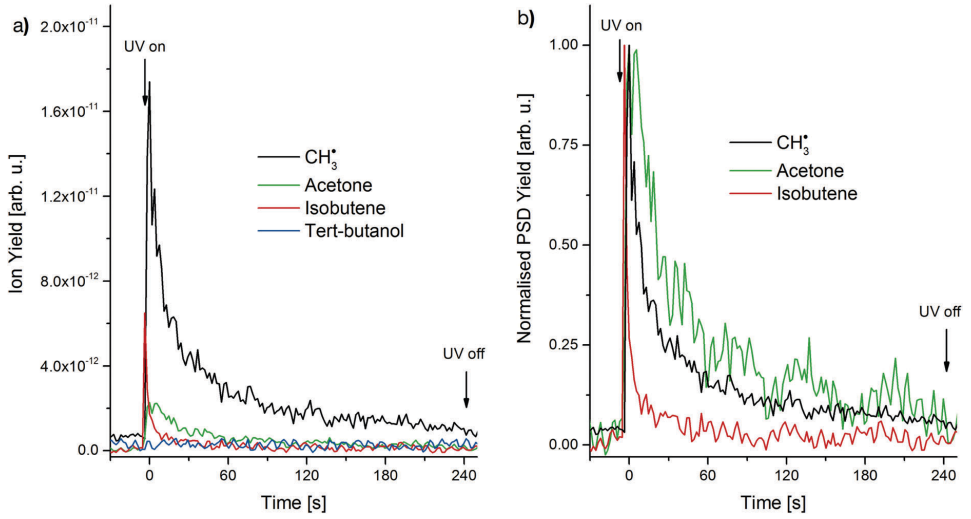

Fig. 3 (a) Isothermal photodesorption yield *vs.* time for 0.18 ML of *tert*-butanol-OD at 293 K on a r-TiO_2(110) surface. When the sample is irradiated with UV light, CH_3-radical ejection is observed similar to the experiment at cryogenic conditions. Furthermore, the photoreaction product acetone also desorbs under illumination at this temperature. In addition, isobutene formation and desorption is observed at 293 K. In panel (b), the normalized PSD yields from the same experiment as in (a) are shown for a qualitative comparison of decay rates. All the decay-rates follow a multi-exponential behavior. The acetone signal shows a small delay with respect to the methyl-radical ejection and then a slightly slower decay, which is attributed to thermal desorption behavior after the photoreaction to acetone. The isobutene decay is faster than the methyl-ejection, which may be attributed to a photochemical desorption as observed in the literature.[28]

demonstrates that at least one reaction step, only accessible by thermal chemistry, is of importance. To study the temperature dependence further, PSD experiments of 0.18 ML *tert*-butanol are carried out at several temperatures between 239 K and 330 K (Fig. S5, ESI†). The analysis of this data shows (Fig. 4) that at 239 K about equal amounts of isobutene and acetone are formed. An increase in the temperature of the photoreaction enhances the formation of both products. However, while for isobutene only a modest increase in the yield is detected, the signal of acetone strongly rises. We attribute this observation to originate from the superposition of two different effects, which are an enhanced thermal desorption of acetone and the diffusion of *tert*-butanol to the photoactive site. The changes in product yields are further reflected in the selectivity of the photoreaction (Fig. 4b). While at low temperatures about 50% selectivity toward acetone is found, this value increases to over 80% at room temperature and above.

The absence of a distinct low-energy structure as the η^2(C,O)-enolate for aldehydes and ketones[20,21,27] suggests that the transfer of the hole immediately leads to the abstraction of a methyl group regardless of the exact adsorption geometry in the defect. While this process rules out temperature-induced geometric transformations, diffusion of the alcohol molecules into the defects plays an important role in the reactivity. This is supported by STM studies, which show that alcohol molecules are also bound on TiO_2 rows even when BBO vacancies are still accessible.[32,36] Furthermore, the accompanied production of acetone (eqn (2)) is also found to be slow at 100 K and the yield only saturates after 30 min of illumination.

$$\underset{\textit{tert}\text{-butanol}}{(CH_3)_3COH} + Vac_{BBO} + O_{BBO} \rightarrow (CH_3)_3CO - Vac_{BBO} + OH_{BBO} \quad (1)$$

$$(CH_3)_3CO - Vac_{BBO} + OH_{BBO} \xrightarrow{h\nu} \underset{\text{acetone}}{C_3H_6O} + CH_3^{\bullet}\uparrow + Vac_{BBO} + OH_{BBO} \quad (2)$$

On the other hand, the resultant increase in methyl ejection at 293 K is not only due to a higher diffusion rate of the alcohol molecules into defects that remained empty, but also by a clearance of the defect by the thermal desorption of acetone. This subsequent desorption step of the ketone is also reflected by a slower decay of the acetone signal with respect to the methyl one, as for the latter this thermal reaction step does not occur.

In comparison with the products originating from methyl ejection, the desorption of isobutene is a very fast process, which is clearly evidenced by the rapid decay in the signal (Fig. 3b). While a very fast photodesorption behavior on the n-type semiconductor may be attributed to a photohole induced charge redistribution on the surface, the reaction is obviously temperature-dependent, as the formation of this molecule does not occur at 100 K. Otherwise, photodesorption of this molecule would have been observed at this temperature.[28] This temperature-dependence suggests, that a barrier to an activated

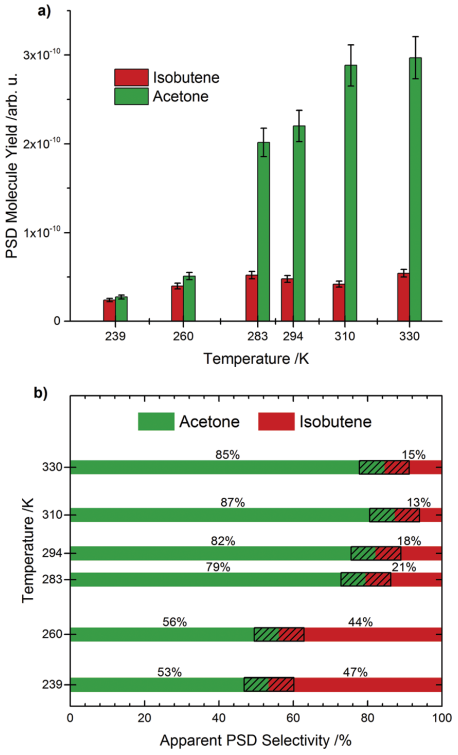

Fig. 4 (a) Resembles the integrated molecule yields of the first 100 s including all correction factors (see ESI†) for the different PSD yields from Fig. S5 (ESI†). For higher temperatures, the overall reaction yield is increased. In (b), the selectivities based on the integral yields are displayed. For higher temperatures, an enhanced apparent PSD selectivity towards acetone is obtained.

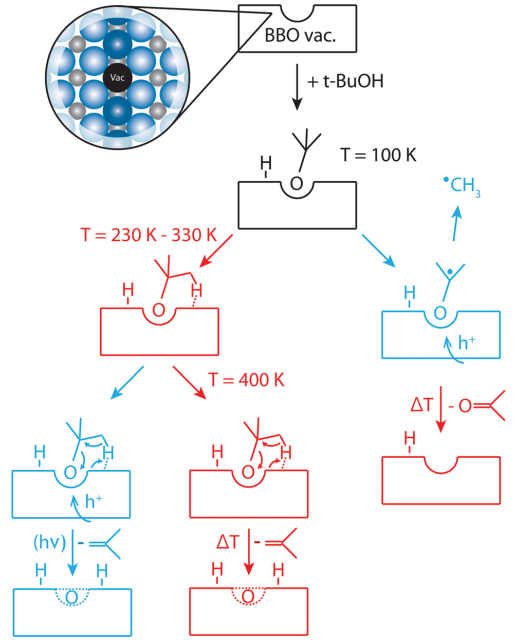

Fig. 5 Photochemical (blue) and thermal (red) reaction pathways of *tert*-butanol on the r-TiO_2(110) surface. When the photo-holes react at cryogenic conditions with *tert*-butanol, methyl ejection is observed. Consecutively, a thermal desorption of acetone is observed. When the photo-reaction is initiated at room temperature, thermally formed isobutene is observed at lower temperatures than that expected from the reaction temperature. The isobutene is either photo-desorbed in the illumination case or thermally desorbed. A representation of the BBO-vacancy from the surface normal is shown for the bare vacancy, while the BBO vacancy is shown in black. The Ti atoms are given in grey and the oxygen ones in blue.

transition state for the H_2O-elimination of *tert*-butanol exists, which can already be overcome at lower temperatures than that of the complete thermal reaction to isobutene. UV illumination seems to propel the consecutive chemical reaction steps and, as the desorption is not thermally hindered, the fastest kinetics of all the observed products results. In the thermal reaction pathway the production of isobutene by water-elimination has previously been attributed to be an E2-type reaction *via* a 5-membered cyclic structure involving the BBO-vacancy.[14] Thus, it seems reasonable that this transition state is only formed after a certain temperature, while the formal abstraction of water is eventually done by the photoreaction (eqn (5)).

$$\underset{\textit{tert}\text{-butanol}}{(CH_3)_3COH} + Vac_{BBO} + O_{BBO} \rightarrow (CH_3)_3CO - Vac_{BBO} + OH_{BBO} \quad (3)$$

$$(CH_3)_3CO - Vac_{BBO} + OH_{BBO} \xrightarrow{\Delta T} \underset{\text{isobutene}}{C_4H_8} + H_2O + Vac_{BBO} + O_{BBO} \quad (4)$$

$$(CH_3)_3CO - Vac_{BBO} + OH_{BBO} \xrightarrow{h\nu} \underset{\text{isobutene}}{C_4H_8} \uparrow + H_2O + Vac_{BBO} + O_{BBO} \quad (5)$$

Both reactions, the formation of acetone by methyl ejection and the production of isobutene by dehydration, comprise thermal as well as photochemical steps, which are summarized in Fig. 5.

The water-free conditions also demonstrate, that such photoreactions do not necessarily need to occur *via* the generation of the OH-radical and the subsequent oxidation of the alcohol. Instead, a direct hole transfer to the organic molecule is observed. This mechanism may also work under aqueous conditions, as long as the defects are not blocked or oxygen ad-atoms exist on the semiconductor. In addition, our findings also explain perfectly the detected products from a previous study concerning the photooxidation of *tert*-butanol on co-catalyst loaded TiO_2 (Degussa P25) in a reactor at 373 K.[11,12] In line with our observations, acetone was also identified as the main reaction product from the photoreaction, while isobutene was the

View Article Online
Paper PCCP

sole thermal decomposition product. Based on our study, we expected these properties to originate from the peculiar chemistry of TiO_2.

4 Conclusions

In summary, we have shown that the photooxidation for alcohols without an α-H moiety opens up new mechanistic pathways such as the splitting of C–C-bonds. In general, all photochemical processes observed can be associated with BBO-vacancy sites. Similar to ketones, the photooxidation of tertiary alcohols (*i.e. tert*-butanol) is attributed to be initiated by photoholes, which travel to the alcohol species to enable the ejection of a methyl radical. As the photochemical product evolution saturates at a certain amount, which can directly be related to the defect concentration, it is evidenced that the reaction occurs directly at the BBO-vacancy site. Increased reaction kinetics for the methyl ejection at higher temperatures suggest that diffusion and the clearance of defects play an important role in the reaction rate. While at 100 K only the reaction pathway to the formation of acetone occurs, an additional one is open for the illumination at 293 K. At this temperature, irradiation facilitates the formation of isobutene originating from a dehydration of the alcohol. However, the desorption of isobutene is observed at surprisingly low temperatures, as the thermal desorption is generally believed to take place immediately after the isobutene formation.[14,28] The temperature-dependent behavior of this reaction can be attributed to a cyclic transition state involving the BBO-vacancy,[14] and a redistribution of charges upon illumination, which may facilitate the reaction and product desorption. For all reaction channels, it is evident that both thermal as well as photochemical effects are important for the yield of a particular product. Furthermore, it is demonstrated that even a seemingly simple system such as rutile and a tertiary alcohol offers a rich chemistry with two different reaction pathways, dehydrogenation and dehydration, which can be tuned by the judicious choice of the appropriate reaction parameters.

Conflicts of interest

There are no conflicts to declare.

Acknowledgements

The authors thank the DFG for grant HE3435/22-1. C. A. W., S. L. K. and M. T. express gratitude to Christian Steiffen for keeping up the good mood during the experiments.

References

1 M. A. Henderson, *Surf. Sci. Rep.*, 2011, **66**, 185–297.
2 R. Rinaldi and F. Schüth, *Energy Environ. Sci.*, 2009, **2**, 610–626.
3 F. Frusteri, F. Arena, G. Bonura, C. Cannilla, L. Spadaro and O. D. Blasi, *Appl. Catal., A*, 2009, **367**, 77–83.
4 N. Rahmat, A. Z. Abdullah and A. R. Mohamed, *Renewable Sustainable Energy Rev.*, 2010, **14**, 987–1000.
5 C. L. Pang, R. Lindsay and G. Thornton, *Chem. Rev.*, 2013, **113**, 3887–3948.
6 M. Shen and M. A. Henderson, *J. Phys. Chem. Lett.*, 2011, **2**, 2707–2710.
7 K. R. Phillips, S. C. Jensen, M. Baron, S.-C. Li and C. M. Friend, *J. Am. Chem. Soc.*, 2013, **135**, 574–577.
8 C. A. Walenta, S. L. Kollmannsberger, J. Kiermaier, A. Winbauer, M. Tschurl and U. Heiz, *Phys. Chem. Chem. Phys.*, 2015, **17**, 22809–22814.
9 D. Brinkley and T. Engel, *J. Phys. Chem. B*, 1998, **102**, 7596–7605.
10 K. P. C. Vollhardt and N. E. Schore, *Organische Chemie*, Wiley-VCH Verlag GmbH & Co. KGaA, 5th edn, 2011.
11 S. Preis and J. Falconer, *Water Sci. Technol.*, 2004, **49**, 141–145.
12 S. Preis, J. L. Falconer, R. del Prado Asensio, N. C. Santiago, A. Kachina and J. Kallas, *Appl. Catal., B*, 2006, **64**, 79–87.
13 V. Augugliaro, H. Kisch, V. Loddo, M. J. López-Muñoz, C. Márquez-Álvarez, G. Palmisano, L. Palmisano, F. Parrino and S. Yurdakal, *Appl. Catal., A*, 2008, **349**, 182–188.
14 Y. Kim, B. D. Kay, J. White and Z. Dohnálek, *Catal. Lett.*, 2007, **119**, 1–4.
15 L. Chen, R. S. Smith, B. D. Kay and Z. Dohnalek, *ACS Catal.*, 2017, **7**, 2002–2006.
16 C. Walenta, S. Kollmannsberger, A. Winnerl, S. Weiszer, R. N. Pereira, M. Tschurl, M. Stutzmann and U. Heiz, *J. Phys. Chem. C*, 2017, **121**, 16291–16299.
17 S. Kollmannsberger, C. A. Walenta, A. Winnerl, F. Knoller, R. N. Pereira, M. Tschurl, M. Stutzmann and U. Heiz, *J. Chem. Phys.*, 2017, **147**, 124704.
18 M. A. Henderson, *Langmuir*, 1996, **12**, 5093–5098.
19 Z. Li, R. S. Smith, B. D. Kay and Z. Dohnálek, *J. Phys. Chem. C*, 2011, **115**, 22534–22539.
20 N. G. Petrik, M. A. Henderson and G. A. Kimmel, *J. Phys. Chem. C*, 2015, **119**, 12273–12282.
21 N. G. Petrik, M. A. Henderson and G. A. Kimmel, *J. Phys. Chem. C*, 2015, **119**, 12262–12272.
22 R. T. Zehr and M. A. Henderson, *Phys. Chem. Chem. Phys.*, 2010, **12**, 8085–8092.
23 M. Shen and M. A. Henderson, *J. Phys. Chem. C*, 2011, **115**, 5886–5893.
24 M. D. Kershis, D. P. Wilson and M. G. White, *J. Chem. Phys.*, 2013, **138**, 204703.
25 M. A. Henderson, *Surf. Sci.*, 2008, **602**, 3188–3193.
26 M. A. Henderson, *J. Phys. Chem. C*, 2008, **112**, 11433–11440.
27 M. D. Kershis and M. G. White, *Phys. Chem. Chem. Phys.*, 2013, **15**, 17976–17982.
28 M. A. Henderson, *J. Phys. Chem. C*, 2013, **117**, 14113–14124.
29 M. Setvin, X. Shi, J. Hulva, T. Simschitz, G. S. Parkinson, M. Schmid, C. Di Valentin, A. Selloni and U. Diebold, *ACS Catal.*, 2017, 7081–7091.
30 M. Shen and M. A. Henderson, *J. Phys. Chem. C*, 2012, **116**, 18788–18795.

31 G. Kolesov, D. Vinichenko, G. A. Tritsaris, C. M. Friend and E. Kaxiras, *J. Phys. Chem. Lett.*, 2015, **6**, 1624–1627.
32 Z. Zhang, O. Bondarchuk, B. D. Kay, J. M. White and Z. Dohnálek, *J. Phys. Chem. C*, 2007, **111**, 3021–3027.
33 M. A. Henderson, *J. Phys. Chem. B*, 2004, **108**, 18932–18941.
34 M. A. Henderson, M. Shen, Z.-T. Wang and I. Lyubinetsky, *J. Phys. Chem. C*, 2013, **117**, 5774–5784.
35 T. L. Thompson and J. T. Yates, *Chem. Rev.*, 2006, **106**, 4428–4453.
36 M. Shen, D. P. Acharya, Z. Dohnálek and M. A. Henderson, *J. Phys. Chem. C*, 2012, **116**, 25465–25469.

Electronic Supplementary Material (ESI) for Physical Chemistry Chemical Physics.

Supporting Information: Photocatalytic Selectivity Switch to C-C Scission: α-Methyl Ejection of tert-Butanol on TiO_2(110)

Constantin A. Walenta,[†,‡,¶] Sebastian L. Kollmannsberger,[†,¶] Carla Courtois,[†]

Martin Tschurl,[†] and Ueli Heiz[*,†,‡]

† Chair of Physical Chemistry, Department of Chemistry & Catalysis Research Center, Technische Universität München, Lichtenbergstr. 4, 85748 Garching, Germany

‡ Nanosystems Initiative Munich, Schellingstr. 4, 80799 München, Germany

¶ The authors contributed equally to this work

*corresponding author: ulrich.heiz@mytum.de

Data Analysis:

During the thermal and photo-desorption experiments, the potential products were monitored with several masses: Isobutene with masses 56, 41 and 39; acetone with 58 and 43; tert-butanol with 59 and 31; tert-butanol-OD with 59, 31 and 32. The methyl-radical was detected during the experiments on mass 15. Further molecules and corresponding masses including H_2 (2), HD (3), CH_4 (16), H_2O (18), HDO (19), CO (28), CO_2 (44) were recorded, but found to be insignificant with the exception of water (see Fig. S2). To quantify the results, the coverages of tert-butanol normalized to the H_2O-TPD of a

monolayer according to the convention in the literature.[1] The tert-butanol-OD was quantified using masses 31 and 32, because some isotope exchange could not be avoided in the gas line and on the single crystal. Isobutene and acetone were quantified using masses 56 and 58 as well as by considering the fragmentation of tert-butanol and the respective other molecules. For the quantification, all molecule yields were corrected for their fragmentation pattern, their transmission through the quadrupole mass spectrometer, and their ionization cross-sections (see Fig. S3 and S4).[2-4]

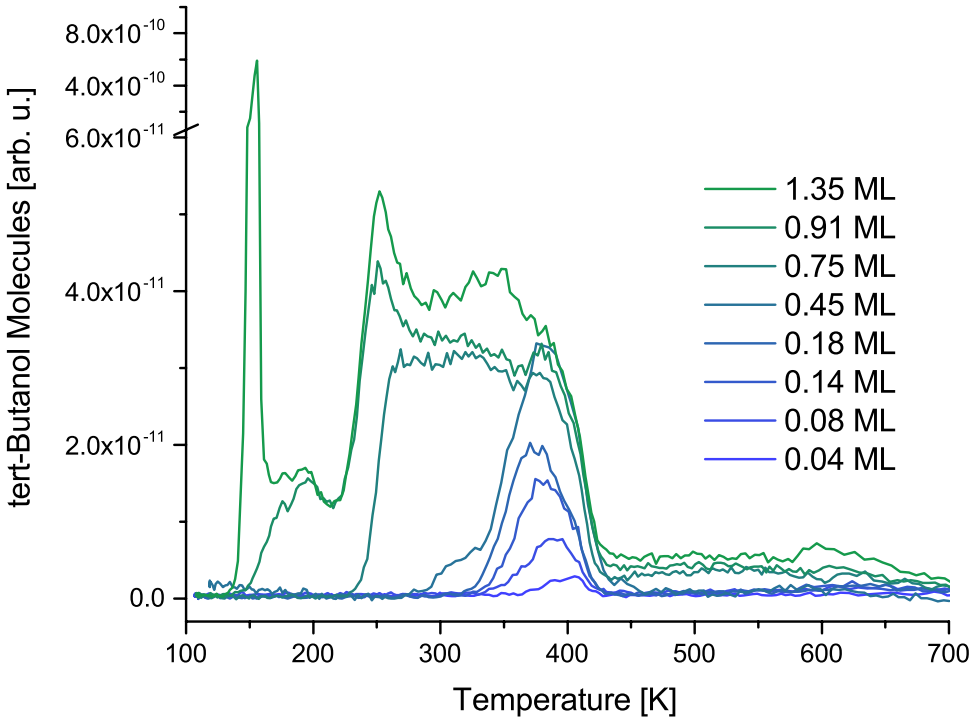

Figure S1: Coverage dependent TPD-series of tert-butanol-OD on a reduced TiO_2(110)-surface [r-TiO_2(110)]. At small coverages, a desorption feature at around 400 K arises, that is attributed to tert-butanol binding to the Ti-lattice sites. With higher coverages this feature saturates and a shoulder is growing to a peak at 250 K, which is assigned to the desorption from bridge-bonding oxygen (BBO) surface atoms. Another feature appearing below 200 K is attributed to multilayer desorption. The coverages are referenced to the

coverage determination of Dohnalek and co-workers and in very good agreement with their work.[1]

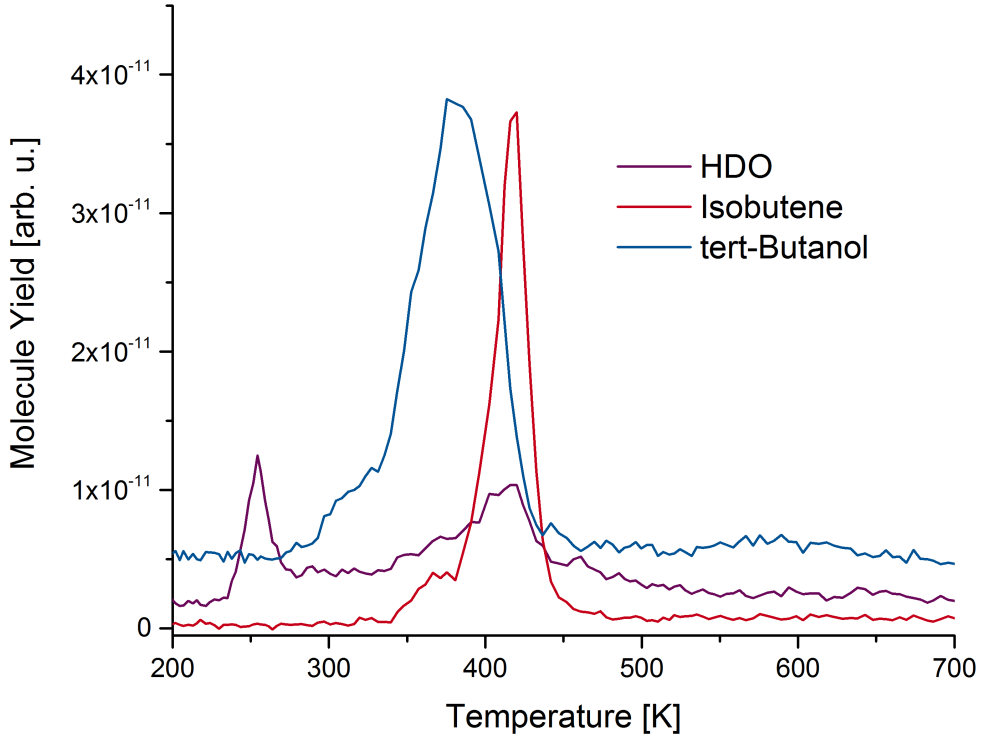

Figure S2: TPD of 0.45 ML tert-butanol-OD on r-TiO_2(110). Tert-butanol desorbs from the Ti-lattice sites, while a dehydration pathway to isobutene is observed at around 425 K, which is in agreement with previous studies.[5-6] Additionally, the HDO (m/z = 19) was also monitored and two peaks occur: One is attributed to the direct dehydration pathway of tert-butanol-OD at 425 K, for which HDO is the by-product. In additional, another peak is observed at 250 K, which is attributed to the desorption of BBO-sites. It arises from water adsorption from the background and some dissociative adsorption, since some exchange to background adsorption from water is obtained.

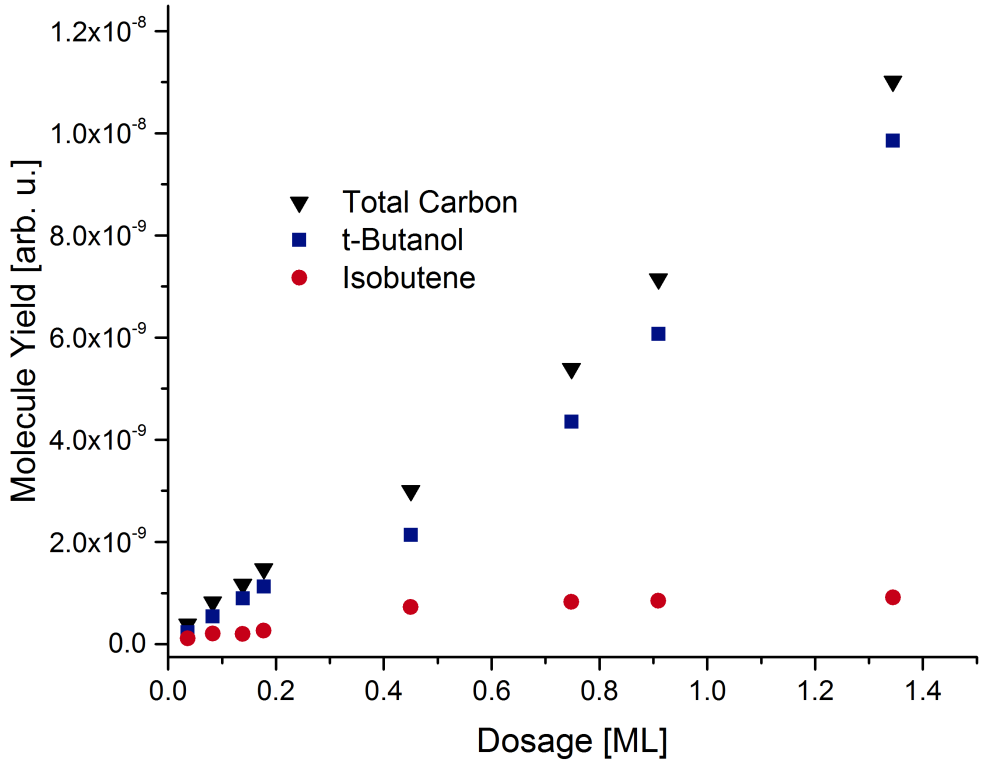

Figure S3: Integrated amounts of tert-butanol-OD and Isobutene for different coverages. While tert-butanol is shown in blue squares, the amount of isobutene is given in red circles. Auger electron spectroscopy and earlier studies[1] indicate that there are no carbon deposits for all alcohols on r-TiO_2(110). Hence, the carbon balance can be closed, which is addressed by black triangles showing the total carbon dosage by addition of the carbon containing desorbing molecules.

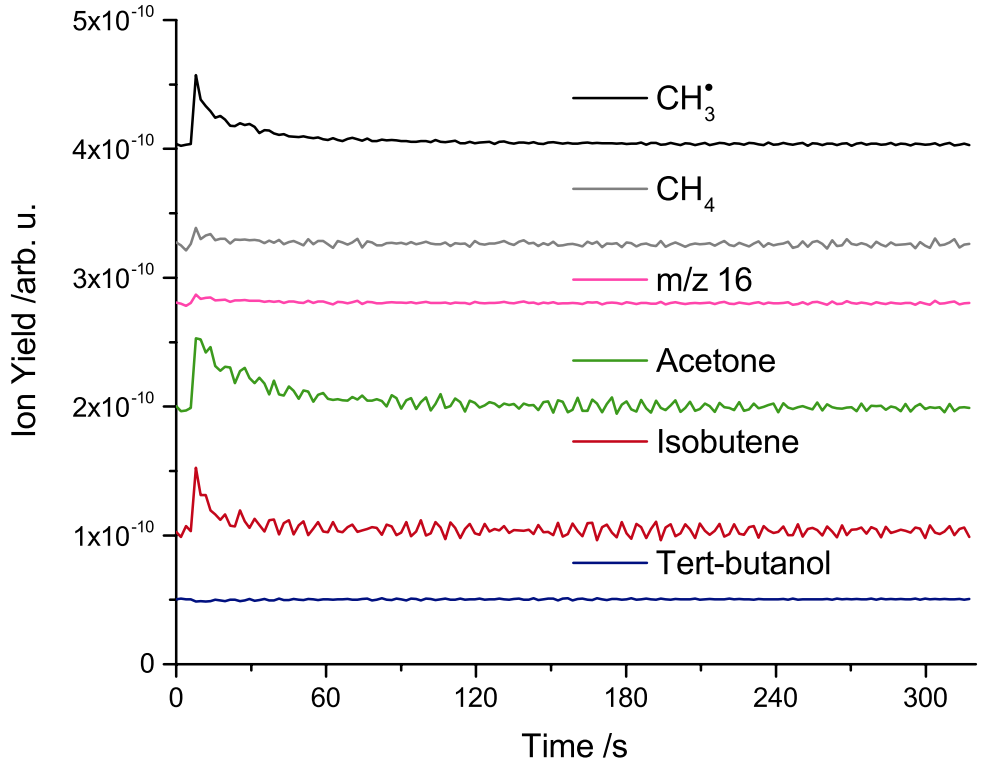

Figure S4: Isothermal photodesorption yield vs time for 0.18 ML of tert-butanol at 295 K on the r-TiO_2(110) surface. Note, that for the fully stated molecules, cracking pattern contributions are already accounted for. The traces are offset for clarity. The signal of m/z 15 is more than 8 times as much as for m/z 16. This is a clear indicator, that really a methyl radical is ejected during the photoreaction, while only trace amounts of methane are observed. The purple trace represents the raw data for mass 16. Note, that all correction factors as described above are included in that data, which increases also the noise in this data set.

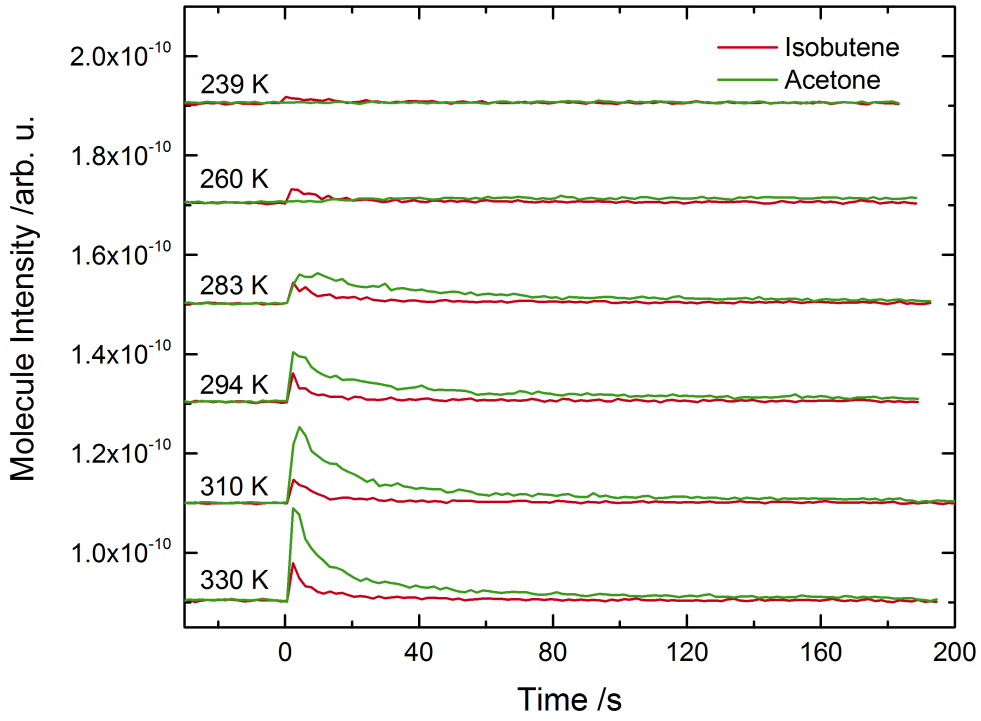

Figure S5: Isothermal photodesorption yield vs time for 0.18 ML of tert-butanol at different temperatures on a r-TiO_2(110) surface. The UV illumination is started at 0 s and ended after 180 s. For all temperatures, some desorption of both isobutene and acetone is observed, while no tert-butanol desorbs by irradiation. By increasing the temperature, both the overall apparent desorption rate is increased as well as the selectivity towards acetone. The traces are offset for clarity.

Notes and references:

1 Li, Z.; Smith, R. S.; Kay, B. D.; Dohnálek, Z., *J. Phys. Chem C,* 2011**, 115**, 22534-22539.
2 Bull, J. N.; Harland, P. W.; Vallance, C., *J. Phys. Chem. A,* 2012**, 116**, 767-777.
3 Irikura, Y.-K. K. K. K. In *BEB*, Proc. 2nd Int. Conf. on Atom. Molec. Data and Their Applications, Bell, K. A. B. K. L., Ed. AIP, New York, NY: 2000.

4 Hudson, J. E.; Hamilton, M. L.; Vallance, C.; Harland, P. W., *Phys. Chem. Chem. Phys.*, 2003, **5**, 3162-3168.
5 Kim, Y. K.; Kay, B. D.; White, J. M.; Dohnálek, Z., *J. Phys. Chem. C*, 2007**, 111**, 18236-18242.
6 Kim, Y. K.; Kay, B. D.; White, J. M.; Dohnálek, Z., *Catal. Lett.*, 2007**, 119**, 1-4.

A.2 Regulating Photochemical Selectivity with Temperature: Isobutanol on TiO_2(110)

JACS
JOURNAL OF THE AMERICAN CHEMICAL SOCIETY
pubs.acs.org/JACS Article

Regulating Photochemical Selectivity with Temperature: Isobutanol on TiO_2(110)

Carla Courtois,[$] Constantin A. Walenta,[$] Martin Tschurl, Ueli Heiz, and Cynthia M. Friend*

Cite This: J. Am. Chem. Soc. 2020, 142, 13072−13080 Read Online

ACCESS | Metrics & More | Article Recommendations | Supporting Information

ABSTRACT: Selective photocatalytic transformations of chemicals derived from biomass, such as isobutanol, have been long envisioned for a sustainable chemical production. A strong temperature dependence in the reaction selectivity is found for isobutanol photo-oxidation on rutile TiO_2(110). The strong temperature dependence is attributed to competition between thermal desorption of the primary photoproduct and secondary photochemical steps. The aldehyde, isobutanal, is the primary photoproduct of isobutanol. At room temperature, isobutanal is obtained selectively from photo-oxidation because of rapid thermal desorption. In contrast, secondary photo-oxidation of isobutanal to propane dominates at lower temperature (240 K) due to the persistence of isobutanal on the surface after it is formed. The byproduct of isobutanal photo-oxidation is CO, which is evolved at higher temperature as a consequence of thermal decomposition of an intermediate, such as formate. The photo-oxidation to isobutanal proceeds after thermally induced isobutoxy formation. These results have strong implications for controlling the selectivity of photochemical processes more generally, in that, selectivity is governed by competition of desorption vs secondary photoreaction of products. This competition can be exploited to design photocatalytic processes to favor specific chemical transformations of organic molecules.

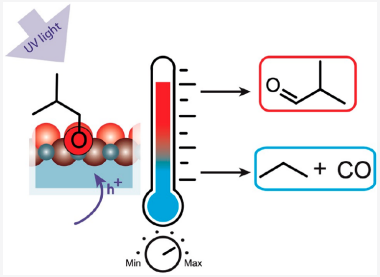

INTRODUCTION

Photocatalytic reforming of alcohols and biomass is a potential source of renewable hydrogen and value-added oxygenates that is not based on natural gas.[1−3] Isobutanol specifically has a high potential for producing renewable H_2 and carbon-based feedstock chemicals because of the recent progress in biologically assisted fermentation of cellulose at room temperature to produce high energy-density alcohols, including isobutanol.[4−6] Isobutanol can also be stored easily, since it is not hygroscopic and is liquid in a broad temperature range. Thermal reforming of isobutanol yields molecular hydrogen and syngas, providing feedstocks for further chemical production,[7] but it requires high temperatures. Photoreforming has the advantage that valuable chemicals can be produced at room temperature,[3,8,9] providing a sustainable pathway from alcohols (such as isobutanol). Photoreforming of alcohols for hydrogen production has been shown for a variety of alcohols[3,10−12] and can also lead to very selective, value-added oxidation products such as aldehydes, carboxylic acids, and esters.[12−15]

TiO_2-based photocatalysts are models for the elucidation of fundamental photochemical reaction mechanisms, both for the hydrogen evolution as well as the selective oxidation chemistry.[13,16,17] Studies in well-defined environments have mostly focused on the short-chain alcohols, methanol[16,18,19] or ethanol.[20,21] Generally, the photo-oxidation on bulk TiO_2 proceeds via a direct hole-transfer from the n-type semiconductor to a surface alkoxy species, since the photohole travels predominantly to the surface in the space charge region upon UV illumination.[22] Adsorbed alkoxy species predominantly form from thermal O−H bond dissociation of the alcohol on the surface and especially on defect sites.[18,22] The first photo-oxidation step, the α-H abstraction to yield formaldehyde, has been studied in detail for methanol, both theoretically[23,24] and experimentally.[18,25−28] For high coverages of methoxy, formaldehyde further reacts in a second consecutive photo-oxidation pathway leading to coupling with the residual methoxy to produce methylformate.[16,29] The selectivity of this process is dependent on the reaction temperature.[13,16,30] However, less is known for other alcohols about the ensuing reaction pathways especially for longer-chain alcohols,[13,16,29,31] although a variety of products from hydrocarbons to CO_2 have been observed.[3,32]

Herein, the selectivity for photochemical decomposition of isobutanol ($(CH_3)_2C(H)CH_2OH$) is shown to be drastically affected by reaction temperature. The underlying reason for

Received: April 22, 2020
Published: June 29, 2020

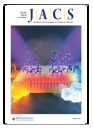

https://dx.doi.org/10.1021/jacs.0c04411
J. Am. Chem. Soc. 2020, 142, 13072−13080

dependence of selectivity on reaction temperature is that a consecutive photo-oxidation step is in direct competition with thermal desorption of the initial photoproduct, the aldehyde. Similar to other alcohols, isobutanol forms alkoxy species, which thermally react at high temperature. Upon UV illumination, isobutoxy is oxidized to the aldehyde, isobutanal, which can either desorb or undergo further hole-mediated photo-oxidation to propane and CO. The selectivity for these two pathways depends on the surface temperature: At low temperature, the primary photoproduct, isobutanal, has a long surface lifetime and, therefore, is further photo-oxidized. The results show that the overall selectivity of photocatalytic reactions can be strongly influenced by temperature effects even if they are purely photochemical and not thermal. This fundamental mechanistic understanding provides valuable insight in the manipulation of selectivity in photocatalytic processes.

EXPERIMENTAL SECTION

The experiments were performed in an ultrahigh vacuum (UHV) system with a base pressure of $<9 \times 10^{-11}$ Torr equipped for thermal reactivity and photoreaction studies.[33,34] The crystal was mounted on top of a W filament in contact to a copper sample mount, which allowed a temperature control between 140−825 K through LN_2-cooling and resistive heating. The slightly blue $TiO_2(110)$ single crystal (SurfaceNet GmbH) was prepared by several Ar^+-sputtering (1.0 keV, 5×10^{-6} Torr, 10 min) and vacuum annealing (800 K, 15 min) cycles until no contaminations were observed in the Auger electron spectrum (AES, Physical Electronics Industries, PHI 10−805), and high quality H_2O desorption spectra were obtained.[35]

Annealing in vacuum produces a reduced $TiO_2(110)$ surface, named r-$TiO_2(110)$. The absence of a high temperature feature in a temperature-programmed desorption experiment of H_2O indicated a bridge-bonded oxygen vacancy concentration of ≤2% of a monolayer (ML) (Figure S1). Further, the crystal showed the characteristic photon-stimulated desorption of molecular oxygen at cryogenic temperatures (Figure S2).[36−38] The oxidized $TiO_2(110)$ surface was prepared by dosing 40 L O_2 at cryogenic temperatures on the freshly prepared r-$TiO_2(110)$ followed by an annealing step to 300 K and is labeled o-$TiO_2(110)$. This results in O_{ad} on Ti_{5c} rows[39] and some filled bridge-bonded oxygen vacancies.[39] The hydroxylated surface was accomplished by dosing 1.5 ML of H_2O at 140 K on the r-$TiO_2(110)$, and an annealing step to 300 K leading to the desorption of molecular water leaving behind only surface hydroxyls scaling with the bridge-bonded oxygen vacancy concentration (h-$TiO_2(110)$).[40]

Isobutanol (Sigma-Aldrich, BioUltra ≥99.5%), isobutanal (Sigma-Aldrich, ≥ 99%), O_2 (Matheson, research grade), and H_2O (VWR, HPLC grade) were dosed through a needle doser at 140 K prior to an experiment. Isobutanol, isobutanal, and water were purified through several pump-freeze-thaw cycles.

The desorption and reactivity measurements were performed in a line-of-sight geometry to a quadrupole mass spectrometer (QMS, Hiden Analytical). The molecules were identified by their characteristic fragmentation patterns and quantified by correcting for their fragmentation pattern, ionization cross sections, and transmission (more details are given in the SI). Temperature-programmed desorption and reaction experiments used a heating ramp of 1 K/s. Photochemical experiments at cryogenic temperatures were initiated by illuminating the sample for a defined period of time prior to a temperature-programmed desorption/reaction experiment. Isothermal photoreactions were performed at a chosen temperature, where the sample is thermalized prior to the illumination and the gas-phase is monitored by the QMS. The annealing pretreatment for photochemistry studies consists of dosing isobutanol at 140 K, heating and thermalizing the sample at 300 K for 3 min, cooling it down to desired temperature, and initiating the photoreaction by illuminating the sample with UV light. The annealing pretreatment promotes the formation of the photoactive alkoxy species.[18,41] A UV-LED light source (AmScope) with wavelength of 365 nm and a power of 150 mW was used for the illumination experiments. The UV spectrum of the LED is shown in the Figure S3. With the lack of coherence, scattering losses, the distance between light source and sample (∼18 cm), and the crystal position, the effective light intensity on the crystal is estimated to be less than 5 mW/cm^2.

RESULTS AND DISCUSSION

The thermal chemistry of isobutanol is similar to those of other alcohols and is readily separable from photochemistry. The majority of isobutanol desorbs from r-$TiO_2(110)$ in a coverage-dependent peak between 300 and 350 K that is predominantly ascribed to molecular binding to Ti_{5c} sites, in analogy to other alcohols.[42] There is a shoulder at 230 K in the desorption peak from hydroxylated $TiO_2(110)$ only for a monolayer coverage (Figure 1c), the origin of which is not known. The saturation coverage regarding the Ti_{5c} sites is estimated to be 0.55 ML based on previous work for other butanol isomers.[42]

A small percentage (∼2%) reacts to yield isobutoxy and bridge-bonded surface hydroxyl (OH_{br}) based on parallels to temperature-programmed reaction studies of other alcohols.[39,42,43] The isobutoxy reacts to yield isobutanal, isobutene, and isobutanol at 600 K (Figure 1a−c), while the dehydration pathway is attributed to reaction at bridge-bonding oxygen vacancies.[44]

The behavior of isobutanol is similar for various surface preparations (reduced-, oxidized-, and hydroxylated-$TiO_2(110)$) with only minor differences in the high temperature reactivity (Figure 1). The isobutoxy species undergo two parallel reaction pathways at 600 K (Figure 2): a disproportionation reaction yielding isobutanol and isobutanal, and a dehydration reaction leading to isobutene and water (Figure S6).[44] The disproportionation reaction of two isobutoxy species yields stoichiometric amounts of the alcohol and the aldehyde (Table S2). All the reaction pathways take place independent of the surface preparation, but only around 2% ML isobutanol reacts in the high temperature regime. Coverage-dependent temperature-programmed reaction experiments show that the high temperature reactivity reaches a saturation above an initial isobutanol coverage of 0.2 ML and the yield of molecular isobutanol increases linearly as a function of alcohol exposure (Figure S5).

Isobutoxy species are photo-oxidized to gas-phase isobutanal on $TiO_2(110)$ upon UV excitation at room temperature (Figure 3). The highest photo-oxidation yield at 300 K is attained on oxidized-$TiO_2(110)$ (Figure 3), most likely because O_{ad} on $TiO_2(110)$ promotes the formation of alkoxy species.[16,18,22,41] Alkoxy species have been identified in several studies as the photoactive intermediate both experimentally and theoretically,[16,18,23,24,48] while the photochemical oxidation of molecular alcohols remains controversial.[18,28,49]

The disproportionation reaction pathway at 600 K is completely absent after exposure of the surfaces containing isobutoxy to UV light for 5 min, providing strong evidence that isobutoxy is the photoactive species (Figure 3b). The reaction proceeds on all three surface terminations (oxidized, reduced, and hydroxylated) in the same fashion, while the isobutanal yield is the highest on o-$TiO_2(110)$ presumably due to the enhanced alkoxy formation.[16,18,22,26] There are no qualitative differences among the three different surface preparations.

The photo-oxidation of isobutoxy is similar to formation of aldehydes from other alkoxides on titania. The photo-oxidation

https://dx.doi.org/10.1021/jacs.0c04411
J. Am. Chem. Soc. 2020, 142, 13072−13080

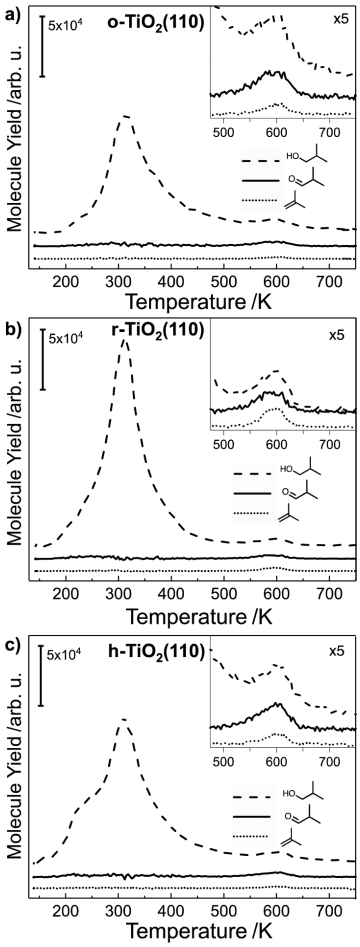

Figure 1. Temperature-programmed reaction spectra of isobutanol on (a) oxidized-, (b) reduced-, and (c) hydroxylated-TiO_2(110) showing the desorption of molecular isobutanol at 315 K and a minor amount of reaction products at 600 K. The coverages of the isobutanol are 0.44 ML on the oxidized surface (o-TiO_2(110)), 0.55 ML on the reduced surface (r-TiO_2(110)), and 0.54 ML on hydroxylated titania (h-TiO_2(110)). The traces shown are fragments characteristic of isobutanol (m/z 33, dashed lines), isobutanal (m/z 43, solid line), and isobutene (m/z 56, dotted line). Mass 33 is a unique fragment of isobutanol. Mass 43 and 56 are corrected for the alcohol contribution. All data shown are corrected for fragmentation, ionization efficiency, and spectrometer transmission differences (see Experimental Section). For ease of display, the three different curves are offset for clarity. The insets magnify the high temperature region by a factor of 5.

of isobutoxy is induced by a photohole that travels to the surface in the space charge region, since TiO_2(110) is an n-type semiconductor (Figure 4).[22,23] The photo-oxidation proceeds via α-C-H dissociation and isobutanal forms and thermally desorbs at 300 K.

Not all isobutoxy species are converted upon illumination, based on the persistence of dehydration to isobutene in subsequent temperature-programmed reaction experiments. Unreacted isobutoxy might either diffuse or is already bound to a bridge-bonded oxygen vacancy that was previously identified as the active site for the dehydration reaction.[43,50] The photoreaction leads to a hydroxylation of the surface, leaving two hydrogen atoms per reacted isobutanol molecule by stoichiometry and forming two bridge-bonded hydroxyl species (OH_{br}). These OH_{br} can recombine and form water around 450 K (Figure S7) resulting in an oxygen vacancy on the surface in analogy to previously detailed photo-oxidation studies with ethanol.[20,48] After the desorption of all carbon species, oxygen and titanium diffusion are possible at 700 K and re-equilibrate the surface vacancy concentration.[51] The carbon mass balance in all of the experiments can be closed based on repeated experiments, subsequent H_2O temperature-programmed desorption, and the absence of a carbon deposit in Auger electron spectra.

The highest conversion in the photo-oxidation of isobutanol to isobutanal is obtained at 300 K, as a temperature dependent photoreaction study above room temperature shows (Figure S8). The almost constant yield of isobutanal above 350 K, which is above the desorption temperature of isobutanol, emphasizes that isobutoxy is the main photoactive species. It is possible that there is some coadsorbed molecular isobutanol, as suggested in the literature;[52] however, the disappearance of the features at 600 K is strong evidence that the alkoxy is depleted through photoreaction. Sum-frequency generation studies of methanol likewise show that the dissociation equilibrium of methanol on the TiO_2(110) may be temperature-dependent, which should analogously hold for isobutanol.[53,54]

The photo-oxidation products are substantially different when isobutoxy is illuminated at 145 K: a temperature where isobutanal is thermally trapped on the surface. Specifically, propane and CO are formed in addition to isobutanal during temperature-programmed reaction after 15 min of illumination at 145 K (Figure 5). Some unreacted isobutanol is also detected. No gas-phase products are detected during illumination. In these experiments, isobutanol is adsorbed at 145 K, subsequently heated to 300 K for 3 min, followed by cooling again to 145 K and illumination. This procedure promotes the formation of alkoxy species[18,41] and induces a substantial amount of molecular isobutanol desorption. Water as a byproduct of the photoreaction (Figure S9) is also observed around 450 K.

The product yields are highly sensitive to the surface temperature during illumination. For example, propane is directly ejected into the gas phase during illumination at 240 K after creation of isobutoxy (Figure 6). Propane is unequivocally identified by its fragmentation pattern as the sole desorbing product at 240 K (Figure S10). In the postillumination temperature dependent desorption experiment (Figure 6b), isobutanal and isobutanol are observed as well as a high temperature peak of CO at 550 K and water at 450 K (Figure S11). The reaction occurs on all three surface preparations qualitatively similar, and isobutanal, propane, and CO are always obtained (Figure S13). The observation of gaseous propane shows that hydrogen is abstracted from the surface during this process, in agreement with the alkane formation from the photoreforming of tertiary alcohols on TiO_2(110) via a C−C split.[55]

https://dx.doi.org/10.1021/jacs.0c04411
J. Am. Chem. Soc. 2020, 142, 13072−13080

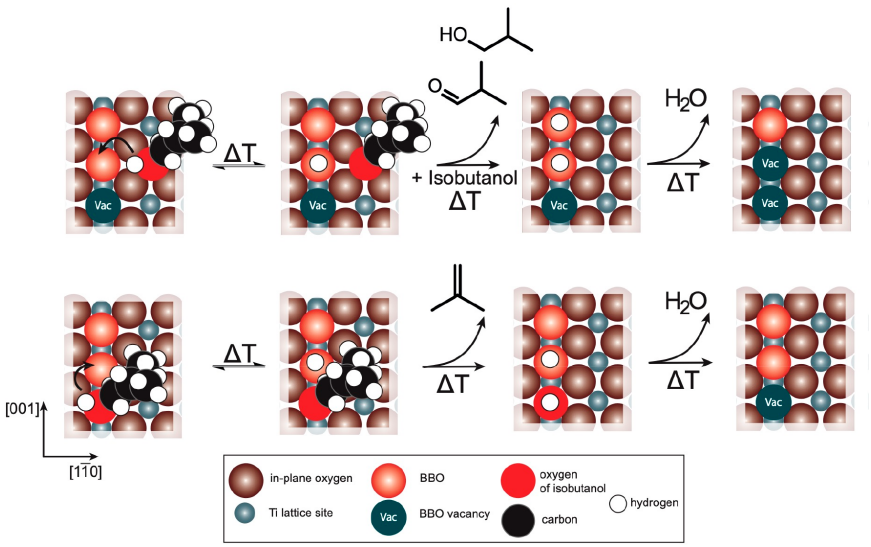

Figure 2. Schematic of isobutanol adsorption and reaction on TiO_2(110) (top view of surface). A small amount of adsorbed isobutoxy is formed in defects and on regular surface sites.[43,45,46] Competing disproportionation to isobutanol and isobutanal and dehydration to isobutene thermally induced above 500 K. The hydroxyl species either remain on the surface or desorb as water.[44,47]

The formation of propane is solely attributed to photo-oxidation of the primary photoproduct, isobutanal, when it is trapped on the surface. Independent investigations of isobutanal adsorbed on TiO_2(110) demonstrate that propane formation occurs in a consecutive photo-oxidation step where a C−C bond is cleaved photochemically (Figures S14 and S15). The photoreactions of isobutanol on TiO_2(110) lead to a photo-oxidation product isobutanal in the first reaction step and isobutanal is further photo-oxidized via a C−C split to propane and a formyl (HC=O) species that reacts with a lattice oxygen to formate (Figure 7) in analogy to formaldehyde (photo)chemistry on TiO_2(110).[56,57] Since molecular CO is only physisorbed on TiO_2(110),[58] CO from formate decomposition at 550 K is proposed to form from decomposition of adsorbed formate based on prior work.[56,59]

Propane and CO formation is observed for all three surface preparations for isobutanal photo-oxidation, showing that the reaction to propane and eventually CO is independent of the surface preparation (Figure S14). In agreement with the alcohol photo-oxidation, the oxidized surface shows the highest reactivity with respect to propane formation from isobutanal. A detailed analysis of the high temperature decomposition pathways shows that CO is the major product on all three surface preparations. On the o- and r-TiO_2(110), some minor signals assigned to CO_2 and formaldehyde are observed. Potentially, they are below the detection limit for the h-TiO_2(110) surface as also the least amount of propane is obtained. The observed products and intensities match the desorption products of formate on TiO_2(110).[56,59,60] On the basis of the repeatability of the experiments and a subsequent water desorption, no carbon deposits remain on the surface consistent with the decomposition of a formate species at 550 K.

Similar to acetaldehyde,[61] a bidentate configuration is likely formed prior to UV illumination. Upon UV irradiation, the photohole leads to a split in the C−C bond and an alkyl species is ejected leaving behind a formyl-species bound to a lattice oxygen atom.[61]

In summary, the aldehyde, isobutanal, and adsorbed OH are the primary photo-oxidation products of isobutanol under UV irradiation at room temperature. In analogy to other alcohols, the isobutanal is proposed to form via a direct photohole-transfer to isobutoxy followed by thermal desorption (Figure 7). The high-temperature disproportionation channel is completely suppressed after UV-irradiation, indicating that the isobutoxy species yielding these products are quantitatively photo-oxidized to isobutanal (Figure 3). The persistence of the dehydration pathway to form isobutene and surface hydroxyls may indicate that some of the alkoxides are not or less photoactive.[20] The origin of this phenomenon is not established. The byproducts from photochemical alcohol oxidation, surface hydroxyls,[48,62] ultimately disproportionate to water leading to a formal reduction of the surface.[20,48]

A secondary photo-oxidation pathway yielding propane and CO from C−C bond scission in the primary product, isobutanal, is observed at low temperatures where the isobutanal remains trapped on the surface. Propane is formed from isobutanal by a consecutive oxidation by photoholes in contrast to the assumption that an alkane reaction product may involve a reduction by photoelectrons. The CO is formed at higher temperature and is likely formed via formation of formate on the basis of an analogy with the literature.[56,59]

A consequence of these two parallel pathways is that the overall selectivity for the photo-oxidation of isobutanol is strongly temperature dependent. Formation of propane requires that the isobutanal produced in the first photo-chemical step has a significant surface lifetime. The surface

https://dx.doi.org/10.1021/jacs.0c04411
J. Am. Chem. Soc. 2020, 142, 13072−13080

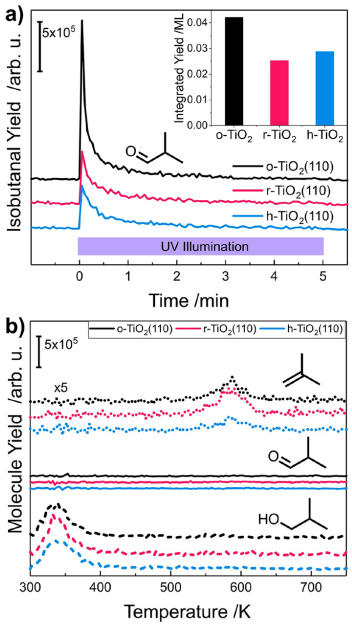

Figure 3. Photo-oxidation of isobutoxy at 300 K yields gas-phase isobutanal with the inset showing integrated yields of isobutanal on the three different surface preparations. a) Photon-stimulated production of gaseous isobutanal (m/z 72, solid line) from isobutanol (m/z 74, dashed line) oxidation at 300 K is observed using mass spectrometry. b) Ensuing temperature-programmed reaction spectra yielding isobutene (m/z 56, dotted line) and unreacted isobutanol (m/z 74, dashed line) on o-, r-, and h-TiO_2(110). The photoreaction is initiated by illuminating the sample for 5 min with a 365 nm LED after exposure of the various surfaces to 0.55 ML isobutanol at 145 K followed by heating to 300 K and thermalizing for 3 min. After the illumination experiment, a temperature-programmed reaction experiment was carried out to identify the remaining surface species. No other products are detected apart from the expected byproduct water (S7). All data shown are corrected for fragmentation, ionization efficiency and spectrometer transmission differences (see Experimental Section).

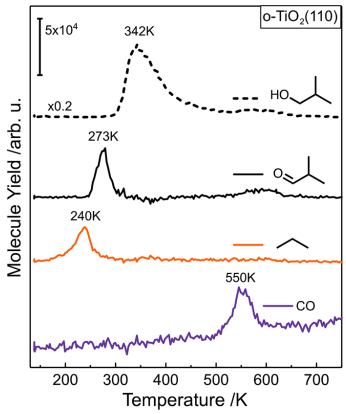

Figure 5. Photochemical products change if isobutoxy species are created before the illumination is carried out at low temperature. No gas phase products are detected during illumination; however, new photoproducts—propane (m/z 29, orange) and CO (m/z 28, purple)—are observed in ensuing temperature-programmed experiments. Isobutanal (m/z 72, solid line) and unreacted isobutanol (m/z 74, dashed line) are also detected. The temperature-programmed reaction data shown were obtained after illumination for 15 min. After exposure of o-TiO_2(110) to 1 L isobutanol at 145 K, subsequent heating to 300 K and recooling to 145 K prior to the illumination was carried out for 15 min with a 365 nm LED. All data shown are corrected for fragmentation, ionization efficiency, spectrometer transmission differences, and contributions from the other products (see Experimental Section).

lifetime of isobutanal at 240 K is estimated to be ~420 s compared to a lifetime of ~0.2 s at 300 K. The surface lifetime under ultrahigh vacuum, $t_{1/2}$, is estimated by assuming first-order desorption and a prefactor, ν_d, of 10^{13} s^{-1},[30]

$$t_{1/2} = \frac{\ln(2)}{\nu_d \times e^{-\Delta H/RT}} \quad (1)$$

Hence, the steady-state concentration of isobutanal at room temperature is extremely low, resulting in no detectable propane formation from secondary oxidation. Conversely, the long surface lifetime of the isobutanal at 240 K favors the secondary photochemical step. A temperature dependence for consecutive photoreactions in the photocatalytic self-coupling

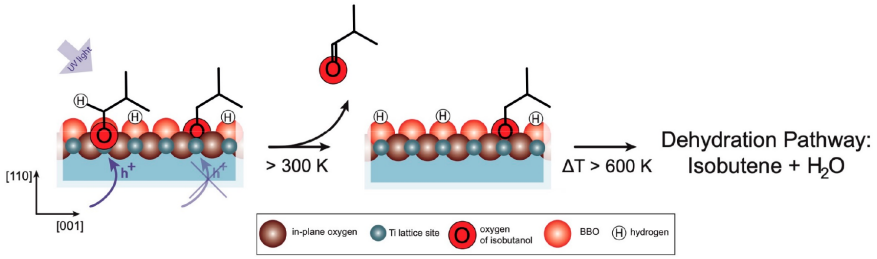

Figure 4. Schematic showing two distinct isobutoxy species, only one of which is photoactive (side-view). The photoactive isobutoxy is oxidized to isobutanal in a hole-driven photoreaction. Isobutanal subsequently desorbs thermally. At 600 K, photoinactive isobutoxy species is dehydrated leading to the formation and desorption of isobutene. The high temperature disproportionation reaction does not occur (Figure 3b).

https://dx.doi.org/10.1021/jacs.0c04411
J. Am. Chem. Soc. 2020, 142, 13072−13080

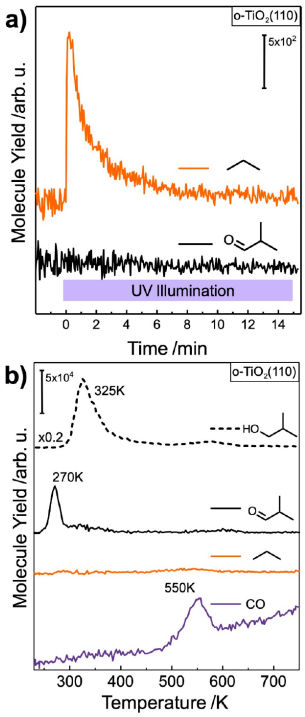

Figure 6. At 240 K, photoproduced isobutanal is thermally hindered to desorb and is oxidized ejecting propane into the gas-phase. (a) Photon-stimulated production of propane (m/z 29, orange) from the photoreaction of isobutanol at 240 K and a consecutive (b) temperature-programmed reaction spectra yielding isobutanal (m/z 72, solid line), propane (m/z 29, orange), and nonreactive isobutanol (m/z 74, dashed line) on o-TiO_2(110). The total UV illumination time is 15 min with a 365 nm LED. No other products are detected. All data shown are corrected for fragmentation, ionization efficiency, spectrometer transmission differences, and contributions from the other products (see Experimental Section).

of methanol to methyl formate vs evolution of formaldehyde has previously been reported, establishing that this is a general principle.[13,16,30]

These results underscore the importance of temperature in determining the selectivity of photocatalytic transformations. Under catalytic conditions, the steady-state concentration of photoactive adsorbed species will depend on operating temperature, reactant pressures, and flow rate. A detailed microkinetic analysis for this system, that it not under catalytic conditions, is not feasible, as detailed in earlier work.[16] Hence, conditions and reactor design can be configured to optimize desired reaction selectivity.

The surface preparations modeling the presence of anaerobic conditions, oxygen, or water do not show a significant effect on the observed photochemical selectivity under these extremely low-pressure conditions, although the overall yield of the processes did change. Oxygen is known to promote alkoxy formation,[6,18,22,41] the key intermediate for the first photo-oxidation step and, consequently, the largest yield in photoproducts are observed on oxidized-TiO_2(110). Surface hydroxylation resembling water present on the surface did not change the photochemical conversion of alkoxy species in line with observations for other alcohols.[26,55] Therefore, the pressure of O_2 during photocatalytic transformation of alcohols will be a critical factor in determining rates.

Although only rutile TiO_2(110) was investigated here, it is likely that these phenomena will be qualitatively similar for more complex materials, even containing other phases of titania, such as anatase[63] and brookite.[64] Previous studies have demonstrated that the same photochemical reaction pathways apply to nanostructured TiO_2 materials such as nanowires[41,64,65] or nanocrystals,[66,67] supporting this argument. Accordingly, the temperature dependence of reaction selectivity is likely to be a general phenomenon. Indeed, a previous study of room temperature photoreforming of butanol on Pd/TiO_2 (based on P25 TiO_2) in aqueous solution found the formation of propane among other expected reaction products and also related it to recombination of an alkyl species with a hydrogen atom.[10]

CONCLUSION

The overall selectivity for photochemical reforming of isobutanol using titania is strongly dependent on surface temperature. The underlying reason for this effect is that thermal desorption of the primary photoproduct competes with a sequential photochemical reaction. For the case of isobutanol, the products are completely different at 240 vs 300 K. Isobutanal, an aldehyde, is the initial photoproduct and predominates at room temperature and above where thermal desorption is fast. In contrast, propane and CO are formed at

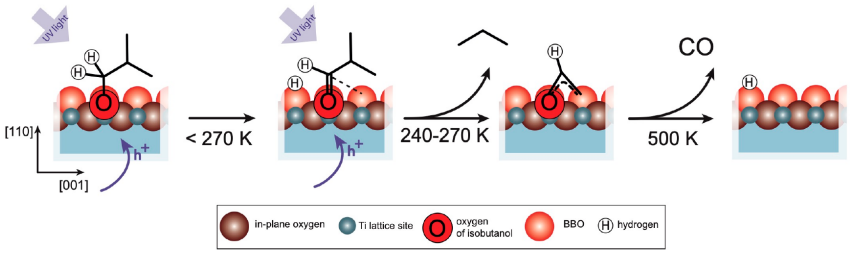

Figure 7. The photoreaction scheme shows the hole-driven oxidation of isobutoxy to isobutanal, which is photo-oxidized in a consecutive reaction yielding propane and a CO intermediate. The adsorbed CO-intermediate is desorbing as CO at 500 K.

https://dx.doi.org/10.1021/jacs.0c04411
J. Am. Chem. Soc. 2020, 142, 13072−13080

240 K, where thermal desorption of isobutanal is slow, allowing the sequential photoreaction step to dominate. Competition between thermal desorption and secondary photochemical reactions should generally be considered in photocatalysis.

While the observation of an alkane from the photochemistry could be ascribed to a reduction reaction with photoelectrons, the alkane in the presented reaction mechanisms stems from a consecutive photo-oxidation reaction and recombination with a surface hydroxyl. This showcases the importance of a mechanistic understanding of photochemical elementary steps and mechanisms to understand catalytic transformations on the example of isobutanol photo-oxidation. This knowledge is a prerequisite to design sustainable photocatalysts and photocatalytic reactors for selective transformations from biomass or biofuels for feedstock chemicals or energy purposes.

■ ASSOCIATED CONTENT

Supporting Information

The Supporting Information is available free of charge at https://pubs.acs.org/doi/10.1021/jacs.0c04411.

Detailed description of the product identification and quantification along with standard reactivity benchmarks of TiO_2(110) including temperature-programmed desorption of H_2O and photon-stimulated desorption of O_2; coverage-dependent thermal desorption data for isobutanol and a quantitative evaluation; further photoreaction data of isobutanol and isobutanal show the temperature-dependent behavior, the formed byproducts such as water and the identification of the reaction products on all surface preparations (PDF)

■ AUTHOR INFORMATION

Corresponding Author

Cynthia M. Friend − *Department of Chemistry and Chemical Biology, Harvard University, Cambridge, Massachusetts 02138, United States;* orcid.org/0000-0002-8673-9046; Email: friend@fas.harvard.edu

Authors

Carla Courtois − *Chair of Physical Chemistry & Catalysis Research Center, Technical University of Munich, 85748 Garching, Germany*

Constantin A. Walenta − *Department of Chemistry and Chemical Biology, Harvard University, Cambridge, Massachusetts 02138, United States;* orcid.org/0000-0001-9879-5101

Martin Tschurl − *Chair of Physical Chemistry & Catalysis Research Center, Technical University of Munich, 85748 Garching, Germany;* orcid.org/0000-0001-6618-7312

Ueli Heiz − *Chair of Physical Chemistry & Catalysis Research Center, Technical University of Munich, 85748 Garching, Germany;* orcid.org/0000-0002-9403-1486

Complete contact information is available at: https://pubs.acs.org/10.1021/jacs.0c04411

Author Contributions

[$]The authors contributed equally to this work.

Notes

The authors declare no competing financial interest.

■ ACKNOWLEDGMENTS

C.C. acknowledges the support by the Luxembourg National Research Fund (FNR), project code 12531916 and by the TUM International Graduate School of Science and Engineering (TUM-IGSSE). C.A.W. and C.M.F. gratefully acknowledge support of this work by the U.S. Army Research Office under Grant No. W911NF1820143 and by the Defense Threat Reduction Agency under Program No. CB3934. C.C., M.T., and U.H. thank the DFG for financial support through HE3435/22-1 and under Germany's Excellence Strategy − EXC 2089/1-390776260.

■ REFERENCES

(1) Christoforidis, K. C.; Fornasiero, P. Photocatalytic Hydrogen Production: A Rift into the Future Energy Supply. *ChemCatChem* **2017**, *9* (9), 1523−1544.

(2) Kuehnel, M. F.; Reisner, E. Solar Hydrogen Generation from Lignocellulose. *Angew. Chem., Int. Ed.* **2018**, *57* (13), 3290−3296.

(3) Cargnello, M.; Gasparotto, A.; Gombac, V.; Montini, T.; Barreca, D.; Fornasiero, P. Photocatalytic H_2 and Added-Value By-Products − The Role of Metal Oxide Systems in Their Synthesis from Oxygenates. *Eur. J. Inorg. Chem.* **2011**, *2011* (28), 4309−4323.

(4) Lee, S. Y.; Kim, H. U.; Chae, T. U.; Cho, J. S.; Kim, J. W.; Shin, J. H.; Kim, D. I.; Ko, Y.-S.; Jang, W. D.; Jang, Y.-S. A Comprehensive Metabolic Map for Production of Bio-Based Chemicals. *Nat. Catal.* **2019**, *2* (1), 18−33.

(5) Peralta-Yahya, P. P.; Zhang, F.; del Cardayre, S. B.; Keasling, J. D. Microbial Engineering for the Production of Advanced Biofuels. *Nature* **2012**, *488* (7411), 320−328.

(6) Higashide, W.; Li, Y.; Yang, Y.; Liao, J. C. Metabolic Engineering of Clostridium Cellulolyticum for Production of Isobutanol from Cellulose. *Appl. Environ. Microbiol.* **2011**, *77* (8), 2727.

(7) Chakrabarti, R.; Kruger, J. S.; Hermann, R. J.; Schmidt, L. D. Autothermal Reforming of Isobutanol. *RSC Adv.* **2012**, *2* (6), 2527−2533.

(8) Butburee, T.; Chakthranont, P.; Phawa, C.; Faungnawakij, K. Beyond Artificial Photosynthesis: Prospects on Photobiorefinery. *ChemCatChem* **2020**, *12* (7), 1873.

(9) Navarro, R. M.; Sánchez-Sánchez, M. C.; Alvarez-Galvan, M. C.; Valle, F. d.; Fierro, J. L. G. Hydrogen Production from Renewable Sources: Biomass and Photocatalytic Opportunities. *Energy Environ. Sci.* **2009**, *2* (1), 35−54.

(10) Bowker, M. Sustainable Hydrogen Production by the Application of Ambient Temperature Photocatalysis. *Green Chem.* **2011**, *13* (9), 2235−2246.

(11) Bowker, M. Photocatalytic Hydrogen Production and Oxygenate Photoreforming. *Catal. Lett.* **2012**, *142* (8), 923−929.

(12) McClelland, K. P.; Weiss, E. A. Selective Photocatalytic Oxidation of Benzyl Alcohol to Benzaldehyde or C−C Coupled Products by Visible-Light-Absorbing Quantum Dots. *ACS Appl. Energy Mater.* **2019**, *2* (1), 92−96.

(13) Kollmannsberger, S. L.; Walenta, C. A.; Courtois, C.; Tschurl, M.; Heiz, U. Thermal Control of Selectivity in Photocatalytic, Water-Free Alcohol Photoreforming. *ACS Catal.* **2018**, *8*, 11076−11084.

(14) Jiang, Y.; Wang, C.; Rogers, C. R.; Kodaimati, M. S.; Weiss, E. A. Regio- and Diastereoselective Intermolecular [2 + 2] Cycloadditions Photocatalysed by Quantum Dots. *Nat. Chem.* **2019**, *11* (11), 1034−1040.

(15) Kominami, H.; Sugahara, H.; Hashimoto, K. Photocatalytic Selective Oxidation of Methanol to Methyl Formate in Gas Phase over Titanium(IV) Oxide in a Flow-Type Reactor. *Catal. Commun.* **2010**, *11* (5), 426−429.

(16) Phillips, K. R.; Jensen, S. C.; Baron, M.; Li, S.-C.; Friend, C. M. Sequential Photo-Oxidation of Methanol to Methyl Formate on TiO_2(110). *J. Am. Chem. Soc.* **2013**, *135* (2), 574−577.

(17) Henderson, M. A. A Surface Science Perspective on TiO_2 Photocatalysis. *Surf. Sci. Rep.* **2011**, *66* (6), 185−297.

(18) Shen, M.; Henderson, M. A. Identification of the Active Species in Photochemical Hole Scavenging Reactions of Methanol on TiO_2. *J. Phys. Chem. Lett.* **2011**, *2* (21), 2707−2710.
(19) Walenta, C. A.; Kollmannsberger, S. L.; Courtois, C.; Pereira, R. N.; Stutzmann, M.; Tschurl, M.; Heiz, U. Why Co-Catalyst-Loaded Rutile Facilitates Photocatalytic Hydrogen Evolution. *Phys. Chem. Chem. Phys.* **2019**, *21* (3), 1491−1496.
(20) Hansen, J. Ø.; Bebensee, R.; Martinez, U.; Porsgaard, S.; Lira, E.; Wei, Y.; Lammich, L.; Li, Z.; Idriss, H.; Besenbacher, F.; Hammer, B.; Wendt, S. Unravelling Site-Specific Photo-Reactions of Ethanol on Rutile TiO_2(110). *Sci. Rep.* **2016**, *6*, 21990.
(21) Harrison, G.; Katsiev, K.; Alsalik, Y.; Thornton, G.; Idriss, H. Switch in Photocatalytic Reaction Selectivity: The Effect of Oxygen Partial Pressure on Carbon-Carbon Bond Dissociation over Hydroxylated TiO_2(110) Surfaces. *J. Catal.* **2018**, *363*, 117−127.
(22) Walenta, C. A.; Tschurl, M.; Heiz, U. Introducing Catalysis in Photocatalysis: What can be Understood from Surface Science Studies of Alcohol Photoreforming on TiO_2. *J. Phys.: Condens. Matter* **2019**, *31* (47), 473002.
(23) Kolesov, G.; Vinichenko, D.; Tritsaris, G. A.; Friend, C. M.; Kaxiras, E. Anatomy of the Photochemical Reaction: Excited-State Dynamics Reveals the C−H Acidity Mechanism of Methoxy Photo-oxidation on Titania. *J. Phys. Chem. Lett.* **2015**, *6* (9), 1624−1627.
(24) Chu, W.; Saidi, W. A.; Zheng, Q.; Xie, Y.; Lan, Z.; Prezhdo, O. V.; Petek, H.; Zhao, J. Ultrafast Dynamics of Photongenerated Holes at a CH_3OH/TiO_2 Rutile Interface. *J. Am. Chem. Soc.* **2016**, *138* (41), 13740−13749.
(25) Shen, M.; Acharya, D. P.; Dohnálek, Z.; Henderson, M. A. Importance of Diffusion in Methanol Photochemistry on TiO_2(110). *J. Phys. Chem. C* **2012**, *116* (48), 25465−25469.
(26) Shen, M.; Henderson, M. A. Role of Water in Methanol Photochemistry on Rutile TiO_2(110). *J. Phys. Chem. C* **2012**, *116* (35), 18788−18795.
(27) Zhou, C.; Ren, Z.; Tan, S.; Ma, Z.; Mao, X.; Dai, D.; Fan, H.; Yang, X.; LaRue, J.; Cooper, R.; Wodtke, A. M.; Wang, Z.; Li, Z.; Wang, B.; Yang, J.; Hou, J. Site-Specific Photocatalytic Splitting of Methanol on TiO_2(110). *Chem. Sci.* **2010**, *1* (5), 575−580.
(28) Guo, Q.; Zhou, C.; Ma, Z.; Ren, Z.; Fan, H.; Yang, X. Elementary Photocatalytic Chemistry on TiO_2 Surfaces. *Chem. Soc. Rev.* **2016**, *45* (13), 3701−3730.
(29) Guo, Q.; Xu, C.; Yang, W.; Ren, Z.; Ma, Z.; Dai, D.; Minton, T. K.; Yang, X. Methyl Formate Production on TiO_2(110), Initiated by Methanol Photocatalysis at 400 nm. *J. Phys. Chem. C* **2013**, *117* (10), 5293−5300.
(30) Walenta, C. A.; Courtois, C.; Kollmannsberger, S. L.; Eder, M.; Tschurl, M.; Heiz, U. Surface Species in Photocatalytic Methanol Reforming on Pt/TiO_2(110): Learning from Surface Science Experiments for Catalytically Relevant Conditions. *ACS Catal.* **2020**, *10*, 4080−4091.
(31) Lang, X.; Wen, B.; Zhou, C.; Ren, Z.; Liu, L.-M. First-Principles Study of Methanol Oxidation into Methyl Formate on Rutile TiO_2(110). *J. Phys. Chem. C* **2014**, *118* (34), 19859−19868.
(32) Puga, A. V.; Forneli, A.; García, H.; Corma, A. Production of H_2 by Ethanol Photoreforming on Au/TiO_2. *Adv. Funct. Mater.* **2014**, *24* (2), 241−248.
(33) Walenta, C. A.; Crampton, A. S.; Xu, F.; Heiz, U.; Friend, C. M. Chemistry of Methanol and Ethanol on Ozone-Prepared α-Fe_2O_3(0001). *J. Phys. Chem. C* **2018**, *122* (44), 25404−25410.
(34) Xu, F.; Chen, W.; Walenta, C. A.; O'Connor, C. R.; Friend, C. M. Dual Lewis Site Creation for Activation of Methanol on Fe_3O_4(111) Thin Films. *Chem. Sci.* **2020**, *11*, 2448−2454.
(35) Zehr, R. T.; Henderson, M. A. Influence of O_2-induced Surface Roughening on the Chemistry of Water on TiO_2(110). *Surf. Sci.* **2008**, *602* (8), 1507−1516.
(36) Henderson, M. A. Relationship of O_2 Photodesorption in Photooxidation of Acetone on TiO_2. *J. Phys. Chem. C* **2008**, *112* (30), 11433−11440.
(37) Henderson, M. A.; Shen, M.; Wang, Z.-T.; Lyubinetsky, I. Characterization of the Active Surface Species Responsible for UV-Induced Desorption of O_2 from the Rutile TiO_2(110) Surface. *J. Phys. Chem. C* **2013**, *117* (11), 5774−5784.
(38) Rusu, C. N.; Yates, J. T. Defect Sites on TiO_2(110): Detection by O_2 Photodesorption. *Langmuir* **1997**, *13* (16), 4311−4316.
(39) Dohnálek, Z.; Lyubinetsky, I.; Rousseau, R. Thermally-Driven Processes on Rutile TiO_2(110)-(1 × 1): A Direct View at the Atomic Scale. *Prog. Surf. Sci.* **2010**, *85* (5), 161−205.
(40) Kim, B.; Li, Z.; Kay, B. D.; Dohnalek, Z.; Kim, Y. K. The Effect of Oxygen Vacancies on the Binding Interactions of NH_3 with Rutile TiO_2(110)-1 × 1. *Phys. Chem. Chem. Phys.* **2012**, *14* (43), 15060−15065.
(41) Crampton, A. S.; Cai, L.; Janvelyan, N.; Zheng, X.; Friend, C. M. Methanol Photo-Oxidation on Rutile TiO_2 Nanowires: Probing Reaction Pathways on Complex Materials. *J. Phys. Chem. C* **2017**, *121* (18), 9910−9919.
(42) Li, Z.; Smith, R. S.; Kay, B. D.; Dohnálek, Z. Determination of Absolute Coverages for Small Aliphatic Alcohols on TiO_2(110). *J. Phys. Chem. C* **2011**, *115* (45), 22534−22539.
(43) Kim, Y. K.; Kay, B. D.; White, J. M.; Dohnálek, Z. Inductive Effect of Alkyl Chains on Alcohol Dehydration at Bridge-bonded Oxygen Vacancies of TiO_2(110). *Catal. Lett.* **2007**, *119* (1), 1−4.
(44) Kim, Y. K.; Kay, B. D.; White, J. M.; Dohnálek, Z. Alcohol Chemistry on Rutile TiO_2(110): The Influence of Alkyl Substituents on Reactivity and Selectivity. *J. Phys. Chem. C* **2007**, *111* (49), 18236−18242.
(45) Bondarchuk, O.; Kim, Y. K.; White, J. M.; Kim, J.; Kay, B. D.; Dohnalek, Z. Surface Chemistry of 2-Propanol on TiO_2(110): Low- and High-Temperature Dehydration, Isotope Effects, and Influence of Local Surface Structure. *J. Phys. Chem. C* **2007**, *111* (29), 11059−11067.
(46) Zhang, Z.; Bondarchuk, O.; Kay, B. D.; White, J. M.; Dohnálek, Z. Direct Visualization of 2-Butanol Adsorption and Dissociation on TiO_2(110). *J. Phys. Chem. C* **2007**, *111* (7), 3021−3027.
(47) Walenta, C. A.; Kollmannsberger, S. L.; Pereira, R. N.; Tschurl, M.; Stutzmann, M.; Heiz, U. Anhydrous Ethanol Dehydrogenation on Metal−Organic Chemical Vapor Deposition Grown GaN(0001). *J. Phys. Chem. C* **2017**, *121* (30), 16393−16398.
(48) Walenta, C. A.; Kollmannsberger, S. L.; Kiermaier, J.; Winbauer, A.; Tschurl, M.; Heiz, U. Ethanol Photocatalysis on Rutile TiO_2(110): the Role of Defects and Water. *Phys. Chem. Chem. Phys.* **2015**, *17* (35), 22809−22814.
(49) Guo, Q.; Zhou, C.; Ma, Z.; Ren, Z.; Fan, H.; Yang, X. Elementary Chemical Reactions in Surface Photocatalysis. *Annu. Rev. Phys. Chem.* **2018**, *69* (1), 451−472.
(50) Kim, Y. K.; Kay, B. D.; White, J. M.; Dohnálek, Z. 2-Propanol dehydration on TiO_2(110): The effect of bridge-bonded oxygen vacancy blocking. *Surf. Sci.* **2008**, *602* (2), 511−516.
(51) Henderson, M. A. A Surface Perspective on Self-Diffusion in Rutile TiO_2. *Surf. Sci.* **1999**, *419* (2), 174−187.
(52) Henderson, M. A.; Otero-Tapia, S.; Castro, M. E. The Chemistry of Methanol on the TiO_2(110) Surface: the Influence of Vacancies and Coadsorbed Species. *Faraday Discuss.* **1999**, *114* (0), 313−329.
(53) Liu, S.; Liu, A.-a.; Wen, B.; Zhang, R.; Zhou, C.; Liu, L.-M.; Ren, Z. Coverage Dependence of Methanol Dissociation on TiO_2(110). *J. Phys. Chem. Lett.* **2015**, *6* (16), 3327−3334.
(54) Zhang, R.; Wang, H.; Peng, X.; Feng, R.-r.; Liu, A.-a.; Guo, Q.; Zhou, C.; Ma, Z.; Yang, X.; Jiang, Y.; Ren, Z. In Situ Studies on Temperature-Dependent Photocatalytic Reactions of Methanol on TiO_2(110). *J. Phys. Chem. C* **2019**, *123* (15), 9993−9999.
(55) Courtois, C.; Eder, M.; Schnabl, K.; Walenta, C. A.; Tschurl, M.; Heiz, U. Reactions in the Photocatalytic Conversion of Tertiary Alcohols on Rutile TiO_2(110). *Angew. Chem., Int. Ed.* **2019**, *58* (ja), 14255.
(56) Cremer, T.; Jensen, S. C.; Friend, C. M. Enhanced Photo-Oxidation of Formaldehyde on Highly Reduced o-TiO_2(110). *J. Phys. Chem. C* **2014**, *118* (50), 29242−29251.
(57) Haubrich, J.; Kaxiras, E.; Friend, C. M. The Role of Surface and Subsurface Point Defects for Chemical Model Studies on TiO2: A

https://dx.doi.org/10.1021/jacs.0c04411
J. Am. Chem. Soc. 2020, 142, 13072−13080

First-Principles Theoretical Study of Formaldehyde Bonding on Rutile TiO2(110). *Chem. - Eur. J.* **2011**, *17* (16), 4496−4506.
(58) Dohnálek, Z.; Kim, J.; Bondarchuk, O.; White, J. M.; Kay, B. D. Physisorption of N_2, O_2, and CO on Fully Oxidized TiO_2(110). *J. Phys. Chem. B* **2006**, *110* (12), 6229−6235.
(59) Henderson, M. A. Complexity in the Decomposition of Formic Acid on the TiO_2(110) Surface. *J. Phys. Chem. B* **1997**, *101* (2), 221−229.
(60) Henderson, M. A. Formic Acid Decomposition on the {110}-Microfaceted Surface of TiO_2(100): Insights Derived from ^{18}O-Labeling Studies. *J. Phys. Chem.* **1995**, *99* (41), 15253−15261.
(61) Zehr, R. T.; Henderson, M. A. Acetaldehyde Photochemistry on TiO_2(110). *Surf. Sci.* **2008**, *602* (13), 2238−2249.
(62) Ma, Z.; Guo, Q.; Mao, X.; Ren, Z.; Wang, X.; Xu, C.; Yang, W.; Dai, D.; Zhou, C.; Fan, H.; Yang, X. Photocatalytic Dissociation of Ethanol on TiO_2(110) by Near-Band-Gap Excitation. *J. Phys. Chem. C* **2013**, *117* (20), 10336−10344.
(63) Setvin, M.; Shi, X.; Hulva, J.; Simschitz, T.; Parkinson, G. S.; Schmid, M.; Di Valentin, C.; Selloni, A.; Diebold, U. Methanol on Anatase TiO_2(101): Mechanistic Insights into Photocatalysis. *ACS Catal.* **2017**, *7* (10), 7081−7091.
(64) Pepin, P. A.; Diroll, B. T.; Choi, H. J.; Murray, C. B.; Vohs, J. M. Thermal and Photochemical Reactions of Methanol, Acetaldehyde, and Acetic Acid on Brookite TiO_2 Nanorods. *J. Phys. Chem. C* **2017**, *121* (21), 11488−11498.
(65) Pepin, P. A.; Lee, J. D.; Murray, C. B.; Vohs, J. M. Thermal and Photocatalytic Reactions of Methanol and Acetaldehyde on Pt-Modified Brookite TiO_2 Nanorods. *ACS Catal.* **2018**, *8*, 11834−11846.
(66) Bennett, D. A.; Cargnello, M.; Diroll, B. T.; Murray, C. B.; Vohs, J. M. Shape-Dependence of the Thermal and Photochemical Reactions of Methanol on Nanocrystalline Anatase TiO_2. *Surf. Sci.* **2016**, *654*, 1−7.
(67) Pepin, P. A.; Lee, J. D.; Foucher, A. C.; Murray, C. B.; Stach, E. A.; Vohs, J. M. The Influence of Surface Platinum Deposits on the Photocatalytic Activity of Anatase TiO_2 Nanocrystals. *J. Phys. Chem. C* **2019**, *123* (16), 10477−10486.

https://dx.doi.org/10.1021/jacs.0c04411
J. Am. Chem. Soc. 2020, 142, 13072−13080

Supporting Information: Regulating Photochemical Selectivity with Temperature: Isobutanol on TiO_2(110)

Carla Courtois[¶,‡], Constantin A. Walenta[§,‡], Martin Tschurl[¶], Ueli Heiz[¶] and Cynthia M. Friend[§,*]

¶ Chair of Physical Chemistry & Catalysis Research Center, Technical University of Munich, Lichtenbergstr. 4, 85748 Garching, Germany
§ Department of Chemistry and Chemical Biology, Harvard University, 12 Oxford Street, Cambridge, Massachusetts 02138, United States

*Corresponding Author: friend@fas.harvard.edu
‡ The authors contributed equally to this work

Experimental Details

The products are identified and quantified with the QMS by taking into account the fragmentation pattern, the electron impact ionization cross-section and the transmission coefficient. The ionization cross section and the masses used for data evaluation are listed in Table S1. Monitored masses for the experiments with isobutanol are 101, 99, 89, 88, 74, 73, 72, 71, 57, 56, 55, 44, 43, 42, 41, 40, 39, 33, 32, 31, 30, 29, 28, 27, 26, 18, 16, 15, 2 and with isobutanal 112, 101, 99, 89, 88, 74, 73, 72, 71, 69, 57, 56, 55, 44, 43, 42, 41, 40, 39, 33, 32, 31, 30, 29, 28, 27, 26, 18, 16, 15, 2. Isobutene is identified as the dehydration product both from a logic of the alcohol structure as well as its fragmentation pattern, that is different from other 1-butene and 2-butene.

Table S1. Mass fragments and respective electron impact ionization cross-section of the molecules used for data evaluation.

Molecule	m/z	ICS [Å^2]
Isobutanol	33/74	12.6[1]
Isobutanal	43/72	11.4[2]
Isobutene	56	11.9[3]
Propane	29/44	11.6[4]
CO	28	2.5[5]

Complementary Data

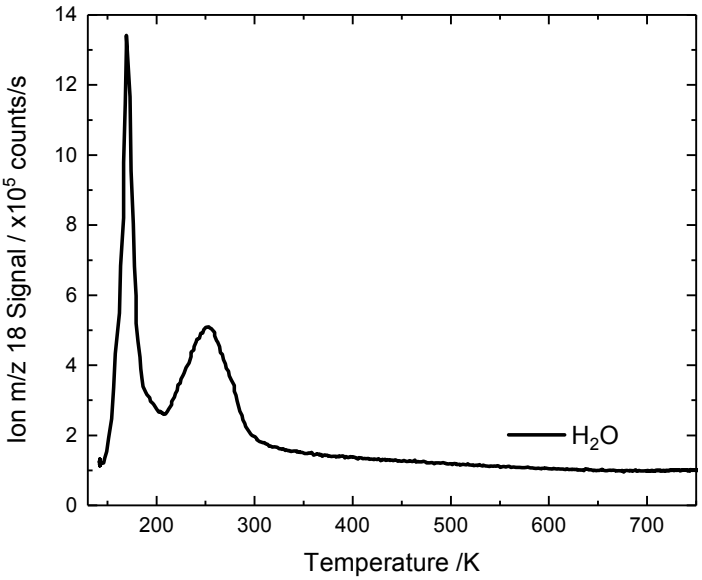

Figure S1. Thermal programmed desorption spectrum of H_2O (*m/z* 18) from r-TiO_2(110). Water is molecularly desorbing from BBO and Ti_{5c} sites. No BBO_v feature is discernable, which indicates a BBO_v concentration of ≤2% ML. The titania crystal shows the very light blue color.

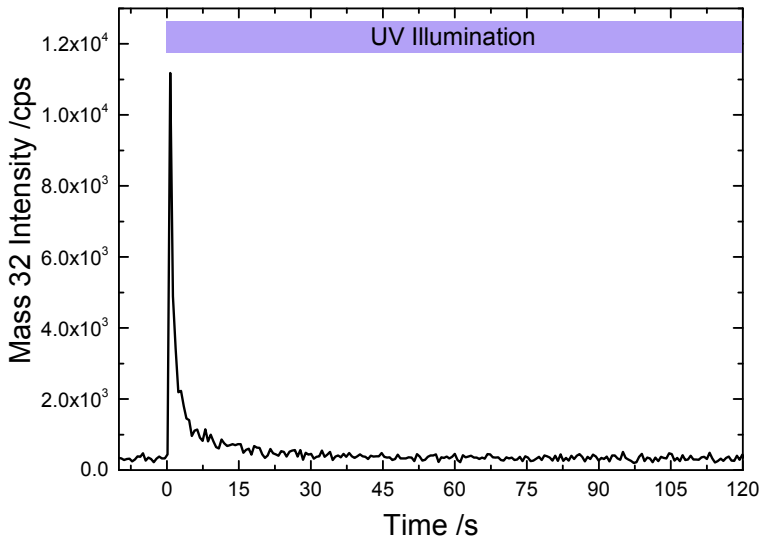

Figure S2. Photon-stimulated desorption of O_2 (*m/z* 32) at 145 K from the pale blue r-TiO_2(110). 20 L O_2 is dosed at 145 K prior to the illumination with a 365 nm LED, characterized in Figure S3.

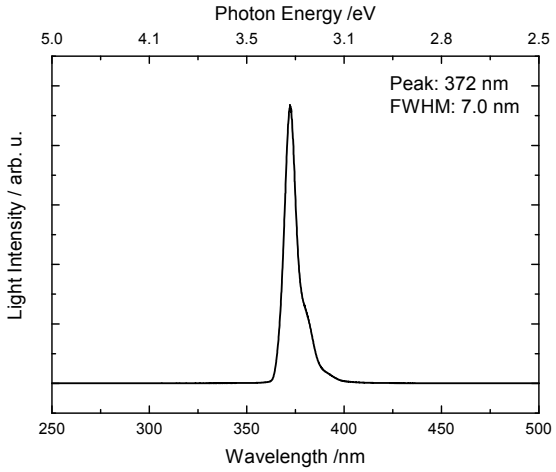

Figure S3. UV-spectrum of the 365 nm LED. The total LED intensity is measured to be 0.15 W directly at the light source.

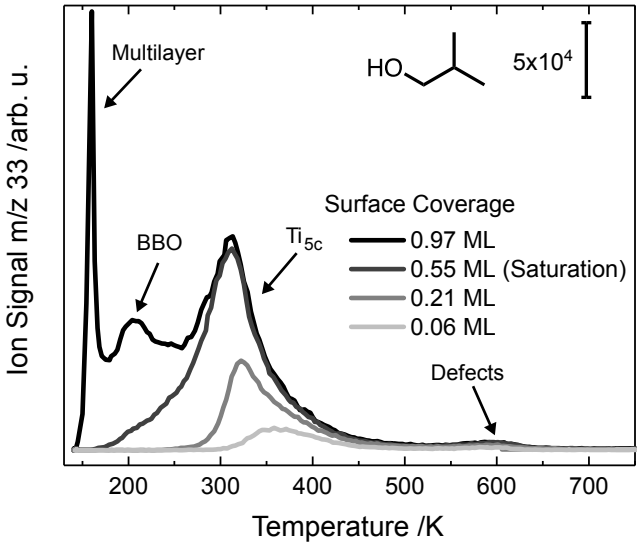

Figure S4. The majority of isobutanol molecularly desorbs from reduced TiO_2(110) below 400 K. Mass 33 is an unequivocal ionization fragment of isobutanol. Isobutanol is dosed at 145 K and the heating ramp is 1 K/s. The desorption peaks are in analogy to prior work by which the saturation coverage of isobutanol is estimated to be 0.55 ML with respect to Ti_{5c} sites.[6] The peak at 165 K attributed to sublimation of condensed isobutanol. The peak at 200 K is assigned to isobutanol adsorbed to bridge-bonded oxygen (BBO) sites, whereas the coverage-dependent peak observed between 300 and 350 K is ascribed to mostly molecular binding to Ti_{5c} sites, in analogy to other alcohols described in the literature.[6] This peak shifts to lower temperature as a function of coverage (0.06 ML - 0.97 ML), which is characteristic of alcohols on TiO_2(110).[6]

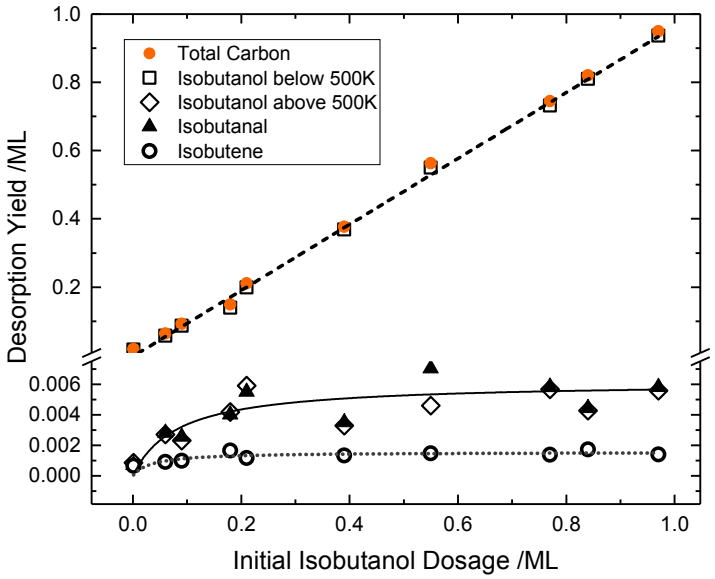

Figure S5. The integrated yields measured from temperature-programmed reaction experiments show that the selectivity for the high temperature products is independent of the initial coverage. The reactivity saturates at ~0.2 ML. Integrated yields of isobutanol below and above 500 K, isobutanal and isobutene from several temperature programmed reaction spectra with different initial isobutanol coverages on r-TiO_2(110).

Table S2. Comparison of the yields of isobutanol, isobutanal and isobutene in the low and high temperature regime from the temperature-programmed reaction spectra of isobutanol on o-, r- and h-TiO_2(110) in Figure 1. Whereas the quantity of disproportionation products, isobutanal and isobutanol, is not changing significantly, the conversion of isobutoxy to isobutene is decreased by approximately 50% for the o- and h-TiO_2(110). This corroborates that BBO_v are blocked to some extend by the filling with oxygen or hydroxyls, as they have been attributed to be the active site for the dehydration reaction of small alcohols.[7-9]

	o-TiO_2	**r-TiO_2**	**h-TiO_2**
Isobutanol 145-750 K	0.44 ML	0.55 ML	0.54 ML
Isobutanol 500-675 K	0.0079 ML	0.0073 ML	0.0071 ML
Isobutanal 500-675 K	0.0084 ML	0.0073 ML	0.0070 ML
Isobutene 500-675 K	0.0022 ML	0.0048 ML	0.0025 ML

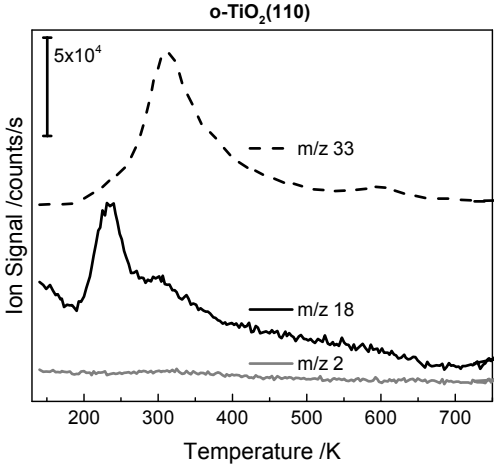

Figure S6. Complementary temperature-programmed reaction spectrum of isobutanol on oxidized-TiO_2(110) showing the raw *m/z* signals of isobutanol (*m/z* 33, dashed lines), H_2O (*m/z* 18, solid line) and *m/z* 2 (grey line). Molecular isobutanol is desorbing at 315 K and is a product of the high temperature reaction at 600 K. Molecular water is desorbing at 235 K, which stems either from alkoxy formation, background adsorption or from impurities in the reactant. The peak at 315 K in the *m/z* 18 trace results from the fragmentation of isobutanol in the QMS. The *m/z* 18 background is decreasing during the experiment. This data is complementary to Figure 1 a). 0.44 ML isobutanol is adsorbed on o-TiO_2(110) and the traces are offset for clarity. Water is formed from the reaction pathways at 600 K, but since the overall amount of reaction is only ≤2% of a monolayer, the detection in the background is not feasible.

Table S3. Comparison of the yields of isobutanol, isobutanal and isobutene high temperature regime from the consecutive temperature-programmed reaction spectra after the photon-stimulated production of isobutanal on o-, r- and h-TiO_2(110) in Figure 3b. Isobutoxy species responsible for the dehydration reaction, are not or less photo-active, respectively based on the integrated product amounts.

	o-TiO_2	**r-TiO_2**	**h-TiO_2**
Isobutanol 500-675 K	< 0.0001 ML	< 0.0001 ML	< 0.0001 ML
Isobutanal 500-675 K	< 0.0001 ML	< 0.0001 ML	< 0.0001 ML
Isobutene 500-675 K	0.0043 ML	0.0047 ML	0.0029 ML

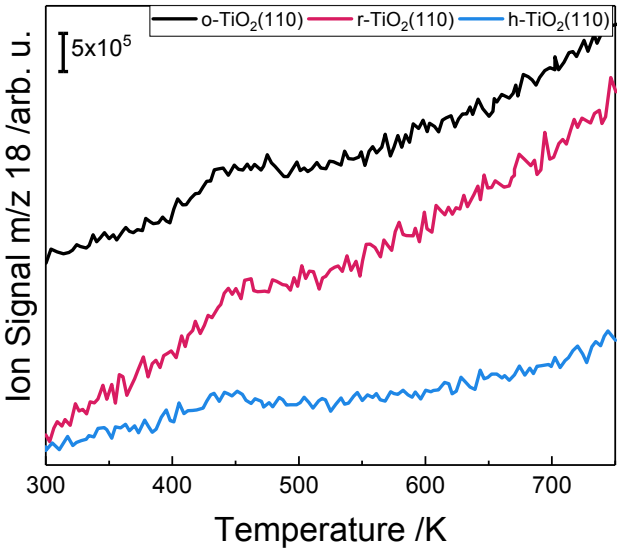

Figure S7. Water is desorbing at 450 K originating from hydroxyl species created during the reaction. Mass traces *m/z 18* (H_2O^+) completing the data from Figure 3. Consecutive TPR spectra after the photon-stimulated production of isobutanal from isobutanol oxidation at 300 K on on o-, r-, and h-TiO_2(110). The graph shows the raw signals of *m/z 18.* The background is rising due to an outgazing of the sample holder.

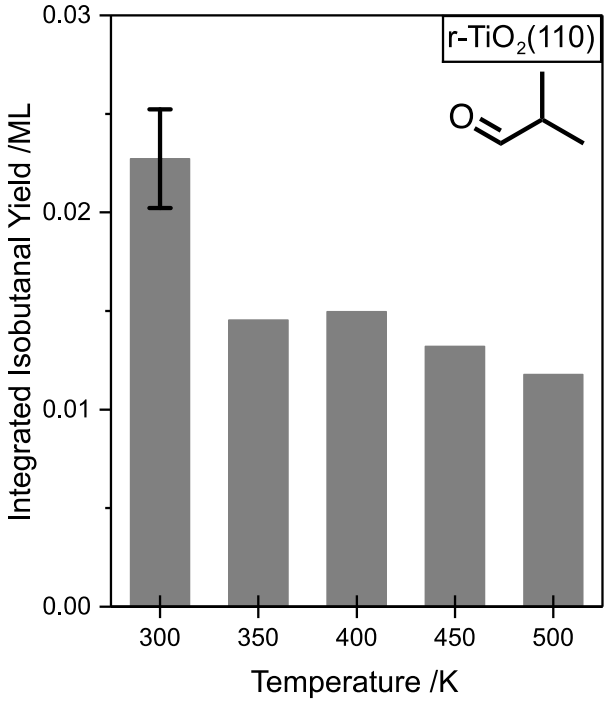

Figure S8. The highest yield of isobutanal in the photo-oxidation of isobutanol is obtained at room temperature. The plot shows the integrated yield of isobutanal in the photon-stimulated reaction experiment of isobutanol on r-TiO_2(110) as function of the reaction temperature. 1 L isobutanol is dosed at 145 K and the sample is thermalized to the reaction temperature. The photo-reaction is initiated by illuminating the sample for 5 min with a 365 nm LED. No other products are detected upon illumination. The PSR at 300 K was repeated 3 times and the value represents the average.

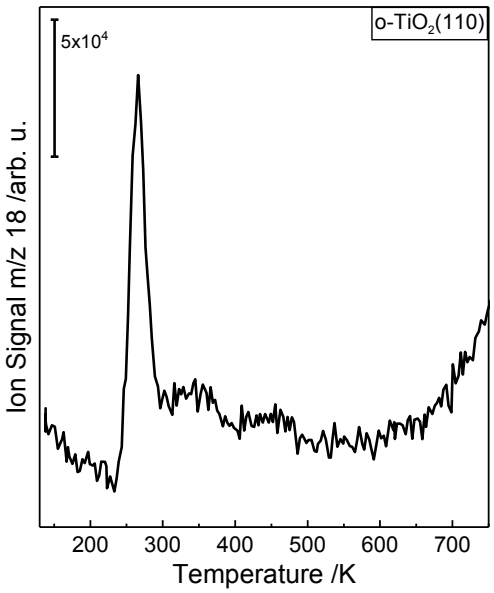

Figure S9. Molecular water, stemming from the background is desorbing at 275 K, recombinative water, originating from hydroxyl species created during the reaction, is desorbing from at 450 K. The mass trace *m/z* 18 (H_2O^+) is completing the data from Figure 5. TPR spectrum after illumination of the sample for 15 min. 1 L isobutanol is dosed at 145 K on o-TiO_2(110) and the sample is thermalized to 300 K and cooled down to 145 K prior to illumination for 15 min. The graph shows the raw signals of *m/z* 18. The background is rising due to an outgasing of the sample holder above 650 K.

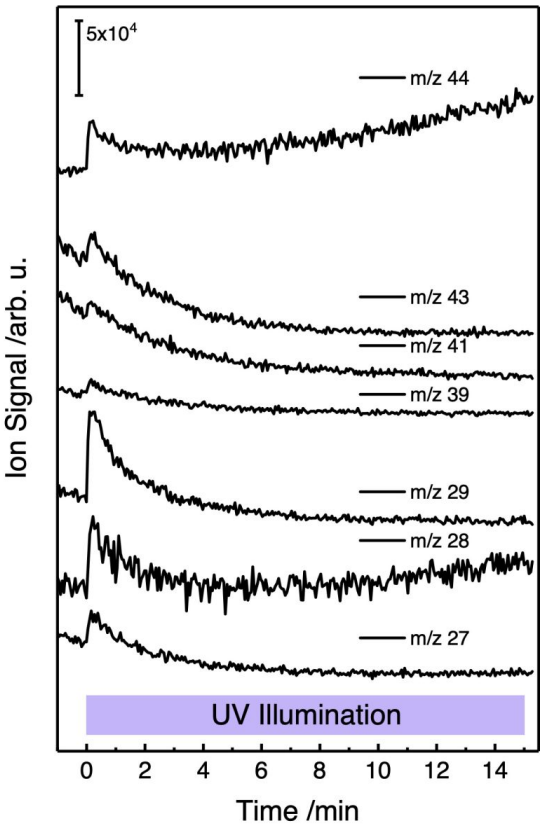

Figure S10. Mass fragments desorbing upon UV illumination of the pre-annealed to 300 K sample at 240 K identifies propane as the sole desorbing product. These mass fragments complement the data shown in Figure 6a). Comparing the mass fragments with the fragmentation pattern of propane from NIST identifies propane as the sole desorbing product.

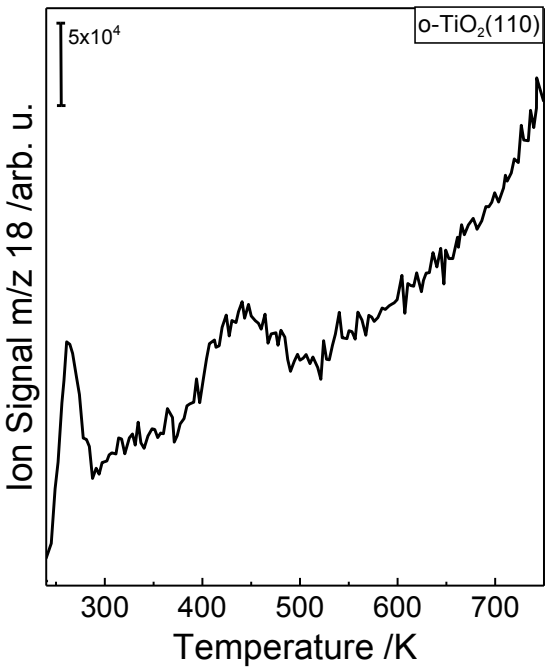

Figure S11. Molecular water, stemming from the background is desorbing at 280 K, and water, originating from hydroxyl species recombination created during the reaction, is desorbing around 450 K. The mass traces *m/z 18* (H_2O^+) is complementary to the data from Figure 6b. TPR spectrum after illumination of the sample at 240 K for 15 min, where solely propane is desorbing. 1 L isobutanol is dosed at 145 K on o-TiO_2(110) and the sample is thermalized to 300 K and cooled down to 240 K prior to illumination for 15 min. The graph shows the raw signals of *m/z 18.* The background is rising due to an outgazing of the sample holder.

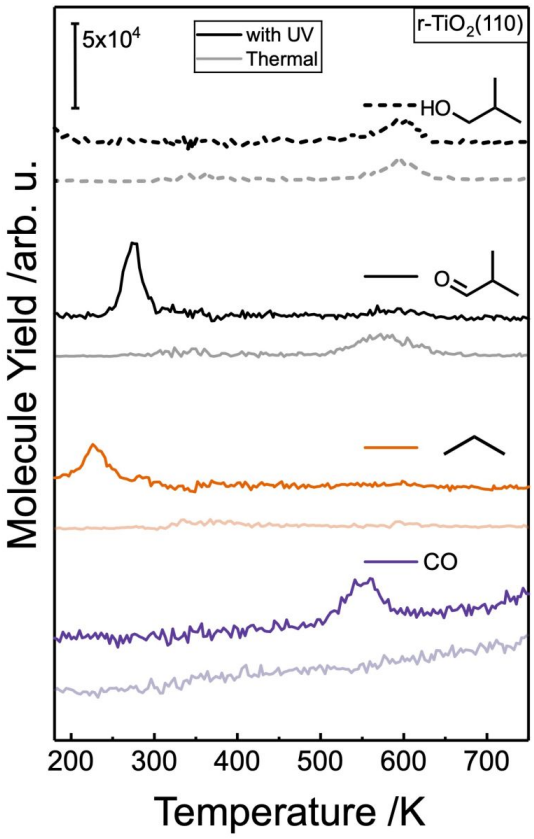

Figure S12. Temperature-programmed reaction spectra of an annealing pre-treated to 300 K sample pre-dosed with alcohol. The conditions with UV-irradiation for 15 min are the same as in Fig. 5 and “thermal” represents a control-experiment without any UV irradiation. Isobutanal, propane and CO are photo-products and not formed thermally through the annealing protocol.

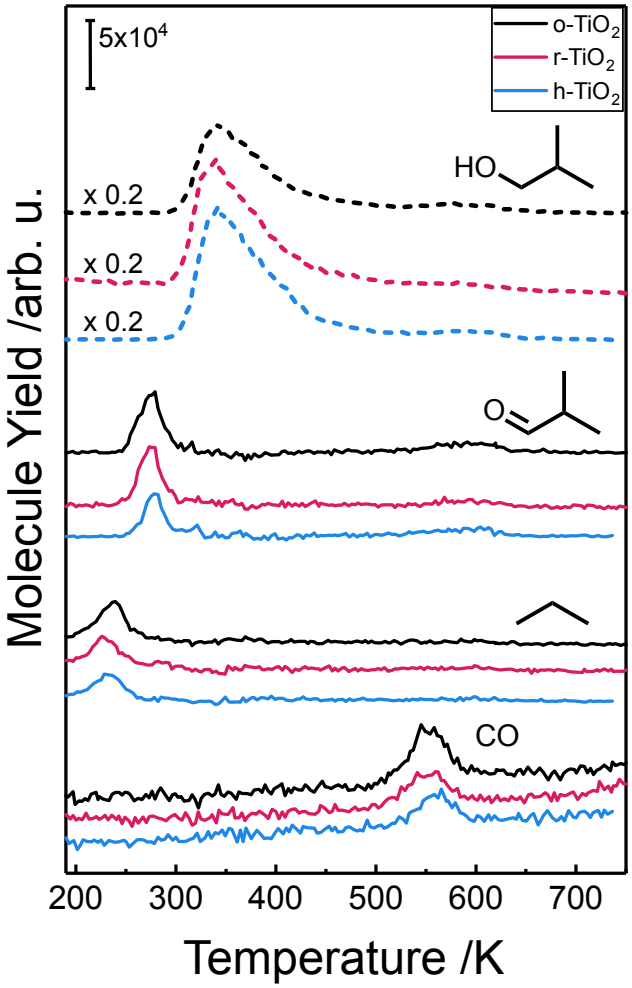

Figure S13. Annealing pre-treatment to 300 K prior to 15 min UV illumination at cryogenic temperatures lead to the formation of propane (*m/z* 29) and CO (*m/z* 28) in addition to the isobutanal (*m/z* 72) in the photo-reaction of isobutanol, desorbing in a consecutive temperature-programmed reaction spectrum o-, r-, and h-TiO_2(110). No specific type of defect is responsible for the formation of propane and CO. No products are desorbing into the gas-phase upon illumination at 145 K. Non-reactive molecular isobutanol (*m/z* 74) is further desorbing. The baselines are off-set for clarity.

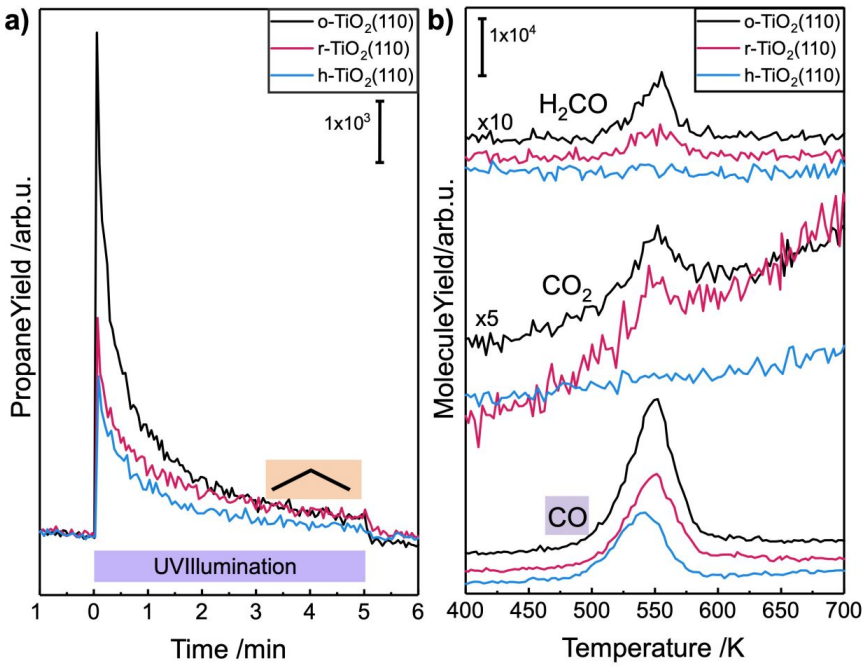

Figure S14. a) Photon-stimulated reaction of isobutanal at 240 K leading to the evolution of propane (*m/z* 29) on o-, r-, and h-TiO_2(110). b) The high temperature regime indicates the formation of a formate species in the consecutive temperature-programmed desorption spectra. CO (*m/z* 28), CO_2 (*m/z* 44) and formaldehyde (*m/z* 30) are characteristic desorption products resulting from formate species.

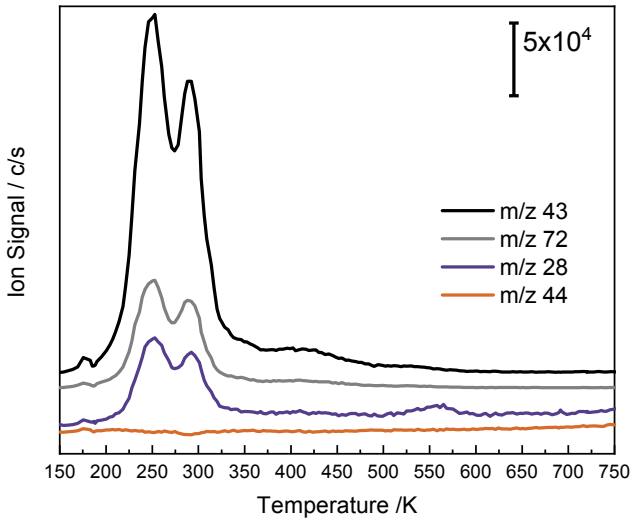

Figure S15. The majority of the aldehyde, isobutanal, desorbs from the reduced TiO_2(110) below 350 K and does not undergo reaction. Temperature-programmed studies of isobutanal (*m/z* 43 and *m/z* 72) from r-TiO_2(110) reveals that *no* propane (*m/z* 44) forms thermally. A CO desorption occurs at 550 K resulting from the aldehyde decomposition analogously observed for acetaldehyde[10]. Further peaks in the high temperature regime at 430 K and 515 K are observed for *m/z* 72 and *m/z* 43, which stem from a reductive coupling reaction.[11]

References

1. Hudson, J. E.; Hamilton, M. L.; Vallance, C.; Harland, P. W., Absolute Electron Impact Ionization Cross-Sections for the C_1 to C_4 Alcohols. *Phys. Chem. Chem. Phys.* **2003,** *5* (15), 3162-3168.
2. Bull, J. N.; Harland, P. W., Absolute Electron Impact Ionization Cross-Sections and Polarisability Volumes for C_2 to C_4 Aldehydes, C_4 and C_6 Symmetric Ethers and C_3 to C_6 Ketones. *Int. J. Mass Spectrom.* **2008,** *273* (1), 53-57.
3. https://physics.nist.gov/cgi-bin/Ionization/table.pl?ionization=C4H8xx2 (accessed 03.12.2019).
4. Harrison, A. G.; Jones, E. G.; Gupta, S. K.; Nagy, G. P., Total Cross Sections for Ionization by Electron Impact. *Can. J. Chem.* **1966,** *44* (16), 1967-1973.
5. https://physics.nist.gov/cgi-bin/Ionization/table.pl?ionization=CO (accessed 03.12.2019).
6. Li, Z.; Smith, R. S.; Kay, B. D.; Dohnálek, Z., Determination of Absolute Coverages for Small Aliphatic Alcohols on TiO_2(110). *J. Phys. Chem. C* **2011,** *115* (45), 22534-22539.
7. Kim, Y. K.; Kay, B. D.; White, J. M.; Dohnálek, Z., Alcohol Chemistry on Rutile TiO_2(110): The Influence of Alkyl Substituents on Reactivity and Selectivity. *J. Phys. Chem. C* **2007,** *111* (49), 18236-18242.
8. Kim, Y. K.; Kay, B. D.; White, J. M.; Dohnálek, Z., Inductive Effect of Alkyl Chains on Alcohol Dehydration at Bridge-bonded Oxygen Vacancies of TiO_2(110). *Catal. Lett.* **2007,** *119* (1), 1-4.
9. Kim, Y. K.; Kay, B. D.; White, J. M.; Dohnálek, Z., 2-Propanol dehydration on TiO_2(110): The effect of bridge-bonded oxygen vacancy blocking. *Surf. Sci.* **2008,** *602* (2), 511-516.
10. Zehr, R. T.; Henderson, M. A., Acetaldehyde Photochemistry on TiO_2(110). *Surf. Sci.* **2008,** *602* (13), 2238-2249.
11. Clawin, P. M.; Friend, C. M.; Al-Shamery, K., Defects in Surface Chemistry—Reductive coupling of Benzaldehyde on Rutile TiO_2(110). *Chem. - Eur. J.* **2014,** *20* (25), 7665-7669.

A.3 Origin of Poisoning in Methanol Photoreforming on TiO_2(110): The Importance of Thermal Back-Reaction Steps in Photocatalysis

ACS Catalysis

pubs.acs.org/acscatalysis Letter

Origin of Poisoning in Methanol Photoreforming on TiO_2(110): The Importance of Thermal Back-Reaction Steps in Photocatalysis

Carla Courtois,[†] Moritz Eder,[†] Sebastian L. Kollmannsberger, Martin Tschurl, Constantin A. Walenta, and Ueli Heiz*

Cite This: ACS Catal. 2020, 10, 7747−7752 Read Online

ACCESS | Metrics & More | Article Recommendations | Supporting Information

ABSTRACT: Alcohol photoreforming on titania represents a perfect model system for elucidating fundamental processes in the heterogeneous photocatalysis of semiconductors. One important but open question is the origin of poisoning during the photoreaction of primary alcohols on a bare, reduced rutile TiO_2(110) crystal under ultrahigh vacuum conditions. By comparing the photocatalytic properties of methanol and 2-methyl-2-pentanol, it is demonstrated that the fading activity in methanol photoreforming does not originate from the often-assigned increase of trap states for photon-generated charge carriers. Instead, we attribute the apparent catalyst poisoning to an increased rate of thermal back reactions, particularly to that of the photochemical oxidation step. While overall back reactions are generally considered in photocatalysis, back reactions of individual steps are largely neglected so far. Our work shows that their inclusion in the reaction scheme is inevitable for the comprehensive modeling of photocatalytic processes.

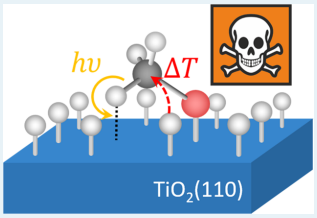

KEYWORDS: *photocatalysis, titania, poisoning, mechanism, alcohol reforming*

Rutile titania is one of the most explored (and applied) heterogeneous photocatalysts,[1] but a complete understanding of the fundamental photochemical surface processes is still lacking. Nevertheless, research on titania under ambient[1,2] and vacuum conditions[3,4] has already demonstrated the value of this material not only for application but also as a model system for the elucidation of fundamental effects in photocatalysis. One advantageous property of the model system TiO_2 is its availability as highly defined, single-crystalline material. Because of extensive research, the thermal surface chemistry is already fairly well understood, particularly on rutile TiO_2(110). For example, the formation of species at different sites and temperatures have been thoroughly elucidated.[5−7] This holds especially for alcohols,[8−11] which are often employed as hole scavengers (i.e., sacrificial agents) in the testing of photocatalysts, with respect to their H_2 evolution performance for photocatalytic water splitting.[12−14] However, the surface chemistry of the materials represents a property often neglected in photocatalysis, and certain phenomena are, in most cases, related solely to charge carrier dynamics. Studies about TiO_2(110) single crystals in particular highlight the importance of such an understanding.[4] The knowledge about thermal phenomena is crucial for disentangling photocatalytic and thermal reaction steps for a comprehensive understanding of catalytic processes. In this regard, Henderson identified thermally formed methoxy as the photoactive species in methanol photo-oxidation on TiO_2(110).[15] Consistent with the upward band-bending toward the TiO_2(110) semiconductor surface, the photo-oxidation mechanism of methoxy is driven by a direct hole transfer, leading to a C−H bond cleavage.[15−17] This yields formaldehyde and a hydroxyl group with a bridging oxygen atom (OH_{br}) from the lattice. The mechanism mediated by photoholes was further suggested for other alcohols, since it comprehensively explains the formation of all corresponding products.[3,18−22] In the same sense, we have only recently demonstrated that alcohol photoreforming on platinum-loaded TiO_2(110) occurs through an unexpected (thermal) mechanism for hydrogen formation succeeding the photoreaction[19,23] and not by the usually assumed set of redox reactions. Furthermore, we discovered a similarly unexpected reaction of tertiary alcohols,[22] corroborating our proposed mechanism.

Although the described photo-oxidation pathway seems generally valid for alcohols,[3] important questions still need to be resolved. In this regard, the different photoactivity of methanol and other primary alcohols on bare and co-catalyst-loaded titania over time still remains elusive. Their photoconversion is truly catalytic on platinum-decorated TiO_2(110),[19,23] while an upper limit in the conversion of different primary alcohols is observed on the bare semiconductor.[15,18,24] These conversions range between 5% and

Received: April 9, 2020
Revised: May 29, 2020
Published: June 25, 2020

https://dx.doi.org/10.1021/acscatal.0c01615
ACS Catal. 2020, 10, 7747−7752

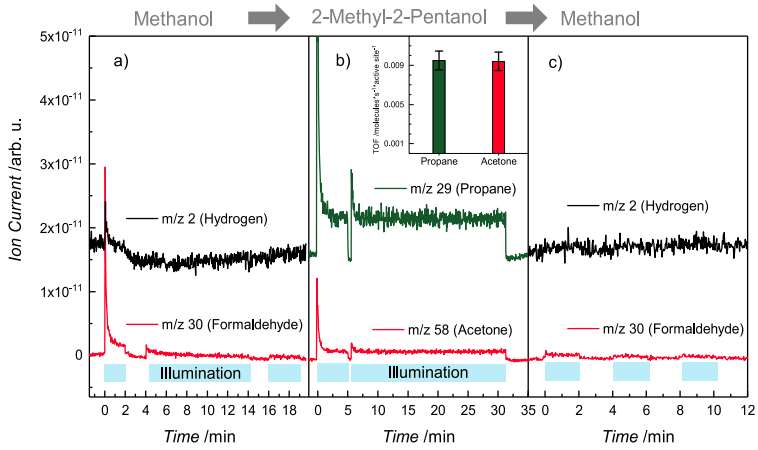

Figure 1. Photochemical reaction of methanol and photocatalysis of 2-methyl-2-pentanol on r-TiO_2(110) at 300 K in an alcohol background of 5×10^{-8} mbar in consecutive experiments. The blue region highlights the period of UV irradiation. (a) Photochemical product formation of methanol oxidation on a freshly prepared r-TiO_2(110). Upon UV excitation, methoxy species are oxidized to formaldehyde (m/z 30), which thermally desorbs. The amount of formaldehyde decreases continuously as the photoreaction progresses. Note that the small spike in the hydrogen trace is not stoichiometric by 2 orders of magnitude and is attributed to fragmentation in the ionization process.[23] This state of the surface will be referred to as "poisoned". (b) The consecutive photocatalytic conversion of 2-methyl-2-pentanol on the poisoned r-TiO_2(110). Upon UV illumination, acetone (m/z 58) and propane (m/z 29) are formed catalytically without any deactivation. The initial spike of the signals of the photoproducts is attributed to a saturation of photoactive alkoxy species in darkness. The catalyst is active over the entire illumination time of 30 min. The inset shows the turnover frequencies (TOFs) of the products. (c) Consecutive photo-oxidation of methanol after photocatalysis of the tertiary alcohol. Upon illumination, only very low amounts of formaldehyde are formed, and the activity of the freshly prepared surface has not been restored by the reforming of the tertiary alcohol. Note that the traces are offset for the sake of clarity.

20% of the initial alcohol coverage and are attributed to result from the accompanying hydroxylation of the surface.[15,18,25] So far, it is most commonly believed that surface hydroxyls act as electron traps and promote charge recombination.[26] This seems conceivable, because the photoconversion of methanol amounts to ~20% at most.[27] At these conversions, by far not all O_{br}-sites are covered by H atoms. Yet, another work only recently ascribed the poisoning during the photoreaction to the mutual repulsion of surface OH-groups, which inhibits the formation of additional surface hydroxyls.[28] Thus, the exact role of OH_{br} in the photochemistry of methanol and other primary alcohols remains unclear and deactivation phenomena are likewise attributed to either a site-blocking or an electronic effect (or both).[3,18,23,26,28,29]

In this Letter, we report strong evidence that thermal backreactions are mainly responsible for the deactivation in alcohol photo-oxidation. Instead of site-blocking or electronic effects, we attribute the thermal back-reactions of carbonyl and surface hydroxyls to cause this deactivation on bare, reduced rutile TiO_2(110) (r-TiO_2(110))—an interpretation that is based on the differences in the photochemistry of tertiary (exemplified by 2-methyl-2-pentanol) and primary alcohols (represented by methanol).

The deactivation of the photocatalyst in a steady methanol background on r-TiO_2(110) under illumination at room temperature is shown in Figure 1a. While the reactant is continuously replenished, the formation of formaldehyde as the product of the photoreaction step decays over time. The eventual photoinactive state of the catalyst, with respect to methanol conversion, is referred to as "poisoned" in the following. A similar poisoning is also observed for experiments with a repeated dosage of methanol (see Figure S1 in the Supporting Information), in which the initial conversion decreases to ~20%, compared to the first photoreaction cycle. The absence of stoichiometric molecular hydrogen desorption (Figure 1a), the second reaction product next to formaldehyde, indicates hydroxylation of the titania surface. This hydroxylation from photo-oxidation of primary alcohols previously was observed directly by means of scanning tunneling microscopy.[27,30,31] Therefore, the removal of this hydroxylation, which is observed on TiO_2(110) only, facilitated in the presence of a Pt co-catalyst[23,32] or via the desorption of water from recombining OH_{br} occurring only at higher temperatures, is inhibited at room temperature.[33] Thus, the overall reaction is given as follows:

$$CH_3OH + 2O_{br} \xrightarrow{h\nu} CH_2O\uparrow + 2OH_{br} \quad (1)$$

As shown in Figure 1b, the disproportionation of 2-methyl-2-pentanol to propane and acetone occurs photocatalytically even on the poisoned r-TiO_2(110) surface.[22] The abstracted propyl group formed by photo-oxidation recombines with a surface hydrogen (e.g., originating from the dissociative adsorption of the alcohol), which opens up a reaction channel chemically closing the photocatalytic cycle and enables the overall net reaction:[22]

$$CR_3OH \xrightarrow{h\nu} CR_2O\uparrow + RH\uparrow \quad (2)$$

In contrast to the formation of molecular hydrogen from two hydrogen surface species in the photoreaction of methanol, this consecutive thermal reaction (i.e., alkyl and surface hydrogen recombination) occurs at room temperature, averting further

https://dx.doi.org/10.1021/acscatal.0c01615
ACS Catal. 2020, 10, 7747−7752

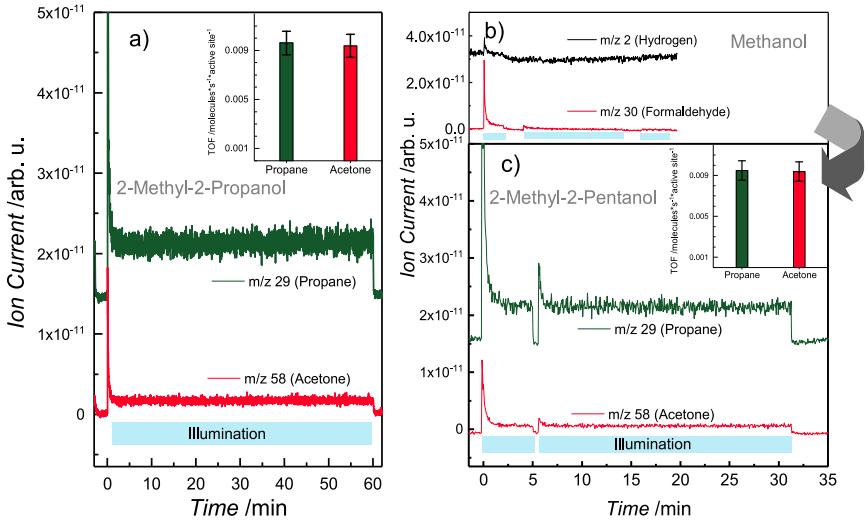

Figure 2. Photochemical reaction of 2-methyl-2-pentanol and methanol on r-TiO_2(110) at 300 K in an alcohol background of 5×10^{-8} mbar. The blue region highlights the period of UV irradiation. The TOFs of 2M2P photocatalytic conversion are in quantitative agreement on a freshly prepared r-TiO_2(110) surface and on one with prior methanol photoconversion. (a) Photocatalytic disproportionation of 2-methyl-2-pentanol on a freshly prepared, bare r-TiO_2(110). Upon UV illumination, acetone (m/z 58) and propane (m/z 29) are formed catalytically. The inset shows the TOFs of the products. (b) Photochemical oxidation of methanol to formaldehyde (m/z 30) leading to a deactivation caused by surface hydroxylation. (c) Consecutive experiment (immediately performed after experiment described in panel (b)) of photocatalytic conversion of 2-methyl-2-pentanol on the poisoned r-TiO_2(110). Upon UV illumination, acetone (m/z 58) and propane (m/z 29) are formed catalytically without any deactivation. The inset shows the TOFs of the products, which remain unchanged from the freshly prepared to the poisoned surface. Note that the traces are offset for the sake of clarity.

accumulation of hydroxyl groups on the surface and rendering the reaction stoichiometric.[22]

While the disproportionation reaction of the tertiary alcohol is not hampered by the hydroxylation of the surface, the crystal remains in its poisoned state for a succeeding methanol photoconversion (Figure 1c). As the photoreforming of the tertiary alcohol proceeds stoichiometrically, neither the concentration of OH_{br} groups on the surface nor the photoactivity toward methanol is altered.

In order to evaluate potential changes in the photocatalytic behavior of the tertiary alcohol quantitatively, the activity of the TiO_2(110) crystal in this reaction is expressed by the TOF.[19,22] Clearly, the product formation remains quantitatively unaffected by a preceding methanol photo-oxidation (Figure 2). This demonstrates that OH_{br} groups do not affect the charge-driven process significantly enough to influence the photochemical reaction itself.

Therefore, other effects must be taken into account for the poisoning in photocatalytic methanol oxidation, which we postulate to result mainly from the thermal back reaction of formaldehyde with surface hydroxyls to methoxy. In order to describe the complete reaction sequence occurring on the titania surface thoroughly, at least three different steps must be considered (see eqs 3−5):

$$CH_3OH_{ad} + O_{br} \rightleftharpoons CH_3O_{ad} + OH_{br} \quad (3)$$

$$CH_3O_{ad} + O_{br} \underset{T}{\overset{h\nu}{\rightleftharpoons}} CH_2O_{ad} + OH_{br} \quad (4)$$

$$CH_2O_{ad} + 2OH_{br} \rightarrow CH_2O\uparrow + 2OH_{br} \quad (5)$$

First, dissociation of the adsorbed alcohol into a methoxy species and an OH_{br} occurs on r-TiO_2(110) (eq 3).[8,34] This represents the first reaction step,[15] which must be considered to be reversible by thermal recombination. Second, the succeeding α-H abstraction is a photon-driven reaction, initiated by holes migrating to the surface of the n-type semiconductor (eq 4). This step embodies the oxidation of methoxy to formaldehyde upon C−H bond cleavage[15,17,23] and the concomitant hydroxyl formation on the titania surface.[29] Third, formaldehyde desorbs into the gas phase at room temperature, whereas hydrogen remains bound to lattice oxygen on the surface (eq 5). Low degrees of hydroxylation by water adsorption (see Figure S7 in the Supporting Information) do not lead to a detectable change in photoactivity (see Figure S3 in the Supporting Information), in excellent agreement with the literature,[29] while continuous alcohol adsorption and photoconversion is instead accompanied by surface hydroxyl accumulation. This favors thermal back-reactions in the reaction network (see eqs 3 and 4). The back-reaction of the α-H cleavage (eq 4) was indeed shown to occur thermally[35] and directly observed via STM by Mao and co-workers.[27,30,31] Furthermore, it is considered to be exothermic, because of the overall endergonic (and endothermic) forward reaction ($\Delta_R G° = +59.8$ kJ/mol ≈ 0.62 eV).[36] Only the thermal desorption of formaldehyde may be simplified to a formally irreversible reaction, because of the low readsorption probability of the molecule at the reaction conditions.

The photocatalytic conversion of 2-methyl-2-pentanol still occurs after the hydroxylation of the TiO_2(110) crystal

https://dx.doi.org/10.1021/acscatal.0c01615
ACS Catal. 2020, 10, 7747−7752

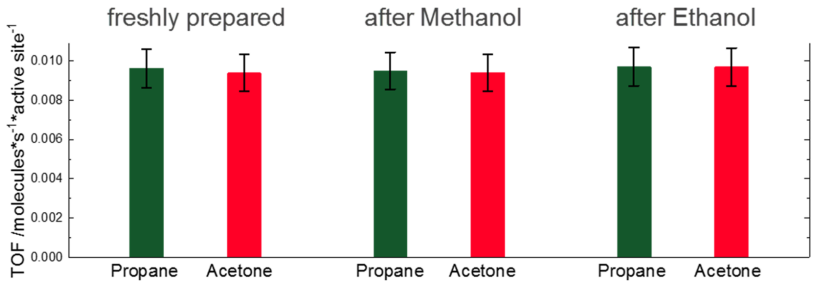

Figure 3. Turnover frequencies for the photoreforming of 2-methyl-2-propanol at 300 K on the freshly prepared r-TiO_2(110), after methanol poisoning and ethanol poisoning. It is found that, in each case, the photocatalytic reaction proceeds stoichiometrically and with the same activity.

(through methanol photo-oxidation), in contrast to the photo-oxidation of methanol (Figure 1). This demonstrates that a blocking of photoactive sites by OH_{br} is not the main reason for the decline in the photoactivity toward methanol. A mutual repulsion of OH-groups is also unlikely decisive for poisoning,[28] since this would also inhibit the dissociative adsorption of the tertiary alcohol, preventing its photo-oxidation completely. Similarly, the role of surface OH-groups as potential trap and recombination sites for photon-generated charge carriers seems improbable, because the amount of hydroxylation does not have a quantifiable effect on the photoreforming TOF of the tertiary alcohol. Instead, thermal back-reactions should be considered for other photodecomposition reaction (e.g., that of trimethyl acetate[26]) apart from changes in the behavior of the photogenerated charges.

The different surface chemistry of these alcohols under illumination can comprehensively explain their different behavior. However, the adsorption properties of methanol and 2-methyl-2-pentanol are very similar to each other, based on STM work for methanol and longer chain, branched alcohols by Dohnálek and co-workers.[8,37,38] Independent of the nature of the photoactive site, both alkoxy species are expected to occupy the same (photoactive) Ti-sites and undergo a hole-mediated oxidation.[15,22] If dosed successively, the respective alcohol concentration on the titania surface sites is determined by the adsorption strengths of the alcohols and their displacement kinetics (see Figures S4 and S5 in the Supporting Information). Obviously, photoreforming of tertiary alcohols (eq 2) occurs by a photochemical C−C cleavage of the alkoxy (eq 6),[22] in contrast to the photo-oxidation of methanol (eq 4), where a C−H bond is cleaved.[3,15,17,39]

$$CR_3OH + O_{br} \rightleftharpoons CR_3O_{ad} + OH_{br} \overset{h\nu}{\underset{T}{\rightleftharpoons}} CR_2O_{ad} + R_{ad} + OH_{br} \rightarrow CR_2O\uparrow + RH\uparrow + O_{br} \quad (6)$$

The potential thermal back-reaction of the photo-oxidation of 2-methyl-2-pentanol does not involve hydrogen atoms from hydroxyls, which perfectly agrees with the alcohol's unaffected TOF upon an increasing hydroxylation of the TiO_2(110) crystal. This unaltered catalytic behavior further points to a similar concentration of photoactive tertiary alkoxy species. This suggests that increasing hydroxylation does not affect the dissociative adsorption of the tertiary alcohol significantly. While a similar thermal chemistry and gas phase acidities[40] are observed, there is a strong difference in the thermal back-reaction of the photo-oxidation, resulting in their different catalytic behavior.

To generalize the findings, ethanol is investigated as another poisoning agent. The photochemical oxidation occurs analogously to methanol by the conversion of ethoxy to acetaldehyde.[18,20] The dissociative adsorption and the photoreaction thus lead to an accumulation of hydroxyls on the surface and the TOF of acetaldehyde decreases over time (Figure S6a in the Supporting Information).[18] In a subsequent photocatalytic oxidation of 2-methyl-2-pentanol (Figure S6b in the Supporting Information), the same TOF as in all other photocatalytic experiments of the tertiary alcohol is obtained (see Figure 3). Consequently, charge carriers are not responsible for the poisoning in alcohol photo-oxidation on TiO_2(110), which may also hold for other photodecomposition reactions.

In conclusion, the presented findings strongly suggest that the limited conversion of primary alcohols on TiO_2(110) results from the back-reaction of the aldehyde with a surface hydroxyl. The catalytic photoreforming of tertiary alcohols demonstrates that the charge carrier dynamics are not altered significantly enough to account for the poisoning effect. Therefore, surface OH groups as trap states/recombination sites have only a negligible effect on these photoreactions. Instead, the different photo-oxidation chemistry of primary and tertiary alcohols allows the assignment of the deactivation to thermal back reactions. In methanol photo-oxidation, two different thermal back reactions were identified, in which hydrogen atoms from surface hydroxyl groups are involved in the reaction scheme. Based on the differences and similarities in the photoreaction steps of methanol and 2-methyl-2-pentanol, we attribute the back-reaction from formaldehyde to methoxy as being mainly responsible for the vanishing photoactivity of TiO_2(110) in methanol photoreforming. For tertiary alcohols, the forward reaction represents a photochemical C−C bond cleavage, instead of the splitting of a C−H bond. Consequently, the thermal back-reaction is completely different from that of primary alcohols.

While overall back-reactions are sometimes considered in photocatalysis, as e.g. in the prominent example of Maeda et al. in full water splitting,[41] back-reactions of individual reaction steps are so far largely ignored. Given the abundance of hydroxyls on the titania surface in the liquid phase,[4] the similar photochemical behavior of other TiO_2 surfaces,[42] modifications (i.e., anatase(101))[43,44] and morphologies (i.e., nanowires)[45−47] suggests that similar effects may also play an important role for these systems. Our work demonstrates that

https://dx.doi.org/10.1021/acscatal.0c01615
ACS Catal. 2020, 10, 7747−7752

individual back-reaction steps must be included in a comprehensive modeling of photocatalytic systems.

■ ASSOCIATED CONTENT

Supporting Information

The Supporting Information is available free of charge at https://pubs.acs.org/doi/10.1021/acscatal.0c01615.

Description of experimental procedures, consecutive isothermal photoreaction experiments of methanol, consecutive photochemical reaction data of ethanol and 2-methyl-2-pentanol on r-TiO_2(110) at 300 K and corresponding TOFs, temperature-programmed desorption of H_2O on r-TiO_2(110), general description of TOF calculation (PDF)

■ AUTHOR INFORMATION

Corresponding Author

Ueli Heiz − *Chair of Physical Chemistry, Department of Chemistry & Catalysis Research Center, Technische Universität München, 85748 Garching, Germany;* orcid.org/0000-0002-9403-1486; Email: ulrich.heiz@mytum.de

Authors

Carla Courtois − *Chair of Physical Chemistry, Department of Chemistry & Catalysis Research Center, Technische Universität München, 85748 Garching, Germany*

Moritz Eder − *Chair of Physical Chemistry, Department of Chemistry & Catalysis Research Center, Technische Universität München, 85748 Garching, Germany*

Sebastian L. Kollmannsberger − *Chair of Physical Chemistry, Department of Chemistry & Catalysis Research Center, Technische Universität München, 85748 Garching, Germany*

Martin Tschurl − *Chair of Physical Chemistry, Department of Chemistry & Catalysis Research Center, Technische Universität München, 85748 Garching, Germany;* orcid.org/0000-0001-6618-7312

Constantin A. Walenta − *Chair of Physical Chemistry, Department of Chemistry & Catalysis Research Center, Technische Universität München, 85748 Garching, Germany;* orcid.org/0000-0001-9879-5101

Complete contact information is available at: https://pubs.acs.org/10.1021/acscatal.0c01615

Author Contributions

†These authors contributed equally to this work.

Notes

The authors declare no competing financial interest.

■ ACKNOWLEDGMENTS

The authors thank the DFG for financial support through the Germany's Excellence Strategy − EXC 2089/1-390776260. C.C. acknowledges the support from the Luxembourg National Research Fund (FNR) (Project Code No. 12531916) and that from the TUM International Graduate School of Science and Engineering (No. TUM-IGSSE).

■ REFERENCES

(1) Schneider, J.; Matsuoka, M.; Takeuchi, M.; Zhang, J.; Horiuchi, Y.; Anpo, M.; Bahnemann, D. W. Understanding TiO_2 Photocatalysis: Mechanisms and Materials. *Chem. Rev.* **2014**, *114* (19), 9919−9986.

(2) Nosaka, Y.; Nosaka, A. Y. Generation and Detection of Reactive Oxygen Species in Photocatalysis. *Chem. Rev.* **2017**, *117* (17), 11302−11336.

(3) Walenta, C. A.; Tschurl, M.; Heiz, U. Introducing Catalysis in Photocatalysis: What can be Understood from Surface Science Studies of Alcohol Photoreforming on TiO_2. *J. Phys.: Condens. Matter* **2019**, *31* (47), 473002.

(4) Henderson, M. A. A Surface Science Perspective on TiO_2 Photocatalysis. *Surf. Sci. Rep.* **2011**, *66* (6), 185−297.

(5) Diebold, U. The Surface Science of Titanium Dioxide. *Surf. Sci. Rep.* **2003**, *48* (5), 53−229.

(6) Lun Pang, C.; Lindsay, R.; Thornton, G. Chemical reactions on rutile TiO_2(110). *Chem. Soc. Rev.* **2008**, *37* (10), 2328−2353.

(7) Dohnálek, Z.; Lyubinetsky, I.; Rousseau, R. Thermally-Driven Processes on Rutile TiO_2(110)-(1 × 1): A Direct View at the Atomic Scale. *Prog. Surf. Sci.* **2010**, *85* (5), 161−205.

(8) Zhang, Z.; Bondarchuk, O.; White, J. M.; Kay, B. D.; Dohnálek, Z. Imaging Adsorbate O-H Bond Cleavage: Methanol on TiO_2(110). *J. Am. Chem. Soc.* **2006**, *128* (13), 4198−4199.

(9) Kim, Y. K.; Kay, B. D.; White, J. M.; Dohnálek, Z. Alcohol Chemistry on Rutile TiO_2(110): The Influence of Alkyl Substituents on Reactivity and Selectivity. *J. Phys. Chem. C* **2007**, *111* (49), 18236−18242.

(10) Kim, Y. K.; Kay, B. D.; White, J. M.; Dohnálek, Z. Inductive Effect of Alkyl Chains on Alcohol Dehydration at Bridge-bonded Oxygen Vacancies of TiO_2(110). *Catal. Lett.* **2007**, *119* (1), 1−4.

(11) Li, Z.; Smith, R. S.; Kay, B. D.; Dohnálek, Z. Determination of Absolute Coverages for Small Aliphatic Alcohols on TiO_2(110). *J. Phys. Chem. C* **2011**, *115* (45), 22534−22539.

(12) Lee, Y. J.; Joo, J. B.; Yin, Y.; Zaera, F. Evaluation of the Effective Photoexcitation Distances in the Photocatalytic Production of H_2 from Water using Au@Void@TiO_2 Yolk−Shell Nanostructures. *ACS Energy Lett.* **2016**, *1* (1), 52−56.

(13) Hainer, A. S.; Hodgins, J. S.; Sandre, V.; Vallieres, M.; Lanterna, A. E.; Scaiano, J. C. Photocatalytic Hydrogen Generation Using Metal-Decorated TiO_2: Sacrificial Donors vs True Water Splitting. *ACS Energy Lett.* **2018**, *3* (3), 542−545.

(14) Joo, J. B.; Dillon, R.; Lee, I.; Yin, Y.; Bardeen, C. J.; Zaera, F. Promotion of atomic hydrogen recombination as an alternative to electron trapping for the role of metals in the photocatalytic production of H_2. *Proc. Natl. Acad. Sci. U. S. A.* **2014**, *111* (22), 7942.

(15) Shen, M.; Henderson, M. A. Identification of the Active Species in Photochemical Hole Scavenging Reactions of Methanol on TiO_2. *J. Phys. Chem. Lett.* **2011**, *2* (21), 2707−2710.

(16) Phillips, K. R.; Jensen, S. C.; Baron, M.; Li, S.-C.; Friend, C. M. Sequential Photo-Oxidation of Methanol to Methyl Formate on TiO_2(110). *J. Am. Chem. Soc.* **2013**, *135* (2), 574−577.

(17) Kolesov, G.; Vinichenko, D.; Tritsaris, G. A.; Friend, C. M.; Kaxiras, E. Anatomy of the Photochemical Reaction: Excited-State Dynamics Reveals the C−H Acidity Mechanism of Methoxy Photo-oxidation on Titania. *J. Phys. Chem. Lett.* **2015**, *6* (9), 1624−1627.

(18) Walenta, C. A.; Kollmannsberger, S. L.; Kiermaier, J.; Winbauer, A.; Tschurl, M.; Heiz, U. Ethanol Photocatalysis on Rutile TiO_2(110): the Role of Defects and Water. *Phys. Chem. Chem. Phys.* **2015**, *17* (35), 22809−22814.

(19) Kollmannsberger, S. L.; Walenta, C. A.; Courtois, C.; Tschurl, M.; Heiz, U. Thermal Control of Selectivity in Photocatalytic, Water-Free Alcohol Photoreforming. *ACS Catal.* **2018**, *8*, 11076−11084.

(20) Hansen, J. Ø.; Bebensee, R.; Martinez, U.; Porsgaard, S.; Lira, E.; Wei, Y.; Lammich, L.; Li, Z.; Idriss, H.; Besenbacher, F.; Hammer, B.; Wendt, S. Unravelling Site-Specific Photo-Reactions of Ethanol on Rutile TiO_2(110). *Sci. Rep.* **2016**, *6*, 21990.

(21) Walenta, C. A.; Kollmannsberger, S. L.; Courtois, C.; Tschurl, M.; Heiz, U. Photocatalytic selectivity switch to C-C scission: 2-methyl ejection of tert-butanol on TiO_2(110). *Phys. Chem. Chem. Phys.* **2018**, *20* (10), 7105−7111.

(22) Courtois, C.; Eder, M.; Schnabl, K.; Walenta, C. A.; Tschurl, M.; Heiz, U. Reactions in the Photocatalytic Conversion of Tertiary

https://dx.doi.org/10.1021/acscatal.0c01615
ACS Catal. 2020, 10, 7747−7752

Alcohols on Rutile TiO_2(110). *Angew. Chem., Int. Ed.* **2019**, *58* (ja), 14255.
(23) Walenta, C. A.; Kollmannsberger, S. L.; Courtois, C.; Pereira, R. N.; Stutzmann, M.; Tschurl, M.; Heiz, U. Why Co-Catalyst-Loaded Rutile Facilitates Photocatalytic Hydrogen Evolution. *Phys. Chem. Chem. Phys.* **2019**, *21* (3), 1491−1496.
(24) Guo, Q.; Xu, C.; Yang, W.; Ren, Z.; Ma, Z.; Dai, D.; Minton, T. K.; Yang, X. Methyl Formate Production on TiO_2(110), Initiated by Methanol Photocatalysis at 400 nm. *J. Phys. Chem. C* **2013**, *117* (10), 5293−5300.
(25) Guo, Q.; Xu, C.; Ren, Z.; Yang, W.; Ma, Z.; Dai, D.; Fan, H.; Minton, T. K.; Yang, X. Stepwise Photocatalytic Dissociation of Methanol and Water on TiO_2(110). *J. Am. Chem. Soc.* **2012**, *134* (32), 13366−13373.
(26) Wang, Z.-T.; Henderson, M. A.; Lyubinetsky, I. Origin of Coverage Dependence in Photoreactivity of Carboxylate on TiO_2(110): Hindering by Charged Coadsorbed Hydroxyls. *ACS Catal.* **2015**, *5* (11), 6463−6467.
(27) Guo, Q.; Zhou, C.; Ma, Z.; Ren, Z.; Fan, H.; Yang, X. Elementary Photocatalytic Chemistry on TiO_2 Surfaces. *Chem. Soc. Rev.* **2016**, *45* (13), 3701−3730.
(28) Zhang, R.; Wang, H.; Peng, X.; Feng, R.-r.; Liu, A.-a.; Guo, Q.; Zhou, C.; Ma, Z.; Yang, X.; Jiang, Y.; Ren, Z. In Situ Studies on Temperature-Dependent Photocatalytic Reactions of Methanol on TiO_2(110). *J. Phys. Chem. C* **2019**, *123* (15), 9993−9999.
(29) Shen, M.; Henderson, M. A. Role of Water in Methanol Photochemistry on Rutile TiO_2(110). *J. Phys. Chem. C* **2012**, *116* (35), 18788−18795.
(30) Mao, X.; Wei, D.; Wang, Z.; Jin, X.; Hao, Q.; Ren, Z.; Dai, D.; Ma, Z.; Zhou, C.; Yang, X. Recombination of Formaldehyde and Hydrogen Atoms on TiO_2(110). *J. Phys. Chem. C* **2015**, *119* (2), 1170−1174.
(31) Guo, Q.; Ma, Z.; Zhou, C.; Ren, Z.; Yang, X. Single Molecule Photocatalysis on TiO_2 Surfaces. *Chem. Rev.* **2019**, *119* (20), 11020−11041.
(32) Hao, Q.; Wang, Z.; Wang, T.; Ren, Z.; Zhou, C.; Yang, X. Role of Pt Loading in the Photocatalytic Chemistry of Methanol on Rutile TiO_2(110). *ACS Catal.* **2019**, *9* (1), 286−294.
(33) Henderson, M. A. Structural Sensitivity in the Dissociation of Water on TiO2 Single-Crystal Surfaces. *Langmuir* **1996**, *12* (21), 5093−5098.
(34) Oviedo, J.; Sánchez-De-Armas, R.; San Miguel, M. Á.; Sanz, J. F. Methanol and Water Dissociation on TiO_2 (110): The Role of Surface Oxygen. *J. Phys. Chem. C* **2008**, *112* (46), 17737−17740.
(35) Yuan, Q.; Wu, Z.; Jin, Y.; Xiong, F.; Huang, W. Surface Chemistry of Formaldehyde on Rutile TiO_2(110) Surface: Photocatalysis vs Thermal-Catalysis. *J. Phys. Chem. C* **2014**, *118* (35), 20420−20428.
(36) Rumble, J. R.; Lide, D. R.; Bruno, T. J. *CRC Handbook of Chemistry and Physics*; CRC Press: Boca Raton, FL, 2017.
(37) Zhang, Z.; Bondarchuk, O.; Kay, B. D.; White, J. M.; Dohnálek, Z. Direct Visualization of 2-Butanol Adsorption and Dissociation on TiO_2(110). *J. Phys. Chem. C* **2007**, *111* (7), 3021−3027.
(38) Zhang, Z.; Rousseau, R.; Gong, J.; Kay, B. D.; Dohnálek, Z. Imaging Hindered Rotations of Alkoxy Species on TiO_2(110). *J. Am. Chem. Soc.* **2009**, *131* (49), 17926−17932.
(39) Walenta, C. A.; Courtois, C.; Kollmannsberger, S. L.; Eder, M.; Tschurl, M.; Heiz, U. Surface Species in Photocatalytic Methanol Reforming on Pt/TiO_2(110): Learning from Surface Science Experiments for Catalytically Relevant Conditions. *ACS Catal.* **2020**, *10*, 4080−4091.
(40) Lias, S. G.; Bartmess, J. E.; Liebman, J. F.; Holmes, J. L.; Levin, R. D.; Mallard, W. G. Ion Energetics Data. In *NIST Chemistry WebBook, NIST Standard Reference Database*, No. 69; Lindstrom, P. J., Mallard, W. G., Eds.; National Institute of Standards and Technology: Gaithersburg, MD, 2019, DOI: 10.18434/T4D303.
(41) Maeda, K.; Teramura, K.; Lu, D.; Saito, N.; Inoue, Y.; Domen, K. Noble-Metal/Cr_2O_3 Core/Shell Nanoparticles as a Cocatalyst for Photocatalytic Overall Water Splitting. *Angew. Chem., Int. Ed.* **2006**, *45* (46), 7806−7809.
(42) Wilson, J. N.; Idriss, H. Effect of Surface Reconstruction of TiO_2(001) Single Crystal on the Photoreaction of Acetic Acid. *J. Catal.* **2003**, *214* (1), 46−52.
(43) Katsiev, K.; Harrison, G.; Alghamdi, H.; Alsalik, Y.; Wilson, A.; Thornton, G.; Idriss, H. Mechanism of Ethanol Photooxidation on Single-Crystal Anatase TiO_2(101). *J. Phys. Chem. C* **2017**, *121* (5), 2940−2950.
(44) Setvin, M.; Shi, X.; Hulva, J.; Simschitz, T.; Parkinson, G. S.; Schmid, M.; Di Valentin, C.; Selloni, A.; Diebold, U. Methanol on Anatase TiO_2(101): Mechanistic Insights into Photocatalysis. *ACS Catal.* **2017**, *7* (10), 7081−7091.
(45) Crampton, A. S.; Cai, L.; Janvelyan, N.; Zheng, X.; Friend, C. M. Methanol Photo-Oxidation on Rutile TiO_2 Nanowires: Probing Reaction Pathways on Complex Materials. *J. Phys. Chem. C* **2017**, *121* (18), 9910−9919.
(46) Pepin, P. A.; Diroll, B. T.; Choi, H. J.; Murray, C. B.; Vohs, J. M. Thermal and Photochemical Reactions of Methanol, Acetaldehyde, and Acetic Acid on Brookite TiO_2 Nanorods. *J. Phys. Chem. C* **2017**, *121* (21), 11488−11498.
(47) Pepin, P. A.; Lee, J. D.; Murray, C. B.; Vohs, J. M. Thermal and Photocatalytic Reactions of Methanol and Acetaldehyde on Pt-Modified Brookite TiO_2 Nanorods. *ACS Catal.* **2018**, *8*, 11834−11846.

https://dx.doi.org/10.1021/acscatal.0c01615
ACS Catal. 2020, 10, 7747−7752

Supporting Information:

Origin of Poisoning in Methanol Photoreforming on TiO_2(110): The Importance of Thermal Back Reaction Steps in Photocatalysis

Carla Courtois‡,¶, Moritz Eder‡,¶, Sebastian L. Kollmannsberger¶, Martin Tschurl¶, Constantin A. Walenta¶, Ueli Heiz¶,*

¶ Chair of Physical Chemistry & Catalysis Research Center, Technical University of Munich, Lichtenbergstr. 4, 85748 Garching, Germany

‡ The authors contributed equally.

*Corresponding Author: ulrich.heiz@mytum.de

Experimental

The details of the experimental setup are described elsewhere.[1-3] The experiments are performed in an ultra-high vacuum apparatus with a base pressure of < 9.8×10^{-11} mbar. The quadratic rutile TiO_2(110) single crystal (SurfaceNet GmbH, 9.95 mm x 9.95 mm x 0.3 mm) is mounted on a sample holder, which is heated by resistive heating and cooled with liquid N_2 to set the sample on a defined temperature. The crystal is prepared by several sputter-annealing cycles, which consist of Ar^+ sputtering (20 min, 1 keV, 1×10^{-5} mbar Ar), oxygen annealing (20 min, 800 K, 5×10^{-6} mbar O_2) and vacuum annealing (10 min, 800 K), until a clean and flat surface is obtained. The cleanliness is verified by Auger electron spectroscopy (Omicron Nanotechnology). The defect concentration and the flatness of the reduced surface is determined by H_2O temperature-programmed desorption experiments.[4, 5] The blueish TiO_2(110) has a bridge-bonded oxygen vacancy concentration of 6 ± 1% ML with respect to Ti-lattice sites (Fig. S7). Photochemical experiments are carried out by illuminating the sample with a Nd:YAG-pumped (3rd harmonic, Innolas Spitlight HighPower 1200, 7 ns pulse width, 20 Hz repetition rate) frequency-doubled OPO (GWU, premiScan ULD/400) laser beam at a wavelength of 242 nm with a power of 5.9 ± 0.3 mW at the crystal surface. Product evolution, as well as the purity of the alcohol background, are monitored with a line of sight quadrupole mass spectrometer (QMA 430, Pfeiffer Vacuum GmbH). Catalytic experiments are carried out in a defined alcohol background pressure, where the chamber is filled with reactant via a leak valve. Single coverage measurements are conducted via Langmuir dosing at cryogenic temperatures. A representative set of raw data is shown in Fig. S8. 2-methyl-2-pentanol (99%, Sigma Aldrich), ethanol (Chromasolv, ≥99.8%, Sigma-Aldrich) and methanol

(Chromasolv, ≥99.9%, Sigma-Aldrich) are degasified by several freeze-pump-thaw cycles.

Additional Data

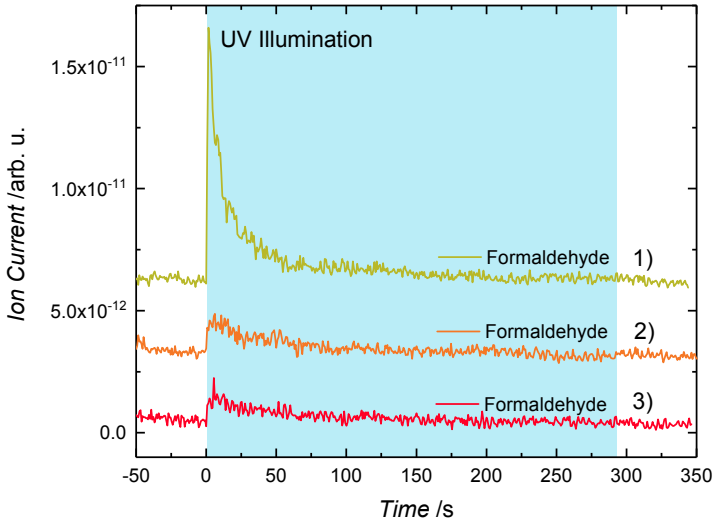

Figure S1. Isothermal mass traces (*m*/*z* 30) of the photoreaction of 1 L methanol on r-TiO_2(110) at 300 K for consecutive dosages. In experiment 1), 1 L methanol is adsorbed on the freshly prepared crystal at 130 K, the sample is thermalized to 300 K, and UV illumination starts at t = 0 s. Upon excitation, an immediate formation of formaldehyde is observed. The methoxy is oxidized by the photo-hole forming formaldehyde, which is thermally desorbing at the reaction temperature of 300 K. Other photoproducts, as well as water, are not observed during illumination. In experiment 2) and 3), the sample is cooled down to 130 K immediately after experiment 1). 1 L methanol is adsorbed and the sample is thermalized to 300 K. Upon illumination, about 20% of the initial amount of formaldehyde is observed in experiment 2) and 3). 2) and 3) show a poisoning of the catalyst towards formaldehyde production with respect to experiment 1). The blue region shows the time of UV illumination.

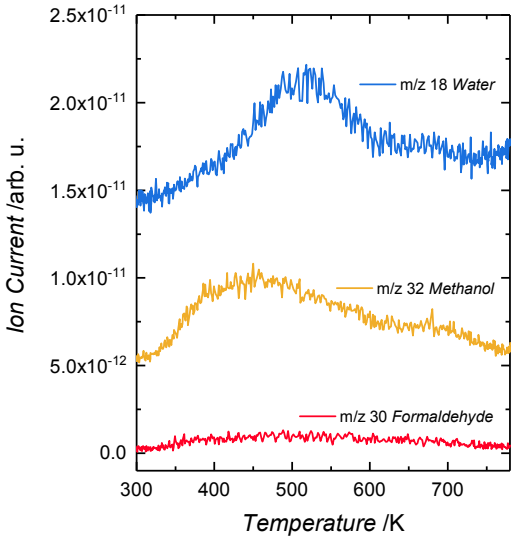

Figure S2. Temperature-programmed desorption experiment after isothermal photoreaction of 1 L methanol on r-TiO_2(110) at 300 K, analogue to Figure S1). 1 L methanol is adsorbed on r-TiO_2(110) at 130 K, the sample is thermalized to 300 K and illuminated with UV light for 5 min. Subsequently, a temperature-programmed desorption experiment shows remaining methanol and the expected water peak around 530 K resulting from recombinative desorption of OH_{br}. No other products were observed in TPD.

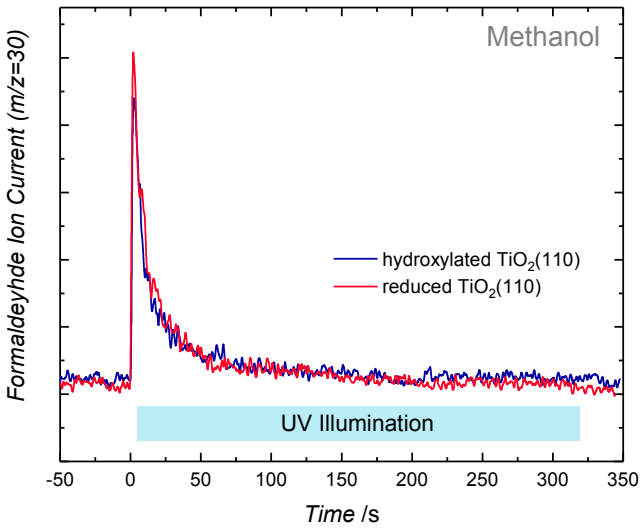

Figure S3. Isothermal mass traces of formaldehyde (m/z 30) of the photoreaction of 1L methanol on r-TiO_2(110) and pre-hydroxylated TiO_2(110) at 300 K. 1 L methanol is adsorbed on the prepared crystal at 130 K, the sample is thermalized at 300 K, and UV illumination starts at t = 0 s. The hydroxylated TiO_2(110) is prepared by adsorbing a saturation layer of water, heating the sample to 350 K, so that all molecular water is desorbing, and is cooled down to cryogenic temperatures. For both surfaces, upon excitation, an immediate formation of formaldehyde is observed. The methoxy is oxidized by the photo-hole yielding formaldehyde, which is thermally desorbing at 300 K. Other photo-products, as well as water, are not observed at these conditions. The blue region shows the time of UV illumination.

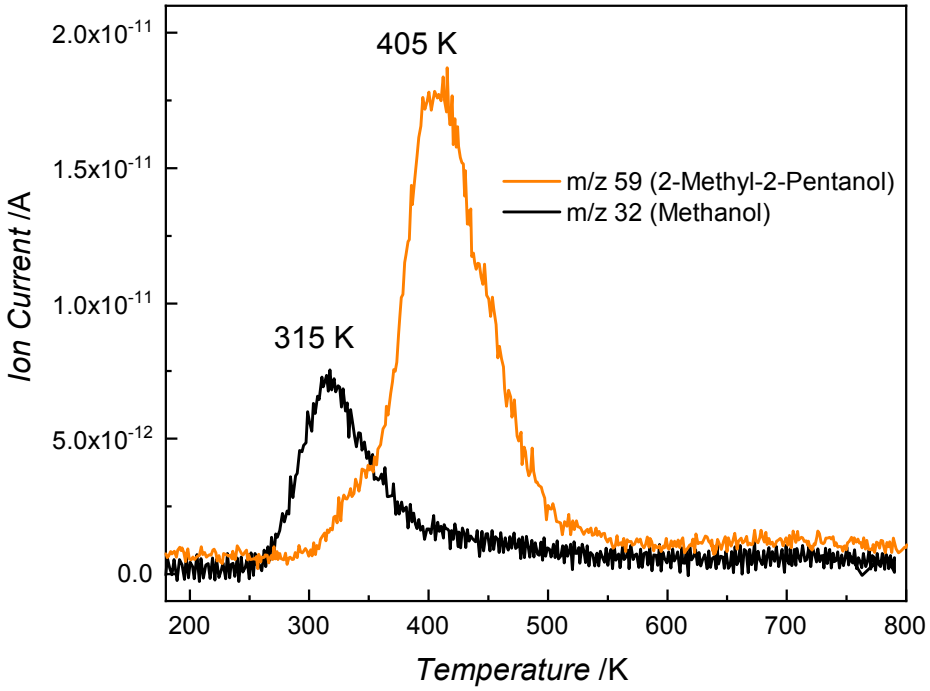

Figure S4. Temperature programmed desorption experiments for methanol (black) and 2-methyl-2-pentanol (orange) on a freshly prepared r-TiO_2(110), respectively. Alcohol exposures (1 L for methanol and 5 L for 2M2P) are carried out at 150 K with a heating rate of 1.5 K/s.

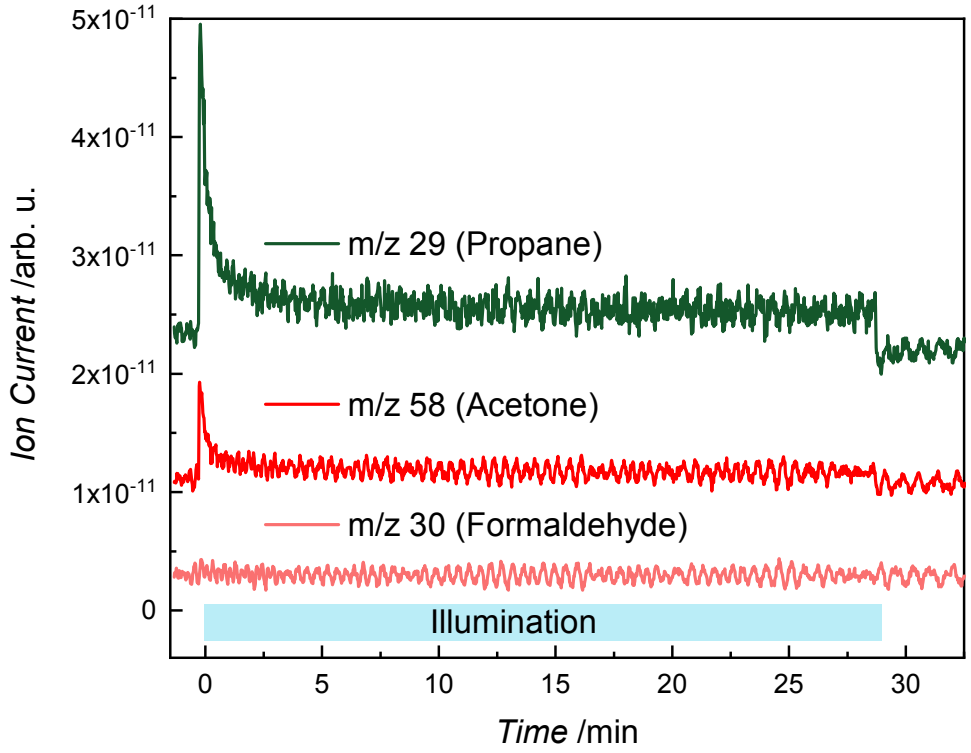

Figure S5. Photocatalysis of 2-methyl-2-pentanol on r-TiO_2(110) at 300 K in an alcohol background of 5×10^{-8} mbar after a dosage of 5 L (i.e. 5×10^{-8} mbar for 133 s) of methanol at 300 K. The blue region highlights the period of UV irradiation. Upon UV illumination, acetone (m/z 58) and propane (m/z 29) are formed catalytically without any deactivation. The catalyst is active over the whole illumination time of 28 min. Upon illumination, significant amounts of formaldehyde from methanol photooxidation are not detected, showing that the tertiary alcohol replaces methanol completely due to its higher binding energy (see Fig. S4). Note that the traces are offset for clarity.

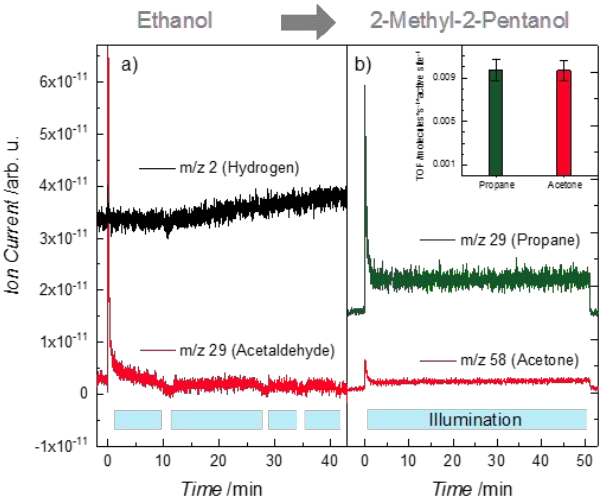

Figure S6. Photochemical reaction of ethanol and 2-methyl-2-pentanol on r-TiO_2(110) at 300 K in an alcohol background of 5×10^{-8} mbar in consecutive experiments. The blue region highlights the period of UV irradiation. a) Photochemical product of ethanol oxidation on a freshly prepared r-TiO_2(110). Upon UV excitation, ethoxy species are oxidized to acetaldehyde (*m*/*z* 29), which thermally desorbs. The amount of acetaldehyde decreases continuously due to the hydroxylation of the titania surface. b) Consecutive experiment of photocatalytic conversion of 2-methyl-2-pentanol on the ethanol-poisoned r-TiO2(110). Upon UV illumination, acetone (*m*/*z* 58) and propane (*m*/*z* 29) are formed catalytically without deactivation. The catalyst is active over the whole illumination time of 50 min towards 2-methyl-2-pentanol conversion. The inset shows the TOFs of acetone and propane. Note that the traces are offset for clarity.

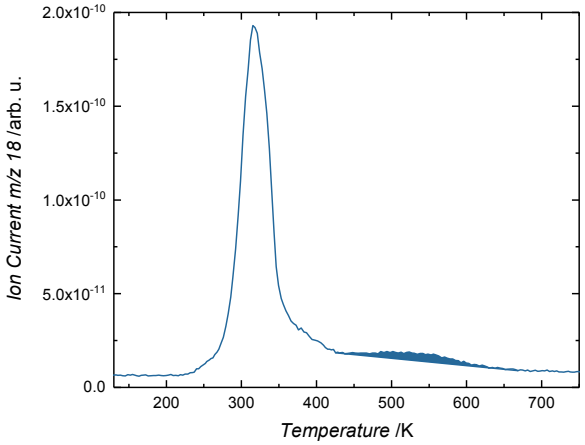

Figure S7. Temperature-programmed desorption of 1 ML H_2O from reduced TiO_2(110). 1 ML H_2O is dosed at 145 K with a molecular beam doser. Molecular water is desorbing at 310 K from Ti-lattice sites. The broad feature at 530 K originates from dissociatively adsorbed water in BBO vacancies forming two OH_{br} species. The integral of the high temperature feature yields a BBO vacancy concentration of 6 $\pm$ 1% ML following the titration method established by Henderson.[4]

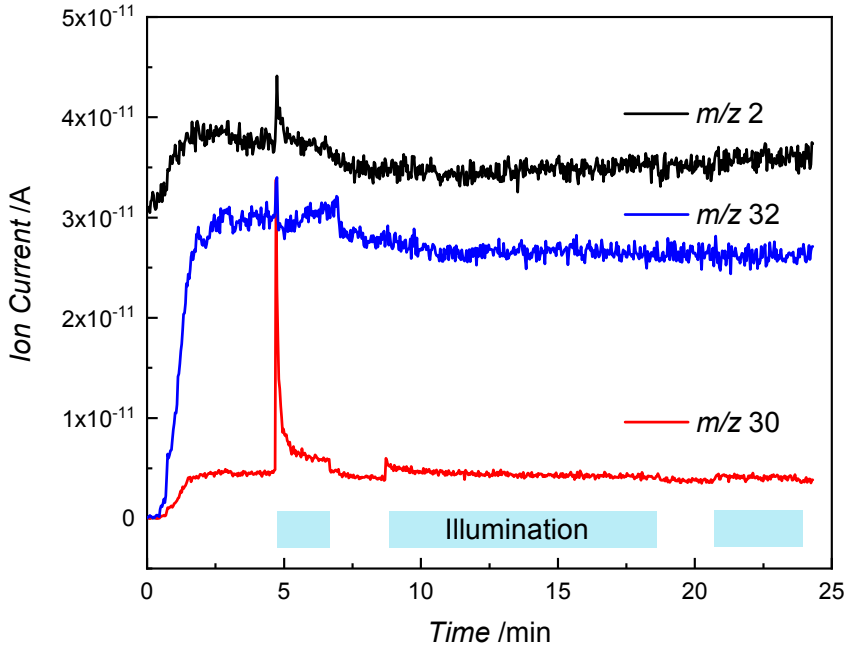

Figure S8. Raw data of the isothermal photooxidation experiment with methanol as shown in Fig. 1a.

Calculation of the turn-over-frequency

The evaluation of the turn-over-frequency allows for a quantification of the product formation with the help of an unequivocal mass fragment. The baseline corrected signal of the QMS is integrated in the steady-state regime. This value is corrected for the m/z-dependent transmission through the QMS, the electron impact ionization cross section (ICS), as well as with a factor considering the ion fragmentation taken from a reference mass spectrum. The ICS values as well as the *m*/*z*-values are given in table S1.

Table S1. Electron impact ionization cross section values at 70 eV and m/z-value of the respective fragment used for quantification.

Molecule	*m*/*z* fragment	ICS [Å]^6
Acetone	58	10.2
Propane	29	11.6

References

1. Walenta, C. A.; Kollmannsberger, S. L.; Courtois, C.; Tschurl, M.; Heiz, U., Photocatalytic Selectivity Switch to C-C scission: α-Methyl Ejection of tert-Butanol on TiO_2(110). *Phys. Chem. Chem. Phys.* **2018,** *20* (10), 7105-7111.
2. Kollmannsberger, S. L.; Walenta, C. A.; Courtois, C.; Tschurl, M.; Heiz, U., Thermal Control of Selectivity in Photocatalytic, Water-Free Alcohol Photoreforming. *ACS Catal.* **2018**, 11076-11084.
3. Walenta, C. A.; Kollmannsberger, S. L.; Pereira, R. N.; Tschurl, M.; Stutzmann, M.; Heiz, U., Anhydrous Ethanol Dehydrogenation on Metal–Organic Chemical Vapor Deposition Grown GaN(0001). *J. Phys. Chem. C* **2017,** *121* (30), 16393-16398.
4. Henderson, M. A., Structural Sensitivity in the Dissociation of Water on TiO2 Single-Crystal Surfaces. *Langmuir* **1996,** *12* (21), 5093-5098.
5. Zehr, R. T.; Henderson, M. A., Influence of O_2-induced Surface Roughening on the Chemistry of Water on TiO_2(110). *Surf. Sci.* **2008,** *602* (8), 1507-1516.
6. Harrison, A. G.; Jones, E. G.; Gupta, S. K.; Nagy, G. P., Total Cross Sections for Ionization by Electron Impact. *Can. J. Chem.* **1966,** *44* (16), 1967-1973.

A.4 Surface Species in Photocatalytic Methanol Reforming on $Pt/TiO_2(110)$: Learning from Surface Science Experiments for Catalytically Relevant Conditions

ACS Catalysis

pubs.acs.org/acscatalysis Research Article

Surface Species in Photocatalytic Methanol Reforming on Pt/TiO_2(110): Learning from Surface Science Experiments for Catalytically Relevant Conditions

Constantin A. Walenta, Carla Courtois, Sebastian L. Kollmannsberger, Moritz Eder, Martin Tschurl, and Ueli Heiz*

Cite This: *ACS Catal.* 2020, 10, 4080−4091 Read Online

ACCESS | Metrics & More | Article Recommendations | Supporting Information

ABSTRACT: Photocatalytic hydrogen evolution from methanol is a standard test reaction for photocatalyst materials. Surprisingly, the exact chemical mechanism is still widely discussed in the literature. In order to disentangle photochemical from thermal reaction steps and gain insights on the atomic level, we use a Pt cluster-loaded TiO_2(110) photocatalyst in very well-defined environments. Using Auger electron spectroscopy, temperature-programmed desorption/reaction, isotopic labeling, and isothermal photoreactions, it is possible to identify the surface species present on the catalyst under photocatalytic conditions. Furthermore, an initial conditioning of the photocatalyst is observed and attributed to thermal dehydrogenation of methanol to CO species on the cluster. The analysis of the isothermal photoreactions reveals that the photo-oxidation kinetics are not significantly affected by cocatalyst loading. The observed conversion and product distribution of formaldehyde and methyl formate can be rationalized with kinetic parameters gained from the bare TiO_2(110) crystal. The work leads to a detailed mechanistic understanding of the surface species and paves the way for an educated microkinetic modeling approach, which may be extended to a variety of noble metal cocatalysts and other TiO_2 modifications.

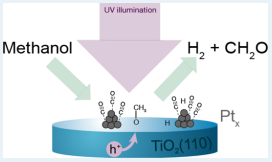

KEYWORDS: *surface species, photocatalytic conditions, Pt cluster loaded TiO_2(110)*

INTRODUCTION

Driving catalytic reactions with light has been envisioned for a long time to replace fossil feedstock for hydrogen production,[1] upgrade biomass to chemical feedstock,[2] or decompose waste in an environmentally benign way.[3] In this regard, understanding the key factors limiting the photocatalytic hydrogen evolution and fathoming the selectivity of the corresponding reactions still remain a great scientific challenge, especially because the concomitant oxidation products may influence the hydrogen evolution reaction.[4] This effect has been observed for the photo-electrocatalytic reforming of alcohol already decades ago[5,6] and is commonly known as "current doubling".[4,7] Thus, a key role for the design of better photocatalysts will be the understanding of the underlying reaction mechanisms and identification of the kinetics of photochemical and thermal reactions. In this regard, the judicious choice of particular reaction conditions (e.g., the temperature and reaction environment) may allow for the disentanglement of the elemental processes on the catalyst surface.

Methanol has been used frequently as a hole scavenger in order to investigate the photocatalytic hydrogen evolution of new catalyst materials.[2,4,8,9] This approach is fostered by the hope to improve the partial reaction of hydrogen evolution separately from the (far more complex) oxidation of water. It is, however, based on the (controversial) assumption that some of the elementary steps are the same or similar to photocatalytic water splitting.[4,10,11] For widely employed titania-based catalysts, the presence of a cocatalyst on the surface has been found to be inevitable for significant photocatalytic hydrogen evolution under ideal and real conditions.[12] The elucidation of the cocatalysts' properties and their exact role in the photoreaction thus represent important goals in the understanding of photocatalysis in general and for the photocatalytic hydrogen evolution in particular.

Zaera and co-workers deconstructed the mechanism of the photocatalytic hydrogen evolution reaction from a methanol/water mixture and found that the role of the cocatalyst is the promotion of the dimerization of surface hydrogen atoms rather than to act as charge traps.[13−15] Additionally, they showed that a thermodynamic approach, only taking conduction and valence band edges into account, is not sufficient to understand hydrogen evolution from NiO_x cocatalysts supported on TiO_2.[16] Further evidence for the

Received: January 16, 2020
Revised: March 3, 2020
Published: March 4, 2020

https://dx.doi.org/10.1021/acscatal.0c00260
ACS Catal. 2020, 10, 4080−4091

thermal hydrogen recombination on the cocatalyst has been presented using H/D-exchange experiments on the photocatalyst material without illumination.[16] Nevertheless, similar systems are still often interpreted in a different way, and to obtain stronger evidence for such a reaction mechanism, the study of more defined systems has proven to be advantageous. In this regard, platinum cocatalyst-loaded TiO_2(110) synthesized under ultrahigh vacuum conditions represents a very well-defined model system to probe photocatalytic reactions. Because rutile TiO_2(110) is one of the best understood materials under very well-defined conditions,[17,18] the surface physics of the semiconductor and thermal chemistry are very well-known.[17−20] We recently reported the hydrogen evolution from photocatalytic alcohol reforming to occur catalytically under ultrahigh vacuum conditions on Pt_x/TiO_2.[21,22] Similar to the studies of Zaera and co-workers,[16] molecular hydrogen is evolved by thermal recombination of surface hydroxyls, but in contrast to those studies, we ruled out the reduction of protons by photoelectrons.[22]

In this study, we further deconstruct the photoreforming of methanol in "snapshots" of the catalytic cycle in order to determine the surface species present under catalytic conditions and their stability. For this purpose, we use Pt-loaded rutile titania (110) because of the advantages of the system mentioned above. We apply Auger electron spectroscopy, temperature-programmed desorption/reaction (TPD/R), isotopic labeling, isothermal photoreactions, and a kinetic analysis to unravel the surface species, their stability, and the driving force for the observed selectivity under photocatalytic conditions. Although only recently photochemical studies have emerged for cocatalyst-loaded rutile TiO_2(110),[23,24] the present work explicitly addresses the characteristics of the cocatalyst under (photo)catalytic conditions and the resulting material's properties in photocatalysis (i.e., the selectivity and stability).

EXPERIMENTAL SECTION

Materials and Methods. All experiments were carried out under ultrahigh vacuum conditions with a backpressure of $<1 \times 10^{-10}$ mbar in a home-built setup for studying photocatalytic reactions.[21,25] An overview of the apparatus is shown elsewhere.[21] Briefly, it consists of surface preparation methods, including a sputter gun (SPECS IQE 11/35) and a molecular beam doser,[26] and surface analysis was performed with Auger electron spectroscopy (CMA 100, Omicron Nanotechnology GmbH). It is further equipped with a quadrupole mass spectrometer (QMS, QMA 430, Pfeiffer Vacuum GmbH) and a home-built time-of-flight mass spectrometer[27] for the analysis of reaction products. A load lock enables the transfer of samples and a laser ablation cluster source[28] creates metal clusters from 1 up to 100 atoms, which can be mass-selected and subsequently landed on various support materials.

Methanol (Chromasolv, ≥99.9%, Sigma-Aldrich), ethanol (absolute, HPLC grade, ≥99.8%, Sigma-Aldrich), and H_2O (Milli-Q, 18.2 MΩ·cm) were extensively degassed and further purified by pump−freeze cycles. D_2 (99% purity, Westfalen, Germany), O_2 (5.0, Westfalen), and CO (4.7, Air Liquide) were used without further purification. All adsorptions were carried out at 100 K sample temperature, unless otherwise indicated. A Pt target (99.95% purity, ESG Edelmetalle, Germany) was used for the generation of the Pt_x clusters and no contaminants in the clusters were found in the mass spectra before each deposition.

The reactivity measurements were carried out with an electron ionization QMS. The molecules were identified by their respective fragmentation patterns. Quantification with the fragmentation pattern correction, QMS sensitivity, and ionization cross section has been established in previous studies.[21,29] TPD experiments were carried out with a heating rate of 1.2 K/s from 100 K to the indicated temperature. Isothermal photoreaction experiments were performed at chosen temperatures of the photocatalyst, in which illumination was only started after the thermalization of the sample. As a source for this illumination, a laser with a wavelength of 242 nm was used with an intensity of 4.6 mW/cm^2. As we previously showed, the photoreactivity is independent on the used wavelength (355 or 369 nm was also tested), as long as the photon energy is above the band gap of rutile TiO_2 (3.0 eV).[22] The time resolution in the photoreaction experiments is limited by the detection time of the QMS and the number of mass traces followed in the experiment. Typically, time resolutions of a couple hundred milliseconds are achieved in the experiments presented, as multiple reaction products are recorded at the same time.

Catalyst Preparation and Characterization. The rutile TiO_2(110) single crystal (SurfaceNet GmbH) was cleaned by cycles of sputtering (Ar, 1.0 keV, 1×10^{-5} mbar, 20 min), oxygen annealing (820 K, 1×10^{-6} mbar), and annealing in vacuum (820 K), which is known to result in a flat and clean surface as determined by Auger electron spectroscopy (Figure S1) and H_2O TPD.[30,31] The concentration of bridge-bonded oxygen (BBO) vacancies was determined to be 6 ± 1% with respect to Ti-lattice sites (5.2×10^{14}/cm^2) based on the evaluation of H_2O TPDs.[22,31]

The deposition of the Pt_x (x = 8−32) clusters was facilitated by the operation of the quadrupole in the ion-guide mode, followed by the soft landing of the clusters on the TiO_2(110) single crystal at 110 K, as described in an earlier study.[22] The catalyst loading is controlled using a picoammeter (Keithley 6587) measuring the neutralization current of the cationic clusters when being deposited on the surface. The total loading is controlled using home-written software, integrating over the current leading to a highly precise cluster coverage determination.[32]

Unless specified differently, the Pt cluster coverage investigated in this work was chosen to be 1% of a monolayer. This value corresponds to a Pt cluster coverage of 1.5×10^{13} e/cm^2 or 0.15 e/nm^2 for the deposition of singly charged clusters and assumes that every surface site (1.5×10^{15}/cm^2) of the single crystal represents an adsorption site. The size distribution was decided to be the same as in our previous studies.[21,22] Furthermore, previous work with scanning probe microscopy[33−37] and X-ray photoelectron spectroscopy[36,37] demonstrated that the clusters are randomly distributed on the surface and do not bind to any specific defect site at room temperature and below. The successful deposition of the platinum cocatalyst is also observed in the Auger electron spectrum at 64 eV (see Figure S1). The complete removal of the Pt clusters from the surface requires an excessive cleaning procedure with multiple sputter−annealing cycles because Pt is very persistent on the surface because of strong metal support interaction.[38,39] The detection of molecular hydrogen from a water TPD proved to be a highly sensitive indicator for the smallest amount of Pt contaminations of the TiO_2(110) single crystal, which was also demonstrated by Geng et al.[40]

https://dx.doi.org/10.1021/acscatal.0c00260
ACS Catal. 2020, 10, 4080−4091

ACS Catalysis pubs.acs.org/acscatalysis Research Article

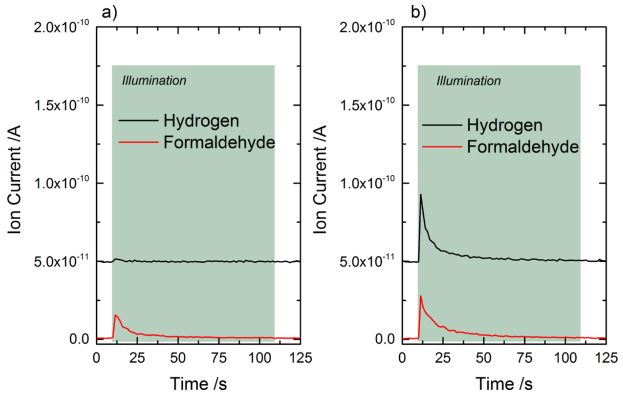

Figure 1. Photochemical products of 1 L of CH_3OH on r-TiO_2(110) (a) and on Pt_x/TiO_2(110) (b) at 260 K. Upon UV illumination (shown as a gray background), methoxy species are photo-oxidized to formaldehyde, which desorb thermally. In (a), only trace amounts of H_2 are formed upon illumination, while the catalyst poisoning is observed in subsequent illumination cycles.[22] The Pt-loaded photocatalyst (b) shows formaldehyde desorption accompanied by significant production of H_2 during illumination. The hydrogen trace is offset to 5×10^{-11} A for clarity. Note that the traces in this figure represent raw data of the masses m/z = 2 for H_2 and 30 for formaldehyde.

RESULTS AND DISCUSSION

A side-by-side comparison (Figure 1) of the photochemical reactions of methanol on the same semiconductor single crystal shows almost exclusively formaldehyde production for r-TiO_2(110) (Figure 1a). In contrast, H_2 evolution in addition to formaldehyde formation is observed for Pt-loaded TiO_2(110) (Figure 1b). This behavior is known from previous studies on bare TiO_2(110)[41,42] and on Pt-loaded TiO_2(110).[21,22] Clearly, the role of the Pt_x cocatalyst is to facilitate molecular hydrogen evolution from methanol during illumination. This completes the dehydrogenation reaction of methanol, which is in fact a hole-mediated disproportion, and makes the reaction truly catalytic.[22] To further investigate the surface chemistry on the Pt cocatalyst, we used isotopically labeled methanol-d_3 on the Pt-loaded photocatalyst and monitored the isothermal photoreaction (Figure 2). Upon the first illumination period at 260 K, desorption of formaldehyde (mass 30) and all mass traces of molecular hydrogen (mass 2, 3, and 4) are observed. All traces decay almost to the baseline within an illumination time of 2 min. Consecutive isothermal irradiation experiments on the same surface resaturated with methanol (obtained by again dosing 1 L of CD_3OH after the previous illumination) revealed that the mass trace for formaldehyde remains unchanged in all dosing illumination cycles. All hydrogen mass traces, although persistent, are less intense than those in the first illumination experiment. This observation points to conditioning of the catalyst. As neither the intensity nor the decay kinetics in the mass traces change in consecutive cycles of methanol dosage and illumination, the conditioning of the catalyst seems to be already completed after the first cycle. In the conditioned state, deuterium atoms for D_2 formation exclusively originate from the photo-oxidation reaction of the alcohol.

Catalyst conditioning proceeds most likely not photochemically but by a thermal mechanism. Initially, a significant amount of hydrogen is on the surface, originating from either the dissociative adsorption of CD_3OH (i.e., hydrogen and methoxy formation) on the TiO_2(110) surface or the thermal decomposition of methanol on the Pt_x clusters. The second

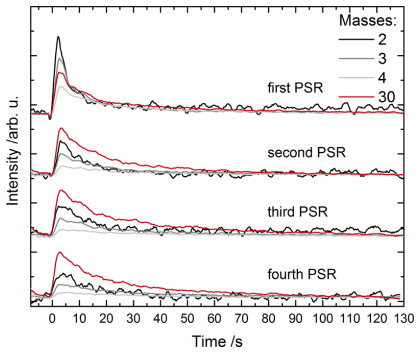

Figure 2. Consecutive isothermal irradiation experiments at 260 K on a Pt_x/TiO_2(110) catalyst. The reaction is started by illumination after adsorption of 1 L of CD_3OH at cryogenic temperatures. Between every photochemical experiment, the surface is recovered with 1 L of methanol-d_3 at the reaction temperature, which is enough to saturate the surface at 260 K. Upon illumination, formaldehyde (mass 30) and hydrogen desorb (masses 2, 3, and 4). After an initial conditioning of the catalyst, where an increased amount of hydrogen desorbs, further illumination cycles result in stable intensities and decay kinetics for all observed products. Note that the Pt_x cluster coverage in this experiment is 0.75% of a monolayer.

pathway yields carbon monoxide and hydrogen species, based on prior work on Pt(111).[43] Both reactions must be considered to give rise to the hydrogen traces in Figure 2. The conditioning is largely finished after the first photochemical reaction cycle, which shows that the time needed for thermalization (in the order of some minutes) is longer than the time scale of the methanol decomposition reaction. In order to analyze the thermal chemistry on the Pt_x cocatalyst, a TPR experiment with isotopically labeled methanol CD_3OH on a Pt_x/TiO_2(110) photocatalyst was performed (Figure 3), which is in good agreement with a very recent study of Hao et al.[23] Methanol adsorbed on the semiconductor surface shows

https://dx.doi.org/10.1021/acscatal.0c00260
ACS Catal. 2020, 10, 4080−4091

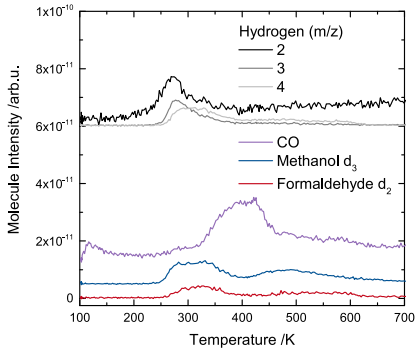

Figure 3. TPR experiment from 100 to 700 K on a $Pt_x/TiO_2(110)$ photocatalyst with a CD_3OH coverage of 1 L without illumination. Upon Pt loading of the catalyst, hydrogen evolution around 250 K from methanol dehydrogenation is observed. Additionally, an intense peak of CO around 400 K is observed, which is assigned to CO desorbing from the Pt clusters.[35,48] The traces are offset for clarity, and the hydrogen species represent raw mass traces, while CO (m/z = 28), methanol (m/z = 35), and formaldehyde (m/z = 30) are corrected for fragmentation patterns.

the well-known desorption chemistry of bare $TiO_2(110)$, with the alcohol leaving the surface at mainly around 300 K, as reported before.[44−46] Some methanol, however, is adsorbed on the Pt clusters and undergoes complete dehydrogenation to CO, similar as in the reaction on a Pt(111) single crystal.[43,47] In contrast, the TPD of the bare titania surface neither shows a high-temperature CO peak nor thermal hydrogen evolution during methanol desorption. Interestingly, only one broad desorption feature of molecular hydrogen is obtained between 220 and 350 K, while Hao et al. observed an additional feature around 550 K.[23] This difference may originate from different preparation techniques of the Pt cocatalysts, yielding clusters in a different size distribution and of potentially different morphologies, both of which affect their local chemical environment. Based on a careful analysis of all fragmentation patterns, we rule out the formation of significant amounts of any other products from methanol chemistry such as methyl formate (Figure S2).

The TPR results present evidence that the active hydrogen recombination cocatalysts in the photocatalytic reaction are apparently not the bare Pt clusters. On the conditioned catalyst, the clusters are rather covered by carbon monoxide, which stems from methanol dehydrogenation.

The thermal evolution of molecular hydrogen from methanol, which is not observed on bare $TiO_2(110)$,[22,45] occurs at around 250 K (Figure 3) in agreement with H_2 desorption from Pt clusters on other oxide supports (e.g., SiO_2)[49] and the D_2 desorption from $Pt_x/TiO_2(110)$ (see Figure S3). This indicates that the dehydrogenation chemistry takes place around or below 250 K because the peak temperature also matches the hydrogen desorption feature upon D_2 adsorption (see Fig. S3). The same desorption temperature is observed for the thermal hydrogen evolution from surface hydroxyl recombination resulting from water adsorption on $Pt_x/TiO_2(110)$ (Figure S3).[40] As mentioned before, molecular water dosed onto the $Pt_x/TiO_2(110)$ surface dissociates in BBO vacancies on the surface and, consequently, two surface hydroxyls are formed.[31] These hydrogen atoms, bound to BBO atoms on the $TiO_2(110)$ surface, are able to diffuse[50] and eventually recombine at the Pt clusters, while the oxygen "heals" the surface defects (see also Figure S4). Other than for bare $TiO_2(110)$, water desorption originating from hydroxyl recombination around 450 K is not observed when the cocatalyst is present on the surface (Figure S4).

In order to observe photochemical evolution of molecular hydrogen formed on the Pt cocatalyst, an isothermal photoreaction experiment is carried out at 250 K. It is followed by a TPD run immediately after the illumination to identify the surface species present on the photocatalyst (Figure 4). Upon illumination, all possible isotopomers of molecular hydrogen are observed (Figure 4a) accompanied by formaldehyde desorption. No significant desorption of carbon monoxide, water, or methanol is detected upon illumination. The immediate increase also in the D_2 signal (mass 4) is indicative for the diffusion of surface hydroxyls and the H atom recombination being fast processes, which is in agreement with

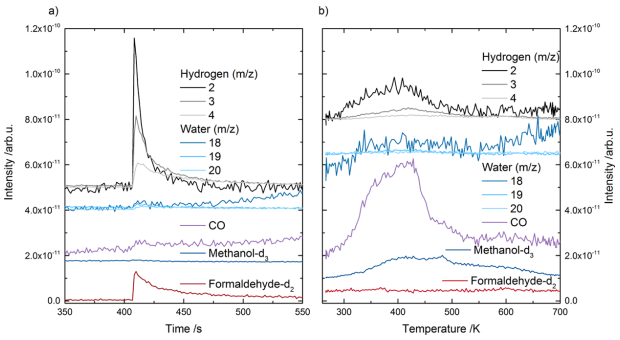

Figure 4. (a) Photon-stimulated reaction of 1 L of methanol (CD_3OH) on a $Pt_x/TiO_2(110)$ catalyst at 250 K. Upon illumination, formaldehyde and hydrogen, which are products from methanol photoreforming, are observed. The traces are offset for clarity. (b) TPR after the isothermal photoreaction (in a) from 250 to 700 K. The traces are again offset for clarity. Mostly, CO is desorbing as a result from thermal methanol dehydrogenation. All the products desorbing are in excellent agreement with the thermal chemistry reported in Figure 3. The photochemical reaction temperature was chosen to be below the onset of methanol desorption.

https://dx.doi.org/10.1021/acscatal.0c00260
ACS Catal. 2020, 10, 4080−4091

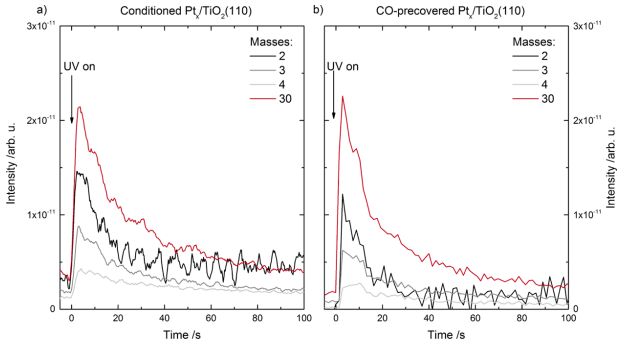

Figure 5. Comparison between isothermal photoreaction experiments at 262 K showing that a conditioned Pt_x/TiO_2 photocatalyst and an artificially CO-saturated Pt_x/TiO_2 lead to very similar desorption characteristics for methanol photocatalysis. (a) Photoreaction of the third cycle (Figure 2) with the photocatalyst prepared without any treatment of the catalyst before the photo-experiments. In (b), the $Pt_x/TiO_2(110)$ catalyst is exposed to 10 L of CO at 110 K and then annealed to 155 K. At this temperature, physisorbed CO on $TiO_2(110)$ either desorbs[53] or diffuses to the Pt_x clusters, where it chemisorbs and remains strongly bound.[54] Subsequently, 1 L of CD_3OH is dosed onto the surface at 120 K after which the catalyst is set to 262 K, where the photoreaction is carried out. The initial temperature for both experiments was chosen again to ensure the best comparability of the measurements with the different pretreatments of the catalyst. Although the Pt clusters are saturated with carbon monoxide, molecular hydrogen evolution is observed, and the intensities are similar to those on the conditioned catalyst (Molecular hydrogen is indicated by the mass traces 2, 3, and 4, while the CDO^+ fragment of formaldehyde is identified by m/z = 30).

the literature.[51] A TPR measurement of the catalyst after the isothermal photoreaction shows (Figure 4b) that all of the formed formaldehyde is already thermally desorbed and that the majority of the methanol molecules were either photo-oxidized or dehydrogenated on the Pt cluster. The latter pathway is supported by the desorption of CO observed around 400 K.

To gain further insights into the hydrogen evolution and the conditioning of the Pt cocatalyst, we artificially exposed clean $Pt_x/TiO_2(110)$ to a saturation coverage of CO directly after cluster deposition, dosed methanol-d_3, and carried out an isothermal illumination experiment at 262 K (Figure 5). Formaldehyde and all hydrogen species were found to desorb upon illumination, indicating that even a carbon monoxide-saturated platinum cocatalyst is active for molecular hydrogen evolution. The observed intensities and isotope distributions (Figure 5) of the molecular hydrogen evolution are in excellent agreement with the isothermal photoreactions from the conditioned catalyst, as shown in Figure 2. This behavior is similar as in a previous study by Berto et al., in which photocatalytic hydrogen evolution from water was observed from CO-covered noble metal nanoparticles on a nitride-based semiconductor.[52] This result further infers that CO from methanol dehydrogenation is most likely adsorbed onto the Pt cocatalyst during the photoreaction and represents a spectator species on the metal clusters for the photocatalytic hydrogen evolution on a conditioned catalyst.

Although Pt loading clearly changes the reactivity of the semiconductor by enabling hydrogen evolution, it may be suspected that the cocatalyst also affects the photo-oxidation reaction of methanol. To evaluate this potential influence of the clusters in the photo-oxidation mechanism, the formaldehyde traces of the bare and the metal-covered surface are compared in the following. The CH_2O peak exhibits a lower intensity and a smaller integral value on the bare semiconductor with respect to the Pt-decorated one (see Figure 1). The well-known poisoning of the photoreaction of methanol (see Figure 1a) on bare $TiO_2(110)$,[22,55] which was first reported for ethanol,[56] makes a kinetic analysis of the peak height gratuitous because it does not represent the amount of active sites directly. It is influenced by the deactivation mechanism (i.e., the hydroxylation of the surface) from the photoreaction on the bare catalyst and the decrease in the coverage of methanol by the initial photoconversion. A complete quantitative microkinetic description is therefore not feasible, as shown by Phillips et al. previously.[42]

On the other hand, both photoreaction products can desorb from $Pt_x/TiO_2(110)$ at the reaction temperature (Figure 1b), leading to a higher observed conversion for formaldehyde. To dissect kinetic information, a qualitative comparison of the rate constants can be performed. The overall photoreforming of methanol can be written in the following kinetic description

$$r = -\frac{\mathrm{d[methanol]}_t}{\mathrm{d}t} = \frac{\mathrm{d[formaldehyde]}_t}{\mathrm{d}t} = k \times [h\nu] \times [\mathrm{methanol}]_t \quad (1)$$

This expression includes that only the charges created from one photon are needed to oxidize methanol to formaldehyde because the dissociative adsorption of methanol is a thermal process on the semiconductor surface.[41] This is in perfect agreement with our postulated mechanism from catalytic experiments[21,22] and all the current doubling observations in the literature for alcohol photochemistry on titania.[5−7]

Under constant illumination, one can simplify eq 1 further by employing $k' = k \times [h\nu]$. Following the reaction mechanism,[21,41,42,57,58] the decay of the product can be assumed in the first approximation to be of first order with the methanol concentration, yielding the typical exponential decay function

$$[\mathrm{methanol}]_t = [\mathrm{methanol}]_0 \times \exp(-k't) \quad (2)$$

with $[\mathrm{methanol}]_0$ being the initial methanol concentration in photo-active sites.

As

https://dx.doi.org/10.1021/acscatal.0c00260
ACS Catal. 2020, 10, 4080−4091

$$[\text{formaldehyde}]_t = [\text{methanol}]_0 - [\text{methanol}]_t \quad (3)$$

this results in the following expression for the integral product yield

$$[\text{formaldehyde}]_t = [\text{methanol}]_0 \times (1 - \exp(-k't)) \quad (4)$$

and its differential form, which represents the signal in the desorption measurements, being

$$\frac{\mathrm{d}[\text{formaldehyde}]_t}{\mathrm{d}t} = [\text{methanol}]_0 \times k' \times \exp(-k't) \quad (5)$$

Therefore, it is evident that the rate constants (k' and k for constant photon fluxes) are reflected in the respective exponential decays, which are very similar for the bare and the cocatalyst-loaded semiconductor (Figure 6).

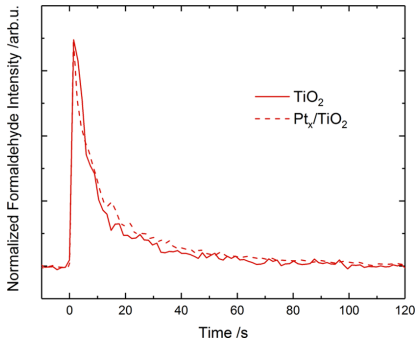

Figure 6. Isothermal illumination experiments at 260 K of the r $TiO_2(110)$ surface and the $Pt_x/TiO_2(110)$ catalyst of 1 L of methanol with normalized intensities to compare the decays. It can be seen that a loading with Pt cocatalysts does not change the exponential decay significantly within the accuracy of the measurements. Illumination is initiated at the time of 0 s.

Because the formaldehyde desorption is a thermal process, it is crucial to keep the sample at the exact temperature of 260 K (with an estimated error of ±0.5 K) to avoid temperature-related effects in the exponential decay. This is in particular of importance as the reaction is quite complex with at least the desorption and photoreaction being important reaction steps (more details are given in Phillips et al. in the Supporting Information).[42] The complexity is also reflected in the decay of the formaldehyde signal, which deviates from the simple first-order behavior assumed above. Consequently, the detected decline becomes multi-exponential and the rate constant cannot be directly obtained. Nevertheless, the similarity of the formaldehyde decays of the bare and Pt-loaded titania crystal indicates that the photo-oxidation of methoxy species is the rate-determining step in methanol photocatalysis and that the thermal H-atom recombination is a consecutive thermal reaction, as known from previous studies.[21,22]

Although the Pt cocatalyst is generally known to promote the hydrogen evolution reaction, the qualitative analysis of the apparent kinetics reveals that the photo-oxidation reaction stays largely unaltered. Consequently, at least at this coverage of 1% Pt_x on $TiO_2(110)$, an electronic effect induced by the cocatalyst (e.g., the controversial charge accumulation in the metal particles[14,16,24,59,60]) on the photo-oxidation reaction is not observed to play an important role.

The photoreaction of methanol to formaldehyde and molecular H_2 can be rationalized in a scheme corroborating knowledge from semiconductor physics (Figure 7). Upon

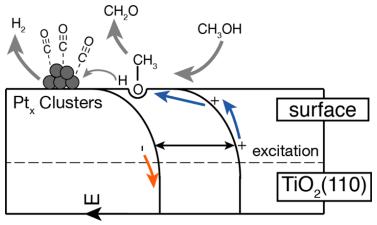

Figure 7. Photochemical mechanism upon illumination of the methanol-covered $Pt_x/TiO_2(110)$ catalyst proceeds via a direct hole transfer to the methoxy species on the surface to form formaldehyde and consecutive thermal hydrogen evolution. The cocatalyst for the hydrogen evolution carries adsorbed CO species from the initial thermal methanol dehydrogenation on the Pt cluster. Thermal steps in the reaction mechanism are depicted in gray arrows, while the known pathways for the photogenerated holes and electrons are shown in the respective colors, blue and orange. Note that the position of the Pt cluster does not reflect its position with respect to the band energy diagram but rather a physical location on the surface.

excitation with UV light, an electron−hole pair is formed in the $TiO_2(110)$ single crystal. Because the latter is an n-type semiconductor, the holes formed in the space charge region are subject to a driving force from a Coulomb attraction toward the surface, while the electrons preferentially travel toward the bulk. Methoxy species form thermally at a variety of defect sites[41,61] including the negatively charged BBO vacancies.[62−64]

In previous photocatalytic studies on a cocatalyst-loaded $TiO_2(110)$ photocatalyst with methanol[21,22] and ethanol,[24] the dependence of the photocatalytic hydrogen evolution with regard to the photon flux was found to be close to 1, meaning that only one absorbed photon leads to the formation of one H_2 molecule. This observation is in very good agreement with the "current-doubling" effect that has been observed for the same materials.[10,65] Furthermore, methoxy species adsorbed on the $TiO_2(110)$ surface were identified in systematic studies as the photo-active intermediate by various groups,[41,42,57,66,67] while a photon-driven O−H dissociation mechanism of molecular methanol remains controversial.[41,58,68−70]

Furthermore, formaldehyde desorption from photo-oxidation is observed at 250 K immediately upon illumination because this molecule desorbs thermally around 240 K.[71] Hydrogen evolution is also observed around that temperature (also see Figures 3 and S3). The methoxy species are directly photo-oxidized by the photohole to form formaldehyde via a split of the C−H bond.[57,66,72] The photoreaction from tertiary alcohols evidences[21,29] that the abstracted H species is most likely a radical (in analogy to $^{\bullet}CH_3$ from *tert*-butanol photo-oxidation), while the extinguished charge corresponds to the electron from the carbon atom in a Lewis-type formalism. Although formaldehyde desorbs thermally, the hydrogen atoms on the surface diffuse to the Pt cocatalyst and thermally recombine.[22] The dimerization on the metal cocatalyst of the surface-bound hydrogen species was also suggested to be present in solution.[14,16,73] Some CO is chemisorbed on the cocatalyst from thermal methanol dehydrogenation on the Pt clusters, but the cocatalyst is active for the photocatalytic

https://dx.doi.org/10.1021/acscatal.0c00260
ACS Catal. 2020, 10, 4080−4091

hydrogen evolution nonetheless. The finding that the cocatalyst loading does not alter the photo-oxidation kinetics further corroborates the scheme in Figure 7 because the hydrogen evolution in this picture is a fast, consecutive thermal reaction to the photo-oxidation of the methoxy species.

The chemical catalytic cycle can be closed in this picture because methanol reacts stoichiometrically to molecular hydrogen and formaldehyde. The photocatalytic methanol reforming can be rationalized using the following set of reaction equations (eqs 6−8). Here, methoxy species are photo-oxidized to formaldehyde, while molecular hydrogen desorbs.

$$CH_3OH \xrightarrow[TiO_2(110)]{} CH_3O^* + H^* \quad (6)$$

$$CH_3O^* + h\nu \xrightarrow[TiO_2(110)]{} CH_2O \uparrow + H^* \quad (7)$$

$$2H^* \xrightarrow[Pt_x]{} H_2 \quad (8)$$

The electronic catalytic cycle can be also closed because the methanol predominantly dissociates on the negatively charged surface states and gets subsequently oxidized by the photohole. Closing this electronic cycle and, thus, leaving the catalyst electronically unchanged require the recharging of the surface states.[70]

Below 250 K, another reaction channel opens up under catalytic conditions: formaldehyde gets photo-oxidized and couples with methanol in a consecutive photoreaction to form methyl formate and another H_2 molecule (eq 9)

$$CH_2O + CH_3OH + h\nu \xrightarrow[Pt_x/TiO_2(110)]{} HCOOCH_3 \uparrow + H_2\uparrow \quad (9)$$

In order to discriminate between photochemical and thermal reaction steps in the low-temperature methanol photo-oxidation pathway, the photoreaction may be carried out at cryogenic temperatures, and postirradiation temperature-programmed desorption (PI-TPD) experiments may then be used to quantify the conversion of methanol and product formation.[41,42,74] A methanol-covered, bare TiO_2(110) surface facilitates under such conditions the formation of methyl formate, which was demonstrated by isotopic labeling experiments to occur via a transient formyl species, as evidenced in the literature.[42] The results from such PI-TPDs on bare r-TiO_2(110) and turnover frequencies (TOFs) from methanol photocatalysis on Pt_x/TiO_2(110) are shown in Figure 8. In (a), the PI-TPD from 15 min illumination of 1 L of CD_3OH at 100 K between 220 and 300 K is displayed. As seen there, methyl formate desorbs around 235 K, formaldehyde desorbs around 245 K, and methanol desorbs around 275 K, which is consistent with the literature.[42,74,75] The full PI-TPD after illumination of methanol on r-TiO_2(110) is given in Figure S5. The dependence of formaldehyde and methyl formate production as a function of illumination time (Figure S6) is in excellent agreement with a previous study.[74]

The observed photo-oxidation products and their respective desorption temperatures in the PI-TPD of methanol on r-TiO_2(110) (Figure 8a) are the same as observed under catalytic conditions in the investigated temperature range from 230 to 273 K on the Pt_x/TiO_2(110) photocatalyst. This supplies further evidence that the platinum cocatalyst does not open another reaction pathway for photo-oxidation. On the high temperature side, the overall product evolution is

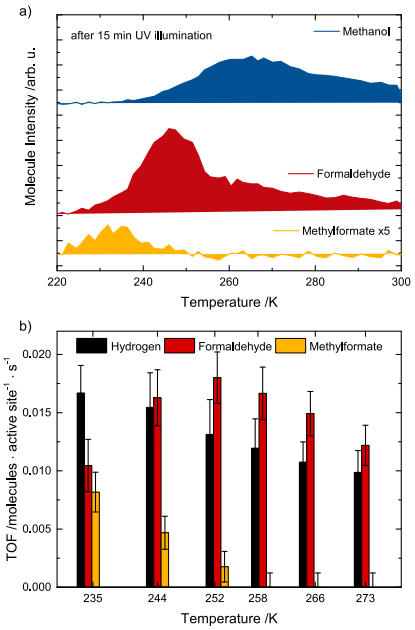

Figure 8. (a) Relevant TPD region of 1 L of CD_3OH on the TiO_2(110) surface after 15 min of UV illumination at 100 K. The full temperature range of the postirradiation experiment is shown in Figure S5. (b) TOFs of methanol photocatalysis in a methanol background pressure of 1×10^{-8} mbar on a Pt_x/TiO_2(110) photocatalyst as reported in a previous study.[21] A direct correlation between the observed product species under photocatalytic conditions with peaks from postirradiation TPDs is suggested from a joint interpretation of these results.

quantitatively lower because the majority of methanol already desorbs at 275 K. Around 255 K, a peak in the formaldehyde TOF is obtained (Figure 8b). In the PI-TPD (Figure 8a), however, the majority of methanol still remains adsorbed on the surface, while formaldehyde desorption is already facilitated. Photocatalysis at even lower temperatures around 235 K changes the selectivity of the reaction, as methyl formate is obtained from the sequential photo-oxidation of formaldehyde. The selectivity of the photochemical processes clearly depends on available intermediates at the surface and can be altered by the reaction temperature (Figure 8b).[21] In this regard, the PI-TPD can be used to calculate the surface lifetime of adsorbates from their peak in TPD experiments. The surface residence time of an adsorbate can be estimated by the following expression, whose detailed derivation is given in the Supporting Information

$$t_{1/2} = \frac{\ln(2)}{\nu_d \times e^{-\Delta H/RT}} \quad (10)$$

In this regard, ΔH is the desorption energy, T is the temperature, ν_d is the pre-exponential factor from the Arrhenius equation, and R is the gas constant. The residence times for methanol, formaldehyde, and methyl formate are shown in Table 1 along with the observed selectivity of the

https://dx.doi.org/10.1021/acscatal.0c00260
ACS Catal. 2020, 10, 4080−4091

methanol photoreforming on cocatalyst-loaded TiO_2(110) at the reaction temperature obtained from Figure 8b.

Table 1. Calculated Surface Residence Times of Methanol, Formaldehyde, and Methyl Formate from PI-TPD Experiments on r-TiO_2(110) and Observed Selectivities from Methanol Photoreforming on Pt_x/TiO_2(110)

	surface residence time/s			observed selectivity/%	
temperature/K	CH_3OH	CH_2O	CH_3OOCH	CH_2O	CH_3OOCH
235	497.80	18.48	3.52	56.1	43.9
244	103.93	4.45	0.85	77.7	22.3
252	28.36	1.36	0.26	91.1	8.9
258	11.29	0.59	0.11	99.9	<0.1
265	4.06	0.23	0.04	99.9	<0.1
273	1.35	0.09	0.02	100	

The observed selectivity of photo-oxidation is dependent on the probability of a consecutive photo-oxidation of the formaldehyde intermediate on the surface, which is in competition with thermal formaldehyde desorption.[21] To visualize this dependence, the methyl formate TOF under catalytic conditions on Pt_x/TiO_2(110) is shown as a function of the surface residence time of both reactants, methanol and formaldehyde, forming the ester (Figure 9). Because methanol

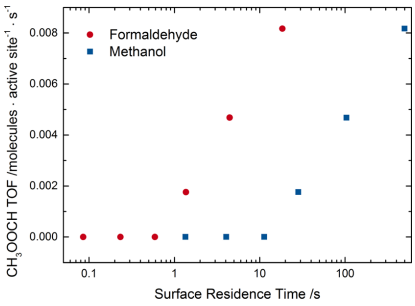

Figure 9. Correlation of the calculated surface residence times from Table 1 with the observed TOFs of methanol photoreforming from Figure 8b. Photocoupling to methyl formate is only observed at formaldehyde surface residence times of more than 1 s on the semiconductor surface. By the nature of adsorption properties, methanol has a surface lifetime that is an order of magnitude higher compared to formaldehyde.

is abundant on the surface at the temperatures where photocoupling to methyl formate is observed, formaldehyde photo-oxidation is believed to be the selectivity-determining step (eq 9). Only when formaldehyde is present for longer than 1 s on the surface, significant methyl formate evolution is observed (see Figure 9). This further emphasizes the importance of the chemical reaction kinetics on photoreforming processes because the charge carrier dynamics occur on much faster time scales of picoseconds for single crystals[76] and microseconds for nanoparticles.[77]

The importance of surface residence time on the observed selectivity may reasonably be transferable to gas-phase, water-free methanol reforming under more applied conditions, as similar reaction pathways and products formed are observed under such conditions.[78−80] Furthermore, this may not only hold true for other rutile surfaces,[81,82] as a very similar thermal and photochemistry for methanol has been observed on anatase[83−89] and brookite modifications.[90,91] The adsorption properties and desorption temperatures for the alcohols and their photo-oxidation products are very similar in general on the investigated TiO_2 surfaces. Especially on anatase, the majority phase[92] in Degussa P25, the same photo-oxidation pathway of methanol to methyl formate has been reported recently.[93]

Stability is one of the major requirements for any future application of photocatalysts.[94] We reported that the Pt_x/TiO_2(110) model catalyst is highly stable and demonstrated this for 4 h of methanol photoreforming at a temperature of 262 K, in which no decline in activity was observed.[21] However, while Pt_x/TiO_2 photocatalysts are generally perceived as stable,[8] recent work from Haselmann et al. reported a deactivation mechanism within the first hour for small platinum loadings.[95] Chung et al. observed a similar deactivation phenomenon after 30 min of photoreforming of methanol on their Pt/TiO_2 catalysts based on Degussa P25, in addition to an induction period lasting a couple of minutes.[96] Therefore, we further investigated the stability under reaction and vacuum conditions. A further sign of the long-term stability of the Pt_x/TiO_2(110) photocatalyst under the investigated conditions is demonstrated by the measurements presented in Figure 10. The catalyst is not only stable for more than 200 min as reported previously;[21] there is also no decline in activity in subsequent catalytic experiments (Figure 10a,b). Furthermore, the storage of the photocatalyst in vacuo for 70 h did not lead to any change in the catalytic activity, neither qualitatively as in the formation of products (Figure 10c) nor quantitatively as in the overall TOF (Figure 10d). Furthermore, deactivation by unavoidable adsorption of residual gases such as CO and H_2O was not observed, which happens because of the long exposure time of 70 h and despite the low pressure of $<1 \times 10^{-10}$ mbar. This again corroborates the findings summed up in Figure 7 that the Pt cocatalyst gets conditioned quickly and most likely by CO adsorbed on the Pt clusters. These CO species may also contribute to the long-term stability of the particle[52] in a similar way as previously observed for Pt clusters on an iron oxide support.[97]

CONCLUSIONS

In summary, the extensive analysis of isothermal photoreactions, TPD, and postirradiation TPDs leads to a complete picture of all the surface species present under photocatalytic conditions in the gas phase. The results supply evidence that the Pt cocatalyst, which acts as a center for thermal hydrogen recombination,[14,16,22,98] is most likely covered by CO under the reaction conditions. Although these spectator species do not inhibit H_2 formation, they may even lead to the protection of the cocatalysts giving rise to high stability, which is observed for the photocatalyst. This observation may not only be important for the interpretation of reactions under applied conditions but also explain or tune the stability of cocatalysts comprising other metals with a strong binding of CO, such as Ni, Pd,[99] and Ru.

Concerning the surface chemistry of the semiconductor, the full understanding of all surface species and the determination of thermal activation barriers and pre-exponentials set the necessary foundation for a meaningful description by microkinetic modeling or ab initio theory investigations. The surface science experiments and their connection to catalytic

https://dx.doi.org/10.1021/acscatal.0c00260
ACS Catal. 2020, 10, 4080−4091

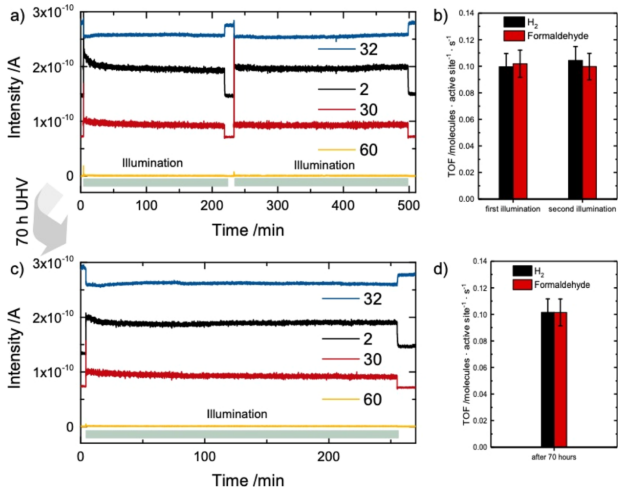

Figure 10. Methanol (m/z = 32), hydrogen (m/z = 2), formaldehyde (m/z = 30), and methyl formate (m/z = 60) traces at 262 K in a methanol background pressure of 7×10^{-8} mbar (a) and corresponding TOFs (b). The gray bars indicate the period of UV illumination. The presented traces are in quantitative agreement with previous studies.[21] Storing in vacuo at room temperature leads to the same catalytic activity as evidenced in the raw mass traces (c) and the quantitative agreement in the TOFs (d). Note that at this temperature, the mass trace 60 of methyl formate is too low in intensity for the calculation of a meaningful TOF.

conditions offer a new toolbox for photocatalysis research, which can be exploited by chemical reaction dynamics and to estimate selectivities under catalytic conditions. For example, the latter may be governed by the residence time of photoproducts on the surface enabling consecutive photoreactions, as we demonstrated for methyl formate formation. We were further able to show that under gas-phase reaction conditions, the photo-oxidation of methoxy is not affected by the Pt cocatalyst loading in the 1% range and that the photo-oxidation is the rate-determining step in the photocatalytic hydrogen evolution from methanol.[22] Clearly, the photocatalytic H_2 evolution cannot be analyzed decoupled from the photo-oxidation reaction in this reaction network, where the photogenerated charge is directly involved in the methanol photo-oxidation. However, one may speculate that a strong similarity in the hydrogen evolution mechanism between water and methanol exists because both reactions presumably proceed via the diffusion of hydroxyls and an eventual H dimerization at the Pt cocatalyst.

A complete kinetic understanding of the thermal processes on the catalyst surface will further set a path for a detailed investigation under different illumination conditions and semiconductor doping in very well-defined materials to investigate the influence of charge carrier dynamics on photocatalytic reactions. The kinetic insight from TPD experiments for catalytic conditions shows that the chemical surface reaction kinetics dominate the overall conversion and selectivity in catalysis,[100] which holds true for photocatalytic reactions as well.

■ ASSOCIATED CONTENT

Supporting Information

The Supporting Information is available free of charge at https://pubs.acs.org/doi/10.1021/acscatal.0c00260.

Auger electron spectra of the clean TiO_2(110) sample before and after photocatalysis; TPD data of methanol-d_3, D_2, and H_2O on Pt_x/TiO_2(110); exemplary postillumination TPD data of methanol-d_3 after 15 min of UV irradiation and the integrated values of an illumination-dependent TPD series of methanol on bare TiO_2(110); derivation of the surface lifetime values for the different species given along with a table; and summary of the kinetic parameters (PDF)

■ AUTHOR INFORMATION

Corresponding Author

Ueli Heiz − *Chair of Physical Chemistry & Catalysis Research Center, Technical University of Munich, Garching 85748, Germany;* orcid.org/0000-0002-9403-1486; Email: ulrich.heiz@mytum.de

Authors

Constantin A. Walenta − *Chair of Physical Chemistry & Catalysis Research Center, Technical University of Munich, Garching 85748, Germany;* orcid.org/0000-0001-9879-5101

Carla Courtois − *Chair of Physical Chemistry & Catalysis Research Center, Technical University of Munich, Garching 85748, Germany*

Sebastian L. Kollmannsberger − *Chair of Physical Chemistry & Catalysis Research Center, Technical University of Munich, Garching 85748, Germany*

Moritz Eder − *Chair of Physical Chemistry & Catalysis Research Center, Technical University of Munich, Garching 85748, Germany*

Martin Tschurl − *Chair of Physical Chemistry & Catalysis Research Center, Technical University of Munich, Garching 85748, Germany;* orcid.org/0000-0001-6618-7312

Complete contact information is available at:
https://pubs.acs.org/10.1021/acscatal.0c00260

Notes

The authors declare no competing financial interest.

■ ACKNOWLEDGMENTS

The authors thank the DFG for financial support through HE3435/22-1 and under Germany's Excellence Strategy—EXC 2089/1-390776260. C.C. acknowledges the support from the Luxembourg National Research Fund (FNR), project code 12531916 and that from the TUM International Graduate School of Science and Engineering (TUM-IGSSE).

■ REFERENCES

(1) Wang, Q.; Hisatomi, T.; Jia, Q.; Tokudome, H.; Zhong, M.; Wang, C.; Pan, Z.; Takata, T.; Nakabayashi, M.; Shibata, N.; Li, Y.; Sharp, I. D.; Kudo, A.; Yamada, T.; Domen, K. Scalable Water Splitting on Particulate Photocatalyst Sheets with a Solar-to-Hydrogen Energy Conversion Efficiency Exceeding 1%. *Nat. Mater.* **2016**, *15*, 611−615.
(2) Cargnello, M.; Gasparotto, A.; Gombac, V.; Montini, T.; Barreca, D.; Fornasiero, P. Photocatalytic H_2 and Added-Value By-Products − The Role of Metal Oxide Systems in Their Synthesis from Oxygenates. *Eur. J. Inorg. Chem.* **2011**, 4309−4323.
(3) Uekert, T.; Kuehnel, M. F.; Wakerley, D. W.; Reisner, E. Plastic Waste as a Feedstock for Solar-driven H_2 Generation. *Energy Environ. Sci.* **2018**, *11*, 2853−2857.
(4) Hainer, A. S.; Hodgins, J. S.; Sandre, V.; Vallieres, M.; Lanterna, A. E.; Scaiano, J. C. Photocatalytic Hydrogen Generation Using Metal-Decorated TiO_2: Sacrificial Donors vs True Water Splitting. *ACS Energy Lett.* **2018**, *3*, 542−545.
(5) Maeda, Y.; Fujishima, A.; Honda, K. The Investigation of Current Doubling Reactions on Semiconductor Photoelectrodes by Temperature Change Measurements. *J. Electrochem. Soc.* **1981**, *128*, 1731−1734.
(6) Baba, R.; Konda, R.; Fujishima, A.; Honda, K. Photoelectrochemical Deposition of Metals on TiO_2 Powders in the Presence of Alcohols. *Chem. Lett.* **1986**, 1307−1310.
(7) Yamagata, S.; Nakabayashi, S.; Sancier, K. M.; Fujishima, A. Photocatalytic Oxidation of Alcohols on TiO_2. *Bull. Chem. Soc. Jpn.* **1988**, *61*, 3429−3434.
(8) Kandiel, T. A.; Ivanova, I.; Bahnemann, D. W. Long-term Investigation of the Photocatalytic Hydrogen Production on Platinized TiO_2: an Isotopic Study. *Energy Environ. Sci.* **2014**, *7*, 1420−1425.
(9) Berr, M. J.; Vaneski, A.; Mauser, C.; Fischbach, S.; Susha, A. S.; Rogach, A. L.; Jäckel, F.; Feldmann, J. Delayed Photoelectron Transfer in Pt-Decorated CdS Nanorods under Hydrogen Generation Conditions. *Small* **2012**, *8*, 291−297.
(10) Schneider, J.; Bahnemann, D. W. Undesired Role of Sacrificial Reagents in Photocatalysis. *J. Phys. Chem. Lett.* **2013**, *4*, 3479−3483.
(11) Kamat, P. V.; Jin, S. Semiconductor Photocatalysis: "Tell Us the Complete Story!". *ACS Energy Lett.* **2018**, *3*, 622−623.
(12) Liu, N.; Zhou, X.; Nguyen, N. T.; Peters, K.; Zoller, F.; Hwang, I.; Schneider, C.; Miehlich, M. E.; Freitag, D.; Meyer, K.; Fattakhova-Rohlfing, D.; Schmuki, P. Black Magic in Gray Titania: Noble-Metal-Free Photocatalytic H_2 Evolution from Hydrogenated Anatase. *ChemSusChem* **2017**, *10*, 62−67.
(13) Joo, J. B.; Dillon, R.; Lee, I.; Yin, Y.; Bardeen, C. J.; Zaera, F. Promotion of Atomic Hydrogen Recombination as an Alternative to Electron Trapping for the Role of Metals in the Photocatalytic Production of H_2. *Proc. Natl. Acad. Sci. U.S.A.* **2014**, *111*, 7942.
(14) Lee, Y. J.; Joo, J. B.; Yin, Y.; Zaera, F. Evaluation of the Effective Photoexcitation Distances in the Photocatalytic Production of H_2 from Water using Au@Void@TiO_2 Yolk−Shell Nanostructures. *ACS Energy Lett.* **2016**, *1*, 52−56.
(15) Zaera, F. Gold-Titania Catalysts for Low-Temperature Oxidation and Water Splitting. *Top. Catal.* **2018**, *61*, 336−347.
(16) Joo, J. B.; Dillon, R.; Lee, I.; Yin, Y.; Bardeen, C. J.; Zaera, F. Promotion of atomic hydrogen recombination as an alternative to electron trapping for the role of metals in the photocatalytic production of H_2. *Proc. Natl. Acad. Sci. U.S.A.* **2014**, *111*, 7942.
(17) Diebold, U. The Surface Science of Titanium Dioxide. *Surf. Sci. Rep.* **2003**, *48*, 53−229.
(18) Henderson, M. A. A surface science perspective on TiO_2 photocatalysis. *Surf. Sci. Rep.* **2011**, *66*, 185−297.
(19) Thompson, T. L.; Yates, J. T. TiO_2-based Photocatalysis: Surface Defects, Oxygen and Charge Transfer. *Top. Catal.* **2005**, *35*, 197−210.
(20) Zhang, Z.; Yates, J. T. Band Bending in Semiconductors: Chemical and Physical Consequences at Surfaces and Interfaces. *Chem. Rev.* **2012**, *112*, 5520−5551.
(21) Kollmannsberger, S. L.; Walenta, C. A.; Courtois, C.; Tschurl, M.; Heiz, U. Thermal Control of Selectivity in Photocatalytic, Water-Free Alcohol Photoreforming. *ACS Catal.* **2018**, *8*, 11076−11084.
(22) Walenta, C. A.; Kollmannsberger, S. L.; Courtois, C.; Pereira, R. N.; Stutzmann, M.; Tschurl, M.; Heiz, U. Why Co-catalyst-loaded Rutile Facilitates Photocatalytic Hydrogen Evolution. *Phys. Chem. Chem. Phys.* **2019**, *21*, 1491−1496.
(23) Hao, Q.; ZhiqiangWang; Wang, T.; Ren, Z.; Zhou, C.; Yang, X. Role of Pt Loading in the Photocatalytic Chemistry of Methanol on Rutile TiO_2(110). *ACS Catal.* **2019**, *9*, 286−294.
(24) Katsiev, K.; Harrison, G.; Al-Salik, Y.; Thornton, G.; Idriss, H. Gold Cluster Coverage Effect on H_2 Production over Rutile TiO_2(110). *ACS Catal.* **2019**, *9*, 8294−8305.
(25) Kollmannsberger, S. L.; Walenta, C. A.; Winnerl, A.; Weiszer, S.; Pereira, R. N.; Tschurl, M.; Stutzmann, M.; Heiz, U. Doping-Dependent Adsorption and Photon-Stimulated Desorption of CO on GaN(0001). *J. Phys. Chem. C* **2017**, *121*, 8473−8479.
(26) Bozack, M. J.; Muehlhoff, L.; Russell, J. N.; Choyke, W. J.; Yates, J. T. Methods in Semiconductor Surface Chemistry. *J. Vac. Sci. Technol., A* **1987**, *5*, 1−8.
(27) Winbauer, A.; Kollmannsberger, S. L.; Walenta, C. A.; Schreiber, P.; Kiermaier, J.; Tschurl, M.; Heiz, U. Isomer-Selective Detection of Aromatic Molecules in Temperature-Programmed Desorption for Model Catalysis. *Anal. Chem.* **2016**, *88*, 5392−5397.
(28) Heiz, U.; Vanolli, F.; Trento, L.; Schneider, W.-D. Chemical Reactivity of Size-Selected Supported Clusters: An Experimental Setup. *Rev. Sci. Instrum.* **1997**, *68*, 1986−1994.
(29) Walenta, C. A.; Kollmannsberger, S. L.; Courtois, C.; Tschurl, M.; Heiz, U. Photocatalytic selectivity switch to C-C scission: α-Methyl Ejection of tert-Butanol on TiO_2(110). *Phys. Chem. Chem. Phys.* **2018**, *20*, 7105−7111.
(30) Zehr, R. T.; Henderson, M. A. Influence of O_2-Induced Surface Roughening on the Chemistry of Water on TiO_2(110). *Surf. Sci.* **2008**, *602*, 1507−1516.
(31) Henderson, M. A. Structural Sensitivity in the Dissociation of Water on TiO_2 Single-Crystal Surfaces. *Langmuir* **1996**, *12*, 5093−5098.
(32) Crampton, A. S.; Rötzer, M. D.; Landman, U.; Heiz, U. Can Support Acidity Predict Sub-Nanometer Catalyst Activity Trends? *ACS Catal.* **2017**, *7*, 6738−6744.
(33) Sasahara, A.; Pang, C. L.; Onishi, H. Local Work Function of Pt Clusters Vacuum-Deposited on a TiO_2 Surface. *J. Phys. Chem. B* **2006**, *110*, 17584−17588.
(34) Bonanni, S.; Aït-Mansour, K.; Brune, H.; Harbich, W. Overcoming the Strong Metal−Support Interaction State: CO Oxidation on TiO_2(110)-Supported Pt Nanoclusters. *ACS Catal.* **2011**, *1*, 385−389.
(35) Bonanni, S.; Aït-Mansour, K.; Harbich, W.; Brune, H. Effect of the TiO2 Reduction State on the Catalytic CO Oxidation on Deposited Size-Selected Pt Clusters. *J. Am. Chem. Soc.* **2012**, *134*, 3445−3450.

(36) Isomura, N.; Wu, X.; Watanabe, Y. Atomic-Resolution Imaging of Size-Selected Platinum Clusters on TiO_2(110) Surfaces. *J. Chem. Phys.* **2009**, *131*, 164707.
(37) Watanabe, Y.; Wu, X.; Hirata, H.; Isomura, N. Size-Dependent Catalytic Activity and Geometries of Size-Selected Pt Clusters on TiO_2(110) Surfaces. *Catal. Sci. Technol.* **2011**, *1*, 1490−1495.
(38) Dulub, O.; Hebenstreit, W.; Diebold, U. Imaging Cluster Surfaces with Atomic Resolution: The Strong Metal-Support Interaction State of Pt Supported on TiO_2(110). *Phys. Rev. Lett.* **2000**, *84*, 3646−3649.
(39) Pesty, F.; Steinrück, H.-P.; Madey, T. E. Thermal Stability of Pt Films on TiO_2(110): Evidence for Encapsulation. *Surf. Sci.* **1995**, *339*, 83−95.
(40) Geng, Z.; Jin, X.; Wang, R.; Chen, X.; Guo, Q.; Ma, Z.; Dai, D.; Fan, H.; Yang, X. Low-Temperature Hydrogen Production via Water Conversion on Pt/TiO_2. *J. Phys. Chem. C* **2018**, *122*, 10956−10962.
(41) Shen, M.; Henderson, M. A. Identification of the Active Species in Photochemical Hole Scavenging Reactions of Methanol on TiO_2. *J. Phys. Chem. Lett.* **2011**, *2*, 2707−2710.
(42) Phillips, K. R.; Jensen, S. C.; Baron, M.; Li, S.-C.; Friend, C. M. Sequential Photo-oxidation of Methanol to Methyl Formate on TiO_2(110). *J. Am. Chem. Soc.* **2013**, *135*, 574−577.
(43) Sexton, B. A. Methanol Decomposition on Platinum (111). *Surf. Sci.* **1981**, *102*, 271−281.
(44) Osmić, M.; Mohrhusen, L.; Al-Shamery, K. Bulk Defect Dependence of Low-Temperature Partial Oxidation of Methanol and High-Temperature Hydrocarbon Formation on Rutile TiO_2(110). *J. Phys. Chem. C* **2019**, *123*, 7615.
(45) Henderson, M. A.; Otero-Tapia, S.; Castro, M. E. The Chemistry of Methanol on the TiO_2(110) Surface: the Influence of Vacancies and Coadsorbed Species. *Faraday Discuss.* **1999**, *114*, 313−329.
(46) Guo, Q.; Xu, C.; Ren, Z.; Yang, W.; Ma, Z.; Dai, D.; Fan, H.; Minton, T. K.; Yang, X. Stepwise Photocatalytic Dissociation of Methanol and Water on TiO_2(110). *J. Am. Chem. Soc.* **2012**, *134*, 13366−13373.
(47) Gibson, K. D.; Dubois, L. H. Step Effects in the Thermal Decomposition of Methanol on Pt(111). *Surf. Sci.* **1990**, *233*, 59−64.
(48) Heiz, U.; Sherwood, R.; Cox, D. M.; Kaldor, A.; Yates, J. T. CO Chemisorption on Monodispersed Platinum Clusters on SiO_2: Detection of CO Chemisorption on Single Platinum Atoms. *J. Phys. Chem.* **1995**, *99*, 8730−8735.
(49) Crampton, A. S.; Rötzer, M. D.; Ridge, C. J.; Schweinberger, F. F.; Heiz, U.; Yoon, B.; Landman, U. Structure Sensitivity in the Nonscalable Regime Explored via Catalysed Ethylene Hydrogenation on Supported Platinum Nanoclusters. *Nat. Commun.* **2016**, *7*, 10389.
(50) Dohnálek, Z.; Lyubinetsky, I.; Rousseau, R. Thermally-Driven Processes on Rutile TiO_2(110)-(1×1): A Direct View at the Atomic Scale. *Prog. Surf. Sci.* **2010**, *85*, 161−205.
(51) Karim, W.; Spreafico, C.; Kleibert, A.; Gobrecht, J.; VandeVondele, J.; Ekinci, Y.; van Bokhoven, J. A. Catalyst Support Effects on Hydrogen Spillover. *Nature* **2017**, *541*, 68−71.
(52) Berto, T. F.; Sanwald, K. E.; Byers, J. P.; Browning, N. D.; Gutiérrez, O. Y.; Lercher, J. A. Enabling Overall Water Splitting on Photocatalysts by CO-Covered Noble Metal Co-Catalysts. *J. Phys. Chem. Lett.* **2016**, *7*, 4358−4362.
(53) Dohnálek, Z.; Kim, J.; Bondarchuk, O.; White, J. M.; Kay, B. D. Physisorption of N_2, O_2, and CO on Fully Oxidized TiO_2(110). *J. Phys. Chem. B* **2006**, *110*, 6229−6235.
(54) Bonanni, S.; Aït-Mansour, K.; Hugentobler, M.; Brune, H.; Harbich, W. An Experimental Setup Combining a Highly Sensitive Detector for Reaction Products with a Mass-Selected Cluster Source and a Low-Temperature STM for Advanced Nanocatalysis Measurements. *Eur. Phys. J. D* **2011**, *63*, 241−249.
(55) Zhang, R.; Wang, H.; Peng, X.; Feng, R.-r.; Liu, A.-a.; Guo, Q.; Zhou, C.; Ma, Z.; Yang, X.; Jiang, Y.; Ren, Z. In Situ Studies on Temperature-Dependent Photocatalytic Reactions of Methanol on TiO_2(110). *J. Phys. Chem. C* **2019**, *123*, 9993−9999.
(56) Walenta, C. A.; Kollmannsberger, S. L.; Kiermaier, J.; Winbauer, A.; Tschurl, M.; Heiz, U. Ethanol Photocatalysis on Rutile TiO_2(110): the Role of Defects and Water. *Phys. Chem. Chem. Phys.* **2015**, *17*, 22809−22814.
(57) Kolesov, G.; Vinichenko, D.; Tritsaris, G. A.; Friend, C. M.; Kaxiras, E. Anatomy of the Photochemical Reaction: Excited-State Dynamics Reveals the C−H Acidity Mechanism of Methoxy Photo-oxidation on Titania. *J. Phys. Chem. Lett.* **2015**, *6*, 1624−1627.
(58) Shen, M.; Henderson, M. A. Role of Water in Methanol Photochemistry on Rutile TiO_2(110). *J. Phys. Chem. C* **2012**, *116*, 18788−18795.
(59) Takanabe, K. Photocatalytic Water Splitting: Quantitative Approaches toward Photocatalyst by Design. *ACS Catal.* **2017**, *7*, 8006−8022.
(60) Subramanian, V.; Wolf, E. E.; Kamat, P. V. Catalysis with TiO_2/Gold Nanocomposites. Effect of Metal Particle Size on the Fermi Level Equilibration. *J. Am. Chem. Soc.* **2004**, *126*, 4943−4950.
(61) Zhang, Z.; Bondarchuk, O.; White, J. M.; Kay, B. D.; Dohnálek, Z. Imaging Adsorbate O−H Bond Cleavage: Methanol on TiO_2(110). *J. Am. Chem. Soc.* **2006**, *128*, 4198−4199.
(62) Henderson, M. A.; Epling, W. S.; Peden, C. H. F.; Perkins, C. L. Insights into Photoexcited Electron Scavenging Processes on TiO_2 Obtained from Studies of the Reaction of O_2 with OH Groups Adsorbed at Electronic Defects on TiO_2(110). *J. Phys. Chem. B* **2003**, *107*, 534−545.
(63) Henderson, M. A.; Szanyi, J.; Peden, C. H. F. Conversion of N_2O to N_2 on TiO_2(110). *Catal. Today* **2003**, *85*, 251−266.
(64) Papageorgiou, A. C.; Beglitis, N. S.; Pang, C. L.; Teobaldi, G.; Cabailh, G.; Chen, Q.; Fisher, A. J.; Hofer, W. A.; Thornton, G. Electron Traps and Their Effect on the Surface Chemistry of TiO_2(110). *Proc. Natl. Acad. Sci. U.S.A.* **2010**, *107*, 2391.
(65) Bingham, M.; Mills, A. Photonic Efficiency and Selectivity Study of M (M=Pt, Pd, Au and Ag)/TiO2 Photocatalysts for Methanol Reforming in the Gas Phase. *J. Photochem. Photobiol., A* **2020**, *389*, 112257.
(66) Chu, W.; Saidi, W. A.; Zheng, Q.; Xie, Y.; Lan, Z.; Prezhdo, O. V.; Petek, H.; Zhao, J. Ultrafast Dynamics of Photongenerated Holes at a CH_3OH/TiO_2 Rutile Interface. *J. Am. Chem. Soc.* **2016**, *138*, 13740−13749.
(67) Jensen, S. C.; Friend, C. M. The Dynamic Roles of Interstitial and Surface Defects on Oxidation and Reduction Reactions on Titania. *Top. Catal.* **2013**, *56*, 1377−1388.
(68) Guo, Q.; Zhou, C.; Ma, Z.; Ren, Z.; Fan, H.; Yang, X. Elementary photocatalytic chemistry on TiO_2 surfaces. *Chem. Soc. Rev.* **2016**, *45*, 3701−3730.
(69) Guo, Q.; Zhou, C.; Ma, Z.; Ren, Z.; Fan, H.; Yang, X. Elementary Chemical Reactions in Surface Photocatalysis. *Annu. Rev. Phys. Chem.* **2018**, *69*, 451−472.
(70) Walenta, C. A.; Tschurl, M.; Heiz, U. Introducing Catalysis in Photocatalysis: What Can Be Understood from Surface Science Studies of Alcohol Photoreforming on TiO_2. *J. Phys.: Condens. Matter* **2019**, *31*, 473002.
(71) Cremer, T.; Jensen, S. C.; Friend, C. M. Enhanced Photo-Oxidation of Formaldehyde on Highly Reduced o-TiO_2(110). *J. Phys. Chem. C* **2014**, *118*, 29242−29251.
(72) Shen, M.; Henderson, M. A. Impact of Solvent on Photocatalytic Mechanisms: Reactions of Photodesorption Products with Ice Overlayers on the TiO_2(110) Surface. *J. Phys. Chem. C* **2011**, *115*, 5886−5893.
(73) Méndez-Medrano, M. G.; Kowalska, E.; Lehoux, A.; Herissan, A.; Ohtani, B.; Rau, S.; Colbeau-Justin, C.; Rodríguez-López, J. L.; Remita, H. Surface Modification of TiO_2 with Au Nanoclusters for Efficient Water Treatment and Hydrogen Generation under Visible Light. *J. Phys. Chem. C* **2016**, *120*, 25010−25022.
(74) Guo, Q.; Xu, C.; Yang, W.; Ren, Z.; Ma, Z.; Dai, D.; Minton, T. K.; Yang, X. Methyl Formate Production on TiO_2(110), Initiated by Methanol Photocatalysis at 400 nm. *J. Phys. Chem. C* **2013**, *117*, 5293−5300.

https://dx.doi.org/10.1021/acscatal.0c00260
ACS Catal. 2020, 10, 4080−4091

(75) Yuan, Q.; Wu, Z.; Jin, Y.; Xu, L.; Xiong, F.; Ma, Y.; Huang, W. Photocatalytic Cross-Coupling of Methanol and Formaldehyde on a Rutile TiO_2(110) Surface. *J. Am. Chem. Soc.* **2013**, *135*, 5212−5219.
(76) Maity, P.; Mohammed, O. F.; Katsiev, K.; Idriss, H. Study of the Bulk Charge Carrier Dynamics in Anatase and Rutile TiO_2 Single Crystals by Femtosecond Time-Resolved Spectroscopy. *J. Phys. Chem. C* **2018**, *122*, 8925−8932.
(77) Bahnemann, D. W.; Hilgendorff, M.; Memming, R. Charge Carrier Dynamics at TiO_2 Particles: Reactivity of Free and Trapped Holes. *J. Phys. Chem. B* **1997**, *101*, 4265−4275.
(78) Chiarello, G. L.; Aguirre, M. H.; Selli, E. Hydrogen Production by Photocatalytic Steam Reforming of Methanol on Noble Metal-Modified TiO_2. *J. Catal.* **2010**, *273*, 182−190.
(79) Chiarello, G. L.; Ferri, D.; Selli, E. Effect of the CH_3OH/H_2O Ratio on the Mechanism of the Gas-Phase Photocatalytic Reforming of Methanol on Noble Metal-Modified TiO_2. *J. Catal.* **2011**, *280*, 168−177.
(80) Kominami, H.; Sugahara, H.; Hashimoto, K. Photocatalytic Selective Oxidation of Methanol to Methyl Formate in Gas Phase over Titanium(IV) Oxide in a Flow-type Reactor. *Catal. Commun.* **2010**, *11*, 426−429.
(81) Kim, K. S.; Barteau, M. A. Reactions of Methanol on TiO_2(001) Single Crystal Surfaces. *Surf. Sci.* **1989**, *223*, 13−32.
(82) Idriss, H.; Kim, K. S.; Barteau, M. A. Surface-Dependent Pathways for Formaldehyde Oxidation and Reduction on TiO_2(001). *Surf. Sci.* **1992**, *262*, 113−127.
(83) Setvin, M.; Shi, X.; Hulva, J.; Simschitz, T.; Parkinson, G. S.; Schmid, M.; Di Valentin, C.; Selloni, A.; Diebold, U. Methanol on Anatase TiO_2(101): Mechanistic Insights into Photocatalysis. *ACS Catal.* **2017**, *7*, 7081−7091.
(84) Setvin, M.; Hulva, J.; Wang, H.; Simschitz, T.; Schmid, M.; Parkinson, G. S.; Di Valentin, C.; Selloni, A.; Diebold, U. Formaldehyde Adsorption on the Anatase TiO_2(101) Surface: Experimental and Theoretical Investigation. *J. Phys. Chem. C* **2017**, *121*, 8914−8922.
(85) Xu, C.; Yang, W.; Guo, Q.; Dai, D.; Chen, M.; Yang, X. Molecular Hydrogen Formation from Photocatalysis of Methanol on Anatase-TiO_2(101). *J. Am. Chem. Soc.* **2014**, *136*, 602−605.
(86) Xiong, F.; Yu, Y.-Y.; Wu, Z.; Sun, G.; Ding, L.; Jin, Y.; Gong, X.-Q.; Huang, W. Methanol Conversion into Dimethyl Ether on the Anatase TiO_2(001) Surface. *Angew. Chem., Int. Ed.* **2016**, *55*, 623−628.
(87) Xiong, F.; Yin, L.-L.; Wang, Z.; Jin, Y.; Sun, G.; Gong, X.-Q.; Huang, W. Surface Reconstruction-Induced Site-Specific Charge Separation and Photocatalytic Reaction on Anatase TiO_2(001) Surface. *J. Phys. Chem. C* **2017**, *121*, 9991−9999.
(88) Bennett, D. A.; Cargnello, M.; Diroll, B. T.; Murray, C. B.; Vohs, J. M. Shape-Dependence of the Thermal and Photochemical Reactions of Methanol on Nanocrystalline Anatase TiO_2. *Surf. Sci.* **2016**, *654*, 1−7.
(89) Pepin, P. A.; Lee, J. D.; Foucher, A. C.; Murray, C. B.; Stach, E. A.; Vohs, J. M. The Influence of Surface Platinum Deposits on the Photocatalytic Activity of Anatase TiO_2 Nanocrystals. *J. Phys. Chem. C* **2019**, *123*, 10477−10486.
(90) Pepin, P. A.; Diroll, B. T.; Choi, H. J.; Murray, C. B.; Vohs, J. M. Thermal and Photochemical Reactions of Methanol, Acetaldehyde, and Acetic Acid on Brookite TiO_2 Nanorods. *J. Phys. Chem. C* **2017**, *121*, 11488−11498.
(91) Pepin, P. A.; Lee, J. D.; Murray, C. B.; Vohs, J. M. Thermal and Photocatalytic Reactions of Methanol and Acetaldehyde on Pt-Modified Brookite TiO_2 Nanorods. *ACS Catal.* **2018**, *8*, 11834−11846.
(92) Ohtani, B.; Prieto-Mahaney, O. O.; Li, D.; Abe, R. What is Degussa (Evonik) P25? Crystalline Composition Analysis, Reconstruction from Isolated Pure Particles and Photocatalytic Activity Test. *J. Photochem. Photobiol., A* **2010**, *216*, 179−182.
(93) Setvin, M.; Shi, X.; Hulva, J.; Simschitz, T.; Parkinson, G. S.; Schmid, M.; Di Valentin, C.; Selloni, A.; Diebold, U. Methanol on Anatase TiO2 (101): Mechanistic Insights into Photocatalysis. *ACS Catal.* **2017**, *7*, 7081−7091.
(94) Bae, D.; Seger, B.; Hansen, O.; Vesborg, P. C. K.; Chorkendorff, I. Durability Testing of Photoelectrochemical Hydrogen Production under Day/Night Light Cycled Conditions. *ChemElectroChem* **2019**, *6*, 106−109.
(95) Haselmann, G. M.; Eder, D. Early-Stage Deactivation of Platinum-Loaded TiO_2 Using in Situ Photodeposition During Photocatalytic Hydrogen Evolution. *ACS Catal.* **2017**, *7*, 4668−4675.
(96) Chung, Y.-H.; Han, K.; Lin, C.-Y.; O'Neill, D.; Mul, G.; Mei, B.; Yang, C.-M., Photocatalytic Hydrogen Production by Photo-Reforming of Methanol with One-Pot Synthesized Pt-Containing TiO_2 Photocatalysts. *Catal. Today* **2019**.
(97) Bliem, R.; van der Hoeven, J. E. S.; Hulva, J.; Pavelec, J.; Gamba, O.; de Jongh, P. E.; Schmid, M.; Blaha, P.; Diebold, U.; Parkinson, G. S. Dual Role of CO in the Stability of Subnano Pt Clusters at the Fe_3O_4(001) Surface. *Proc. Natl. Acad. Sci. U.S.A.* **2016**, *113*, 8921.
(98) Luna, A. L.; Dragoe, D.; Wang, K.; Beaunier, P.; Kowalska, E.; Ohtani, B.; Bahena Uribe, D.; Valenzuela, M. A.; Remita, H.; Colbeau-Justin, C. Photocatalytic Hydrogen Evolution Using Ni−Pd/TiO_2: Correlation of Light Absorption, Charge-Carrier Dynamics, and Quantum Efficiency. *J. Phys. Chem. C* **2017**, *121*, 14302−14311.
(99) Al-Mazroai, L. S.; Bowker, M.; Davies, P.; Dickinson, A.; Greaves, J.; James, D.; Millard, L. The Photocatalytic Reforming of Methanol. *Catal. Today* **2007**, *122*, 46−50.
(100) Reece, C.; Redekop, E. A.; Karakalos, S.; Friend, C. M.; Madix, R. J. Crossing the Great Divide Between Single-Crystal Reactivity and Actual Catalyst Selectivity with Pressure Transients. *Nat. Catal.* **2018**, *1*, 852−859.

https://dx.doi.org/10.1021/acscatal.0c00260
ACS Catal. 2020, 10, 4080−4091

Supporting Information for:
Surface Species in Photocatalytic Methanol Reforming on Pt/TiO_2(110): Learning from Surface Science Experiments for Catalytically Relevant Conditions

Constantin A. Walenta[¶], Carla Courtois[¶], Sebastian L. Kollmannsberger[¶], Moritz Eder[¶], Martin Tschurl[¶], Ueli Heiz[¶,*]

¶ Chair of Physical Chemistry & Catalysis Research Center, Technical University of Munich, Lichtenbergstr. 4, 85748 Garching, Germany

*Corresponding Author: ulrich.heiz@mytum.de

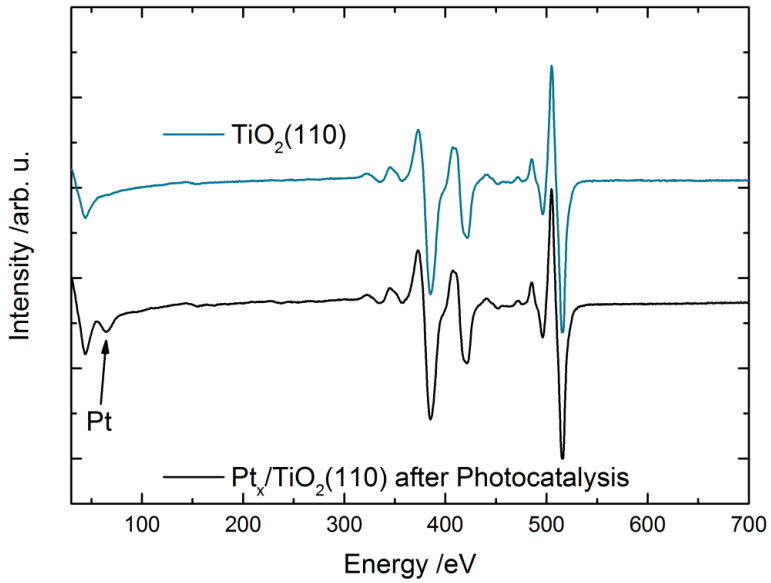

Fig. S1: Auger electron spectrum of the freshly prepared TiO_2(110) semiconductor (blue) and the Pt_x/TiO_2(110) catalyst (black) after photocatalytic experiments for 2 h and 15 min of additional illumination at the reaction temperature without reactant atmosphere. Within the detection limit, no significant carbon containing species (expected at 272 eV) are detected on the surface. Platinum is detected around 64 eV, while the characteristic peaks for titanium and oxygen are located between 350 and 525 eV.

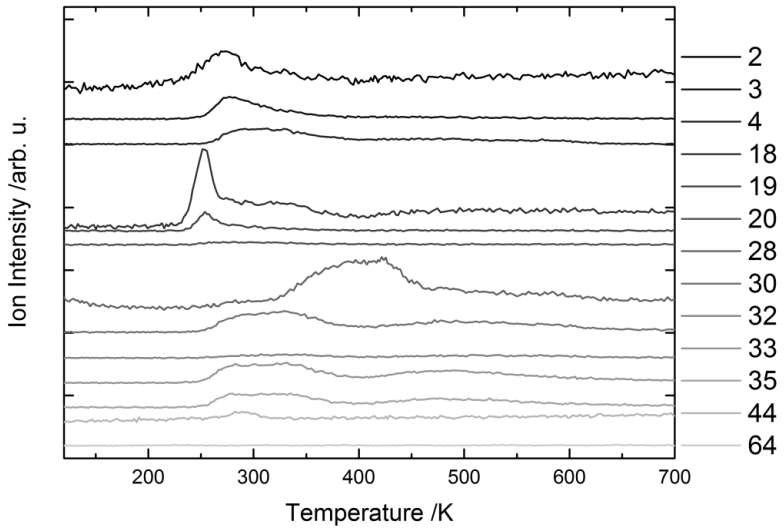

Fig S2: Temperature-programmed desorption of 1 L of methanol-d_3 on Pt_x/TiO_2(110). The traces represent raw data and are not corrected. The observations are in excellent agreement in all mass traces with the work of Hao *et al.*[1], with the exception of the absence of hydrogen at higher temperatures. We relate this difference in the desorption of H_2 to the co-catalyst due to different cluster loadings, cluster size and treatment procedure, further supporting the role of the platinum clusters as recombination sites for H_2.[2-3] In both works, potential molecules such as methyl formate-d_6 (mass 64), methane-d_3 (mass 19) and methane-d_4 (mass 20) are not observed. Mass 35 (methanol-d_3) and mass 32 (formaldehyde-d_2) follow the trend observed in Fig. 3, corroborated by the joint mass fragment 30 of methanol-d_3 and formaldehyde-d_2. Mass 18 is mainly attributed to water as an impurity in the methanol source and mass 19 is attributed to the scrambling products, since methanol decomposition already sets in below the observed temperature of 275 K, evident by the hydrogen signals (2, 3 and 4).

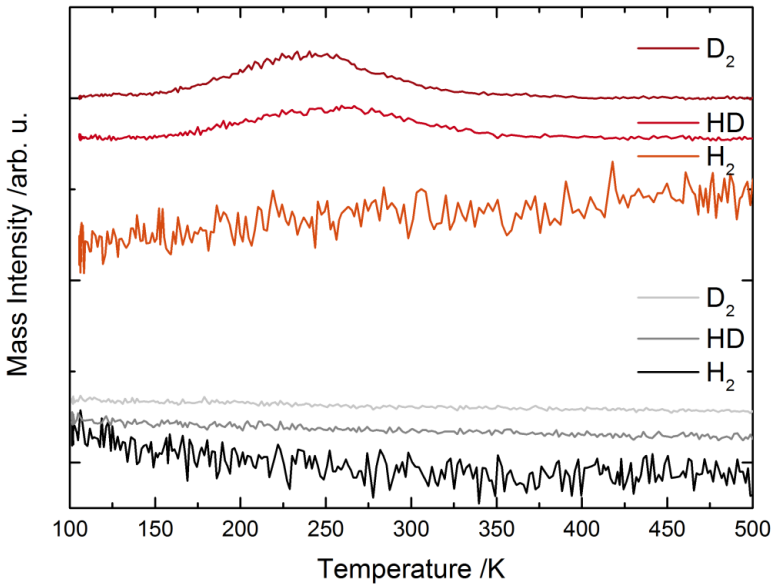

Fig. S3: Temperature programmed desorption of 1 L of D_2 on the TiO_2(110) surface (grey traces) and the Pt_x/TiO_2(110) photocatalyst (red traces). On bare TiO_2(110), Deuterium does not adsorb on the surface at 100 K in agreement with literature.[4-5] On the Pt cluster-loaded TiO_2(110), Deuterium does adsorb on the Pt clusters and desorbs in a broad feature around 240 K. A similar peak is observed for the HD trace, indicating some HD scrambling in agreement with literature.[6-7]

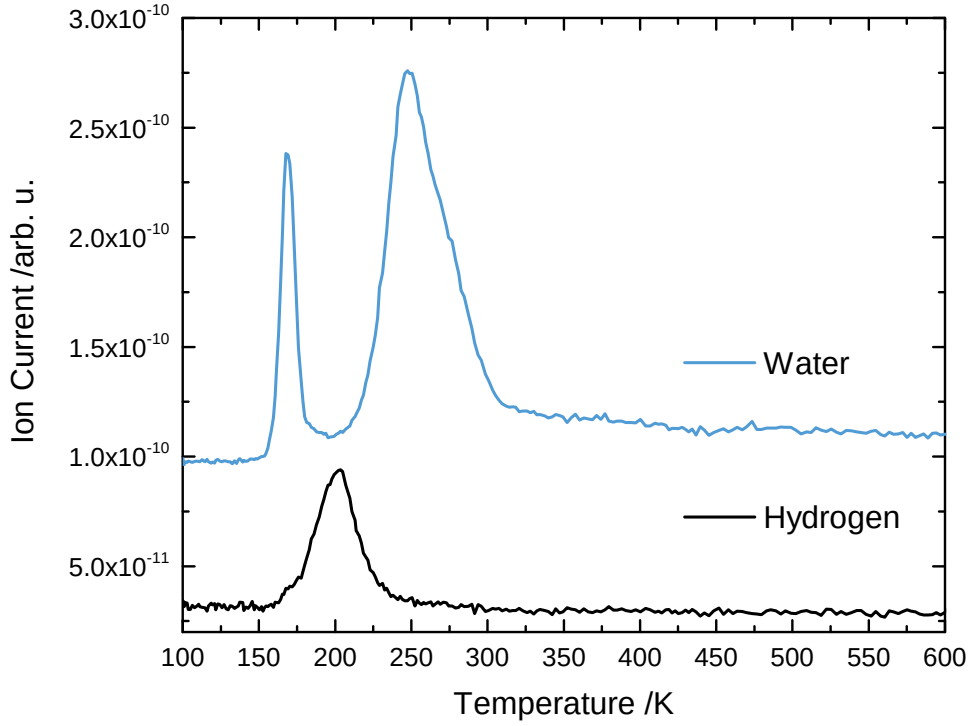

Fig. S4: Temperature programmed desorption measurement of 1.31 ML of H_2O adsorbed at 100 K on $Pt_x/TiO_2(110)$. Water from the O-lattice sites desorbs around 160 K, while H_2O from the Ti-lattice sites desorbs around 255 K. Hydrogen desorbs between 180 K and 250 K in a peak centered around 210 K in very good agreement with a previous report.[3]

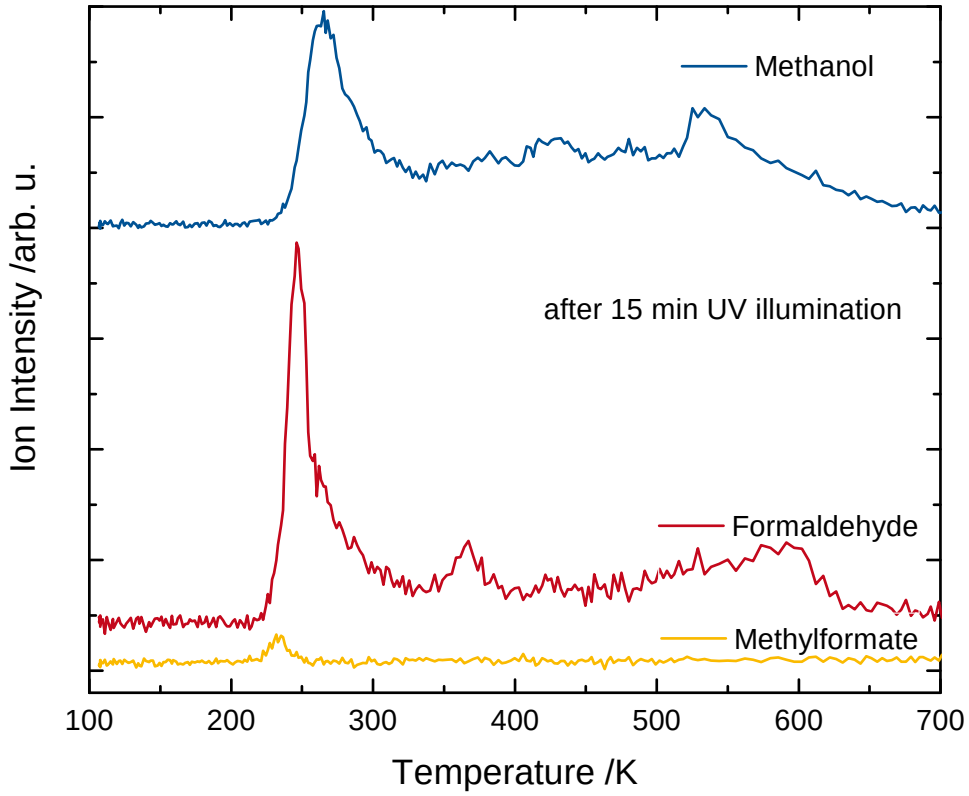

Fig. S5: Post-Irradiation TPD of 1 L of CD_3OH on r-TiO_2(110) after 15 min of UV illumination at 110 K. Note, that methanol is oxidized to formaldehyde and in a second photo-oxidation to methyl formate, in excellent agreement with a previous report.[8] Methanol is identified by mass 35, formaldehyde by mass 30 and methyl formate by mass 64. All traces are corrected for the fragmentation patterns.[8-10]

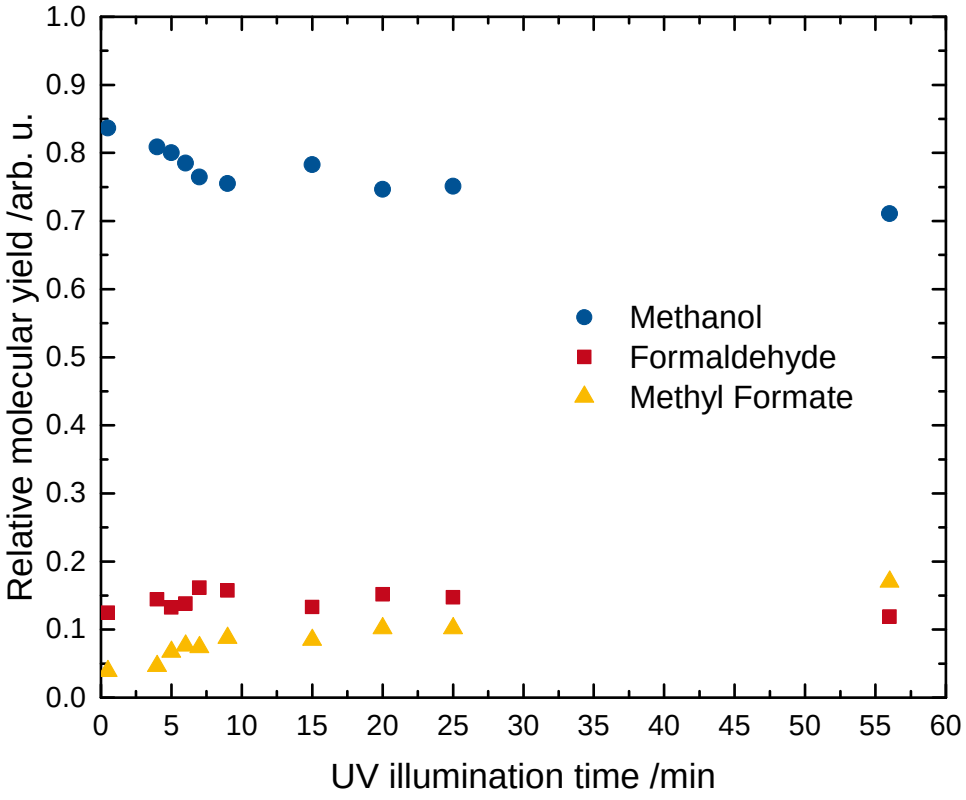

Fig. S6: Product evolution of the PI-TPDs with varied illumination time at 110 K. Methanol is adsorbed on the bare r-TiO_2(110) surface and illuminated for a certain time period with UV light. PI-TPD is used to quantify the photoreaction products. Formaldehyde forms even at the shortest illumination times, while the consecutive photocoupling reaction becomes more dominant at larger illumination times in very good agreement with literature.[8] Note, that not all methanol can be converted in these experiments, indicating a poisoning of the reaction at cryogenic temperatures.

The surface lifetime of a species can the estimated from an evaluation of the rate of desorption from a surface. The rate of desorption is given by:

$$-\frac{d\theta}{dt} = \nu_d \times f(\theta) \times exp^{-\frac{\Delta H}{RT}} \qquad \text{(Eq. S1)}$$

While the exponential term (with the desorption energy ΔH) together with pre-exponential factor ν_d reflects the temperature-dependent rate constant, $f(\theta)$ considers the concentration-dependence of the rate. Assuming a first desorption process and that the desorption is coverage-independent, one can rewrite the formula to:

$$-\frac{d\theta}{dt} = \nu_d \times \theta \times exp^{-\frac{\Delta H}{RT}} \qquad \text{(Eq. S2)}$$

$$-\int_{\theta_i}^{\theta_f} \frac{d\theta}{\theta} = \int_0^{t_f} \nu_d \times exp^{-\frac{\Delta H}{RT}} dt \qquad \text{(Eq. S3)}$$

$$t = \ln\left(\frac{\theta_i}{\theta_f}\right) \times \frac{1}{\nu_d \times exp^{-\frac{\Delta H}{RT}}} \qquad \text{(Eq. S4)}$$

Using the $\left(\theta_f / \theta_i\right)$ = 2 by definition, the surface lifetime is then given by:

$$t_{1/2} = \frac{\ln(2)}{\nu_d \times e^{\frac{-\Delta H}{RT}}} \qquad \text{(Eq. S5)}$$

The pre-exponential factors are determined by a method established by Campbell *et al*. and can be obtained from the gas-phase entropies of the molecules.[11-12] These pre-exponential factors can be used in a Redhead formalism[13] to calculate and apparent desorption enthalpy. All of these values are given in Table S1 and set the foundation to calculate the surface residence time at a given temperature.

Table S1: Tabulated values for the gas phase entropy and the resulting pre-exponential factors as well as the activation barriers.

Molecule	Gasphase Entropy S_0[J/mol × K]	Reference	Pre-exponential Factor ν_d [s^{-1}]	Desorption Enthalpy ΔH [kJ/mol]
Methanol	236.12	14	3.8771E+15	82.9786
Formaldehyde	219.00	15	2.2297E+15	75.4629
Methyl Formate	282.31	15	1.1253E+16	75.3847

References

1. Hao, Q.; Zhiqiang, W.; Wang, T.; Ren, Z.; Zhou, C.; Yang, X., Role of Pt Loading in the Photocatalytic Chemistry of Methanol on Rutile TiO_2(110). *ACS Catal.* **2019,** *9*, 286-294.
2. Walenta, C. A.; Kollmannsberger, S. L.; Courtois, C.; Pereira, R. N.; Stutzmann, M.; Tschurl, M.; Heiz, U., Why Co-Catalyst-loaded Rutile Facilitates Photocatalytic Hydrogen Evolution. *Phys. Chem. Chem. Phys.* **2019,** *21*, 1491-1496.
3. Geng, Z.; Jin, X.; Wang, R.; Chen, X.; Guo, Q.; Ma, Z.; Dai, D.; Fan, H.; Yang, X., Low-Temperature Hydrogen Production via Water Conversion on Pt/TiO_2. *J. Phys. Chem. C* **2018,** *122*, 10956-10962.
4. Chen, L.; Li, Z.; Smith, R. S.; Kay, B. D.; Dohnálek, Z., Molecular Hydrogen Formation from Proximal Glycol Pairs on TiO_2(110). *J. Am. Chem. Soc.* **2014,** *136*, 5559-5562.
5. Zhang, Z.; Yates, J. T., A New Form of Chemisorbed Photo- and Electro-Active Atomic H Species on the TiO_2(110) surface. *Surf. Sci.* **2016,** *652*, 195-199.
6. Riedel, J. N.; Rötzer, M. D.; Jørgensen, M.; Vej-Hansen, U. G.; Pedersen, T.; Sebok, B.; Schweinberger, F. F.; Vesborg, P. C. K.; Hansen, O.; Schiøtz, J.; Heiz, U.; Chorkendorff, I., H2/D2 Exchange Reaction on Mono-Disperse Pt Clusters: Enhanced Activity from Minute O_2 Concentrations. *Catal. Sci. Technol.* **2016,** *6*, 6893-6900.
7. Joo, J. B.; Dillon, R.; Lee, I.; Yin, Y.; Bardeen, C. J.; Zaera, F., Promotion of Atomic Hydrogen Recombination as an Alternative to Electron Trapping for the Role of Metals in the Photocatalytic Production of H_2O. *Proc. Natl. Acad. Sci.* **2014,** *111*, 7942.
8. Guo, Q.; Xu, C.; Yang, W.; Ren, Z.; Ma, Z.; Dai, D.; Minton, T. K.; Yang, X., Methyl Formate Production on TiO_2(110), Initiated by Methanol Photocatalysis at 400 nm. *J. Phys. Chem. C* **2013,** *117*, 5293-5300.
9. Phillips, K. R.; Jensen, S. C.; Baron, M.; Li, S.-C.; Friend, C. M., Sequential Photo-Oxidation of Methanol to Methyl Formate on TiO_2(110). *J. Am. Chem. Soc.* **2013,** *135*, 574-577.
10. Yuan, Q.; Wu, Z.; Jin, Y.; Xu, L.; Xiong, F.; Ma, Y.; Huang, W., Photocatalytic Cross-Coupling of Methanol and Formaldehyde on a Rutile TiO_2(110) Surface. *J. Am. Chem. Soc.* **2013,** *135*, 5212-5219.
11. Campbell, C. T.; Sellers, J. R. V., The Entropies of Adsorbed Molecules. *J. Am. Chem. Soc.* **2012,** *134*, 18109-18115.
12. Campbell Charles, T.; Árnadóttir, L.; Sellers Jason, R. V., Kinetic Prefactors of Reactions on Solid Surfaces. In *Z. Phys. Chem.*, 2013, 227, p 1435.
13. Redhead, P. A., Thermal Desorption of Gases. *Vacuum* **1962,** *12*, 203-211.
14. Chao, J.; Hall, K. R.; Marsh, K. N.; Wilhoit, R. C., Thermodynamic Properties of Key Organic Oxygen Compounds in the Carbon Range C1 to C4. Part 2. Ideal Gas Properties. *J. Phys. Chem. Ref. Data* **1986,** *15*, 1369-1436.
15. NIST Chemistry WebBook, NIST Standard Reference Database Number 69. Mallard, P. J. L. a. W. G., Ed. National Institute of Standards and Technology, Gaithersburg MD, 20899. (accessed retrieved June 5, 2018).

A.5 Thermal Control of Selectivity in Photocatalytic, Water-Free Alcohol Photoreforming

ACS Catalysis
Research Article
Cite This: ACS Catal. 2018, 8, 11076−11084
pubs.acs.org/acscatalysis

Thermal Control of Selectivity in Photocatalytic, Water-Free Alcohol Photoreforming

Sebastian L. Kollmannsberger,[†,§] Constantin A. Walenta,[†,‡,§] Carla Courtois,[†] Martin Tschurl,[†] and Ueli Heiz*[,†,‡]

[†]Chair of Physical Chemistry, Department of Chemistry & Catalysis Research Center, Technische Universität München, Lichtenbergstraße 4, 85748 Garching, Germany

[‡]Nanosystems Initiative Munich, Schellingstraße 4, 80799 München, Germany

Supporting Information

ABSTRACT: The selective oxidation of alcohols has attracted a great deal of attention. While most photocatalytic studies focus on the generation of hydrogen from alcohols, there is also a great potential to replace inefficient thermal reaction pathways (as e.g. the formox process) by light-driven reactions. In this work we focus on the photoreforming of methanol, ethanol, cyclohexanol, benzyl alcohol, and *tert*-butanol on well-defined $Pt_x/TiO_2(110)$ under UHV. It is found that, with the exception of *tert*-butanol, alcohol oxidation can produce the respective water-free aldehydes and ketones along with the formation of stoichiometric molecular hydrogen with 100% selectivity. While α-H-containing alcohols usually exhibit only a disproportionation reaction with the release of H_2, another reaction pathway is detected for methanol (and to a much lower extent benzyl alcohol) to yield the respective ester, methyl formate (or benzyl benzoate, respectively). The formation of this product occurs via a consecutive photoreaction and is strongly influenced by temperature. In general, higher temperatures lead to a higher selectivity toward formaldehyde, as product desorption is favored over the consecutive photoreaction. For *tert*-butanol two parallel photoreactions occur. In addition to the splitting of a C−C bond yielding a methyl radical, hydrogen, and acetone, dehydration to isobutene is observed. The branching ratios of both reaction pathways can be strongly controlled by temperature, by changing the reaction regime from adsorption to desorption limited. The high selectivities toward aldehydes are attributed to the absence of O_2 and water, which inhibits an unwanted overoxidation to acids or CO/CO_2. This study shows that photocatalysis under such conditions provides a prospective approach for a highly selective and water-free aldehyde production under mild conditions.

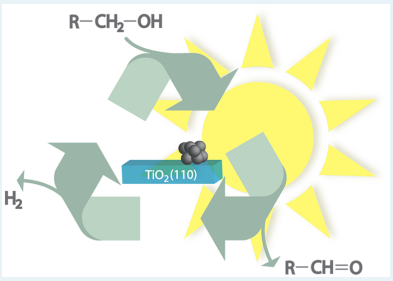

KEYWORDS: *titania, alcohol oxidation, photocatalysis, selectivity, photoreforming, hydrogen production*

INTRODUCTION

Selective oxidation of alcohols has attracted extensive attention in the past decade.[1−3] In this regard tuning the selectivity of photocatalytic reactions has been the focus of current research.[4,5] A key step to high selectivities is a fundamental understanding of photocatalytic mechanisms. Therefore, studies on perfectly defined semiconductor single crystals are of utmost importance. Not only do titania-based systems represent the most heavily used semiconductors in photocatalytic applications but also TiO_2 (110) is a readily available, heavily studied single-crystalline material. Therefore, it represents an ideal material to elucidate fundamental mechanisms in photocatalysis. Similarly, Pt is a very prominent and often used cocatalyst for photocatalytic hydrogen evolution.[6] In alcohol reforming, the photocatalytic synthesis of highly industrial relevant products such as benzaldehyde, formaldehyde, and cyclohexanone is particularly attractive. Benzaldehyde is among the most important molecules in the cosmetics and flavor industries.[7] Formaldehyde is, in addition to its application as a building block chemical, also needed as a precursor for potential ultralow-emission fuels.[8] In particular, the formation of water-free formaldehyde as an alternative to the commonly used formox process, which requires a complex procedure to be freed from water and other impurities, is of great interest.[9] Cyclohexanone is a precursor molecule for the production of nylon-6 and is industrially synthesized by either a high-temperature and high-pressure oxidation of cyclohexane or a two-step process starting from phenol.[10] Consequently, the development of a one-step photoprocess may receive great attention. Ethanol oxidation is highly relevant, as it is easily available in large amounts from biomass conversion. Its photooxidation to produce solar hydrogen from bio-ethanol is environmentally benign.[11]

Received: August 30, 2018
Revised: October 10, 2018
Published: October 17, 2018

DOI: 10.1021/acscatal.8b03479
ACS Catal. 2018, 8, 11076−11084

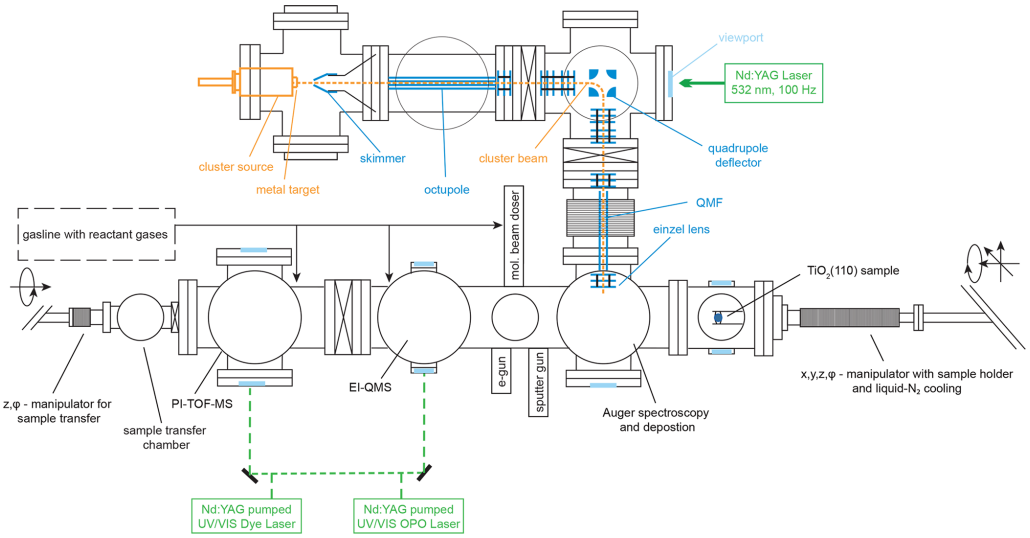

Figure 1. Chamber scheme of the UHV apparatus including the laser vaporization cluster source and the laser system.

As it is generally known that photo-oxidation of primary and secondary alcohols proceeds via abstraction of the α-H,[12−15] the investigation of a tertiary alcohol such as *tert*-butanol is therefore mechanistically interesting, because the conventional pathway is not feasible. Therefore, we have chosen four alcohols, whose conversions are industrially relevant, and the mechanistically interesting *tert*-butanol for photocatalytic reforming.

The vast majority of studies concerning alcohol photoreforming address the evolution of hydrogen, and less focus has been placed on the oxidation products; this is also the case for rather defined systems.[16] When the selectivity of the reaction is considered, it is usually observed that photocatalysis of alcohol with cocatalyst-loaded TiO_2 leads to several different oxidation products, even to CO and CO_2 (examples are shown in a microreview by Cargnello et al.[17]). However, in the quantitative analysis of photoreaction products in an aqueous solutions of methanol, it was found that, under shorter illumination times (15 min in comparison to 3 h), high selectivities toward formaldehyde could be achieved.[18] For gas-phase reactions, Selli and co-workers have performed several studies. For methanol, they found varying selectivities for different mole fractions of alcohol and water. One result from these studies was that water serves as an oxygen donor for the oxidation of formaldehyde.[19] Consequently, the highest selectivity was achieved for pure methanol, but only a value of 60% with respect to the H_2 yield was found.[20] While for all of these studies principal mechanisms have been formulated to explain the observed reaction behavior, detailed insights into the parameters governing the selectivity are still missing and have fostered research activities in this field.[21] In this regard surface science studies may be helpful, because they enable investigations of highly defined materials under highly defined conditions.

While alcohol oxidations have been explored in great depth on bare TiO_2(110) single-crystal surfaces in single-coverage experiments,[14,15,22−32] investigations with cocatalyst-loaded semiconductors under catalytic conditions are scarce. However, such studies enable unique insights into mechanistic details. In the following we demonstrate the determination of stoichiometric mechanisms for the photo-oxidation of alcohols, photo-oxidative coupling reactions, the formation of hydrogen, and temperature-induced selectivity changes.

EXPERIMENTAL SECTION

The experimental setup for photocatalytic measurements, which is shown schematically in Figure 1, consists of a UHV chamber with a background pressure better than 9.8×10^{-11} mbar and a laser vaporization cluster source for the deposition of size-selected metal clusters. The main chamber includes a manipulator (VAB Vakuum GmbH), a surface preparation and surface analysis part, a reaction part with an electron ionization quadrupole mass spectrometer (EI-QMS) (QMA 430, Pfeiffer Vacuum GmbH), and a home-built photoionization time-of-flight mass spectrometer (PI-TOF-MS), which enables the selective ionization of isobaric molecules.[33] Furthermore, a sample transfer chamber and a gas line with reactant gases, which contains a leak valve and a molecular beam doser, are attached to the chamber.

The sample holder, which is described in detail elsewhere,[14] enables liquid nitrogen cooling and heating. The laser system consists of a Nd:YAG pumped dye laser and a Nd:YAG pumped UV/vis OPO laser. The photoexcitation of the semiconductor is carried out with a wavelength of 242 nm, obtained by the frequency-doubled OPO laser (GWU, premiScan ULD/400), which is pumped by the third harmonic of a Nd:YAG laser (Innolas Spitlight HighPower 1200, 7 ns pulse width, 20 Hz repitition rate). If not otherwise noted, illumination intensities in the saturation regime of 4.5 ± 0.7 mW are applied.

The rutile TiO_2(110) single crystal (SurfaceNet GmbH) was prepared by cycles of Ar^+ sputtering (1.5 keV, 1×10^{-5}

DOI: 10.1021/acscatal.8b03479
ACS Catal. 2018, 8, 11076−11084

mbar, 30 min), oxygen annealing (800 K, 1×10^{-6} mbar, 20 min), and vacuum annealing (800 K, 10 min) until no contamination was detected by Auger electron spectroscopy (AES). The resulting TiO_2(110) is light blue with a bridge-bonded oxygen (BBO) vacancy concentration, determined with H_2O TPD, of 6 ± 1% of Ti lattice sites.[34]

The laser vaporization cluster source was operated by a Nd:YAG laser (532 nm, 100 Hz, Innolas), which ablated a Pt target (99.95% purity, ESG Edelmetalle, Germany). The resulting plasma was cooled by a He pulse and expanded into the vacuum. The resulting cationic clusters were guided and bent into a quadrupole mass filter (QMF) (Extrel, USA) to enable cluster size selection.[35] With these settings a size distribution from Pt_7 to Pt_{35} with a maximum from Pt_{11} to Pt_{13} (see Figure S1 in the Supporting Information) resulted. In this work, the QMF was operated with ac potential only during deposition and acted as an ion guide, discarding all masses lower than Pt_8. The deposition of 1% ML Pt (respective to the surface atoms) onto the TiO_2(110) single crystal occurred under soft-landing conditions (<1 eV/atom in kinetic energy), as checked with retarding field analysis. The cluster loadings were determined by recording the cluster current during deposition with a picoammeter (Keithley, 6587). The samples are named Pt_x/TiO_2(110) in the following. With this type of cluster deposition, several studies by different groups using different characterization methods revealed that highly defined samples are obtained regarding cluster size and coverage.[36−38]

Methanol (Chromasolv, ≥99.9%, Sigma-Aldrich), ethanol (absolute, HPLC grade, ≥99.8%, Sigma-Aldrich), cyclohexanol (99%, Sigma-Aldrich), *tert*-butanol (2-methyl-2-propanol, ≥99.5%, Sigma-Aldrich), and benzyl alcohol (99.8%, Sigma-Aldrich) were degasified by several freeze−pump−thaw cycles prior to their insertion via a leak valve into the UHV chamber.

RESULTS

In order to study the process of alcohols in photoreforming, UV illumination experiments have been carried out under alcohol background pressure.

Figure 2 shows the QMS traces of methanol, hydrogen, formaldehyde and methyl formate during laser irradiation of the Pt_x/TiO_2(110) at 262 K under a methanol background pressure of 7×10^{-8} mbar. On the one hand, the intensity of the methanol fragment drops drastically with the start of the illumination and goes back to the initial value when the illumination is stopped. On the other hand, the irradiation leads to an immediate increase in molecular hydrogen, formaldehyde, and methyl formate. After about 10 s a steady state in the formation of formaldehyde and all other molecules is reached, which is then constant over the whole illumination time. From a baseline-corrected integral of the constant region of formation, a turnover frequency (TOF) is determined. The QMS is calibrated for methanol to obtain quantitative values from the ion currents. In this quantitative analysis of the respective molecule, its fragmentation pattern, its electron impact ionization cross sections (see Table S1 in the Supporting Information), and the m/z-dependent transmission through the QMS are considered. Moreover, for the determination of TOFs the amount of active sites is attributed to the number of BBO vacancies. The TOFs of the other alcohols are determined in identical experiments with the same procedure of quantification.

In Figure 3 the pressure-dependent TOFs of five different alcohols are depicted in the range from 1×10^{-8} to 1×10^{-7}

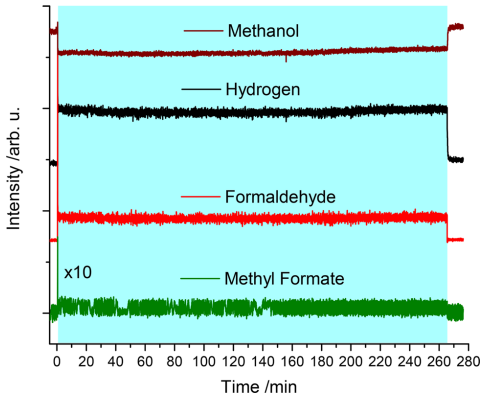

Figure 2. Methanol (m/z 32), hydrogen (m/z 2), formaldehyde (m/z 30), and methyl formate (m/z 60) signals at 262 K under a methanol background pressure of 7×10^{-8} mbar. The blue region highlights the period of laser irradiation. Note that the methyl formate signal is multiplied by a factor of 10 for better visibility.

mbar. Higher pressures were not studied to ensure that ion−molecule reactions after electron impact ionization in the QMS do not deteriorate a quantitative determination of the products. From all α-H-containing alcohols, the respective aldehyde or ketone and H_2, corresponding to the stoichiometry of the reaction, are observed. With higher reactant pressure the TOFs rise linearly, with the exception of methanol, for which a flattening may be observed. Furthermore, other byproducts are not detected at the investigated temperatures for all α-H-containing alcohols. This is again different for methanol, for which photoreforming leads to the formation of methyl formate. The TOF of this reaction shows a saturation behavior, starting at a pressure of 5×10^{-8} mbar (see Figure S2 in the Supporting Information for an enlargement of methyl formate TOF). A comparison of both carbon-based products (i.e., methyl formate and formaldehyde) as a function of laser power reveals that a further photon is needed for the reaction to methyl formate (see Figure S3 in the Supporting Information). For ethanol other reaction pathways can be ruled out, as different mass fragments (see Figure S4 in the Supporting Information) do not exhibit any change in signal during illumination after cracking pattern correction. Similarly, also for cyclohexanol and benzyl alcohol a selectivity of 100% toward the ketone and the aldehyde occurs.

An exception to those α-H-containing alcohols is *tert*-butanol, for which the standard oxidation pathway is excluded. Therefore, only 1/2 H_2 is obtained from the oxidation of one *tert*-butanol to acetone, accompanied by stoichiometric methyl radical ejection. Furthermore, an additional side reaction forming isobutene and water is observed. The photoreforming of each alcohol is stoichiometric in long-term experiments (≥200 min) and exhibits no changes in the TOFs.

For all alcohols the reaction has been investigated for their temperature dependence under isobaric conditions. Figure 4 shows the product distribution for methanol and ethanol oxidation as a function of temperature but otherwise constant conditions. For methanol photoreforming about the same amounts of formaldehyde and methyl formate are produced at 235 K (Figure 4a). However, the selectivity of the reaction

DOI: 10.1021/acscatal.8b03479
ACS Catal. 2018, 8, 11076−11084

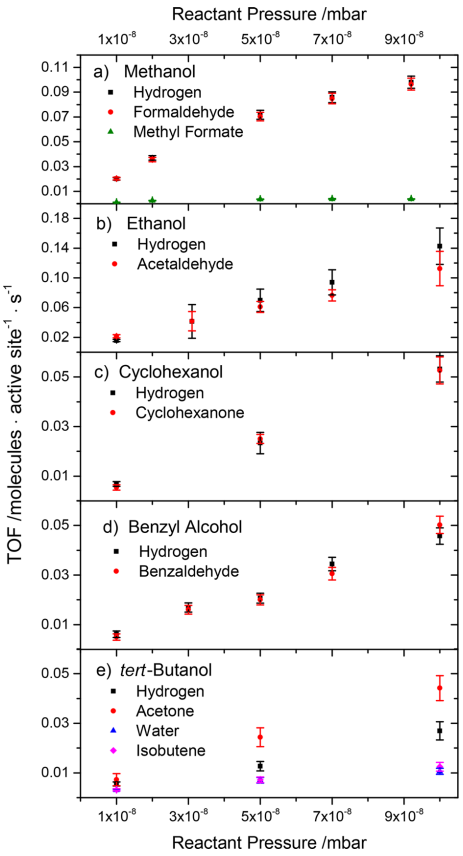

Figure 3. Pressure-dependent TOFs for photocatalytic reforming of (a) methanol, (b) ethanol, (c) cyclohexanol, (d) benzyl alcohol and (e) *tert*-butanol. The temperature is 260 K in (a), 280 K in (b), (c), and (e), and 300 K in (d). The temperatures have been chosen in order to be above the desorption temperature of the aldehyde (or ketone) and below that of alcohol desorption. In general the TOFs rise linearly in the investigated pressure range and a saturation behavior is not observed. Note that products other than those displayed are not observed.

changes drastically with higher temperatures. The TOF of methyl formate drops to zero at around 260 K, while that of formaldehyde remains high. More precisely this means that a temperature-dependent selectivity toward $A_{\text{formaldehyde}}$, defined as $S_{\text{formaldehyde}} = \frac{A_{\text{formaldehyde}}}{A_{\text{total product}}}$, is obtained from 56% at 235 K and 100% at 273 K. While the reaction becomes more selective, the conversion of methanol decreases at temperatures higher than 250 K.

For the conversion of ethanol it can be seen that no byproducts are observed over the whole investigated temperature range (Figure 4b). As a result a 100% selectivity to acetaldehyde is always achieved. Furthermore, a change in the TOF is only visible at temperatures lower than 200 K (see Figure S5 in the Supporting Information), while it stays constant at elevated values. The differences in the TOFs of formaldehyde and acetaldehyde of about a factor of 10 are only related to different background pressures of the respective reactant, which were chosen to completely rule out a consecutive photoreaction for ethanol.

Figure 5a shows the cyclohexanone TOFs in the range from 240 to 300 K and Figure 5b the benzaldehyde TOFs in the range from 210 to 340 K. An increase in the turnover is observed for both alcohols in the lower temperature region up to ~260 K. In the region above this temperature the investigated TOFs remain almost constant. Furthermore, a 100% selectivity to cyclohexanone and nearly a 100% selectivity to benzaldehyde during the respective photoreforming is found. For the latter molecule, a minor byproduct is detected at a m/z 92 fragment (see Figure S6a in the Supporting Information), which can be attributed to benzyl benzoate. Its very low signal to noise intensity excludes a reliable product quantification. Therefore, only a qualitative evaluation is shown in Figure S6b in the Supporting Information.

The temperature dependence of the TOFs in the photoreforming of *tert*-butanol shows a complex behavior. On the one hand, an increase in the TOFs of acetone, methyl radical, and H_2 is observed with increasing temperatures from 230 to 305 K (blue region in Figure 6). Afterward, the turnover of those products is constant or decreases slightly (ocher region). On the other hand, the TOFs of isobutene and H_2O show a slow decrease over the entire temperature range. Consequently, the selectivity to acetone is increasing strongly from 66% at 234 K to 96% at 306 K (blue region) and increases only very weakly in the ocher part.

DISCUSSION

Oxidation Reaction. Photocatalytic alcohol reforming on $Pt_x/TiO_2(110)$ produces water-free aldehyde or ketone of the respective alcohol and stoichiometrically molecular hydrogen. The first step is the thermal reaction by dissociative adsorption, resulting formally in the formation of an alkoxy group and a hydrogen atom.[39] The following photo-oxidation of the alkoxy species proceeds via a hole-mediated α-H abstraction.[22,25,40] The resulting aldehyde or ketone desorbs thermally at a sufficiently high temperature. The remaining two hydrogen atoms diffuse on the $TiO_2(110)$ surface, recombine at a Pt cluster, and finally desorb.[41] All of these processes are thermally driven, with the exception of the α-H abstraction. The reaction equations are shown for the general alcohol oxidation (eq 1), hydrogen recombination (eq 2) and the total reaction (eq 3).

$$R_1R_2CHOH(g) \rightarrow R_1R_2CHO_{ad}/TiO_2 + H(ad)/TiO_2 \xrightarrow{h\nu} R_1R_2CO\uparrow + H(ad)/TiO_2 \quad (1)$$

$$2H(ad)/TiO_2 \xrightarrow{\text{diff}} 2H(ad)/Pt \rightarrow H_2\uparrow \quad (2)$$

and the total reaction:

$$R_1R_2CHOH(g) \xrightarrow[Pt@TiO_2]{h\nu} R_1R_2CO\uparrow + H_2\uparrow \quad (3)$$

This mechanism is used for the interpretation of all α-H-containing alcohols. From the determined TOFs it can be seen, that a stoichiometric aldehyde (or ketone) to hydrogen ratio is observed.

DOI: 10.1021/acscatal.8b03479
ACS Catal. 2018, 8, 11076−11084

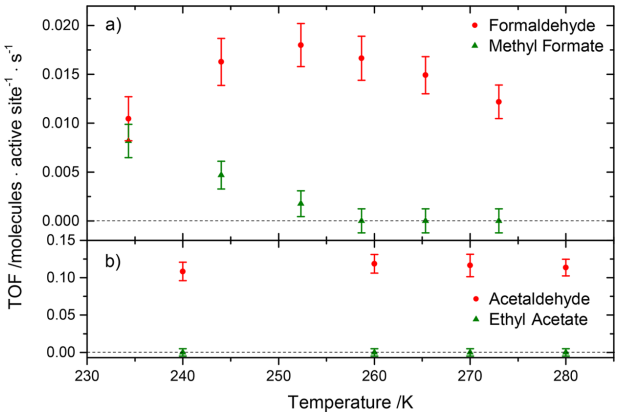

Figure 4. Temperature-dependent TOFs for (a) methanol (1×10^{-8} mbar) and (b) ethanol (1×10^{-7} mbar) photoreforming. Methanol (a) shows a temperature-induced selectivity change from formaldehyde to methyl formate. However, ethanol (b) does not exhibit a reaction to ethyl acetate and the TOFs are temperature independent in the investigated temperature range from 240 to 280 K.

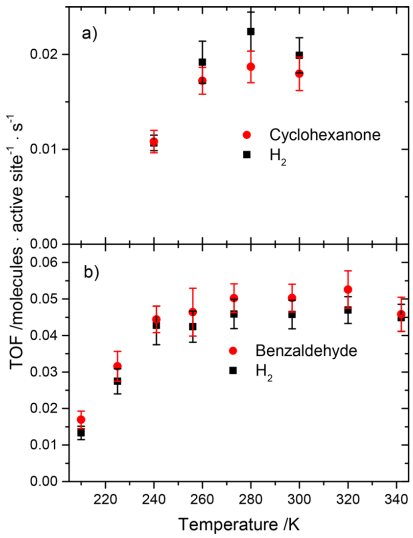

Figure 5. Temperature-dependent TOFs for (a) cyclohexanol (1×10^{-8} mbar) and (b) benzyl alcohol (5×10^{-8} mbar) photoreforming. Secondary products are not observed from cyclohexanol and benzyl alcohol reforming. The TOFs in (a) and (b) increase with temperature and saturate at around 260 K.

Pressure Dependence. In the investigated pressure range a linear increase in the TOFs is visible for all investigated alcohols. Only for methanol may a flattening of the curve occur at the maximum TOF. From the linear increase, an adsorption limitation of the reaction can be concluded.[42] Consequently, the alcohol photoreforming is a first-order reaction with the reactant pressure in the investigated pressure range. A saturation of the reactive surface sites with reactant is not obtained.

In order to compare the rates of the different alcohol photoreforming reactions, the reaction rate k, normalized to the pressure of the alcohol, is determined (see Table 1). For *tert*-butanol the sum of acetone and isobutene TOFs reflect the overall rate for *tert*-butanol conversion. As the formation of methyl formate does not change the methanol conversion significantly at the investigated temperature, it is omitted for the determination of the reaction rate constant. Although the temperature is the lowest for formaldehyde production, the largest rate constant is obtained. In general, a decrease in the rate constant with the steric demand of the alcohol is visible. This can be ascribed to a steric hindrance of the active site required geometry, which is in good accordance with the adsorption limitation of the reaction rate.

Temperature Dependence. At the applied alcohol pressure, the TOF increases for all investigated alcohols in the low-temperature regime. After this regime, the TOFs stay constant or slightly decrease at higher temperatures. This behavior can by explained by the following: an increase in the TOF with temperature results from increasing product formation due to a faster product desorption. As soon as the curve flattens, not enough substrate is available at the surface in order to enable a further increase in the TOF. This adsorption limitation can be counteracted with higher substrate pressures. The increased availability of reactant thus results in a later flattening of the curve.[43] The activation energies, which can be obtained from the slope of the linear region in an Arrhenius plot are very low (<20 kJ/mol) (see SI Figure S7 and Table S2 in the Supporting Information). This is expected for photocatalytic reactions[44] and is strong evidence for a limitation by product desorption. Furthermore, the observed adsorption limitation at higher temperatures is in very good accordance with the determined pressure-dependent behavior.

Oxidative Coupling Reaction. A further reaction pathway is found for methanol, for which a coupling to methyl formate occurs. This consecutive oxidation reaction is the only additionally observed pathway for methanol photoreforming. The formation of this coupling product is in good agreement with non-steady-state photocatalytic studies on bare TiO_2(110),.[25,28,30] However, the exact coupling mechanism

DOI: 10.1021/acscatal.8b03479
ACS Catal. 2018, 8, 11076−11084

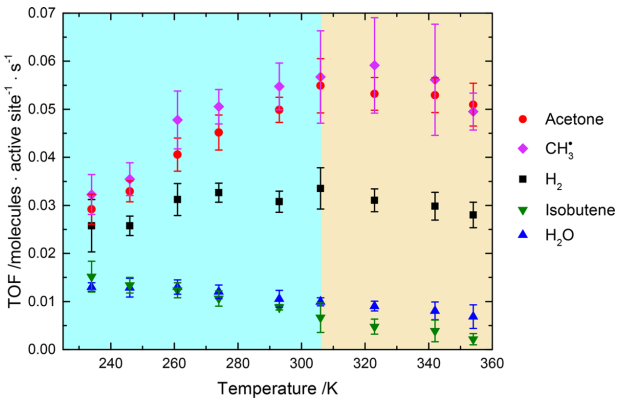

Figure 6. Temperature-dependent TOFs for *tert*-butanol (1×10^{-7} mbar) photoreforming. The lower temperature region up to ~305 K, in which the turnover to acetone increase, is depicted in blue. The upper temperature region, with a constant or slight decrease in the acetone TOF, is depicted in ocher. Over the whole investigated temperature region, the turnover of isobutene and H_2O decreases with increasing temperature.

Table 1. Rate Constants (k) at a Temperature (T) of Maximum Rate, Referenced to the Alcohol Pressure

product	$10^5 k$	T (K)
formaldehyde	16.6 ± 1.8	260
acetaldehyde	10.6 ± 1.2	280
acetone	4.6 ± 0.3	280
isobutene	1.5 ± 0.4	280
acetone + isobutene	6.1 ± 0.7	280
cyclohexanone	5.1 ± 0.1	280
benzaldehyde	4.6 ± 0.2	300

producing methyl formate is still under discussion. It has been suggested that either a formyl or a hemiacetal intermediate is formed to produce methyl formate.[25,28,45] Both pathways represent photoactivated mechanisms, in which a photon is needed for the coupling of formaldehyde and methanol. This is also observed by the illumination dependence in this study (see Figure S3 in the Supporting Information). The resulting reaction equation is given in eq 4:

$$CH_2O(ad)/TiO_2 + CH_3O(ad)/TiO_2 \xrightarrow[Pt@TiO_2]{h\nu} HCO_2CH_3\uparrow + H(ad)/TiO_2 \quad (4)$$

The total reaction can be written as

$$2CH_3OH(g) \xrightarrow[Pt@TiO_2]{h\nu} HCO_2CH_3(ad)\uparrow + 2H_2\uparrow \quad (5)$$

A strong temperature dependence is observed for the selectivity toward methyl formate. It is related to the residence time of formaldehyde on the TiO_2 surface, which has to be long enough in order to enable the consecutive reaction. As the formaldehyde desorption maximum from a reduced $TiO_2(110)$ surface is around 260 K,[22,30,46] the drop in the methyl formate TOF can be related to a higher desorption rate, resulting in a significant decrease in the residence time of the molecule. For photoreforming of benzyl alcohol a similar coupling mechanism occurs, resulting in the production of benzyl benzoate, but with a strongly reduced rate. Similarly to the formation of methyl formate, the consecutive photo-oxidation step is strongly dependent on temperature. Therefore, only in a small temperature range is a small amount of benzyl benzoate detected.

In contrast to formaldehyde and benzaldehyde the second photo-oxidation step does not occur for adsorbed acetaldehyde under anaerobic conditions. This is in good accordance with previous work of Henderson and Friend, who showed that photo-oxidation of acetaldehyde is not possible on reduced $TiO_2(110)$, in contrast to the photo-oxidation of formaldehyde.[46,47] Our study demonstrates that the pathway of photoinduced decomposition of acetaldehyde on reduced $TiO_2(110)$ proposed by Yang and co-workers[48] is not relevant under catalytic conditions.

From cyclohexanol photoreforming a coupling product will only be possible if a ring opening would occur. However, such a reaction can be ruled out, as no product other than cyclohexanone is detected.

***tert*-Butanol Photoreforming.** In contrast to the α-H-containing alcohols, *tert*-butanol photo-oxidation leads to methyl ejection and the desorption of hydrogen and acetone. Furthermore, isobutene and water are formed via a photo-activated thermal reaction pathway. Both pathways are reflected in the stoichiometry of the photoreaction and were observed also on bare TiO_2 previously,[49] but without the evolution of molecular hydrogen. The reactions on Pt-loaded TiO_2 are given in eq 6 and 7

$$(CH_3)_3COH(g) \rightarrow (CH_3)_3CO(ad)/TiO_2 + H(ad)/TiO_2 \xrightarrow{h\nu} (CH_3)_2CO\uparrow + CH_3\uparrow + \frac{1}{2}H_2\uparrow \quad (6)$$

$$(CH_3)_3COH(g) \rightarrow (CH_3)_3CO(ad)/TiO_2 + H(ad)/TiO_2 \xrightarrow{h\nu} C_4H_8\uparrow + H_2O\uparrow \quad (7)$$

with the formation of water resulting from a dehydroxylation of the semiconductor:

$$HO(ad)/TiO_2 + H(ad)/TiO_2 \rightarrow H_2O\uparrow \quad (8)$$

The selectivity of *tert*-butanol photoreforming shows also a pronounced temperature dependence. While the acetone

DOI: 10.1021/acscatal.8b03479
ACS Catal. 2018, 8, 11076−11084

pathway is thermally hindered, which is attributed to a limitation for the thermal butoxy formation, the isobutene formation decreases continuously with increasing temperature. This is due to the required transition state of the photothermal reaction, which has previously been attributed to be a five-membered cyclic structure involving the BBO vacancy.[49] While the transition state may be thermodynamically favored, the probability for molecules exhibiting this particular geometry decreases with increasing temperature for entropic reasons. Furthermore, the ejection of the methyl radical under illumination shows that the photoreaction occurs via a homolytic bond cleavage.

CONCLUSION

In summary, water-free alcohol photoreforming on $Pt_x/TiO_2(110)$ at room temperature is shown for five alcohols (methanol, ethanol, cyclohexanol, benzyl alcohol, and *tert*-butanol) under anaerobic conditions. The absence of oxygen results in the generation of aldehydes and ketones with high selectivities, as further oxidation reactions on the semiconductor (e.g., for ethanol to formate[50]) and on the cocatalyst are avoided. This leads to a pathway in which the main reaction products of all α-H-containing alcohols are the respective aldehyde or ketone and stoichiometric molecular hydrogen. The photo-oxidation mechanism proceeds via a hole-mediated α-H abstraction of dissociatively adsorbed alcohol on the TiO_2 surface and recombination of abstracted hydrogen at Pt_x clusters. The reaction of *tert*-butanol shows that the photoreaction occurs via homolytic bond cleavages.

In general, the reaction behavior of all alcohols very much reflects the findings from the bare semiconductor but under catalytic conditions. This is in good agreement with the aforementioned reaction mechanism. Furthermore, it shows that the oxidation reaction pathways are not influenced by the deposition of the platinum clusters and occur on sites of the reduced TiO_2 crystal.

The surface chemistry also reveals that, by a choice of suitable conditions (i.e., water and oxygen free), consecutive reactions can be suppressed for α-H-containing alcohols and 100% selectivity toward the aldehyde or the ketone can be obtained. For aldehydes and particularly methanol, temperature is also an important parameter, as a consecutive oxidative coupling reaction may happen. At lower temperatures this subsequent reaction step becomes important, because the aldehyde (i.e., formaldehyde) desorption is decreased, which enables the oxidative coupling with the alcohol (i.e., methanol). At higher temperature, a prompt desorption of the aldehyde is enabled, which prevents the consecutive photoreaction step. While the reaction may be conducted with a high selectivity for formaldehyde under conventional conditions, conditions with an increased residence time of the aldehyde may instead enable the formation of methyl formate. This can be achieved by the addition of O_2 into the feed, as was shown for example for bare anatase particles,[51] which however comes at the expense of the formation of water instead of molecular hydrogen.

ASSOCIATED CONTENT

Supporting Information

The Supporting Information is available free of charge on the ACS Publications website at DOI: 10.1021/acscatal.8b03479.

Size distribution of the deposited Pt clusters, electron impact ionization cross sections of the investigated molecules, enlargement of the pressure-dependent TOFs to methyl formate and change in this TOF as a function of illumination intensity in comparison to the TOF of formaldehyde, CH_3 fragment intensity in comparison to the acetaldehyde turnover in a pressure-dependent ethanol photoreforming experiment, low-temperature region of the ethanol photoreforming TOFs, water, oxygen, benzaldehyde, and benzyl benzoate QMS traces for a temperature-dependent benzyl alcohol photoreforming experiment with the coupling product benzyl benzoate depicted qualitatively, Arrhenius plots for acetaldehyde, cyclohexanone, benzaldehyde, and acetone, and activation energies (PDF)

AUTHOR INFORMATION

Corresponding Author

*U.H.: e-mail, ulrich.heiz@mytum.de; tel, +49 (0) 89 289 13391; fax, +49 (0) 89 289 13389.

ORCID

Martin Tschurl: 0000-0001-6618-7312

Author Contributions

§S.L.K. and C.A.W. contributed equally to this work.

Notes

The authors declare no competing financial interest.

ACKNOWLEDGMENTS

The authors thank the DFG through grant HE3435/22-1. C.A.W., S.L.K., C.C., and M.T. express gratitude to Christian Steiffen for keeping up a good mood during the experiments.

REFERENCES

(1) Davis, S. E.; Ide, M. S.; Davis, R. J. Selective Oxidation of Alcohols and Aldehydes Over Supported Metal Nanoparticles. *Green Chem.* **2013**, *15*, 17−45.

(2) Parmeggiani, C.; Cardona, F. Transition Metal Based Catalysts in the Aerobic Oxidation of Alcohols. *Green Chem.* **2012**, *14*, 547−564.

(3) Vinod, C. P.; Wilson, K.; Lee, A. F. Recent Advances in the Heterogeneously Catalysed Aerobic Selective Oxidation of Alcohols. *J. Chem. Technol. Biotechnol.* **2011**, *86*, 161−171.

(4) Sanwald, K. E.; Berto, T. F.; Eisenreich, W.; Gutiérrez, O. Y.; Lercher, J. A. Catalytic Routes and Oxidation Mechanisms in Photoreforming of Polyols. *J. Catal.* **2016**, *344*, 806−816.

(5) Yang, X.; Zhao, H.; Feng, J.; Chen, Y.; Gao, S.; Cao, R. Visible-Light-Driven Selective Oxidation of Alcohols Using a Dye-Sensitized TiO_2-Polyoxometalate Catalyst. *J. Catal.* **2017**, *351*, 59−66.

(6) Chen, X.; Shen, S.; Guo, L.; Mao, S. S. Semiconductor-Based Photocatalytic Hydrogen Generation. *Chem. Rev.* **2010**, *110*, 6503−6570.

(7) Della Pina, C.; Falletta, E.; Rossi, M. Highly Selective Oxidation of Benzyl Alcohol to Benzaldehyde Catalyzed by Bimetallic Gold−Copper Catalyst. *J. Catal.* **2008**, *260*, 384−386.

(8) Omari, A.; Heuser, B.; Pischinger, S. Potential of Oxymethylenether-Diesel Blends for Ultra-Low Emission Engines. *Fuel* **2017**, *209*, 232−237.

(9) Su, S.; Zaza, P.; Renken, A. Catalytic Dehydrogenation of Methanol to Water-Free Formaldehyde. *Chem. Eng. Technol.* **1994**, *17*, 34−40.

(10) Claus, P.; Berndt, H.; Mohr, C.; Radnik, J.; Shin, E.-J.; Keane, M. A. Pd/MgO: Catalyst Characterization and Phenol Hydrogenation Activity. *J. Catal.* **2000**, *192*, 88−97.

DOI: 10.1021/acscatal.8b03479
ACS Catal. 2018, 8, 11076−11084

(11) Ni, M.; Leung, D. Y.; Leung, M. K. A Review on Reforming Bio-Ethanol for Hydrogen Production. *Int. J. Hydrogen Energy* **2007**, *32*, 3238−3247.
(12) Pillai, U. R.; Sahle-Demessie, E. Selective Oxidation of Alcohols in Gas Phase Using Light-Activated Titanium Dioxide. *J. Catal.* **2002**, *211*, 434−444.
(13) Tomita, O.; Otsubo, T.; Higashi, M.; Ohtani, B.; Abe, R. Partial Oxidation of Alcohols On Visible-Light-Responsive WO_3Photocatalysts Loaded With Palladium Oxide Cocatalyst. *ACS Catal.* **2016**, *6*, 1134−1144.
(14) Walenta, C. A.; Kollmannsberger, S. L.; Kiermaier, J.; Winbauer, A.; Tschurl, M.; Heiz, U. Ethanol Photocatalysis on Rutile TiO_2(110): The Role of Defects and Water. *Phys. Chem. Chem. Phys.* **2015**, *17*, 22809−22814.
(15) Brinkley, D.; Engel, T. Photocatalytic Dehydrogenation of 2-Propanol on TiO2(110). *J. Phys. Chem. B* **1998**, *102*, 7596−7605.
(16) Yamakata, A.; Ishibashi, T.; Onishi, H. Electron- and Hole-Capture Reactions on Pt/TiO_2 Photocatalyst Exposed to Methanol Vapor Studied with Time-Resolved Infrared Absorption Spectroscopy. *J. Phys. Chem. B* **2002**, *106*, 9122−9125.
(17) Cargnello, M.; Gasparotto, A.; Gombac, V.; Montini, T.; Barreca, D.; Fornasiero, P. Photocatalytic $H_2$and Added-Value By-Products - The Role of Metal Oxide Systems in their Synthesis of Oxygenates. *Eur. J. Inorg. Chem.* **2011**, *2011*, 4309.
(18) Kandiel, T. A.; Dillert, R.; Robben, L.; Bahnemann, D. W. Photonic Efficiency and Mechanism of Photocatalytic Molecular Hydrogen Production over Platinized Titanium Dioxide from Aqueous Methanol Solutions. *Catal. Today* **2011**, *161*, 161.
(19) Chiarello, G. L.; Ferri, D.; Selli, E. Effect of the CH_3OH/H_2O Ratio on the Mechanism of the Gas-Phase Photocatalytic Reforming of Methanol on Noble Metal-Modified TiO_2. *J. Catal.* **2011**, *280*, 168−177.
(20) Chiarello, G. L.; Aguirre, M. H.; Selli, E. Hydrogen Production by Photocatalytic Steam Reforming of Methanol on Noble Metal-Modified TiO2. *J. Catal.* **2010**, *273*, 182−190.
(21) Chiarello, G. L.; Ferri, D.; Selli, E. In Situ Attenuated Total Reflection Infrared Spectroscopy Study of the Photocatalytic Steam Reforming of Methanol on Pt/TiO_2. *Appl. Surf. Sci.* **2018**, *450*, 146−154.
(22) Shen, M.; Henderson, M. A. Identification of the Active Species in Photochemical Hole Scavenging Reactions of Methanol on TiO_2. *J. Phys. Chem. Lett.* **2011**, *2*, 2707−2710.
(23) Shen, M.; Henderson, M. A. Role of Water in Methanol Photochemistry on Rutile TiO_2(110). *J. Phys. Chem. C* **2012**, *116*, 18788−18795.
(24) Kolesov, G.; Vinichenko, D.; Tritsaris, G. A.; Friend, C. M.; Kaxiras, E. Anatomy of the Photochemical Reaction: Excited-State Dynamics Reveals the C−H Acidity Mechanism of Methoxy Photo-Oxidation on Titania. *J. Phys. Chem. Lett.* **2015**, *6*, 1624−1627.
(25) Phillips, K. R.; Jensen, S. C.; Baron, M.; Li, S.-C.; Friend, C. M. Sequential Photo-Oxidation of Methanol to Methyl Formate on TiO_2(110). *J. Am. Chem. Soc.* **2013**, *135*, 574−577.
(26) Nadeem, A. M.; Muir, J. M. R.; Connelly, K. A.; Adamson, B. T.; Metson, B. J.; Idriss, H. Ethanol Photo-Oxidation on a Rutile TiO_2(110) Single Crystal Surface. *Phys. Chem. Chem. Phys.* **2011**, *13*, 7637−7643.
(27) Guo, Q.; Xu, C.; Ren, Z.; Yang, W.; Ma, Z.; Dai, D.; Fan, H.; Minton, T. K.; Yang, X. Stepwise Photocatalytic Dissociation of Methanol and Water on TiO_2(110). *J. Am. Chem. Soc.* **2012**, *134*, 13366−13373.
(28) Guo, Q.; Xu, C.; Yang, W.; Ren, Z.; Ma, Z.; Dai, D.; Minton, T. K.; Yang, X. Methyl Formate Production on TiO_2(110), Initiated by Methanol Photocatalysis at 400 nm. *J. Phys. Chem. C* **2013**, *117*, 5293−5300.
(29) Ma, Z.; Guo, Q.; Mao, X.; Ren, Z.; Wang, X.; Xu, C.; Yang, W.; Dai, D.; Zhou, C.; Fan, H.; Yang, X. Photocatalytic Dissociation of Ethanol on TiO_2(110) by Near-Band-Gap Excitation. *J. Phys. Chem. C* **2013**, *117*, 10336−10344.
(30) Yuan, Q.; Wu, Z.; Jin, Y.; Xu, L.; Xiong, F.; Ma, Y.; Huang, W. Photocatalytic Cross-Coupling of Methanol and Formaldehyde on a Rutile TiO_2(110) Surface. *J. Am. Chem. Soc.* **2013**, *135*, 5212−5219.
(31) Zhou, C.; Ren, Z.; Tan, S.; Ma, Z.; Mao, X.; Dai, D.; Fan, H.; Yang, X.; LaRue, J.; Cooper, R.; Wodtke, A. M.; Wang, Z.; Li, Z.; Wang, B.; Yang, J.; Hou, J. Site-Specific Photocatalytic Splitting of Methanol on TiO_2(110). *Chem. Sci.* **2010**, *1*, 575−580.
(32) Xu, C.; Yang, W.; Guo, Q.; Dai, D.; Chen, M.; Yang, X. Molecular Hydrogen Formation from Photocatalysis of Methanol on TiO_2(110). *J. Am. Chem. Soc.* **2013**, *135*, 10206−10209.
(33) Winbauer, A.; Kollmannsberger, S. L.; Walenta, C. A.; Schreiber, P.; Kiermaier, J.; Tschurl, M.; Heiz, U. Isomer-Selective Detection of Aromatic Molecules in Temperature-Programmed Desorption for Model Catalysis. *Anal. Chem.* **2016**, *88*, 5392−5397.
(34) Henderson, M. A. Structural Sensitivity in the Dissociation of Water on TiO_2Single-Crystal Surfaces. *Langmuir* **1996**, *12*, 5093−5098.
(35) Heiz, U.; Vanolli, F.; Trento, L.; Schneider, W.-D. Chemical Reactivity of Size-Selected Supported Clusters: An Experimental Setup. *Rev. Sci. Instrum.* **1997**, *68*, 1986−1994.
(36) Watanabe, Y.; Wu, X.; Hirata, H.; Isomura, N. Size-Dependent Catalytic Activity and Geometries of Size-Selected Pt Clusters on TiO_2(110) Surfaces. *Catal. Sci. Technol.* **2011**, *1*, 1490−1495.
(37) Berr, M. J.; Schweinberger, F. F.; Döblinger, M.; Sanwald, K. E.; Wolff, C.; Breimeier, J.; Crampton, A. S.; Ridge, C. J.; Tschurl, M.; Heiz, U.; Jäckel, F.; Feldmann, J. Size-Selected Subnanometer Cluster Catalysts on Semiconductor Nanocrystal Films for Atomic Scale Insight into Photocatalysis. *Nano Lett.* **2012**, *12*, 5903−5906.
(38) Bonanni, S.; Aït-Mansour, K.; Harbich, W.; Brune, H. Effect of the TiO2 Reduction State on the Catalytic CO Oxidation on Deposited Size-Selected Pt Clusters. *J. Am. Chem. Soc.* **2012**, *134*, 3445−3450.
(39) Henderson, M. A.; Otero-Tapia, S.; Castro, M. E. The Chemistry of Methanol on the TiO_2(110) Surface: The Influence of Vacancies and Coadsorbed Species. *Faraday Discuss.* **1999**, *114*, 313−329.
(40) Hansen, J. Ø.; Bebensee, R.; Martinez, U.; Porsgaard, S.; Lira, E.; Wei, Y.; Lammich, L.; Li, Z.; Idriss, H.; Besenbacher, F.; Hammer, B.; Wendt, S. Unravelling Site-Specific Photo-Reactions of Ethanol on Rutile TiO_2(110). *Sci. Rep.* **2016**, *6*, 21990.
(41) Geng, Z.; Jin, X.; Wang, R.; Chen, X.; Guo, Q.; Ma, Z.; Dai, D.; Fan, H.; Yang, X. Low-Temperature Hydrogen Production via Water Conversion on Pt/TiO_2. *J. Phys. Chem. C* **2018**, *122*, 10956−10962.
(42) Moulijn, J. A.; van Leeuwen, P. W. N. M.; van Santen, R. Catalysis: An Integrated Approach to Homogeneous, Heterogeneous and Industrial Catalysis. *Stud. Surf. Sci. Catal.* **1993**, *79*, 69−86.
(43) Goodman, D. W. Single Crystals as Model Catalysts. *J. Vac. Sci. Technol.* **1982**, *20*, 522−526.
(44) Cant, N. W.; Cole, J. R. Photocatalysis of the Reaction Between Ammonia and Nitric Oxide on TiO_2Surfaces. *J. Catal.* **1992**, *134*, 317−330.
(45) Lang, X.; Wen, B.; Zhou, C.; Ren, Z.; Liu, L.-M. First-Principles Study of Methanol Oxidation into Methyl Formate on Rutile TiO_2(110). *J. Phys. Chem. C* **2014**, *118*, 19859−19868.
(46) Cremer, T.; Jensen, S. C.; Friend, C. M. Enhanced Photo-Oxidation of Formaldehyde on Highly Reduced o-TiO_2(110). *J. Phys. Chem. C* **2014**, *118*, 29242−29251.
(47) Zehr, R.; Henderson, M. Acetaldehyde Photochemistry on TiO_2(110). *Surf. Sci.* **2008**, *602*, 2238−2249.
(48) Xu, C.; Yang, W.; Guo, Q.; Dai, D.; Yang, X. Photoinduced Decomposition of Acetaldehyde on a Reduced TiO_2(110) Surface: Involvement of Lattice Oxygen. *Phys. Chem. Chem. Phys.* **2016**, *18*, 30982.
(49) Walenta, C. A.; Kollmannsberger, S. L.; Courtois, C.; Tschurl, M.; Heiz, U. Photocatalytic Selectivity Switch to C-C Scission: α-Methyl Ejection of *tert*-Butanol on TiO_2(110). *Phys. Chem. Chem. Phys.* **2018**, *20*, 7105−7111.
(50) Harrison, G.; Katsiev, K.; Alsalik, Y.; Thornton, G.; Idriss, H. Switch in Photocatalytic Reaction Selectivity: The Effect of Oxygen

DOI: 10.1021/acscatal.8b03479
ACS Catal. 2018, 8, 11076−11084

ACS Catalysis Research Article

Partial Pressure on Carbon-Carbon Bond Dissociation over Hydroxylated TiO_2(110)Surfaces. *J. Catal.* **2018**, *363*, 117−127.
(51) Kominami, H.; Sugahara, H.; Hashimoto, K. Photocatalytic Selective Oxidation of Methanol to Methyl Formate in Gas Phase over Titanium(IV) Oxide in a Flow-Type Reactor. *Catal. Commun.* **2010**, *11*, 426−429.

DOI: 10.1021/acscatal.8b03479
ACS Catal. 2018, 8, 11076−11084

Supporting Information: Thermal control of selectivity in photocatalytic, water-free alcohol photo-reforming

Sebastian L. Kollmannsberger,[†,¶] Constantin A. Walenta,[†,‡,¶] Carla Courtois,[†] Martin Tschurl,[†] and Ueli Heiz[*,†,‡]

†*Chair of Physical Chemistry, Department of Chemistry & Catalysis Research Center, Technische Universität München, Lichtenbergstr. 4, 85748 Garching, Germany*

‡*Nanosystems Initiative Munich, Schellingstr. 4, 80799 München, Germany*

¶*The authors contributed equally to this work*

E-mail: ulrich.heiz@mytum.de

Phone: +49 (0) 89 289 13391. Fax: +49 (0) 89 289 13389

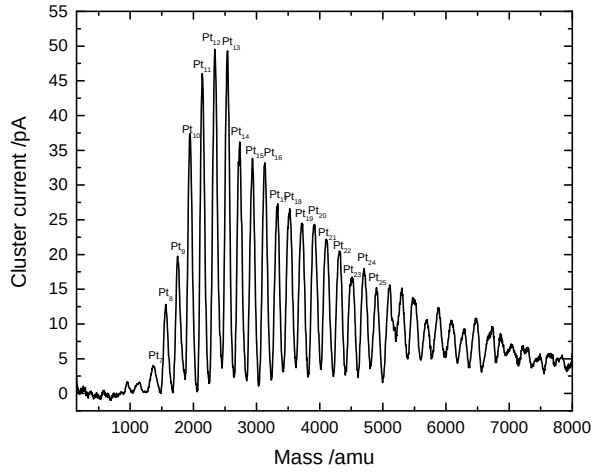

Figure S1: Size-distribution from Pt_7 to Pt_{35} with a maximum from Pt_{11} to Pt_{13} from the laser vaporization cluster source. The cluster size is about 1 nm and the distribution shows a log-normal behaviour.[S1]

Table S1: Electron impact ionization cross sensitivity values at 70 eV and m/z fragments used for quantification.

substance	ICS [Å^2]	m/z fragment
methanol	4.61[S2]	31
formaldehyde	4.14[S3]	30
acetaldehyde	6.7[S2]	44
benzaldehyde	20.1[S4]	106
cyclohexanone	17.6[S4]	70
methyl-radical	2.99[S5]	15
acetone	9.0[S2]	58
isobutene	11.889[S6]	56
water	2.275[S6]	18
hydrogen	1.021[S6]	2
methyl formate	6.8[S7]	60

The QMS ion current is calibrated via the desorption integral of a saturation coverage of the Ti-lattice sites with methanol in a TPD experiment. To obtain quantitative values for other molecules than methanol the fragmentation pattern, the electron impact ionization cross sensitivities (ICS) and the m/z dependent transmission through the QMS must be considered. The fragmentation pattern are obtained from mass spectra from the National Institute of Standards and Technology for all molecules[S8] besides methyl.[S9] The ICS values and the m/z fragments used for the quantification can be found in table S1.

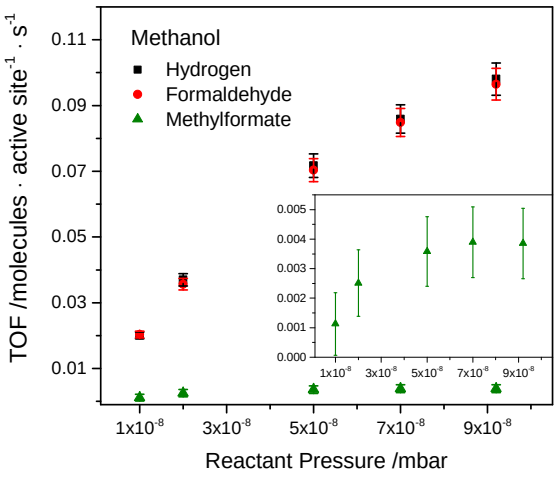

Figure S2: Pressure-dependent methanol photo-reforming at 260 K. Note that the methyl formate TOFs are multiplied with a factor of 15 for better visibility.

The TOFs of methyl formate from methanol photo-reforming show a saturation behavior, starting at a pressure of 5×10^{-8} mbar (see Figure S2).

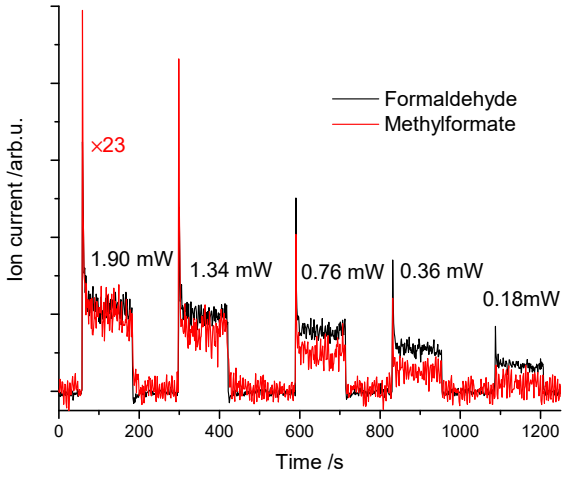

Figure S3: Laser power-dependent photo-catalytic methanol conversion. Note that the m/z = 60 trace is enlarged by a factor of 23 to optimize the comparability between the two products. The indictated energies refer to the light energy directly before the UHV chamber.

From laser power-dependent photo-catalytic methanol conversion (Figure S3), it can be seen that the yield of the coupling product methyl formate is stronger reduced than the yield of formaldehyde with lower laser power. Consequently, the coupling of an adsorbed formaldehyde and a methoxy is a consecutive photo-catalytic process.

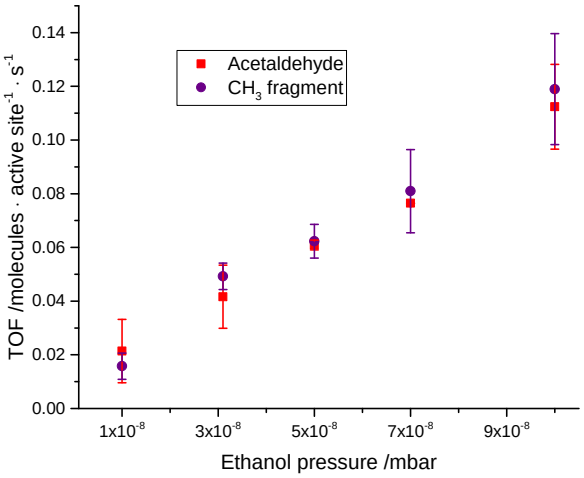

Figure S4: Pressure-dependent TOFs for ethanol photo-reforming at 280 K. Plotted are the acetaldehyde TOFs obtained from evaluation of the m/z=15 QMS signal (CH_3-fragment) and the m/z=44 QMS signal. As both are identically the formation of other molecules containing CH_3-fragments can be ruled out.

From ethanol photo-reforming other reaction products containing CH_3-fragments are ruled out by comparison of the acetaldehyde TOFs obtained from two different m/z QMS signals, as shown in figure S4.

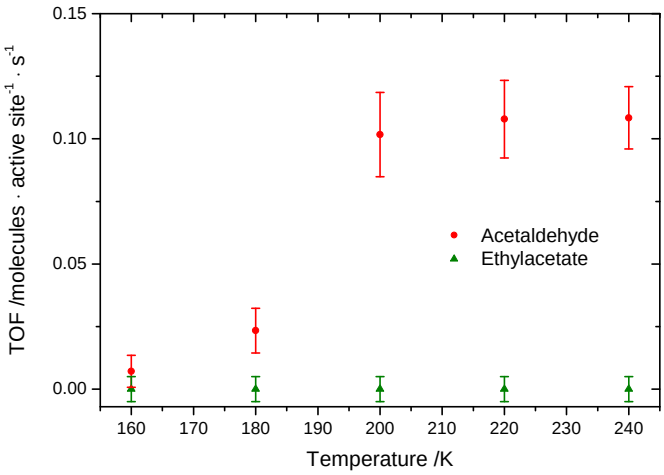

Figure S5: Low temperature region of acetaldehyde and ethylacetate TOFs from ethanol photo-reforming at 1×10^{-7} mbar.

It can clearly be seen from figure S5, that the acetaldehyde TOFs rise from 160 K to 200 K. From this temperature on the following TOFs are constant. Furthermore it is visible, that no ethylacetate is formed.

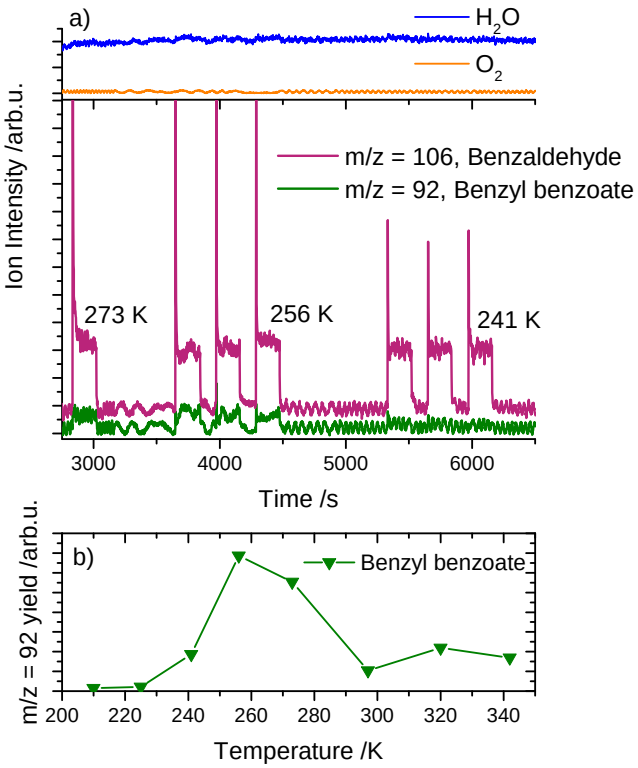

Figure S6: Temperature-dependent benzyl alcohol photo-reforming at 5×10^{-8} mbar. In a) the water, oxygen, benzaldehyde and benzyl benzoate raw data QMS traces are shown for three different temperatures. b) shows a qualitative evaluation of the coupling product benzyl benzoate.

For benzyl alcohol it is found that the m/z=92 fragment is formed in a small temperature range from ≈240 K to ≈300 K, which can either result from toluene (deoxygenation of benzyl alcohol[S10]) or from benzyl benzoate (coupling product). Note that no oxygen or water desorption is observed during catalysis (see SI Fig. S6a). Consequently, the formation of toluene can be ruled out as a potential side product to this pathway does not occur and poisoning effects are also not observed. Therefore, a coupling reaction to benzyl benzoate is proposed. However, we refrain from a quantitative analysis as the m/z=92 fragment is only a minor fragment of benzyl benzoate resulting in a large error, when being quantified.

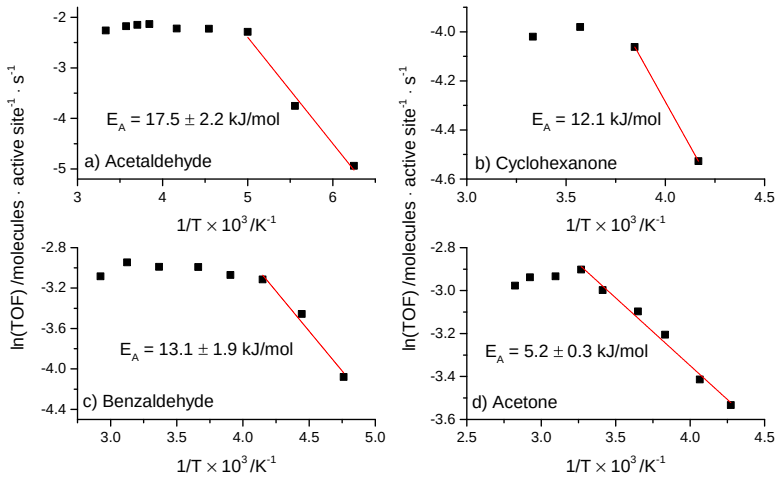

Figure S7: Arrhenius plots for a) acetaldehyde (at 1×10^{-7} mbar), b) cyclohexanone (at 1×10^{-8} mbar), c) benzaldehyde (at 5×10^{-8} mbar) and d) acetone (at 1×10^{-7} mbar) photo-reforming of the respective alcohol. The activation energy E_A is determined from the slope of the linear rise in the Arrhenius plot.

The obtained activation energies (see figure S7) are all less than 20 $\frac{kJ}{mol}$ and are summarized in table S2. We refrain from an Arrhenius type activation energy evaluation of the formaldehyde formation, as this reaction competes with the methyl formate formation.

Table S2: Activation energies of acetaldehyde, cyclohexanone, benzaldehyde and acetone formation from figure S7

Product	E_A $[\frac{kJ}{mol}]$
Acetaldehyde	17.5 ± 2.2
Cyclohexanone	12.1
Benzaldehyde	13.1 ± 1.9
Acetone	5.2 ± 0.3

References

(S1) Crampton, A. S.; Rötzer, M. D.; Schweinberger, F. F.; Yoon, B.; Landman, U.; Heiz, U. Ethylene Hydrogenation on Supported Ni, Pd and Pt Nanoparticles: Catalyst Activity, Deactivation and the d-Band Model. *J. Catal.* **2016**, *333*, 51–58.

(S2) Bull, J. N.; Harland, P. W.; Vallance, C. Absolute Total Electron Impact Ionization Cross-Sections for Many-Atom Organic and Halocarbon Species. *J. Phys. Chem. A* **2012**, *116*, 767–777.

(S3) Gupta, D.; Antony, B. Electron Impact Ionization of Cycloalkanes, Aldehydes, and Ketones. *J. Chem. Phys.* **2014**, *141*, 054303.

(S4) Harrison, A. G.; Jones, E. G.; Gupta, S. K.; Nagy, G. P. Total Cross Sections for Ionization by Electron Impact. *Can. J. Chem.* **1966**, *44*, 1967–1973.

(S5) Peng, X.; Viswanathan, R.; Smudde Jr., G. H.; Stair, P. C. A Methyl Free Radical Source for Use in Surface Studies. *Rev. Sci. Instrum.* **1992**, *63*, 3930–3935.

(S6) Kim, Y.-K.; Irikura, K. K.; Rudd, M. E.; Ali, M. A.; Stone, P. M.; Chang, J.; Coursey, J. S.; Dragoset, R. A.; Kishore, A. R.; Olsen, K. J.; Sansonetti, A. M.; Wiersma, G. G.; Zucker, D. S.; Zucker, M. A. Electron-Impact Ionization Cross Section for Ionization and Excitation Database. `http://physics.nist.gov/ionxsec`, 2004 version 3.0; 2018, February 12.

(S7) Hudson, J. E.; Weng, Z. F.; Vallance, C.; Harland, P. W. Absolute Electron Impact Ionization Cross-Sections and Polarizability Volumes for the C_2 to C_6 Methanoates and C_3 to C_7 Ethanoates. *Int. J. Mass Spectrom.* **2006**, *248*, 42 – 46.

(S8) Linstrom, P., Mallard, W., Eds. *NIST Chemistry WebBook, NIST Standard Reference Database Number 69*, retrieved December 12, 2017 ed.; National Institute of Standards and Technology: Gaithersburg MD, 20899, 2017.

(S9) Langer, A.; Hipple, J. A.; Stevenson, D. P. Ionization and Dissociation by Electron Impact; Methylene, Methyl, and Methane. *J. Chem. Phys.* **1954**, *22*, 1836–1844.

(S10) Chen, L.; Smith, R. S.; Kay, B. D.; Dohnalek, Z. Direct Deoxygenation of Phenylmethanol to Methylbenzene and Benzyl Radicals on Rutile TiO_2(110). *ACS Catal.* **2017**, *7*, 2002–2006.

A.6 Why Co-Catalyst-Loaded Rutile Facilitates Photocatalytic Hydrogen Evolution

PCCP

PAPER

View Article Online
View Journal | View Issue

Cite this: *Phys. Chem. Chem. Phys.*, 2019, **21**, 1491

Received 10th September 2018,
Accepted 15th December 2018

DOI: 10.1039/c8cp05513k

rsc.li/pccp

Why co-catalyst-loaded rutile facilitates photocatalytic hydrogen evolution†

Constantin A. Walenta,‡[ab] Sebastian L. Kollmannsberger,‡[a] Carla Courtois,[a] Rui N. Pereira,[c] Martin Stutzmann,[bc] Martin Tschurl[a] and Ueli Heiz*[ab]

As the conduction band edge of rutile is close to the reduction potential of hydrogen, there is a long-lasting discussion on whether molecular hydrogen can be evolved from this semiconductor. Our study on methanol photoreforming in the ultra-high vacuum reveals that photocatalysts comprising a TiO_2(110) single crystal decorated with platinum clusters indeed enable the evolution of H_2. This is attributed to a new type of mechanism, in which the co-catalyst acts as a recombination center for hydrogen and not as a reduction site of a photoreaction. This mechanism is an alternative pathway to the commonly used mechanism derived from photoelectrochemistry and must particularly be considered for systems, in which reducible semiconductors enable the surface diffusion of hydrogen species.

Introduction

Hydrogen generated from renewable feedstocks is envisioned to act as a potential fuel for clean transportation.[1] In the last decade research focusing on increasing the efficiency of hydrogen production has tremendously been intensified by following both conventional and novel approaches.[2,3] Photocatalytic water splitting facilitated by co-catalyst loaded semiconductor particles is one promising way for clean hydrogen production. Recently, such systems have been reported to exceed efficiencies of over 1% in a scalable solar-to-hydrogen production.[4] Surprisingly, detailed mechanistic insights are still scarce despite the intense research efforts undertaken in the past. Such knowledge, however, may be vital for the development of devices, which are economically competitive. So far, there has been a general agreement that two different effects contribute to the hydrogen evolution rate, the charge carrier dynamics and the chemical reactions. For the latter, both partial reactions are usually treated somewhat independently from each other, following the concepts of photoelectrocatalysis. For most of the systems it is believed that the oxidation reaction is the rate-determining step, while the evolution of hydrogen occurs on a much faster time scale. The latter is usually viewed as a two-electron reduction of H^+. If such a separate picture of both half-reactions is valid, the choice of particular semiconductor materials is subject to certain restrictions, for example the position of the band edges with respect to the electrochemical potential of the two half-reactions. In this regard, there is still a lively discussion on whether rutile is capable of enabling the evolution of molecular hydrogen or whether its conduction band edge is too low in energy.[5,6]

On the other hand, the commonly used picture of explaining photocatalytic reactions is based on the mechanisms observed in two electrochemical half-cells, for which only the energetics of the materials are taken into account. Contributions related to their surface chemistry are usually completely ignored, despite their potential importance. For illustration, gallium nitride exhibits a similar valence band edge and even a conduction band edge higher in energy to rutile TiO_2.[7] However, GaN(0001) does not enable alcohol photooxidation in the ultra-high vacuum (UHV),[8] despite its activity in the charge-carrier driven photodesorption of CO.[9] With the established model based on electrochemical half-cells only a straightforward explanation of these observations cannot readily be given.

Experimental

In order to study photocatalytic reactions in a highly defined environment with highly defined catalysts, all experiments were performed in an UHV apparatus[10–12] with an attached laser-vaporization cluster source. The focused 2nd harmonic of a Nd:YAG laser (Spitlight DPSS, Innolas) ablates a rotating platinum target creating a plasma, which is cooled by the introduction of a helium gas (He 6.0, Air Westfalen) pulse *via* a home-built

[a] *Chair of Physical Chemistry, Department of Chemistry & Catalysis Research Center, Technische Universität München, Lichtenbergstr. 4, 85748 Garching, Germany. E-mail: ulrich.heiz@mytum.de*
[b] *Nanosystems Initiative Munich, Schellingstr. 4, 80799 München, Germany*
[c] *Walter Schottky Institute and Physics Department, Technische Universität München, Am Coulombwall 4, 85748 Garching, Germany*

† Electronic supplementary information (ESI) available: Details of catalyst preparation and characterization; the analysis of thermal reaction products, a detailed description of photocatalytic activity measurements and more results concerning methanol photocatalysis. See DOI: 10.1039/c8cp05513k

‡ These authors contributed equally to this work.

piezo valve into the vacuum. The cationic clusters of the resulting beam are guided by an octupole ion guide and several einzel lenses to a quadrupole bender. This bender enables the separation of cations from neutral clusters prior to their guidance through a quadrupole mass spectrometer and subsequent cluster deposition (details on the deposition method and materials used are given in "1. Catalyst Preparation" in the ESI†). The main chamber with a typical base pressure more than 9.1×10^{-11} mbar is equipped with a leak valve (Pfeiffer Vacuum) for Langmuir dosing and a molecular beam doser. A sputter gun (SPECS IQE11/35) enables crystal cleaning by cycles of argon sputtering. The cleaning procedure is evaluated by Auger Electron Spectroscopy (AES) with a respective spectrometer (Omicron Nanotechnology). The typical spectrum of a clean TiO_2 crystal is shown in Fig. S1a in the ESI.† The sample holder, which is attached to a manipulator, can be cooled to liquid nitrogen temperatures and heated resistively to more than 1000 K.

The photocatalysts are prepared by using a reduced rutile TiO_2(110) single crystal, which is prepared by sputtering and oxygen annealing cycles and a subsequent vacuum annealing step for 10 min (more details are given in the ESI,† in the section "1. Catalyst Preparation") prior to the deposition of soft-landed Pt clusters. This results in a stable oxygen vacancy concentration of 6% (for details see Fig. S2 in the ESI†).

Methanol is either dosed at cryogenic temperatures or *via* a constant background, while all relevant masses are monitored with a QMS (QMA 430, Pfeiffer Vacuum GmbH), which can be placed right above the photocatalyst. Given a certain temperature, the photoreaction is facilitated using a nanosecond pulsed OPO-laser, operated at 241.8 nm after frequency doubling. Changes in the composition of the gas phase above the photocatalyst are then detected in the QMS. The photoreaction is shown to be independent of UV wavelength and pulsed or continuous excitation, as long as the photon energy is above the band gap (see Fig. S8 in the ESI†).

Results

The photochemical behavior of methanol and other alcohols on bare TiO_2(110) has already been extensively investigated, which makes them excellent systems for studying the hydrogen evolution reaction. As alcohols are known to efficiently facilitate hole-reactions, they have vastly been used in different studies as hole-scavengers in the past.[13,14] From studies in UHV it is known that on a reduced titania crystal the main photochemical reaction pathway is a disproportionation reaction yielding formaldehyde and the hydroxylated semiconductor (see eqn (1)).[14–16] At best only very small amounts of molecular hydrogen are detected.[17]

$$CH_3OH_{ad}/TiO_2 \xrightarrow{h\nu} CH_2O\uparrow + 2H_{ad}/TiO_2 \qquad (1)$$

Therefore, the semiconductor surface becomes significantly hydroxylated during the photoreaction. Furthermore, only a fraction of the initial methanol adsorbed at the surface can be converted.[18,19] Amongst other effects, this is attributed to the poisoning of the crystal due to its hydroxylation,[10,14] whose details however still remain elusive. The deposition of small platinum clusters on the semiconductor completely changes this behavior (see Fig. 1). A strong production of molecular hydrogen is observed, which is stoichiometric to formaldehyde formation. In contrast to the reaction on the bare semiconductor, catalyst poisoning does not occur anymore after the deposition of Pt clusters. The absence of poisoning in Pt_x/TiO_2(110) enables the reaction to occur under steady-state conditions. This allows for the determination of a turnover frequency (TOF) of the photocatalyst (Fig. 2a). The photoreaction is found to be stoichiometric for several investigated pressures (Fig. 2a).

Surprisingly, it is found that higher coverages of co-catalysts only lead to very small changes in the TOF (Fig. 2b). In this regard, changing the Pt cluster loading over almost two orders

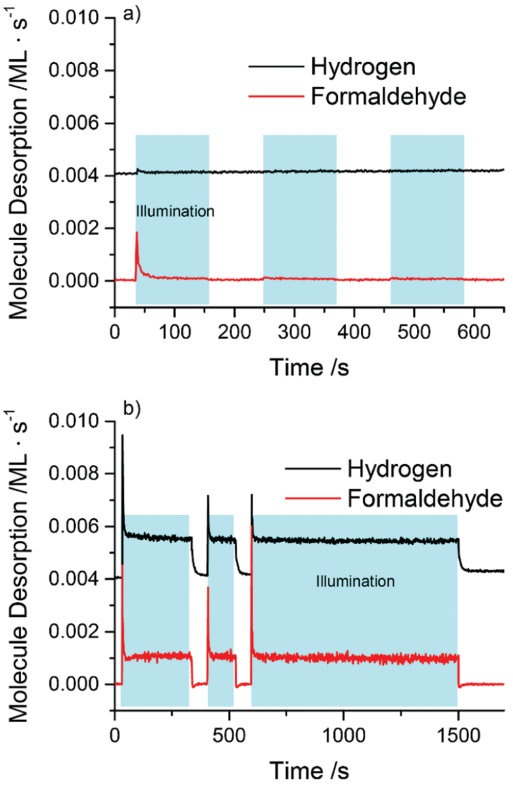

Fig. 1 Photochemical products of methanol photo-reforming on r-TiO_2(110) [a] and on Pt_x/TiO_2(110) (0.1% cluster coverage) [b] at 260 K in a methanol background of 1×10^{-8} mbar. Upon UV illumination (shown as blue background), methoxy species are photo-oxidized to formaldehyde, which desorbs thermally. In [a] only trace amounts of H_2 are formed upon illumination, while poisoning of the catalyst is immediately observed upon illumination. The Pt-loaded photocatalyst [b] shows an evolution of formaldehyde as well as hydrogen without deactivation. The stoichiometry of the reaction products is in perfect agreement with the expected one. Note that the H_2 trace is offset by 0.004 ML s^{-1} for clarity.

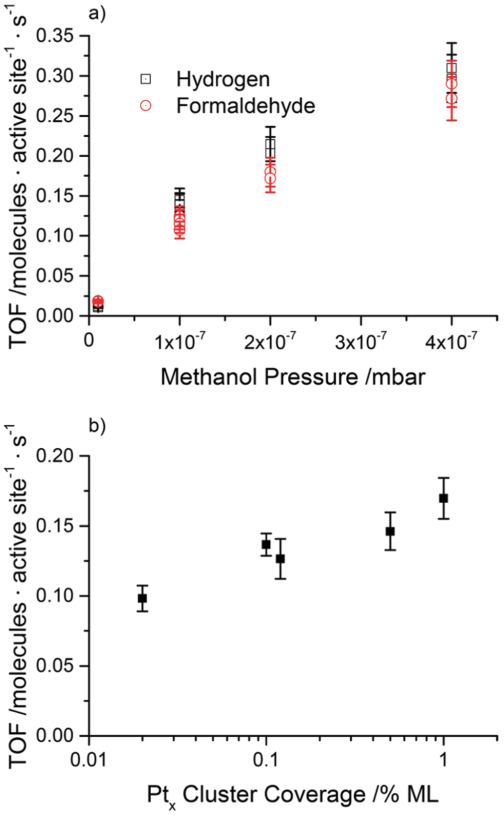

Fig. 2 Photocatalytic conversion of methanol on Pt-loaded r-TiO_2(110). In (a), the background pressure-dependent TOFs for Pt_x/r-TiO_2(110) are shown for several photocatalytic experiments. The catalyst was prepared with a coverage of 1‰ clusters per TiO_2(110) surface atom and methanol was introduced in the chamber at 260 K. The reaction stoichiometry is independent of the pressure. Every square and circle pair resembles a photocatalytic experiment. In (b), the cluster coverage is varied on the semiconductor and the reaction even occurs with an appreciable TOF for a Pt cluster coverage of 0.02% of a monolayer.

of magnitude (from 0.02% to 1% of a monolayer) only leads to a 2-fold increase in the TOF. If a typical spherical rutile nanoparticle of 20 nm in diameter is considered, this coverage amounts to weight loadings of less than 0.01 to over 0.3 wt% of platinum (assuming the bulk density of rutile TiO_2 and Pt_{15} as the average cluster size). Indeed, in a recent study on colloidal systems it was reported that very little amounts of platinum loading already result in high hydrogen production rates.[20] This is also in good agreement with a previous work of Haruta and co-workers, who found an increase in H_2 production in the lower loading regime, similar to our results.[21]

The observed behavior of the Pt coverage-dependent TOFs suggests that the photo-oxidation to formaldehyde is the rate-determining step and that hydrogen diffusion and recombination are significantly faster. Therefore, it is vital that the active sites for the photo-oxidation on the semiconductor remain unblocked by the metal co-catalyst. This gives rise to a previously mentioned maximum at higher co-catalyst loadings. In our study, clusters are randomly distributed on the surface due to the applied deposition method (soft-landing of clusters from a cluster source) as evidenced by different microscopy techniques (*i.e.* scanning tunneling microscopy, Kelvin probe force microscopy and transmission electron microscopy).[22–24]

In addition, photon-stimulated desorption of oxygen is a powerful tool to probe the concentration of accessible photo-active surface sites on TiO_2(110).[25] The application of this method further confirms the accessibility of photo-active sites after cluster deposition and even after catalysis, as it does not significantly change after both events (see Fig. S11, ESI†). This is in good agreement with the random cluster distribution and different to the formation of clusters *via* the evaporation of metals on the semiconductor. Using the latter deposition method it was found that it strongly inhibits the photo-oxidation of CO in the case of Pt[26] or the O_2 photodesorption in the case of gold.[27] This is a clear indication that the migration to or the formation of metal centers in or near photoactive surface sites will inhibit the photooxidation pathway on the semiconductor.

Varying the incident pulse energy of UV illumination shows that a saturation regime is reached at high photon fluxes, while for small illumination intensities a linear dependence is obtained (Fig. S6, ESI†). The observed trend suggests a transition from a 1st order regime to a 0th one, which indicates that only a one-photon process is involved in the evolution of a hydrogen molecule.

This is a similar observation to that for the so-called ''current doubling'', which aims to describe an increase in the observed charge-carrier generation in the reaction of methanol with photoanodes.[28] However, it was also used to interpret the purely photocatalytic reaction of methanol vapor.[29] Current doubling is usually explained by the decomposition of a CH_3O-radical and an injection of an electron into the semiconductor's conduction band. While this mechanism is capable of describing the reaction in photoelectrocatalysis,[28,31] it can be excluded in the present work. On the one hand, this is due to the reaction conditions, but on the other hand, we found in one of our previous works that the bond cleavage occurs in a homolytic manner for tertiary alcohols.[11,12]

Discussion

The comparison of the photocatalytic reaction behavior of the bare semiconductor with the Pt-loaded one leads to the following reaction mechanism, which is illustrated in Fig. 3. From the methanol chemistry on the bare semiconductor it is generally accepted that methoxys act as photoactive species for a hole-mediated α-H abstraction.[15] In many studies of different research groups the authors came to the conclusion that the adsorption of alcohols onto the TiO_2(110) surface occurs *via* a

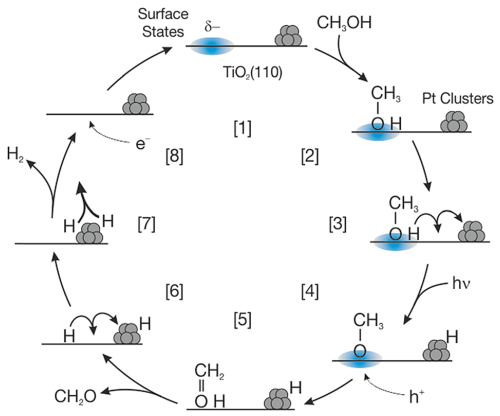

Fig. 3 Photocatalytic reaction mechanism for methanol conversion at a co-catalyst-loaded r-TiO_2(110)-surface. Upon adsorption, methoxy species [2] are formed thermally, while hydroxyls may diffuse on the surface [3]. The methoxy gets oxidized by the photohole[30] originating from the illumination of the semiconductor [4]. This causes the formation of formaldehyde [5], which eventually desorbs thermally. The formed atomic hydrogen diffuses on the surface [6] and recombines at a co-catalyst, where it also desorbs thermally [7]. Note that the reaction mechanism facilitates an overall charge-neutral disproportionation reaction, which is triggered by the irreversible photo-oxidation step. The negatively charged surface states (attributed to maybe BBO vacancies or Ti^{3+} interstitials) of the n-type semiconductor get replenished by photoelectrons [8] and the catalyst remains unchanged after the completion of the cycle [1].

dissociative adsorption of alkoxy species.[15,30,32–35] For example, the O–H bond cleavage in oxygen vacancies has been studied in detail by STM studies.[36] The change in the TOF as a function of illumination intensity in the present study similarly favors the thermal over photochemical pathway of methoxy formation, as a second order behavior required for a two-photon process is never observed, even not at low illumination intensities.

The appearance of the stoichiometric amounts of formaldehyde and H_2 demonstrates that the role of the co-catalyst in the chemical reaction is only to enable the recombination of hydrogen atoms of the hydroxylated TiO_2 crystal (eqn (2) and (3)):

$$CH_3OH_{ad}/TiO_2 \xrightarrow{h\nu} CH_2O\uparrow + 2H_{ad}/TiO_2 \quad (2)$$

$$2H_{ad}/TiO_2 \xrightarrow{Pt_n} H_2\uparrow + TiO_2 \quad (3)$$

As seen from these reaction equations, an electron-consuming reduction of H^+ at the metal clusters can be excluded due to the conservation of charges. This is also in agreement with the reaction conditions of our experiments, in which solvated H^+ moieties do not appear.

With the hole-mediated disproportionation reaction mechanism, a straightforward interpretation of the observations in this work can readily be given:

As the platinum co-catalysts only act as recombination centers for atomic hydrogen, which also has been proposed previously,[37] charge carrier dynamics do not significantly influence the reaction step of hydrogen formation. Instead, the migration of hydrogen atoms to the co-catalysts plays a crucial role. In this regard, it has only recently been shown that the diffusion of hydrogen is efficiently facilitated over large distances on TiO_2, which has been attributed to the redox properties of the semiconductor.[38] As a result, the distance of the co-catalyst to the center of the photoreaction is not of paramount importance for the H_2 evolution rate.

The comparison of eqn (2) and (3) with eqn (1) demonstrates that the release of H_2 occurs *via* the recombination of hydrogen atoms on the co-catalyst, which has already been facilitated thermally (see Fig. S10, ESI†). This is further evidenced by the decay in product formation after the illumination is stopped. As the removal of the hydroxylation represents a consecutive thermal reaction of the photoreaction, the H_2 signal decays slower than that of formaldehyde (see Fig. 1b).

The reaction requires only one photon per hydrogen molecule, which is further evidenced in the illumination dependent TOFs, which show a first-order behavior transferring into a saturation regime at higher illumination intensities (Fig. S6, ESI†). This is in excellent agreement with previous reports on hydrogen evolution from alcohols.[39,40]

The proposed mechanism does not only consider the charge balance and catalytic reaction behavior, but is also in good agreement with findings from semiconductor physics. As the TiO_2 single crystal represents a bulk oxide n-type semiconductor, surface band bending must strongly be considered, which is different to nano-structured systems. On an n-type semiconductor, photoholes highly tend to migrate to the negatively charged surface states, while photogenerated electrons preferentially move toward the bulk. Consumption of these photoholes causes flattening of the semiconductor bands, which results in an increased rate of surface state regeneration by the corresponding photoelectrons. Note that negative surface states resulting from point defects are about 0.3 eV lower in energy than the conduction band edge.[41,42]

The resulting neutral charge balance is fully compatible with the mechanism described above. These consequences from semiconductor physics for the surface photochemistry are illustrated in Fig. 4.

In summary, some important consequences result from these findings:

1. The new mechanism for molecular hydrogen evolution extends the range of possible semiconductor materials. In particular, hydroxyl-forming oxides may be potential candidates and their conduction band edges do not necessarily have to match the reduction potential of hydrogen, as it is illustrated here in the case of rutile decorated with co-catalysts.[6]

2. The amount of co-catalyst for the H_2 evolution has only a very weak influence on the TOF. While vital for the formation of molecular hydrogen, a coverage of 0.02% (which amounts to a loading of 0.01 wt% for typical 20 nm rutile particles) results in a considerably strong H_2 signal. This effect can readily be explained with the reaction mechanism: as the co-catalyst only enables hydrogen recombination, its loading only plays a minor role in comparison to the formation of formaldehyde, which is the rate-determining step.

View Article Online
PCCP Paper

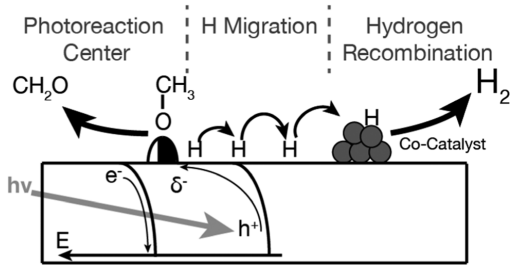

Fig. 4 The photocatalytic mechanism governed by the negative surface states of the n-type semiconductor. By light absorption, the methoxy species is photooxidized by one hole in the partially negatively charged surface states, leading to formaldehyde desorption from the photoreaction center. The co-generated H-atoms migrate on the surface to the co-catalysts (in this case Pt clusters), which act as a recombination center. As the dissociative adsorption of methanol already occurs thermally in the dark on the semiconductor, only one photon is needed for the photocatalytic reaction in the case of TiO_2.

3. As photoactive sites on the semiconductor enable the α-H abstraction from alcohols, it is vital that the co-catalyst does not block them. While the exact site for the photo-oxidation may be a BBO vacancy[10] or a regular Ti_{5c} site,[14,15] it is certainly closely associated with the negative surface states of the semiconductor as they are the driving force for the photoholes to migrate to the surface.[43] Consequently, the procedure of co-catalyst preparation may be essential for the photoreaction yield.[44] The optimal preparation procedure may differ for different metals, depending on the metal mobility on the semiconductor.[23]

4. The mechanism also illustrates that there may exist intrinsic differences of photocatalysis in comparison to photoelectrocatalysis other than the absence of voltage. These differences may be associated with disadvantages (*e.g.* significant contributions of the back reaction), but also with advantages as both half-reactions are not strictly separated from each other.

While these findings are obtained for the hydrogen evolution reaction from alcohol reforming, the thermal reaction steps (abstraction of the first hydrogen atom,[45] H-migration[45] and -recombination) may similarly contribute to the hydrogen evolution reaction in photocatalytic water splitting. This is evidenced by a recent study, in which it has been demonstrated that H_2 has been released thermally in water already at low temperatures.[46] Similarly, the hydroxylation of the TiO_2 single crystal upon water treatment[47] gets removed in the loaded platinum cluster, after which the same TOF for the reaction with methanol is observed (see Fig. S12, ESI†). In addition, based on studies of H. Idriss and co-workers, we speculate that the generation of molecular hydrogen in the photocatalysis of alcohols occurs *via* a similar mechanism on palladium and gold loaded TiO_2 [48] and maybe even on anatase,[49] as it is reported that the reaction pathways are the same and only the reaction rate is affected. Concerning further earth-abundant metals, a recent study of Montoya and Gillan shows that also cobalt, nickel and copper facilitate alcohol reforming in a similar way.[50] As all these metals (Pt, Au, Pd, Co, Ni, Co and Cu) are typical hydrogenation catalysts they enable the cleavage of H_2 and, consequently, also its formation from H-atoms. Therefore, these studies further support our proposed reaction mechanism.

Conclusions

In this work we present an alternative reaction mechanism in alcohol photoreforming, which is significantly different to the commonly used one derived from photoelectrochemistry. It comprises three different reaction steps, which are the photoreaction at one photocatalytic center, the migration of hydrogen on the surface and their thermal recombination at the cluster. In contrast to the established mechanism, it considers the surface chemistry of the material and describes the reaction pathway under the reaction conditions applied in this work. Furthermore, it explains the observed one-photon dependence and includes concepts from semiconductor physics. While the mechanism may be transferred to other semiconductors, in particular to other reducible oxides, it also highlights that photocatalytic systems may behave completely different to photoelectrocatalytic ones.

Conflicts of interest

There are no conflicts to declare.

Acknowledgements

We thank the DFG through grants HE3435/22-1 and STU139/12-1 for financial support.

Notes and references

1 J. A. Turner, *Science*, 2004, **305**, 972–974.
2 K. Maeda, K. Teramura, D. Lu, T. Takata, N. Saito, Y. Inoue and K. Domen, *Nature*, 2006, **440**, 295.
3 T. Hisatomi, J. Kubota and K. Domen, *Chem. Soc. Rev.*, 2014, **43**, 7520–7535.
4 Q. Wang, T. Hisatomi, Q. Jia, H. Tokudome, M. Zhong, C. Wang, Z. Pan, T. Takata, M. Nakabayashi, N. Shibata, Y. Li, I. D. Sharp, A. Kudo, T. Yamada and K. Domen, *Nat. Mater.*, 2016, **15**, 611–615.
5 S. Chen and L.-W. Wang, *Chem. Mater.*, 2012, **24**, 3659–3666.
6 T. R. Esch and T. Bredow, *Surf. Sci.*, 2017, **665**, 20–27.
7 V. J. Babu, S. Vempati, T. Uyar and S. Ramakrishna, *Phys. Chem. Chem. Phys.*, 2015, **17**, 2960–2986.
8 C. A. Walenta, S. L. Kollmannsberger, R. N. Pereira, M. Tschurl, M. Stutzmann and U. Heiz, *J. Phys. Chem. C*, 2017, **121**, 16393–16398.
9 S. L. Kollmannsberger, C. A. Walenta, A. Winnerl, S. Weiszer, R. N. Pereira, M. Tschurl, M. Stutzmann and U. Heiz, *J. Phys. Chem. C*, 2017, **121**, 8473–8479.
10 C. A. Walenta, S. L. Kollmannsberger, J. Kiermaier, A. Winbauer, M. Tschurl and U. Heiz, *Phys. Chem. Chem. Phys.*, 2015, **17**, 22809–22814.

11 C. A. Walenta, S. L. Kollmannsberger, C. Courtois, M. Tschurl and U. Heiz, *Phys. Chem. Chem. Phys.*, 2018, **20**, 7105–7111.
12 S. L. Kollmannsberger, C. A. Walenta, C. Courtois, M. Tschurl and U. Heiz, *ACS Catal.*, 2018, **8**, 11076–11084.
13 D. M. Fabian, S. Hu, N. Singh, F. A. Houle, T. Hisatomi, K. Domen, F. E. Osterloh and S. Ardo, *Energy Environ. Sci.*, 2015, **8**, 2825–2850.
14 J. Ø. Hansen, R. Bebensee, U. Martinez, S. Porsgaard, E. Lira, Y. Wei, L. Lammich, Z. Li, H. Idriss, F. Besenbacher, B. Hammer and S. Wendt, *Sci. Rep.*, 2016, **6**, 21990.
15 M. Shen and M. A. Henderson, *J. Phys. Chem. Lett.*, 2011, **2**, 2707–2710.
16 K. R. Phillips, S. C. Jensen, M. Baron, S.-C. Li and C. M. Friend, *J. Am. Chem. Soc.*, 2013, **135**, 574–577.
17 C. Xu, W. Yang, Q. Guo, D. Dai, M. Chen and X. Yang, *J. Am. Chem. Soc.*, 2013, **135**, 10206–10209.
18 W. Chu, W. A. Saidi, Q. Zheng, Y. Xie, Z. Lan, O. V. Prezhdo, H. Petek and J. Zhao, *J. Am. Chem. Soc.*, 2016, **138**, 13740–13749.
19 Q. Guo, C. Xu, W. Yang, Z. Ren, Z. Ma, D. Dai, T. K. Minton and X. Yang, *J. Phys. Chem. C*, 2013, **117**, 5293–5300.
20 K. Wang, Z. Wei, B. Ohtani and E. Kowalska, *Catal. Today*, 2018, **303**, 327–333.
21 G. R. Bamwenda, S. Tsubota, T. Nakamura and M. Haruta, *J. Photochem. Photobiol., A*, 1995, **89**, 177–189.
22 N. Isomura, X. Wu and Y. Watanabe, *J. Chem. Phys.*, 2009, **131**, 164707.
23 A. Sasahara, C. L. Pang and H. Onishi, *J. Phys. Chem. B*, 2006, **110**, 17584–17588.
24 M. Nesselberger, M. Roefzaad, R. Fayçal Hamou, P. Ulrich Biedermann, F. F. Schweinberger, S. Kunz, K. Schloegl, G. K. H. Wiberg, S. Ashton, U. Heiz, K. J. J. Mayrhofer and M. Arenz, *Nat. Mater.*, 2013, **12**, 919.
25 C. N. Rusu and J. T. Yates, *Langmuir*, 1997, **13**, 4311–4316.
26 A. Linsebigler, C. Rusu and J. T. Yates, *J. Am. Chem. Soc.*, 1996, **118**, 5284–5289.
27 Z. Zhang, W. Tang, M. Neurock and J. T. Yates, *J. Phys. Chem. C*, 2011, **115**, 23848–23853.
28 N. Hykaway, W. M. Sears, H. Morisaki and S. R. Morrison, *J. Phys. Chem.*, 1986, **90**, 6663–6667.
29 A. Yamakata, T.-a. Ishibashi and H. Onishi, *J. Phys. Chem. B*, 2002, **106**, 9122–9125.
30 G. Kolesov, D. Vinichenko, G. A. Tritsaris, C. M. Friend and E. Kaxiras, *J. Phys. Chem. Lett.*, 2015, **6**, 1624–1627.
31 N. Hykaway, W. M. Sears, H. Morisaki and S. R. Morrison, *J. Phys. Chem.*, 1986, **90**, 6663–6667.
32 P. M. Jayaweera, E. L. Quah and H. Idriss, *J. Phys. Chem. C*, 2007, **111**, 1764–1769.
33 U. Martinez, J. Ø. Hansen, E. Lira, H. H. Kristoffersen, P. Huo, R. Bechstein, E. Lægsgaard, F. Besenbacher, B. Hammer and S. Wendt, *Phys. Rev. Lett.*, 2012, **109**, 155501.
34 E. Farfan-Arribas and R. J. Madix, *J. Phys. Chem. B*, 2002, **106**, 10680–10692.
35 M. Shen, D. P. Acharya, Z. Dohnálek and M. A. Henderson, *J. Phys. Chem. C*, 2012, **116**, 25465–25469.
36 Z. Zhang, O. Bondarchuk, J. M. White, B. D. Kay and Z. Dohnálek, *J. Am. Chem. Soc.*, 2006, **128**, 4198–4199.
37 J. B. Joo, R. Dillon, I. Lee, Y. Yin, C. J. Bardeen and F. Zaera, *Proc. Natl. Acad. Sci. U. S. A.*, 2014, **111**, 7942–7947.
38 W. Karim, C. Spreafico, A. Kleibert, J. Gobrecht, J. VandeVondele, Y. Ekinci and J. A. van Bokhoven, *Nature*, 2017, **541**, 68–71.
39 A. S. Hainer, J. S. Hodgins, V. Sandre, M. Vallieres, A. E. Lanterna and J. C. Scaiano, *ACS Energy Lett.*, 2018, **3**, 542–545.
40 T. Ohno, S. Izumi, K. Fujihara, Y. Masaki and M. Matsumura, *J. Phys. Chem. B*, 2000, **104**, 6801–6803.
41 W. Göpel, J. A. Anderson, D. Frankel, M. Jaehnig, K. Phillips, J. A. Schäfer and G. Rocker, *Surf. Sci.*, 1984, **139**, 333–346.
42 C. M. Yim, C. L. Pang and G. Thornton, *Phys. Rev. Lett.*, 2010, **104**, 036806.
43 Z. Zhang and J. T. Yates, *Chem. Rev.*, 2012, **112**, 5520–5551.
44 G. M. Haselmann and D. Eder, *ACS Catal.*, 2017, **7**, 4668–4675.
45 Z. Zhang, O. Bondarchuk, B. D. Kay, J. M. White and Z. Dohnálek, *J. Phys. Chem. B*, 2006, **110**, 21840–21845.
46 Z. Geng, X. Jin, R. Wang, X. Chen, Q. Guo, Z. Ma, D. Dai, H. Fan and X. Yang, *J. Phys. Chem. C*, 2018, **122**, 10956–10962.
47 M. A. Henderson, *Langmuir*, 1996, **12**, 5093–5098.
48 Z. H. N. Al-Azri, W.-T. Chen, A. Chan, V. Jovic, T. Ina, H. Idriss and G. I. N. Waterhouse, *J. Catal.*, 2015, **329**, 355–367.
49 M. Murdoch, G. I. N. Waterhouse, M. A. Nadeem, J. B. Metson, M. A. Keane, R. F. Howe, J. Llorca and H. Idriss, *Nat. Chem.*, 2011, **3**, 489–492.
50 A. T. Montoya and E. G. Gillan, *ACS Omega*, 2018, **3**, 2947–2955.

Electronic Supplementary Material (ESI) for Physical Chemistry Chemical Physics.

Supporting Information: Why Co-Catalyst-Loaded Rutile Facilitates Photocatalytic Hydrogen Evolution

Constantin A. Walenta [a,b,†], Sebastian L. Kollmannsberger[a,†], Carla Courtois[a], Rui N. Pereira[c], Martin Stutzmann[b,c], Martin Tschurl[a], Ueli Heiz[a,b,*]

[a]Chair of Physical Chemistry, Department of Chemistry & Catalysis Research Center, Technische Universität München, Lichtenbergstr. 4, 85748 Garching, Germany
[b]Nanosystems Initiative Munich, Schellingstr. 4, 80799 München, Germany
[c]Walter Schottky Institute and Physics Department, Technische Universität München, Am Coulombwall 4, 85748 Garching

*corresponding author: email ulrich.heiz@tum.de
† The authors contributed equally to this work

1. Catalyst Preparation

A rutile TiO_2(110) single crystal (Surface-net GmbH) was cleaned by several cycles of sputtering (Ar, 1.0 keV, 7×10^{-6} mbar) and annealing at 850 K in vacuum, which results in an atomically flat surface, while the crystal shows a light blue color indicating a slightly reduced surface [r-TiO_2(110)]. Over the course of the experiments, the crystal was sputtered (same conditions), annealed in oxygen atmosphere (1×10^{-6} mbar, 820 K) for 20 min and vacuum annealed at 820 K for 10 min. This recipe is known to result in a clean surface with a constant bridge-bonding oxygen (BBO) vacancy concentration.[1]
The Pt (99.95% purity, ESG Edelmetalle, Germany) clusters are generated by a laser vaporization source coupled with a quadrupole mass spectrometer (Extrel, USA). In this work, the quadrupole mass spectrometer was operated with the AC-potential only, acting as an ion guide. The resulting size-distribution is then determined by the pressure and voltage settings and kept constant over the course of the experiments.[2] The Pt clusters are deposited on the r-TiO_2(110) surface under soft-landing conditions (< 1eV/atom in kinetic energy). The resulting catalyst is therefore named Pt_x/TiO_2(110) in the following. Between the experiments, a few cycles in sputtering, lasting in total more than 1h, were employed to facilitate a clean surface. The surface purity is verified by D_2-TPD, since also the smallest contamination of Pt clusters on the surface leads to a desorption feature in a TPD between 200 K and 300 K.

The platinum cluster coverages investigated in this work are displayed in Table 1. The coverages are given in %ML respective to the 1.5×10^{15} surface atoms of the TiO_2(110) surface.[3] They are determined by the neutralization current of soft-landed cationic Pt clusters measured by a picoammeter (Keithley 6587).

Table 1: Cluster coverages used in this work on the TiO_2(110) surface.

%ML [cm^2]	Number of clusters [e/nm^2]	Number of clusters [e/cm^2]
0.02	0.003	3×10^{11}
0.1	0.015	1.5×10^{12}
0.12	0.018	1.8×10^{12}
0.5	0.075	7.5×10^{12}
1.0	0.15	1.5×10^{13}

Methanol (Chromasolv, ≥99.9% purity) and Methanol-d_3 (Sigma Aldrich, 99.8 atom % D) are cleaned via several pump-freeze cycles and either introduced by dosing or in a constant background.

2. Catalyst Characterization

The absence of contaminants from the r-TiO_2(110) surface is deduced from Auger Electron Spectroscopy (AES) as shown in Figure S1. Further, the surface of a light blue crystal shows a certain BBO vacancy concentration. The vacancies can be observed either by STM[4] or by titration experiments.[3, 5, 6] In this study, the BBO-vacancy density was about 6±1% of the Ti-lattice sites as determined by temperature programmed desorption (TPD) of H_2O (Fig. S2).
The cluster size distribution is checked before every experiment and determined by a mass scan over all sizes. The resulting mass spectrum is displayed in Figure S3. The clusters are deposited randomly on the surface and show no preferential adsorption as evidenced by Kelvin Probe Force Microscopy and STM.[7-9]

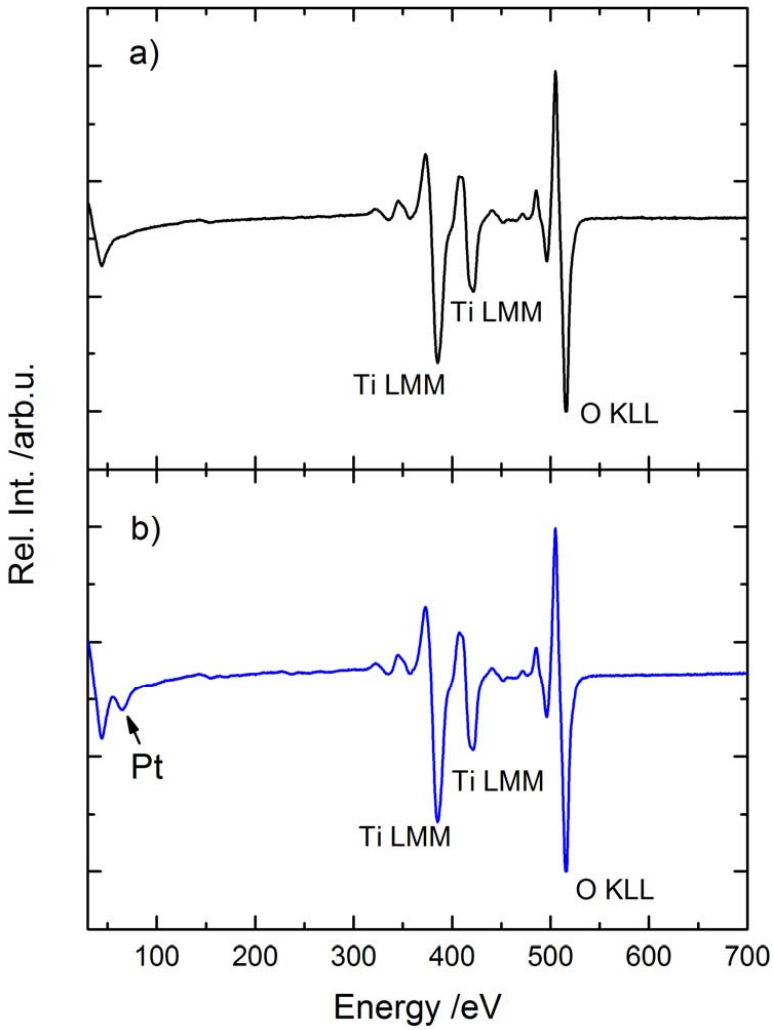

Fig. S1: Auger Electron Spectrum of the r-TiO_2(110) surface (a) and Pt_x/r-TiO_2(110) (b). Titanium and oxygen are observed for the rutile TiO_2(110) surface, while a small feature of Pt NOO Peak is observed at 64 eV. The coverage is 1% Pt_x/ML.

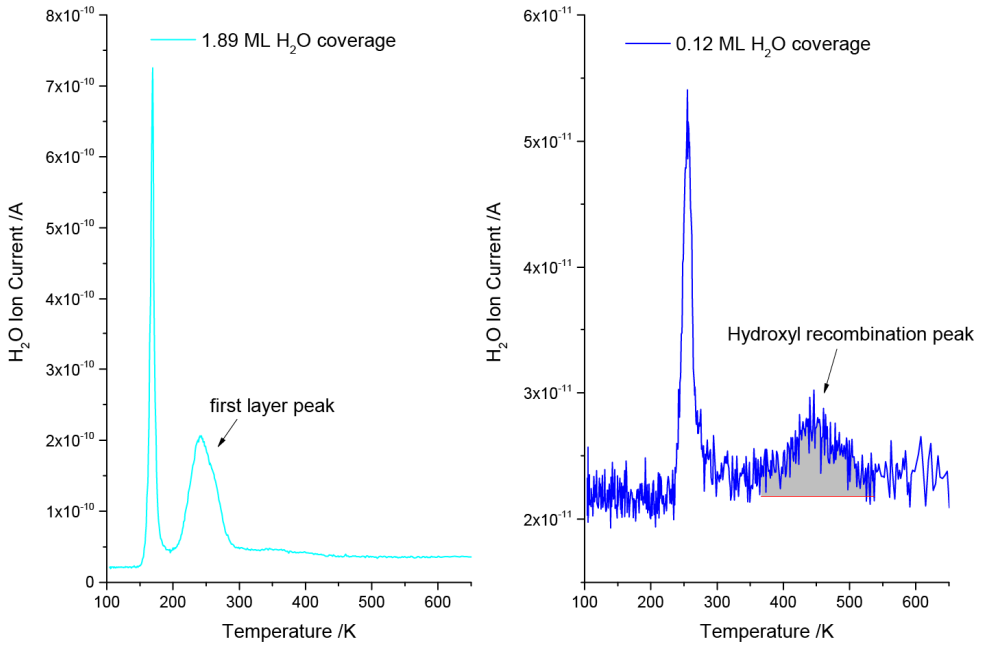

Fig. S2: TPD spectra of H_2O on the r-TiO_2(110) surface. In S2a, the TPD of 1.89 ML of H_2O dosed on the surface is shown and is in excellent agreement with literature.[5, 10, 11] The first layer peak is assigned to water desorbing from Ti-lattice sites, while the feature at around 170 K is attributed to water on BBO-sites and multilayer adsorption. Figure S2b shows a smaller coverage, where the hydroxyl recombination peak is clearly observed around 460 K. The grey area indicate the integrated area, that is compared to the integral of the first layer peak in S2a, to obtain a BBO-vacancy concentration of 6 ±1% of Ti-lattice sites.

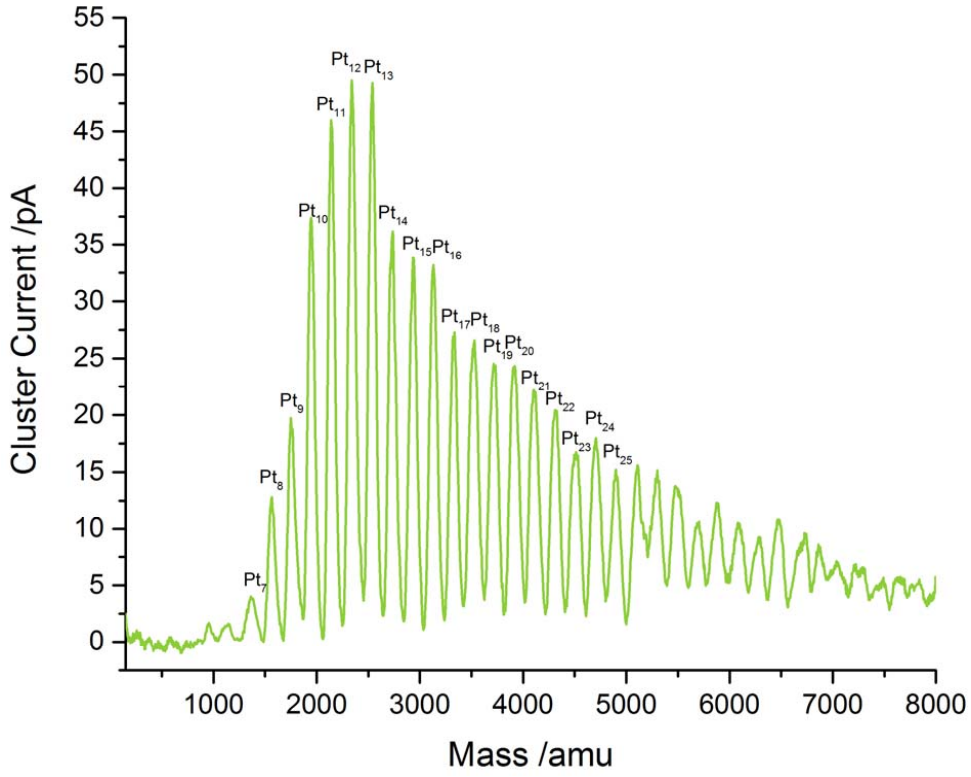

Fig. S3: Mass spectrum of the cluster size distribution of Pt clusters from the laser vaporization source. The spectrum is taken after the quadrupole mass filter and shows a size-distribution of Pt_7 up to Pt_{32}. When depositing in the ion guide mode, all masses lower than Pt_8 are discarded. The clusters show a log-normal distribution and have a size of about 1 nm in diameter.[2]

3. Thermal Reaction Products

To understand photocatalytic mechanism on an atomic scale, first the methanol chemistry on r-TiO_2(110) is explored (see Fig. S4) which is found to be in very good agreement with literature.[12-14] In comparison with Fig. S4, a TPD of 1 L of methanol-d_3 on Pt_x/r-TiO_2(110) (1% cluster coverage) (Fig. S5) shows significant thermal hydrogen desorption between 250 K and 350 K, accompanied by significant CO desorption between 350 K and 500 K from the Pt clusters.

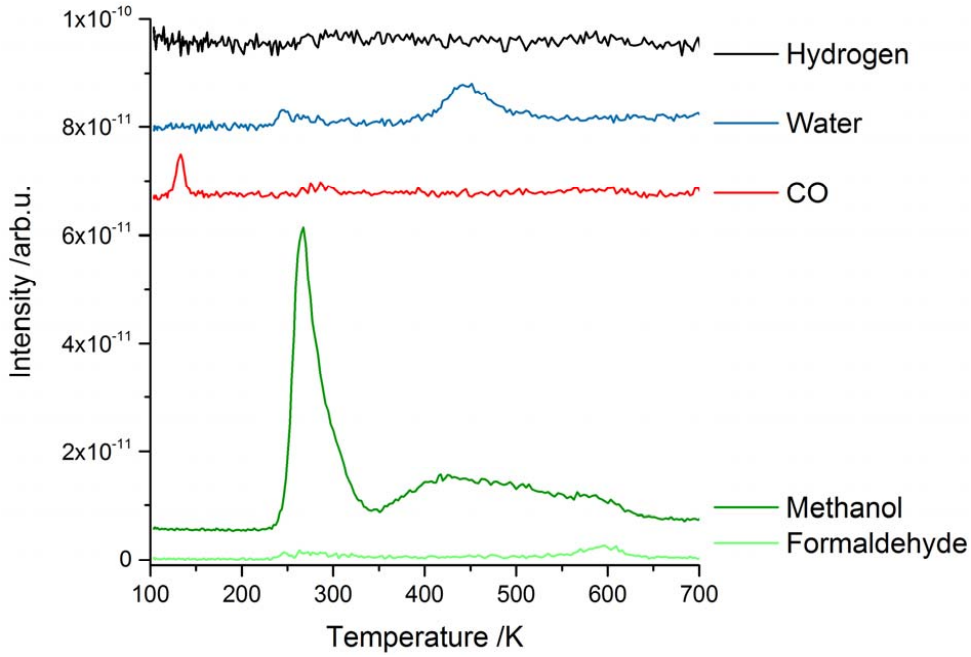

Fig. S4: TPD of 1 L of methanol on r-TiO_2(110). Molecular methanol mainly desorbs at 270 K from Ti-lattice sites. The high temperature feature at 480 K is associated with recombinative desorption of dissociated methanol and trace amounts of formaldehyde are obtained around 600 K. No molecular hydrogen formation is observed from methanol. The excess hydrogen from formaldehyde formation typically forms water on oxides, as observed from the water desorption at 470 K. The small CO signal at 125 K is attributed to background adsorption. The traces are offset for clarity.

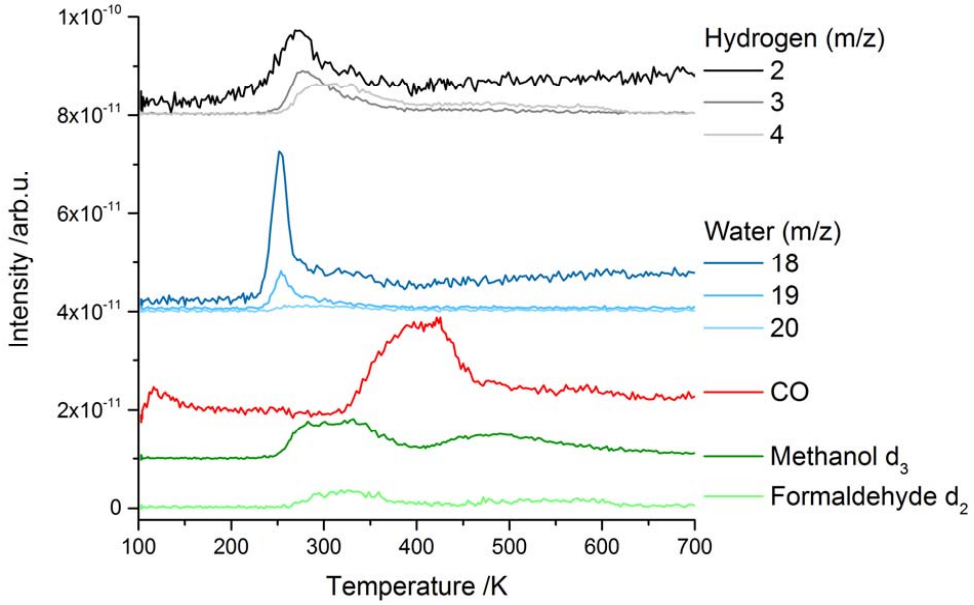

Fig. S5: TPD of 1 L of methanol-d_3 on Pt_x/r-TiO_2(110). In this experiment, isotopically labeled methanol CD_3OH is used to explore the thermal reactions on Pt-loaded TiO_2(110). While the methanol signal is less intense, both molecular and dissociative adsorption are observed on the TiO_2 surface. No intact desorption of methanol or formaldehyde from Pt is observed. Instead, the dehydrogenation products hydrogen and CO ultimately desorb at higher temperature. Methanol-d_3 on Pt is completely decomposed and hydrogen desorbs between 250 K and 350 K. Additionally, CO is observed between 350 and 500 K, as is expected for a CO TPD from Pt nanoparticles on TiO_2(110).[15] Additionally, some water is observed at 240 K. The traces are grouped and offset for clarity.

4. Photocatalytic Activity-Measurements

For the photocatalytic measurements, the catalyst is prepared and moved to the QMS. The pulse energy of the laser is monitored and the reactant is dosed at cryogenic conditions, unless stated otherwise. The crystal is heated to the reaction temperature and then the UV-illumination is started.
To determine turnover-frequencies (TOFs), the catalyst is exposed to a continuous background of a certain methanol pressure and the UV illumination is facilitated and blocked. Areas of constant photoconversion of methanol to H_2 (m/z=2) and formaldehyde (m/z=30) are chosen and both signals are integrated over time. For both species, transmission of the calibrated QMS, ionization cross sections and cracking pattern contributions are taken into account. The following integral area is normalized by the integral of a methanol TPD peak of the Ti-lattice sites (1 ML = 5.2×10^{14}).[10] To calculate the TOF or site time yield (STY), this integral is divided by the time and by the number of active sites for formaldehyde production (0.06 ML, in this case for the BBO-vacancies[14] [see Fig. S2]) to yield a number of molecules per active site per second. Stoichiometry was checked for every catalytic experiment (see Fig. S8). This TOF is possibly still limited by mass transport, but pressures higher than 4×10^{-7} mbar were not investigated to ensure the proper detection by QMS.
The apparent quantum yield (AQY) can be calculated by relating the number of evolved molecules per second to the photon flux:[16, 17]

$$AQY\ (\%) = \frac{Product\ molecules\ (s^{-1})}{Photons\ (s^{-1})} \times 100 \quad (1)$$

In this work, the amount of product molecules (either formaldehyde or hydrogen) is divided by the number of incident photons from the laser.
In the classical picture, two charges are needed to oxidize methanol to formaldehyde as well as reduce protons to H_2.[17-19] For the lowest photon fluxes (compare to Fig. 3b), a quantum yield of 3.2% is obtained, while in the saturation regime (see Fig. 3b), the quantum yield is about 0.11%.

5. Methanol Photocatalysis on $Pt_x/TiO_2(110)$

Photocatalytic measurements were performed on the r-TiO_2(110) surface with different loadings of Pt clusters on the surface. Then a background pressure of methanol is applied and the reaction temperature is chosen. The photocatalytic reaction is then started by the UV illumination.
Figure S7 shows, that upon the first illumination a conditioning of the catalyst is observed, that is then constant with every additional illumination. The obtained reaction products are stoichiometric. A one-photon dependence for the H_2 evolution is found for the lowest light intensities, while for the higher ones a saturation regime is observed (Fig. S6).
In Figure S8, it is shown that the photocatalytic reaction is independent on the used wavelength, when the energy of the photon is higher than the semiconductor's band gap and furthermore independent on pulsed or continuous illumination, at least to a ns-Laser with 20 Hz. In Fig. S10 the thermal H_2 peak from dissociatively adsorbed methanol is shown prior to a photocatalytic experiment with Pt loaded TiO_2(110). The

comparison of O_2 photon-stimulated desorption (PSD) on a bare surface and after the used photocatalyst gives evidence that it is possible to empty all active sites for the oxidation reaction.[14]

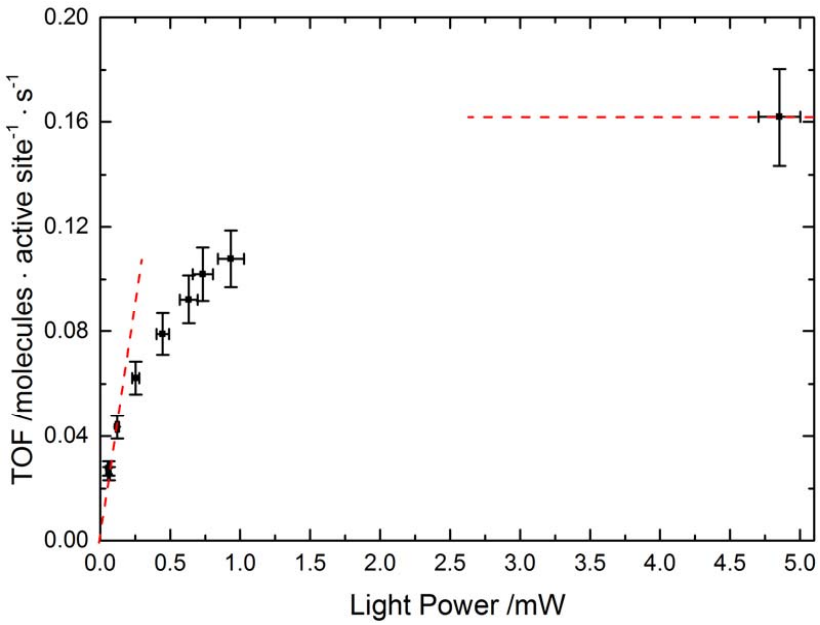

Fig. S6: The TOF of formaldehyde as a function of the illumination intensity is shown. While for low illumination intensities a linear behavior is found, the signal saturates at higher values. This observation is not in line with a two-photon process, for which a quadratic dependence with light power would arise. The dotted red lines indicate the transition from the regime of first order behavior into the one of saturation. The error bars in energy are determined by the standard deviation of the laser power, while the TOF errors bars are of 10%, except for the one at 5 mW, which represents the standard deviation of four measurements.

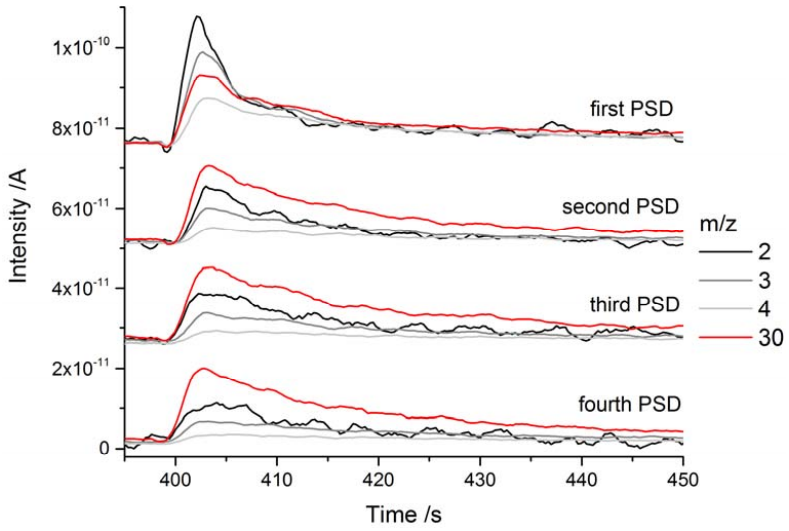

Fig. S7: Consecutive photocatalytic experiments with methanol on Pt_x/r-TiO_2(110). The Pt coverage is 0.75% cluster per surface atom and the reaction is carried out at 260 K after adsorption of 1L methanol-d_3. In contrast to Fig. 1(a), no catalyst poisoning is observed after an initial conditioning of the catalyst. Formaldehyde is measured with mass 30, while all hydrogen species are measured on the masses 2, 3 and 4. Between the cycles, the surface is recovered with 1 L of methanol-d_3. In the first experiments, more H_2 is observed, which is attributed to dissociative methanol adsorption and an unknown degree of pre-hydroxylation of the semiconductor. In all runs, the formaldehyde intensity and kinetic decay stays the same and after the conditioning in the first shot, the same holds true for all hydrogen traces.

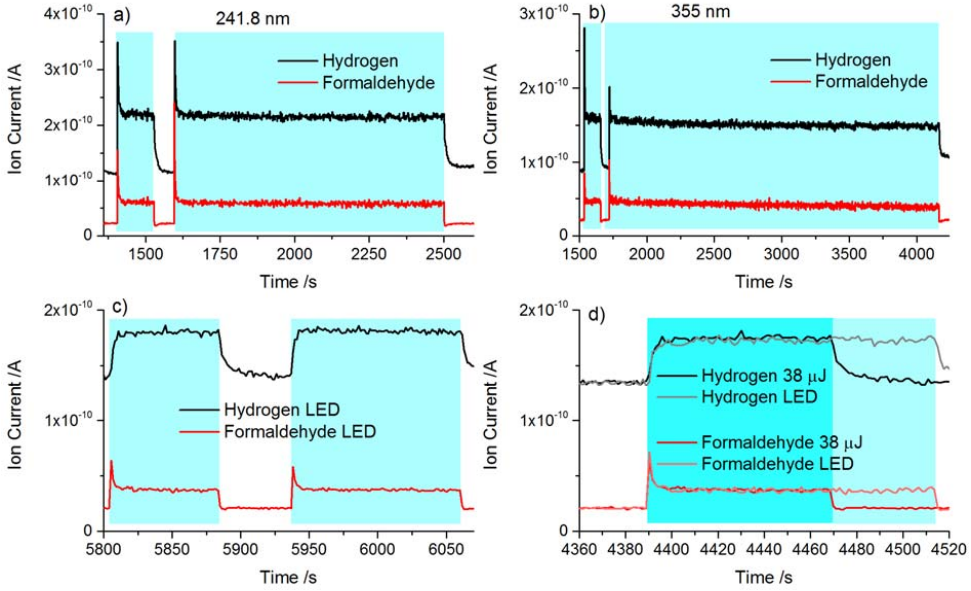

Fig. S8: Photocatalytic experiments depending on wavelength and illumination conditions with $Pt_x/TiO_2(110)$ and a cluster coverage of 1% in a background of 1×10^{-7} mbar methanol are shown. In a), the sample is illuminated with 250 µJ pulse energy (this corresponds to 5 mW) at 241.8 nm, and with illumination the reaction starts immediately. The reaction stops immediately, when the light is switched off and also runs constant. In panel b), the pulse energy is also hold constant at 250 µJ, but the wavelength is changed to 355 nm. The same amounts of hydrogen and formaldehyde are obtained, also in the second illumination over a time of 45 min. In c), the light source is exchanged from the ns-Laser with 20 Hz to a continuous light source. In this case, this light source is a UV-LED that emits light around 367 nm (see Fig. S9 for details), well above the band gap value for rutile TiO_2 of 3.0 eV. The photocatalytic reaction of methanol shows the same behavior as in a) and b). In panel d), a direct comparison of the LED to laser excitation is shown, while the pulse energy of the laser is only 38 µJ at 241.8 nm and the characteristics show no appreciable difference.

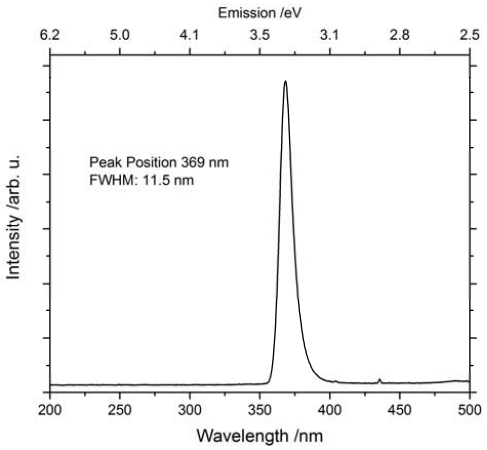

Fig. S9: Light emission characteristics of the UV-LED. The emission is centered around 369 nm with a full-width half maximum of 11.5 nm.

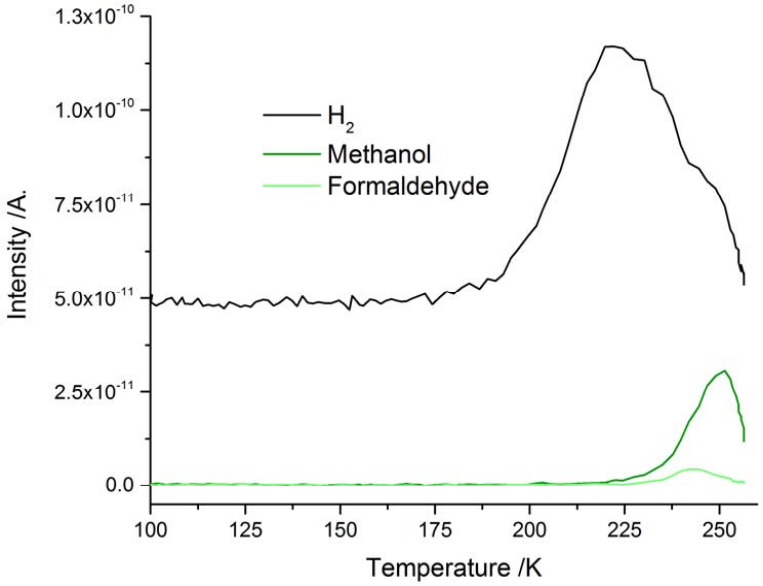

Fig. S10: TPD in a background of 1×10^{-7} mbar methanol on 1‰ $Pt_x/TiO_2(110)$ from 100 K to the reaction temperature at 260 K. After oversaturation of the surface at cryogenic temperatures, some methanol desorption occurs around 250 K as it is expected from Fig. S4. In agreement with Fig. S5, hydrogen desorption from the Pt clusters is observed, too. As methanol adsorbs dissociatively on the $TiO_2(110)$, which is known from STM studies[20], the abstracted hydrogen atoms thermally recombine at the Pt clusters and desorb.

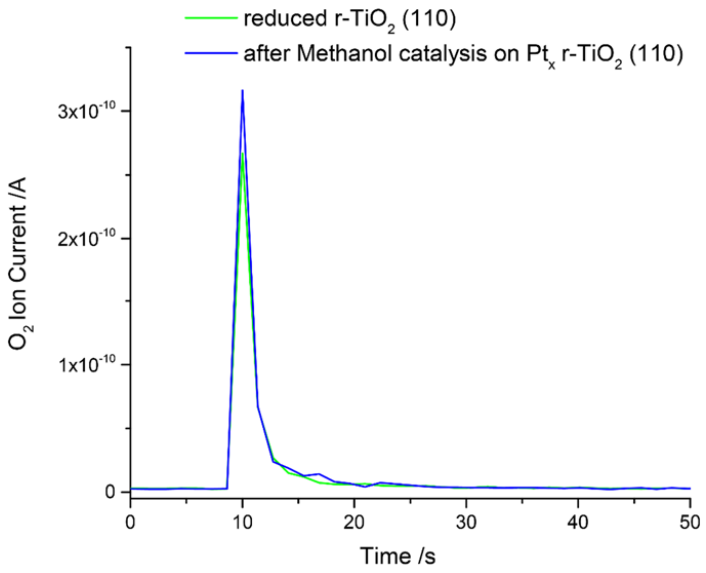

Fig. S11: O_2-Photon Stimulated Desorption at 100 K of the r-TiO_2(110)-surface and the Pt_x/TiO_2(110) catalyst after 2 h of photocatalysis. The green trace represents a O_2 PSD from bare surface, that is in excellent agreement with literature. After the catalytic experiment, the methanol background is turned off and the sample was illuminated for another 15 min to deplete all the methanol from the photo-oxidation sites. After illumination is turned off, the sample was cooled down to 100 K and exposed to 20 L of oxygen, to saturate the surface. Upon UV illumination, the same intensity and kinetics for the O_2 PSD are observed as for the bare sample, indicating that the number of photoactive sites stays constant and that the methanol at least in the active sties was completely converted. (Note that the signals only slightly deviate in their maximum values from each other. This is caused by a higher uncertainty due to the additional uncertainty in the starting time of the illumination.)

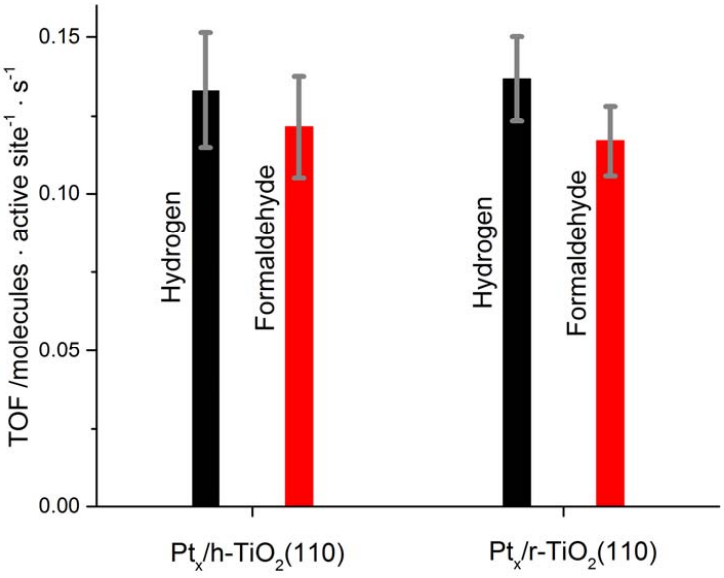

Figure S12: TOFs at 260 K for a background of $1 \cdot 10^{-7}$ mbar methanol on 1‰ Pt_x/TiO2(110) for a reduced and pre-hydroxylated TiO_2(110). The h-TiO_2(110) was prepared in the same way as in a previous study by Kim *et al.*.[21]

References:

1. C. A. Walenta, S. L. Kollmannsberger, J. Kiermaier, A. Winbauer, M. Tschurl and U. Heiz, *Phys. Chem. Chem. Phys.*, 2015, **17**, 22809-22814.
2. A. S. Crampton, M. D. Rötzer, F. F. Schweinberger, B. Yoon, U. Landman and U. Heiz, *J. Catal.*, 2016, **333**, 51-58.
3. U. Diebold, *Surf. Sci. Rep.*, 2003, **48**, 53-229.
4. E. Wahlström, E. K. Vestergaard, R. Schaub, A. Rønnau, M. Vestergaard, E. Lægsgaard, I. Stensgaard and F. Besenbacher, *Science*, 2004, **303**, 511-513.
5. M. A. Henderson, *Langmuir*, 1996, **12**, 5093-5098.
6. G. Lu, A. Linsebigler and J. T. Yates, *J. Phys. Chem.*, 1994, **98**, 11733-11738.
7. A. Sasahara, C. L. Pang and H. Onishi, *J. Phys. Chem. B*, 2006, **110**, 17584-17588.
8. N. Isomura, X. Wu and Y. Watanabe, *J. Chem. Phys.*, 2009, **131**, 164707.
9. S. Bonanni, K. Aït-Mansour, H. Brune and W. Harbich, *ACS Catal.*, 2011, **1**, 385-389.
10. Z. Li, R. S. Smith, B. D. Kay and Z. Dohnálek, *J. Phys. Chem. C*, 2011, **115**, 22534-22539.
11. C. Xu, W. Yang, Q. Guo, D. Dai, M. Chen and X. Yang, *J. Am. Chem. Soc.*, 2013, **135**, 10206-10209.
12. M. A. Henderson, S. Otero-Tapia and M. E. Castro, *Faraday Discuss.*, 1999, **114**, 313-329.
13. M. Shen, D. P. Acharya, Z. Dohnálek and M. A. Henderson, *J. Phys. Chem. C*, 2012, **116**, 25465-25469.
14. M. Shen and M. A. Henderson, *J. Phys. Chem. Lett.*, 2011, **2**, 2707-2710.
15. A. Linsebigler, C. Rusu and J. T. Yates, *J. Am. Chem. Soc.*, 1996, **118**, 5284-5289.
16. A. Kudo and Y. Miseki, *Chem. Soc. Rev.*, 2009, **38**, 253-278.
17. T. Hisatomi, J. Kubota and K. Domen, *Chem. Soc. Rev.*, 2014, **43**, 7520-7535.
18. B. Ohtani, *J. Photochem. Photobiol. C*, 2010, **11**, 157-178.
19. B. Ohtani, *Chem. Lett.*, 2008, **37**, 216-229.
20. Z. Zhang, O. Bondarchuk, J. M. White, B. D. Kay and Z. Dohnálek, *J. Am. Chem. Soc.*, 2006, **128**, 4198-4199.
21. B. Kim, Z. Li, B. D. Kay, Z. Dohnalek and Y. K. Kim, *Phys. Chem. Chem. Phys.*, 2012, **14**, 15060-15065.

A.7 Reactions in the Photocatalytic Conversion of Tertiary Alcohols on Rutile TiO_2(110)

GDCh Communications Angewandte International Edition Chemie

Photocatalysis

International Edition: DOI: 10.1002/anie.201907917
German Edition: DOI: 10.1002/ange.201907917

Reactions in the Photocatalytic Conversion of Tertiary Alcohols on Rutile TiO_2(110)

*Carla Courtois[+], Moritz Eder[+], Kordula Schnabl, Constantin A. Walenta, Martin Tschurl, and Ulrich Heiz**

Abstract: *According to textbooks, tertiary alcohols are inert towards oxidation. The photocatalysis of tertiary alcohols under highly defined vacuum conditions on a titania single crystal reveals unexpected and new reactions, which can be described as disproportionation into an alkane and the respective ketone. In contrast to primary and secondary alcohols, in tertiary alcohols the absence of an α-H leads to a C–C-bond cleavage instead of the common abstraction of hydrogen. Surprisingly, bonds to methyl groups are not cleaved when the alcohol exhibits longer alkyl chains in the α-position to the hydroxyl group. The presence of platinum loadings not only increases the reaction rate but also opens up a new reaction channel: the formation of molecular hydrogen and a long-chain alkane resulting from recombination of two alkyl moieties. This work demonstrates that new synthetic routes may become possible by introducing photocatalytic reaction steps in which the co-catalysts may also play a decisive role. Open access funding enabled and organized by Projekt DEAL.*

The selective oxidation of alcohols to aldehydes and ketones is a fundamental topic in various fields of chemistry ranging from heterogeneous catalysis to synthetic organic chemistry.[1] In contrast to the facile oxidation of primary and secondary alcohols, tertiary alcoholstypically do not react analogously, due to the required cleavage of a C–C instead of a C–H bond to establish the carbonyl functionality.[2] As tertiary alcohol oxidation is generally difficult, in particular in a selective manner, publications on this subject are thus scarce and often a broad product spectrum results.[1c,2,3] Conventional synthetic methods often rely on auxiliary compounds or quantitative amounts of oxidants to enable the reaction in the first place.[4] Often the conversion is conducted with the use of toxic metal oxides such as chromium(VI) oxides.[5]

An alternative approach for alcohol reforming is photocatalysis using semiconductors.[6] For example, Teichner and co-workers successfully photooxidized 2-methyl-2-butanol by means of UV irradiation on a nonporous anatase catalyst in the presence of oxygen. The proposed reaction pathways take place via olefin intermediates, leading to the reaction products acetone, ethanal, and 2-butanone.[7]

In general, titania is by far the most used material in photocatalysis due to its reaction properties and availability.[8] While it is commonly applied in a nanostructure form (e.g. as P25), the material's structural complexity often prevents the elucidation of exact reaction mechanisms.[9] As in thermal catalysis, defined single-crystal surfaces under highly defined conditions in ultra-high vacuum (UHV) are more suitable for this purpose.[10] In heterogeneous photocatalysis, rutile TiO_2-(110) surfaces have been comprehensively employed in alcohol conversion thermally[11] and photochemically.[12] Thus, this material represents the best-suited model system, even though other titania systems (e.g. anatase) may exhibit better photoactivities.

For this report, we investigated the photochemical reaction behavior of longer-chain tertiary alcohols (3-methyl-3-hexanol, 2-methyl-2-pentanol, and 2-methyl-2-butanol) on bare and platinum-loaded rutile TiO_2(110) in an UHV environment in the absence of oxygen and water. We demonstrate that the alcohols undergo unexpected and new photocatalytic reactions, which enable general mechanistic insights. Furthermore, we show that the rich chemistry of tertiary alcohols makes them an interesting model system for photocatalysis. For example, they enable the elucidation of the behavior of alkyl radicals on surfaces, important for the photo-Kolbe reaction[13] and the Fischer–Tropsch process.[14] In the latter, TiO_2 represents a common support material.[15]

The UV illumination of a TiO_2(110) crystal, decorated with a defined coverage (0.1 % monolayer (ML)) of platinum clusters ranging in size range from Pt_8 to about Pt_{25}, leads to a photocatalytic reaction of 3-methyl-3-hexanol, which results in a complex fragmentation pattern in the mass spectrum. However, a detailed analysis reveals (see Figure S2) that only two parallel reactions occur, both of which are an oxidation to a ketone and a corresponding alkane (2-pentanone and ethane, 2-butanone and propane, see Scheme 1). While the formation of higher alkanes is observed, a reaction yielding methane is not. Monitoring mass traces specific for a particular molecule (Figure 1) demonstrates that the reaction is truly catalytic under illumination and formation of unwanted surface species leading to catalyst poisoning does not occur.

[*] C. Courtois,[+] M. Eder,[+] K. Schnabl, Dr. C. A. Walenta, Dr. M. Tschurl, Prof. Dr. U. Heiz
Chair of Physical Chemistry
Department of Chemistry & Catalysis Research Center
Technische Universität München
Lichtenbergstraße 4, 85748 Garching (Germany)
E-mail: ulrich.heiz@mytum.de

[+] These authors contributed equally to this work

Supporting information and the ORCID identification number(s) for the author(s) of this article can be found under: https://doi.org/10.1002/anie.201907917.

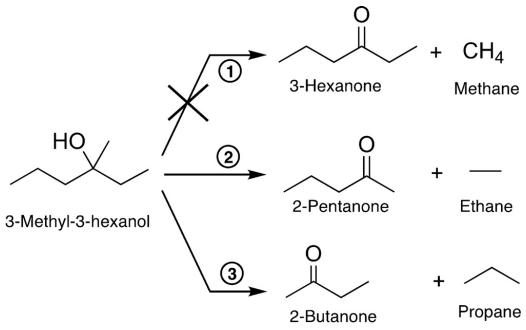

Scheme 1. Reaction scheme for the photoreforming of 3-methyl-3-hexanol on Pt_x/r-TiO_2(110) and on r-TiO_2(110) under UV illumination. The reaction can be seen formally as a hole-mediated disproportionation yielding an alkane and the respective ketone; however, this does not occur for the formation of methane.

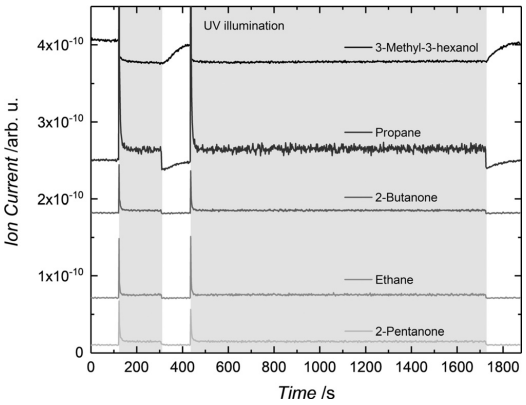

Figure 1. Photocatalytic products of 3-methyl-3-hexanol photoreforming on Pt_x/r-TiO_2(110) (0.1% monolayer (ML) cluster coverage). Signals for 3-methyl-3-hexanol (*m*/*z* 73), propane (*m*/*z* 29), 2-butanone (*m*/*z* 72), ethane (*m*/*z* 30), and 2-pentanone (*m*/*z* 86) are shown at 340 K under a 3-methyl-3-hexanol background pressure of 1.7×10^{-7} mbar. The gray region highlights the period of UV laser irradiation. The initial burst of the signal originates from higher surface concentrations of the alcohol before the start of the illumination. Note that the traces are offset for clarity. The traces demonstrate that two different photocatalytic reactions occur in parallel yielding a ketone and the respective alkane.

Compared to the photoreforming of other alcohols, the observed reaction pathways are unexpected. The absence of an α-H precludes the common C–H cleavage to form H_2 and the respective aldehyde or ketone, as detected for primary and secondary alcohols.[2,16] Therefore, the ejection of radicals and concomitant stoichiometric production of H_2 is expected in analogy to *tert*-butanol photoreforming.[17] Neither radical abstraction nor significant molecular hydrogen formation is detected for prolonged reaction times. Instead, this reaction, which to the best of our knowledge has never been described before, can be viewed as a photocatalytic disproportionation yielding higher alkanes and the respective ketones. Interestingly, reaction products originating from the cleavage of the methyl group are not observed (Figure S9). In the same way, dehydration reactions, common in thermal reactions, also do not occur (Figure S9). The same reaction is observed for tertiary alcohols with two methyl groups at the α-C position (namely, 2-methyl-2-butanol and 2-methyl-2-pentanol), for which only the long carbon chain is abstracted with 100% selectivity (see Figures S3 and S4). Consequently, the formation of acetone and the respective alkane results exclusively. This demonstrates the generality of our findings. The same products are observed under ambient conditions even for 2-methy-2-butanol, but the presence of oxygen and water leads to additional by-products.[7,18]

This new reaction can be explained with the mechanism we suggested for the photoreforming of alcohols on TiO_2 in the gas phase.[17a] The photoactive alkoxy species, which are already formed upon surface adsorption in the dark[12,19] undergo a hole-mediated oxidation reaction, resulting in the cleavage of a C–C bond. The role of alkoxy compounds as the photoactive species on TiO_2(110) in alcohol photoreforming has been demonstrated convincingly in the works of Henderson and others.[12,20] Methyl radical ejection observed with *tert*-butanol demonstrates that the photocatalytic oxidation reaction occurs via a homolytic C–C bond scission. In contrast to methyl groups, longer alkyl chains such as ethyl and propyl exhibit stronger interactions with the TiO_2 surface in their adsorption geometry and thus remain on the surface. This is in perfect agreement with their absence in the mass spectra.

These surface alkyl radicals undergo recombination in a consecutive thermal reaction step with hydrogen atoms originating from the dissociative adsorption of the alcohol. This reaction is also facilitated on bare TiO_2(110) (i.e., in the absence of Pt) in contrast to the recombination of two hydrogen atoms. Consequently, photoreforming of higher tertiary alcohols occurs in a photocatalytic manner even without any co-catalyst (Figure 2a) and on a hydroxylated surface (as shown in Figure S13 for 2-methyl-2-pentanol photoreforming), in contrast to α-H-containing alcohols. For the latter, surface hydroxylation results in the poisoning of the photocatalyst.[17a] The deposition of small amounts of Pt clusters significantly increases the overall reaction rate, with higher loadings leading only to a small increase in the turnover frequency (TOF) (Figure 2a). This trend is in good agreement with findings from methanol photoreforming in UHV[17a] and with colloidal systems.[21]

In good accordance with the interpretation of the photooxidation on the semiconductor and a consecutive alkane formation, the selectivity of the reaction of 3-methyl-3-hexanol remains unaffected by the degree of Pt coverage (Figure 2b). It also remains constant at temperatures (Figure S8b) between 230 and 360 K, further demonstrating the photocatalytic nature of the reaction. In order to explain the observed selectivity of pentanone to butanone of about 2:1 (i.e., the preferred cleavage of ethyl over propyl and the general absence of methyl), the thermochemistry of the reactions may be used to obtain qualitative insights. All three possible reactions displayed in Scheme 1 are endothermic by about 20 to 30 kJ mol^{-1} (see the corresponding chapter in the

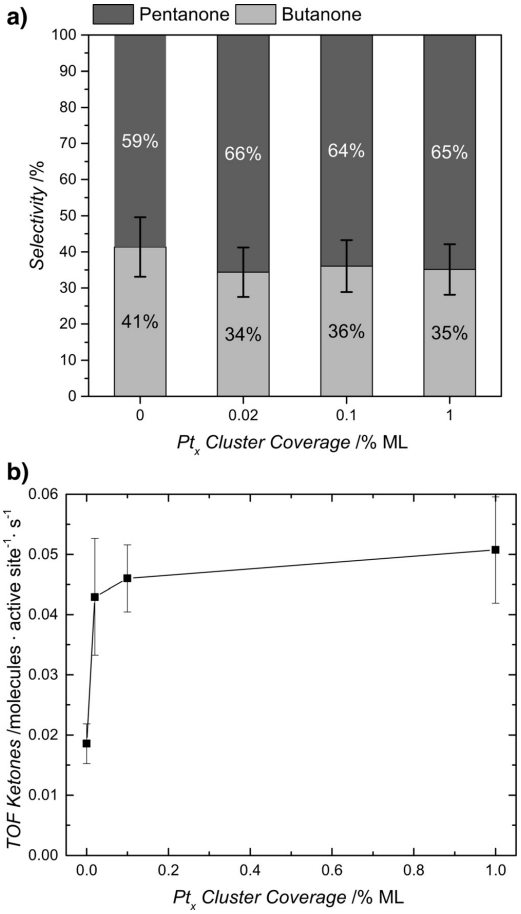

Figure 2. Photocatalytic conversion of 3-methyl-3-hexanol on Pt-decorated r-TiO_2(110). In (a) the TOF of the ketones (sum of 2-butanone and 2-pentanone) is shown for different Pt_x cluster coverages. In (b) the selectivities for 2-pentanone and 2-butanone based on the TOFs are displayed for bare r-TiO_2(110) and for different Pt loadings on r-TiO_2(110). A monolayer ML refers to the surface atoms. 0% ML stands for the bare r-TiO_2(110). While the deposition of Pt clusters does not affect the reaction's selectivity, it initially increases the TOF. However, higher loadings do not have a similar effect.

Supporting Information). Model reactions for the photocatalytic C–C bond cleavage suggest that the formation of methyl radicals requires significantly more energy than ethyl or propyl formation (see details in the Supporting Information). In addition, longer-chain alkyl moieties than methyl exhibit stronger interactions with the surface. These radicals are therefore not detected in the gas phase, in contrast to the ejection of methyl radicals in *tert*-butanol photoreforming. For ethyl and propyl formation, the difference in thermochemistry is less pronounced compared to methyl. However, reactions yielding ethyl are generally more endothermic than propyl formation. This trend is reflected in the observed selectivity of the reaction; pentanone and an ethyl radical are preferentially formed over butanone and a propyl radical. Therefore, thermodynamic values may be used as a rule-of-thumb to predict preferential bond cleavage in similar photoreactions.

Performing the reaction at different pressures (3×10^{-8} mbar to 5×10^{-6} mbar) with the Pt-loaded photocatalyst does not affect the branching ratio for the two reactions (Figure S8a). The overall TOFs exhibit typical 1st order behavior when the reaction is limited by reactant adsorption and 0th order in the case of limitation by product desorption (see Figures S5 and S6). Similarly, the illumination-dependent TOFs (see Figure S7) suggest a first-order behavior at lower irradiation illumination intensities, which transfer into a saturation regime (zeroth order) at higher photon fluxes, as in the photoreforming of other alcohols.[17a] However, and more importantly, for platinum-decorated TiO_2(110) an additional side reaction becomes evident at higher pressures. This is best illustrated for 2-methyl-2-pentanol photoreforming (Scheme 2), for which all reaction products can clearly be

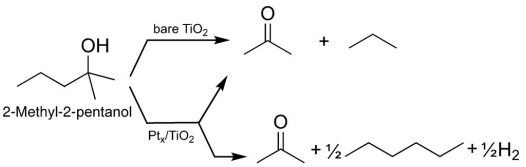

Scheme 2. Reaction scheme for the photoreforming of 2-methyl-2-pentanol on bare r-TiO_2(110) and Pt_x/r-TiO_2(110) under UV illumination. While on bare titania only the hole-mediated disproportionation yielding acetone and propane occurs, a second reaction pathway is enabled for Pt-decorated TiO_2 above 2.0×10^{-7} mbar alcohol pressure. In the latter reaction, hydrogen recombines on the Pt clusters and two propyl radicals recombine forming hexane.

quantified and their analysis is not affected by isobaric interference. As deposited platinum clusters enable the efficient thermal recombination of hydrogen atoms,[17a] the surface coverage of alkyl increases in the steady state with increasing pressure. Consequently, the recombination product of two radicals (i.e., hexane) accompanied by H_2 formation is detected at 5×10^{-6} mbar of alcohol pressure (Figure 3a).

As the formation of H_2 is not facilitated on bare titania, this side reaction is not observed in the absence of a co-catalyst (Figure 3b). Consequently, this result also demonstrates that with the addition of noble-metal clusters, not only unwanted consecutive reactions (as for example the hydrogenation of ketones recently studied mechanistically by electrochemistry[22]), but also an intrinsically different outcome of the photoreaction cycle must be considered in applied systems.

To summarize, we discovered a new reaction for the photoreforming of tertiary alcohols on rutile, which can be described as hole-mediated disproportionation yielding an alkane and the respective ketone. Surprisingly, the abstraction of methyl groups does not occur and only α-C bonds to longer alkyl chains are selectively cleaved, in contrast to the reaction

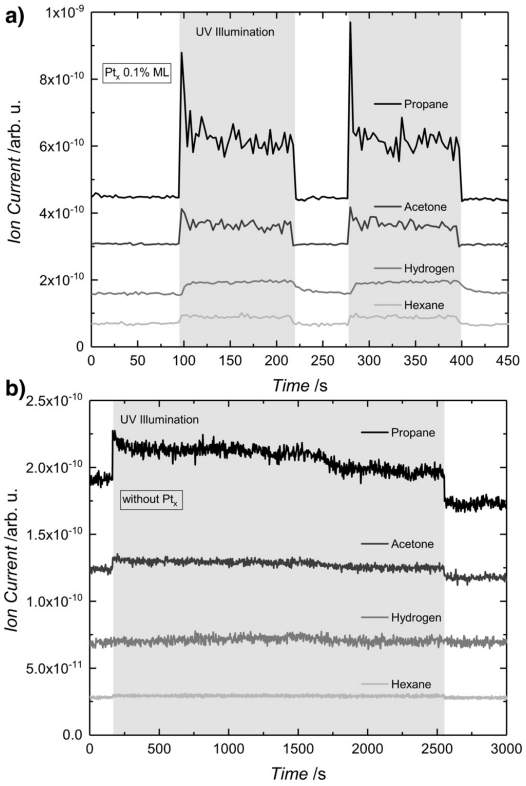

Figure 3. Photocatalytic products of 2-methyl-2-pentanol photoreforming on a) Pt_x/r-TiO_2(110) (0.1% ML cluster coverage) and b) r-TiO_2-(110). Propane (m/z 29), acetone (m/z 58), hydrogen (m/z 2), and hexane (m/z 86) signals are shown at 336 K under a 2-methyl-2-pentanol background pressure of 5.0×10^{-6} mbar. The gray region highlights the period of UV laser irradiation. Note that the traces are offset for clarity. In contrast to bare TiO_2(110), the co-catalyst-loaded semiconductor enables another side reaction, alkyl radical recombination and molecular hydrogen formation.

of *tert*-butanol. The thermochemistry of radical formation may supply a qualitative measure to predict the selectivity of the photoreaction. As the recombination of the alkyl radical and hydrogen is enabled on bare titania, in contrast to the recombination of two hydrogen atoms, the reaction is fully catalytic even without a co-catalyst. While already small amounts of Pt clusters on the rutile crystal increase the overall reaction rate, they also induce another reaction pathway yielding molecular hydrogen and the recombination product of two radicals observed at increasing pressures.

The observed mechanisms may explain the variety of product distributions from ambient pressure and liquid photoreforming studies and have set mechanistic research in photocatalysis on a solid foundation.

Acknowledgements

We thank Martin Stutzmann (TU Munich) for helpful discussions and the DFG for project funding via grant HE3435/22-1. C.C. acknowledges the support by the Luxembourg National Research Fund (FNR), project code 12531916 and by the TUM International Graduate School of Science and Engineering (TUM-IGSSE). Open access funding enabled and organized by Projekt DEAL.

Conflict of interest

The authors declare no conflict of interest.

Keywords: alcohol reforming · photocatalysis · reaction mechanisms · tertiary alcohols · titania

How to cite: *Angew. Chem. Int. Ed.* **2019**, *58*, 14255–14259
Angew. Chem. **2019**, *131*, 14393–14397

[1] a) J. H. J. Kluytmans, A. P. Markusse, B. F. M. Kuster, G. B. Marin, J. C. Schouten, *Catal. Today* **2000**, *57*, 143; b) G. Tojo, M. I. Fernández, *Oxidation of Alcohols to Aldehydes and Ketones: A Guide to Current Common Practice*, 1st ed., Springer, New York, **2006**; c) M. N. Kopylovich, A. P. C. Ribeiro, E. C. B. A. Alegria, N. M. R. Martins, L. M. D. R. S. Martins, A. J. L. Pombeiro, *Adv. Organomet. Chem.* **2015**, *63*, 91; d) R. A. Sheldon, H. v. Bekkum, *Fine chemicals through heterogeneous catalysis*, 1st ed., Wiley-VCH, Weinheim, **2001**.

[2] K. Wietzerbin, J. Bernadou, B. Meunier, *Eur. J. Inorg. Chem.* **2000**, 1391.

[3] a) D. F. Chen, Y. C. Zhang, X. Y. Pan, F. Wang, S. L. Huang, *Adv. Synth. Catal.* **2018**, *360*, 3607; b) K. Matsunaga, H. Hirajima, A. Kishida, K. Takatori, H. Nagaoka, *Tetrahedron Lett.* **2015**, *56*, 5941.

[4] a) E. Brenna, M. Crotti, M. De Pieri, F. G. Gatti, G. Manenti, D. Monti, *Adv. Synth. Catal.* **2018**, *360*, 3677; b) H. G. Yayla, H. J. Wang, K. T. Tarantino, H. S. Orbe, R. R. Knowles, *J. Am. Chem. Soc.* **2016**, *138*, 10794; c) J. M. Vatèle, *Tetrahedron* **2010**, *66*, 904.

[5] a) G. Cainelli, G. Cardillo, *Chromium oxidations in organic chemistry*, Springer, Berlin, New York, **1984**; b) S. V. Ley, A. Madin, in *Comprehensive Organic Synthesis* (Eds.: B. M. Trost, I. Fleming), Pergamon, Oxford, **1991**, p. 251; c) F. A. Luzzio in *Organic Reactions* (Eds.: P. A. Evans, S. Weinreb), Vol. 53, Wiley, **1998**, DOI: 10.1002/0471264180.or053.01.

[6] "Photocatalytic Synthesis of Chemicals": M. Kobielusz, P. Mikrut, W. Macyk, in *Materials for Sustainable Energy*, *Vol. 72*, Academic Press, San Diego, **2018**, pp. 93–144.

[7] A. Walker, M. Formenti, P. Meriaudeau, S. J. Teichner, *J. Catal.* **1977**, *50*, 237.

[8] a) M. A. Henderson, *Surf. Sci. Rep.* **2011**, *66*, 185; b) A. Fujishima, X. T. Zhang, D. A. Tryk, *Surf. Sci. Rep.* **2008**, *63*, 515; c) J. Schneider, M. Matsuoka, M. Takeuchi, J. L. Zhang, Y. Horiuchi, M. Anpo, D. W. Bahnemann, *Chem. Rev.* **2014**, *114*, 9919.

[9] B. Ohtani, O. O. Prieto-Mahaney, D. Li, R. Abe, *J. Photochem. Photobiol. A* **2010**, *216*, 179.

[10] a) U. Diebold, *Appl. Phys. A* **2003**, *76*, 681; b) U. Diebold, *Surf. Sci. Rep.* **2003**, *48*, 53.

[11] a) Y. K. Kim, B. D. Kay, J. M. White, Z. Dohnalek, *J. Phys. Chem. C* **2007**, *111*, 18236; b) Z. Dohnálek, I. Lyubinetsky, R. Rousseau, *Prog. Surf. Sci.* **2010**, *85*, 161; c) Z. J. Li, R. S. Smith, B. D. Kay, Z. Dohnalek, *J. Phys. Chem. C* **2011**, *115*, 22534.

[12] a) M. A. Henderson, I. Lyubinetsky, *Chem. Rev.* **2013**, *113*, 4428; b) M. Shen, D. P. Acharya, Z. Dohnalek, M. A. Henderson, *J. Phys. Chem. C* **2012**, *116*, 25465; c) M. M. Shen, M. A. Henderson, *J. Phys. Chem. Lett.* **2011**, *2*, 2707.
[13] a) B. Kraeutler, C. D. Jaeger, A. J. Bard, *J. Am. Chem. Soc.* **1978**, *100*, 4903; b) D. Yang, X. Y. Ni, W. K. Chen, Z. Weng, *J. Photochem. Photobiol. A* **2008**, *195*, 323.
[14] W. A. Herrmann, *Angew. Chem. Int. Ed. Engl.* **1982**, *21*, 117; *Angew. Chem.* **1982**, *94*, 118.
[15] E. Iglesia, *Appl. Catal. A* **1997**, *161*, 59.
[16] M. B. Smith, *March's Advanced Organic Chemistry: Reactions, Mechanisms, and Structure*, 7th ed., John Wiley & Sons, Inc, Hoboken, **2013**, pp. 1433 – 1497.
[17] a) C. A. Walenta, S. L. Kollmannsberger, C. Courtois, R. N. Pereira, M. Stutzmann, M. Tschurl, U. Heiz, *Phys. Chem. Chem. Phys.* **2019**, *21*, 1491; b) S. L. Kollmannsberger, C. A. Walenta, C. Courtois, M. Tschurl, U. Heiz, *ACS Catal.* **2018**, *8*, 11076.
[18] J. Cunningham, B. K. Hodnett, A. Walker, *Proc. R. Ir. Acad. Sect. B* **1977**, *77*, 411.
[19] a) Z. R. Zhang, R. Rousseau, J. L. Gong, B. D. Kay, Z. Dohnalek, *J. Am. Chem. Soc.* **2009**, *131*, 17926; b) E. Farfan-Arribas, R. J. Madix, *J. Phys. Chem. B* **2002**, *106*, 10680; c) M. A. Henderson, S. Otero-Tapia, M. E. Castro, *Faraday Discuss.* **1999**, *114*, 313.
[20] K. R. Phillips, S. C. Jensen, M. Baron, S.-C. Li, C. M. Friend, *J. Am. Chem. Soc.* **2013**, *135*, 574.
[21] G. R. Bamwenda, S. Tsubota, T. Nakamura, M. Haruta, *J. Photochem. Photobiol. A* **1995**, *89*, 177.
[22] C. J. Bondue, M. T. M. Koper, *J. Catal.* **2019**, *369*, 302.
[23] U. Heiz, F. Vanolli, L. Trento, W. D. Schneider, *Revi. Sci. Instruments* **1997**, *68*, 1986.
[24] C. A. Walenta, S. L. Kollmannsberger, J. Kiermaier, A. Winbauer, M. Tschurl, U. Heiz, *Phys. Chem. Chem. Phys.* **2015**, *17*, 22809.
[25] M. A. Henderson, *Langmuir* **1996**, *12*, 5093.
[26] Z. H. Geng, X. C. Jin, R. M. Wang, X. Chen, Q. Guo, Z. B. Ma, D. X. Dai, H. J. Fan, X. M. Yang, *J. Phys. Chem. C* **2018**, *122*, 10956.
[27] a) Y. Watanabe, X. Y. Wu, H. Hirata, N. Isomura, *Catal. Sci. Technol.* **2011**, *1*, 1490; b) N. Isomura, X. Y. Wu, H. Hirata, Y. Watanabe, *J. Vac. Sci. Technol. A* **2010**, *28*, 1141.

Manuscript received: June 25, 2019
Accepted manuscript online: August 7, 2019
Version of record online: August 28, 2019

Angewandte Chemie
Eine Zeitschrift der Gesellschaft Deutscher Chemiker

Supporting Information

Reactions in the Photocatalytic Conversion of Tertiary Alcohols on Rutile TiO_2(110)

*Carla Courtois[+], Moritz Eder[+], Kordula Schnabl, Constantin A. Walenta, Martin Tschurl, and Ulrich Heiz**

anie_201907917_sm_miscellaneous_information.pdf

Supporting Information:

Experimental Overview

The details of the experimental setup are described below and also elsewhere.[S1] In brief, measurements are performed with a complex UHV apparatus featuring a laser vaporization cluster source for the deposition of clusters with an atomically precise number of atoms.[S2] The cluster coverage is controlled by the deposition time and determined by recording the neutralization current with a picoammeter. The UHV chamber is equipped with an Auger spectrometer and an ion gun for Ar^+ sputtering for the preparation of a defined semiconductor surface. The sample is mounted on a sample holder,[S3] which is attached to a heatable and

liquid-N_2-coolable manipulator in order to set the sample on a selected and defined temperature. The TiO_2(110) crystal is cleaned following established procedures of sputtering and annealing cycles. The degree of surface reduction and absence of platinum is determined by H_2O temperature-programmed desorption and the evaluation of traces of water[S4] and H_2,[S5] respectively. The Pt/TiO_2(110) model catalysts have been thoroughly characterized by a variety of local and integral techniques.[S6] Photocatalytic measurements are performed by illuminating the sample with a Nd:YAG-pumped, frequency-doubled OPO laser beam at 242 nm in an alcohol background. Product evolution is followed by a quadrupole mass spectrometer placed in line of sight with the photocatalyst.

Experimental Details

The setup consists of a laser vaporization cluster generation source and an ultra-high vacuum (UHV) setup. For cluster generation, a focused beam of the frequency-doubled of a Nd:YAG (532 nm, 100 Hz, Spitlight DPSS, Innolas) ablates a rotating Pt target (99.96% purity, ESG Edelmetalle, Germany). The resulting plasma is cooled by the expansion of a He gas pulse (He 6.0, Air Westfalen) into the vacuum. The cationic cluster beam is guided and bent into a quadrupole mass filter (QMF; Extrel, USA), which enables either the selection of a particular cluster size or the guidance of the clusters in ion-guide mode.[S2] For this study, the latter mode was used and was operated as high-pass filter transmitting only ions larger than Pt_7. The settings resulted in a cluster size distribution with a maximum from Pt_{11} to Pt_{13} (see S1). 0.1% monolayer (ML) of Pt_x clusters (respective to surface atoms) were deposited onto a TiO_2(110) single crystal under soft landing conditions (<1eV/atom in kinetic energy). Cluster loadings were determined by recording the cluster neutralization current during the deposition with a picoammeter (Keithley, 6587). For experiments with different cluster coverages, the desired amount of platinum, which is specified in the presented data, was deposited by varying the deposition time (in the order of minutes). The as-obtained Pt-

decorated TiO_2(110) catalysts have been been well-characterized in previous works by means of scanning probe microscopy and photoelectron spectroscopy.[S6–S9]

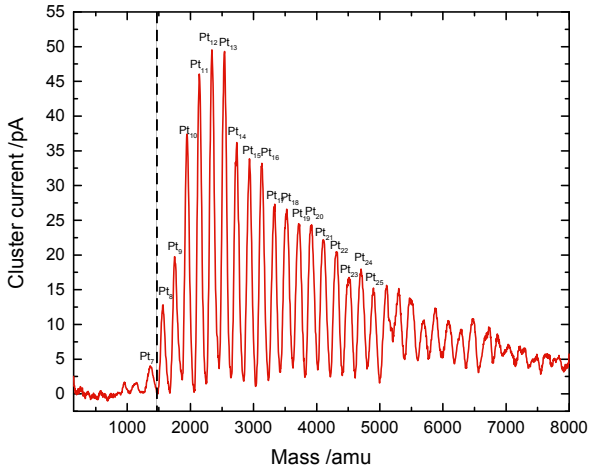

Figure S1: Size-distribution of platinum clusters from Pt_7 to Pt_{35} with a maximum from Pt_{11} to Pt_{13} from the laser vaporization cluster source. The solid black line denotes the cut-off mass of the quadrupole mass filter during deposition.

In the UHV setup, a base pressure lower than $9.8 \cdot 10^{-11}$ mbar is achieved. The sample in the chamber is mounted on a sample holder,[S3] which is attached to a (ϕ,x,y,z)-manipulator (VAB Vakuum GmbH) in order to enable the movement of the sample to different positions. The sample holder enables liquid nitrogen cooling and the resistive heating of the crystal. For analysis, an auger spectroscope (MDC, HLM-275-3), an electron ionization quadrupole mass spectrometer (EI-QMS; QMA 430, Pfeiffer Vacuum GmbH) and a home-built photoionization time-of-flight mass spectrometer (PI-TOF-MS) are attached to the main chamber. The chamber is further equipped with a leak valve (Pfeiffer Vacuum) for Langmuir dosing and a molecular beam doser in order introduce reactant gases into the vacuum via a gas line. The vapor pressure of 3-methyl-3-hexanol (99%, Alfa Aesar), 2-methyl-2-pentanol (99%, Sigma Aldrich) and 2-methyl-2-butanol ($\geq$ 99%, Sigma Aldrich) is exploited in order to introduce the reactants in the reaction chamber via a leak valve twith a constant background pressure.

The surface of the rutile TiO_2(110) single crystal (SurfaceNet GmbH) is prepared by cycles of Ar^+ (100% N60; Air Liquide) sputtering (1 keV, $4 \cdot 10^{-5}$ mbar for several hours), oxygen ($\geq$ 99%; Westfalen) annealing (800 K, $1 \cdot 10^{-6}$ mbar, 20 min) and vacuum annealing (800 K, 10 min) until no contamination is observed by Auger electron spectroscopy with a respective spectrometer (Omicron Nanotechnology). The absence of Pt is further confirmed by the evaluation of the H_2 trace in a H_2O thermal programmed desorption (TPD) experiment.[S5] The resulting light blue TiO_2 has a bridge-bonded oxygen (BBO) vacancy concentration of $6 \pm 1\%$ of Ti lattice sites, which is determined by H_2O TPD.[S4] All the experiments are performed on such a reduced TiO_2(110) crystal. Photoexcitation experiments are conducted with a frequency doubled OPO laser (GWU, premiScan ULD/400), which is pumped with the third harmonic of a Nd:YAG (Innolas Spitlight HighPower 1200, 7 ns pulse width, 20 Hz repetition rate), in order to achieve a wavelength of 242 nm (with a power of 3.6 ± 0.3 mW at the crystal surface, if not otherwise noted). Product identification is performed with the above-mentioned QMS with mass scans under catalytic conditions (see for example figure S2) and the recording of specific mass traces for the quantification of the reaction rates (see for example figure S11). The QMS ion current is calibrated via the desorption integral of a saturation coverage of the Ti-lattice sites with methanol in a TPD experiment.

The turnover frequency (TOF) values are calculated by integrating the baseline corrected signals of the QMS. These are further corrected with the m/z-dependent transmissions through the QMS, electron impact ionization cross sections (ICS) as well as with a factor considering ion fragmentation which are taken from reference mass spectra. The fragmentation pattern are obtained from recording the mass spectra of the respective molecules. The ICS values and the m/z-value of the respective fragment used for the quantification are given in table S1.

Table S1: Electron impact ionization cross sensitivity values at 70 eV and m/z-value of the respective fragment used for quantification.

substance	ICS [Å^2]	m/z fragment
2-butanone	12.9[S10]	72
2-pentanone	15.2[S10]	86
propane	11.6[S10]	29
ethane	8.39[S10]	30
acetone	10.2[S10]	58
hydrogen	1.021[S11]	2
hexane	20.8[S10]	86

Evaluation of Mass Spectra

The products are identified by the evaluation the mass scans. Firstly, a mass scan **I** over the whole mass range with potential product masses, is carried out at a certain alcohol background pressure, which is given in the caption of the respective figure. This mass scan **I** includes the fragmentation pattern of the alcohol and possible contaminations from the residual gas in the UHV chamber (mainly H_2, CO, CO_2 and H_2O). Secondly, the sample is illuminated and a mass scan **II** under steady-state condition is recorded. This mass scan **II** includes the fragmentation pattern of the alcohol and its photo products. Subtracting mass scan **I** (dark) from mass scan **II** (illuminated) reveals a mass scan of the photocatalytic reaction. These spectra are named as difference spectra an are shown in Figure S2a, S3a and S4a. Positive values indicate that these masses arise from photo products and negative values originate from the consumed alcohol. In order to demonstrate that the resulting mass peaks are due to the presence of the ketones and the respective alkanes, self-recorded mass spectra of the reactant and products are added or subtracted from the difference spectrum

a).

In a first step, from spectrum **a)** to **b)**, the mass spectrum of the alcohol is added to the difference spectrum. This results spectrum **b)**, which only includes reaction products (i.e. positive signals). Subsequently, the mass peaks of one product after the other is subtracted from **b)** so that a baseline spectrum **d)** is obtained. Before every addition or subtraction, the mass spectrum is normalized to a unique mass fragment of the respective molecule. All the products can be clearly identified and it can be demonstrated, that no other products result.

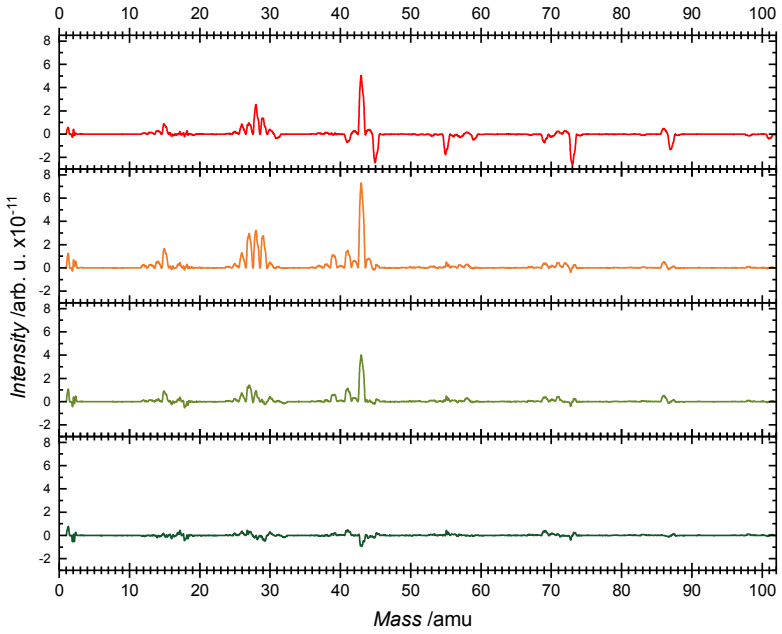

Figure S2: Mass spectra for the product analysis of the photocatalytic reforming of 3-methyl-3-hexanol (0.1% ML Pt_x/TiO_2, 300 K, alcohol background pressure $1.7 \cdot 10^{-7}$ mbar). The difference spectrum is shown in **a)**. Positive peaks originate from the products (2-butanone, propane, 2-pentanone and ethane), and the negative peaks stem from consumed 3-methyl-3-hexanol. Spectrum **b)** is obtained by adding the mass spectrum of 3-methyl-3-hexanol to the difference spectrum (both spectra were normalized to $m/z = 73$ prior to the addition). **c)** depicts the mass spectrum after the subtraction of the spectra of 2-butanone (normalized to $m/z = 72$) and propane (normalized to $m/z = 44$). Spectrum **d)** shows a baseline after subtracting the spectra of 2-pentanone (normalized to $m/z = 86$) and ethane (normalized to $m/z = 28$) from spectrum **c)**.

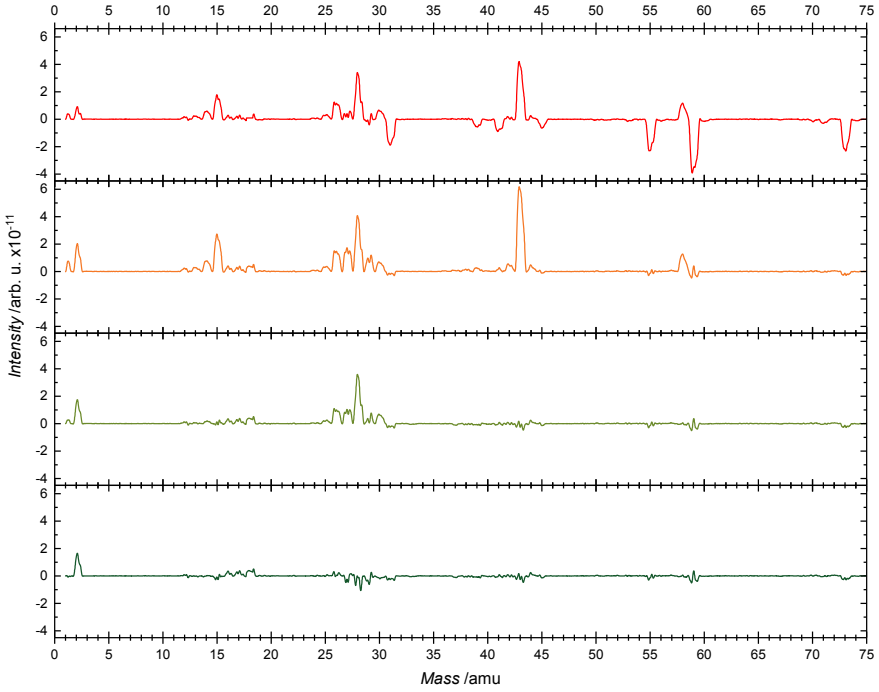

Figure S3: Mass spectra for the product analysis of the photocatalytic reforming of 2-methyl-2-butanol (0.1% ML Pt_x/TiO_2, 263 K, alcohol background pressure $2.0 \cdot 10^{-7}$ mbar). The difference spectrum is shown in **a)**. Positive peaks originate from the products (acetone and ethane), and the negative peaks stem from consumed 2-methyl-2-butanol. Spectrum **b)** is obtained by adding the mass spectrum of 2-methyl-2-butanol to the difference spectrum (both spectra were normalized to $m/z = 59$ prior to the addition). **c)** depicts the mass spectrum after the subtraction of the spectrum of acetone (normalized to $m/z = 43$). Spectrum **d)** shows a baseline after subtracting the spectrum of ethane (normalized to $m/z = 28$) from spectrum **c)**.

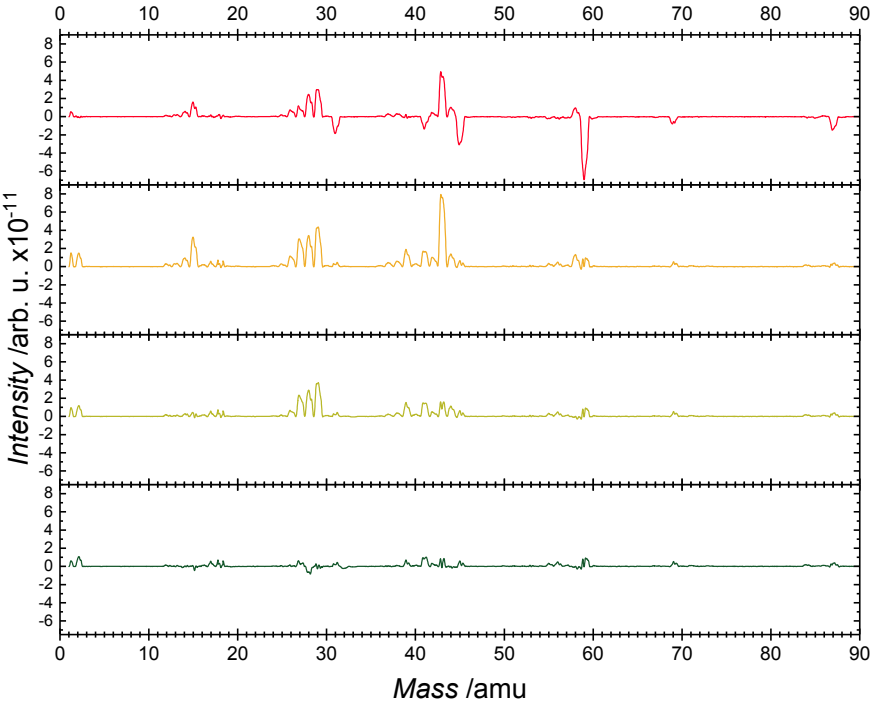

Figure S4: Mass spectra for the product analysis of the photocatalytic reforming of 2-methyl-2-pentanol (0.1% ML Pt_x/TiO_2, 321 K, alcohol background pressure $2.0 \cdot 10^{-7}$ mbar). The difference spectrum is shown in **a)**. Positive peaks originate from the products (acetone and propane), and the negative peaks stem from consumed 2-methyl-2-pentanol. Spectrum **b)** is obtained by adding the mass spectrum of 2-methyl-2-pentanol to the difference spectrum (both spectra were normalized to $m/z = 59$ prior to the addition). **c)** depicts the mass spectrum after the subtraction of the spectrum of acetone (normalized to $m/z = 58$). Spectrum **d)** shows a baseline after subtracting the spectrum of ethane (normalized to $m/z = 29$) from spectrum **c)**.

Turnover Frequencies

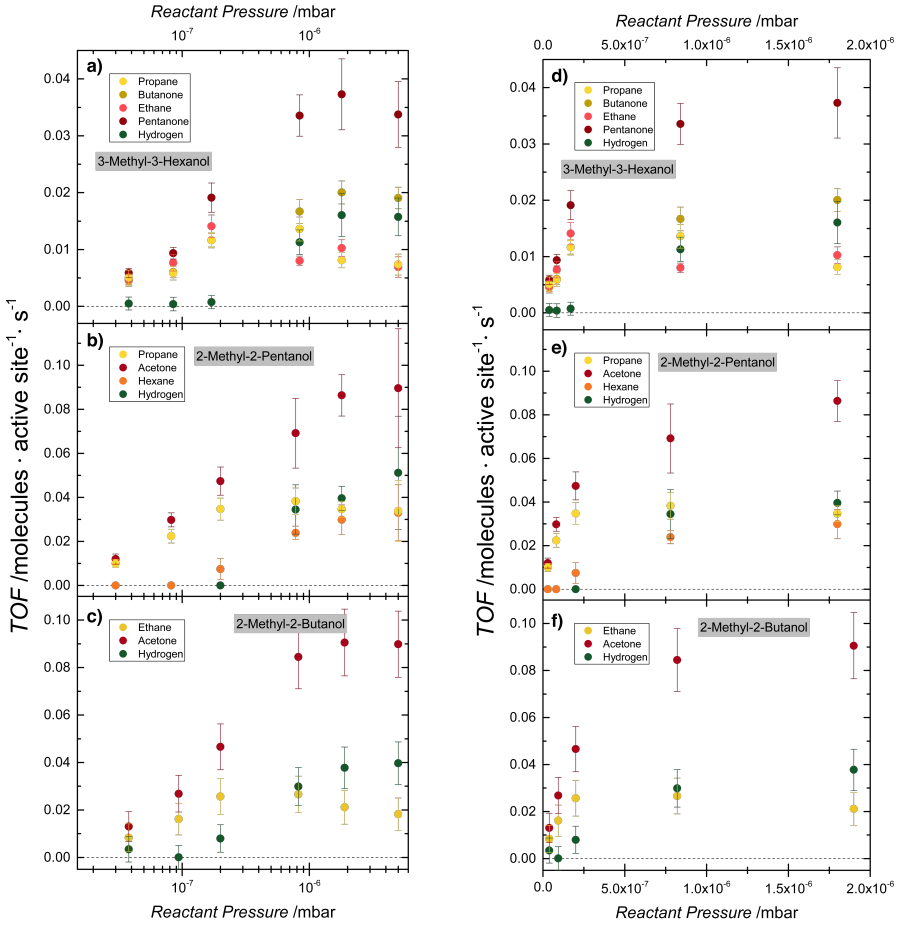

Figure S5: Pressure-dependent Turnover Frequencies (TOFs) for photocatalytic reforming of **a)** and **d)** 3-methyl-3-hexanol, **b)** and **e)** 2-methyl-2-pentanol, **c)** and **f)** 2-methyl-2-butanol over 0.1% ML Pt_x/TiO_2. The photocatalytic experiments are performed at 253 K, so that the temperature is above the desorption temperature of the ketones and alkanes and below the desorption temperature of the alcohol. The TOF exhibit a 1^{st} order behavior until the regime changes from reactant adsorption to product desorption limitation. The latter results in a 0^{st} order behavior. In **a)**, **b)** and **c)**, the pressure-dependent TOFs are plotted on a logarithmic scale and in **d)**, **e)** and **f)**, a section of the TOFs are plotted linearly to demonstrate a linear rise before the saturation behaviour.

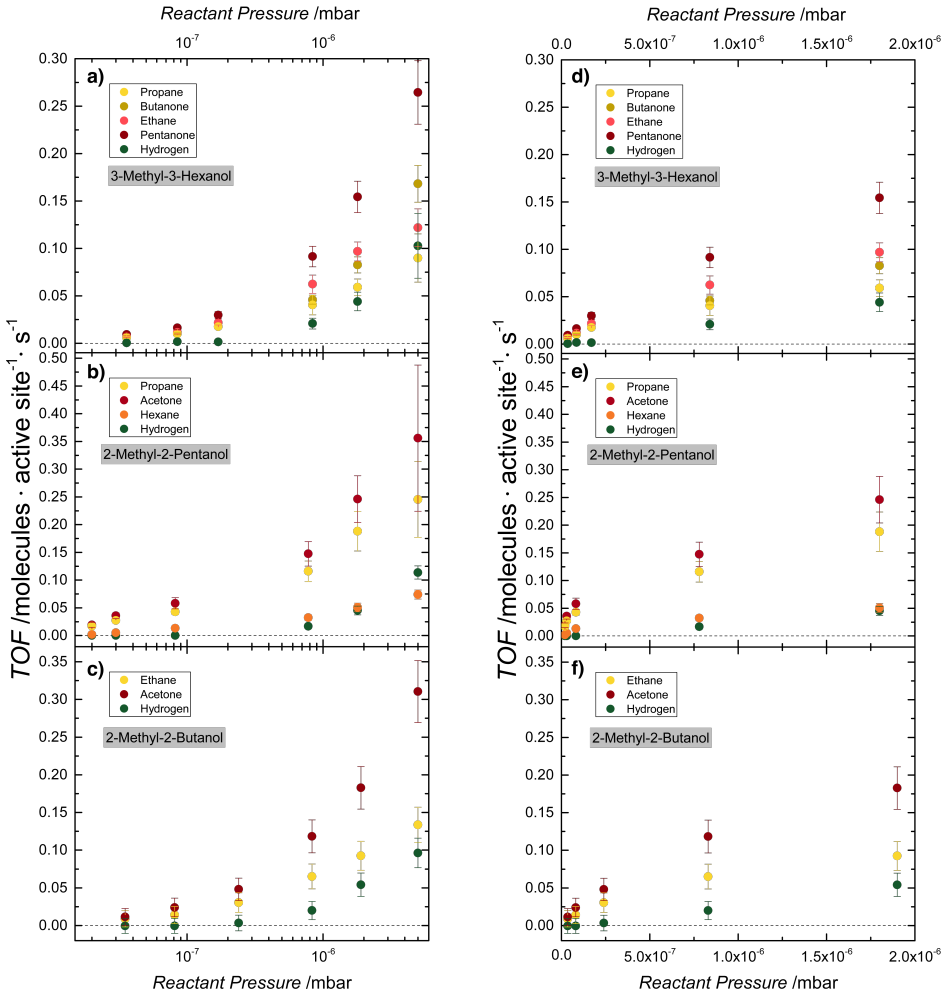

Figure S6: Pressure-dependent TOFs for photocatalytic reforming of **a)** and **d)** 3-methyl-3-hexanol, **b)** and **e)** 2-methyl-2-pentanol, **c)** and **f)** 2-methyl-2-butanol over 0.1% ML Pt_x/TiO_2. The catalytic experiments are performed at 336 K, so that the temperature is above the desorption temperature of the ketones and alkanes and below the desorption temperature of the alcohol. The TOFs exhibit a 1^{st} order behaviour since the reaction is limited by reactant adsorption at 336 K. Due to higher temperature, a desorption limited regime is not reached, which is different to figure S5. In **a)**, **b)** and **c)**, the pressure-dependent TOFs are plotted on a logarithmic scale and in **d)**, **e)** and **f)**, a section of the TOFs are plotted linearly to demonstrate a linear rise with increasing alcohol pressure.

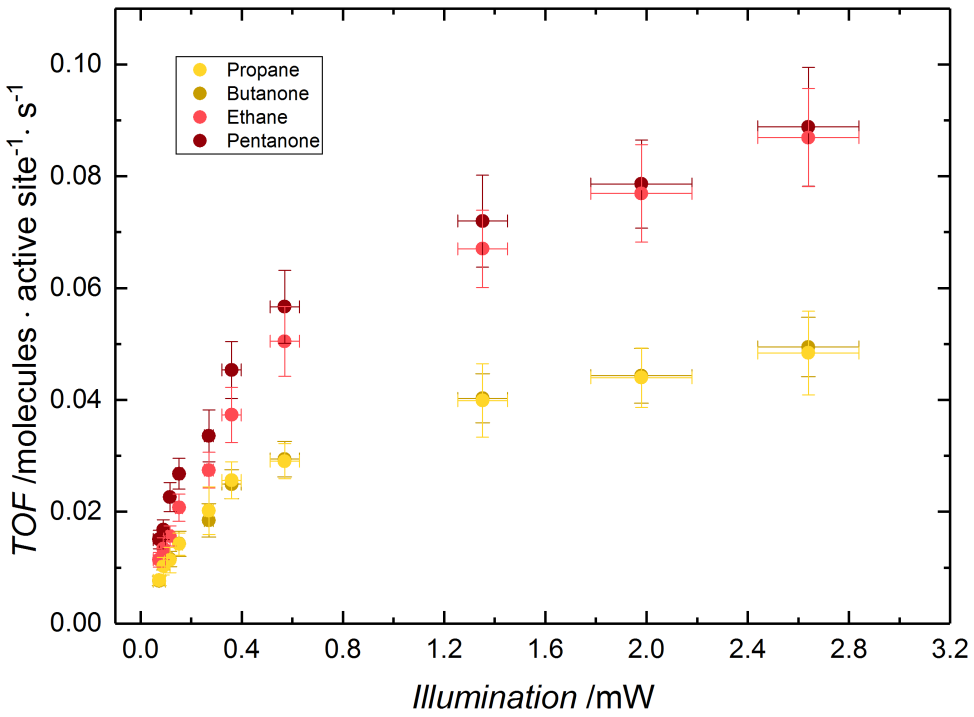

Figure S7: Power-dependent TOFs for photoreforming of 3-methyl-3-hexanol on 0.1% ML $Pt_x/TiO_2(110)$ at 336 K in an alcohol background pressure of $8.4 \cdot 10^{-7}$ mbar. The reaction exhibits a first-order dependence, which transfers into a zeroth-order regime at higher illumination intensities. This behavior, which is similar to the reaction of other alcohols,[S12] supplies evidence for a one photon process. Note that the overall apparent quantum yield ranges from 0.67 % for low illumination intensities (0.74 μW) to 0.11 % for higher photon fluxes (2.64 mW), when the calculations follow the generally applied procedure via the number of evolved molecules per second with respect to the photon flux[S12–S14] and assuming the usually assumed two-photon process for a direct comparison with literature values.

Selectivities

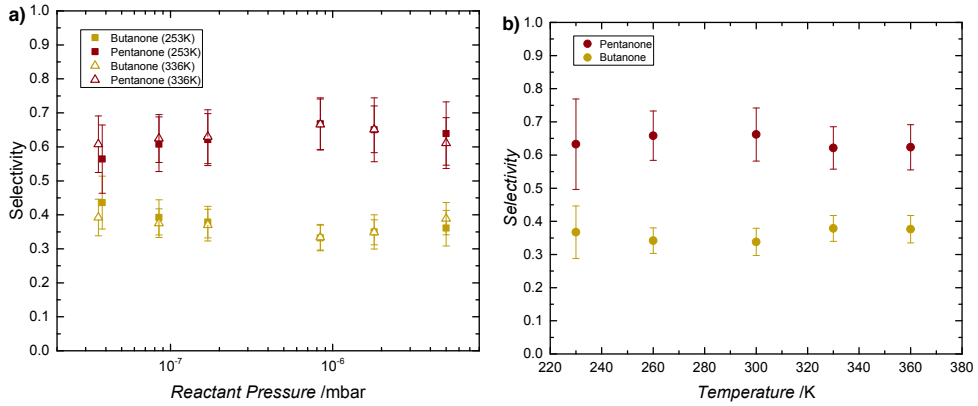

Figure S8: Photocatalytic conversion of 3-methyl-3-hexanol on 0.1% ML $Pt_x/TiO_2(110)$. In **a)**,the selectivities for 2-pentanone and 2-butanone based on the TOFs from figure S5 and figure S6 are displayed for different reactant pressures at two different temperatures 253 K and 336 K, respectively. The two temperatures typify the temperature regime limited by product desorption, respectively by reactant adsorption. In **b)**, the selectivities for 2-pentanone and 2-butanone are shown for different temperatures. It is found, that the selectivities are temperature and concentration independent.

QMS traces

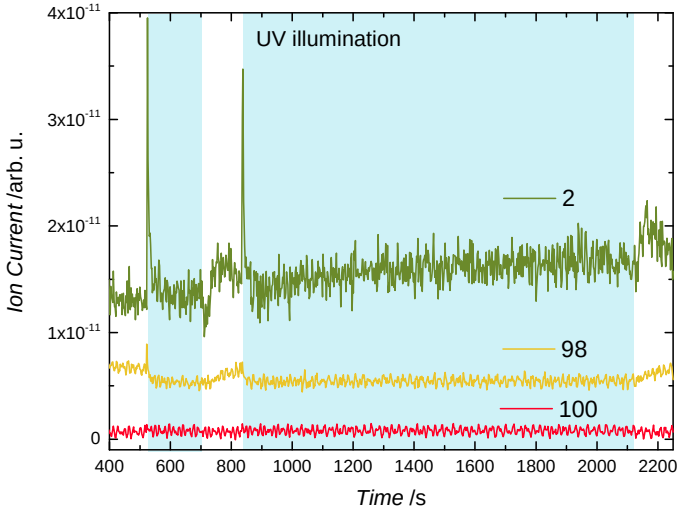

Figure S9: Photocatalytic alcohol reforming of 3-methyl-3-hexanol on $Pt_x/TiO_2(110)$ (0.1% ML cluster coverage). The masses *m/z = 2* for hydrogen, *m/z = 98* for the dehydration products, hexene and methylene hexane, and *m/z = 100* for 3-hexanone are displayed at 340 K under a 3-methyl-3-hexanol pressure of $1.7 \cdot 10^{-7}$ mbar. The blue region highlights the period of UV irradiation. It can be clearly seen that neither of these products are quantitatively formed. Note that the decrease in the *m/z = 98* during illumination is due to the consumption of the alcohol (the substrate), which exhibits a fragment of this particular mass in its fragmentation pattern.

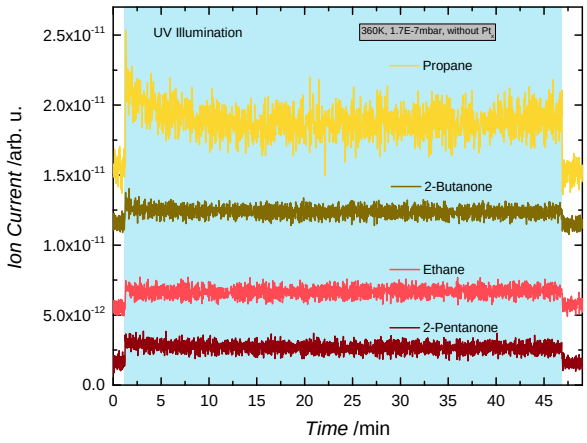

Figure S10: Photocatalytic products of 3-methyl-3-hexanol photoreforming on bare r−TiO_2(110). 3-methyl-3-hexanol (*m/z=73*), propane (*m/z=29*), 2-butanone (*m/z=72*), ethane (*m/z=30*), and 2-pentanone (*m/z=86*) signals are shown at 360 K under a 3-methyl-3-hexanol pressure of $1.7 \cdot 10^{-7}$ mbar. The blue region highlights the period of UV irradiation. Note that the traces are offset for clarity.

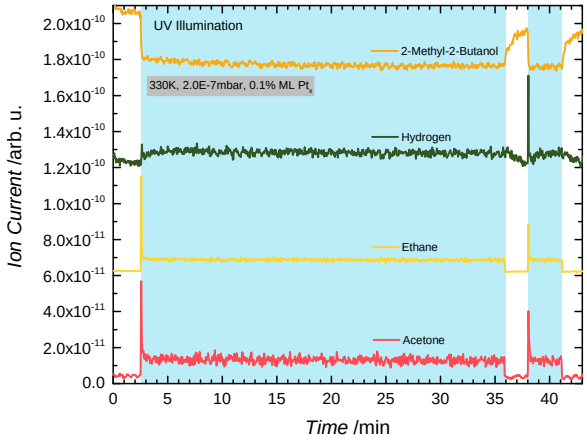

Figure S11: Photocatalytic products of 2-methyl-2-butanol photoreforming on 0.1% ML Pt_x/TiO_2(110). 2-methyl-2-butanol (*m/z=73*), hydrogen (*m/z=2*), ethane (*m/z=30*), and acetone (*m/z=58*) signals are shown at 330 K under a 2-methyl-2-butanol pressure of $2.0 \cdot 10^{-7}$ mbar. The blue region highlights the period of UV irradiation. Note that the traces are offset for clarity. Under these reactions conditions, a third reaction product next to acetone and ethane, namely hydrogen is observed.

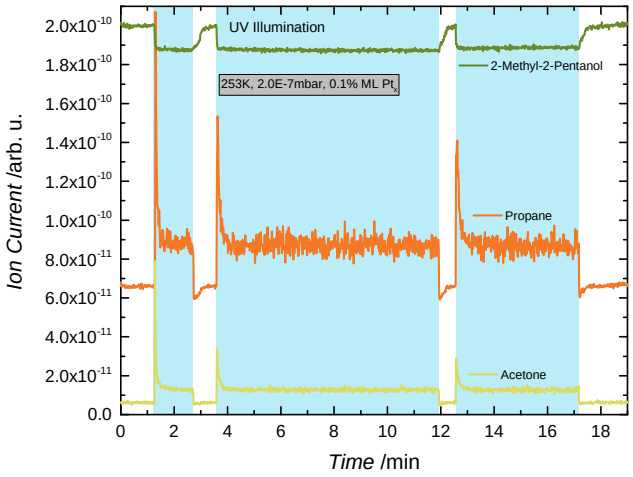

Figure S12: Photocatalytic products of 2-methyl-2-pentanol photoreforming on 0.1% ML $Pt_x/TiO_2(110)$. 2-methyl-2-pentanol (*m/z=87*), propane (*m/z=29*), and acetone (*m/z=58*) signals are shown at 253 K under a 2-methyl-2-pentanol pressure of $2.0 \cdot 10^{-7}$ mbar. The blue region highlights the period of UV irradiation. Note that the traces are offset for clarity.

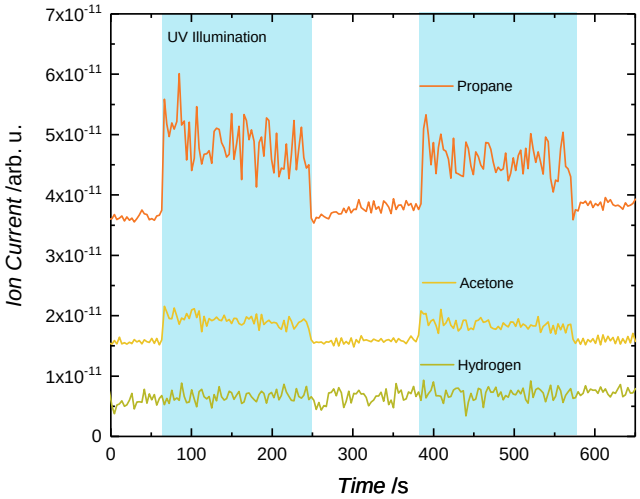

Figure S13: Photocatalytic products of 2-methyl-2-pentanol photoreforming on hydroxylated-TiO_2(110). Propane (*m/z=29*), acetone (*m/z=58*) and molecular hydrogen (*m/z=2*) signals are shown at 270 K under a 2-methyl-2-pentanol background pressure of $1.7 \cdot 10^{-7}$ mbar. The hydroxylated-TiO_2(110) crystal was exposed to water at cryogenic temperatures and annealed to 270 K. This leads to hydroxyl groups on the surface, while residual water molecules are being desorbed.[S15] The photoreaction occurs very similar to that on reduced-TiO_2(110) (see Fig. 3a) showing that the hydroxylation does not lead to significant changes in the reaction behavior. Note that the traces are offset for clarity.

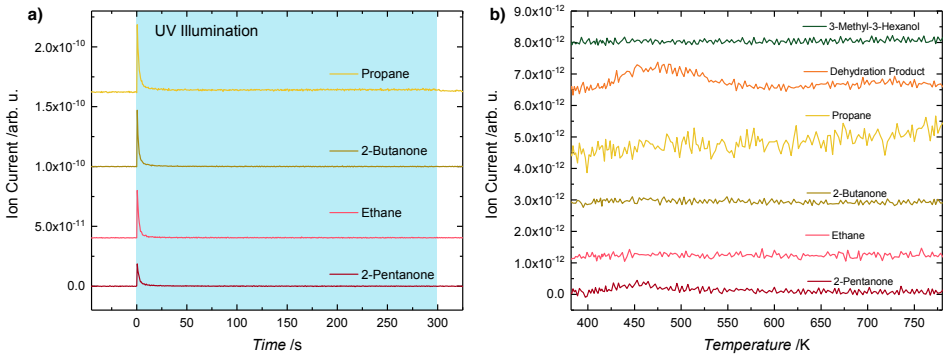

Figure S14: **a)** Isothermal photoreaction experiment of 5 L 3-methyl-3-hexanol on r-TiO_2(110) at 340 K. The catalyst is exposed to 3-methyl-3-hexanol at 150 K and then brought to 340 K. Upon illumination (blue region), propane (*m/z=44*), 2-butanone (*m/z=72*), ethane (*m/z=30*), and 2-pentanone (*m/z=86*) are formed.
b) Temperature programmed desorption spectroscopy (TPD) experiment after the isothermal photoreaction at 340 K. It is found that no alkanes and ketones appear in the TPD spectrum, which shows that the photoproducts have desorbed completely during illumination. Furthermore, no other photoproducts are detected. Only the formation of small amounts of dehydration products (*m/z=98*) are observed. They originate from the thermal water elimination of alcohol residues, a general property of the thermal reactivity of alcohols,[S16] and may lead to three different structural isomers for which an unambiguous assignment cannot be given by EI-QMS. (Note that in both plots the traces are offset for clarity.)

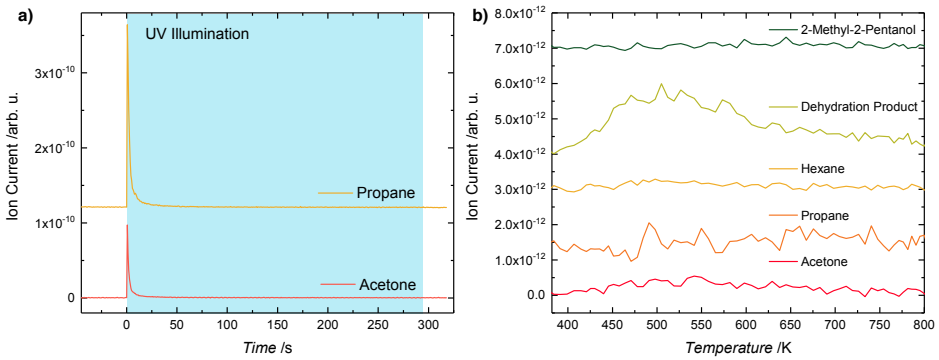

Figure S15: **a)** Isothermal photoreaction experiment of 5 L 2-methyl-2-pentanol on r-TiO_2(110) at 340 K. The catalyst is exposed to 2-methyl-2-pentanol at 150 K and then brought to 340 K. Upon illumination (blue region), propane (*m/z=29*) and acetone (*m/z=58*) are formed.
b) Temperature programmed desorption spectroscopy (TPD) experiment after the isothermal photoreaction at 340 K. It is found that acetone and propane do not appear in the TPD spectrum, which shows that the photoproducts have desorbed completely during illumination. Furthermore, no other photoproducts (e.g. product from alkyl recombination, i.e. hexane (*m/z=86*)) are detected. Only the formation of small amounts of dehydration products (*m/z=84*) are observed. They originate from the thermal water elimination of alcohol residues, a general property of the thermal reactivity of alcohols,[S16] and may lead to three different structural isomers for which an unambiguous assignment cannot be given by EI-QMS. (Note that in both plots the traces are offset for clarity.)

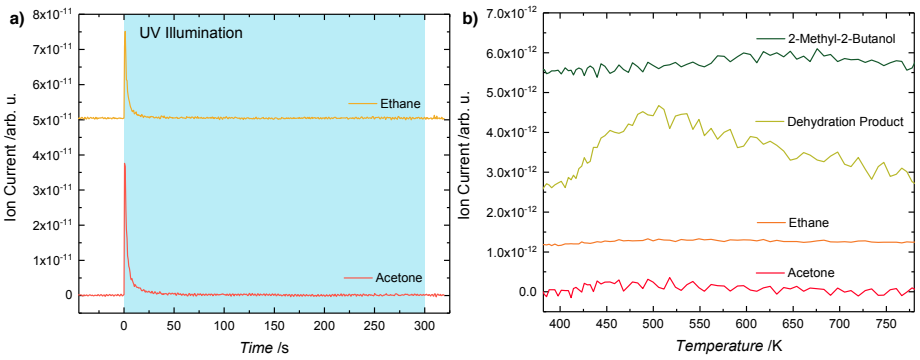

Figure S16: **a)** Isothermal photoreaction experiment of 5 L 2-methyl-2-butanol on r-TiO_2(110) at 340 K. The catalyst is exposed to 2-methyl-2-butanol at 150 K and then brought to 340 K. Upon illumination (blue region), ethane (*m/z=30*) and acetone (*m/z=58*) are formed.
b) Temperature programmed desorption spectroscopy (TPD) experiment after the isothermal photoreaction at 340 K. It is found that acetone and ethane do not appear in the TPD spectrum, which shows that the photoproducts have desorbed completely during illumination. Furthermore, no other photoproducts are detected. Only the formation of small amounts of dehydration products (*m/z=70*) are observed. They originate from the thermal water elimination of alcohol residues, a general property of the thermal reactivity of alcohols,[S16] and may lead to three different structural isomers for which an unambiguous assignment cannot be given by EI-QMS. (Note that in both plots the traces are offset for clarity.)

Auger Electron Spectroscopy

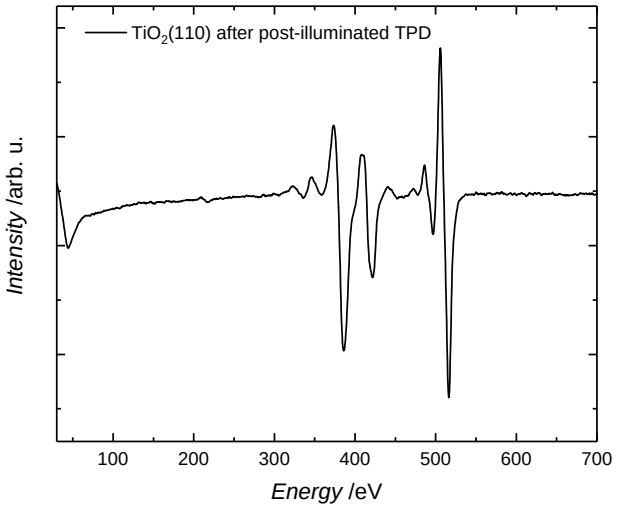

Figure S17: Auger Electron Spectrum of the reduced-TiO_2(110) after the isothermal photoreaction experiment of 5 L 3-methyl-3-hexanol at 340 K followed by a thermal programmed desorption from $340 - 800$ K, shown in S14. No carbon containing species (expected at 272 eV) are detected.

Thermochemistry

Table S2: Standard enthalpy of formation (ΔH_f°) for molecules, which may be formed in different reactions.

Molecule	ΔH_f° [kJ/mol]
methane	-74.6[S17]
ethane	-84.0[S17]
propane	-103.8[S17]
butane	-125.6[S17]
pentane	-146.9[S17]
hexane	-167.1[S17]
acetone	-217.1[S17]
2-butanone	-238.5[S17]
2-pentanone	-259.0[S17]
3-hexanone	-277.6[S18]
2-methyl-2-butanol	-329.3[S18]
2-methyl-2-propanol	-352.1[S19]
3-methyl-3-hexanol	-372.8[S19]
atomic hydrogen	217.998[S17]
methyl radical	146.427[S20]
ethyl radical	119.87[S21]
propyl radical	100.87[S21]

Table S3: Standard enthalpy of reaction (ΔH_R°) calculated from the standard enthalpy of formation (ΔH_f°) of the respective reactants and products.

Reaction	ΔH_R° [kJ/mol]
2−methyl−2−butanol ⟶ methane + 2−butanone	16.2
2−methyl−2−butanol ⟶ ethane + acetone	28.2
2−methyl−2−butanol ⟶ $\frac{1}{2}$ butane + acetone	98.8
2−methyl−2−propanol ⟶ methane + 2−pentanone	18.5
2−methyl−2−propanol ⟶ propane + acetone	31.2
2−methyl−2−propanol ⟶ $\frac{1}{2}$ hexane + acetone	102.9
3−methyl−3−hexanol ⟶ methane + 3−hexanone	20.6
3−methyl−3−hexanol ⟶ ethane + 2−pentanone	29.8
3−methyl−3−hexanol ⟶ propane + 2−butanone	30.5

All potential overall reactions are endothermic and elementary reaction steps are considered to require even more energy due to the cleavage of C-C bonds (see below).

The thermochemistry of three different model reactions is evaluated (see Table S4) in order to relate it to the selectivity of 3-methly-3-hexanol photoreforming. First, the required energy for a radical formation from the respective alkane via a C-H bond cleavage is calculated. Second, the scission of a C−C bond is addressed by the evaluation of the heat of reaction for the formation of two radicals from the respective alkane. Third, it is assumed that the reaction of the alcohol leads to a ketone, an alkyl radical and atomic hydrogen.

Table S4: Standard Enthalpy of Reaction (ΔH_R°) for three model reactions in order of evaluate the selectivity in 3-methyl-3-hexanol photoreforming (values calculated from Table S2).

Reaction	ΔH_R° [kJ/mol]
Model Reaction 1	
$CH_4 \longrightarrow CH_3^{\cdot} + H^{\cdot}$	439
$C_2H_6 \longrightarrow CH_3CH_2^{\cdot} + H^{\cdot}$	422
$C_3H_8 \longrightarrow CH_3CH_2CH_2^{\cdot} + H^{\cdot}$	423
Model Reaction 2	
$C_2H_6 \longrightarrow 2CH_3^{\cdot}$	377
$C_4H_{10} \longrightarrow 2CH_3CH_2^{\cdot}$	365
$C_6H_{14} \longrightarrow 2CH_3CH_2CH_2^{\cdot}$	369
Model Reaction 3	
$3-methyl-3-hexanol \longrightarrow 3-hexanone + CH_3^{\cdot} + H^{\cdot}$	460
$3-methyl-3-hexanol \longrightarrow 2-pentanone + CH_3CH_2^{\cdot} + H^{\cdot}$	452
$3-methyl-3-hexanol \longrightarrow 2-butanone + CH_3CH_2CH_2^{\cdot} + H^{\cdot}$	453

The reactions yielding a methyl radical require significantly more energy than those for the other two radicals. Reactions for the formation of propyl and ethyl radicals are very similar in energy, but in every case the formation of ethyl is energetically favoured over that of propyl. This is the same trend as for the observed selectivity in 3-methly-3-hexanol photoreforming.

References

(S1) Kollmannsberger, S. L.; Walenta, C. A.; Courtois, C.; Tschurl, M.; Heiz, U. Thermal Control of Selectivity in Photocatalytic, Water-Free Alcohol Photoreforming. *ACS Catal.* **2018**, *8*, 11076 – 11084.

(S2) Heiz, U.; Vanolli, F.; Trento, L.; Schneider, W.-D. Chemical Reactivity of Size-Selected Supported Clusters: An Experimental Setup. *Review of Scientific Instruments* **1997**, *68*, 1986–1994.

(S3) Walenta, C. A.; Kollmannsberger, S. L.; Kiermaier, J.; Winbauer, A.; Tschurl, M.; Heiz, U. Ethanol Photocatalysis on Rutile TiO_2(110): the Role of Defects and Water. *Phys. Chem. Chem. Phys.* **2015**, *17*, 22809–22814.

(S4) Henderson, M. A. Structural Sensitivity in the Dissociation of Water on TiO_2 Single-Crystal Surfaces. *Langmuir* **1996**, *12*, 5093–5098.

(S5) Geng, Z.; Jin, X.; Wang, R.; Chen, X.; Guo, Q.; Ma, Z.; Dai, D.; Fan, H.; Yang, X. Low-Temperature Hydrogen Production via Water Conversion on Pt/TiO_2. *J. Phys. Chem. C* **2018**, *122*, 10956–10962.

(S6) Isomura, N.; Wu, X.; Hirata, H.; Watanabe, Y. Cluster Size Dependence of Pt Core-Level Shifts for Mass-Selected Pt Clusters on TiO_2(110) Surfaces. *J. Vac. Sci. Technol., A* **2010**, *28*, 1141–1144.

(S7) Watanabe, Y.; Isomura, N. A New Experimental Setup for High-Pressure Catalytic Activity Measurements on Surface Deposited Mass-Selected Pt Clusters. *J. Vac. Sci. Technol., A* **2009**, *27*, 1153–1158.

(S8) Isomura, N.; Wu, X.; Watanabe, Y. Atomic-Resolution Imaging of Size-Selected Platinum Clusters on TiO_2(110) Surfaces. *J. Chem. Phys.* **2009**, *131*.

(S9) Bonanni, S.; Aït-Mansour, K.; Harbich, W.; Brune, H. Effect of the TiO_2 Reduction State on the Catalytic CO Oxidation on Deposited Size-Selected Pt Clusters. *J. Am. Chem. Soc.* **2012**, *134*, 3445–3450.

(S10) Harrison, A. G.; Jones, E. G.; Gupta, S. K.; Nagy, G. P. Total Cross Sections for Ionization by Electron Impact. *Can. J. Chem.* **1966**, *44*, 1967–1973.

(S11) Kim, Y.-K. et al. Electron-impact ionization cross section for ionization and excitation database. `http://physics.nist.gov/ionxsec`, 2004 version 3.0; 2018, February 12.

(S12) Walenta, C. A.; Kollmannsberger, S. L.; Courtois, C.; Pereira, R. N.; Stutzmann, M.; Tschurl, M.; Heiz, U. Why Co-Catalyst-Loaded Rutile Facilitates Photocatalytic Hydrogen Evolution. *Phys. Chem. Chem. Phys.* **2019**, *21*, 1491–1496.

(S13) Kudo, A.; Miseki, Y. Heterogeneous Photocatalyst Materials for Water Splitting. *Chem. Soc. Rev.* **2009**, *38*, 253 – 278.

(S14) Hisatomi, T.; Kubota, J.; Domen, K. Recent Advances in Semiconductors for Photocatalytic and Photoelectrochemical Water Splitting. *Chem. Soc. Rev.* **2014**,

(S15) Kim, B.; Li, Z.; Kay, B. D.; Dohnalek, Z.; Kim, Y. K. The Effect of Oxygen Vacancies on the Binding Interactions of NH_3 with Rutile TiO_2(110)-(1x1). *Phys. Chem. Chem. Phys.* **2012**, *14*, 15060–15065.

(S16) Kim, Y. K.; Kay, B. D.; White, J. M.; Dohnalek, Z. Alcohol Chemistry on Rutile TiO_2(110) The Influence of Alkyl Substituents on Reactivity and Selectivity. *J. Phys. Chem. C* **2007**, *111*, 18236–18242.

(S17) Dean, J. A.; Lange, N. A. *Lange's Handbook of Chemistry, 15th Edition*; New York: McGraw-Hill, 1999.

(S18) CRC Handbook, In *CRC Handbook of Chemistry and Physics, 85th Edition*; Lide, David R.„ Ed.; CRC Press, 2004.

(S19) Alberty, R. A.; Chung, M. B.; Flood, T. M. Standard Chemical Thermodynamic Properties of Alkanol Isomer Groups. *J. Phys. Chem. Ref. Data* **1987**, *16*, 391.

(S20) Baghal-Vayjooee, M. H.; Colussi, A. J.; Benson, S. W. Very Low Pressure Reactor. A New Technique for Measuring Rates and Equilibria of Radical-Molecule Reactions at Low Temperature. Heat of Formation of the Methyl Radical. *J. Am. Chem. Soc.* **1978**, *100*, 3214–3215.

(S21) Houle, F. A.; Beauchamp, J. L. Photoelectron Spectroscopy of Methyl, Ethyl, Isopropyl, and *tert*-Butyl Radicals. Implications for the Thermochemistry and Structures of the Radicals and Their Corresponding Carbonium Ions. *J. Am. Chem. Soc.* **1979**, *101*, 4067–4074.

A.8 Nickel Clusters on TiO_2(110): Thermal Chemistry and Photocatalytic Hydrogen Evolution of Methanol

Catalysis Science & Technology

ROYAL SOCIETY OF CHEMISTRY

PAPER

View Article Online
View Journal | View Issue

Cite this: *Catal. Sci. Technol.*, 2020, **10**, 7630

Nickel clusters on TiO_2(110): thermal chemistry and photocatalytic hydrogen evolution of methanol†

Moritz Eder,‡[a] Carla Courtois,‡[a] Tim Kratky,[b] Sebastian Günther,[b] Martin Tschurl[a] and Ueli Heiz*[a]

Received 21st July 2020,
Accepted 9th September 2020

DOI: 10.1039/d0cy01465f

rsc.li/catalysis

In heterogeneous photocatalysis, noble metals such as Au, Pt, or Pd are most commonly used as co-catalysts to facilitate H_2 evolution, yet their costs are problematic for applications on a large scale. In this work, we show that the cheaper, more abundant transition metal nickel as co-catalyst material reacts accordingly, when being deposited as small clusters onto rutile TiO_2. Different to noble metal systems the photocatalysts undergo photocorrosion, depicted in a declining activity during the photoreforming of methanol. The reaction being performed in an ultra-high vacuum environment allows for a more detailed elucidation of the deactivation processes. Supported by reactivity studies under different conditions, Auger electron spectroscopy reveals that coking of the clusters occurs, while nickel oxide formation is not observed. The study thus shows that nickel co-catalysts are indeed prospective systems for the photocatalytic hydrogen evolution reaction, similar to platinum clusters, but instead may also feature unexpected photon-driven deactivation pathways.

Introduction

Hydrogen is a key element in the intent to decarbonize major sectors of the economy. It is not only an ideal substrate for fuel cells which are used for transportation or for industry energy supply,[1] but its relevance has tremendously increased since the development of hydrogen gas turbines,[2] which may fill the gap of dispatchable generation in the carbon-free energy ecosystem.[3] However, most of the world's hydrogen production (>95%) is based on carbon-emitting processes, such as steam reforming of natural gas.[4] Photocatalytic hydrogen production from alcohols or water under mild conditions is a sustainable approach to guarantee the rising demand for hydrogen. This accounts all the more since the development of bioalcohol generation from renewable sources.[5–7] In addition, photocatalytic alcohol reforming on titania-based systems provides ketones and aldehydes as valuable oxidation side products and even facilitates the selective photocatalytic conversion of tertiary alcohols.[8] TiO_2 is the most often used and best understood semiconductor in photocatalytic applications,[9] because single-crystalline studies on TiO_2(110) under highly defined conditions in ultra-high vacuum (UHV) allow the investigation of fundamental mechanisms in photocatalysis and the disentanglement of thermal- and photochemical steps. The highly systematic works by Henderson, Dohnálek and others have provided reliable preparation recipes of the photocatalyst and its surface.[10–14] These procedures provide a defined, reproducible thermal and photochemical reactivity of the TiO_2(110) surface which is widely established in the field.[8,15–20] Loading the titania photocatalyst with a co-catalyst is indispensable for the system to be able to significantly evolve H_2.[21,22] For single crystals in UHV, laser-ablation cluster sources have proven to be outstanding tools for the *in situ* deposition of small, size-selected metal clusters.[23] It allows for a more precise size and coverage control than *e.g.* evaporation techniques, since soft-landing of the clusters ensures a destruction-free surface coverage.[24] A very prominent, stable and widely used co-catalyst is platinum. The photocatalytic oxidation of methanol on (Pt-loaded) rutile titania has been identified to be a hole-driven process.[25,26] On the well-investigated TiO_2(110) model surface, methanol is to a certain extent adsorbed dissociatively by O–H bond cleavage, yielding a photo-active methoxy and a hydrogen species. Upon illumination this photo-active methoxy is oxidized to formaldehyde through a C–H bond cleavage.[25] In a previous study, we demonstrated that Pt facilitates H_2

[a] *Chair of Physical Chemistry & Catalysis Research Center, Technical University of Munich, Lichtenbergstr. 4, 85748 Garching, Germany.*
E-mail: ulrich.heiz@mytum.de
[b] *Department of Chemistry, Technical University of Munich, Lichtenbergstr. 4, 85748 Garching, Germany*

† Electronic supplementary information (ESI) available: Mass scan of Ni clusters, methanol photochemistry on titania, oxygen PSD on titania, AES reference spectra. See DOI: 10.1039/d0cy01465f

‡ The authors contributed equally to this work.

evolution such that both abstracted hydrogen atoms recombine thermally on the metal cluster.[21] Although deviating from the widespread electrochemical 2-photon-process, which includes H^+ reduction by an electron, this pathway even comprehensively explains the photochemical reactivity of tertiary alcohols.[27] However, the high costs and low abundance of Pt hamper its implementation into applied systems on a larger scale. As its only role in the catalytic cycle is the thermal hydrogen recombination, a more abundant metal such as nickel, whose surface is able to thermally desorb hydrogen,[28,29] is a promising candidate for replacing it. Single crystal studies reveal that methanol decomposes thermally to H_2 and CO on nickel as it was observed for methanol on Pt clusters.[30,31]

The photocatalytic activity of Ni-loaded TiO_2 powder mixtures in methanol– or ethanol–water mixtures has been subject in several studies.[32–40] Chen *et al.* report a comparable photocatalytic hydrogen production rate from ethanol–water solutions for Ni/TiO_2 and Au/TiO_2.[41] In contrast, Bahruji *et al.* present a vanishingly small rate of hydrogen production for Ni/TiO_2 in methanol photoreforming.[33] There is, however, no consensus about whether metallic nickel, nickel hydroxide or nickel oxide is the active phase. In addition, hydrogen production rates are strongly dependent on the various preparation methods. The different conditions and the heterogeneity of the employed catalysts make it difficult to compare the results among each other and to draw systematic conclusions. Apart from titania, NiO_x is used as co-catalyst on Ga_2O_3 and various other support materials for overall water splitting, where the nickel-containing phase might act as hydrogen evolution catalyst, although the focus of these works often lies on the support and the exact role of the co-catalyst remains elusive.[42–44] Those studies imply that the key factors limiting the photocatalytic hydrogen evolution remain an open scientific question. As in the case of noble metals, these open questions can be approached from a fundamental level in order to clarify the role of Ni clusters as co-catalysts for heterogeneous photocatalysis.

In this work, we report the photocatalytic hydrogen evolution from methanol reforming on Ni_x-loaded $TiO_2(110)$ using size-selected metal clusters in a water-free, anaerobe environment under highly defined conditions in UHV. The absence of a solution underlines the direct hole transfer mechanism without involving any additional intermediate species, which allows to draw a complete picture of methanol photoreforming.

Conventional characterization methods cannot be applied to ideal single crystals in UHV. For example, the $TiO_2(110)$ sample is too thick for TEM analysis, and the cluster surface concentration is too low for a detection by Raman spectroscopy or X-ray diffraction. Instead, analytic procedures typical for surface science studies are used. We apply temperature programmed desorption (TPD) to investigate the thermal reaction pathways and Auger electron spectroscopy (AES) to characterize surface species. This method is extremely surface sensitive and in some cases even allows a better disentanglement of Ni and carbon species than *e.g.* X-ray photoelectron spectroscopy (XPS).[45–47] The photocatalytic activity is probed by well-defined reaction conditions to unravel elemental processes on the catalysts surface on a molecular level. The thoughtful choice of defined reaction conditions then allows a disentanglement of elemental thermal- and photochemical processes on a molecular level on the catalysts surface.

Experimental

All experiments were carried out in a home built ultra-high vacuum setup with a base pressure lower than 9.9×10^{-11} mbar.[8] Briefly, it consisted of a liquid N_2-cooled (x, y, z, φ) – manipulator (VAB Vakuum GmbH), an Auger spectrometer (CMA 100, Omicron Nanotechnology GmbH), a sputter gun (IQE 11/35, SPECS GmbH), a line-of-sight quadrupole mass spectrometer (QMS) (QMA 430, Pfeiffer Vacuum GmbH), a leak valve (Pfeiffer Vacuum GmbH), and a home-built gasline (base pressure 5.0×10^{-9} mbar). A laser vaporization cluster source, which allowed the generation and *in situ* deposition of metal cluster cations with an atomically precise number of atoms, was connected with the analysis chamber. Generally, the experimental parameters for the cluster deposition were chosen to ensure soft-landing conditions to eventually yield Ni^0 clusters on the reduced titania (Ni_x/r-$TiO_2(110)$) surface, as determined by Aizawa *et al.* by means of X-ray photoelectron spectroscopy (XPS).[24]

For cluster generation, a focused beam of a frequency-doubled Nd:YAG (532 nm, 100 Hz, Spitlight DPSS, Innolas) ablated a rotating Ni target (99.96% purity, ESG Edelmetalle, Germany). The as-generated plasma was cooled down by pulses of He gas (He 6.0, Air Westfalen) synchronized with the laser pulses. This way, the expansion of the cluster beam into the vacuum was facilitated. The cationic cluster beam was orthogonally deflected by a quadrupole bender and guided through a quadrupole mass filter (QMF; Extrel, USA), which enabled either the selection of a particular cluster size or the guidance of the clusters in ion-guide mode. For this study, the latter mode was used and the device was operated as high-pass filter transmitting only ions larger than Ni_{10}. The settings resulted in a cluster size distribution with a maximum from Ni_{20} to Ni_{23} (see Fig. S1†). Cluster loadings were determined by monitoring and integrating the cluster neutralization current during the deposition with a picoammeter (Keithley, 6587). The amount of metal clusters deposited onto the titania surface was 1% of a monolayer (ML) with respect to the total number of $TiO_2(110)$ surface atoms on the crystal in every experiment if not indicated differently. For experiments with different cluster coverages, the desired amount of nickel, which was specified in the presented data, were deposited by varying the deposition time (in the order of minutes).

The rutile $TiO_2(110)$ crystal plate (Surface-net GmbH, 0.995 cm × 0.995 cm × 0.3 mm) was mounted in a

molybdenum sample holder, whose temperature was controlled by resistive heating and liquid N_2 cooling and measured by a thermocouple attached to the bottom of the mounting plate. Crystal preparation and cleaning was done by repeated cycles of Ar^+ (100% N60; Air Liquide) sputtering (20 min, 1.0 keV, 1×10^{-5} mbar Ar), O_2 (≥99%, Westfalen) annealing (20 min, 800 K, 1.0×10^{-6} mbar O_2), and vacuum annealing (15 min, 800 K). The cleanliness was confirmed by AES. With this procedure a reduced, blue, conductive crystal was obtained containing a constant surface defect density of 6 ± 1%, determined by H_2O TPD.[13,19]

The reactants were dosed by Langmuir dosing at 150 K in the case of TPD, photon-stimulated reaction (PSR) and subsequent post-illumination TPD (PI-TPD) experiments. The TPD and PI-TPD measurements used a heating rate of 1–2 K s^{-1}. For the PSR experiment, the reactant-covered crystal was thermalized to 250 K prior to an illumination of 10 min at 250 K. Subsequently a PI-TPD was performed. For catalytic studies, the crystal was illuminated in a constant methanol background pressure of 5.0×10^{-7} mbar at 300 K. Mass signals in the QMS of thermal and photochemically desorbing species were identified by a fragmentation pattern analysis. The ion signals were corrected for the fragmentation contribution taken from reference mass spectra,[48] the transmission through the QMS, and the electron-impact ionization cross section. Methanol (absolute, HPLC grade, 99.8%, Sigma-Aldrich) was purified by several freeze–pump–thaw cycles and repeated flushing of the gasline prior to use. Its purity was confirmed by QMS analysis at a constant methanol background pressure.

The light source for the illumination of the photocatalyst was a frequency-doubled optical parametric oscillator (242 nm, GWU, premiScan ULD/400), pumped by the third harmonic of a Nd:YAG (Innolas Spitlight HighPower 1200, 20 Hz repetition rate, 7 ns pulse width). A pulse energy of 600 ± 50 μJ of the incident light beam guaranteed the saturation of the absorbing crystal with photons. No laser induced thermal heating effects were observed.

Results

Thermal chemistry on Ni-decorated titania

The thermal reactivity of methanol on Ni cluster loaded reduced-titania was investigated by means of TPD. Five consecutive methanol TPD spectra were taken in order to observe possible changes induced by the heat treatment, shown in Fig. 1 in comparison to a methanol TPD spectrum on bare r-TiO_2(110).

The bare surface (dashed lines) yields only one peak of the methanol fragment m/z 31 at ~340 K, which corresponds to the desorption of molecular methanol, as expected in this temperature range for an exposure of 1 L.[13] The TPDs on Ni_x/r-TiO_2(110) (solid lines) show the same peak, whose intensity is initially lower but increases consecutively in the following experiments. Additionally, the cluster-loaded surface shows an H_2 signal (~370 K) as well as a high temperature CO peak (~470 K). These two TPD profiles in Fig. 1 are in accordance with H_2 and CO TPD spectra published by Raupp and Dumesic using Ni evaporated on titania,[49] and with CO TPD studies by the Anderson group on Ni_x/TiO_2 using size-selected clusters.[24] Contrariwise to the methanol feature, their intensities are initially highest but decrease consecutively in the first three experiments. The desorption temperatures of H_2 and CO observed in Fig. 1 are close to literature desorption temperatures of these molecules from Ni nanoparticles.[49,50]

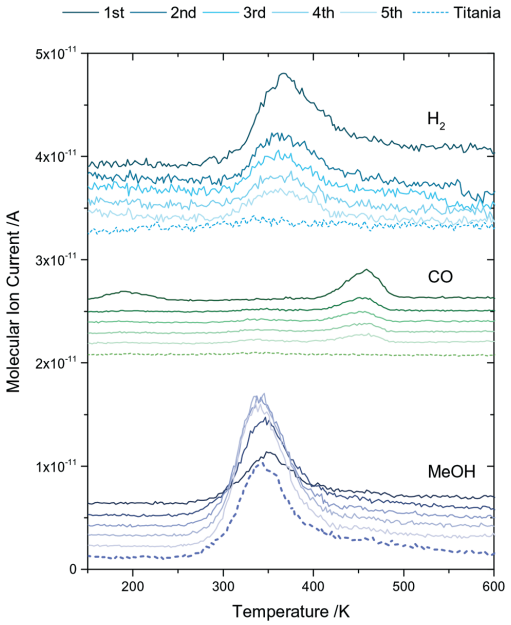

Fig. 1 Five consecutive TPD experiments with 1 L of methanol from 150 to 600 K on Ni_x/r-TiO_2(110) (solid lines) and an identical TPD experiment on bare r-TiO_2(110) (dashed lines) with traces for hydrogen (m/z 2), carbon monoxide (m/z 28) and methanol (m/z 31) are shown. The brightness of the graphs increases in the consecutive running order of the TPD experiments (see top legend). The signals are corrected for ionization cross section, QMS transmission, and cracking contributions by other molecules. After dosing 1 L of methanol onto the surface at 150 K, the catalyst was heated to 600 K at a rate of 1–2 K s^{-1}. After cooling to 150 K, the next TPD experiment was started immediately. Note that the traces are offset for sake of clarity.

Photochemistry on Ni-decorated titania

In order obtain insights into the photochemical properties of Ni_x/TiO_2(110), methanol photoconversion was investigated at 250 K. Isothermal PSR experiments are shown in the top of Fig. 2.

Upon illumination of the photocatalyst with 1 L of methanol adsorbed, the bare semiconductor surface (dark lines) shows no desorbing species other than formaldehyde

(orange). In contrast, the formaldehyde trace and the H_2 signal (blue) exhibit a sudden increase upon the illumination of the cluster-loaded semiconductor. Since both quantitatively corrected formaldehyde traces are virtually congruent, the molecule is detected in equal amounts in both experiments. Methyl formate, which is a common product upon irradiation at low-temperature, is not at all detected.[15]

Since more strongly bound adsorbates will not desorb at the chosen photoreaction temperature of 250 K, a PI-TPD was conducted subsequently. The PI-TPD spectrum (bottom Fig. 2) shows methanol desorption from both, the bare and the cluster-loaded surface, in similarly high amounts, whereas again no methyl formate and only negligible amounts of formaldehyde are detected. In contrast to the bare surface, $Ni_x/TiO_2(110)$ PI-TPDs show broad features of molecular hydrogen starting at 300 K as well as carbon monoxide desorption starting at 350 K.

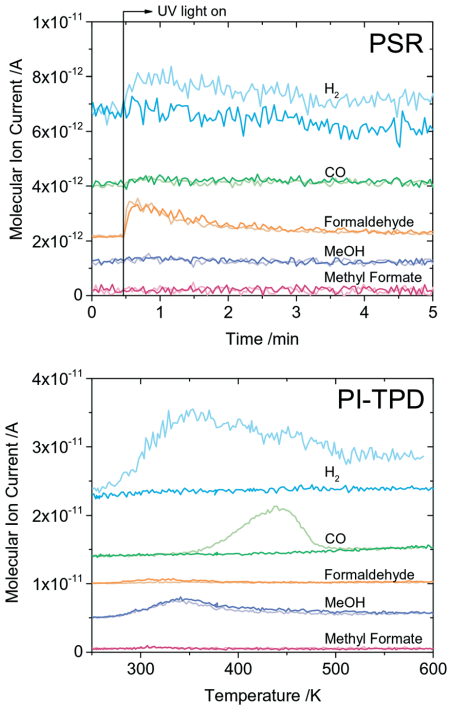

Fig. 2 Top: Isothermal photon stimulated reaction (PSR) experiments with 1 L of methanol at 250 K on $Ni_x/r\text{-}TiO_2(110)$ (bright graphs) and the bare $r\text{-}TiO_2(110)$ (dark graphs), with traces for hydrogen (m/z 2), water (m/z 18), carbon monoxide (m/z 28), formaldehyde (m/z 30), methanol (m/z 31) and methyl formate (m/z 60) shown. The signals are corrected for ionization cross section, QMS transmission, and cracking contributions by other molecules. Note that the traces are offset for sake of clarity. After dosing 1 L methanol onto the surface at 150 K, the catalyst was heated to 250 K and illuminated for 10 min. Bottom: PI-TPD spectrum taken subsequently to the PSR experiment at a heating rate of at a rate of 1–2 K s^{-1}. Contrary to the bare titania, the Ni loaded semiconductor facilitates both, thermal and photochemical hydrogen evolution by methanol (photo) conversion.

Photocatalysis on Ni-decorated titania

The photochemical investigations of $Ni_x/r\text{-}TiO_2(110)$ were extended to photocatalytic methanol oxidation under steady-state conditions. The photocatalytic conversion was conducted in a steady methanol background of 5×10^{-7} mbar near room temperature (300 K). The results are shown in Fig. 3.

Upon illumination (yellow background), an increase in both, the H_2 and formaldehyde trace, is observed, which drops back to its former level as the light is turned off (white background). Superimposing the quantitatively corrected traces (see inset in Fig. 3) shows that the molecules are generated in stoichiometrically equal amounts under irradiation. The intensities of formaldehyde and hydrogen traces taper off in parallel during repeated illumination intervals over time, which can be regarded as a deactivation process of the photocatalyst. This deactivation occurs in a non-linear fashion, *i.e.* the intensities of the traces under illumination approach their respective baseline in the dark asymptotically.

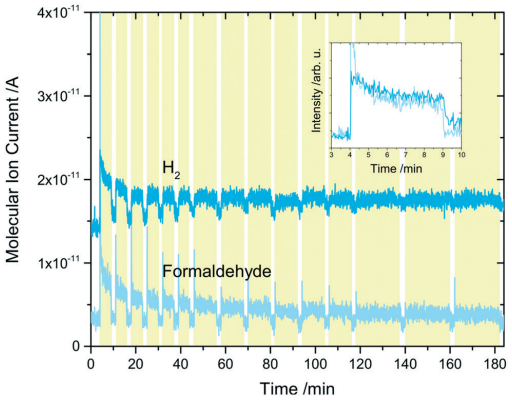

Fig. 3 Products of methanol photoreforming on $Ni_x/r\text{-}TiO_2(110)$ at 5×10^{-7} mbar alcohol background pressure at 300 K. The traces for hydrogen (m/z 2) and formaldehyde (m/z 30) are shown. The signals are corrected for ionization cross section, QMS transmission, and cracking contributions by other molecules. The yellow background highlights the illumination periods (242 nm), where the initial bursts stem from an enhanced methanol concentration on the surface due to its accumulation in the dark. Note that the traces are offset for sake of clarity. The inset shows both graphs superimposed within the first ten minutes. The equal area under the curves shows a stoichiometric formation of H_2 and formaldehyde as the respective traces have been corrected for their sensitivities. With increasing duration of the experiment, deactivation of the catalyst is evident as hydrogen and formaldehyde formation under illumination declines.

While the photocatalytic activity thus approaches zero, photocatalytic hydrogen and formaldehyde evolution is again feasible after heat treatment of the catalyst as depicted in Fig. 4. Annealing to 800 K recovers its photocatalytic activity to a considerable extent, even though the initial activity after cluster deposition is not reached. As in the case of the fresh catalyst, the traces of hydrogen and formaldehyde are congruent when superimposed as shown by the inset in Fig. 4.

To elucidate a possible change in the elemental surface composition in the course of the experiment, we employed Auger electron spectroscopy (AES) as a very surface-sensitive technique (Fig. 5). A loading of 3% ML of Ni clusters ensured pronounced and visible signals of the metal. For clarity, the insets show excerpts of the C KLL (left) and the Ni LMM peaks (right).

In the Auger spectrum shortly after the deposition of Ni clusters at 150 K (black), only the expected signals for Ti, O, and Ni are detected.[47] In the red spectrum recorded 16 h after catalysis a carbon peak is additionally observed while the intensities of the Ni transitions have decreased. As the carbon peak might originate from residual surface methoxy or carbonyl species, the crystal was treated with two cycles of annealing to 800 K and a spectrum was recorded while cooling (blue and green). While the Ni signals barely lose in intensity, the carbon signal persists in the spectra.

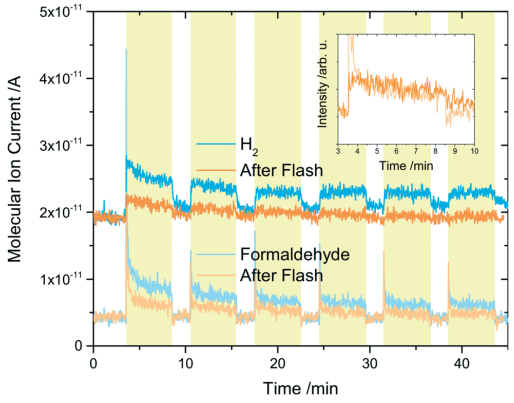

Fig. 4 Products of methanol photoreforming on $Ni_x/r\text{-}TiO_2(110)$ at 5×10^{-7} mbar alcohol background pressure at 300 K. The signals are corrected for ionization cross section, QMS transmission, and cracking contributions by other molecules. The H_2 and formaldehyde trace were recorded during the catalytic experiment after cluster deposition (blue). Subsequently, the catalyst was annealed to 800 K, cooled to room temperature and another catalytic experiment was conducted (orange). The yellow background highlights the illumination periods (242 nm). The initial bursts stem from an enhanced methanol concentration on the surface due to its accumulation in the dark. Note that the traces are offset for sake of clarity. With increasing duration of the experiment, deactivation of the catalyst is evident in all curves as hydrogen and formaldehyde formation under illumination declines. Flashing the catalyst to high temperatures partially regenerates the catalytic activity.

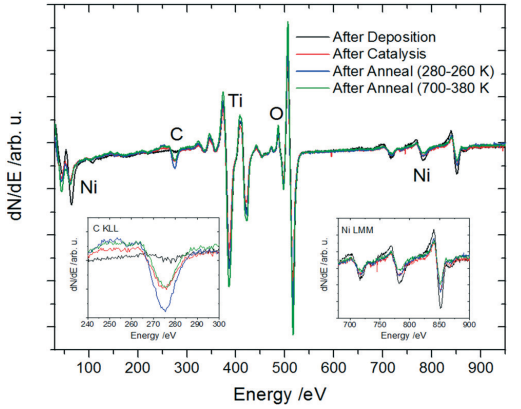

Fig. 5 Auger spectra of $Ni_x/r\text{-}TiO_2(110)$ (3% ML cluster coverage) taken consecutively: directly after deposition (black), after two catalytic experiments and storage *in vacuo* for 16 h (red), annealed to 800 K and cooled to 270 K (blue); while cooling down after annealing to 800 K and recording from 700 K on (green). The insets show excerpts of the spectrum with magnified C KLL peak (left) and Ni LMM peaks (right), respectively. The peaks were assigned using ref. 47.

While prolonged illumination in the presence of methanol leads to deactivation, the impact of methanol exposure on the catalytic activity was investigated in the absence of illumination. Fig. 6 shows a direct comparison of the hydrogen and formaldehyde traces between two catalytic experiments, which were started either directly after the cluster deposition (blue graphs) or after pre-exposing the catalyst to a steady methanol background for one hour. The congruency of the H_2 and formaldehyde traces from the two experiments show their formation in quantitatively equal amounts.

Discussion

Thermal chemistry on Ni-decorated titania

The TPDs of 1 L of methanol (Fig. 1) represent a direct comparison of the purely thermal chemistry of bare and Ni-decorated $TiO_2(110)$. During five consecutive methanol TPDs on $Ni_x/TiO_2(110)$, the declining intensity of the molecular alcohol trace and rise of the H_2/CO traces suggest that the alcohol decomposes into the latter. The fact that both decomposition products are absent in TPD spectra on bare titania indicates that the metal clusters on $Ni_x/TiO_2(110)$ are their formation sites. On the other hand, both molecules are more strongly bound to the surface than methanol, which supplies evidence for Ni clusters being also their desorption sites. On bare $r\text{-}TiO_2(110)$, surface CO already desorbs below 200 K,[51] while hydrogen does not desorb molecularly but as water from surface hydroxyl

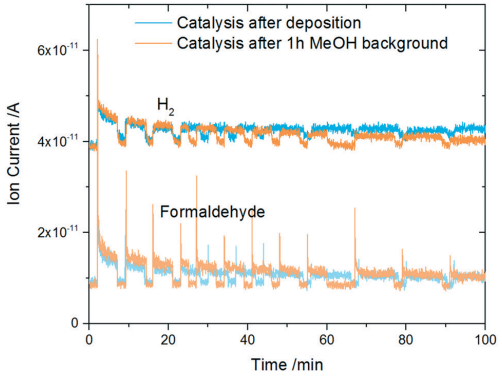

Fig. 6 Products of methanol photoreforming on Ni_x/r-TiO_2(110) at 5 × 10^{-7} mbar alcohol background pressure at room temperature, corrected traces for hydrogen (*m*/*z* 2, dark colors) and formaldehyde (*m*/*z* 30, bright colors) shown. The H_2 and formaldehyde trace were recorded during the catalytic experiment after cluster deposition (blue) and after cluster deposition followed by a constant MeOH background exposure of 5 × 10^{-7} mbar before illumination (orange). The initial bursts stem from an initially enhanced methanol concentration on the surface due to its accumulation in the dark. Note that the traces are offset for sake of clarity. With increasing duration of the experiment, deactivation of the catalyst is evident in all curves as hydrogen and formaldehyde formation under illumination declines. As the superimposed traces reach equal heights upon illumination (elevated traces), product formation remains quantitatively unaffected by MeOH pre-exposure.

recombination above 300 K.[18,52] Ni clusters hence induce additional surface reaction pathways to the thermal reactivity of titania to facilitate thermal H_2 formation. Since the desorption temperatures of H_2 and CO observed in Fig. 1 are close to literature desorption temperatures of these molecules from Ni nanoparticles,[49,50] decomposition already takes place below the desorption temperature. An impact on the clusters by the heat treatment is evident, too, because the peak intensities change with repeated ramping to 600 K.

Thermal H_2 evolution and strongly bound CO species during methanol TPD have also been observed on Au/TiO_2,[53] Pt/TiO_2(110)[17,31] and other noble metal loaded oxides[54,55] under ideal and applied conditions. The results from Fig. 1 confirm that Ni as co-catalyst can indeed react in the same way. As the methanol peak shows reduced intensity on Ni_x/TiO_2 in the first experiments, it is conceivable that the signals of hydrogen and carbon monoxide emerge at the expense of the methanol signal's intensity, *i.e.*, H_2 and CO are generated thermally by partial dehydrogenation of adsorbed methanol in the presence of Ni. These results agree with findings on transition metal surfaces, which can thermally decompose methanol to CO and molecular hydrogen.[56–60] TPD experiments on Ni single crystals have shown that methanol and intermediate methoxy species are decomposed to H_2 and CO.[58,61] In the same sense, the results herein show that methanol on Ni cluster-loaded titania decomposes to H_2 and CO at the metal clusters (pursuant to eqn (1)), which also serve as the desorption sites of these thermal products.

$$CH_3OH \xrightarrow{[Ni_x/TiO_2]} CO + 2H_2. \quad (1)$$

The change in the peak intensities caused by the heat treatment (Fig. 1), suggests a significant alteration of the Ni clusters in the course of the experiments. A possible scenario could be the diffusion of Ni clusters into the titania bulk. However, this process usually occurs at temperatures above 600 K,[62,63] which is the upper threshold of the TPD experiments in this work and is hence discarded as being relevant herein. While other studies in the literature also report a significantly strong metal-support interaction (SMSI) in Ni/TiO_2 systems at high temperatures,[64] Tanner *et al.* observed the growth of Ni nanoislands on TiO_2(110) *via* the Volmer–Weber mode between 295 and 400 K.[65] Based on their results, Anderson and coworkers estimated the size of these islands to 30 atoms, which appears to be a stable number based on their own TPD results in a temperature range from 150 to 600 K.[24] The size distribution of the Ni clusters in this work ranges from 12 to 27 atoms, and thus a growth of these clusters to slightly larger sizes seems likely. Since the last TPD spectra differ less strongly in intensity than the first ones, a majority of the clusters has presumably achieved a stable size after few TPD cycles, in excellent agreement with the results from the literature. This suggests a modification of the Ni clusters by the heat treatment until a thermodynamically more stable conformation is reached, which is accompanied by a lower amount of methanol being decomposed to H_2 and CO.

Photochemistry on Ni-decorated titania

Generally, the photoactivity of the titania photocatalyst appears unaffected by the presence of Ni clusters, because the formaldehyde peaks in the PSR experiments (orange, top of Fig. 2) and the methanol peaks in the PI-TPD (bottom of Fig. 2) are of equal intensity and shape. The latter stems from remaining alcohol species that have not been photo-converted. Formaldehyde is formed in equal amounts in the PSR spectra, which can be seen from the quantitatively corrected QMS traces. As expected from literature studies, TiO_2(110) does not show H_2 evolution under UV light,[21] whereas the Ni cluster-loaded surface leads to a rise of the H_2 trace upon illumination (top of Fig. 2). This result clearly shows that Ni clusters facilitate photochemical hydrogen evolution on TiO_2(110) in methanol photo-oxidation. Although this reactivity had been observed with Ni nanoparticles on P25 in aqueous systems,[32,40] in UHV studies using rutile it was hitherto only achieved with Au or Pt metal clusters.[8,17,21,66] As methyl formate is not detected due to the short residence time of formaldehyde on the surface at 250 K,[15,31] the

overall photoreaction exclusively occurs *via* the following equation:

$$CH_3OH_{ad} + h\nu \xrightarrow{[Ni_x/TiO_2]} CH_2O\uparrow + H_2\uparrow. \quad (2)$$

Since the same reaction products are formed in equal amounts in both experiments (depicted in Fig. 2), it can be concluded that the Ni clusters do not affect the photoreactivity and -activity of the reduced titania surface in the photo-oxidation of the alcohol.

The photocatalyst $Ni_x/TiO_2(110)$ shows parallels to $Pt_x/TiO_2(110)$ in UHV as well as to Ni/TiO_2 in wet-chemical systems. Despite of the photochemical similarities of metal cluster-loaded titania in wet-chemical and UHV conditions, it must be noted that the presence of a liquid environment and, in particular, molecules other than the alcohol (*e.g.* water or oxygen) may facilitate additional reaction pathways (*e.g.* an indirect hole transfer through the solvent).[9,22,67] Since the photoreaction depicted in eqn (2) occurs analogously on Pt_x/TiO_2, it is likely that the surface mechanism is identical, although the rates of individual reaction steps may differ.[21]

Similar as in the TPD experiments in the absence of illumination (Fig. 1), the TPDs after irradiation of bare and cluster-loaded titania also differ from each other (bottom of Fig. 2). In the PI-TPDs, only the Ni cluster-loaded surface shows H_2 and CO desorption, in agreement with the results from the TPD series (Fig. 1). Obviously, only a fraction of H_2 desorbs upon illumination at 250 K on $Ni_x/TiO_2(110)$, as significant amounts still desorb during the PI-TPD at higher temperature. This indicates that the chosen temperature hampers hydrogen recombination and desorption from Ni sites.

Photocatalysis on Ni-decorated titania and auger analysis

$Ni_x/TiO_2(110)$ facilitates steady-state hydrogen and formaldehyde formation by photocatalytic methanol conversion at room temperature as shown in Fig. 3. As no further byproducts are detected, methanol photo-oxidation takes place as described in eqn (2), in a manner as it is known from Pt-loaded $TiO_2(110)$.[21] Contrary to the latter (see Fig. S2†), the intensities of both, the formaldehyde and hydrogen trace under illumination, taper off over time. The photocatalytic activity of Ni-loaded titania hence declines during methanol photoreforming. Bare $TiO_2(110)$ also deactivates during alcohol photoreforming, but the deactivation pattern compared to Ni_x-r-$TiO_2(110)$ is notably different: r-$TiO_2(110)$ does not show any photon-driven hydrogen evolution (see Fig. 2 and S3†) and deactivates more rapidly due to the accumulation of hydrogen on the surface.[18] O_2 photon-stimulated desorption (PSD) measurements on the bare and nickel-loaded titania surface (see Fig. S4†) indicate that nickel clusters do not block photoactive sites to a significant extent (in parallel to Pt clusters).[21] Thus, the activity of the titania photocatalyst itself is not severely affected by cluster decoration. The number of photo-active sites is hence virtually equal to the bare r-$TiO_2(110)$ surface, and deactivation most likely occurs by a decreasing hydrogen recombination activity at the Ni clusters. This might be caused by a chemical change of the metal clusters, which are deposited in the metallic state due to the soft-landing conditions.[24] Apart from deactivation, the reactivity patterns (photochemical as well as thermal) of $Ni_x/TiO_2(110)$ are virtually identical to that of $Pt_x/TiO_2(110)$.[31]

Possible mechanisms for a chemical change of the clusters are sintering,[24,65] encapsulation underneath the surface,[62–64] the formation of oxide species,[24] carbonaceous deposits blocking the sites for hydrogen recombination or carbide formation.[68–70] In a first instance, encapsulation and sintering can be ruled out as origin of deactivation, as these processes would be significantly enhanced by higher temperatures. However, the catalytic activity can in contrast be restored to a certain degree by annealing (Fig. 5). The decrease in intensity of the Ni peaks in the Auger spectrum from before (black) to after photocatalysis (red) indeed points toward a diminished cluster concentration on the surface. However, the persistence of the Ni signal upon further heat treatment (blue and green) indicates that a certain stable conformation is eventually reached. This is in accordance with the observed thermal chemistry (Fig. 1) and literature results.[24] The fact that the metal clusters are still detectable although the photocatalytic activity for H_2 evolution has vanished, indicates that the Ni surface concentration and H_2 formation are not directly correlated. Therefore, a chemical change of the Ni surface species seems the most probable reason for the decline of the product formation rate.

An oxidation of the metallic Ni clusters to an oxide species seems a plausible scenario for deactivation but is contradicted by a more detailed analysis of all four Auger measurements and thermodynamic considerations. Generally, Ni oxidation by reduction of TiO_2 is unfavorable since the heat of formation of NiO (−250 kJ mol^{-1}) is energetically higher than the change in the standard free energy to form Ti^{3+} or Ti^{2+} (−364 kJ mol^{-1} and −483 kJ mol^{-1}, respectively).[71] Superimposing the spectra from Fig. 5 with reference spectra of Ni^0 and NiO (Fig. S4†) clearly demonstrates the dominance of metallic species in this series of experiments. This is in excellent agreement with literature results showing that metallic Ni is detected after various oxygen treatments at high temperatures of the $Ni_3Al(111)$ surface in UHV by means of Auger spectroscopy.[46] Furthermore, a recent *operando* XPS study on a bimetallic NiCu–TiO_2 photocatalyst for H_2 evolution unequivocally shows the metallic state of both co-catalyst metals.[72] While Prahov *et al.* concluded that Ni^0 atoms are required to evolve H_2 in a wet chemical environment, based on comparisons between the freshly reduced catalyst and after its exposure to air,[40] the observed decline in catalytic activity in the present work is not attributed to the oxide formation of the Ni co-catalyst.

On the other hand, the persistence of the carbon signal in the spectra after photocatalysis (orange, bright and dark green) points toward a strongly bound carbon surface compound. Since all common organic species on titania desorb upon heating to 800 K, the formation of strongly

bound carbonaceous species on the Ni clusters seems plausible based on general research on Ni catalysts.[68–70] In contrast, carbon formation is not observed on $Pt_x/TiO_2(110)$ after a similarly long period of photocatalytic methanol conversion (see Fig. S6†). As carbon can be removed by heat treatment as CO (Fig. 1), the residues on Ni clusters can be removed thermally, but only to a certain extent. At the same time, the catalytic activity is partially restored. The fact that $Ni_x/TiO_2(110)$ is not fully regenerated can thus be ascribed to irremovable carbonaceous surface residues as indicated by the still detectable C signal after repeated annealing (Fig. 5 dark green).

This scenario is supported by kinetic considerations on the declining photoactivity of $Ni_x/TiO_2(110)$. TiO_2 is known to show formaldehyde formation but no H_2 evolution in methanol photo-reforming due to the absence of suitable recombination sites. If the rate of hydrogen recombination and desorption is lower than the desorption rate of formaldehyde, hydrogen accumulation on the surface will result. This, in turn, changes the observed steady-state behavior: surface hydrogen and formaldehyde species will be converted back to methanol and methoxy rather than being desorbed from the surface if the hydrogen concentration on the surface becomes sufficiently high.[19] This will occur with an increasing probability as the H_2 recombination activity of Ni decreases, which is likely induced by the formation of a carbonaceous Ni species. The formation of C-species is clearly documented by the Auger spectrum and most likely linked to the declining catalytic activity. Furthermore, Ni clusters are the most plausible site for the formation of carbon species as the observed carbon deposits correlate with the clusters' presence at the TiO_2 crystal. Similarly, the clusters also enable H_2 recombination in the photoreaction, supplying evidence for the two mechanisms being interconnected. Thus, prolonged illumination does not only result in an increase in carbon residues on Ni, but at the same time impedes H_2 formation and deteriorates the photocatalytic activity.

Notably, the deactivation of the photo-catalyst indeed seems to be a purely photon-driven process. In additional experiments, $Ni_x/TiO_2(110)$ was exposed to a constant methanol background without illumination for one hour. The photocatalytic formation of H_2 and formaldehyde was found to be unaffected by prolonged methanol pre-exposure (see Fig. 6). Consequently, the presence of molecular methanol in the absence of UV irradiation does thus not lead to the deactivation of the Ni co-catalyst. Hence, the deactivation represents a phenomenon known as photo-corrosion and appears to originate from intermediate species or products rather than from molecularly adsorbed methanol only.

Conclusion

In summary, the work shows that nickel clusters can indeed facilitate a thermal evolution of H_2 at room temperature and thus enable the photocatalytic hydrogen evolution reaction on $TiO_2(110)$, similarly as observed for Pt clusters. However, nickel-loaded titania exhibits deactivation over time for prolonged illumination in a methanol atmosphere, which is different to the alcohol photoreforming with platinum clusters as co-catalysts. The decline in photoactivity is attributed to photocorrosion, as the activity of the photocatalyst is maintained upon exposure with the alcohol in the absence of light. A closer look onto the changes of the photocatalysts after reaction by Auger electron spectroscopy reveals that carbonaceous species are being formed. In contrast, an oxidation of the nickel clusters is not evident and the clusters largely remain in their metallic oxidation state. While the carbonaceous deposits can partially be desorbed as CO at elevated temperature, only a partial restoration of the photoactivity is possible. In general, nickel clusters may thus represent a more benign alternative in comparison to noble metal particles as hydrogen evolution co-catalysts. However, additional reaction pathways leading to the deactivation of the photocatalyst must be considered, in particular in the presence of carbon-containing molecules.

Conflicts of interest

There are no conflicts to declare.

Acknowledgements

The authors thank the DFG for financial support through the Germany's Excellence Strategy – EXC 2089/1-390776260. C. C. acknowledges the support from the Luxembourg National Research Fund (FNR), project code 12531916 and that from the TUM International Graduate School of Science and Engineering (TUM-IGSSE). M. E. would like to thank C. C. A. for fruitful discussions.

References

1 I. Staffell, D. Scamman, A. Velazquez Abad, P. Balcombe, P. E. Dodds, P. Ekins, N. Shah and K. R. Ward, *Energy Environ. Sci.*, 2019, **12**, 463–491.
2 M. Nose, T. Kawakami, H. Araki, N. Senba and S. Tanimura, *Tech. Rev. - Mitsubishi Heavy Ind.*, 2018, **55**, 1–7.
3 T. Bexten, *et al.*, Optimal Operation of a Gas Turbine Cogeneration Unit With Energy Storage for Wind Power System Integration, *Turbo Expo: Power for Land, Sea, and Air*, American Society of Mechanical Engineers, 2018, vol. 51043.
4 I. E. A., Technology Roadmap Hydrogen and Fuel Cells www.iea.org/t&c/, 2015, (accessed on 26.03.2020).
5 D. S. Thakur and A. Kundu, *J. Am. Oil Chem. Soc.*, 2016, **93**, 1575–1593.
6 S. Pugh, R. McKenna, I. Halloum and D. R. Nielsen, *Metab. Eng. Commun.*, 2015, **2**, 39–45.
7 A. Demirbaş, *Energy Sources*, 2005, **27**, 327–337.
8 S. L. Kollmannsberger, C. A. Walenta, C. Courtois, M. Tschurl and U. Heiz, *ACS Catal.*, 2018, **8**, 11076–11084.
9 M. A. Henderson, *Surf. Sci. Rep.*, 2011, **66**, 185–297.

10 R. T. Zehr and M. A. Henderson, *Surf. Sci.*, 2008, **602**, 1507–1516.
11 Z. Zhang, O. Bondarchuk, J. M. White, B. D. Kay and Z. Dohnálek, *J. Am. Chem. Soc.*, 2006, **128**, 4198–4199.
12 M. Shen and M. A. Henderson, *J. Phys. Chem. C*, 2012, **116**, 18788–18795.
13 M. A. Henderson, S. Otero-Tapia and M. E. Castro, *Faraday Discuss.*, 1999, **114**, 313–319.
14 M. A. Henderson and I. Lyubinetsky, *Chem. Rev.*, 2013, **113**, 4428–4455.
15 K. R. Phillips, S. C. Jensen, M. Baron, S.-C. Li and C. M. Friend, *J. Am. Chem. Soc.*, 2013, **135**, 574–577.
16 Q. Guo, C. Xu, W. Yang, Z. Ren, Z. Ma, D. Dai, T. K. Minton and X. Yang, *J. Am. Chem. Soc.*, 2013, **117**, 5293–5300.
17 Q. Hao, Z. Wang, T. Wang, Z. Ren, C. Zhou and X. Yang, *ACS Catal.*, 2019, **9**, 286–294.
18 C. A. Walenta, S. L. Kollmannsberger, J. Kiermaier, A. Winbauer, M. Tschurl and U. Heiz, *Phys. Chem. Chem. Phys.*, 2015, **17**, 22809–22814.
19 C. Courtois, M. Eder, S. L. Kollmannsberger, M. Tschurl, C. A. Walenta and U. Heiz, *ACS Catal.*, 2020, **10**, 7747–7752.
20 P. M. Clawin, C. M. Friend and K. Al-Shamery, *Chem. – Eur. J.*, 2014, **20**, 7665–7669.
21 C. A. Walenta, S. L. Kollmannsberger, C. Courtois, R. N. Pereira, M. Stutzmann, M. Tschurl and U. Heiz, *Phys. Chem. Chem. Phys.*, 2019, **21**, 1491–1496.
22 G. L. Chiarello, M. H. Aguirre and E. Selli, *J. Catal.*, 2010, **273**, 182–190.
23 U. Heiz, F. Vanolli, L. Trento and W.-D. Schneider, *Rev. Sci. Instrum.*, 1997, **68**, 1986–1994.
24 M. Aizawa, S. Lee and S. L. Anderson, *J. Chem. Phys.*, 2002, **117**, 5001–5011.
25 M. Shen and M. A. Henderson, *J. Phys. Chem. Lett.*, 2011, **2**, 2707–2710.
26 A. Yamakata, T.-a. Ishibashi and H. Onishi, *J. Phys. Chem. B*, 2002, **106**, 9122–9125.
27 C. Courtois, M. Eder, K. Schnabl, C. A. Walenta, M. Tschurl and U. Heiz, *Angew. Chem., Int. Ed.*, 2019, **58**, 14255–14259.
28 I. Chorkendorff, J. N. Russell and J. T. Yates, *Surf. Sci.*, 1987, **182**, 375–389.
29 B. E. Koel, D. E. Peebles and J. M. White, *Surf. Sci.*, 1983, **125**, 709–738.
30 J. N. Russell, I. Chorkendorff and J. T. Yates, *Surf. Sci.*, 1987, **183**, 316–330.
31 C. A. Walenta, C. Courtois, S. L. Kollmannsberger, M. Eder, M. Tschurl and U. Heiz, *ACS Catal.*, 2020, **10**, 4080–4091.
32 W.-T. Chen, A. Chan, D. Sun-Waterhouse, T. Moriga, H. Idriss and G. I. N. Waterhouse, *J. Catal.*, 2015, **326**, 43–53.
33 H. Bahruji, M. Bowker, P. R. Davies, J. Kennedy and D. J. Morgan, *Int. J. Hydrogen Energy*, 2015, **40**, 1465–1471.
34 E. P. Melián, M. N. Suárez, T. Jardiel, J. M. D. Rodríguez, A. C. Caballero, J. Araña, D. G. Calatayud and O. G. Díaz, *Appl. Catal., B*, 2014, **152-153**, 192–201.
35 J. B. Joo, R. Dillon, I. Lee, Y. Yin, C. J. Bardeen and F. Zaera, *Proc. Natl. Acad. Sci. U. S. A.*, 2014, **111**, 7942.
36 A. J. Simamora, F.-C. Chang, H. P. Wang, T. C. Yang, Y. L. Wei and W. K. Lin, *Int. J. Photoenergy*, 2013, **2013**, 419182.
37 P. D. Tran, L. Xi, S. K. Batabyal, L. H. Wong, J. Barber and J. S. Chye Loo, *Phys. Chem. Chem. Phys.*, 2012, **14**, 11596–11599.
38 J. Yu, Y. Hai and B. Cheng, *J. Phys. Chem. C*, 2011, **115**, 4953–4958.
39 W. Wang, S. Liu, L. Nie, B. Cheng and J. Yu, *Phys. Chem. Chem. Phys.*, 2013, **15**, 12033–12039.
40 L. T. Prahov, J. Disdier, J.-M. Herrmann and P. Pichat, *Int. J. Hydrogen Energy*, 1984, **9**, 397–403.
41 W.-T. Chen, A. Chan, D. Sun-Waterhouse, J. Llorca, H. Idriss and G. I. N. Waterhouse, *J. Catal.*, 2018, **367**, 27–42.
42 X. Wang, Q. Xu, M. Li, S. Shen, X. Wang, Y. Wang, Z. Feng, J. Shi, H. Han and C. Li, *Angew. Chem., Int. Ed.*, 2012, **51**, 13089–13092.
43 Y. Takashi, S. Yoshihisa and I. Hayao, *Chem. Lett.*, 2004, **33**, 726–727.
44 Q. Wang and K. Domen, *Chem. Rev.*, 2020, **120**, 919–985.
45 C. Ronning, H. Feldermann, R. Merk and H. Hofsäss, *Phys. Rev. B: Condens. Matter Mater. Phys.*, 1998, **58**, 2207–2215.
46 X. Ma, T. Kratky and S. Günther, *Nanoscale Adv.*, 2019, **1**, 4501–4512.
47 L. E. Davis, N. C. MacDonald, P. W. Palmberg, G. E. Riach and R. E. Weber, *Handbook of Auger Electron Spectroscopy*, Physical Electronics Industries, Inc., 2nd edn, 1976.
48 https://webbook.nist.gov/, 2020.
49 G. B. Raupp and J. A. Dumesic, *J. Catal.*, 1986, **97**, 85–99.
50 Y. Yao and D. W. Goodman, *J. Mol. Catal. A: Chem.*, 2014, **383–384**, 239–242.
51 A. Linsebigler, G. Lu and J. T. Yates, *J. Chem. Phys.*, 1995, **103**, 9438–9443.
52 Y. Du, N. G. Petrik, N. A. Deskins, Z. Wang, M. A. Henderson, G. A. Kimmel and I. Lyubinetsky, *Phys. Chem. Chem. Phys.*, 2012, **14**, 3066–3074.
53 S. A. Tenney, B. A. Cagg, M. S. Levine, W. He, K. Manandhar and D. A. Chen, *Surf. Sci.*, 2012, **606**, 1233–1243.
54 C. Lee, H.-K. Yoon, S.-H. Moon and K. J. Yoon, *Korean J. Chem. Eng.*, 1998, **15**, 590–595.
55 W. Jianxin and L. Laitao, *Catal. Lett.*, 2008, **126**, 325–332.
56 L. J. Richter and W. Ho, *J. Chem. Phys.*, 1985, **83**, 2569–2582.
57 F. L. Baudais, A. J. Borschke, J. D. Fedyk and M. J. Dignam, *Surf. Sci.*, 1980, **100**, 210–224.
58 S. R. Bare, J. A. Stroscio and W. Ho, *Surf. Sci.*, 1985, **150**, 399–418.
59 J. A. Gates and L. L. Kesmodel, *J. Catal.*, 1983, **83**, 437–445.
60 G. A. Attard, K. Chibane, H. D. Ebert and R. Parsons, *Surf. Sci.*, 1989, **224**, 311–326.
61 R. Neubauer, C. M. Whelan, R. Denecke and H.-P. Steinrück, *Surf. Sci.*, 2002, **507–510**, 832–837.
62 C. C. Kao, S. C. Tsai, M. K. Bahl, Y. W. Chung and W. J. Lo, *Surf. Sci.*, 1980, **95**, 1–14.
63 J. P. Espinós, A. Fernández and A. R. González-Elipe, *Surf. Sci.*, 1993, **295**, 402–410.
64 S. Takatani and Y.-W. Chung, *J. Catal.*, 1984, **90**, 75–83.
65 R. E. Tanner, I. Goldfarb, M. R. Castell and G. A. D. Briggs, *Surf. Sci.*, 2001, **486**, 167–184.
66 K. Katsiev, G. Harrison, Y. Al-Salik, G. Thornton and H. Idriss, *ACS Catal.*, 2019, **9**, 8294–8305.

67 G. L. Chiarello, D. Ferri and E. Selli, *J. Catal.*, 2011, **280**, 168–177.
68 I. Czekaj, F. Loviat, F. Raimondi, J. Wambach, S. Biollaz and A. Wokaun, *Appl. Catal., A*, 2007, **329**, 68–78.
69 P. K. Debokx, A. J. H. M. Kock, E. Boellaard, W. Klop and J. W. Geus, *J. Catal.*, 1985, **96**, 454–467.
70 M. Ichihashi, T. Hanmura, R. T. Yadav and T. Kondow, *J. Phys. Chem. A*, 2000, **104**, 11885–11890.
71 C. T. Campbell, *Surf. Sci. Rep.*, 1997, **27**, 7–9.
72 D. Spanu, A. Minguzzi, S. Recchia, F. Shahvardanfard, O. Tomanec, R. Zboril, P. Schmuki, P. Ghigna and M. Altomare, *ACS Catal.*, 2020, **10**, 8293–8302.

Electronic Supplementary Material (ESI) for Catalysis Science & Technology.

Supporting Information for

Nickel Clusters on TiO_2(110): Thermal Chemistry and Photocatalytic Hydrogen Evolution of Methanol

Moritz Eder[‡,a], Carla Courtois[‡,a], Tim Kratky[b], Sebastian Günther[b], Martin Tschurl[a], and Ueli Heiz[a,*]

[a] Chair of Physical Chemistry & Catalysis Research Center, Technical University of Munich, Lichtenbergstr. 4, 85748 Garching, Germany

[b] Department of Chemistry & Catalysis Research Center, Technical University of Munich, Lichtenbergstr. 4, 85748 Garching, Germany

‡ The authors contributed equally.
*Corresponding Author: ulrich.heiz@mytum.de

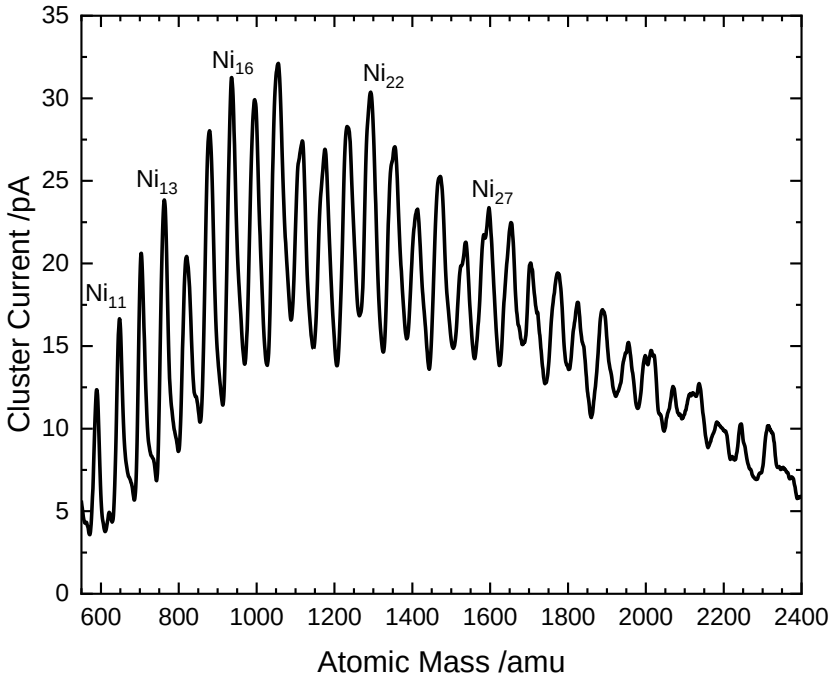

Figure S1. Mass spectrum of the cluster size distribution of Ni clusters from the laser vaporization source. The spectrum is taken after the quadrupole mass filter and shows a size-distribution of Ni_{10} up to Ni_{30}. When depositing in the ion guide mode, all masses lower than Ni_8 are discarded.

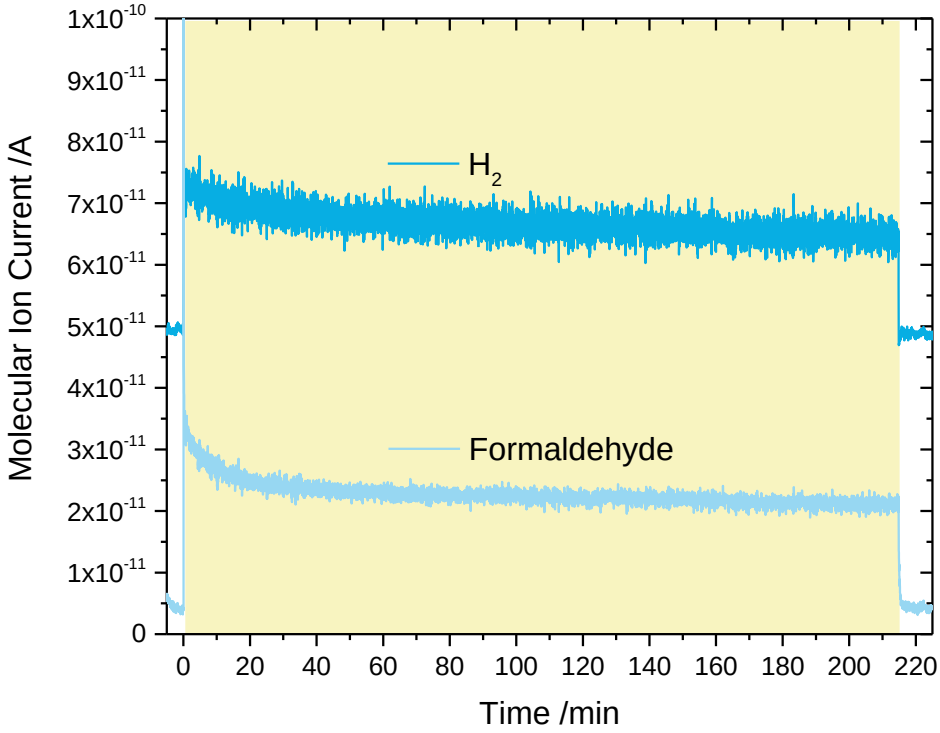

Figure S2. Products of methanol photoreforming on Pt_x/r-TiO_2(110) at 7x10^{-8} mbar alcohol background pressure at 267 K, corrected traces for hydrogen (*m/z 2*), and formaldehyde (*m/z 30)* shown. The colored background highlights the illumination period, where the initial bursts stem from an enhanced methanol concentration on the surface due to its accumulation in the dark. Note that the traces are offset for clarity. With increasing duration of the experiment, no deactivation of the catalyst is evident.

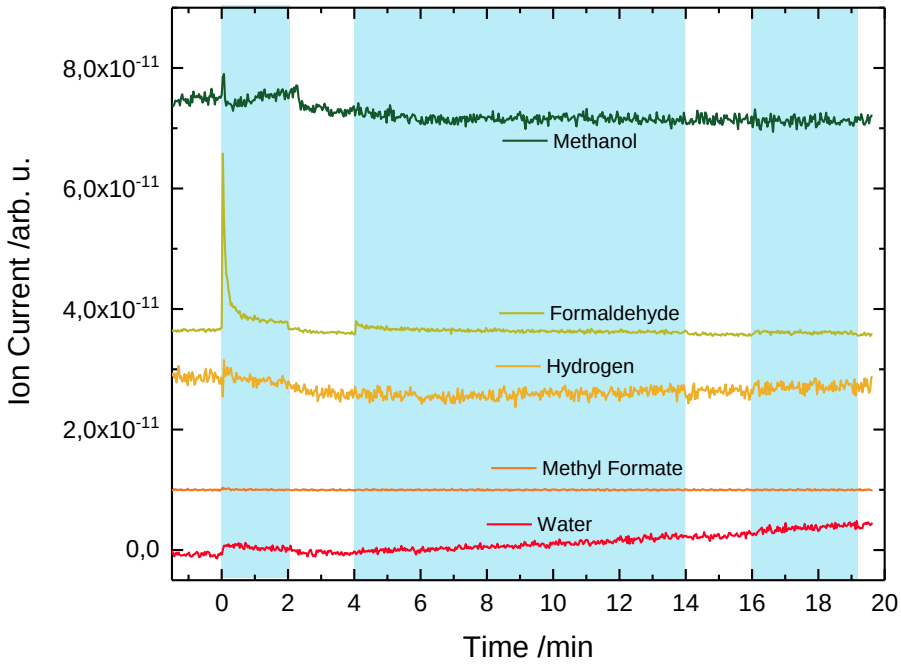

Figure S3. Products of methanol photoreforming on r-TiO_2(110) at 5x10^{-7} mbar alcohol background pressure at room temperature (RT), raw traces for hydrogen (*m/z 2*), water (*m/z* 18) formaldehyde (*m/z 30*), methanol (*m/z* 31), and methyl formate *(m/z* 60) shown. The blue background highlights the illumination periods, where the initial bursts stem from an enhanced methanol concentration on the surface due to its accumulation in the dark. Note that the traces are offset for clarity. With increasing duration of the experiment, deactivation of the catalyst is evident as formaldehyde formation under illumination declines.

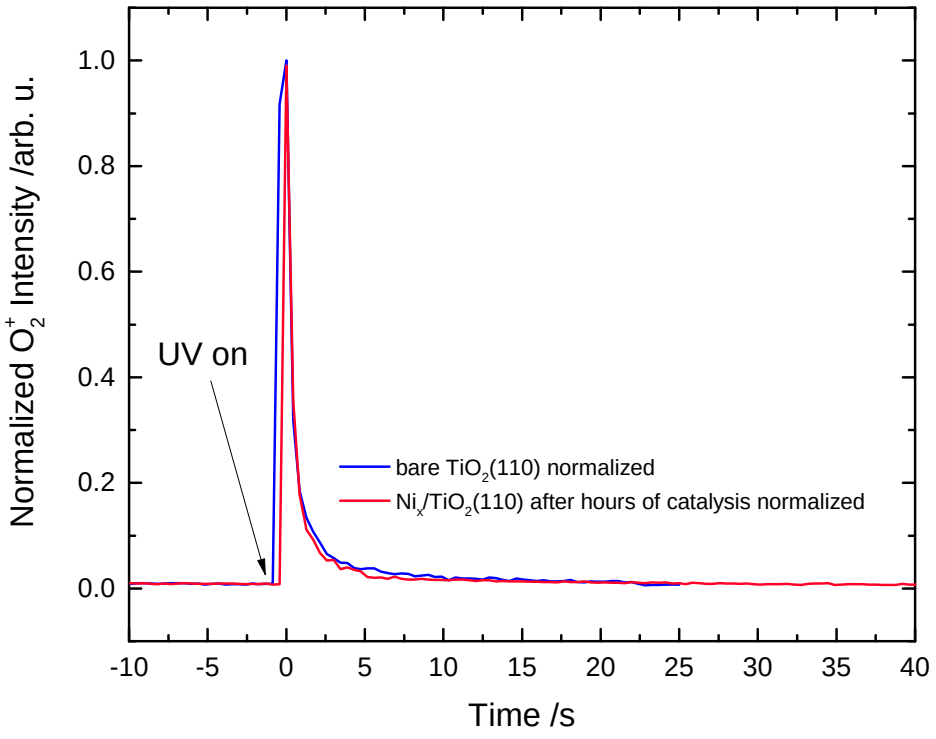

Figure S4. Normalized O_2 photon-stimulated desorption (PSD) spectra on r-TiO_2(110) and Ni_{16-45}/r-TiO_2(110), trace *m/z* 32 shown. For r-TiO_2(110), after dosing 20 L of O2 at cryogenic temperatures, the crystal surface was illuminated at 241.8 nm. For Ni_{16-45}/r-TiO_2(110) after the experiment, the methanol background is turned off and the sample was illuminated for another 15 min to deplete all the methanol from the photo-oxidation sites. The illumination is turned off, the sample cooled down to 130 K and exposed to 20 L of oxygen, to saturate the surface. Upon UV illumination, the same intensity and kinetics for the O2 PSD are observed as for the bare sample, indicating that the number of photoactive sites stays constant and that the methanol at least in the active sties was completely converted. (Note that the signals only slightly deviate in their maximum values from each other. This is caused due to the uncertainty in the starting time of the illumination as well as deviations by the QMS when the recording data points.)

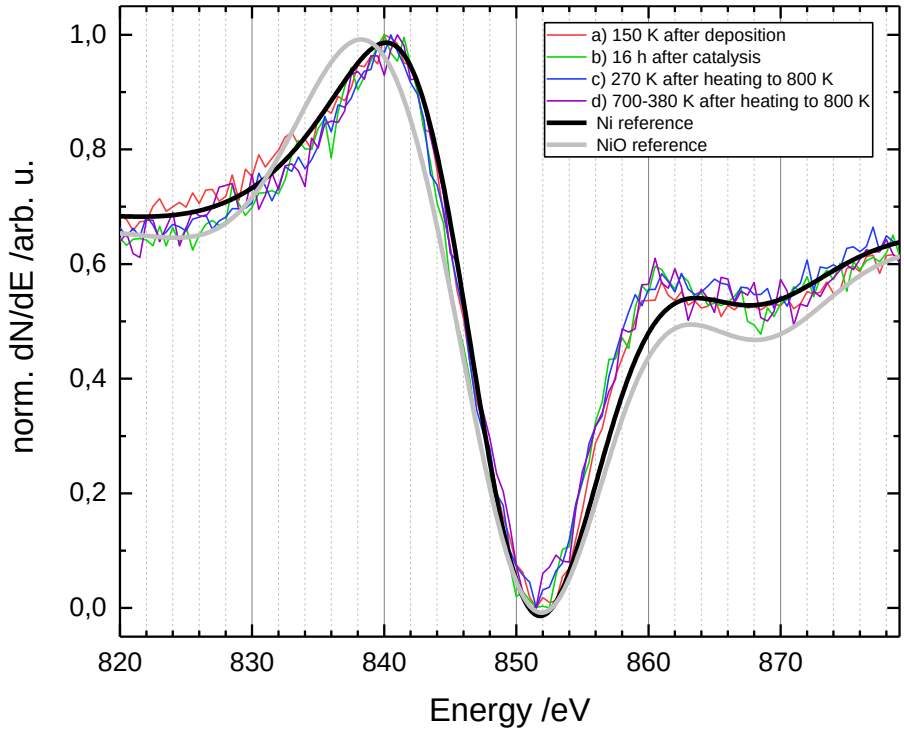

Figure S5. Excerpt of the Auger spectra of the Ni_x/r-TiO_2(110) surface from **Figure 5** in the manuscript, normalized to the maximum peak intensity between 800 eV and 900 eV (Ni). Two reference curves outline the progression of metallic Ni (black) and NiO (grey) references for comparison. The auger spectra were recorded with a primary electron energy of 3 keV.

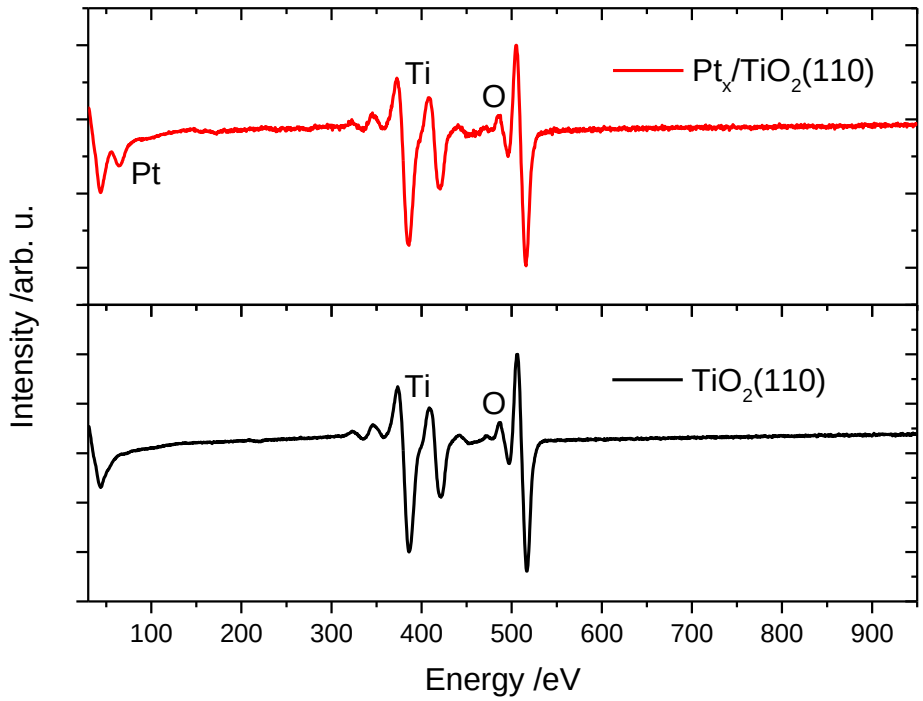

Figure. S6. Auger Electron Spectra of the clean r-TiO_2(110) surface (bottom) and Pt_x/r-TiO_2(110) after methanol photocatalysis and subsequent annealing to 800 K (top). Only titanium and oxygen are observed for the r-TiO_2(110) surface, while a small feature of the Pt NOO Peak appears at 64 eV on Pt_x/r-TiO_2(110). The coverage is 0.3% Pt>47/ML.

B

Reprint Permissions

B.1 Photocatalytic Selectivity Switch to C-C Scission: α-Methyl Ejection of *tert*-butanol on TiO_2(110)

Statement from the Royal Chemical Society:

"If you are the author of this article you still need to obtain permission to reproduce the whole article in a third party publication with the exception of reproduction of the whole article in a thesis or dissertation. Information about reproducing material from RSC articles with different licences is available on our Permission Requests page[1]."

[1] `https://www.rsc.org/journals-books-databases/journal-authors-reviewers/licences-copyright-permissions/#deposition-sharin9`, accessed February 9, 2021

B.2 Regulating Photochemical Selectivity with Temperature: Isobutanol on $TiO_2(110)$

ACS Publications
Most Trusted. Most Cited. Most Read.

Regulating Photochemical Selectivity with Temperature: Isobutanol on TiO2(110)

Author: Carla Courtois, Constantin A. Walenta, Martin Tschurl, et al
Publication: Journal of the American Chemical Society
Publisher: American Chemical Society
Date: Jul 1, 2020

PERMISSION/LICENSE IS GRANTED FOR YOUR ORDER AT NO CHARGE

This type of permission/license, instead of the standard Terms & Conditions, is sent to you because no fee is being charged for your order. Please note the following:

- Permission is granted for your request in both print and electronic formats, and translations.
- If figures and/or tables were requested, they may be adapted or used in part.
- Please print this page for your records and send a copy of it to your publisher/graduate school.
- Appropriate credit for the requested material should be given as follows: "Reprinted (adapted) with permission from (COMPLETE REFERENCE CITATION). Copyright (YEAR) American Chemical Society." Insert appropriate information in place of the capitalized words.
- One-time permission is granted only for the use specified in your request. No additional uses are granted (such as derivative works or other editions). For any other uses, please submit a new request.

BACK CLOSE WINDOW

B.3 Origin of Poisoning in Methanol Photoreforming on $TiO_2(110)$: The Importance of Thermal Back-Reaction Steps in Photocatalysis

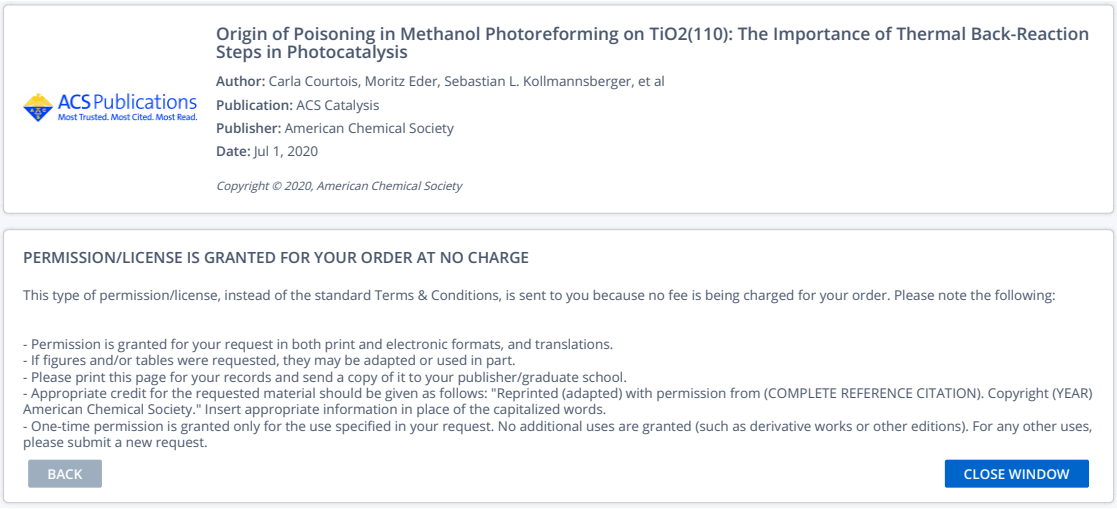

Origin of Poisoning in Methanol Photoreforming on TiO2(110): The Importance of Thermal Back-Reaction Steps in Photocatalysis

Author: Carla Courtois, Moritz Eder, Sebastian L. Kollmannsberger, et al

Publication: ACS Catalysis

Publisher: American Chemical Society

Date: Jul 1, 2020

Copyright © 2020, American Chemical Society

PERMISSION/LICENSE IS GRANTED FOR YOUR ORDER AT NO CHARGE

This type of permission/license, instead of the standard Terms & Conditions, is sent to you because no fee is being charged for your order. Please note the following:

- Permission is granted for your request in both print and electronic formats, and translations.
- If figures and/or tables were requested, they may be adapted or used in part.
- Please print this page for your records and send a copy of it to your publisher/graduate school.
- Appropriate credit for the requested material should be given as follows: "Reprinted (adapted) with permission from (COMPLETE REFERENCE CITATION). Copyright (YEAR) American Chemical Society." Insert appropriate information in place of the capitalized words.
- One-time permission is granted only for the use specified in your request. No additional uses are granted (such as derivative works or other editions). For any other uses, please submit a new request.

BACK CLOSE WINDOW

B.4 Surface Species in Photocatalytic Methanol Reforming on $Pt/TiO_2(110)$: Learning from Surface Science Experiments for Catalytically Relevant Conditions

B.5 Thermal Control of Selectivity in Photocatalytic, Water-Free Alcohol Photoreforming

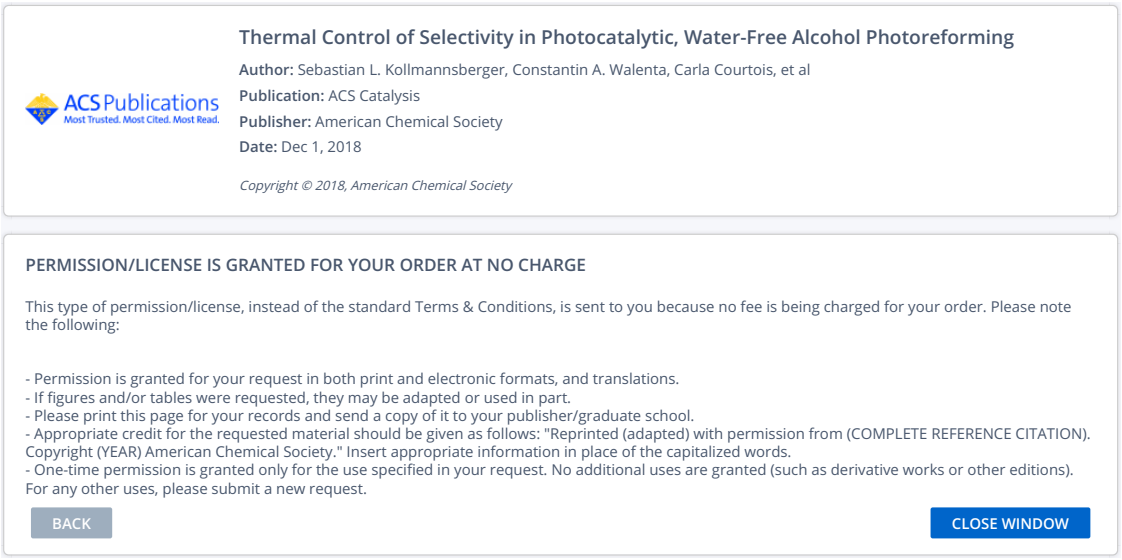

Thermal Control of Selectivity in Photocatalytic, Water-Free Alcohol Photoreforming

Author: Sebastian L. Kollmannsberger, Constantin A. Walenta, Carla Courtois, et al
Publication: ACS Catalysis
Publisher: American Chemical Society
Date: Dec 1, 2018

Copyright © 2018, American Chemical Society

PERMISSION/LICENSE IS GRANTED FOR YOUR ORDER AT NO CHARGE

This type of permission/license, instead of the standard Terms & Conditions, is sent to you because no fee is being charged for your order. Please note the following:

- Permission is granted for your request in both print and electronic formats, and translations.
- If figures and/or tables were requested, they may be adapted or used in part.
- Please print this page for your records and send a copy of it to your publisher/graduate school.
- Appropriate credit for the requested material should be given as follows: "Reprinted (adapted) with permission from (COMPLETE REFERENCE CITATION). Copyright (YEAR) American Chemical Society." Insert appropriate information in place of the capitalized words.
- One-time permission is granted only for the use specified in your request. No additional uses are granted (such as derivative works or other editions). For any other uses, please submit a new request.

BACK CLOSE WINDOW

B.6 Why Co-Catalyst-Loaded Rutile Facilitates Photocatalytic Hydrogen Evolution

Statement from the Royal Chemical Society:

"If you are the author of this article you still need to obtain permission to reproduce the whole article in a third party publication with the exception of reproduction of the whole article in a thesis or dissertation. Information about reproducing material from RSC articles with different licences is available on our Permission Requests page[2]."

[2] `https://www.rsc.org/journals-books-databases/journal-authors-reviewers/licences-copyright-permissions/#deposition-sharin9`, accessed February 9, 2021

B.7 Reactions in the Photocatalytic Conversion of Tertiary Alcohols on Rutile $TiO_2(110)$

B.8 Nickel Clusters on TiO_2(110): Thermal Chemistry and Photocatalytic Hydrogen Evolution of Methanol

Statement from the Royal Chemical Society:

"If you are the author of this article you still need to obtain permission to reproduce the whole article in a third party publication with the exception of reproduction of the whole article in a thesis or dissertation. Information about reproducing material from RSC articles with different licences is available on our Permission Requests page[3]."

[3] `https://www.rsc.org/journals-books-databases/journal-authors-reviewers/licences-copyright-permissions/#deposition-sharin9`, accessed February 9, 2021